



EUROPEAN SOUTHERN OBSERVATORY

# PROPOSAL

FOR THE CONSTRUCTION OF THE

# 16-M VERY LARGE TELESCOPE



March 1987

ESO

ML187/88

A4-2  
120a

ESO Libraries

---



ML 1993 000288

**PROPOSAL**  
**FOR THE CONSTRUCTION OF THE**  
**16-M VERY LARGE TELESCOPE**



**March 1987**

European Southern Observatory  
Karl Schwarzschild Straße 2  
D-8046 Garching  
Federal Republic of Germany

**VLT REPORT No. 57**



# Table of Contents

<b>1</b>	<b>Foreword</b>	<b>1</b>
<b>2</b>	<b>VLT Concept and Performance</b>	<b>5</b>
2.1	Concept Selection	5
2.1.1	Primary Mirror Technology	7
2.1.2	Optical Throughput	9
2.1.3	Wide Field Imaging	10
2.1.4	IR Observing	10
2.1.5	Interferometry	11
2.1.6	Redundancy and Flexibility	12
2.1.7	The Selection of the Basic Concept for the VLT	12
2.2	Summary of the VLT Concept	13
2.2.1	Unit 8 Metre Telescopes	13
2.2.2	Primary Mirrors	14
2.2.3	Active Correction	15
2.2.4	Mechanical Structure	17
2.2.5	Array Configuration and Building	17
2.2.6	Beam Combination and Interferometry	18
2.2.7	Site	20
2.3	Performance Goals and Basis for Specifications	21
2.3.1	Imaging Performance	21
2.3.2	Optical Throughput	24
2.3.3	IR Performance	25
2.3.4	Pointing	25
2.3.5	Tracking	25
2.3.6	Near Ground and Telescope Generated Seeing	26
2.3.7	Day Time Observing	26
2.3.8	Mirror Contamination	27
2.3.9	Environment	27
2.3.10	Operation	29
<b>3</b>	<b>Scientific Programme for the VLT</b>	<b>31</b>
3.1	Introduction	31
3.2	Scientific Opportunities for the VLT	34

3.2.1	Solar Systems Programmes	34
3.2.2	Star Formation	38
3.2.3	Studies of Interstellar Gas Clouds	42
3.2.4	Stellar Astronomy	45
3.2.5	Studies of Galactic Nuclei	49
3.2.6	Cosmological Studies	50
3.3	Conclusions	59
<b>4</b>	<b>Optics</b>	<b>61</b>
4.1	The Unit Telescope	62
4.1.1	Primary Mirror	69
4.1.2	Secondary Mirror	69
4.1.3	Nasmyth Mirror	71
4.1.4	Instrument Interface	72
4.1.5	Sky Baffling and Pupil Alignment	72
4.1.6	Optimization for the Infrared	73
4.1.7	Conversion to Cassegrain Focus	76
4.1.8	Individual Coudé Focus	77
4.1.9	Polarimetry	86
4.2	Beam Combination	86
4.2.1	Combined Coudé Focus	88
4.2.2	Fibre Optics for Beam Combination	94
4.3	Coatings	96
4.3.1	Coatings for Large Telescope Mirrors	96
4.3.2	Coatings for the Beam Combination Optics	97
<b>5</b>	<b>Primary Mirrors</b>	<b>103</b>
5.1	Technologies for Large Monolithic Mirror Blanks and Options for the VLT	103
5.1.1	Zerodur (Glass Ceramic)	104
5.1.2	Borosilicate Glass (BSC, Pyrex, Duran 50)	108
5.1.3	Fused Silica	108
5.1.4	Aluminium	109
5.1.5	Steels	110
5.1.6	Options for the ESO VLT Primary Mirror Blanks	114

5.2	Optical Figuring	115
5.2.1	General	115
5.2.2	Building and Test Tower	116
5.2.3	Milling, Grinding and Polishing Machine	117
5.2.4	Mirror Support During Figuring	117
5.2.5	Nature of the Blanks and Thermal Aspects	118
5.2.6	Optical Testing	118
5.2.7	Leadtime	119
5.3	Active Correction	120
5.3.1	Image Error Sources in Telescopes	120
5.3.2	The Active Optics Control System: Principles	121
5.3.3	The 1m Laboratory Experiment and Demonstration	125
5.3.4	Extrapolation from the NTT to the VLT	129
5.3.5	Active Optics and Wind Buffeting	135
5.3.6	Modal Analysis of a Thin Glass Meniscus Mirror	137
5.4	Primary Mirror Support	138
5.4.1	Specification	138
5.4.2	Axial Support	143
5.4.3	Radial Support	151
5.5	Mirror Cell	156
5.6	Thermal Aspects	161
5.7	Handling	163
<b>6</b>	<b>Mechanical Design</b>	<b>169</b>
6.1	General	169
6.2	Tube	171
6.2.1	Structure	171
6.2.2	Mirror Units	175
6.3	Azimuthal Structure	176
6.3.1	Fork Structure	176
6.3.2	Support Ring and Azimuth Tracks	176
6.3.3	Bearings and Oil System	177
6.4	Drives and Encoders	180

6.5	Structural Performance	180
6.5.1	Static Performance	180
6.5.2	Dynamic Performance	185
6.6	Tracking	189
6.6.1	Model	189
6.6.2	Results	191
<b>7</b>	<b>Control System</b>	<b>199</b>
7.1	Introduction	199
7.2	Distributed Microcontrollers	199
7.2.1	Hardware	201
7.2.2	Microprocessor Software	201
7.2.3	Local Area Network (LAN)	203
7.3	Main Axis Servos	204
7.4	TV-Image Analysis	205
7.5	Instrument Control and Data Acquisition	206
7.5.1	Hardware	206
7.5.2	Software	207
7.6	User End	211
7.7	Computers	212
7.7.1	Control/Instrumentation Minicomputers	212
7.7.2	User End Workstations	212
7.8	Remote Observing	213
<b>8</b>	<b>Building</b>	<b>217</b>
8.1	General	217
8.2	Infrastructure	220
8.2.1	Telescope Pillars	220
8.2.2	Combined Coudé Laboratory	221
8.2.3	Control Room	221
8.2.4	Interferometric Laboratory	223



8.2.5	Mirror Maintenance Building	224
8.3	Upper Structure: Telescope Shelters, Wind Screen, Handling Equipment	227
8.3.1	Telescope Shelters	227
8.3.2	Service Platform	230
8.3.3	Wind Screen	231
8.3.4	Gantry Crane and Other Lifting Equipment	233
8.4	Alternatives	233
<b>9</b>	<b>Site</b>	<b>237</b>
9.1	Requirements for a Site for the VLT	237
9.2	Possible Sites	237
9.2.1	Introduction	237
9.2.2	Comparison between Paranal, La Silla and Other Sites	238
<b>10</b>	<b>Instrumentation</b>	<b>245</b>
10.1	Introduction	245
10.2	Intrumentation Interfaces	245
10.2.1	Available Telescope Foci	245
10.2.2	Nasmyth Platforms	246
10.2.3	Instrumentation Adapters and Rotators	249
10.2.4	Compensation of Atmospheric Dispersion	251
10.2.5	Individual Coudé Focus	251
10.2.6	Combined Coudé Focus	251
10.3	Instruments for Observations in the UV/Visible Spectral Region (320-1000 nm)	252
10.3.1	Definition of General Characteristics of Instruments for Nasmyth and Cassegrain Foci	252
10.3.2	Optical Layouts and Performance of Instruments for Nasmyth/Cassegrain Focus	254
10.3.3	A High Resolution Instrument for the Incoherent Combined Focus	258
10.4	Infrared Instrumentation	264
10.4.1	Imaging at the Nasmyth Foci	265

10.4.2	Spectroscopy and Polarimetry Options at the Nasmyth Foci	267
10.4.3	Near Infrared Spectroscopy at the Combined Focus	268
10.4.4	Summary of Infrared Instrumentation	270
10.5	Conclusions	271
<b>11</b>	<b>Adaptive Optics</b>	<b>273</b>
11.1	Principle of Adaptive Optics	275
11.2	Strategy for Seeing Optimization	277
11.3	Elements of an Adaptive System	279
11.3.1	Wavefront Correction Device	279
11.3.2	Wavefront Sensor	279
11.3.3	Control System	281
11.4	Performance of an Adaptive System	282
11.5	Requirements for Adaptive Correction in Astronomy	283
11.6	Adaptive Optics for the VLT	285
<b>12</b>	<b>Interferometry</b>	<b>291</b>
12.1	Image Formation in Interferometry	293
12.1.1	Measuring the Visibility Amplitude	296
12.1.2	Measuring the Visibility Phase and Image Restoration	298
12.2	Optics	300
12.2.1	Delay Lines	304
12.2.2	Lateral Pupil Geometry	307
12.2.3	Longitudinal Pupil Position	307
12.2.4	Optical Design	307
12.2.5	Adaptive Optics	309
12.2.6	Fibre Optics for Interferometry	311
12.2.7	Instrumentation	312
12.3	Mechanical Stability	313

12.4	Auxiliary Movable Telescopes	313
12.5	Site Aspects	315
12.6	Conclusions	315
<b>13</b>	<b>Management, Schedule and Cost</b>	<b>319</b>
13.1	Management: ESO Project Experience, Means and Organisation	319
13.2	Schedule	321
13.3	Budget	325
13.4	Detailed Cost Estimates (KDM 1986)	326
13.5	Annual Costs	330
<b>Appendix 1</b>	<b>Summary of VLT Design Parameters</b>	<b>333</b>
<b>Appendix 2</b>	<b>VLT Notes and Reports</b>	<b>337</b>
<b>Appendix 3</b>	<b>Institutes and Industrial Firms which have contributed to VLT Studies</b>	<b>341</b>

# Chapter 1

## FOREWORD

This document presents the proposal made by ESO for the construction of the 16m VLT, the facility needed if its leading research capabilities are to be maintained also in the coming decades. *Specifically, it is proposed to construct an array of four 8m telescopes with an equivalent light gathering power of a 16m telescope, to place it on one of the world's best astronomical sites, and to provide it with auxiliary instrumentation needed to maximize its usefulness to the European research community.* As a complement to planned European activities in space, in high energy physics and in other branches of science, it will allow to push back the frontiers of knowledge on the most fundamental issues in our understanding of the Universe, its origin and evolution. At the same time, the VLT will be an ambitious technological undertaking worthy of the European capabilities in engineering and industrial enterprise.

To research the furthest reaches of the Universe in time and in space, ever fainter objects need to be studied in detail. This requires the light collecting power which only a very large telescope can give. To study the physical processes which occur in distant objects, sufficient angular and spectral resolution are needed. Both will be provided by the VLT array with its associated instrumentation. Many phenomena are best studied in the infrared part of the spectrum, where it is possible to penetrate through the veil of dust which obscures much of our Galaxy. Also here the VLT will open up entirely new possibilities.

It is sometimes thought that the future of astronomy is in space where the disturbing effects of the earth's atmosphere are absent. Of course, this is an advantage. But there are many things which cannot realistically be done in space. The Space Telescope, which will perhaps be launched next year, has cost nearly 1500 million US dollars. But it has an aperture of only 2.4 metres. A much larger telescope could be placed in space only at a prohibitively high cost. While the Space Telescope is needed in particular to study the ultraviolet radiation of celestial objects, which cannot penetrate the earth's atmosphere, a VLT which collects fifty times as much light can be built on the ground for one tenth of the cost.

Several other space projects are being planned in Europe for the 1990's at a cost

which far exceeds that of the VLT. The Infrared Space Observatory (ISO) will have an unparalleled sensitivity in the thermal infrared, but a very modest angular resolution. The VLT with its much higher angular resolution and with its high sensitivity in the near infrared will perform essential complementary observations. The high throughput X-ray facility XMM will study the spectra of X-ray sources. Since these sources are very faint optically, the sensitivity of the VLT is needed to study their spectra at optical wavelengths. And later, FIRST, the submillimetre mission, is expected to observe the interstellar medium and possibly galaxy formation. Again, correlated VLT studies will be important in the interpretation of the data obtained. *The VLT therefore is an essential complement to the European space programme of the next two decades.*

The most important discoveries which the VLT will make are likely to be unexpected. But it is clear already now that the VLT will make contributions to the solution of the problems which currently are at the centre of interest of astrophysicists. These include the size and age of the Universe, the distribution and composition of primeval intergalactic matter, the origin of the prodigious energy production in quasars, the formation of galaxies and their evolution, the origin of the chemical elements, the formation of stars and of the solar system, the dynamics and chemistry of planetary atmospheres, and the laws governing physical systems under conditions of high gravity or strong electromagnetic fields not obtainable in the laboratory.

No one has yet constructed an eight metre telescope or an array of such large telescopes. But in different parts of the world a start is being made. Much new technology will be needed to make such an instrument possible at an acceptable cost. The principal aspects of this have been considered during the last years at ESO in cooperation with the European industrial and other organizations listed on p. 339. Perhaps the most important new technology is the "active optics" discussed in Chapter 5 which allows the use of lightweight mirrors, thereby leading to a significant reduction in the weight and cost of telescopes. This technology has been extensively developed and tested at ESO. It is the basic technology for the 3.5m New Technology Telescope which is currently under construction. The NTT serves in many ways as a prototype for the unit telescopes of the VLT.

In an era of rapid technological development, it is important not to choose between various options before it is really necessary. At the same time, it is necessary at the start to know that the project is technically feasible in its entirety and that it can be realized with the funds which are available. As an example of the resulting approach, in Chapter 6 a mechanical design is presented based on steel as the construction material. This is easily costed, while static and dynamic response calculations of the structure to gravity, wind, etc., can be made with confidence. This baseline solution appears to be entirely acceptable. However, studies are conducted at present to see if a replacement of certain parts by carbon fibre elements would be an advantage. If the answer were positive and if the cost aspects were favourable, such a replacement would be implemented. It is important, however, to note that one does not have to do this, and that even without further development a satisfactory solution is available. This applies in other areas as well. *There is no doubt that the basic elements of the VLT can be built within the global*

*budget and that the essential specifications can be met.*

There are other aspects of the VLT which are much more uncertain. For example "adaptive optics", the compensation for the degrading of images by atmospheric turbulence, is actively being pursued within the VLT context. If it can be pushed sufficiently far, the gain will be very large, but at the moment no one knows what will be possible in practice. However, the VLT has been designed primarily for use without adaptive optics, and its success does not depend on the implementation of that feature. But it certainly seemed a good idea to allow for its possible implementation later. Interferometry has recently acquired more importance, also as a result of the large amount of work done by the corresponding ESO Working Group. But no one is yet very certain how far it can be pushed on the ground and at what wavelength. Again, the provisions for making interferometry possible have been made in the VLT design, and there should be no problem in arranging things in an optimal way a decade from now on the basis of the knowledge obtained by then.

Another important area where it appears possible and desirable to postpone a choice for a few years concerns the site for the VLT. The present La Silla site is among the best in the world. But sites have been found and investigated by ESO further north in the Atacama desert which on the basis of the available evidence are superior. The evidence is still incomplete, and because of the variability of climates it seems well to wait with a definitive decision until it is really necessary, so that adequate statistics can be obtained.

The VLT will be in particular complementary to the Hubble Space Telescope. As discussed in Chapter 3, each has its domain of excellence: there are some scientific problems which can only be solved by the HST, while others need the VLT with its large collecting area. Because of the long lead time of space projects, it is not always possible to incorporate newer technologies developed after a project has been started. It is one of the advantages of ground based instruments that newer technology can be adopted rapidly. While it is necessary to have at the start a feasible solution to every aspect, further optimization remains possible along the way. This is particularly true in the area of the auxiliary instrumentation where the detector technology has made remarkable progress in the last five years. Since further developments are in prospect in the next five years, a freezing of the instrumentation package for the VLT at the present time would be unwise. The proposals made in Chapter 10 reflect this. While a feasible instrument package is presently being outlined and costed, future developments may be expected to lead to important improvements.

The present proposals have been elaborated by the VLT project study group, headed by D. Enard. Contributions to this proposal have been made by many persons at ESO, including B. Delabre, S. D'Odorico, F. Merkle, A. Moorwood, G. Raffi, M. Sarazin, M. Schneermann, J. Wampler, R. Wilson, L. Zago and M. Ziebell. Editorial assistance was provided by K. Kjär, S. Lively and R.M. West.

The VLT project is not just a project of ESO as an organization. It is the project of the astronomical community in the ESO countries. In order to ensure the impact

of this community on the definition of the project, a number of Working Groups have considered various aspects: Imaging and Low Resolution Spectroscopy; High Resolution Spectroscopy; Infrared Aspects; Interferometry; Site Selection.

The members of the Working Groups were I. Appenzeller (Heidelberg), A. Ardeberg (Lund), D. Baade (ESO), H.R. Butcher (Groningen), B. Carli (Firenze), O. Citterio (Milano), J. Danziger (ESO), L. Delbouille (Liège), M.-H. Demoulin-Ulrich (ESO), M. Dennefeld (IAP), S. di Serego Alighieri (ST-ECF), S. D'Odorico (ESO), D. Downes (IRAM), D. Dravins (Lund), P. Felenbok (Meudon), B. Fort (Toulouse), T. Gehren (München), C. Jamar (Liège), E. Kreysa (Bonn), A. Labeyrie (CERGA), D. Lemke (MPI Heidelberg), P. Léna (Paris), M. Mayor (Genève), A. Moorwood (ESO), P.E. Nissen (Aarhus), J.E. Noordam (Dwingeloo), G. Olofsson (Stockholm), F. Roddier (Nice/NOAO), P. Salinari (Firenze), M. Sarazin (ESO), P. Shaver (ESO), F. Sibille (Lyon), J. Solf (MPI Heidelberg), H. van der Laan (Leiden), J. Vernin (Nice), G. Weigelt (Erlangen), J.J. Wijnbergen (Groningen), R. Wilson (ESO), H. Wöhl (Freiburg). The activities of the Working Groups were coordinated by J.-P. Swings (Liège).

In addition, two VLT Workshops have been held. The first one, at Cargèse in 1983 with 46 participants, provided an opportunity for discussing the general characteristics of the project. At the second Workshop in October 1986 at the Cini Foundation in Venice with 80 participants, the conclusions of the Working Groups and a preliminary version of this proposal were presented and further feedback was received from the community.

This proposal is concerned mainly with the technological problems of building the VLT. But its main aim is to provide facilities to the scientific community with which the exciting programmes discussed in Chapter 3, as well as many others, may be executed. It is difficult to foresee the technological developments which will take place between now and the completion of the VLT. It is even more difficult to imagine the unexpected scientific discoveries which will be made with the new large telescopes during the coming decades. If the governments of the ESO member countries can come to a rapid decision about the funding of the project, the future share of Europe in these discoveries will be assured.

L. Woltjer  
Director General

# Chapter 2

## VLT CONCEPT AND PERFORMANCE

### 2.1 Concept Selection

The main approaches to a large telescope concept proceed largely from the consideration of primary mirror technologies.

The choice is either to reconstitute one single large aperture from individual contiguous mirror segments, or to consider a set of monolithic mirrors each one being a primary mirror of a smaller telescope. An array of such smaller telescopes can then be assembled in one single mount or have independent mounts. The beams are optically combined in both cases. The former case corresponds to the multi-mirror-telescope (MMT) concept best represented by the existing MMT in Arizona. The latter is the solution retained for the ESO VLT. The segmented mirror solution has been selected for the California 10m Keck telescope project. It should be noted that none of these concepts are really new. The very first attempts to make fixed segmented mirrors are from Horn-D'Arturo in Bologna and Vaisälä in Turku. The first steerable segmented mirror telescope was built at the Meudon observatory in the late 60's [Chevallard et al., 1977] and several segmented light collectors have also been built. The concept of an MMT dates from the early 70's and although the 6 x 1.8m MMT of Mount Hopkins is the only one existing, several large telescope projects, such as the U.S. National New Technology Telescope (NNTT), are based on an MMT concept. The array concept has been discussed on many occasions [Disney, 1978; Grundmann et al., 1980; Learner, 1980; Barr, 1980], but has not yet been applied except for a few specific projects aiming exclusively to Michelson interferometry.

Figure 2.1 shows how the various concepts derive from the mirror technology. There is a nearly infinite number of ways in which the two basic technologies (segmented, and monolithic mirrors) can be combined, trading off size and number of elements. An example of mixed technology is the Themis project [Baranne et al., 1982] which



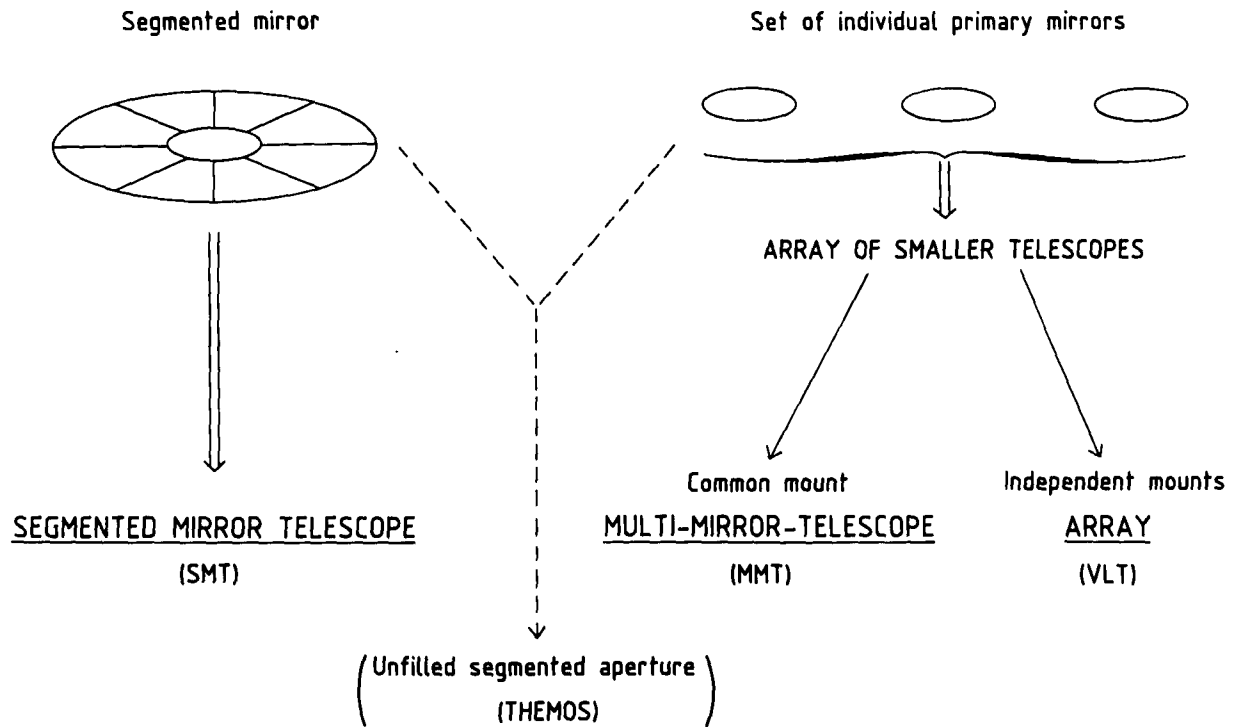


Figure 2.1: Mirror technology and telescope concept.

uses a set of spherical mirrors of circular shape, having the same centre of curvature. The mirrors are part of one single surface as with an SMT but the pupil remains unfilled as with an MMT. Such a mixed technology approach may have some advantages for specific applications but it rather tends to cumulate drawbacks. For instance the Themos approach would have a tube with a cross-section similar to that of an MMT, but a tube length even longer than that of an SMT. The diffraction pattern will be identical to that of an MMT (an unfilled aperture) and the spherical primary will very much limit the effective field of view. The fact that the manufacturing of the mirrors becomes easier does not compensate for the additional cost of the structure and building.

Similarly, it can safely be argued that a combination of an array of SMT's or of MMT's would not at the end present any of the basic advantages of each solution but only cumulate the technical difficulties inherent to each of them.

The number of realistic options is also limited if one considers that:

- A 16m aperture cannot be economically obtained with one single monolithic dish.
- If an array (here defined in its broad sense, i.e. it includes the MMT concept) is

considered, it should be made of the largest unit mirrors.

The reasons for this latest statement are:

- The necessity to have large photon collectors for observations requiring a large field which cannot be obtained at a combined focus of independent telescopes, and to limit the number of identical instruments to be produced,
- IR imaging under diffraction limited conditions,
- The cost of the mirror fabrication which increases less rapidly than the square of the aperture.

The interim report of the VLT Study Group (VLT Report No.44, pp. 8-14) has largely discussed the question of mirror technology. The report shows clearly that 8m is a nearly optimal trade-off between the scientific requirements, which suggest that the mirror diameter should be as large as possible and the optimization of cost, risk, handling and transportation.

Therefore one can restrict the discussion to concepts either based on 8m monolithic mirrors or on a single segmented mirror, 16m in diameter. Although the discussion between the pros and cons of various concepts has been going on for nearly 10 years and is amply documented, we feel it is useful to give an overview of the 3 basic possible options that have been considered for the ESO VLT. The discussion is however limited to the main aspects for which a difference in the performance could, a priori, be expected.

We shall therefore compare:

- A segmented mirror telescope (SMT) 16m diameter (single dish)
- A multi-mirror telescope (MMT) made of four 8m mirrors
- An array of 4 independent 8m telescopes

### 2.1.1 Primary Mirror Technology

The aspects to be considered are cost, reliability and imaging performance.

A segmented mirror is bound to be more expensive than a large monolithic mirror if one assumes the latter is active, that is its thickness is constant and does not increase with the diameter. Its figure must then be controlled by an active support system, which is simpler for a monolithic mirror than for a segmented mirror.

Figure 2.2 shows the dependence of the cost/m<sup>2</sup> upon the mirror diameter. The cost includes mirror blank and optical figuring. The estimate for the VLT 8m mirrors

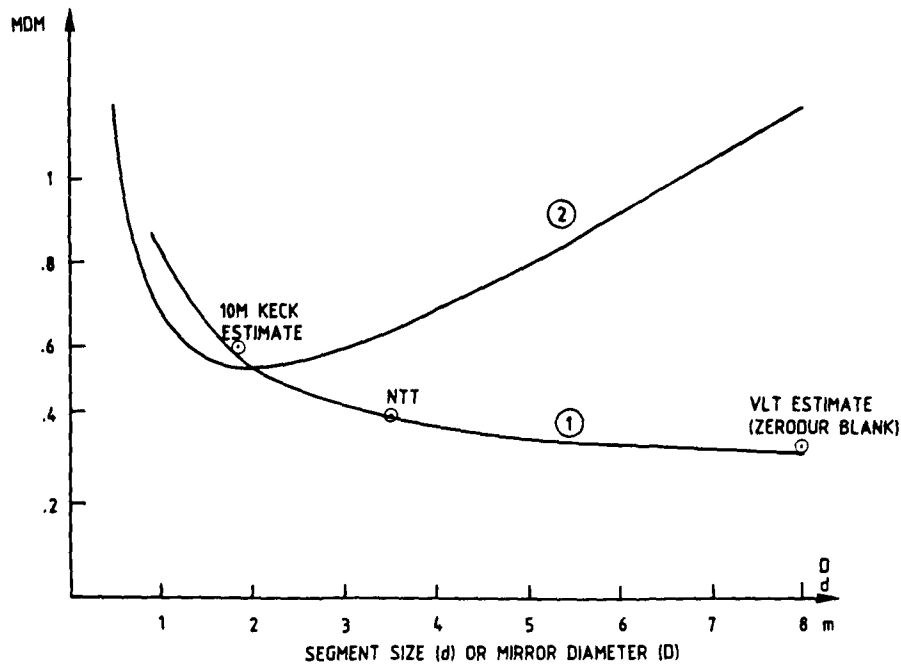


Figure 2.2: Approximative cost/m<sup>2</sup> of a monolithic (1) and a segmented (2) mirror. For a segmented mirror the cost is plotted against the segment size ( $d$ ) and assumes a fully passive internal support for the segments. For the monolithic mirror the cost is plotted against its diameter and the thickness is assumed independent of the diameter.

includes also the investment for the production of the blanks and the figuring on the basis of a total of 8 mirrors.

In the case of a segmented mirror, the cost/m<sup>2</sup> is independent of the final diameter but is dependent on the segment size because the thickness of the segment blanks will increase with their size. The decrease of the cost of monolithic mirrors with the diameter comes essentially from the fact that for an active mirror, the cost/m<sup>2</sup> of blanks is constant whilst the corresponding cost for the polishing decreases with  $D$ .

A monolithic mirror, whether active or not, is bound to be the most reliable because of the relative simplicity of its support system compared with that of a segmented mirror.

Imaging performance should be better with an active mirror than with a passively supported mirror, the former offers an additional possibility of correction in situ that the passive mirror does not have. The segmented mirror is likely to be the poorer because of the tremendous difficulty of manufacturing the segments with the same radius of

curvature and with the required accuracy up to the edge. It must be remembered that the cost of manufacturing an optical mirror is largely driven by the difficulty of producing an optical surface out to the edge of the mirror. A monolithic mirror has only one edge; a segmented mirror has edges everywhere. In whichever way the control system is designed it is likely to introduce an additional noise on the surface. This noise is bound to be more important than for an active monolithic mirror for which the correction can be viewed as a fine tuning. In comparison, errors of the actuators and sensors of a segmented mirror are transmitted directly to the segment position.

Though both MMT's and arrays use monolithic mirrors, a major difference appears when active correction is considered. The combined field of view of an MMT, which cannot exceed a few arcminutes unless the combining mirrors are made exceedingly large, would be too small to find a bright enough star that could serve as a reference for active tracking and correction of the mirror. Therefore an MMT is bound to either not have any real-time active correction or to have an intermediate large field focus. In the first case, the telescope will have to rely on its mechanical and thermal stability and on modelization, in the second case the combining optical system becomes complex and the basic advantage of an MMT over an array is lost.

The ESO approach that has been developed and applied to the NTT consists in relying extensively on active control to correct for various disturbances and achieve ambitious image quality performance. Though in principle there exist alternative ways such as a modelization coupled to a periodic check with a stellar image, an on-line correction is a definitive advantage.

The array concept is likely to provide the best image quality combined with low cost mirrors.

### 2.1.2 Optical Throughput

The SMT is conceptually similar to a classical telescope and the full collecting power is in principle available over the total field of view and with no wavelength limitation. By contrast, the MMT or an array needs a complex optical system to recombine the beams and the field of view at the combined focus is necessarily small. The effective field of view is dependent upon the relative distance between the telescopes; an array will therefore tend to have a combined field of view smaller than an MMT for the same size of combining mirrors.

The beam combining system of an MMT is located inside the telescope structure; it is therefore subject to flexures and the exchange of mirrors that would be necessary for selective high efficiency coatings to be used is much more problematic than for an array for which there is more space available for the combining optics outside the tube structure.

The practical effective field of view would be of the order of 30 arcminutes for an SMT, 2 to 3 arcminutes for an MMT and 0.5 to 1 arcminute for an array (depending

on its geometry). Both MMT and arrays can have wide field capability at foci of unit telescopes. Based on an efficiency of 90% for aluminium and 98% for high efficiency coatings, an MMT with 5 aluminium mirrors would have 59% efficiency and an array with 3 aluminium and 8 high efficiency coatings 62%.

If silver coatings with 98% efficiency in the visible would be used for all mirrors, the MMT would have 90% efficiency and the array 80%. By comparison, an SMT at the Nasmyth focus would have 61% efficiency with aluminium coatings and 94% with silver coatings. High efficiency coatings have therefore a crucial importance, all the more with an array for which they are mandatory for the combining optics.

### 2.1.3 Wide Field Imaging

Because of field limitation at the combined focus, wide field imaging with an MMT as well as with an array is only possible at the focus of unit telescopes. Post detection addition of data becomes then necessary whereas direct images are produced by an SMT.

Both modes lead to equal performance as long as the detector read-out noise can be neglected (which will be the case with a VLT for not too narrow band application owing to the predominance of sky background and likely improvement of detector performance). The total detector area and number of pixels necessary to cover a given field are also identical in both cases. The more complex data processing required for post-detection combination may be seen as the price to pay for smaller detectors and redundancy. One should also consider that it might anyhow be necessary to split long integrations with one single detector into several exposures in order to discriminate real objects from spurious events such as cosmic rays, so that both types of imaging may finally require a similar number of images to be combined.

Altogether the three concepts will probably yield equally satisfying results in wide field imaging observations.

### 2.1.4 IR Observing

The SMT is optically similar to existing telescopes. With 2 warm mirrors for Cassegrain operation and 3 for the Nasmyth it offers fewer warm surfaces that emit at IR wavelengths, but additional and possibly somewhat variable emissivity is introduced by the segment interspaces.

The MMT and the array need additional mirrors to combine the beams. Either these mirrors are warm and correspondingly an additional background can be anticipated or they are cooled at the cost of a considerable complexity (very large vacuum pipes, large scale cryogenics, windows...). With cooled combining mirrors, the 3 concepts would appear roughly equivalent, the emissivity of segment interspaces being balanced by the

presence of extra components with the MMT or the array. The SMT remains however definitely simpler.

An MMT or an SMT would give diffraction limited images about a factor of 2 better than with a single 8m aperture. Full phasing of an 8m aperture appears relatively easy to achieve at IR wavelengths with an adaptive correction. Full phasing of a composite aperture such as an MMT or an SMT requires in addition to control piston and tilt errors of each element of the aperture. It is not clear whether the theoretical gain of synthetic apertures could be fully realized for direct imaging.

### 2.1.5 Interferometry

The limit of resolution of an SMT is given by its aperture, i.e. it is better by a factor of 2 than that of a single 8m dish. This limit can be attained with classical speckle techniques in the visible or by phasing the segments in the IR, when the seeing is smaller than the limit of diffraction.

An MMT can work in an interferometric mode and has the advantage of maintaining equal path lengths between the telescope beams; a real time compensation of mechanical instabilities is necessary. The limit of resolution is that of a dish which would cover the 4 mirrors and is therefore slightly better than for a single 16m dish.

With both the SMT and the MMT, the spatial frequencies plane (so-called  $u,v$  plane) can be continuously covered and an image fully reconstructed up to the resolution limit which, in the case of the MMT, would be about 0.1 arcsec at  $\lambda = 10 \mu\text{m}$  and 5 milliarcsec at  $0.5 \mu\text{m}$ .

With an array of fixed independent telescopes it is necessary to compensate continuously the optical path difference between telescope beams when tracking the object. This, of course, makes interferometry technically more complex. The limit of resolution is given by the maximum distance between telescopes and can be one or two orders of magnitude better than for a single mount telescope. The  $u,v$  frequency plane cannot however be continuously covered, unless telescopes are made mobile. Therefore an array will provide information at a much higher resolution than a single mount but the quality of the reconstructed image may not be as good because of missing intermediate frequencies. Smaller, mobile auxiliary telescopes could be used to fill the gap.

In the IR, considering that mechanical stability tolerances are relaxed and that a single mount would provide a very limited improvement in resolution (merely a factor of 2), with respect to a single 8m dish, it seems that an array is preferable. At visible wavelengths single mounts would perform interferometry much more easily than an array but only for a limited resolution range.

### 2.1.6 Redundancy and Flexibility

No matter which concept is retained, a VLT is likely to be a highly complex instrument involving rigorous maintenance procedures. Reliability and maintenance aspects should be seriously considered during the design phase and a maximum of redundancy for the telescope and its instrumentation is indeed desirable. In that respect, the SMT is the less attractive since any failure of the telescope or of its instrumentation would preclude observation. The MMT is somewhat better since each telescope can be used independently; for instance a defect in one of the wide field instruments would not preclude observing with the three others. The array is obviously the most favourable solution because it offers a large redundancy; even with one telescope out of operation, observation with 3/4 of the collecting power is still possible and repair operations could even take place while observing with other telescopes. It should also be pointed out that by its nature, a segmented mirror is entirely dependent on its servos. A failure would be catastrophic whereas a monolithic mirror could still work even with degraded performance in a passive mode.

Flexibility is also a specific and fundamental advantage of the array which can be used in many different ways; complementary observing of the same object in different modes, partial specialization of the telescopes for certain types of observation for which the full collecting power is not required, and perhaps the more important, independent observing with 1 to 4 telescopes.

### 2.1.7 The Selection of the Basic Concept for the VLT

The necessarily crude analysis of the previous paragraphs shows that an array presents a number of advantages over competitive concepts. In a few areas it is "only" equal to others and only in exceptional cases is it inferior. The preference for a concept depends on the relative weight placed on the scientific goals and the appreciation of their realism. The selection of a concept is however a very complex issue in which factors other than scientific or technical have their place.

Such parameters are for instance the availability or not of certain technologies and of the manpower necessary to carry out the project completion, the type of expertise and experience available in and outside the organisation, the funding and, nearly as important, the cash flow that can be expected.

The success of a project depends usually on the correct appreciation of the difficulties and of the available resources, human, financial, technical. The fact that ESO has developed an actively corrected primary mirror for the 3.5m NTT, and is going to test the whole concept while the VLT will still be on the drawing board is also a key element in the decision and a factor of success.

Balancing altogether the various issues concerned ESO has selected an array of independent 8 m telescopes as the most favourable choice. The main specific arguments

which tilt the balance in favour of the proposed concept can be summarized as follows:

#### Scientific

- flexibility of use
- high resolution imaging (interferometry)
- early availability of an 8m telescope

#### Technical

- most adapted to an active primary mirror (better image, lower cost)
- experience of the NNT
- confidence that an extrapolation of the NNT by a factor 2 (for the unit telescopes) is reasonable and will limit risks

#### Financial

- reproduction of identical units is cost effective

## **2.2 Summary of The VLT Concept**

### **2.2.1 Unit 8 Metre Telescopes**

Altitude-azimuth (alt-az) mounting is now standard for modern telescope designs. It combines compactness, low mass and vertical symmetry of flexures. Its main drawback, which is the need for driving two axes is no longer seen as a problem and the forbidden zone around the zenith where tracking becomes impossible has in practice never been a real difficulty. Altitude-altitude (alt-alt) mountings - where a third servo mirror located at the cross-point of the two telescope axes reflects the beam along a fixed direction - are attractive whenever a Coudé focus is required. This is the case for an array where the beams have to be recombined in a central location. Although for this reason an alt-alt mount has been considered for some time, it has been abandoned because of the much larger mechanical structure it requires. Also, the variable angle of incidence on mirror 3 and its rapidly increasing size with sky coverage makes it rather unattractive for normal operation. If the telescopes were to be mobile, alt-alt mounts could be reconsidered in view of their potential for combining beams with no extra mirrors and no delay lines (case of auxiliary telescopes for interferometry).

The unit telescopes are conceived for single focus operation. This choice results from experience with large telescopes where the prime focus and the conventional Coudé foci



represent a significant fraction of the cost, whilst relatively little used largely because of the difficulties of operation. Prime focus operation with a VLT would be even more difficult and expensive. Existing designs for prime focus correctors (for large telescopes) indicate that very large lenses close to 1m diameter will be needed. Their manufacture and support are likely to create difficult problems. The need for image rotation compensation and off-axis guiding would make the development of a prime focus system very expensive. Due to its complexity, its final efficiency may not be superior to that of a focal reducer located at a Cassegrain or Nasmyth focus. This is confirmed by the recent experience at the ESO 3.6m telescope where a high throughput Cassegrain focal reducer provides more flexibility and in practice a better efficiency than the prime focus. With field segmentation techniques, a large field of view can be covered with small and independent focal reducers; among other advantages this technique eliminates the need for very large single detectors.

For an array, the combined Coudé mode is mandatory. In order to provide a fixed focus and to remain consistent with the philosophy of a single focus telescope priority was given to the Nasmyth focus. From the Nasmyth focus the beam can be easily relayed to the final Coudé focus with a set of fixed mirrors. Therefore, Nasmyth and Coudé operations can be obtained with an identical configuration of the telescope. Keeping constant characteristics of the telescope tube relative to gravity effects and wind load is a particularly important factor of reliability. An additional Cassegrain focus might be attractive because it would have only two reflections and no instrumental polarisation. It would normally require the change of the secondary mirror and the removal of the tertiary mirror. Both mirrors are large and this would increase the cost of the telescope and of its operation. In order to avoid this problem a solution where only the tertiary mirror has to be removed is proposed. It would provide an additional access to the Cassegrain focus, though Nasmyth operation remains the fundamental mode. It is very likely that the possibility of flexible scheduling will be lost during the time the Cassegrain focus is in operation. It is therefore foreseen not to implement it until the need for it is proven.

### **2.2.2 Primary Mirrors**

A monolithic actively corrected primary mirror appears as the best choice in terms of cost, reliability of operation and performance. The main problem lies in the blank procurement and in the investment necessary to figure it.

#### **Mirror blanks**

The realistic options for the primary mirror blanks are the following:

- **Zerodur glass ceramics:** Small scale experiments have demonstrated the possibility to cast or assemble lightweight structures. The most promising approach is however spin-casting of a thin meniscus. An 8m meniscus could be produced with an upgrading only of the existing facility at Schott. Casting of a 4.1m blank in 1987 will demonstrate the validity of the approach.
- **Fused silica:** The primary mirror of the ESO 3.6m telescope as well as a number of other large mirrors have been made of fused segments of silica. Extending this to larger dimensions is a technically feasible and reliable solution. Lead-time for the procurement of a thin meniscus blank would be fully compatible with the VLT schedule. One supplier in the U.S. and one in Europe could compete for the supply of a silica blank.
- **Metal:** A number of experiments on steel and aluminium have been carried out at ESO. First results look encouraging but further tests are necessary to establish the validity of the solution. Metal is attractive because of the relatively low cost compared with any glass solution and the short manufacturing time.

The current plans are to order one or more glass blanks by the end of 1987 and to continue developing the technology of metal mirrors as a back-up solution. It is not decided as yet whether the zerodur or the silica option will finally be selected.

### Figuring and polishing

The various studies performed by European optical firms for ESO have shown that figuring and polishing a single large mirror, even a highly flexible one, is well within the possibility of today's technology. The cost of the polishing machine, control tower and building is rather high and as a consequence it is not yet clear if the construction of one or two such facilities would be most appropriate.

### 2.2.3 Active Correction

The strategy for the unit telescopes is to rely essentially on active correction to compensate various image deteriorating effects such as gravity, temperature variations, hysteresis, wind buffets, etc. This approach is in line with ESO's current efforts to develop and apply an active correction scheme to the 3.5m New Technology Telescope (NTT). The NTT will be able to operate in a semi passive mode, but the VLT will be more dependent on its active correction. We believe this is the only way to obtain optimum image quality at a reasonable cost.

The ESO active correction scheme requires a reference star, whose brightness determines the correcting bandpass. Therefore, a field of view of 20 to 30 arcminutes is an important requirement. This requirement implies that in whichever way the unit



Figure 2.3: Model of the mechanical structure of an 8 metre unit telescope.

telescopes are finally combined an intermediate large field image plane must be available. This restricts considerably the freedom for telescope design innovation. Unless either the optical quality is relaxed or, extremely stable and rigid mirror blanks (hence heavy and/or expensive) are available we see little possibility to compromise with this requirement. The active correction scheme envisaged for the VLT includes a correction of the primary mirror figure through force actuators (as for the NTT) and a correction of fast tracking errors (i.e. beyond the bandpass of the main servos) with the secondary mirror.

### 2.2.4 Mechanical Structure

The general requirements for a modern telescope structure are:

- lightweight
- low thermal inertia
- smallest wind attack cross-section
- very great stiffness and high resonance frequencies
- high reliability and low hysteresis

These requirements necessarily push the design in the direction of a highly optimized space frame structure. Pre-design and computer analysis of several solutions have been performed. The most favourable provisional concept is shown in Figure 2.3. The total moving mass of the telescope will be about 230 tons and the lowest resonance frequencies of the structure about 9 Hz. For comparison, the figures for the 5m Mount Palomar telescope are 500 tons and about 1 Hz.

The drives are of particular importance considering the important wind load on the telescope structure. A conventional gear-wheel system has been analysed. Alternatives are being investigated.

### 2.2.5 Array Configuration and Building

The final configuration of an array should be determined considering the following factors:

- The field of view at the combined focus is a function of the distance between telescopes.
- The aerodynamic coupling and interference between separate buildings and telescopes should be avoided.

- Optimum configuration for interferometry and its compatibility with other requirements such as the site topography.

The particular wind pattern in most sites of Northern Chile shows a quasi constant direction for strong winds so that a linear arrangement facing the prevailing wind becomes attractive. A logical consequence is that if the wind direction can be considered as quasi constant, a protection against strong winds does not need to move with the telescope and could be constructed independently of the building. The present VLT building concept is effectively based on this idea. In this concept, the telescopes have been set at a close distance so as to provide the most compact and cheapest building. There is in principle no technical difficulty to modify the configuration for instance to provide longer baselines for interferometry. The field of view at the combined focus would however be reduced.

Seeing optimization is a long debated issue for which there is no straightforward solution; dome generated seeing and wind load must necessarily be traded off. The proposed approach is to deal in the best possible way with seeing in operating the telescope in open air. The critical problem becomes then the wind loads. Wind loads can be measured and their effects can be objectively analysed and predicted. The cost increase of the telescope structure and drives required to cope with the wind load should be largely compensated by a corresponding decrease in building cost. Thus the seeing optimization will be achieved at no extra cost.

Though operating in the open air, the telescopes need a physical and thermal protection during day time and bad weather periods. An attractive building concept consists of inflatable domes supported by a rigid structure. Operation of the telescope without protection should be possible at least up to wind speeds of 9 m/sec. Beyond this value, a wind screen would reduce the effective mean wind speed on the telescope by a factor of two. Operation should then be possible up to 18 m/sec which corresponds to more than 96% of night time at the sites considered. Figure 2.4 shows a model of this building concept. Alternatives with more conventional enclosures are also considered as potential back-up solutions.

## 2.2.6 Beam Combination and Interferometry

Combining the beams of alt-az telescopes necessarily requires a number of additional mirrors and hence potential light losses. High quality of coatings and protection of surfaces are therefore essential for Coudé operation.

The concept for the beam combination is based on the following principles:

- Relaying the central part of the Nasmyth focal plane to the final Coudé focus. Changing from Nasmyth to Coudé does not require then any change of the telescope configuration.

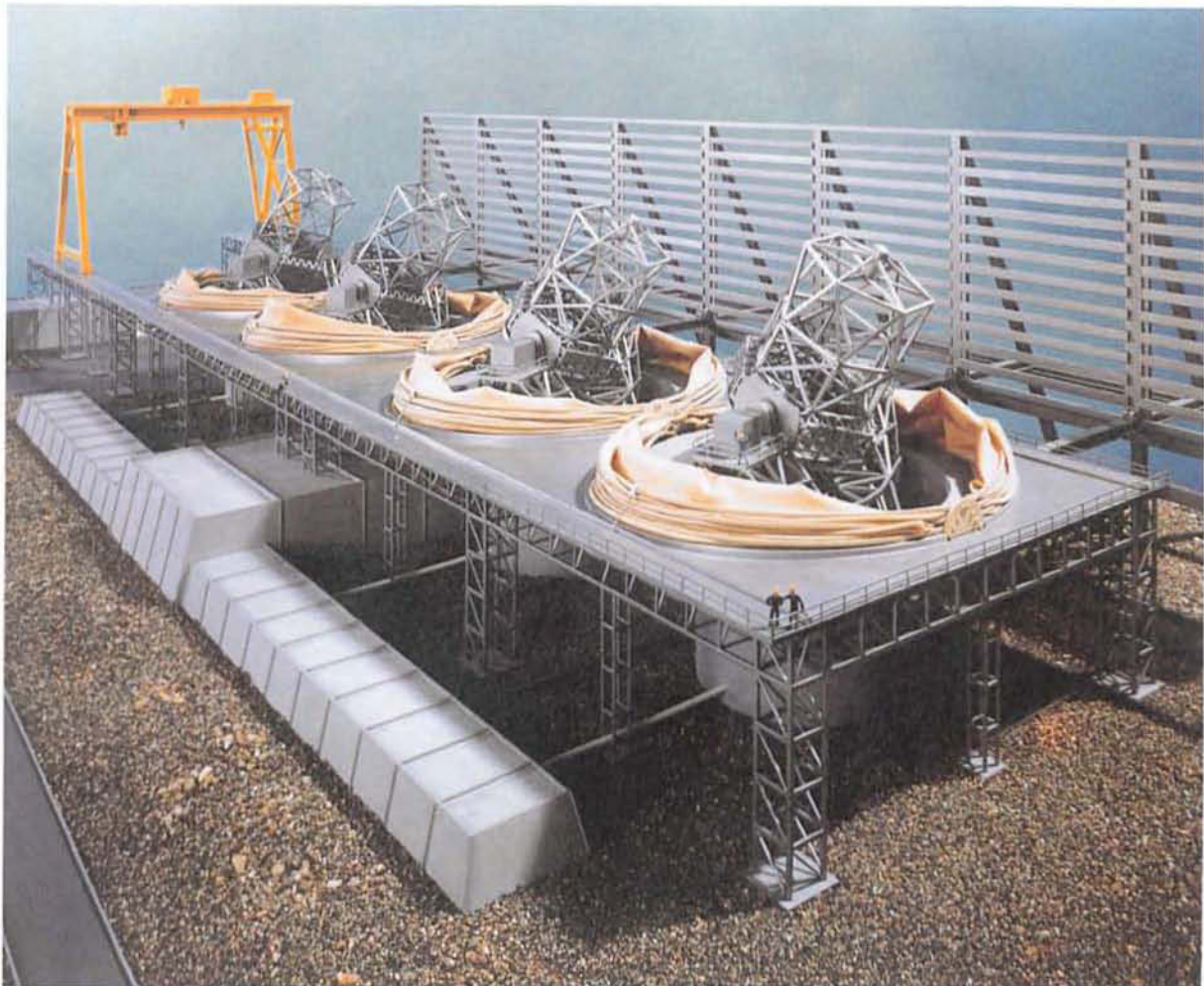


Figure 2.4: Model of the VLT with its present building concept.

- Using sets of moderate size, easily exchangeable mirrors and high efficiency dielectric coatings. The complete spectral range is covered with excellent efficiency with three types of coatings.
- Ensuring a complete sealing of the Coudé beam with protective tubes which are evacuated or filled with Helium in order to avoid any image degradation induced by internal convection.

Figure 2.5 shows schematically the principle of the beam combination for the combined Coudé focus where the 4 beams are simply added and the coherent combination for interferometry where the beams are phased.

Phasing can be achieved with optical delay lines or more simply if only two telescopes are combined at a time, by moving the interferometric set-up.

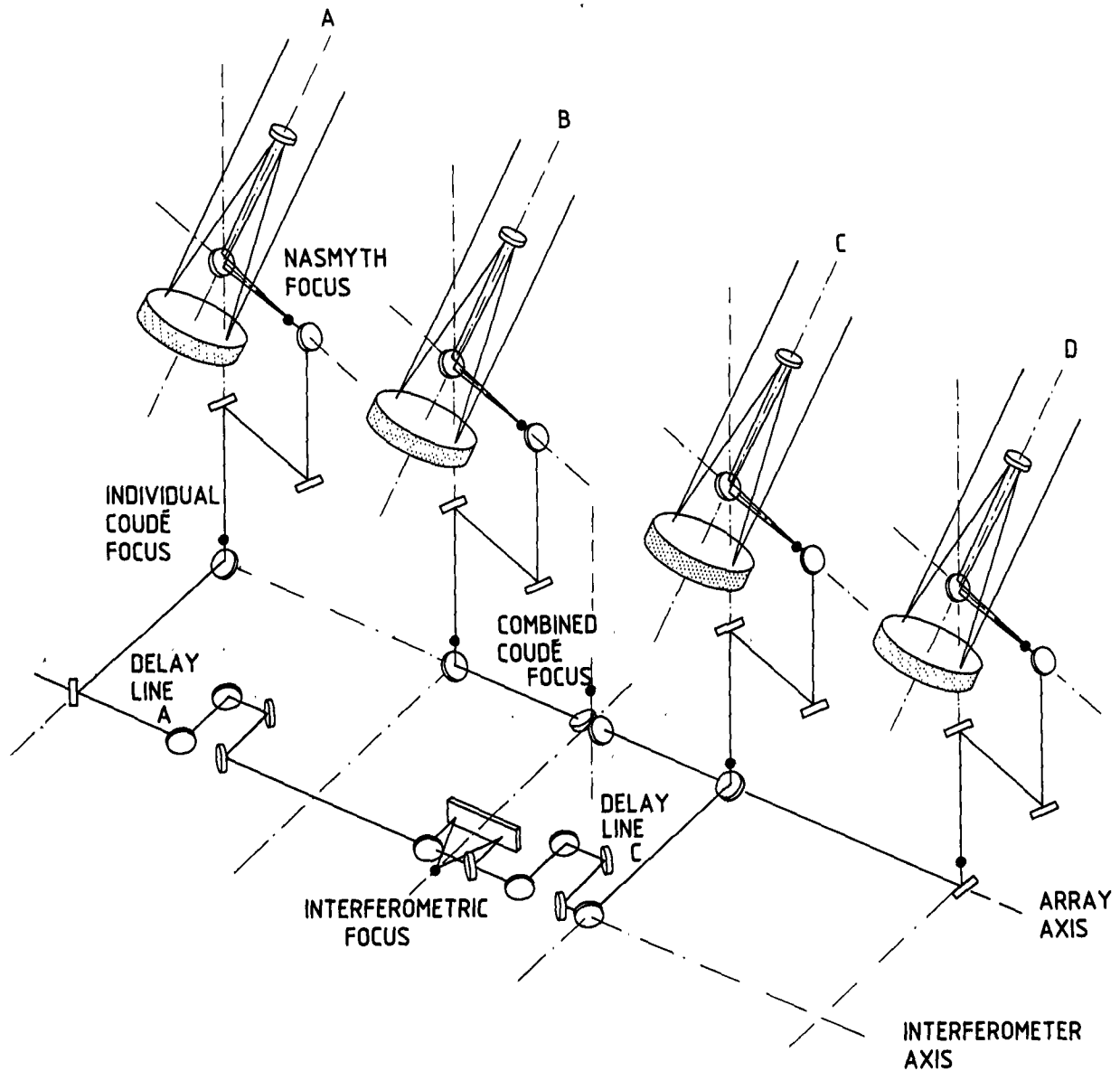


Figure 2.5: Principle of the beam combination.

In addition, each unit telescope may have its own Coudé focus located in the telescope base.

Two smaller size movable ancillary telescopes can also be used to cover continuously the spatial frequency plane. They could work either together or coupled to one of the 8m telescopes.

### 2.2.7 Site

The main requirements for the VLT site are:

- excellent seeing
- high IR transmission and low background (water vapour)
- high percentage of observable nights
- low light pollution and atmospheric scatter
- low wind speed
- large space available for the VLT and its possible extension

The studies are mainly concentrated on a coastal region of Northern Chile and at La Silla. Northern Chile seems to offer an outstanding climatology but space on the available summits is limited. Cerro Paranal located at about 150km south of Antofagasta and at 2650m elevation has been monitored for more than 3 years and appears as an excellent candidate. The immediate surroundings of La Silla provide interesting possibilities. Cerro Vizcachas located at 5km from La Silla can easily be reached with an extension of the existing road. On the basis of presently available data, Paranal appears to be superior to any known site in the world for cloudless nights. It is also extremely dry. Seeing measurements are still needed for a final selection to be made.

## 2.3 Performance Goals and Basis for Specifications

### 2.3.1 Imaging Performance

An error tree budget, shown in Figure 2.6 has been established. Main possible error sources have been identified and plausible values allocated. These values will be the basis for the detailed system specifications.

We have split the errors into two domains, the high spatial frequency errors defined as those beyond the correction range of the active system, and the lower spatial frequencies which are the result of the finite accuracy of the active corrections which are essentially limited by the photometric and spatial noise of the error sensors and by the bandpass of the servo system.

The criterion is the image diameter for 80% enclosed energy expressed in arcseconds. Others have sometimes used the FWHM which for a gaussian distribution is a factor 1.52 smaller. The various errors are added quadratically which implicitly assumes they are random. This is not the case for the support and polishing errors which are usually axisymmetric and may also be radially periodic. Those errors add up to the others in a different way. The specifications for the mirror and its support are under review and the values indicated in the error budget are approximative. The provisional value considered for the influence of the support distribution is an RMS wavefront error lower than 40nm, i.e. 20nm on the mirror surface.



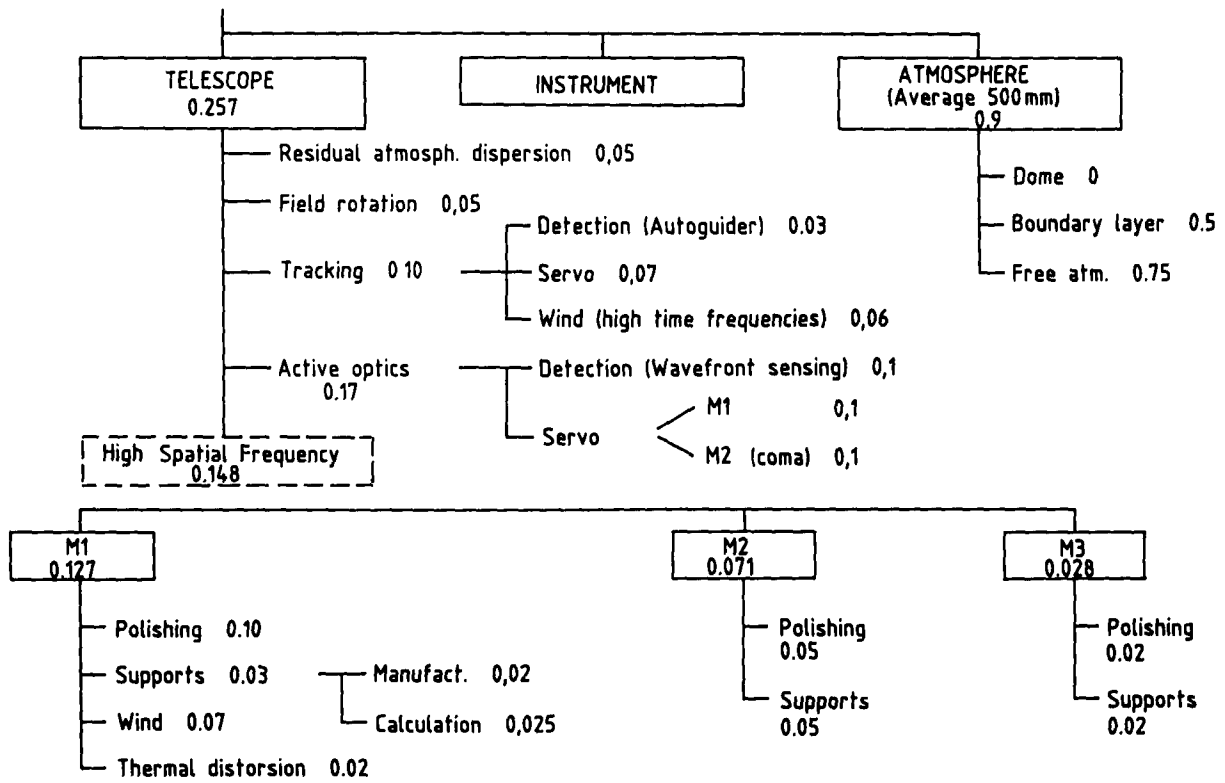


Figure 2.6: Error tree budget for the 8m unit telescopes. Numbers refer to the image diameter for 80% encircled energy and are added quadratically. The budgets for M1, M2, M3 consider only the high spatial frequency errors not correctable with active optics.

The seeing disk diameter varies as  $\lambda^{-0.2}$  and the 80% encircled energy of the diffraction pattern of a circular aperture is  $1.92 \lambda/D$ .

Figure 2.7 shows the wavelength dependence of the image quality for several typical cases and assuming a quadratic addition of all deteriorating effects (image quality as defined by Figure 2.6, diffraction by the aperture, seeing).

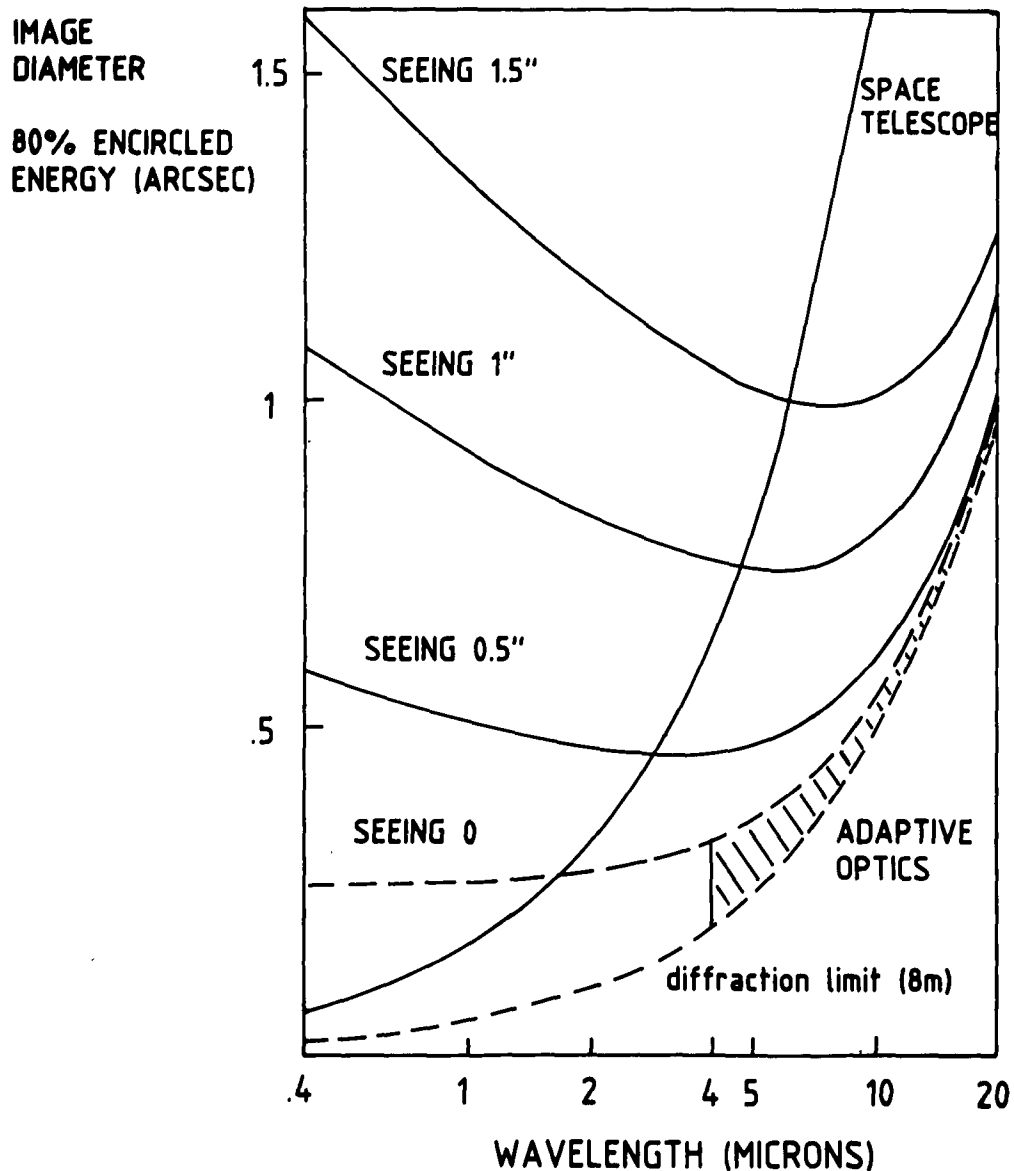


Figure 2.7: Imaging performance of the 8m unit telescopes under various seeing conditions (values indicated are for  $\lambda = 500\text{nm}$  and 80% encircled energy).

Best image quality will be obtained at a wavelength of about 5 microns. For longer wavelengths, diffraction tends to set the limit. Adaptive optics may in the near future compensate totally or partially seeing and telescope errors down to wavelengths of about 4 microns. As the technology evolves it could then be progressively extended to shorter wavelengths. The dashed zone corresponds to the practical system performance that could be expected from an adaptive system. The upper curve would correspond to a correction of seeing only, the lower curve is the diffraction limit of an 8m aperture and corresponds therefore to the ultimate performance.

### 2.3.2 Optical Throughput

It seems that at least in the near future, aluminium coatings will be the only possibility for the mirrors of the telescope (primary, secondary, Nasmyth) unless it would be decided to abandon the UV coverage in one or more telescopes and instead to improve the efficiency at other wavelengths in which case silver coatings could be considered.

The mirrors and other optical elements used for the beam combination which are of moderate size, will receive high efficiency coatings which will cover in three separate bandpasses, the UV/blue, visible and red/IR regions. Such coatings have been used at La Silla for about 8 years and do not show any degradation of performance over time.

Table 2.1 gives the expected efficiencies at the different foci based on commercially available coatings measured at ESO. The optical throughput is mainly limited by the efficiency of the aluminium coatings of the telescope mirrors.

Table 2.1

<b>EFFICIENCIES OF THE NASMYTH AND COUDÉ FOCI</b>			
<b>FOCUS</b>	<b>EFFICIENCY (in %)</b>		
	<b>UV</b>	<b>green-red</b>	<b>IR</b>
<b>NASMYTH</b>	<b>68</b>	<b>68</b>	<b>94</b>
<b>INDIVIDUAL COUDÉ</b>	<b>62</b>	<b>63</b>	<b>88</b>
<b>COMBINED COUDÉ</b>	<b>55</b>	<b>57</b>	<b>81</b>
<b>All telescope mirrors have aluminium coatings</b>			

### 2.3.3 IR Performance

The use of large two-dimensional IR arrays will probably modify in the future some specific IR requirements for the telescope. Conversely, the possibility offered by the VLT to observe in the visible objects which are much fainter than the sky background may push the observing techniques in the IR and in the visible much closer to each other than they are at the moment.

Many IR requirements such as low emissivity of mirrors, reduction of central obstruction are directly or indirectly beneficial to visible observation. The F/15 aperture matches current pixel sizes of IR detectors and minimizes the size of the secondary mirror.

An IR wobbling mirror, if limited to small amplitudes, may be compatible with an active secondary mirror designed to correct fast tracking errors.

It is therefore believed that it is possible to satisfy most IR requirements while meeting the general requirements for the telescope design (no change of configuration, flexible scheduling) and not being detrimental to observing in the visible.

The theoretical telescope emissivity at 10  $\mu\text{m}$  would be about 7%, considering 2% emissivity per mirror (aluminium coating) and 1% for the spiders. Additional measures such as specialized coatings and observation at the Cassegrain could further reduce this value. It should nevertheless be considered that existing telescopes - even IR optimized - have usually much higher emissivity values. Imperfect pupil alignment and mirror pollution are probably responsible for the difference. If those two problems were correctly addressed, one could expect the unit telescope emissivity to be realistically maintained below 10%.

### 2.3.4 Pointing

The main advantage one will draw from the concept of an alt-az mount and of a tube with a fixed configuration is a large reduction of hysteresis effects and the vertical symmetry of gravity forces which will simplify and improve the accuracy of a pointing model. An absolute pointing accuracy of 1 arcsec seems to be a realistic goal. Blind pointing from a nearby reference star should also be possible within 0.1 arcsec or better.

### 2.3.5 Tracking

A computer simulation has shown that with a conventional gear and wheel drive it was not possible to reach quite the accuracy required for observing under sub-arcsec seeing conditions. Fast tracking errors induced under strong winds will be compensated with the secondary mirror which in addition to its centering and focusing functions will have a two axes tilt system. Tracking errors should then be kept below 0.1 arcsec even in the

worst conditions.

### 2.3.6 Near Ground and Telescope Generated Seeing

Air thermal turbulence increases near the ground. This is the reason for which most telescopes are placed in high towers. Recent measurements at La Silla performed at 10, 20, 30m elevation [Sarazin et al., VLT Report to be published] have shown that  $C_T^2$  is nearly constant at 20 and 30m whilst its value is greater and wind dependent at 10m.

Because the optical path concerned is very short, the higher value of  $C_T^2$  at 10m would not have much influence on the final seeing. The contribution of the boundary layer which extends over a few hundred metres is more of concern even if the corresponding  $C_T^2$  value is lower.

Since - apart from the choice of the site - one has little influence on the boundary layer, one can conclude that the elevation of the telescope from the ground is not critical. A minimum elevation of 10 metres may be anyway required by the telescope lower structures and bases. It is essential that the telescope and its utilities do not further deteriorate the quality of the site.

The open air operation aims at eliminating most of the internally generated seeing which depends on the thermal equilibrium of the telescope with the ambient air. It seems relatively easy with the proper choice of materials and coats to reduce the influence of the upper structures. The mirror which will be a thin shell will have a time constant of about 3 hours and it should be possible to limit the temperature difference with the ambient air to less than a degree (see chapter 5.6). Because of the quasi-permanent wind sweeping of the optical path, local seeing should be almost completely eliminated. Attention must however be drawn to the thermal control of the massive lower structures which although located beneath the mirror could release hot air bubbles especially during low wind conditions. Radiative cooling of the part of the floor which is directly facing the sky will help but an air conditioning of the telescope enclosure during the day as well as a good insulation and ventilation of the floor is essential.

### 2.3.7 Day Time Observing

Day time observing is not considered as a driver. The reasons for this are:

- During day time seeing is usually much worse than during the night. An 8m aperture would be diffraction limited in the thermal IR only for best seeing conditions. An important loss of efficiency should then be expected during day time.
- The thermal equilibrium of the telescope cannot be obtained for both day and night time. Diurnal temperature variations are too important for the massive

parts of the telescope to adapt quickly. Not only will the local conditions during day time be poor but the night time is likely to be spoiled.

- Heating up by the sun of telescope structures may have adverse effects on pointing and tracking accuracy. The practicability of day time observing during which blind pointing and passive tracking will be necessary is therefore questionable.

It is nevertheless possible to consider a limited day time observing for a few hours after sunrise where the seeing could still be acceptable and the temperature variation of the telescope moderate. The air conditioning then will have time to adapt the temperature of the structures to that required the following night.

### 2.3.8 Mirror Contamination

Contamination of mirrors by dust and condensation of water and other products is a major source of performance loss. Frequent washings, mainly of the primary mirror, is a way to overcome the problem. It is nevertheless essential to reduce the sources of pollution.

An experimental investigation of the dust contamination problem is being undertaken. The main questions related to the building design are:

- Whether dust is mostly internally generated or carried in by the wind.
- Whether the deposition occurs mainly during operation or penetrates the enclosure during windy or stormy periods.
- What is likely to be the influence of open air operation on dust accumulation on the mirror surface.

It is suspected that an important cause of contamination is the condensation of greasy products which are likely to come from two sources: hydrostatic bearings and air conditioning. Running the bearings at low temperature may help in reducing the first source. Possibly cold traps in the vicinity of the pads could be considered. The air conditioning system should have special filters to decrease its content of oil particles down to an insignificant amount. Similarly, whenever compressed air is used, it must be dry and free of oil particles.

### 2.3.9 Environment

#### Snow and rain falls

Snow falls at La Silla happen occasionally but they never represent a danger for structures. At Paranal no snow and hardly any rain fall has been recorded in three years.

Nevertheless, buildings and telescope enclosures will be conceived to resist relatively important loads, 20cm snow is considered. Rain falls are similarly scarce and do not represent a problem. The telescope enclosures will be designed in such a way that water never falls on the mirrors during rain falls, opening of the enclosure or because of condensation.

### **Winds**

Wind is by far the most serious problem. Statistics recorded at La Silla show that the wind speed is below 9 m/sec during 70% of the night time and below 18 m/sec during 96 to 99% according to year to year variations. The telescope should be expected to work at optimal performance for the latter value, possibly with the help of a wind screen. The maximum wind speed for operation is 28 m/sec or 100 km/hr which means that it must be possible to enclose the telescope safely up to this limit. The survival conditions for the building have been fixed at 250 km/hr.

### **Temperature**

Temperature is relatively stable at the sites which are considered for the VLT. At La Silla diurnal variations are of about 5°, night variations about 2°. Temperature goes occasionally below 0°; absolute minimum close to -10° has been recorded. Paranal in northern Chile is similar to La Silla but slightly warmer.

The range of operation for the telescopes is -10°, +25°. Optimum performance should be obtained for a range of 0°, +15°.

### **Seismic activity**

Chile is a seismically active region. Two problems must be considered: the survival of the equipment and the microseismicity which may affect performance.

It is remarkable that despite many earthquakes, some of great intensity, no destruction has ever been recorded at La Silla. On some occasions telescopes were displaced and only needed to be readjusted.

The specifications considered for survivability are based on a horizontal acceleration of 0.3g and a vertical acceleration of 1.1g. This is more than what could reasonably be expected from a major earthquake, and about a factor 2 above Chilean standards.

Microseismicity has not been found so far to be a problem for normal observing and there is no reason to believe it could become one in the future. Yet, interferometry will be much more sensitive to vibrations and relative movements between telescopes.

Seismicity measured at various sites has shown that time frequencies for natural

sources mostly atmospheric and oceanic are low, of a fraction of a Hertz. Volcanic sources hardly have any permanent effect that can be measured. Major high frequency noise is generated by human activity. Trucks and heavy machinery (compressors, generators) may have a non negligible impact on the performance of an interferometer. A programme of investigation aiming at a quantitative estimate of various sources will begin soon. The results will serve as a basis for detailed specifications and will also indicate what particular constraints should be considered for the site and its surrounding activity (proximity of heavy traffic for instance).

### 2.3.10 Operation

#### Telescope slewing speed

Since the VLT will operate without a dome, its ability to switch rapidly from one object to another is only limited by the slewing speed of the telescope.

A high slewing speed represents an advantage whenever frequent switches between different objects (calibration objects for instance) are necessary. The slewing speed must be more than 2 degrees per sec for both axes. The requirement should in principle be more severe on the azimuth axis than on the elevation axis but to the extent that it can more easily be fulfilled for the elevation axis we chose to take the same value for both. The settling time must be less than 5 seconds.

Considering the relationships of the above values on acceleration limits, it is possible to expect a blind spot at the zenith of about 0.5 degree diameter.

#### Flexible scheduling and remote observing

Like most telescopes of the new generation, the VLT will largely be operated in a remote observing mode. Remote observing, in its broadest sense covers different modes of observing: full remote control of the instrument, eavesdropping, service observing. They are not excluding each other but are complementary to classical observing which remains necessary whenever the presence of the observer at the telescope is justified by the character or the difficulty of the task.

Flexible scheduling is the ultimate goal. Considering that seeing becomes more critical when the telescope diameter increases, it is essential to be able to take advantage of excellent conditions whenever they appear. They can hardly be predicted and they do not necessarily last a long time. The more exceptional, the more fugitive. Flexible scheduling requires very rapid instrument switching. The concept of the VLT has been much influenced by this requirement. We set as a requirement that any standard instrumental mode, including Coudé operation be accessible within a few minutes. Also, the time for instrumental calibrations and settings should be minimized.



### Maintenance and servicing

The goals mentioned above which can be reached with stationary instruments and single focus telescopes will also help to reduce the costs of maintenance and operation. Already, a few single purpose instruments such as the CAT/CES combination have amply demonstrated the efficiency and reliability of dedicated systems.

The NTT also largely follows this approach. As a result it is expected that the maintenance crew will be able to concentrate on preventive maintenance as well as on maintaining the original performance. Advanced means must be foreseen to detect and correct any loss of performance. This includes checking of alignment, measurement of mirrors efficiency and emissivity, detection of detector drifts etc. These aspects should be taken into consideration during the design phase.

### References

- Baranne A., Lemaître G., 1982, *Optica Acta*, **29**, 847.  
Barr L.D., 1980, *Optical and IR telescopes for the 1990's*, KPNO, Tucson, 23.  
Chevallard J.P., Connes P., Cuisenier M., Friteau J., Marlot E., 1977, *Applied Optics*, **16**, 1817.  
Disney M.J., 1978, *Optical Telescopes of the Future*, ESO, Geneva, 145.  
Enard D., Delabre B., 1983, *Proc. SPIE* **445**, 522.  
Enard D., 1984, IAU Colloquium No. 79, ESO, Garching, 439.  
Epps H.W., Angel J.R.P., Anderson E., 1984, IAU Colloquium No. 79, 519.  
Grundmann W., Richardson H., 1980, *Optical and IR telescopes for the 1990's*, KPNO, 905.  
Learner R., 1980, *Optical and IR telescopes for the 1990's*, KPNO, 930.  
Richardson E.H., Morbey C.L., 1984, IAU Colloquium No. 79, ESO, 549.

## Chapter 3

# SCIENTIFIC PROGRAMME FOR THE VLT

### 3.1 Introduction

Optical astronomy is unique among the physical sciences since the machines required to expand our knowledge of the Universe are not only advanced in observational capabilities but are also technical and aesthetic accomplishments. Given here is a description of the expected scientific programme of the VLT, a telescope that will far exceed the light collecting ability of the world's largest telescopes. The VLT, with its unique blend of advanced technology and scientific capability will signal the return of astronomical leadership to Europe.

Astronomy is entering a new turning point in the long history of the development of instrumentation. The gradual evolution of astronomical detectors from the human eye to photographic plates to photoelectric detectors has now reached the stage in which high resolution two-dimensional detectors with nearly 100 per cent efficiency are either available or will soon be available for all wavelengths from the optical ultraviolet to the deep infrared. Coating technology is also rapidly advancing. Nearly perfect coatings are available throughout the infrared. High efficiency coatings with restricted bandpass are available in the optical, and new optical coatings with extended bandpass are being developed. It will soon no longer be possible to upgrade the efficiency of existing telescopes by relatively inexpensive improvements in detector or instrumentation technology. Additional sensitivity will then only be gained by increasing the telescope aperture.

At the present time the great advantage of ground based telescopes is that they can be made very large compared to space telescopes. The 16-metre VLT will cost  $3 \times 10^8$  DM. The Hubble Space Telescope (HST) has 1/40 the light collecting area and costs ten times as much. A second great advantage of ground telescopes is that their instrumentation is relatively easy to modify as technology advances. The instrument

package for the HST was frozen 10 years before it will be put in orbit and it will only be upgraded by other long lead time instruments. As this is occurring during a period of rapid detector development the instrumentation for HST will not be as sensitive as it might have been in the visual and red. HST spectrographs will be approximately 10 to 20 times less efficient than comparable spectrographs for the VLT. In addition there is the factor of 40 increase in light collecting area of the VLT over the HST. Thus in the spectroscopic mode the VLT will collect information at a rate between 400 and 800 times as fast as HST. In the atmospheric windows this enormous increase in speed will more than compensate for the interference caused by the sky glow and image blur that plague ground telescopes. Since the HST with its high angular resolution at short wavelengths and high sensitivity in the vacuum ultraviolet will discover many sources that are too faint for study with HST spectrographs, HST scientists will have to cooperate with the VLT user community to unravel the nature of the new sources that HST finds.

The large aperture of the VLT will make it competitive with even cooled space IR satellites for those problems that can be solved by observations through the atmospheric windows and which require high spectral resolution or high angular resolution imaging. The development of IR arrays will allow the VLT to achieve its imaging potential in the infrared. A very important class of problems for the VLT will be high angular and spectral resolution mapping of extended IR sources. For these problems the VLT will exceed the capabilities of any other telescope.

In general the problems that will require a VLT are those that are either flux or resolution limited. Flux limited objects can be either those that appear very faint or brighter objects that require very high spectral resolution. In the first category are problems connected with distant galaxies, faint stars, etc. Examples from the second category are studies of weak stellar features, doppler imaging of star spots and studies of the cold intergalactic medium. Infrared problems that are limited by angular resolution will benefit from the large size of the individual dishes of the VLT and its array capability if the individual dishes of the VLT can be phased in the infrared. Examples of important problems include those dealing with molecular clouds, studies of galactic nuclei, imaging of planetary atmospheres, asteroids, comets and nearby giant stars.

An important goal will be the capability of the VLT to revolutionize our understanding of the Universe because it will increase the astronomer's technical abilities to the point that significant thresholds now blocking progress can be crossed. It is useful to cite examples. High energy physics is frequently given as a science that profits from the construction of ever larger machines and, indeed, these machines have produced a wealth of new particles. Galileo's telescope also allowed important new thresholds to be crossed. We believe VLT discoveries will rival these examples from physics and history. Galileo's telescope allowed him to see sunspots, mountains on the moon and the satellites of Jupiter. All three of these were considered revolutionary new discoveries. But the Japanese had already recorded sunspot numbers from visual observation, mountains on the moon produce the naked eye phenomena of Bailey's beads during an eclipse of the sun and some people with acute vision are said to be able to see the satellites of Jupiter without a telescope. Galileo's telescope was a turning point in astronomy be-

cause it gave him the capability of seeing phenomena that were previously just at the limit of observational capabilities. Similarly, in the case of high energy particle physics, some cosmic ray collisions exceed the centre of mass energy of even the most powerful accelerators. Many of the sub-atomic particles were first seen in cosmic ray events. The scientific value of each new generation of accelerators was not that it could produce more energetic collisions than were ever seen before but that the flux of high energy events was so great that rare particles could be studied in detail. In the same way the VLT will increase the detectable flux from faint objects to the point that they can be studied in detail. It will create an environment in which unexpected phenomena will become clear to all. Observed reality can then sweep away old ideas. Once this revolution has occurred it is possible to return to previously observed phenomena and re-interpret them in the light of the new advance. Without the VLT we will miss significant phenomena because our thoughts are constrained by incorrect paradigms that existing telescopes do not expose.

At the present time there are two clear problems that seem to be just beyond the reach of 4 metre telescopes: one is the problem of the collapse of molecular clouds that results in the birth of new stars. The other concerns the birth of our own universe and the study of distant galaxies.

Dense molecular clouds are so dusty that their interiors can only be seen at infrared wavelengths. And many phenomena important to their dynamics and chemistry occur in cool regions that only emit infrared radiation. High angular resolution is required to differentiate regions of differing physical conditions. High spectral resolution is needed to map the motions of the cool molecular components of the clouds. The VLT's infrared capabilities will revolutionize this field.

In his book "The Realm of the Nebulae" Hubble concluded by saying: "With increasing distance our knowledge fades, and fades rapidly. Eventually we reach the dim boundary - the utmost limits of our telescopes. There, we measure shadows, and we search among ghostly errors of measurement for landmarks that are scarcely more substantial. The search will continue. Not until the empirical resources are exhausted, need we pass on to the dreamy realms of speculation."

Since he wrote his book we have increased the sensitivity of our telescopes by a factor of almost 100 and extended the volume of the known Universe by a factor of over 1000; yet we must still agree with his description of cosmology for we have not yet pushed the limits to the era when galaxies were first created. We know that the additional increase of sensitivity by the factor of 10 that the VLT represents will allow us either to study the epoch during which the first galaxies and stars were born or we will find that the Big Bang theory is seriously flawed. When we can finally study the epoch of galaxy birth in detail we will be able to adjust our theories to the empirical truth and constrain not only astronomical theories but also the theories of particle physics that govern the development of the Universe during the age before the formation of the galaxies. If we find that the Big Bang theory is incorrect the observations will point us the direction of the new theory and a deeper understanding of our Universe.

The huge advance over present capabilities that the VLT will give, will certainly lead to unexpected findings. Since nature is not constrained by the limitations of human imagination, we can be sure that the technical advance achieved by the VLT over smaller telescopes will lead to unforeseen discoveries which will revolutionize astronomy.

## 3.2 Scientific Opportunities for the VLT

Research in astronomy is advancing very rapidly. The new technical capabilities such as those represented by the space programme and instrument development are leading to new discoveries that can fundamentally alter the stream of research activity. Ten years from now the HST will have been in operation for over 6 years, optical and infrared array detectors will have revolutionized instrumentation capabilities and the techniques for interferometers and adaptive optics will have matured. It is therefore not possible at this time to give an accurate, detailed account of the scientific programme for the VLT during its first years of operation. The programme given here represents our best effort to foresee the nature of astronomical research in the era of the VLT. Our discussion is flawed by our inability to clearly see the future and by our personal biases and inadvertent omissions. While one should not take too literally the details of the scientific programmes given here, the observing capabilities of the VLT ensure that scientific programmes similar in scope and importance to those given here will be successfully mounted. We have made no attempt to organize the discussion according to scientific merit since to a large measure that is a matter of individual taste. Instead, we have decided to list the programmes according to the distance of the astronomical object from the earth.

### 3.2.1 Solar System Programmes

The only concrete possibility now available to us for studying the origins of life in the Universe are studies of the processes that occurred in the primeval solar system. We know that these led to the appearance of life. It is becoming increasingly clear that complex organic molecules were present in the solar nebula out of which the solid bodies in the solar system condensed. For instance, the type I carbonaceous chondrite meteorites contain large amounts of complex organic compounds. There is probably a connection between the chemistry of the solar nebula and the development of life on earth. Many of the products of this early chemistry are likely to be present in a nearly pristine form in cometary nuclei. Because the comets have spent nearly all their lifetime in the extreme outer parts of the solar system, thousands of astronomical units (AU) from the sun, any prebiotic organic materials they might contain would be protected by the natural deep freeze of space.

The comets that we see are those whose orbits have been perturbed by an encounter with a passing star or gas cloud and have been thrown into the inner solar system.

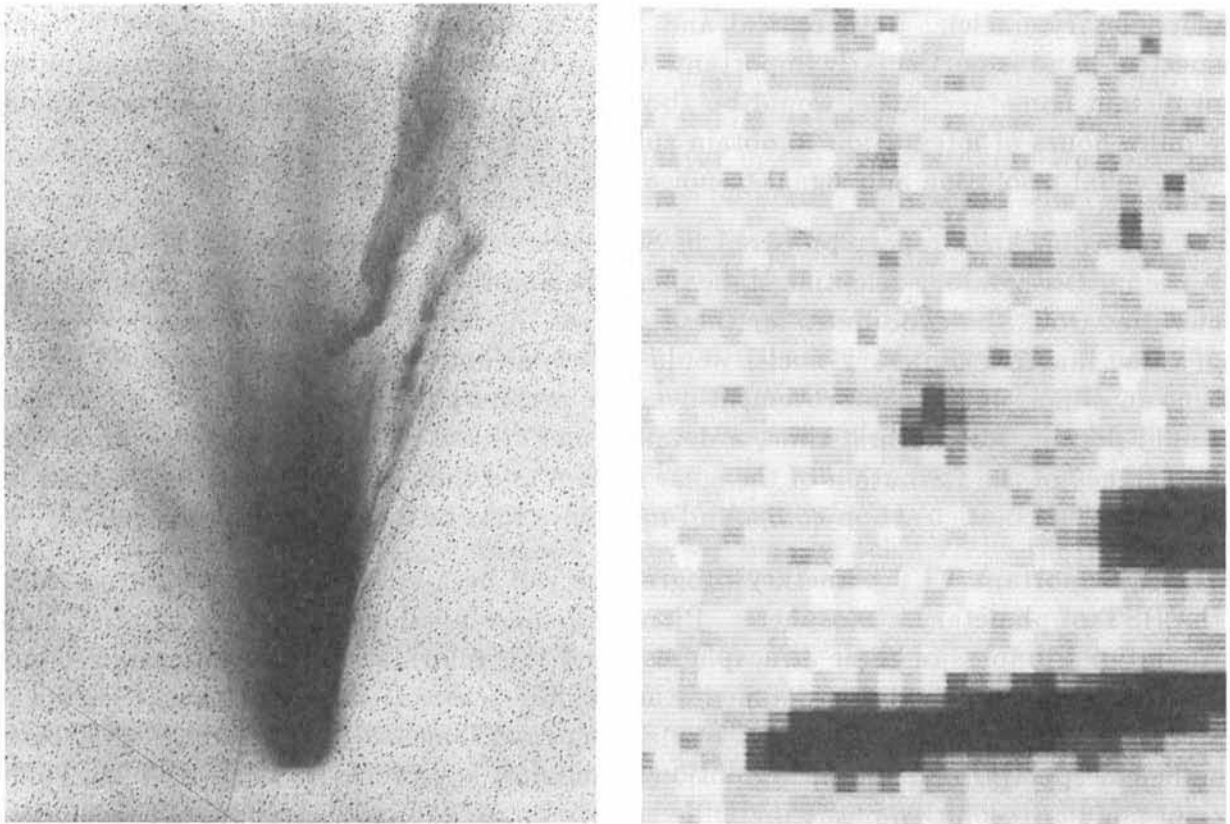


Figure 3.1: Photographs of Comet Halley when it is near the sun (left, ESO 1m Schmidt telescope on March 10, 1986) and when it is beyond the orbit of Jupiter (right, Danish 1.5m telescope on January 14, 1983). Near the sun, the coma blocks any chance of observing the nucleus. Far from the sun, the comet is faint and the VLT is needed for detailed studies.

Here they can interact with the planets and some are deflected into orbits that pass near the sun. The postcard comet with its bright coma and streaming tail is one of these close solar encounters. The tail is formed as solar radiation evaporates volatile cometary materials. This interaction is violent and many fragile chemical species are destroyed in the stripping process. These fragments can be observed in the spectra of the cometary tail. It is important to observe comets before they develop this obscuring halo. Because the comets become active when they are still far from the sun the study must be directed to very faint objects indeed. Spectra taken with the HST or even 4-metre telescopes require very long exposures. And because the comets are moving against the background star fields, contamination of the spectra by the varying background star light is a serious problem. Only the VLT has sufficient aperture to reduce the exposure times to the point that the motion of the comet can be “frozen” against the mottled background light.

Up to now, technical problems have prevented even survey observations of cometary nuclei. Spectral resolution of a few hundred to a thousand is adequate for a first study of cometary nuclei. Both optical and infrared spectra are needed and the 1-3  $\mu\text{m}$  spectral band is particularly important. Using comet Halley as a guide, the magnitudes of distant cometary nuclei would be about 22-23 mag. The 3.6-metre telescope would require hours of integration to obtain suitable spectra. The VLT could obtain spectra with equal resolution and signal-to-noise in a few tenths of an hour.

According to a report prepared in September 1985 by members of the Kitt Peak National Observatory scientific staff, there are approximately 100 known cometary nuclei that would be candidates for these studies. A modest survey of even a few dozen of these inactive cometary nuclei would be important. Data on all 100 would represent an almost infinite improvement over the present state of knowledge. Such studies would permit, for the first time, a detailed and critical examination of the important late stages of the formation of the solar system and the chemical reactions that led to the zoo of prebiotic carbon-compound molecules that lie frozen in cometary nuclei.

An important VLT planetary programme will be a collaborative monitoring with the HST of planetary atmospheres. Planetary space missions have given us brief, high resolution glimpses of these atmospheres. And this information has revolutionized our view of the planets. But a detailed study of the seasonal changes, and the chemical structure and its changes requires monitoring from long lived observatories that have sufficient spectral and spatial resolution to monitor key processes. The HST has sufficient angular resolution in the UV and visual to image Jupiter with about 500 resolution elements. At 3  $\mu\text{m}$  the angular resolution of HST has fallen by about a factor of 5 and is approximately equal to that of the VLT during periods of good seeing. However, only the VLT has sufficient light gathering power to exploit the techniques of doppler imaging to reconstruct a detailed image of a planetary atmosphere. Resolutions of several million would be useful. These are best obtained at the combined focus.

Such studies are useful in understanding the nature of atmospheric flow patterns (weather systems) in situations that are much different from the conditions that prevail on the earth. These differences include different distances from the Sun, different atmospheric chemical compositions, different planetary masses and rotational velocities. In addition, both Jupiter and Saturn have significant internal heat sources released from continuing gravitational contraction. Uranus, because of its very oblique rotational axis (this axis lies almost in the orbital plane), has now had its north pole in darkness for over 40 Earth years. Since the average distribution of solar radiation is a maximum at the poles of Uranus it is expected that an axisymmetric circulation of the Uranian atmosphere will occur. This is similar to the Hadley circulation in the tropics of the earth but is of opposite sign. Small, vertically coherent temperature differences were found during the January 1986 Voyager 2 encounter with Uranus. These observations support the circulation theories. The VLT will be able to measure such temperature differences and will be able to observe wind distributions by tracking infrared clouds. We can then extend our knowledge of the circulation patterns of Uranus and monitor seasonal variations. By deepening our understanding of such weather systems in general

we can hope to improve our understanding of the physical processes responsible for the earth's weather. These studies could then have a direct practical application in our daily lives.

Studies of chemical interactions in planetary atmospheres can similarly lead to a better understanding of the photochemical interaction in the earth's upper atmosphere. The production and destruction of the ozone layer in the upper atmosphere, and the evolution of CO<sub>2</sub> in the earth's atmosphere may be better understood when we have studied the more extreme cases represented by other systems. On Venus the clouds seen in ultraviolet photographs of Venus are now known to be composed of H<sub>2</sub>SO<sub>4</sub> and to be governed by the photochemistry of SO<sub>4</sub> in the Venesian upper atmosphere. Theoretical studies of ground-based optical polarization data gave the solution. A detailed analysis of the chemical composition of the planetary atmospheres is needed. Easily seen differences exist between the atmospheres of Jupiter and Saturn on one hand and Uranus and Neptune on the other. These studies will require a capability for imaging spectrophotometry with rather high resolution as the important processes are molecular transitions with low line-of-sight motions. This will best be achieved by the VLT used in a combined mode.

The NASA planetary probes to the outer planets have found that planetary rings are a common phenomenon. It is not only Saturn that has a ring system. These ring systems can be studied by imaging cameras during planetary probe fly-bys. This technique gives a single "snapshot" of the ring. Much can be learned from a single high resolution photograph but planetary missions are expensive and a single photograph does not show dynamical oscillations and changes in the ring systems. Because the ring system of a planet has dynamical similarities to the solar planetary system their study will deepen our understanding of the origin of planetary systems in general.

The VLT can contribute to this study by observing stellar occultations by the ring systems. Such studies can give information on the ring widths, the separation of rings and possible gaps in ring closure. Because the number of background stars that can be used increases roughly as the aperture of the telescope squared, the VLT could see approximately 20 times as many occultations per year as the 3.6-metre telescope is able to. The Hipparcos satellite will obtain accurate positions for hundreds of thousands of stars. This new positional catalogue will permit an expanded programme of study of the planetary ring systems with the VLT. The array configuration of the VLT will allow the observers to separate atmospheric effects from the diffraction modulation that accompanies the occultation.

Our own solar system is an end product of star birth and it is the only such system that we can study in detail. Frozen in the icy cores of comets are traces of that primeval chemistry and the planetary system with its rings and moons tells us much about the dynamical forces that were important. Guided by our knowledge of the solar system we can extend our studies to other stars and star systems. Most stars are members of binary systems or star groups. It is not known if only isolated single stars can have planetary systems or whether systems containing two or more stars only represent a situation in



which the collapsing interstellar cloud not only produced small mass objects (planets, asteroids, comets) but also two or more larger mass objects that became stars.

While in principle a Jupiter-sized satellite of a nearby star would be bright enough to be detected by the VLT, scattered light from the star makes detection very difficult or impossible. An easier observation is the detection of flattened discs of fine dusty material, similar to a planetary ring, associated with nearby stars. The IRAS satellite has found such disc systems with scales equivalent to that of our solar system associated with 12 nearby stars. For this emerging field even a small increase in capability can have an important scientific payoff. Not only will more objects be added to the source list for statistical studies but the VLT, working at both optical and infrared wavelengths, will set important limits on the physical, chemical and dynamical properties of these systems. At optical wavelengths the image is dominated by light from the central star. The balance slowly changes so that in the far infrared the nebula emits most of the energy. Scientific goals include studies of the angular distribution of the radiation and searches for gaps that could indicate the presence of massive planets. Spectrophotometry is needed to study various chemical species, and polarization studies can determine the size distribution of the particles. This project requires high resolution imaging combined with low scattered light, both in the atmosphere above the site and in the telescope optical train.

### 3.2.2 Star Formation

Interstellar gas clouds collapse under the influence of gravity to form new stars. In this process they pass through a critical and poorly understood phase that establishes the mass of the new star and the division of matter between the star and any new planetary system. Also at this time chemical processes enrich the cloud with prebiotic molecules which seed the new planetary system and, at least in the case of our solar system, led to the development of life. These “molecular clouds” are very dusty and therefore opaque in the optical, but most of their radiation is released at infrared wavelengths where the dust extinction is much less. Spectral features from molecular rotational transitions are very strong. During the earliest stages of protostar formation the emission is best observed at very long infrared wavelengths using space infrared telescopes. But at somewhat later stages in the evolution of the clouds the studies are best carried out using the VLT.

The high angular resolution of the VLT at infrared wavelengths will be critical for untangling the complexities that exist in regions of active star formation. In the solar neighbourhood a newly forming star cluster has typical star densities of  $\sim 100$  objects/(arcminute)<sup>2</sup>. In such highly confused regions it is often difficult to distinguish between stars and small bright patches of reflected light. Since scattered starlight is highly polarized an efficient discriminator would be polarization measurements.

The two nearest regions of star formation, the Ophiuchus and Taurus/Auriga dark clouds are both at a distance of about 150 pc. With an optical resolution of 0.5 arcsecond

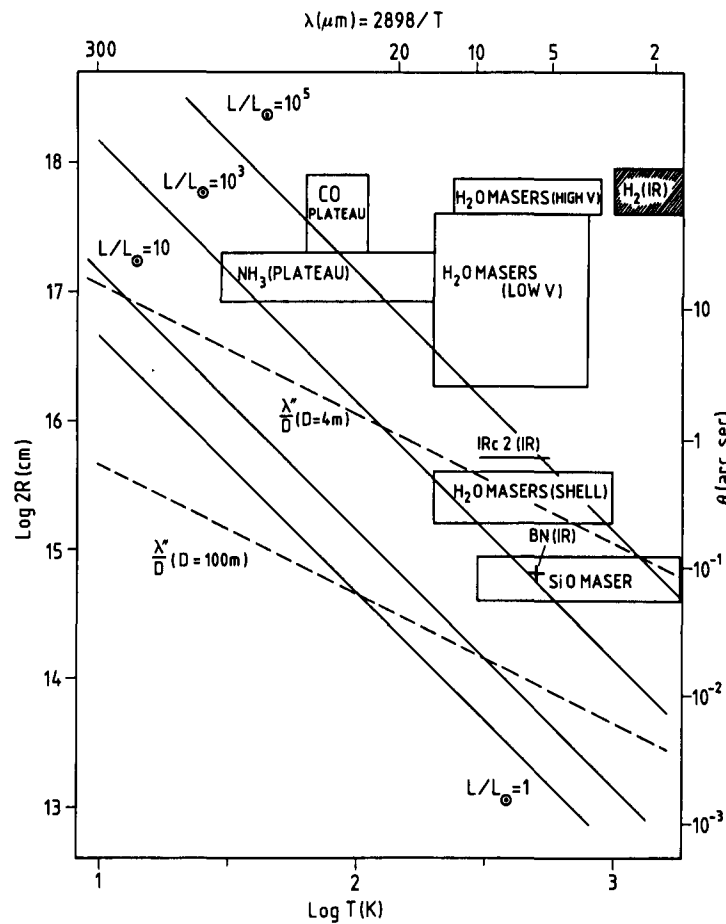


Figure 3.2: Diameter versus temperature for spherical blackbodies with luminosities in the range  $1-10^5 L_{\odot}$ . Such structures are representative of simple models for molecular clouds. The right hand ordinate gives the subtended angle for a distance of 500 pc. The top scale shows the wavelength of peak emission corresponding to the lower temperature scale. The dashed lines indicate the nominal angular resolution achievable with a 4m telescope and with an interferometer having a 100m baseline. Observed IR sizes and temperatures are plotted for two famous molecular clouds, BN ( $\approx 10^3 L_{\odot}$ ) and IRc2 ( $\approx 10^5 L_{\odot}$ ). For IRc2, the temperatures and distances of various molecular phenomena are also shown.

structures as small as 75 AU can be resolved. Even at a distance of 3000 light-years it should be possible to resolve dust shells 1000 AU in diameter. This is approximately the diameter of the inner parts of the cometary clouds accompanying the solar system.

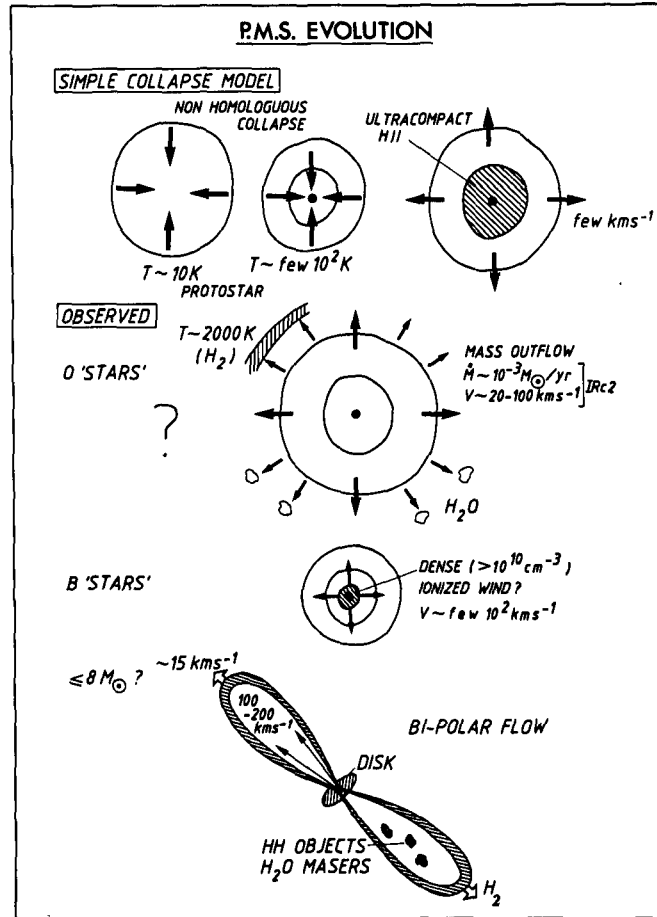


Figure 3.3: A simple molecular cloud collapse model compared to 3 observed pre-main-sequence stars. Hydrodynamic models predict that cloud collapse is non-homologous and that thermonuclear burning can be initiated in the core while the outer part of the cloud is still accreting (cocoon star). At a later stage, radiation pressure results in expansion and eventually dispersion of the cocoon.

Depending on the spacing of the telescopes and the ability to obtain fringes, it might be possible to obtain some imaging information on structures several tens of astronomical units in diameter. Models for protostars by Bertout and York show that it would be possible using the VLT to record spectra in 6 hours with a velocity resolution of 3 km/sec and a S/N ratio  $> 225$  at  $5 \mu\text{m}$  or  $> 60$  at  $10 \mu\text{m}$ . The combination of high sensitivity, high spectral resolution and high spatial resolution is needed to probe the dynamical processes that occur in the interaction between the protostar and the larger gas cloud complex. HI and [NeII] lines can be used to probe the hotter inner regions while in the cooler outer parts the  $\text{H}_2$  line profiles can serve as a probe. In these cooler

parts of the clouds gas motions are slow and the high spectral resolution required for definitive studies is best obtained with the VLT used in the combined mode. Spatially resolved spectroscopy, perhaps obtained using multiple slits, will give the most complete information. Fields of view of several arcminutes will be required in order to adequately examine the protostar - outer cloud interaction. For the more evolved protostars both optical and infrared imaging will prove useful.

One goal will be to obtain high spatial resolution spectral imaging to study gas flows in molecular clouds. An important problem that might be solved by such studies is the problem of stellar angular momentum. Contrary to expectation, stars are not born with random rotational periods. Stars seem to arrive on the main sequence with a rotational period that is a unique function of their mass. The physical reasons for this are not understood. IR spectroscopy that combines high spatial and spectral resolution will be an important tool in trying to understand this mystery.

The origin of the low mass stars is an unsolved problem. They exist in considerable numbers in the solar neighbourhood but are not seen in young clusters. Do they only form outside of clusters? The VLT can detect protostars with  $T > 280^\circ\text{K}$  as faint as  $M_{bol} = +12.5$  in nearby star forming regions. This is equivalent to a late-type dwarf M star. Thus the VLT would be able to provide important information on the formation of very low mass stars.

The inner spiral arm of our Galaxy is a region of greatly enhanced star formation. The radiation and matter density are much higher in the inner arm region than in the local solar neighbourhood. Here the gas is much richer in elements with atomic masses greater than hydrogen than gas clouds near the Sun. Because the inner spiral arm is five times more distant than the local cloud complexes, the higher angular resolution and light gathering power of the VLT is needed to determine the effects of changing the initial conditions on the formation rate of stars. Both the galactic centre and the inner spiral are obscured by foreground interstellar dust. They can only clearly be seen at infrared wavelengths, the spectral region in which the VLT is particularly effective. The next step, once the data are in hand, is to extend the studies to the nearest external galaxies, the Magellanic Clouds. It is important to note that the galactic centre, the inner spiral arm and the Magellanic Clouds are all southern hemisphere objects.

When a star is born, that is, when it begins to convert the hydrogen in its core into helium and support its structure with the resulting energy release, it begins to emerge from its molecular cloud womb and can be seen as a distinct, but still somewhat nebulous star. These new stars, called T-Tauri stars, are unstable, as if they had not yet quite determined their place in the Universe. They seem to have very irregular surfaces. High signal-to-noise optical-near IR spectra with high wavelength resolution promise to give good maps using the technique of doppler imaging. Stars as faint as  $m_K = 9$  could be observed with the VLT operating in the combined mode. A ten metre telescope would be limited to stars brighter than  $m_K = 7.5$ . These latter are only the brightest, least obscured T-Tauri stars.

A major task of the VLT will be to collaborate with a space infrared telescope to

accumulate a large, complete and therefore statistically significant body of data on star formation. These studies will be compared with information coming from solar system studies to trace, for the first time, a complete history of the birth of a star. Only then will we have the empirical evidence needed to estimate the likelihood of other planetary systems or estimate the probability that other life forms exist in our galaxy.

### 3.2.3 Studies of Interstellar Gas Clouds

The molecular clouds, described in the previous Section, condense from a much more diffuse interstellar gas. In this gas ultraviolet starlight, unshielded by dense dust clouds, prevents the accumulation of complex molecules. Although simpler molecules such as  $H_2$ , CN and  $CH^+$  can exist, the medium is mostly composed of single atoms and ions. The interstellar gas is a mixture of the primordial gas, created at the beginning of the Universe, and the products of nuclear synthesis recycled into the interstellar medium by supernova explosions and stellar winds. Roughly speaking, the gas is separated into two phases; a hot component that is highly ionized by shock waves and the ultraviolet light from stars, and a cooler component pulled together by the force of gravity and slowly collapsing to become the new generation of molecular clouds.

The study of this medium tells us much about the sources of energy input and dissipation of the material, the chemical composition and the buildup of heavy ions by stellar processes, the mass distribution within our galaxy and the distribution of gas in intergalactic space.

The VLT in its combined mode will contribute much to the study of this material. Since in most cases the velocity dispersion in cloud complexes is quite low, high resolution spectroscopy is needed to properly understand the situation. The stars used as background light sources must be bright in order to accumulate adequate signal-to-noise spectra. A typical example of these studies is the investigation of the CN molecular spectrum in the nearby star  $\zeta$  Ophiuchi. The lines of CN in this star have been studied since 1941, when Adams noticed that a line from the first fine structure level was present in the spectrum. It had not been expected that the fine structure level would be populated. An early explanation was that diffuse starlight, which has an interstellar energy density equal to that of a 3°K black body, was somehow exciting the level. After the discovery of the cosmic 3°K background radiation, accurate measurements of the fine structure line in nearby stars were used to determine the temperature of the background radiation. The most accurate, modern measurement was made using the La Silla CAT with the Coudé Echelle Spectrograph. Not only was an accurate background temperature obtained, but an additional measurement was made of the interstellar  $C^{12}/C^{13}$  ratio.

We know that the background radiation is isotropic in direction, but we do not know whether measurements of the CN molecule in other, nearby galaxies would give the same value for the background. If, for instance, the VLT had existed in 1986, it would have been possible to measure the fine structure lines due to the interstellar gas

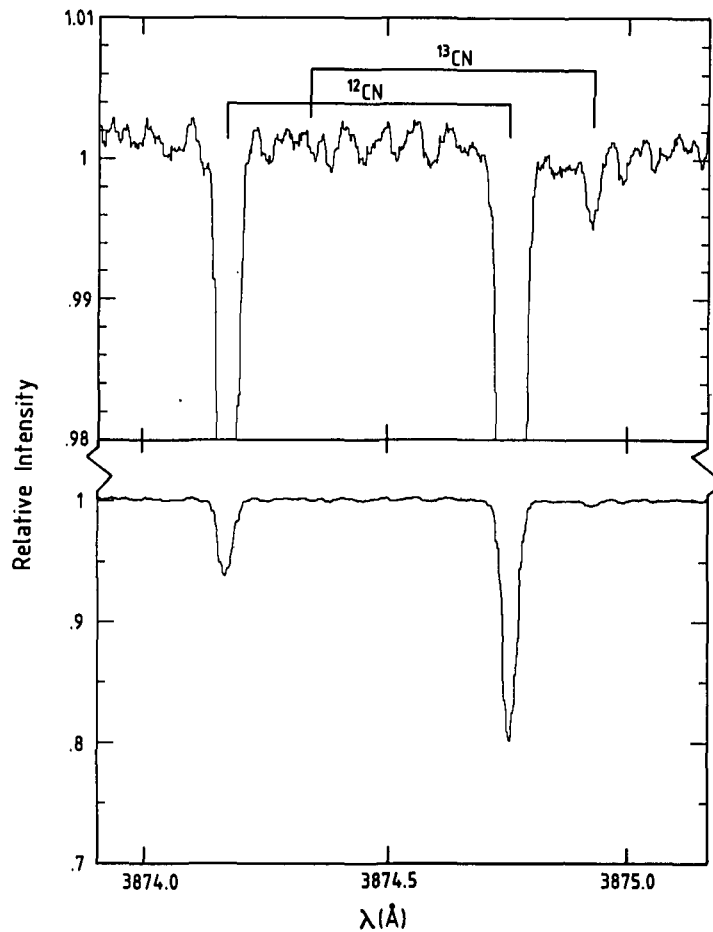


Figure 3.4: The CN fine structure lines in  $\zeta$  Ophiuchi, a 3rd magnitude star. The 3°K background radiation temperature and the  $C^{13}/C^{12}$  isotope ratio can be determined from this CES spectrum obtained with the 1.5m Coudé Auxiliary Telescope.

in the galaxy Centaurus A, using the 1986 supernova in this galaxy as a light source. We would then have been able to investigate the possibility that we live in a closed universe with positive  $\Lambda$  and that the locally measured 3°K background is due to a thermal source at the earth's antipole.

Even without the aid of a supernova, the VLT will be able to study the interstellar lines using bright early-type stars in the Magellanic Clouds. The 1987A supernova in the Large Magellanic Cloud (LMC) showed us how rich in gas the space between us and the Magellanic Clouds really is. The CaII H and K lines were broken into over 20 velocity components, some at the velocity of our galaxy, others at that of LMC, but also many at velocities corresponding to clouds in intergalactic space. Using the bright

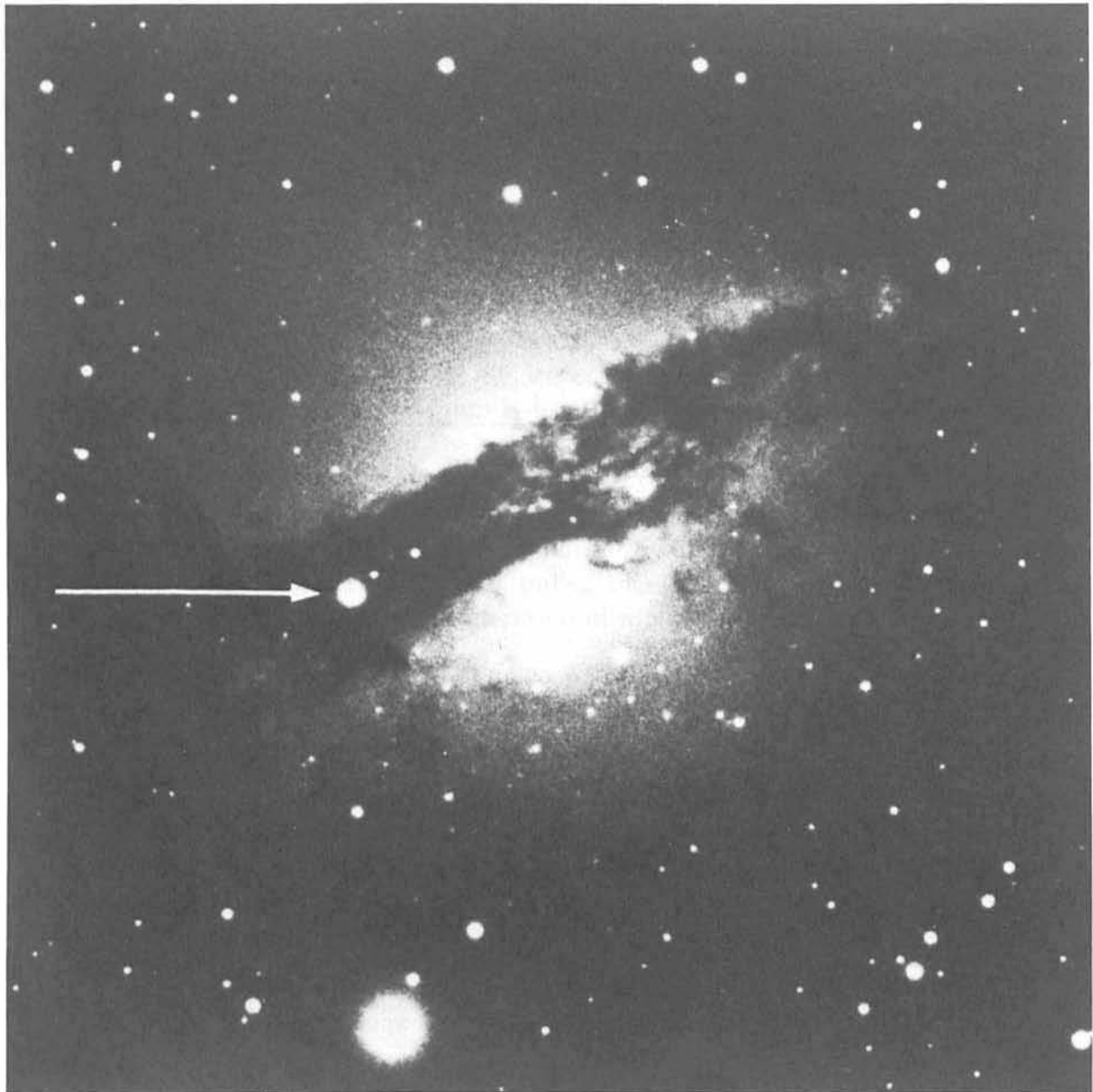


Figure 3.5: The peculiar galaxy Centaurus A, photographed with the ESO GPO telescope. The supernova of 1986 is indicated with an arrow. With the VLT in the combined mode, it will be possible to use such a supernova as a light source to study the interstellar medium in the parent galaxy and also the intervening intergalactic clouds, with high signal-to-noise ratio.

stars distributed over the face of the Magellanic Clouds, the VLT will be able to map the extent and velocity structure of these intergalactic clouds.

### 3.2.4 Stellar Astronomy

In the past decade the importance of high signal-to-noise, high resolution spectroscopy has been increasingly recognized. At Paris Observatory, in July of this year, an IAU Symposium will be devoted to the impact of high precision spectroscopy on stellar physics. Areas of particularly active development include the studies of star spots and rotation, stellar surface oscillations, stellar chromospheres and corona solar like and stellar cycles. It is now possible to use high resolution spectroscopy and doppler imaging to observe transit phenomena on stellar surfaces. No longer is the sun the only star whose surface can be studied in detail. For most imaging studies of stars very high signal-to-noise ratios are required. Often spectra with signal-to-noise ratios of several hundred to one thousand are needed. These signal-to-noise ratios are 10 to 50 times higher than astronomers are used to obtaining. To achieve such accuracies, from 100 to 2500 times as many photons must be detected as for traditional spectroscopy. Because many of the phenomena of interest are transient, often lasting for only a few seconds to several minutes, it is not possible to increase the accuracy by increasing the observing time. The present technology uses detectors with nearly 100% efficiency together with very efficient spectrographs coupled to the world's largest telescopes. Yet only the brightest, nearby stars can be observed. To expand the volume of space that is accessible to observation a larger telescope is needed. The VLT will increase the size of the observable volume by a factor of 50 and will permit the study of rare stars that are beyond the reach of existing telescopes.

Examples of the kinds of stellar studies the VLT might undertake include:

#### Studies of stellar oscillations

Solar astronomers have shown that the interior structures of solar type stars may be inferred directly from observations of low amplitude, stochastically excited, global oscillations. This technique, called stellar seismology, provides for the first time a chance to test whether the physics used to model the internal structure and evolution of such stars is correctly understood in detail. Stars with masses near one solar mass are of fundamental importance both in setting the age scale of the Universe and in determining the integrated spectra of most galaxies. This new development is therefore of profound significance for astronomy. The oscillations may be observed in velocity or luminosity, but most clearly in velocity. For this purpose, enormous numbers of photons are required to achieve measurement accuracies of a few tens of centimetres per second, and a really interesting cross-section of stellar parameter space will only be possible with telescopes much larger than those available today. Because all photon detectors have additional noise at the precision level required by these observations, it will be necessary to combine the beams of the 4 VLT sub-telescopes in order to realize the highest accuracy. Thus for these very high accuracy observations the VLT must be used in the combined mode.



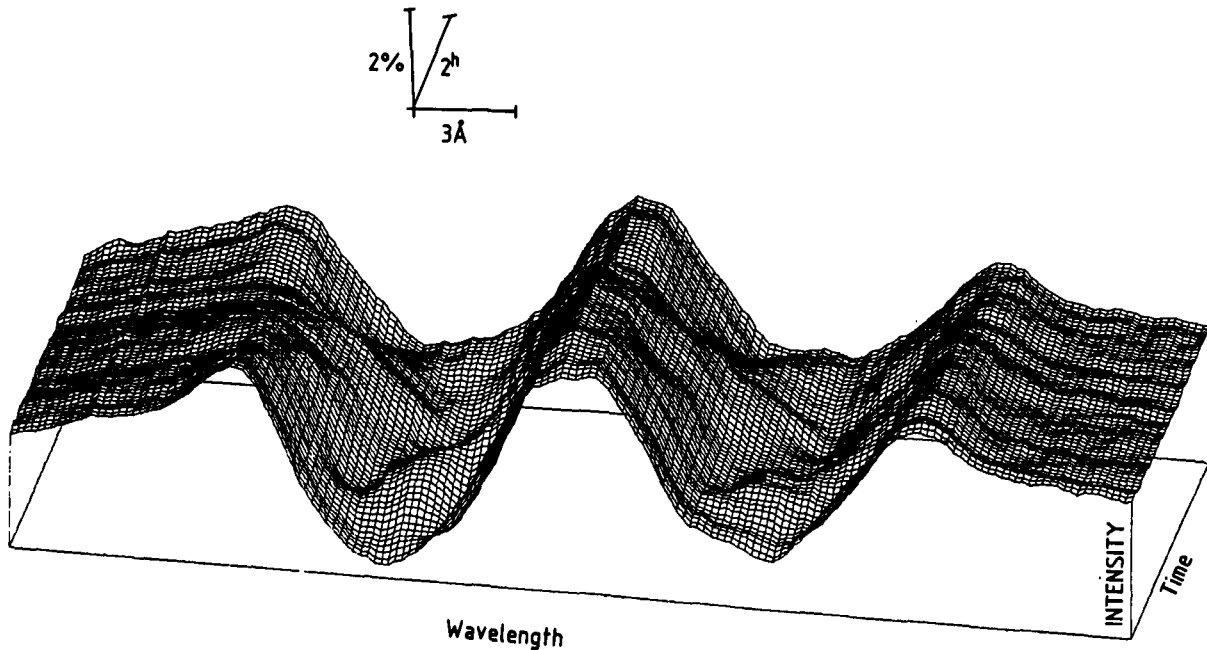


Figure 3.6: Temporal changes in the profiles of the CIV  $\lambda\lambda 5801, 5812$  absorption lines in the 2nd magnitude star  $\zeta$  Puppis (O4 I+). The divisions along the wavelength scale correspond to  $0.2\text{\AA}$  and along the time axis to 7 minutes. The S/N-ratio in this ESO CES spectrum is 500:1. With the VLT and improved instrumentation, similar spectra could be obtained for such stars in the Magellanic Clouds.

### Studies of condensed stars

It has often been supposed that the cataclysmic variable stars and galactic X-ray binaries may also yield insights into the phenomenon of black holes and the behaviour of material around black holes. Indeed, the best candidates to date for bona fide black hole examples are found among the X-ray binaries. Models involving mass transfer from a companion star onto an accretion disc surrounding a compact mass have been rather successful at explaining available data on these stars, at least phenomenologically. Progress in developing physically predictive models, however, will have to be guided by further observations. High precision spectropolarimetry is likely to yield important new information. Observations on timescales from seconds to as short as milliseconds are known to be required.

Sco X-1 data from EXOSAT shows that when the star is in a quiescent stage, it exhibits a 6 Hz quasi-periodic oscillation with about a 5% amplitude. When Sco X-1 is

active this oscillation disappears. Because the satellite only observed Sco X-1 for a short time it is not possible to determine if the oscillations are excited by the active period and would gradually die out or if they represent a true oscillation during the quiescent period that is disrupted when Sco X-1 becomes active. At optical wavelengths accessible to the VLT the phenomena detected by EXOSAT are likely to be diluted but still observable if high signal-to-noise data can be obtained.

Spectroscopy and polarimetry with such high time resolution will provide one of the most demanding applications of the VLT. Atmospheric seeing and scintillation have variations on similar timescales and can cause serious technical problems for such studies. The ESO VLT design, with four widely spaced element-telescopes, each looking through different atmospheric disturbances, should allow reliable separation of fluctuations intrinsic to the source from those induced by the atmosphere. As an aside, we note that the High Speed Photometer on the HST has been provided for making just this sort of observation. It will have advantages over the VLT only in the UV and when high angular resolution is needed in badly crowded stellar fields. On the other hand, spectroscopy at high time resolution, important for distinguishing spatially unresolved features via velocity or other spectral differences, will be the exclusive province of the VLT.

### Studies of pulsars

Pulsars are believed to be rapidly rotating, magnetized neutron, or, possibly, strange particle stars, from which radiation is beamed in highly specific, opposite directions. This causes them to appear to distant observers to pulse periodically. Some of these objects are seen not only in radio waves, but also in the optical. Unfortunately, except for the single example of the Crab pulsar, they are too faint for detailed study with existing telescopes. The increased light gathering power of the VLT will allow precise studies of the structure and polarization properties of the optical pulses of the pulsars in Vela and in the Magellanic Clouds, which seem to show differences from the Crab. Variability of polarization through the pulses, variation of individual pulses, and the implied microstructure (of fraction of a millisecond), including polarization properties, are valuable clues for decoding the location and geometry of the emitting regions and contrasting these to radio emitting regions. And if more optical pulsars are to be found, they will mostly be beyond the reach of current instruments; i.e. more light gathering power is needed.

A fundamental test of the gravitational radiation predictions of the Theory of General Relativity has been made using radio observations of a binary pulsar. The Theory passes the test, but on the assumption that the companion object may be treated as a point mass in the analysis. An optical source is seen at the radio position, and a spectrum might show what kind of object it is; whether it is associated with the pulsar, and whether it really can be considered a point mass. Predictably, it is just beyond the reach of the largest telescopes and the most sensitive of today's detectors. This unique object will clearly be a candidate for early observation with the ESO VLT.

### Galactic structure studies

On a much larger scale we can hope to learn how our Galaxy collapsed. The VLT will be able to obtain  $R = 200$  spectra of dwarf stars in the Galactic halo to a distance of 70 kpc and of giant stars throughout the halo. High-quality abundance determinations of  $[C/H]$  and  $[Fe/H]$  could be obtained for dwarf stars to 20 kpc and for giant stars to about 100 kpc above the galactic plane.

Early studies suggested that the galactic halo collapsed from a single protogalactic cloud. The halo was expected to show a gradient in chemical composition from the centre outward. Recent studies of the composition gradient have not supported this picture. Rather halo stars show a wide range of chemical compositions even for stars with apparently the same dynamical history. It is important to measure the chemical composition for dwarf stars since these stars are believed to have had little mixing of nuclear processed material into their envelopes. The VLT will be able to determine the composition gradient in the halo to a distance of at least twice that of any other facility.

Measurements of the space motions of field stars in the halo require accurate radial velocity determinations. The required proper motion data are largely available now and in any event could be obtained using smaller telescopes. Some of this work will be done for the northern hemisphere by the 10-metre Keck telescope. The VLT will cover the southern hemisphere and reach more distant stars, increasing the observable volume by nearly a factor of 10. When these studies are complete we will for the first time be able to read the historical record of the collapse of the Galactic halo and test for the presence of dark matter.

Galactic rotation curves do not decrease in velocity as expected at the luminous edge of a galaxy. If gravitational theory is correct, an extended “dark” galaxy must co-exist with each luminous galaxy we see. The stellar dynamics of our Galaxy seems to be dominated by this dark material which would be many times more massive than the mass of luminous material we do see. We know that the non-luminous material is not hydrogen gas. Proposed identifications for this unseen matter range from rocks and Jupiter-like objects, to swarms of black holes, to exotic elementary particles supposed to have been produced in the Big Bang creation event. Different possibilities would result in distributions of material that would match the visible mass distribution to different degrees. It is already known for example that the unseen matter inferred to be present in spiral galaxies cannot be distributed like the visible discs of stars; if it were, these discs would be unstable and could not exist.

An important observational problem is to use astronomical test bodies such as stars, star clusters and even galaxies to map the gravitational potential of this unseen matter in as many different situations and on as many different physical scales as possible. This work combines observations of stellar velocity dispersions and rotation curves in galaxies of different masses and forms, virial theorem analyses in groups and clusters of galaxies, and maps of deviations from the general Hubble expansion flow on both small and very large scales.

The largest radii to which galactic rotation curves have been mapped have used radio observations of the trace amounts of neutral hydrogen gas that are present even far from the visible galaxy. To probe even larger radii, one must measure velocities of the very rare individual stars and star clusters which inhabit the thin, extreme outer regions of galaxies. These objects are near the limits of what can be observed at adequate S/N using the HST in nearby Local Group galaxies. The improved angular resolution obtained by HST above the earth's atmosphere increases the contrast of point sources, such as stars, against the sky glow. This allows the 2.4-m HST to compete with the VLT in observing single point sources. Nevertheless, the VLT provides a comparable S/N ratio to the HST for stars, and has in addition the advantage of a dramatically larger field of view. Thus it can observe the spectra of many objects in the field simultaneously. While such studies *can* be done using satellite telescopes, they more likely *will* be done using VLT-class instruments on the ground, principally because of the multiplexing ability of the VLT.

### 3.2.5 Studies of Galactic Nuclei

All symmetric galaxies have a bright central nucleus. Irregular galaxies may have no obvious nucleus or may contain one or even several. It is clear that the star density is very high in galactic nuclei and many astronomers suspect that in all galactic nuclei there is also a black hole. In several per cent of all galaxies the nucleus is very active, releasing enormous amounts of energy throughout the electromagnetic spectrum. The nearest galactic nucleus to us is the southern hemisphere object IRS 16; the nucleus of our own galaxy. Taking 10 kpc as the distance to the centre of the Galaxy and 0.4 arcsecond as the angular resolution of the VLT in the IR it will be able to resolve details of the galactic nucleus 4000 AU in diameter. If, as some believe, there is a black hole of about  $4 \times 10^6 M_{\odot}$  in the centre of our galaxy, gas at that distance would be expected to have a velocity exceeding 1000 km/sec. At present the closest HeI  $\lambda 2.06 \mu\text{m}$  measurement samples a region about 17000 AU in diameter and the nearest [NeII]  $\lambda 12.8 \mu\text{m}$  measurement samples a region nearly 0.35 pc in diameter. The HeI  $\lambda 2.06 \mu\text{m}$  measurements were obtained after deconvolving the original 3.6 arcsecond beam of the UKIRT. The observed emission lines are bright: the total intensity of HeI  $\lambda 2.06 \mu\text{m}$  in a 4.2 arcsecond beam is  $3 \times 10^{-16} \text{ W/m}^2$  while the intensity of the hydrogen Brackett- $\alpha$  line at  $4.05 \mu\text{m}$  is nearly  $10^{-14} \text{ W/m}^2$ . It might be possible to determine the velocity structure of IRS-16 using the VLT in its interferometer mode. If so, we would for the first time be able to map the centre of a galaxy on the scale of several hundreds of AU. Clearly the centre of our own galaxy will be a prime target and for such studies the southern hemisphere site of the VLT gives it an additional advantage over large northern hemisphere telescopes.

Reaching out slightly further there are a number of rare objects which are unique because they are the nearest members of their class. Important examples are Cen A and NGC 1068. Cen A is the nearest example of a giant elliptical radio source and is only half the distance to the next nearest such source, M87. It contains X-ray and radio

jets that cannot be seen at optical wavelengths because of obscuration by a central dust lane. But the VLT can detect and map this nuclear region in infrared wavelengths. It is too far south to be studied by northern large telescopes.

The more distant Seyfert galaxy NGC 1068 has an extended, bright infrared emitting region that is centred on its nucleus. Here the flux is dominated by radiation from dust clouds with temperatures of 170°K. In addition, these clouds emit numerous atomic and molecular emission lines. High spectral resolution studies with the VLT used in a combined mode will be needed to map the dynamical structure of these cool clouds. The currently accepted model is that the dust is not heated by the Seyfert nucleus but rather is a site of rapid star formation. The gas in the cloud is metal rich and may represent, in miniature, the conditions that would prevail in a giant elliptical galaxy after an initial intensive burst of star formation has enriched the gas. With the VLT such regions can be studied in greater detail and more distant objects can be surveyed than can be reached with 4-metre telescopes which are handicapped by comparatively large diffraction patterns. The improved statistical base will help constrain theoretical models. And a better empirical understanding of local star forming regions will aid in the understanding of similar phenomena as that seen in NGC 1068.

Most galaxies which have active nuclei are obviously disturbed by tidal encounters with a neighbouring companion. It has been suggested that the tidal disturbances disrupt the circular motion of disc gas, some of which then falls into the nucleus where it is swallowed by a central black hole. This process, if it actually is occurring, would release huge amounts of gravitational energy and could account for the energetics of these nuclei. But not all interacting galaxies have such active nuclei. More work will be needed before we have a sufficiently large and unbiased sample to understand the connection between an active nucleus, star formation and gravitational interaction with a neighbouring galaxy. Active nuclei are best studied in the far ultraviolet or in the infrared since in these two spectral regions the contrast between the nucleus and the galaxy stellar population is greatest. VLT studies can complement the ultraviolet studies that the HST will undertake by providing high spatial resolution infrared spectrophotometry of the nuclear regions. HST has neither the infrared sensitivity nor the angular resolution to compete with the VLT in the infrared.

### 3.2.6 Cosmological Studies

The VLT will be particularly valuable for extending our ability to study the nature and evolution of the Universe. Existing optical telescopes and instrumentation are capable of studying the Universe in detail out to a distance corresponding to an age of about 1/3 the age of the Universe. Beyond this the difficulties of the observations increase rapidly. The resulting data are of low precision and far too few objects are sampled. The result is a low precision data base that does not strongly constrain theoretical speculations. The increased collecting area of the VLT, together with improved instrumentation, will allow us to extend the frontiers of the known Universe by a factor of about 2. For cosmological

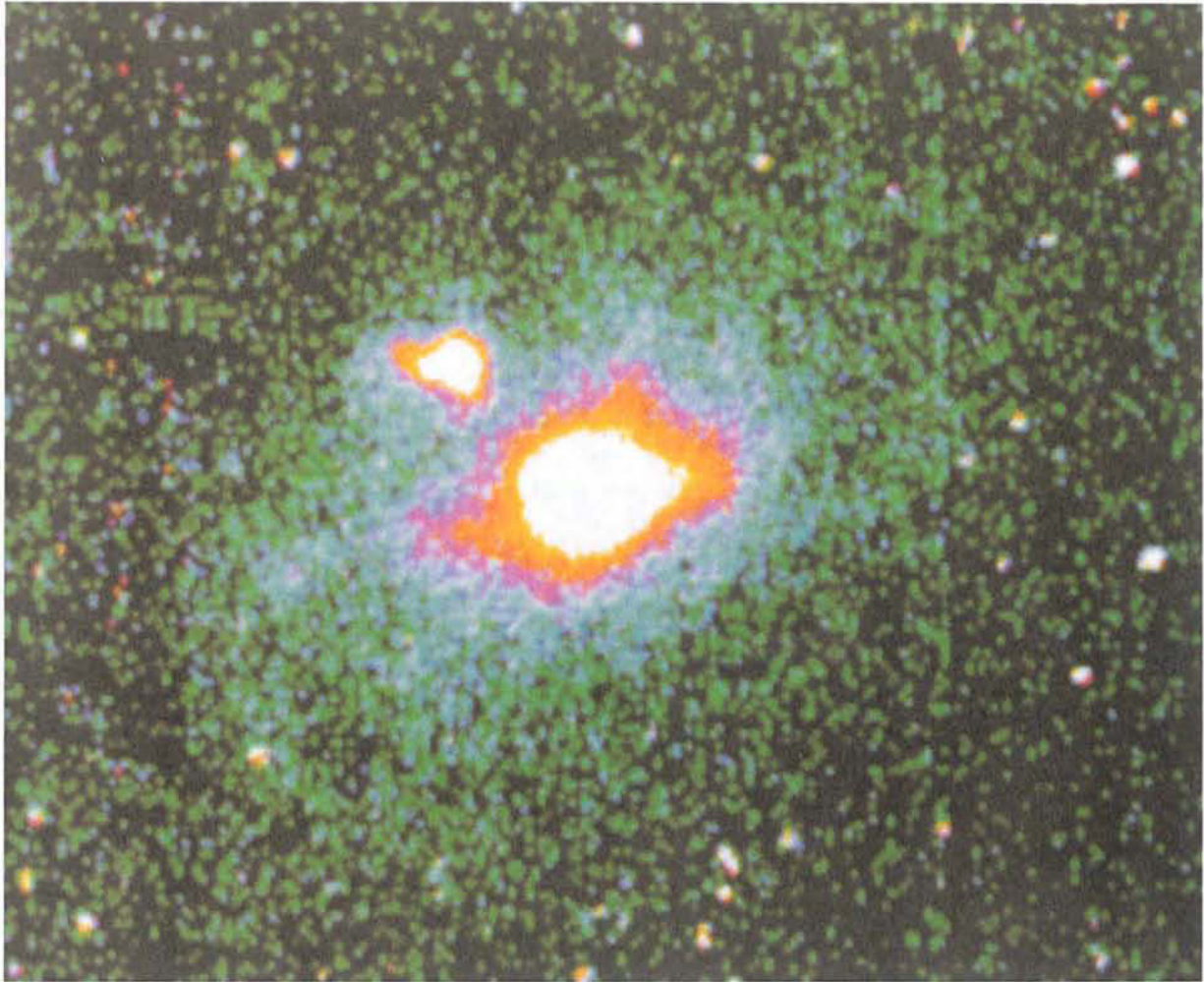


Figure 3.7: A 2.2 metre telescope CCD image of a radio galaxy, 500 million light years from the earth. The bright blob to the upper left of the galaxy is emission from a very hot gas cloud. It is possible that it is ionized by a hot jet of particles from the nucleus of the radio galaxy. The VLT, working with the HST and X-ray telescope can provide higher resolution, high S/N images of this interaction in infrared, UV and X-ray wavelengths.

studies this difference is critical. With existing telescopes we can only study in detail a volume of space that is very similar to the local neighbourhood. With the VLT we can extend these studies back in time to the era that some theories give as the epoch of galaxy formation, when the first stars were formed. It has been suggested that radio and X-ray telescopes have already reached this limit. But optical and infrared data are needed to identify and determine the distance to the mysterious sources identified in

other wavelength regions.

Particularly active areas of research are:

### **X-ray source identification**

We need to solve the problem of the origin of the extragalactic X-ray background radiation. All current interpretations are uncertain but the interpretation most widely believed is that the background radiation is largely made up of discrete sources, such as quasars and active galactic nuclei, with a hint of a contribution from either a new class of objects, or objects with evolved spectral properties. The Einstein X-ray Observatory medium sensitivity and deep field surveys with subsequent optical identifications have not reached faint enough limits to resolve this problem. ROSAT, the new German X-ray observatory to be launched in the next decade, will conduct surveys that yield an anticipated 4 times as many objects per unit area of sky ( $> 80$  per square degree) as Einstein, and therefore contain optical identifications that go  $> 1.6$  magnitudes fainter than those found with Einstein. AXAF, the U.S. X-ray satellite anticipated for the mid to late 1990's, will yield 50 times the number of Einstein detections.

Therefore, a VLT of 16 metre diameter could provide optical identifications for the ROSAT surveys that are more complete than current 4m class telescopes provide for the Einstein deep surveys (which might eventually become 95 per cent complete). VLT spectra for objects as faint as 24 magnitudes could in principle also provide identifications for  $> 25$  per cent of sources found with AXAF. Because of the much larger sampling at fainter magnitudes, these proposed combined X-ray and optical surveys will result in far better statistical data than are currently available. Optical spectroscopy with a VLT will make an important contribution to resolving the problem of whether the populations of fainter X-ray sources contain a proportion of a new type of X-ray source with different spectral characteristics or not. If there are new classes of X-ray sources, clearly the value of optical spectroscopy will be very much enhanced by the need to investigate the physical properties of the sources at all feasible wavelengths.

### **Studies of distant galaxies**

It has recently become evident that the evolutionary histories of normal galaxies are rather more complex than previously imagined, exhibiting in particular important developments during intermediate cosmological epochs. The evidence is now sufficient to demonstrate the inadequacy of current ideas on galaxy evolution, but details are confusing and clearly incomplete. Current technology has, with difficulty, provided data on normal galaxies, like our own, to redshifts near  $z = 0.5$  (that is, over roughly the most recent  $1/3$  of the age of the Universe) and on the very brightest systems to something over  $1/2$  of the total age of the Universe. Star formation significantly stronger than expected is seen in many objects, suggesting major metamorphoses during intermediate epochs. At high redshift many more systems show the strong nuclear activities charac-

teristic of the quasar and radio galaxy phenomena than is seen in nearby samples. Other systems seem relatively dead, in the sense of showing little on-going star formation, but at the same time show huge masses of ionized gas which on any simple scenario should be condensing into new stars.

Some studies have indicated that there is substantial colour evolution of galaxies by  $z = 0.5$ , but even this conclusion is tentative since selection effects may be important. A larger sample at redshift  $z = 1$  that includes intrinsically fainter galaxies will be needed before these issues can be settled.

Clearly, our understanding of the processes governing galaxy evolution is very incomplete. We apparently live in a relatively quiescent period of cosmological time, with most of the important events in the lives of galaxies having occurred at earlier times. Further progress toward developing an understanding of the causes and effects responsible for galaxy evolution will therefore have to be guided by definitive observations. Current estimates suggest that the effect of evolution at  $z = 1$  will be double or triple that seen at  $z = 0.5$ . The needed observational completeness and precision can only be provided by the VLT.

The technical requirements may be understood as follows: The observations will involve very faint galaxies (a fraction of a per cent of the brightness of the night sky) which will be marginally resolvable spatially (one to a few arcsec in size).

Neglecting dynamical evolution, large clusters of galaxies at  $z = 1$  would be expected to subtend about 8 arcminutes. Such clusters would be easily visible on wide angle direct images taken with the VLT. Galaxies with redshifts between 0.5 and 1.0 are best studied in the spectral region between  $0.4 \mu\text{m}$  and  $3 \mu\text{m}$ . The VLT will be the most sensitive telescope for these studies and multi-object spectroscopy will be an important instrumental requirement. This is likely to be best accomplished with multiple apertures rather than using fibre optic feeds. The galaxies will be faint - near the level of the sky background - and fibre optic feeds have to date not exhibited good background subtraction. The required field of view is not excessive and thus lends itself to spectroscopy with a multi-aperture entrance plate. Since most of the galactic light will be at wavelengths to the red of  $0.4 \mu\text{m}$ , the spectrograph for these studies does not need high UV transmission.

Galaxies can also be used to study the large scale distribution of matter in the Universe. Despite the assumption of cosmological theories that matter is uniformly distributed, observations of galaxies in our neighbourhood show that the galaxies are distributed in a network of bubbles, filaments and voids on scales that exceed 100 Mpc. In fact, a recent study of the distribution of low redshift quasars suggests that these inhomogeneities may extend to  $z = 0.5$ ,  $1/3$  the distance to the edge of the Universe. Such studies require a combination of direct images giving the distribution of galaxies on the sky (an easy task) and redshift measurements to give the third dimension, i.e. the depth of the bubbles, their distance from us and the dispersion in velocities of the galaxies at the surface of the bubbles.



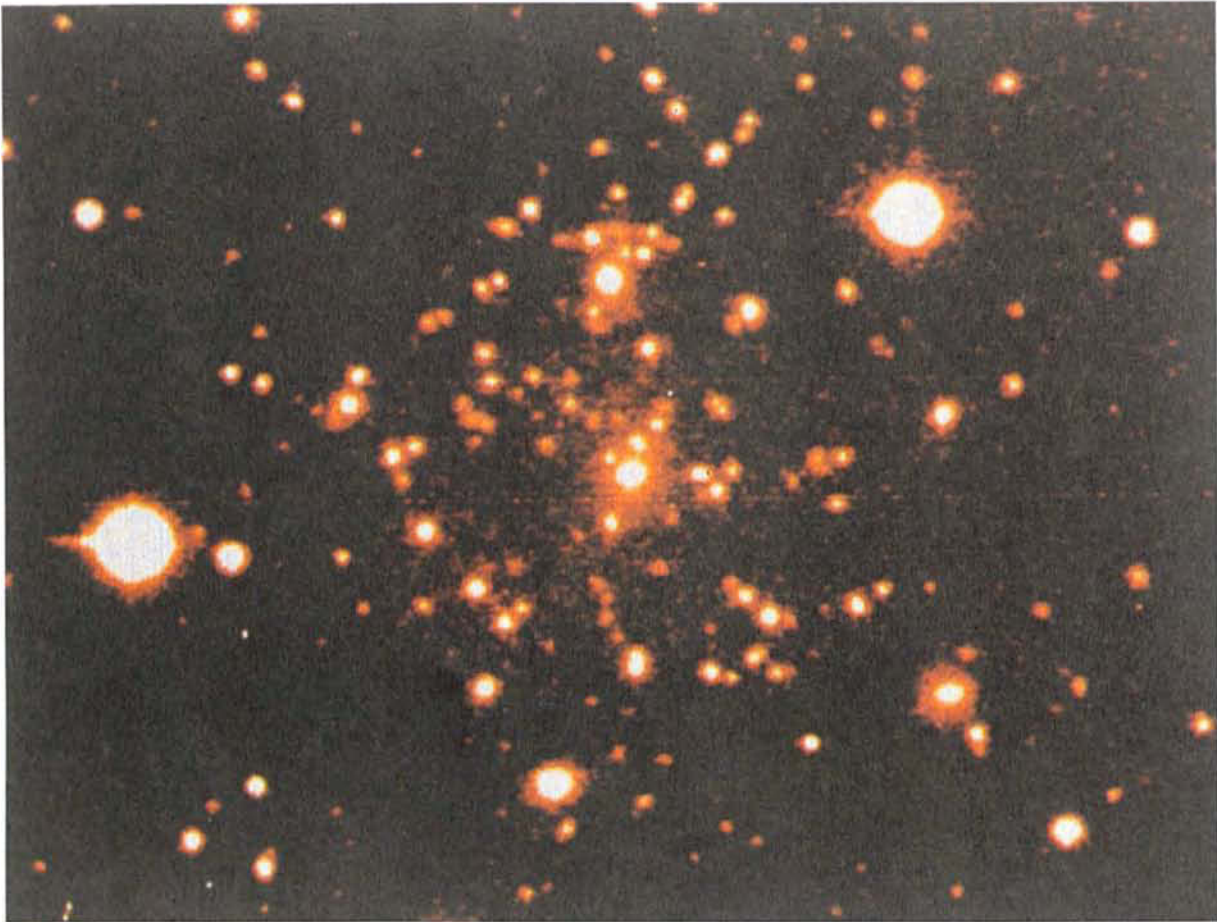


Figure 3.8: The cluster of galaxies A 370 with a redshift equal to 32 per cent of the velocity of light. At this redshift, the brighter member galaxies have red magnitudes equal to 17 - 18 and can be observed with 4m-class telescopes. An interesting feature of this cluster is the bright arc which corresponds to a structure 450.000 light years across. The VLT will be needed for detailed observations of this very faint structure. Bright galaxies of similar clusters, but at twice the distance, can be studied in similar detail with the VLT.

Because of the distribution of the galaxies in bubbles, the histogram of the line-of-sight velocities of galaxies which are projected on the sky in the same direction is not uniformly populated, but instead has pronounced peaks which define the surfaces of the bubbles or the boundaries of the voids. The accuracy with which the velocities must be measured to detect bubbles and voids must therefore be significantly better than the distance  $\Delta v$  between the peaks in the velocity histogram.

The imagery necessary to obtain the distribution on the sky of bright galaxies at  $z = 1$  to  $2$  does not require a VLT. It is almost being done already. The selection of galaxies near a particular redshift can be made by taking narrow band pictures on either side of the redshifted  $0.4\mu\text{m}$  discontinuity. The VLT is needed to obtain accurate measurements of the redshift of the selected galaxies and also study the neighbouring intergalactic gas by measuring the absorption lines in the spectrum of the faint background quasars.

A proper mapping of the distribution of matter at large  $z$  must be done with a sufficient number of galaxies per unit volume, thus including galaxies substantially fainter than the optically brightest one. In the CfA survey some of the bubbles are clearly outlined by galaxies with  $m_B = 15.0$  at  $V = 10000$  km/s. Taking  $H_0 = 100$  km/s/Mpc this corresponds to a galaxy  $M_B = -20.5$ , about two magnitudes fainter than the brightest elliptical galaxies.

We assume that the VLT will be equipped with a combination of spectrograph and detector covering the wavelength range  $0.8 - 1.4 \mu\text{m}$  that has an overall efficiency equal to that of the IR spectrograph considered in the VLT report. It will then be possible to measure the redshift of  $M_B = -20.5$  galaxies. For  $R = 500$ ,  $S/N = 10$  is reached in 1 to 2 hours if the galaxies undergo a luminosity evolution by 1 magnitude between  $z = 1$  and now. Such a luminosity evolution is indicated by current observation and is predicted from theoretical grounds. For  $z = 2$ , and assuming 2 magnitudes in luminosity evolution (for which there is some indirect sign), a signal-to-noise ratio of 10 is reached in 4 to 8 hours.

For these calculations we assumed that the determination of the redshift is based on the measurement of the H and K lines and the discontinuity in the energy distribution at  $0.4\mu\text{m}$  typical of early type galaxies. The measurements of the redshifts will be easier if a significant fraction of these galaxies undergo a spectral evolution in the sense of being richer in young stars in the past. (There is some evidence for this already.) With such evolution, the  $0.4\mu\text{m}$  discontinuity has less contrast but this is more than compensated by the presence of prominent Balmer absorption lines and in some instances strong emission lines.

For reasons related to detector development history, the wavelength region  $0.8 - 1.4 \mu\text{m}$  falls between the traditional optical and infrared ranges. But now, however, there are detectors which can cover the whole range  $0.8 - 1.4 \mu\text{m}$ . For example with HgCdTe detectors one can set the wavelength of the peak in sensitivity by adjusting the relative proportions in the alloy. Developments such as these will make it possible to build spectrographs with maximum throughput in this important wavelength range.

It is always possible to probe much more deeply with broad band imagery than with spectroscopy, and the VLT offers for the first time the possibility of obtaining high quality photometry of systems to the confusion limit, the distance at which individual galactic images overlap each other. In a practical sense this is the distance limit for studies of normal galaxies of the optically explorable Universe. Very roughly, the confusion limit is predicted to be reached at a visual magnitude of 28. At this magnitude the dark night sky is about a thousand times brighter than the galaxies of interest. A

statistically significant detection requires a signal-to-noise (S/N) ratio of 5. To record enough photons to attain this signal-to-noise a nearly perfect detector on today's large telescopes would require at least 70 hours of integration (needing in practice some 20-25 high quality dark nights spread over 3 to 5 years). For extended sources, such as galaxies, the Hubble Space Telescope has no great speed advantage as the night sky is only marginally darker in space, and the instrumental package of the HST will be less efficient than the VLT instrument package in the critical red-infrared spectral regions. Because of its smaller aperture, the HST would require some 200 hours (300-400 orbits) of integration to reach a similar flux level. Its detectors do not in any case promise adequate performance to make such measurements. By contrast, the ESO VLT in its full configuration should be able to probe to the confusion limit in the optical in 4-5 hours of integration. This is in practice a readily obtainable period of time.

*The direct study of galaxies as they evolve over cosmic time will only become practical after construction of a VLT.*

### **The study of quasars**

It is generally supposed that quasars represent extreme examples of active galactic nuclei. A bright quasar can be a thousand times as bright as all the stars in our Galaxy combined. They are very rare objects; we know of no nearby bright quasars. Yet because they are so bright they are easily seen to very great distances. The light from the most distant quasar known left it when the Universe was only 1/5 its present size. It could be that in that epoch galaxies were only just beginning to form and possible connections between the beginnings of galaxy formation and the existence of distant quasars is the subject of widespread speculation in the astronomical community. The luminosity distribution of quasars is uncertain since the samples are still small and the luminosity function may depend on cosmological distance. But roughly speaking for every increase in brightness by a factor of 2 the space density of quasars decreases by a factor of 10.

The most distant quasars, those with the highest redshifts, seem very hard to find compared with somewhat lower redshift quasars. To some extent this may only reflect the fact that quasars are not bright in the far ultraviolet, and the ultraviolet spectral region is shifted to the blue and visible wavelengths by the time the light from a high redshift quasar reaches us. But this cannot be the whole story. Other factors must be important. Because many quasars are strong radio emitters it should be possible, by searching radio fields, to find many very high redshift quasars. Diligent searches of radio fields have not been very successful. In fact, surveys using only optical methods have been at least as successful as the radio surveys. There are a number of explanations for the observed fall-off in density: we could be witnessing the era of galaxy birth and perhaps very high redshift quasars don't exist because there were no galaxies then. Or it could be that the quasar luminosity function changes with redshift in such a way that there were no bright quasars at high redshift. Or, possibly, distant galaxies may be very dusty and galaxy discs, projected against the sky, may be so numerous by redshift  $z = 4$

that a large fraction of the possible sight-lines to more distant eras are blocked by dust extinction. And, finally, it may be that we are using incorrect cosmological models. We could be living in a closed Universe in which by redshift 4 we have seen nearly the entire volume.

The VLT can help to settle these issues. Using infrared array detectors the VLT can search blank radio fields for very red obscured quasars. And with infrared - visible filter photometry it can undertake surveys to find quasars fainter than present telescopes can reach.  $H\alpha$  would be expected to be a strong infrared line in the spectra of high redshift galaxies. For the intermediate luminosity quasar 3C 273 at a redshift  $z = 5$  the flux from  $H\alpha$  would be  $9 \times 10^{-19} \text{ W/m}^2$  ( $q_0 = 0$ ). A 4-metre class telescope in an exposure of about 1 hour has a detection threshold of about  $4 \times 10^{-18} \text{ W/m}^2$ . Only the VLT could easily detect  $H\alpha$  in high redshift quasars if they exist. An IR search of blank fields around faint compact radio sources would either find these high  $z$  quasars or would show that their absence is not caused by foreground obscuration.

Possibly the most important contribution that the VLT might make to cosmological studies would be the exploitation of its ability to collect accurate, high resolution spectra of faint sources such as quasars.

### Studies of intergalactic gas clouds

There are at least a few dozen quasars available to the VLT with  $m < 17$  and  $z > 1.5$ . To 19 mag there may be as many as  $10^4$  quasars with  $z > 1.5$  that can be seen with the VLT. Half of the quasars in the Palomar Bright Quasar Survey with  $z > 1.5$  show at least some narrow absorption lines with equivalent widths greater than  $1 \text{ \AA}$ . For higher redshift objects the incidence of narrow absorption lines increases until at  $z = 2.5$  virtually all quasars show strong narrow absorption. This collection of bright sources is thus an ideal probe of the composition, temperature, ionization and dynamics of gas in galactic halos and the intergalactic region. Because the quasars are bright, high signal-to-noise spectra can be obtained with a VLT even at high resolution. For the brightest sources a resolution of  $10^5$  could be achieved. This resolution is appropriate for these studies since many absorption lines are composed of a cluster of components with individual internal velocity dispersions of less than  $10 \text{ km/sec}$ .

So much information can be obtained from appropriate spectra of intergalactic cloud systems that possibly the best way to study the evolution of the Universe is to study the evolution of these narrow absorption line systems. The absorption lines may be roughly divided into three categories: systems that are clearly associated with a foreground galaxy or quasar, systems in an uncertain environment that are rich in heavy elements created by stellar processes and systems that are deficient in the elements that indicate stellar activity. Spectra of the first category are useful indicators of the development of quasars and galactic haloes and the intergalactic gas in clusters of galaxies. It is to be expected that as the sensitivity of imaging systems develops, particularly with the deployment of HST and the VLT, more and more narrow line systems will be identified

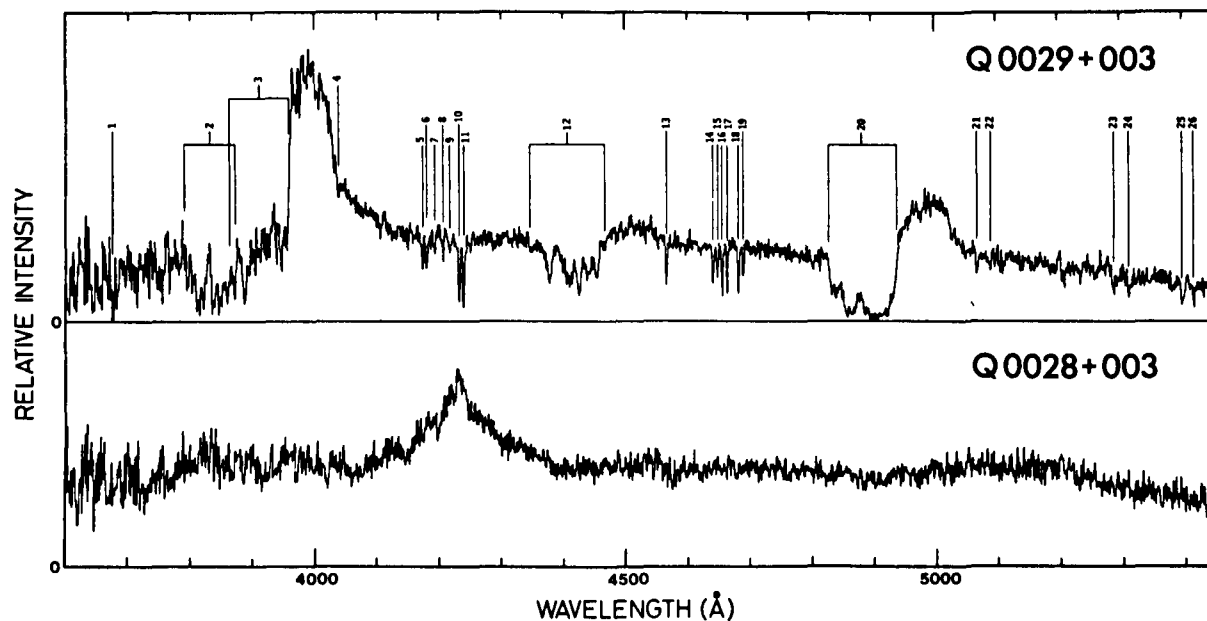


Figure 3.9: Spectra of the 18th magnitude quasar pair Q0028+003/ Q0029+003, obtained with the 3.6 m telescope. The resolution is 2000 and the S/N  $\sim 18$ .

with particular galaxies, quasars or clusters. Studies of the morphology and intergalactic environment of the foreground objects, together with an increased sensitivity to weaker lines, will open a major field of studies connected to the evolution of gas associated with galaxies and quasars.

One spectroscopically identifiable sub-class of metal rich gas clouds do not seem to show strong evolution with cosmic time. Probably their ionization structure cannot be maintained by the diffuse radiation of UV light in the intergalactic medium. These clouds must be closely associated with young stars. One explanation is that they are located in the halos of dwarf galaxies. Their number density and chemical evolution (if any) will shed light on the cosmic evolution of such dwarf galactic systems. A small fraction of these clouds have very strong Ly- $\alpha$  absorption lines. Such systems have been interpreted as gas in a galactic disc superimposed on a background quasar. If this explanation is correct, studies of this material will yield information of the state of the interstellar medium in typical galaxies at large redshift.

Clouds with high column density and low ionization might also provide an opportunity to measure the temperature of the cosmic blackbody radiation at a time when the background radiation temperature is 3-4 times higher than that at the present epoch. Both CI and NII have low lying excited states that might be used for this determination.

For  $T_0 = 3^\circ\text{K}$  at  $z = 2$  the ratio of the population in the excited state to the population in the ground state should be 0.2 for CI and 0.001 for NII. For  $z = 4$  the ratio of the populations becomes 0.6 for CI and 0.009 for NII. One system at  $z = 2$  has been studied with a 4-metre telescope and an upper limit of  $16^\circ\text{K}$  has been found. This is still too high to be interesting except to show that the clouds are cool. High resolution spectra with high signal-to-noise ratios are needed to determine these ratios accurately. A number of systems should be measured to disentangle possible contributions of local radiation fields from the cosmic background. A number of quasars show low excitation absorption systems that would be suitable for this programme. Unfortunately, they are all just a little too faint for definitive studies with 4m-class telescopes.

At high redshift weak Ly- $\alpha$  absorption lines are seen in the spectra of all quasars. Such Ly- $\alpha$  systems seem to be free of associated metal lines. These systems increase rapidly in number with  $z$ . High resolution spectra can determine their velocity structure. Studies of their internal velocity dispersion are necessary for realistic modelling of the clouds. High signal-to-noise ratios will be needed to set meaningful constraints on the abundances of metallic species in these clouds. It will be very important to determine if the clouds are really metal free or are only metal poor.

If it is found that these distant Ly- $\alpha$  absorbing clouds are relatively unmodified by stellar nuclear synthesis processes, it will be important to determine their D/H ratios. This ratio, together with the locally determined He/H ratio is a sensitive indicator of the physical conditions during the early phases of the expansion of our universe when H, D and He were created. With existing 4-metre telescopes and several nights of integration, a low precision measurement of the D/H ratio in one object has been obtained. But the conditions of the cloud producing the line are not well determined. A definitive measurement is simply beyond the reach of existing telescopes.

Intergalactic cloud studies require very high signal-to-noise ratios and high resolution. It is necessary to examine a sufficient number of cloud systems in order that meaningful statistics can be obtained. The full light gathering capability of the VLT operating in the combined mode will be required. Since one is concerned only with the spectra of individual point sources there is no field requirement or even a need for field rotation. However the ultraviolet spectral region is very important as the Ly- $\alpha$  absorption lines lie in the UV, even for high redshift quasars.

### 3.3 Conclusions

If one wished to summarize the scientific programmes for the VLT in a few words, one could say that it will be used to study *beginnings*: the beginning of life in the solar system and by extension the Universe itself. The beginning of new stars condensing out of molecular clouds; and the beginning of the Universe itself, the creation of hydrogen, deuterium and helium, and later the galaxies and their stars which created the heavy elements. Existing telescopes fall short of being able to answer the central questions.

Space telescopes will contribute important knowledge from observations in wavelength bands that are not observable from the surface of the earth. But the VLT, with its great capabilities for observation at optical and infrared wavelengths, will be necessary for making the critical observations needed to answer the central questions relating to these beginnings.

Our 4-metre class telescopes are showing us things that we cannot easily interpret. Much more high accuracy data, as can only be provided by the VLT, are needed for a meaningful advance. The VLT, like Galileo's telescope, will advance knowledge by clarifying our observations. Indeed, we are poised at a new beginning, ready to accept the challenge of Kant:

“A vast field lies open to discoveries, and observation alone will give the key.”

# Chapter 4

## OPTICS

The optical configuration of the VLT is based on a linear array of 4 independently mounted 8m telescopes. This concept allows a flexible and versatile use of the telescopes. They can be operated either independently or in various combination schemes. In the latter case the light collected with the unit telescopes is fed via an optical beam combination system to the combined foci (see Figure 4.1). The various available foci (see Table 4.1) are dedicated to specific instrumentation.

The optics of the individual telescopes is of the Ritchey-Chrétien type. It is foreseen to equip each telescope with two Nasmyth foci, one dedicated to the visible and one to the infrared. Additionally, each telescope will have an individual Coudé focus in the base of the telescope providing telescope access for special instrumentation. Also the possibility to equip one or more telescopes later with a supplementary Cassegrain focus has been included in the design.

The incoherent combination with a combined Coudé focus offers the light collecting power equivalent to a 16m single dish telescope. The coherent combination option opens long baseline interferometry with a resolution span of approximately 0.7 milliarcsec in the blue to approximately 45 milliarcsec at  $20\mu\text{m}$  wavelength in case a 104m baseline (distance between the two extreme telescopes) is selected. The interferometric operation is discussed in more detail in Chapter 12.

The optical design of the beam combination paths is mainly determined by the desired field of view of the combined image and the distance between the single telescopes. Both are desired to be as large as possible, a large field of view and a long baseline for high resolution imaging in the coherent combination mode. However, the field of view and the baseline influence directly the dimensions and the number of the optical elements in the combination path and therefore the cost of the systems. A lot of technical aspects are valid for the incoherent as well as for the coherent combination system, although the interferometric combination has much higher technical requirements, mainly with respect to mechanical stability.



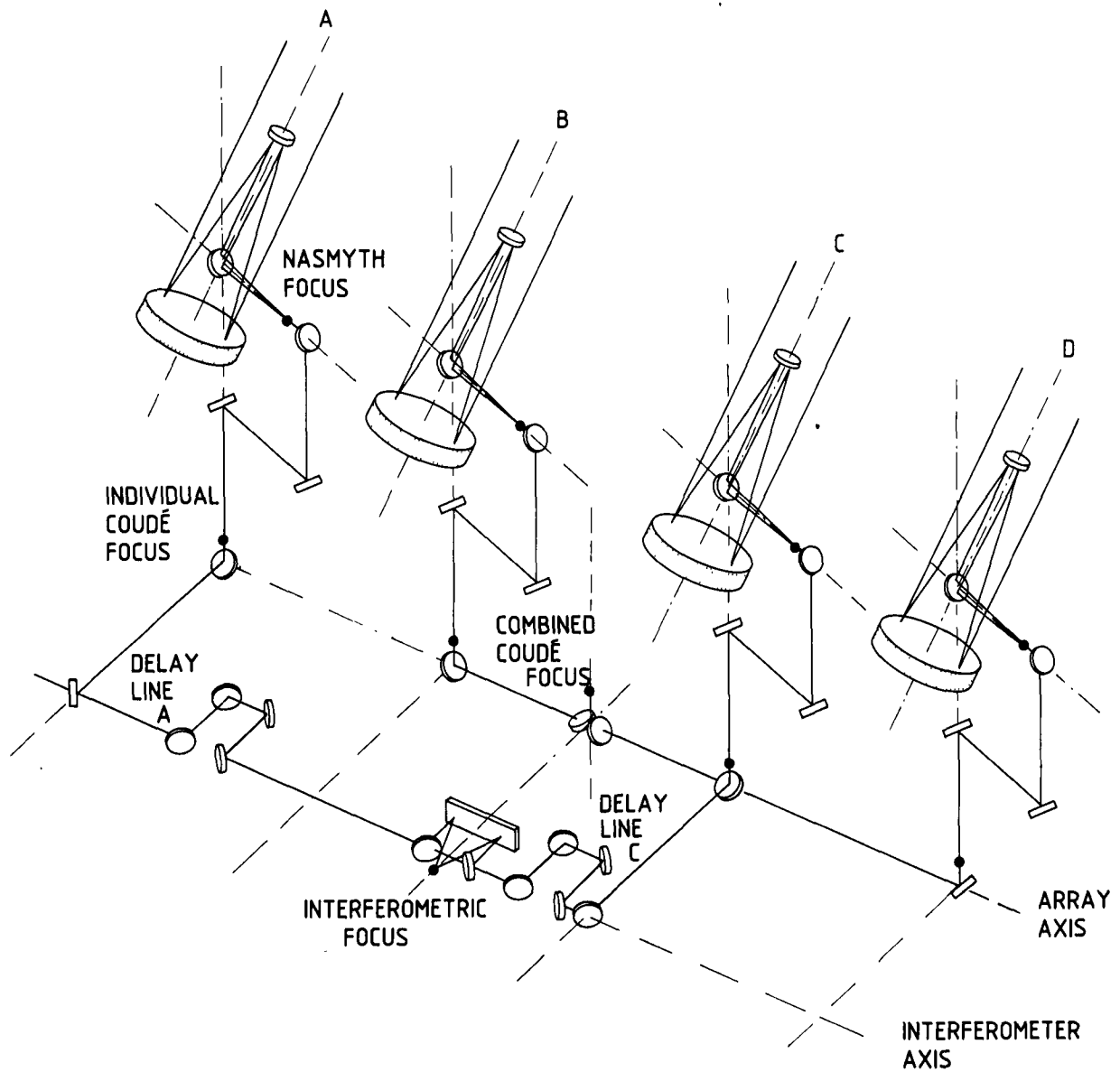


Figure 4.1: Schematics of the VLT optics. The individual foci as well as the combined foci are indicated.

## 4.1 The Unit Telescope

The optics of the individual telescopes is of the Ritchey-Chrétien type with an F-number of 15 (see Figure 4.2). It is foreseen to equip the telescopes only with two Nasmyth foci to reduce the telescope modifications during change-over of observation modes to a rotation of the Nasmyth mirror. Table 4.2 summarizes the major optical design characteristics. The possibility to equip the telescopes additionally with a Cassegrain focus has been

TABLE 4.1

SPECIFICATIONS FOR THE VLT FOCI						
FOCUS	F-RATIO	FOCAL LENGTH	IMAGE SCALE	field of view		FIELD CURV.
				[ <i>arcmin</i> ]	[ <i>mm</i> ]	
		[ <i>m</i> ]	[ $\frac{\mu m}{arcsec}$ ]			[ <i>mm</i> ]
NASMYTH	F/15	120	582	30	1048	2170
INDIVIDUAL COUDÉ						
-visible	F/74	592	2910	0.5	87	
-infrared	F/32	256	1250	2	150	
COMBINED COUDÉ						
-visible	F/26	208	1020	0.5	31	
-infrared	F/18.9	151	740	1	44	
CASSEGRAIN	F/13.3	107	515	15	464	2070
INTERFERO- METRY	tbd			0.05		

investigated and is included in the telescope design in a way that this option could be added later, although it increases the complexity of the total system significantly (see Section 4.1.7). Each telescope is also equipped with an individual Coudé focus in the base of the telescope.

The on-axis performance goal of the optical system for a Nasmyth image is

80% of the light within 0.15 arcsec

and for a combined focus image

80% of the light within 0.20 arcsec

(corresponding to a FWHM of 0.098 arcsec and 0.131 arcsec, respectively) after a full correction of all low frequency errors with active optics.



TABLE 4.2

OPTICAL DESIGN CHARACTERISTICS OF THE VLT UNIT TELESCOPES	
Diameter of primary mirror	8000mm
Radius of curvature (primary)	28800mm
Conic constant (primary)	-1.00487
Diameter of secondary mirror	1270mm
Radius of curvature (secondary)	-4434.9mm → -4734.983
Conic constant (secondary)	-1.66924
Dimensions of tertiary mirror (flat)	1142 × 1615mm <sup>2</sup> (elliptical)
F-ratio of Nasmyth foci	15
Linear scale at Nasmyth foci	1.72 arcsec/mm
Nasmyth field of view	30arcmin ≡ 1048mm
Nasmyth field curvature	2170mm
Equivalent focal length	120m
Distance primary-secondary	12316.6mm
Back focal distance from tertiary	7600mm

For the primary mirror the value 1.8 has been selected as F-number. It could be desirable from a mechanical standpoint to decrease the F-number in order to shorten the tube length. Aside this, there is no strong argument to go below this value because there will be no further gain in the size of the building; the distance between the Nasmyth platforms is becoming the largest dimension. In addition, the cost of the optical figuring increases with the square of the inverse of the F-number, and the optical quality for a mirror of this size would be very uncertain since no experience exists up to now on very fast mirrors of large dimensions (For example the ESO-NTT F/2.2 primary mirror will be the fastest for its size in the near future). The technological risk associated with small F-numbers should not be underestimated. The F-number of the primary mirror is, together with the mirror diameter, the major dimensioning parameter for the telescope structure and building. There is no chance for a later modification without an enormous impact on the total project.

Figures 4.3 and 4.4 give the theoretical spot diagrams for the curved and flat fields. The acceptable field of view without field curvature correction is about 8 arcmin.

The sensitivity of the optical system with respect to pointing and tracking, and focusing errors is given in Table 4.3.  $\alpha$  and  $\beta$  are the mirror tilts in arcmin (around the x- and z- axis, respectively), dx, dy, and dz the mirror displacement in mm (the coordinate system is indicated in Figure 4.2), and the indices denote the mirror numbers.

The availability of a prime focus has not been considered, because it would have a major impact on the telescope mechanics for a marginal gain in efficiency.

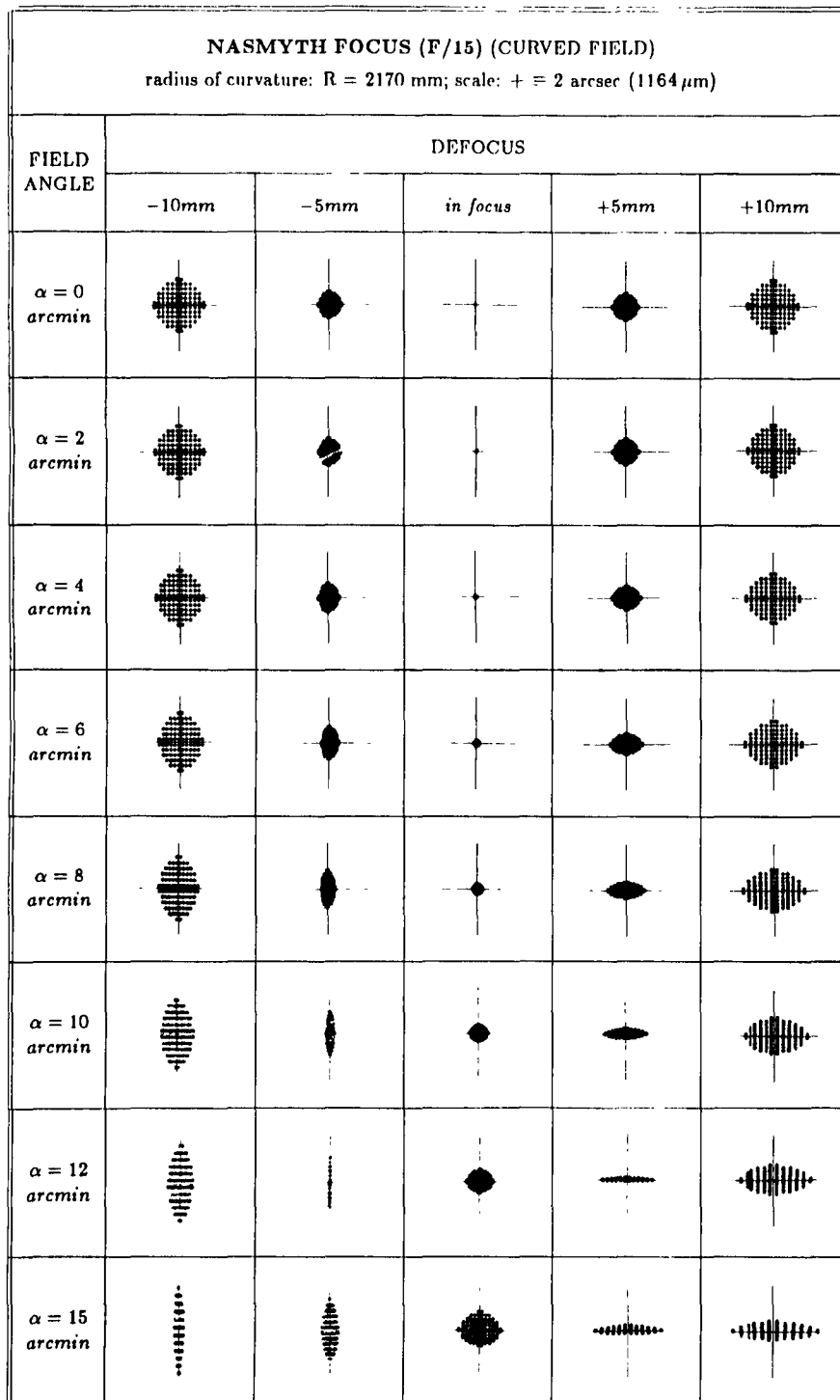


Figure 4.3: Spot diagrams for the curved field at a Nasmyth focus of the VLT unit telescope.

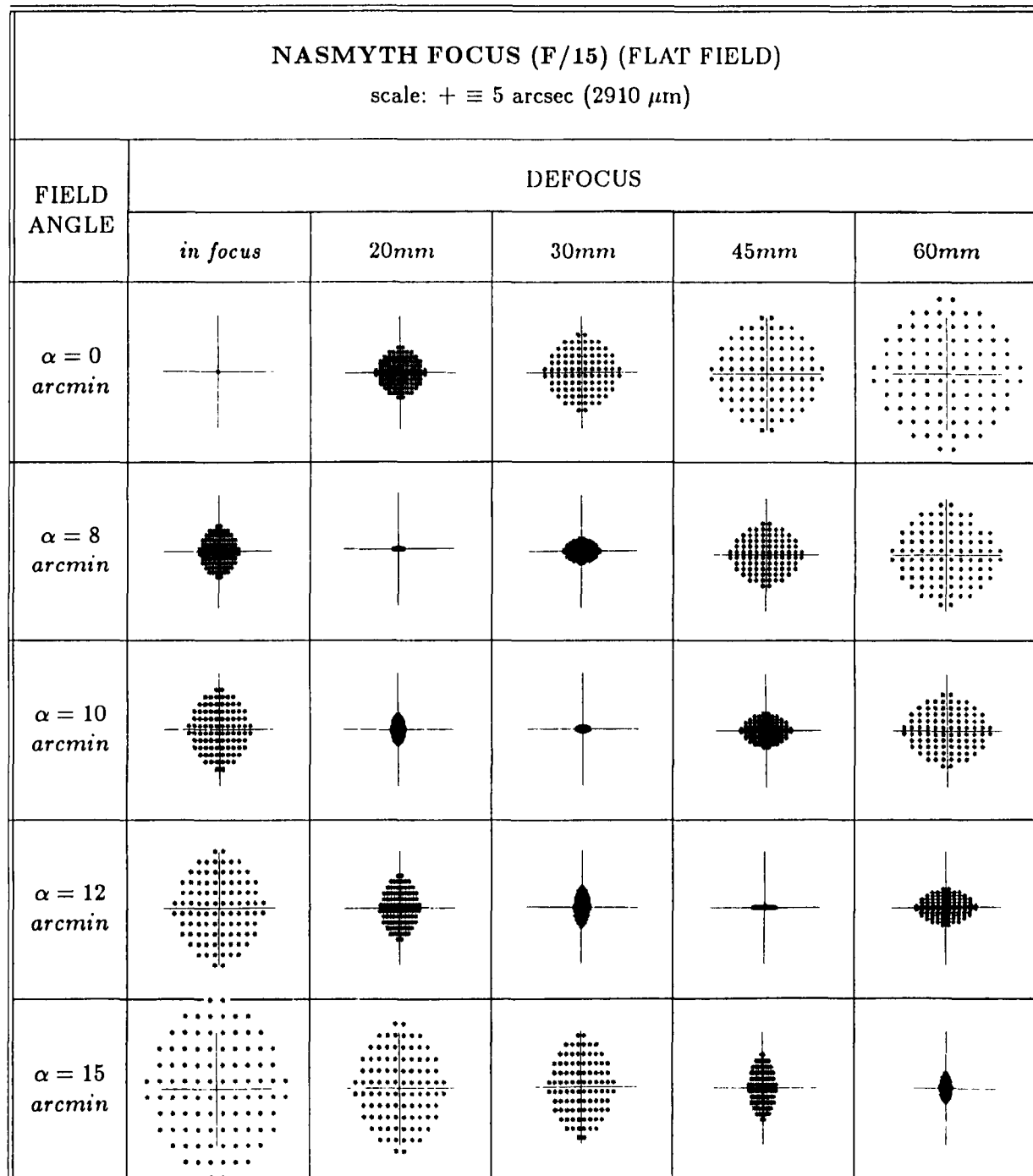


Figure 4.4: Spot diagrams for a flat field at a Nasmyth focus of the VLT unit telescope.

TABLE 4.3

SENSITIVITY OF THE NASMYTH IMAGE TO TILT AND DISPLACEMENT								
MIRROR						NASMYTH IMAGE		
	TILT (in <i>arcmin</i> )		DISPLACEMENT (in <i>mm</i> )			DISPLACEM. (in <i>mm</i> )		DEFOC. (in <i>mm</i> )
	$d\alpha$	$d\beta$	$dy$	$dx$	$dz$	$dy_i$	$dx_i$	$dz_i$
<i>M1</i>	+1	+1	+1	+1	+1	-69.82	-69.82	+69.5
						-8.3	+8.3	
<i>M2</i>	+1	+1	+1	+1	+1	+10.10	+10.10	-70.5
						+7.3	-7.3	
<i>M3</i>	+1	+1	+1	+1	+1	-4.42	-3.13	+1
						+1		+1
						+1		+1

$d\alpha, d\beta$ : rotation of the mirror around the  $x$ -, or  $y$ -axis  
 $dx, dy, dz$ : displacement of the mirror in  $x$ -,  $y$ -, or  $z$ -direction  
 $dx_i, dy_i, dz_i$ : displacement of the image in  $x$ -,  $y$ -, or  $z$ -direction

### 4.1.1 Primary Mirror

One of the most important topics of the whole VLT project is the primary mirror problem, i.e. what type of material, characteristics of the mirror, and its support. These are discussed separately in Chapter 5.

Whatever solution proves to be the ultimate solution, the primary mirror will be actively controlled and corrected. This solution seems currently the only technology which allows to achieve the ambitious imaging quality goal. Additionally it seems to be the only way to stay within realistic weight limits and an affordable cost frame for the entire project.

Table 4.4 summarizes the main characteristics and specifications of the solid meniscus solution which seems to be currently the most promising primary mirror technology.

TABLE 4.4

<b>MAIN PHYSICAL PROPERTIES OF THE PRIMARY MIRROR (M1): THIN MENISCUS OPTION</b>		
Material	ZERODUR	Fused Silica
Shape	Solid Meniscus	
Effective diameter	8000mm	
Thickness	175mm	200mm
Central hole diameter	$\simeq 1.1m$	
Mass	$\simeq 22000kg$	
Number of active supports	150 to 200	
Mass of M1 unit (mirror and cell)	30000kg	

The effective thickness of the blank and the number of supports have to be fixed during the final optimization process. The most important factors which have to be considered are optical quality, polishing, thermal aspects, total mass, handling risk, transport, and cost.

### 4.1.2 Secondary Mirror

For the design of the secondary mirror several aspects have been considered, including active optical correction, focusing, fine tracking, and wobbling in the infrared.



The correction of the decentering coma as part of the active optical system (see Chapter 5) will be achieved by turning the secondary around its centre of curvature. This method has the advantage of introducing no pointing error. To compensate 1 arcsec of coma a tilt of 1.60 arcmin is needed. This value corresponds to a displacement of 2.20mm in the M2 plane.

A general scheme of the secondary unit is shown in Figure 4.5. In addition to coma correction, the secondary mirror may be used to correct for small but fast varying tracking errors. With 2 piezoelectric linear actuators the lightweighted secondary is envisaged to work at frequencies up to 20Hz and an amplitude corresponding to 5 arcsec. The resulting actuator force is in this case small enough that it should be possible to avoid exciting resonance frequencies in the top unit structure. A sophisticated control system would allow to use the secondary also for fine tracking, image motion compensation and to some extent as a chopper for IR observations. Secondary effects of a fast tracking

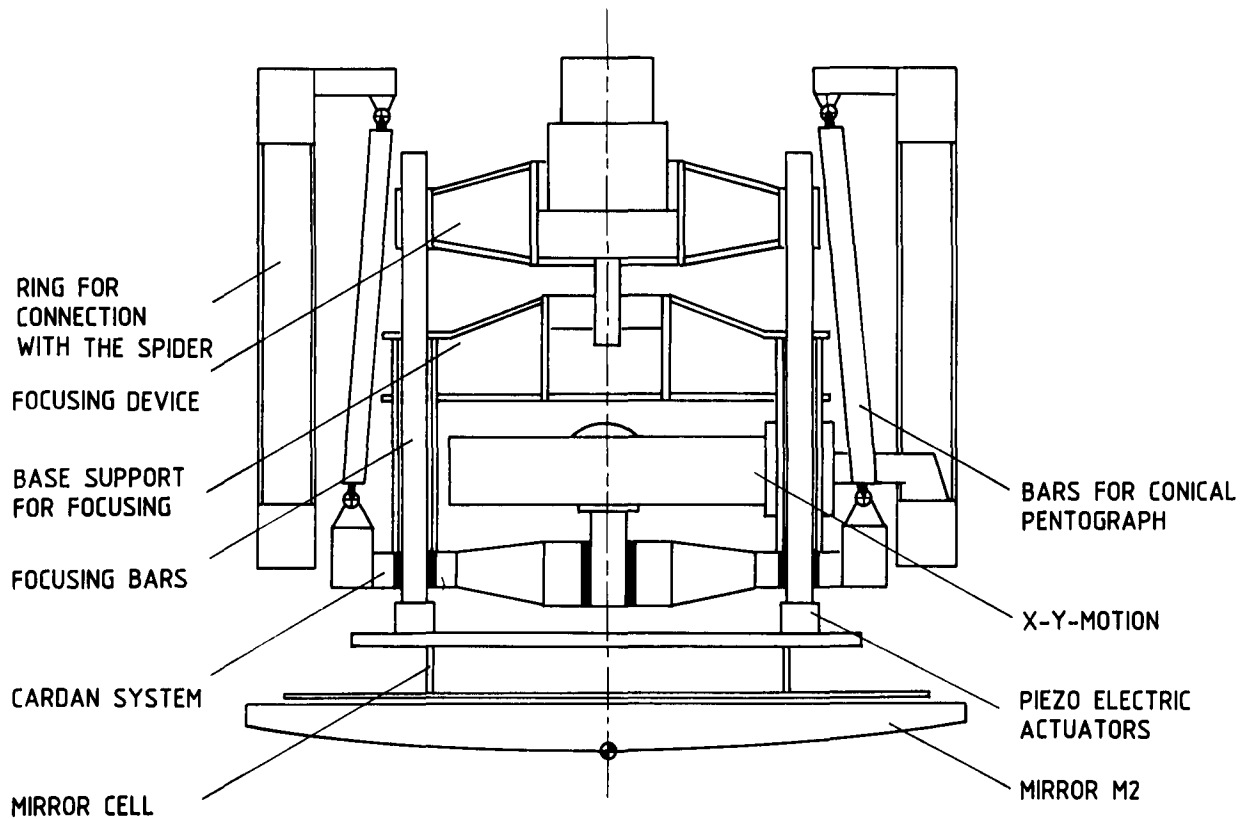


Figure 4.5: Schematics of the secondary mirror (M2) unit. The mirror is supported from its back. Mechanical parts are entirely hidden in the shadow of the mirror. The mirror has 5 degrees of freedom ( $x, y, z$  translation for focus and coma correction;  $\alpha, \beta$  rotation for fast tracking error correction).

correction with the secondary mirror such as possible field distortions and background variations in the IR have however to be assessed. Because the dynamic requirements for a fast tracking correction (or IR wobbling) and in order to minimize the total mass of the secondary unit which is important for the optimization of the telescope tube structure and its dynamic characteristics, it is important to lightweight the secondary mirror.

Provisional characteristics considered in the current state of the proposal as well as the goals if the secondary has to satisfy the requirements of a wobbling secondary are given in Table 4.5.

TABLE 4.5

<b>SECONDARY MIRROR (M2)</b>		
	present specifications	IR wobbling mirror (GOAL)
Diameter	1270mm	1270mm
Thickness	150mm	150mm
Material	glass-ceramics	glass-ceramics
Mass	200kg	70kg
Lightweighting factor	≈ 60%	≈ 80%

### 4.1.3 Nasmyth Mirror

In order to limit the moving mass of the telescope and to increase local eigenfrequencies the Nasmyth mirror will be moderately lightweighted to approximately 40% to 60%. Table 4.6 summarizes the most important parameters.

TABLE 4.6

<b>NASMYTH MIRROR (M3)</b>	
Dimension	1615 × 1142mm <sup>2</sup>
Thickness	150mm
Material	glass-ceramics
Mass	225kg
Lightweighting factor	≈ 60%

#### 4.1.4 Instrument Interface

Two Nasmyth foci are available at opposite ends of the elevation axis, each of which is served by a platform for mounting even large and massive instruments. One of these foci is dedicated to the visible and the other to infrared wavelengths. Both Nasmyth foci have a back focal distance behind the adaptor of 200mm.

Atmospheric dispersion compensation with large telescopes implies severe difficulties, because in case of the VLT the field of view has a diameter of 1047mm. In order to avoid prisms with more than 1m diameter the compensation of the whole field of view has been dropped. Aside this practical reason such large prisms would be very expensive. It has been decided to include the atmospheric dispersion compensation into the instrumentation with moderately sized optical elements (see Chapter 10). These elements compensate only the used part of the field of view.

The problem of field rotation is met by rotating the instrumentation to avoid additional reflecting surfaces or refracting elements. The final definition of the various interface elements (adapters, atmospheric dispersion compensation) and of the details of the Nasmyth platform has to be done in close relationship with detailed definition and design of the instruments.

#### 4.1.5 Sky Baffling and Pupil Alignment

It is considered to avoid the sky baffles because they usually create the following major problems: They increase the central obstruction (from approximately 3% considering only the secondary mirror to about 10% with a baffle designed for a 30 arcmin field of view), they must be removable for IR observation, and they increase considerably the wind cross-section of the telescope. The mechanical unit of the secondary mirror will be smaller in diameter than the mirror itself. From the focal plane only the mirror and the spiders can be seen. Whenever sky baffling is necessary it has to be foreseen in the instrument design. A possible compromise for the visible is shown in Figure 4.6 with baffles inside the adaptor and flange and a black surface on the opposite side of the tube.

Matching the image scale of the F/15 Nasmyth focus to the detector, the typically available pixel sizes will anyway require some kind of focal reducer, which usually provides ample opportunities for internal baffling. However in this case particular attention must be paid to the quality of the pupil image and to diffraction effects of sky apertures, especially in the IR, for which a sharp pupil image and a perfectly aligned cold stop is essential to maintain a low emissivity.

The above mentioned point is even more critical for an alt-az telescope compared with a classical mounting. The instrument rotation which is necessary to compensate for field rotation may introduce pupil decentering if it is not perfectly aligned with the optical axis. It is foreseen to include in the telescope design the possibility to check or

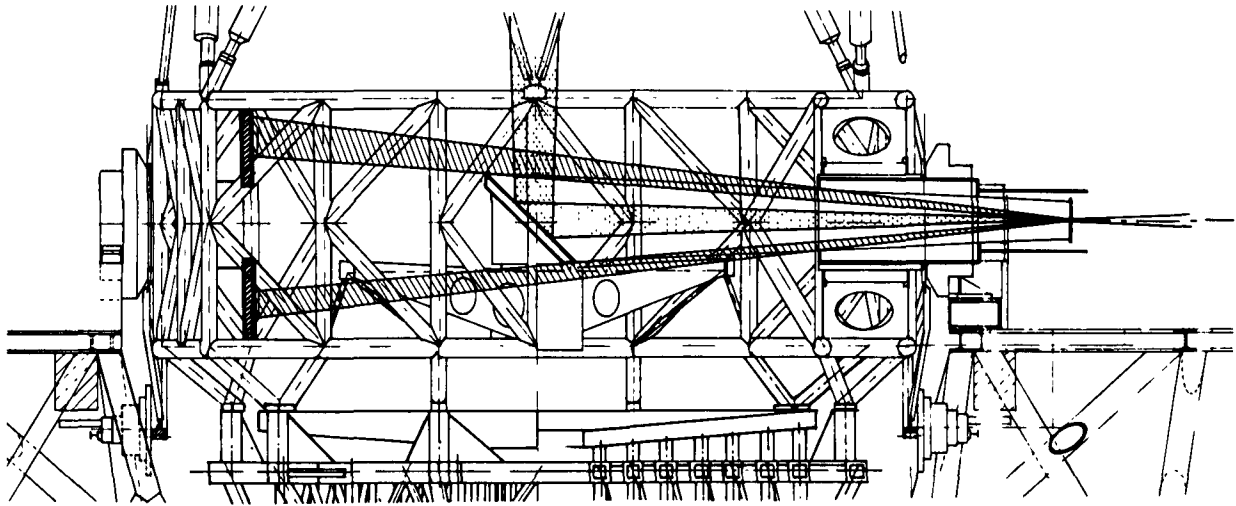


Figure 4.6: Possible scheme for baffling at visible wavelengths.

control the instrument alignment. A possible system could be a light emitting diode located in the centre of the secondary mirror and a quadrant cell detector located in the shadow of the central obstruction of the pupil stop.

#### 4.1.6 Optimization for the Infrared

As described above the unit VLT telescopes are designed for visible and infrared operation without change of the optical configuration. Especially, no time-consuming exchange of the secondary unit is foreseen like in classical telescopes. Therefore, the detailed design has to comply with the requirements for the two observation modes.

##### Minimization of the spider obstruction

The preliminary mechanical design shows that 1.5% spider obstruction is achievable. A further optimization and the use of special composite materials may push it down below 1%. Additional measures such as the use of reflective back surfaces and of slightly inclined walls could further reduce the effective emissivity in the IR.

##### Reduction of the central obstruction

Because all observation modes will require the use of relay optics in order to match the pixel size of detectors, the telescope's relative aperture is not a fundamental parameter.

A large F-number allows minimizing the central obstruction. On the other hand, there are physical parameters which limit the size of the linear field of view, and, therefore, F/15 has been selected as an optimum compromise. The secondary mirror would then have a minimum diameter of 1160mm for the axial beam only and 1270mm for 30 arcmin unvignetted field of view. As mentioned before, the telescope will not have any sky baffles even for the visible, so that the central obstruction will be less than 3% of the light collecting area. All mechanical parts and supports of M2 and M3 will be optically hidden behind the mirrors. The Nasmyth mirror has a smaller cross section than M2, and if the primary mirror has a central hole smaller than M3, a detector located in the focal plane will only see the sky and highly reflective surfaces looking at the sky. A cooled pupil baffling and a field stop inside the instrument will nevertheless be necessary.

### **Undersizing the secondary mirror**

Undersizing the secondary mirror will not be necessary, if the instrument provides a clean and high quality image of the telescope pupil (either M1 or M2), and is therefore not further considered. Additionally, it is possible to provide for the IR observing mode an annular reflective mask on the secondary mirror, which will effectively limit the pupil size. A possible drawback is the vignetting progressively introduced off-axis. Its effect on the active optics wavefront sensor has to be investigated. Limiting M2 to the axial beam size, a vignetting of about 10% would be introduced at 15 arcmin off-axis. Unless there are severe local wavefront aberration effects it is not expected that this would cause a sensible degradation of image quality.

### **Alignment of the telescope and instrument pupils**

Alignment of the telescope and instrument pupils is critical with an alt-az mounting because the compensation of field rotation may offset the pupils if the alignment of the telescope and instrument axes is not perfect. It is proposed to introduce an active control of the instrument pupil (or of the instrument axis) as described in Section 4.1.6.

### **Cleanliness of mirror surfaces**

For several years, distilled water washing of mirrors has been used successfully at La Silla to extend the lifetime of aluminium coatings. The VLT will have an in-situ washing facility. It is expected that cleaning procedures at 2 to 3 month intervals will maintain the emissivity close to its theoretical level. The lifetime of coatings is expected to be between 1 and 2 years. The same washing procedure will also be applied to M3 but not to M2, which - considering its favourable position - is much less subjected to pollution and dust accumulation.

Recently, a new method especially suited for dust and particle removal from mirror surfaces has been proposed. Pressurized CO<sub>2</sub> is expanded through a nozzle in front of the mirror surface to generate dry ice snow. This snow is very adhesive and while sliding down the mirror surface on a thin gas layer it carries away contaminations. This simple dry cleaning method could replace part of the above mentioned wet washing and possibly increase the lifetime of the coatings. Further tests are necessary to study this effect for condensated contaminants on the surfaces.

### Wobbling secondary mirror

From experience it seems to be evident that wobbling the secondary yields better results than focal plane choppers. It is not clear however, whether this results from fundamental limitations or from engineering problems. Another aspect to be considered is the performance (amplitude and frequency of the wobbling mirror) which will be required with future IR detectors, in particular array detectors. It is foreseeable that they will cover a substantial field of view. Their integration times will be somewhat longer than for existing single element detectors. From the present discussion (see VLT Report No. 51 of the IR Working Group) it emerges that wobbling the normal F/15 secondary may be an acceptable solution. Yet the mirror would have to be lightweighted. A 60% factor could be easily achieved, 80% being an upper limit for conventional lightweighting techniques (see Section 5.1.2). If the mirrors were limited in size to provide only an unvignetted field of 15 arcmin, its weight could be reduced to about 70 kg. Adding the supports, the moving mass might be less than 100 kg. Beryllium or composite materials could also be considered. Beryllium mirrors of similar size, high optical quality, and with a density of 34 kg/m<sup>2</sup> after lightweighting have already been manufactured for space applications.

Chopping with frequencies up to about 10 Hz is believed to be possible for beam separations (amplitudes) of the order of 10 to 20 arcsec, which - considering the emphasis on high spatial resolution - appears to be quite acceptable. Although a number of problems have still to be investigated, it seems that the future requirements for sky chopping with the secondary mirror may well be compatible with the standard telescope configuration.

The same chopping mechanism could be used during normal observing for the correction of small and fast tracking errors which cannot be corrected with the telescope drive and servo system. In order to keep the same chopping direction on the sky (and to correct for 2 dimensional tracking errors) a 2-axis system is proposed.

Compatibility of the wobbling secondary with the active correction of the primary has to be analysed. It may be necessary to synchronize the chopping mirror and the active optics correction loop.

## Coatings

If for the VLT a partial or total specialization for infrared observations is envisaged, silver or gold coatings could be used for the telescope mirrors. This would result in a significant gain of performance.

The mirrors used for combining the beams, which are of modest size, will be anyway exchangeable (see Section 5.2.1) and one set will be optimized for the IR (silver coatings). Special measures to preserve the combining mirrors from pollution will also be applied (see Section 5.2).

Coatings aspects are discussed in more detail in Section 5.3.2.

## Possibility for the conversion to a Cassegrain system

The possibility of an additional Cassegrain focus for the unit VLT telescopes has been discussed. Although a Cassegrain focus is not part of the VLT baseline concept, the optical and mechanical design of the unit telescopes foresees a possible later addition of this option. The telescopes could then be converted to Cassegrain systems for a certain period of time (see Section 5.1.7). But for the decision on this option one has to consider the trade-off between cost increase, maintenance, cost of operation, and non-compliance with flexible scheduling on one side, and the gain in performance (lower emissivity, no instrument polarization, etc.) and observing capabilities on the other side.

### 4.1.7 Conversion to Cassegrain Focus

As mentioned in Chapter 2 the unit telescopes of the VLT are conceived for single focus operation. Priority is given to a Nasmyth focus, because the Nasmyth image can be easily relayed to the combined Coudé focus. In a classical telescope a change-over from Nasmyth/Coudé to a Cassegrain focus would require a change of the secondary mirror, because otherwise the backfocal length would make rather long yoke arms necessary. Additionally, the tertiary mirror has to be removed. But the concept of an active primary opens the possibility to switch to Cassegrain operation by only removing the tertiary mirror. With a small translation of the secondary mirror and a spherical aberration correction with the active primary mirror, it is possible to retain a corrected Cassegrain focus in the space between the backside of the primary mirror and the yoke, even in the existing compact mechanical design. Table 4.7 gives the necessary modifications. A maximum of approximately  $16 \mu\text{m}$  surface deformation is necessary to achieve the spherical aberration correction. This value is fully in the range of the rather flexible VLT mirror. An alternative consists of correcting the spherical aberration with a deformable secondary mirror. This solution has been used on the secondary mirror of the CFH Telescope with success. Figure 4.7 presents a possible Cassegrain focus configuration. Figures 4.8 and 4.9 show the corresponding spot diagrams. The sensitivity of this design with respect to tilt and displacement of M1 and M2 is given in Table 4.8.

TABLE 4.7

CONVERSION TO CASSEGRAIN FOCUS				
Focus	F-ratio	Back focal length [mm]	Displacement of M3 [mm]	Surface deformation for spherical aberration correction [ $\mu m$ ]
Nasmyth	15.00	7600	-	-
Cassegrain	13.28	5255	34.2	12.51

Although a Cassegrain focus seems to be possible from the point of view of optical design, it creates additional technical difficulties for the mechanical design:

- the tertiary mirror has to be removed;
- the Cassegrain focus needs a complete adaptor including image rotation compensation, wavefront sensor for the active optics, guide probe, etc., which would be different from the Nasmyth adaptors;
- the Cassegrain adaptor and a reasonable sized instrument box has to be integrated in the rather complex mirror support and cell structure.

All these measures will significantly increase the cost.

In the present proposal, it is considered to take appropriate measures in the detailed design to make a later implementation of the Cassegrain focus possible. The decision to construct and implement the Cassegrain equipment could then be taken later when experience obtained with the first telescope is available.

#### 4.1.8 Individual Coudé Focus

Each unit telescope will have an individual visible and infrared Coudé focus in the telescope base. These foci are mainly dedicated to special instrumentation. The optical design of these foci is part of the design for the beam combining optics which requires anyway an intermediate image in order to keep the optical elements of the combining train reasonably small for the required field of view. The visible and infrared beam



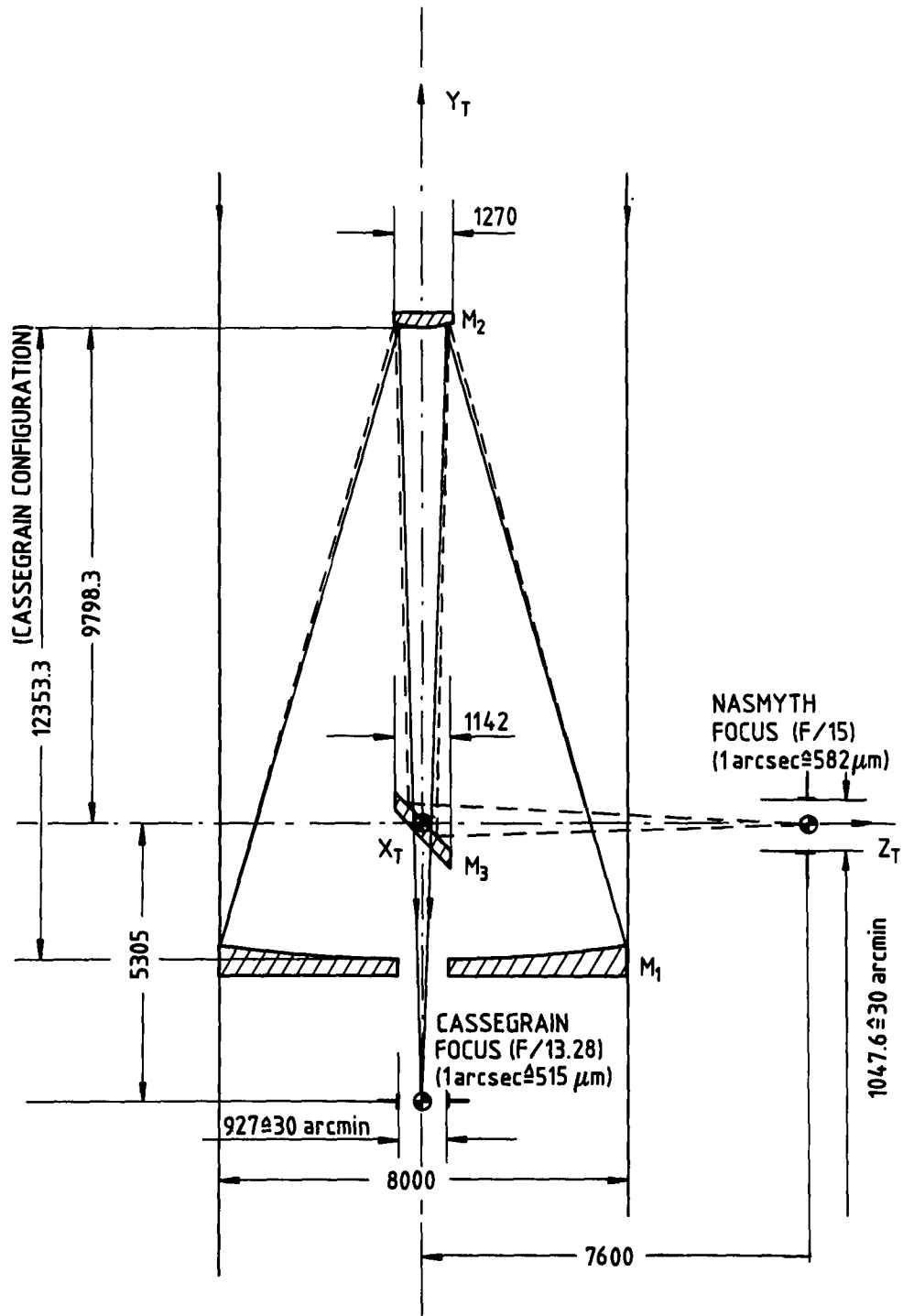


Figure 4.7: Optical design of the 8m unit telescope in the Cassegrain configuration.

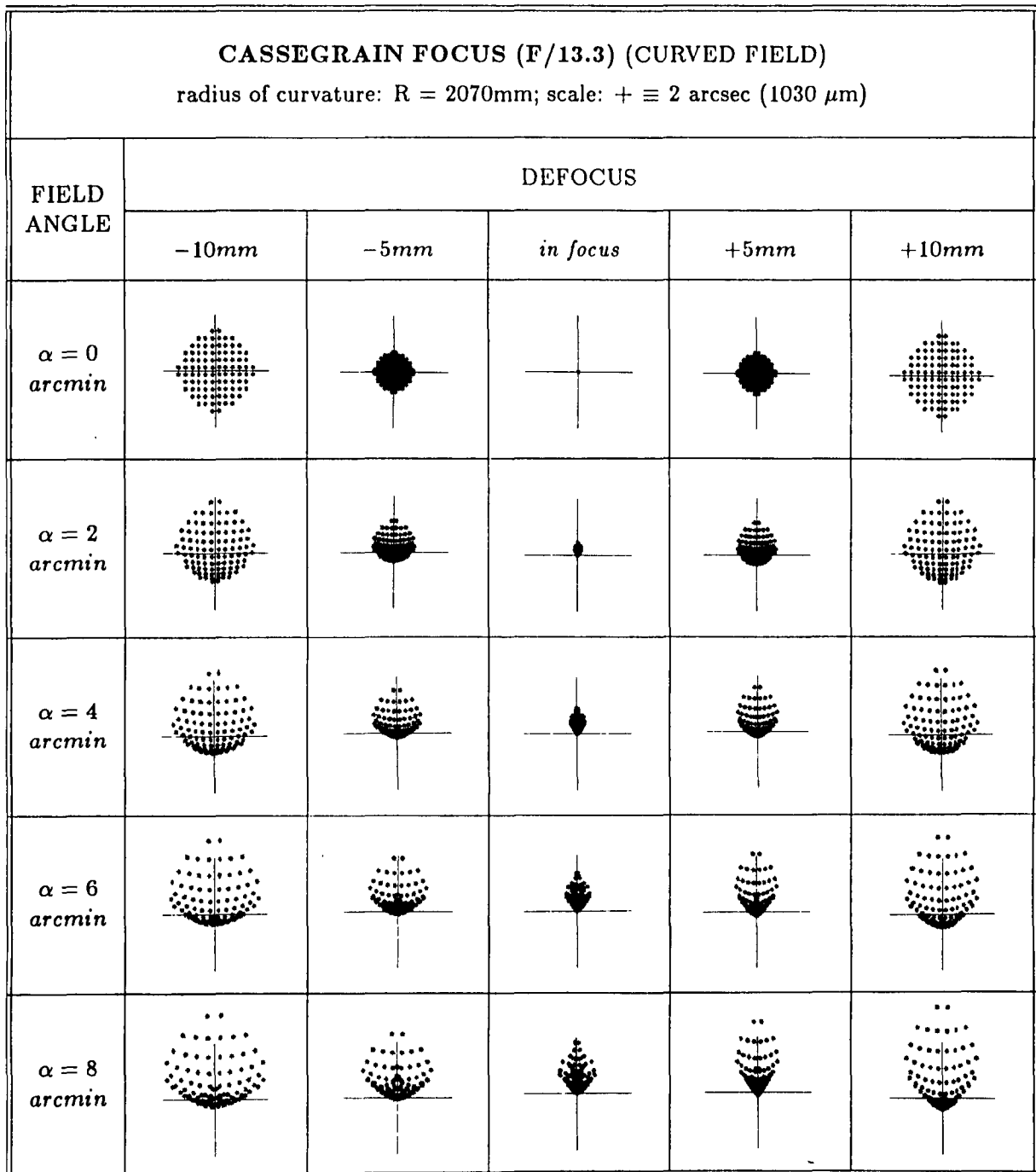


Figure 4.8: Spot diagram for the curved field at the Cassegrain focus of the VLT unit telescope.

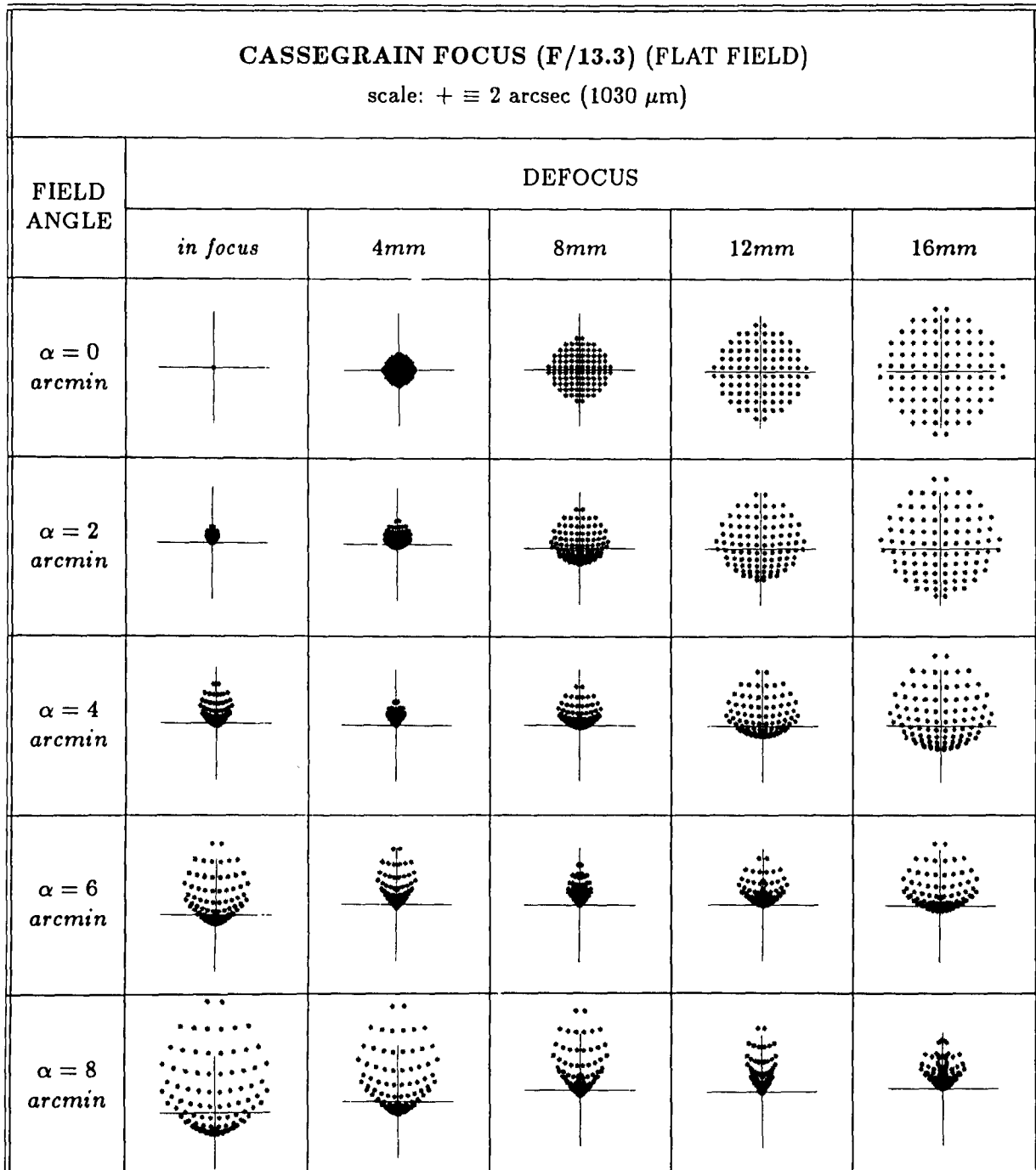


Figure 4.9: Spot diagram for a flat field at the Cassegrain focus of the VLT unit telescope.

TABLE 4.8

SENSITIVITY OF THE CASSEGRAIN IMAGE TO TILT AND DISPLACEMENT								
MIRROR						CASSEGRAIN IMAGE		
	TILT (in <i>arcmin</i> )		DISPLACEMENT (in <i>mm</i> )			DEFOC. (in <i>mm</i> )	DISPLACEM. (in <i>mm</i> )	
	$d\alpha$	$d\beta$	$dy$	$dx$	$dz$	$dy_i$	$dx_i$	$dz_i$
<i>M1</i>	+1	+1	+1	+1	+1	-54.8	-61.82	+61.82
							+7.38	+7.38
<i>M2</i>	+1	+1	+1	+1	+1	-55.8	+8.79	-8.79
							-6.38	-6.38
$d\alpha, d\beta$ : rotation of the mirror around the $x$ -, or $y$ -axis $dx, dy, dz$ : displacement of the mirror in $x$ -, $y$ -, or $z$ -direction $dx_i, dy_i, dz_i$ : displacement of the image in $x$ -, $y$ -, or $z$ -direction								

combination has been designed in a way that these intermediate images will be accessible. The design resulted in an  $F/74$  individual Coudé focus for the visible with 0.5 arcmin field of view (see Figure 4.10) and an  $F/32$  individual Coudé focus with 2 arcmin field of view for the infrared (see Figure 4.11). The optical quality for both foci is given in Figures 4.12 and 4.13 by the spot diagrams, respectively.

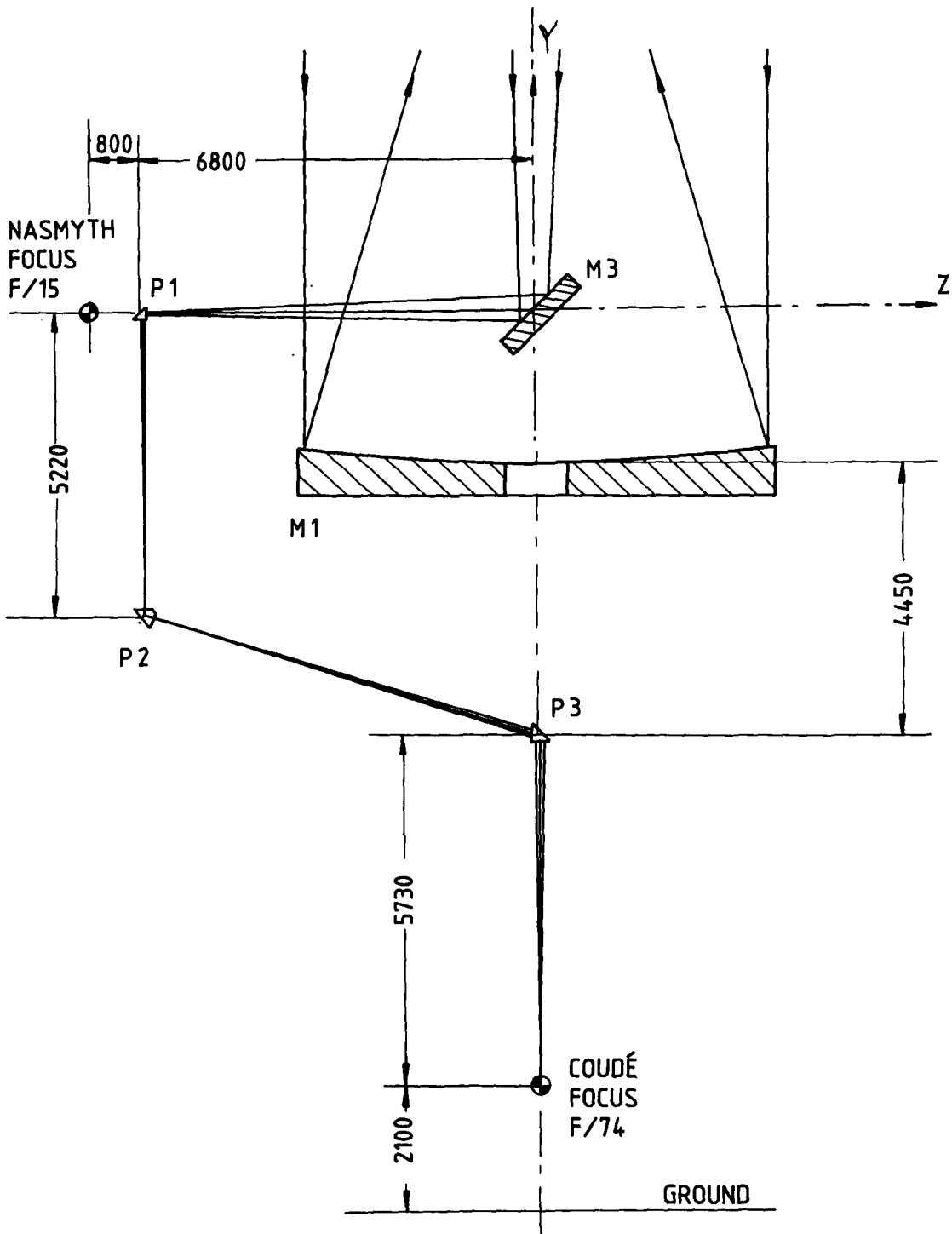


Figure 4.10: Optical design of the visible F/74 individual telescope Coudé focus.

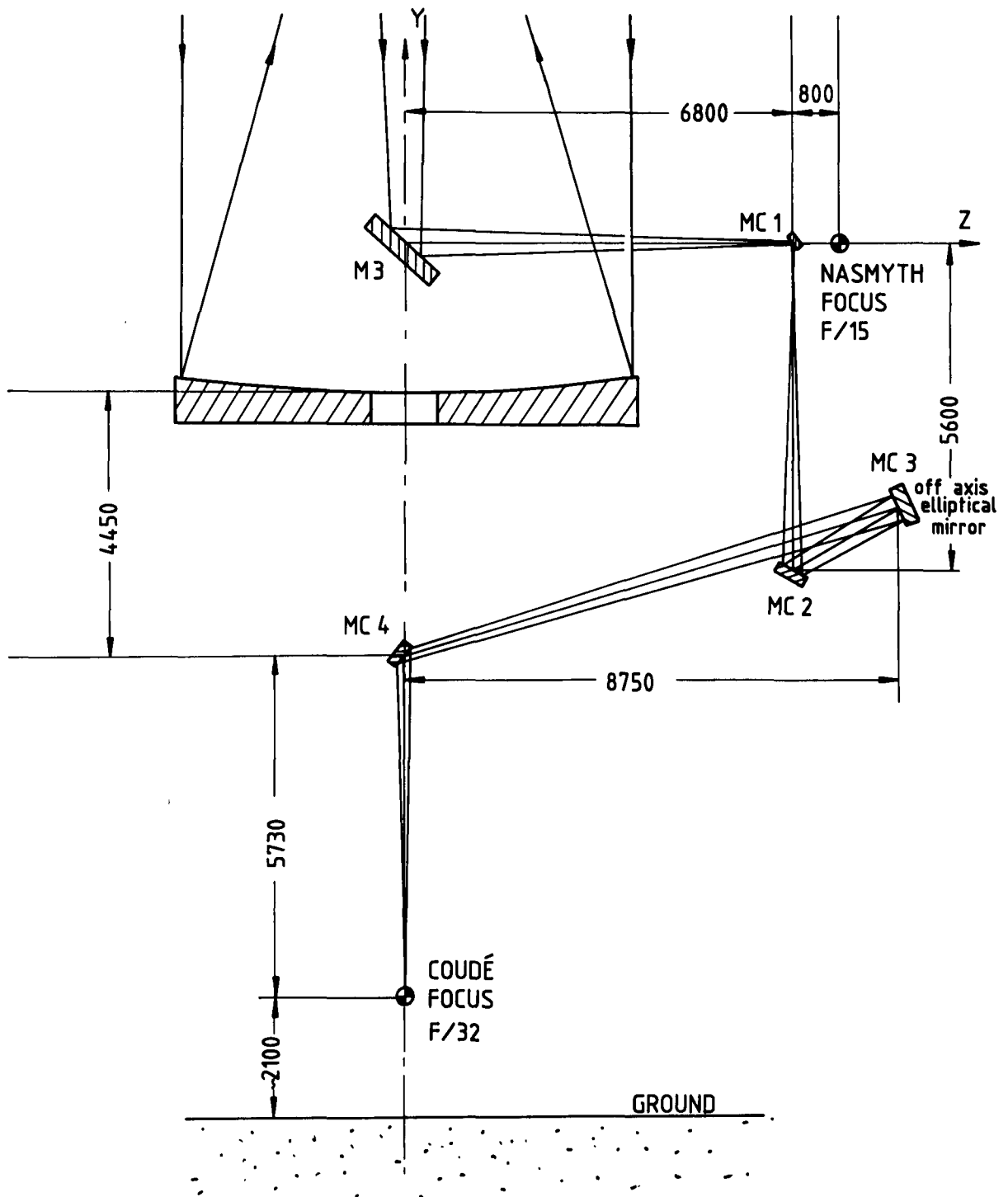


Figure 4.11: Optical design of the infrared F/32 individual telescope Coudé focus.

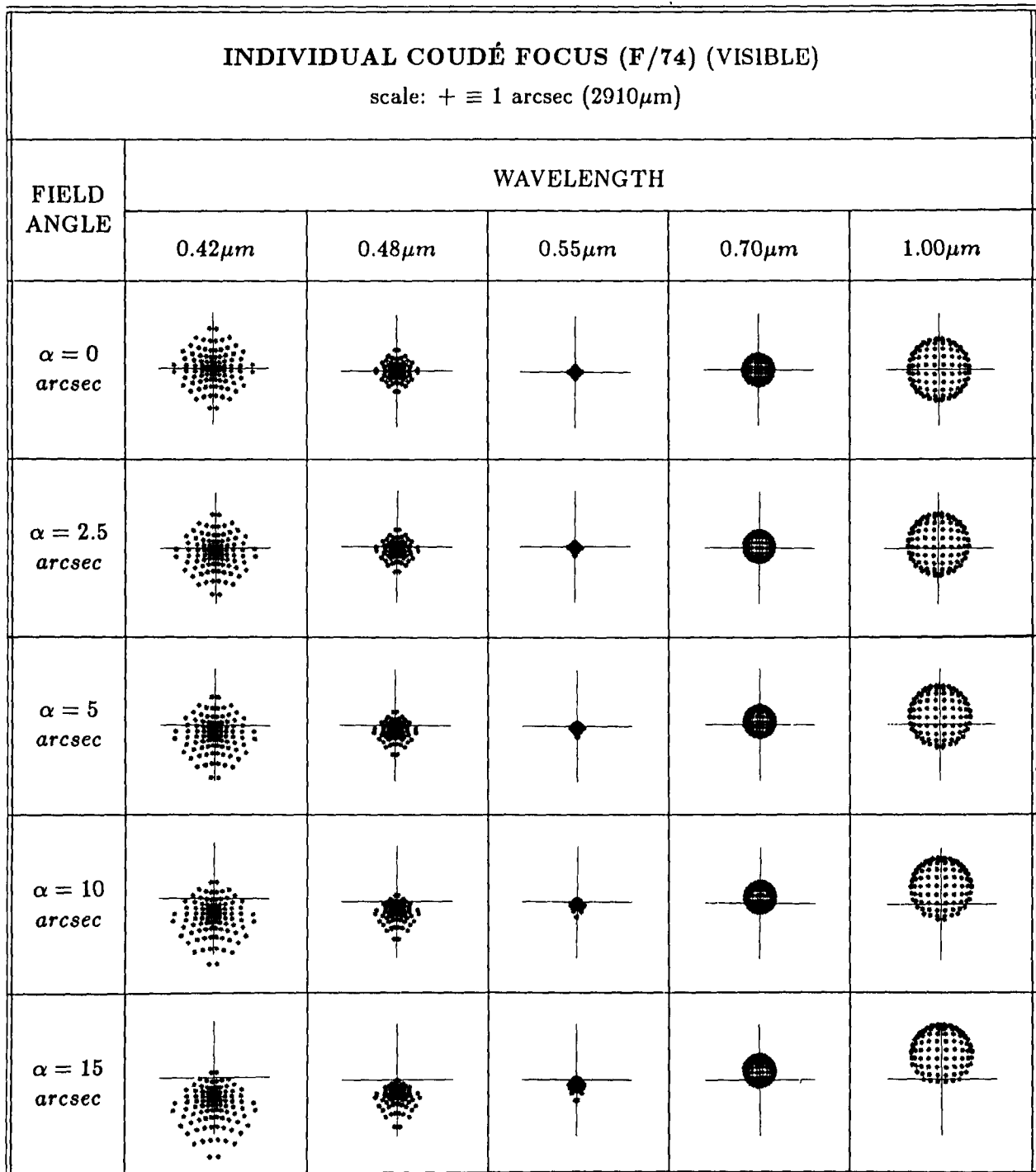


Figure 4.12: Spot diagrams for the visible individual Coudé focus (F/74). This focus is not corrected for chromatic aberrations. It is possible to add a correcting element in front of the focal plane, if the spectral range of the instrument would exceed about 1000 Å. The residual image quality will then be equivalent to the 0.55 $\mu$ m case.

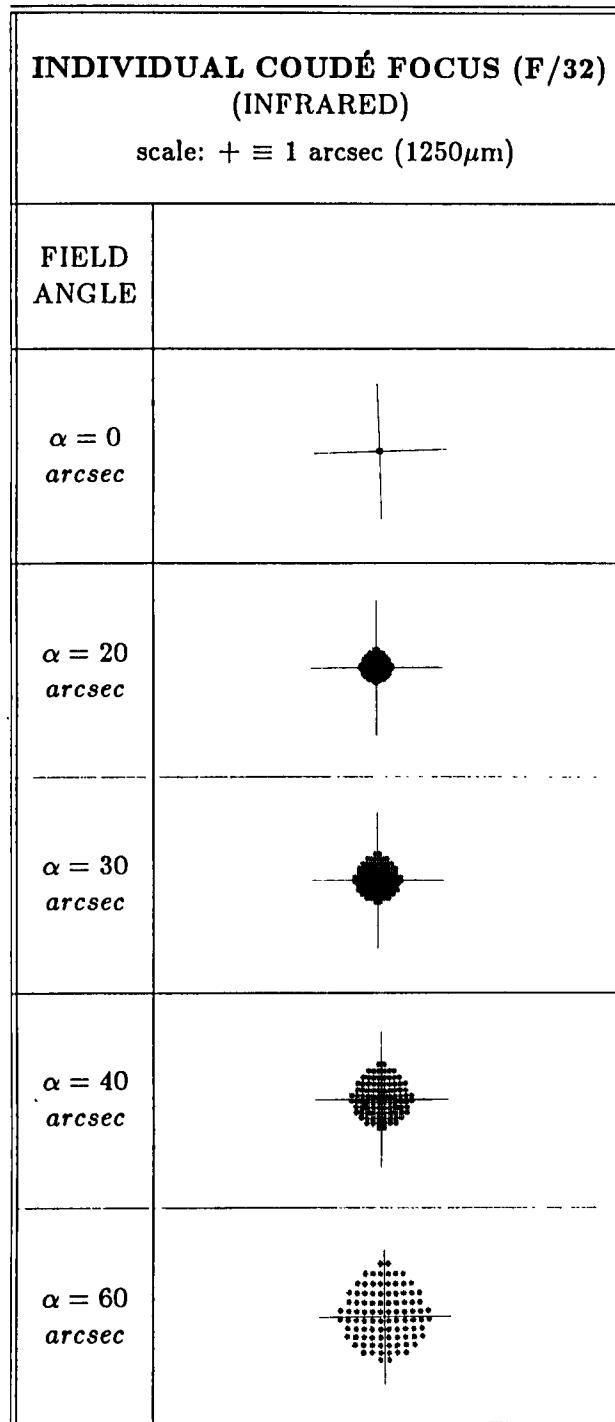


Figure 4.13: Spot diagrams for the infrared individual Coudé focus (F/32).



### 4.1.9 Polarimetry

Accurate polarimetry may require to set the polarimeter on the telescope axis. In this case a Cassegrain Focus is favourable. With an additional mirror, which is placed in front of the Nasmyth mirror M3 a 'pseudo Cassegrain focus' could be created with a field of approximately 1 arcmin. The image pick-up could be combined with fibre-optics. This possibility is not foreseen in the present configuration, but could be introduced in one of the four telescopes. However the image quality would possibly be somewhat lower because the active optics scheme will not be usable, due to the obscuration of the tertiary mirror. As a consequence the active correction for gravity deformation of the primary mirror would have to be preprogrammed, i.e. the active optical system would have to work in open loop, which is currently not foreseen.

It can be assumed that accurate polarimetry is possible with a Nasmyth configuration (even at a Coudé focus) by precalibration. In this case it is important to use mirror coatings with well defined and understood polarization properties, in order to precisely calibrate the three mirror Nasmyth system.

## 4.2 Beam Combination

The VLT linear array concept allows a versatile use of the unit telescopes. The individual telescopes could be used either independently or in various combination schemes. The major beam combination modes are (see Figure 4.1):

- Incoherent beam combination (Combined Coudé Focus)
- Coherent beam combination (Interferometry)

The incoherent combination with a combined Coudé focus offers the light collecting power of a 16m equivalent single dish telescope and is discussed in more detail in this Chapter. The coherent combination opens long baseline interferometry with a resolution span of approximately 0.7 milliarcsec in the blue to 45 milliarcsec at  $20\mu\text{m}$  wavelength in case a 104m baseline (distance between the two extreme telescopes) is selected. The coherent beam combination for interferometry is discussed in more detail in Chapter 12. Of course many technical aspects are valid for the incoherent as well as for the coherent combination modes, although the interferometric combination has much more stringent technical requirements, since extremely high optical stability is needed. Therefore, it seems to be appropriate to start the interferometric combination in the IR range and then gradually extend it towards the visible.

Due to the large number of optical elements necessary in the beam combining beam paths it may be very attractive to use replica techniques for the production of the combining mirrors. Quite a number of elements will be identical. These techniques are in development and first results indicate that the optical loss during replication is less

than  $\lambda/55$  rms ( $\lambda = 632.8\mu m$ ). Diameters of 500mm are present state of the art. With this method a significant cost saving could be achieved. Only one master (negative optical shape) per optical surface would have to be polished. The transfer blanks must be ground to a precision of approximately  $10\mu m$ . They obtain then their final optical shape from the master including the transfer of the coating. Recent results show that even a later recoating is possible.

The optical efficiency of the combined beam modes depends strongly on the coating efficiency. Because of the significant number of optical elements in the combining path, more than one optical train is necessary for the combination mode. Each of these is optimized for a specific wavelength band. The proposed beam combination is based on two different optical designs, one for:

- the visible and the UV range with refractive elements and dielectric mirrors, and one
- for the red and the IR with silver mirrors.

Because the visible and UV range cannot be covered efficiently by one type of coating it is foreseen to have two subsets of optical elements, one optimized for the UV and blue range and one for the green red range. With these combination paths it is possible to achieve an average efficiency for the combining path of  $\geq 0.85$  in the visible and of  $\geq 0.90$  in the IR (see Table 4.9 and Section 4.3.2. for the spectral reflectance curves). The optical elements will be mounted on motorized turrets to allow a fast change from one wavelength range to an other.

In the thermal IR the emissivity of the mirrors might be a limitation. Therefore, it could be necessary to cool the mirrors. This question needs further investigations. In any case, it is of utmost importance to keep the optical elements absolutely clean. New and improved coatings may at least partly solve some emissivity problems.

The beam path in both combination modes has to be protected against air turbulence, which, as laser transmission experiments have shown, are critical in the horizontal sections. Even if not necessary for optical reasons, a protection has to be provided against other environmental effects like dust, humidity, etc. which ruin the efficiency of the optical components and accelerate the ageing of the coatings. Experiments to study the effects of turbulence on horizontal optical propagation near the ground and in tubes are planned.

The solution proposed here consists of sealing the beam combination system and fill it with helium (or nitrogen) under atmospheric pressure. Helium has an index of refraction approximately 10 times lower than air and reduces the influence of turbulence and convection in the same proportion. A vacuum operation has also been investigated (see VLT Report No. 44) and appears quite feasible, though it is more expensive. Incidentally helium is provided for free by the various IR cryostats. This otherwise lost gas can be used to maintain the helium pressure and compensate possible leakage

and diffusion through the walls and joints. Additionally the tubes will be thermally insulated to prevent convection.

The possible application of fibre optics for combining the light from the different telescopes is discussed separately in Section 4.2.2.

### 4.2.1 Combined Coudé Focus

A beam combination in an array of individual alt-az telescopes requires a minimum of 4 to 5 additional optical elements (mirrors or total reflection prisms). For long transfer distances an afocal beam is not recommended because the mirror dimensions become very large. Intermediate images with relay optics is a way to overcome this problem, but this solution increases the number of optical elements in the beam path. In addition it may be necessary to introduce further mirrors or refractive elements to avoid extreme off-axis elements and to ensure a high pupil imaging quality which is particularly important for infrared operation.

It is foreseen to equip the VLT with the following combined Coudé beam systems, one optimized for the visible range and one for the infrared. Both systems are installed permanently to allow a fast and uncomplicated switch-over between the two observing modes:

- Infrared beam combination based only on reflective optical elements;
- Visible beam combination based on total reflection prisms with refracting power on the external surfaces and mirrors with optimized dielectric coatings.

As mentioned above it is necessary for efficiency reasons that, for the visible, two sets of optical elements be provided, one set optimized for the ultraviolet-blue range and one optimized for the green-red range. The proposed coatings for the mirrors and antireflection layers are described in more detail in Section 4.3.2.

Figure 4.14 shows the optical design of the infrared combination path. It uses 8 additional mirrors. The largest optical element has a diameter of 750mm for a distance of 52m between the azimuth axis of the telescope and the combined focus. In this case a total unvignetted field of view of 1 arcmin is achievable. The requirement for IR chopping at the combined focus is probably the determining constraint for the minimum field of view. The optical quality of the infrared combined Coudé focus is given in Figure 4.15.

Figure 4.16 shows the optical design of the visible combination path. In this case 5 total reflection prisms are applied with refracting power at the end surfaces (see Figure 4.17). Additionally, one lens and a spherical mirror with 800mm diameter are necessary. In case of the visible path a total unvignetted field of view of 0.5 arcmin is achievable. The optical quality of the visible combined Coudé focus is given in Figure 4.18.

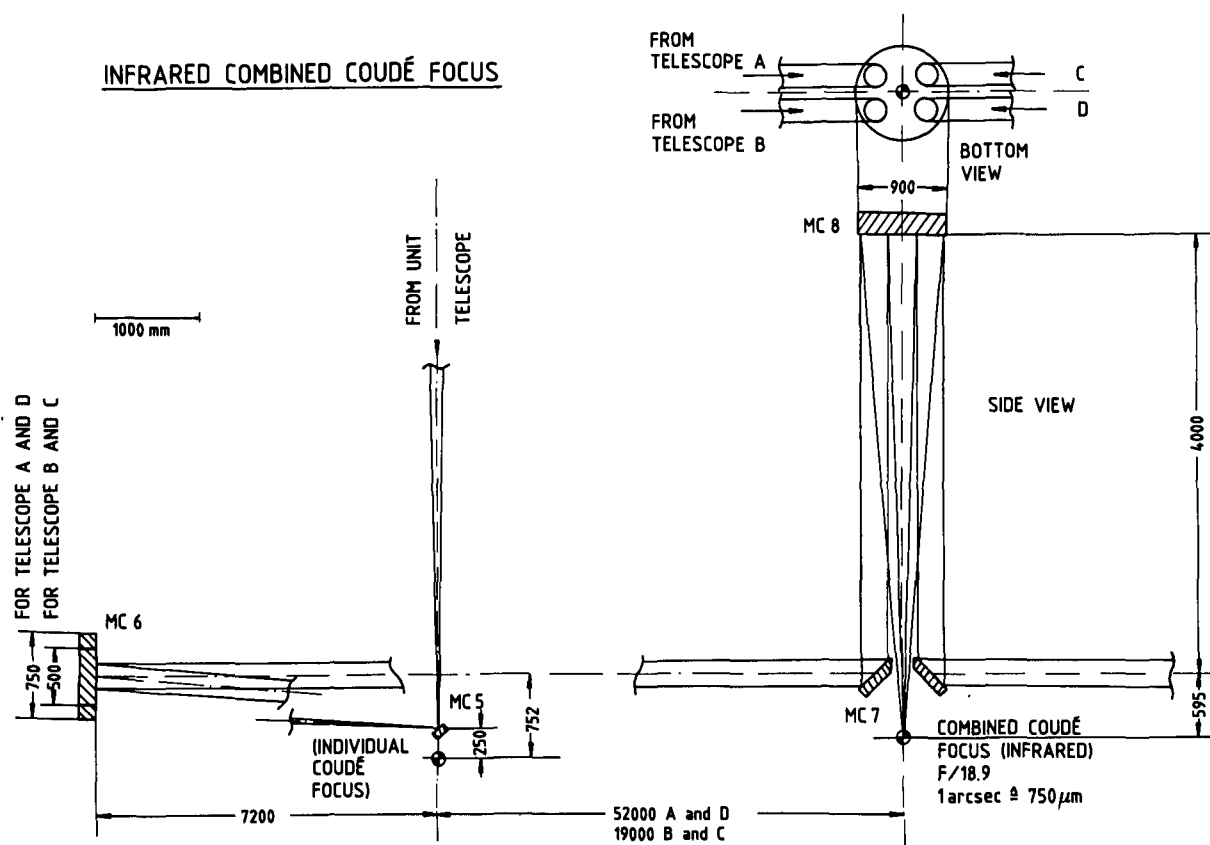


Figure 4.14: Optical design of the infrared beam combination path.

In the infrared as well as in the visible case the stability and alignment requirements can be met by an active control. The alignment of the Coudé train will be initially achieved and periodically checked with a build-in laser alignment and stabilization system, which subsequently could be made active to meet the specific requirements of interferometry if this could not be achieved in a passive mode. The combining mirrors are not subject to variations of gravity forces, and considering the relatively low sensitivity of the optical elements, this should not be necessary too often.

The mirror cells and prism mounts will be supported by motor driven actuators. Though all elements will be remotely adjustable, only one will remain adjustable after the initial alignment is performed. Therefore, the sole purpose of the remote adjustment is to facilitate this initial tuning of the optical system.

The present concept with telescopes in alt-az mount produces both image and pupil rotation. This drawback can be overcome by the use of an image derotator or by synchronously rotating the instruments. It is proposed to apply the latter method to the Nasmyth and individual Coudé foci as described in Chapter 5. The size of

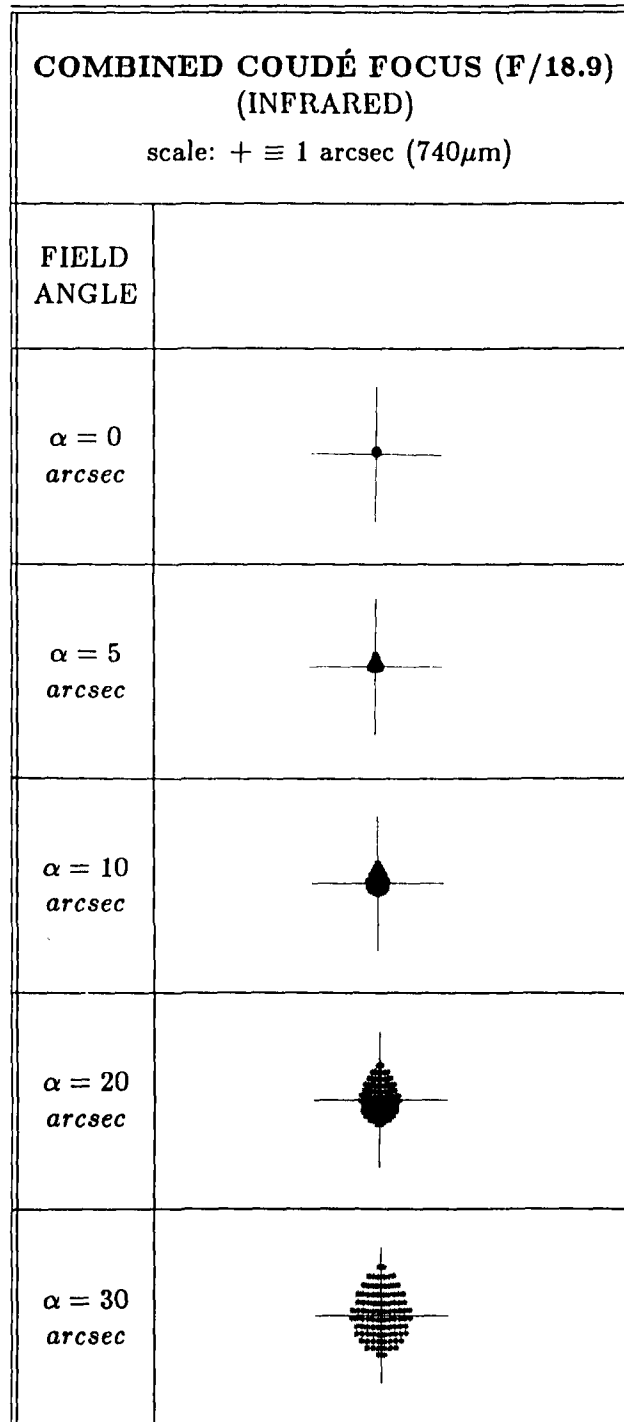


Figure 4.15: Spot diagrams of the infrared combined Coudé focus.

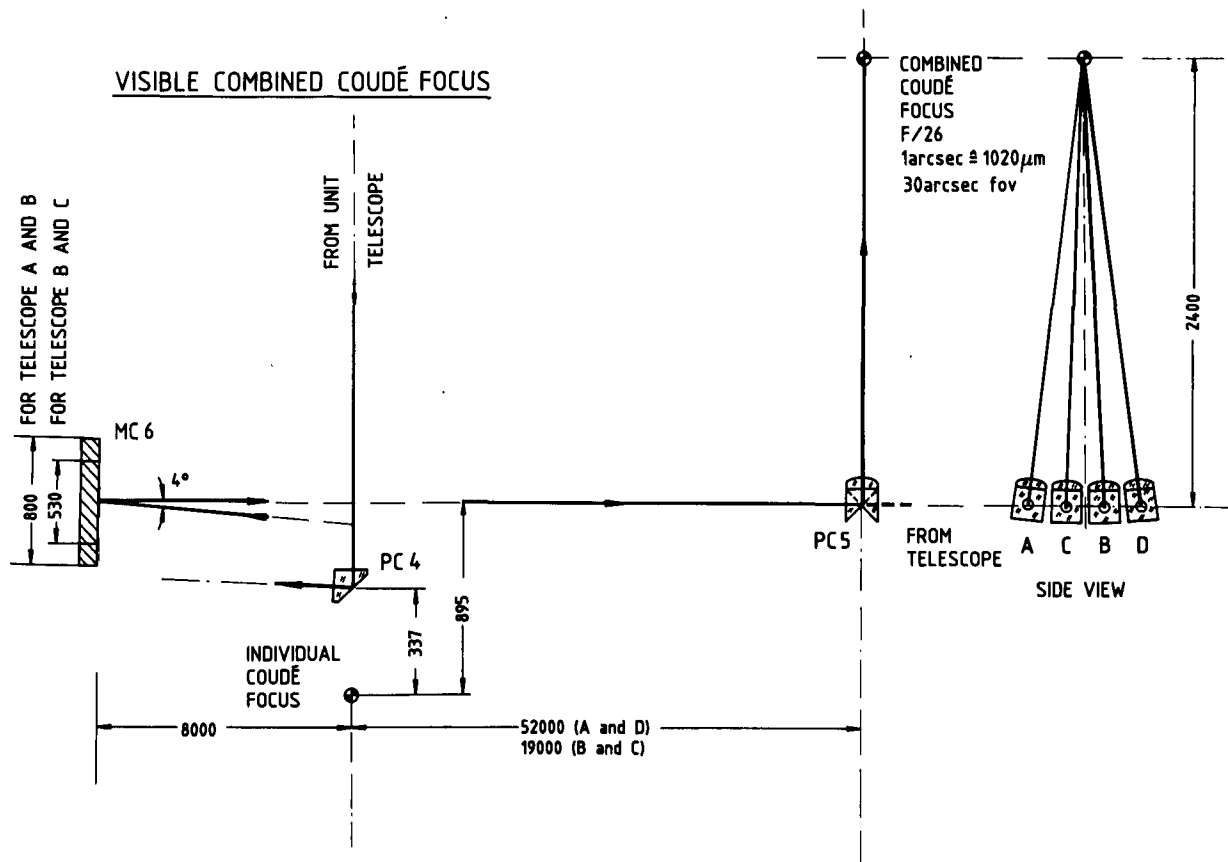


Figure 4.16: Optical design of the visible beam combination path.

the instruments likely to be used at the combined Coudé focus will probably exclude rotating the instrument. In this case an optical derotator could be used but it will necessarily introduce undesirable additional optical elements. It is likely that finally the combined focus will exclusively be used for the spectroscopy of single objects as it is the case with nearly all existing Coudé facilities. Therefore, it is questionable whether an image rotation compensation is necessary at this focus, and none has been foreseen.

An exclusive use for the spectroscopy of single objects may also allow to reduce the field of view to 10 to 20 arcsec. A reduction of the field of view may increase the efficiency by eventually reducing the number of optical elements. But in any case it reduces the cost since the size of the optical elements is proportional to the field of view.

The concept of flexible scheduling has also a strong impact on the optical design. A fast switch-over between the Coudé instrumentation has to be provided. In the present design it will be possible to switch from the visible train to the infrared by exchanging

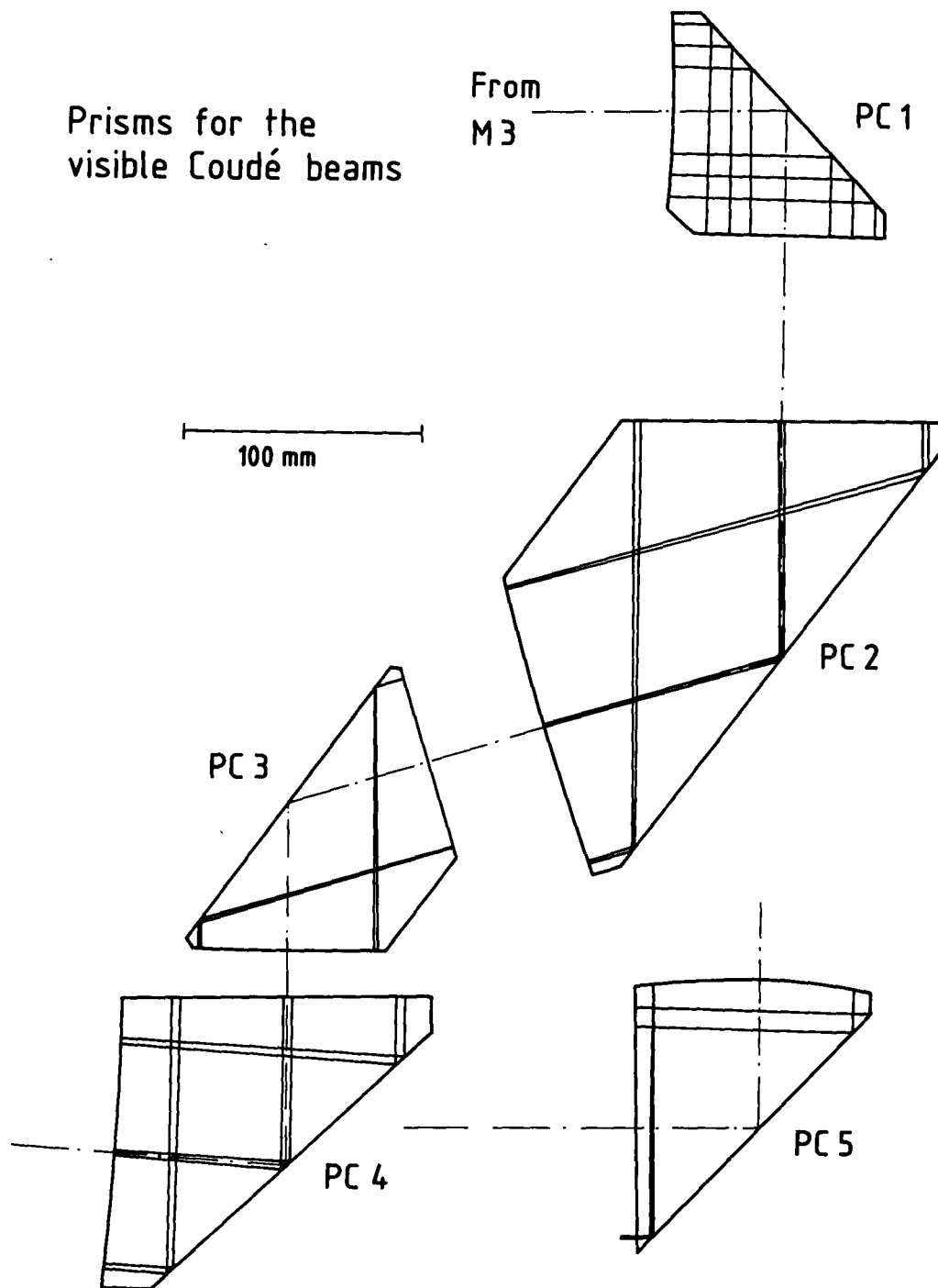


Figure 4.17: Prisms for the visible beam combination path.

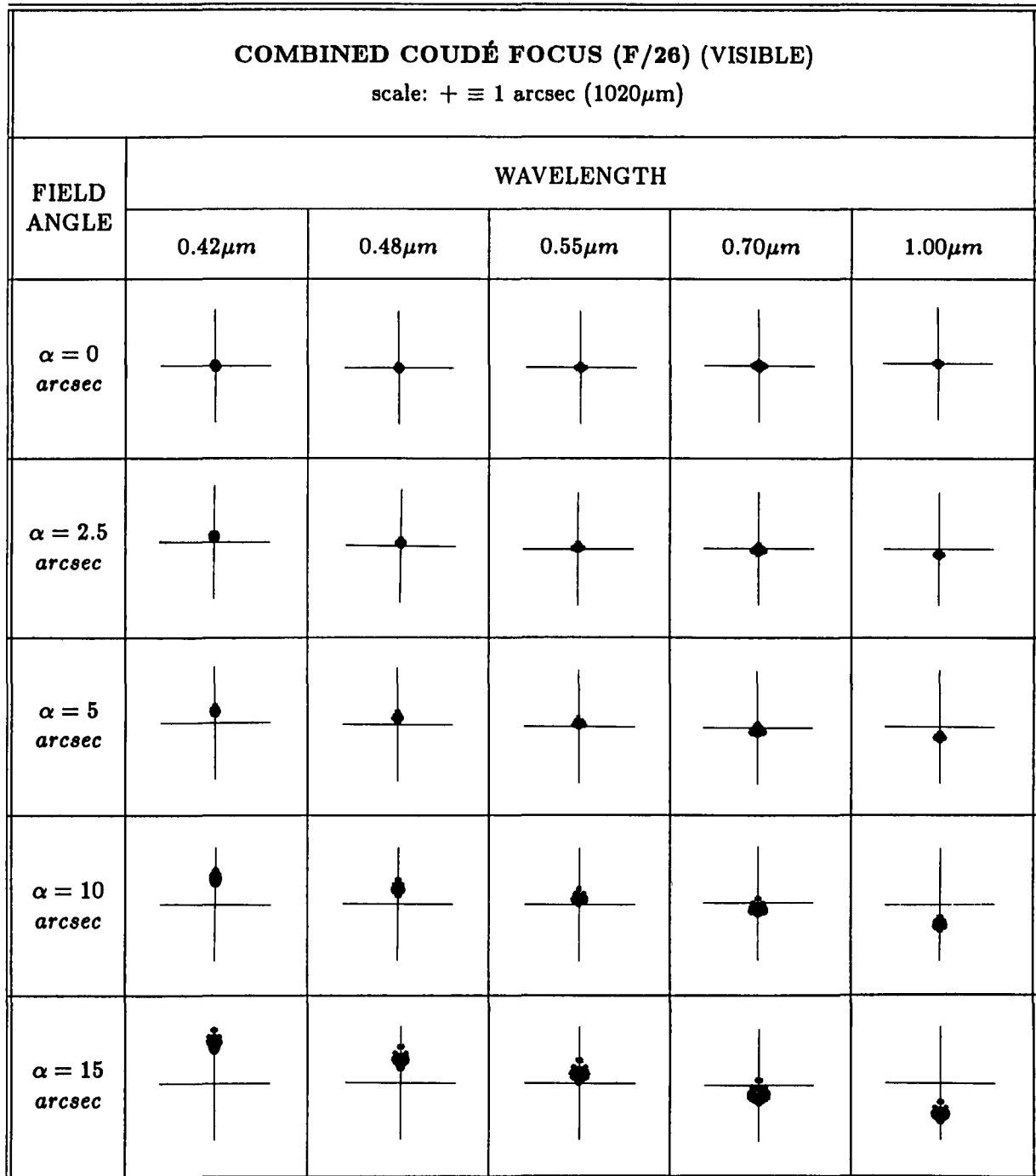


Figure 4.18: Spot diagrams of the visible combined Coudé focus. For this focus, the chromatic aberrations are corrected with prism PC5 used as a folded achromatic doublet.



PC3 with MC4 (see Figures 4.10 and 4.11) both mounted on a remotely controlled turret and by rotating the Nasmyth mirrors. The visible and infrared instrument are both permanently installed in the Coudé laboratory. Figure 4.19 shows a possible fibre feed for instruments. In this case a parabolic mirror with the fibre input end in its foci has to be moved into each beam.

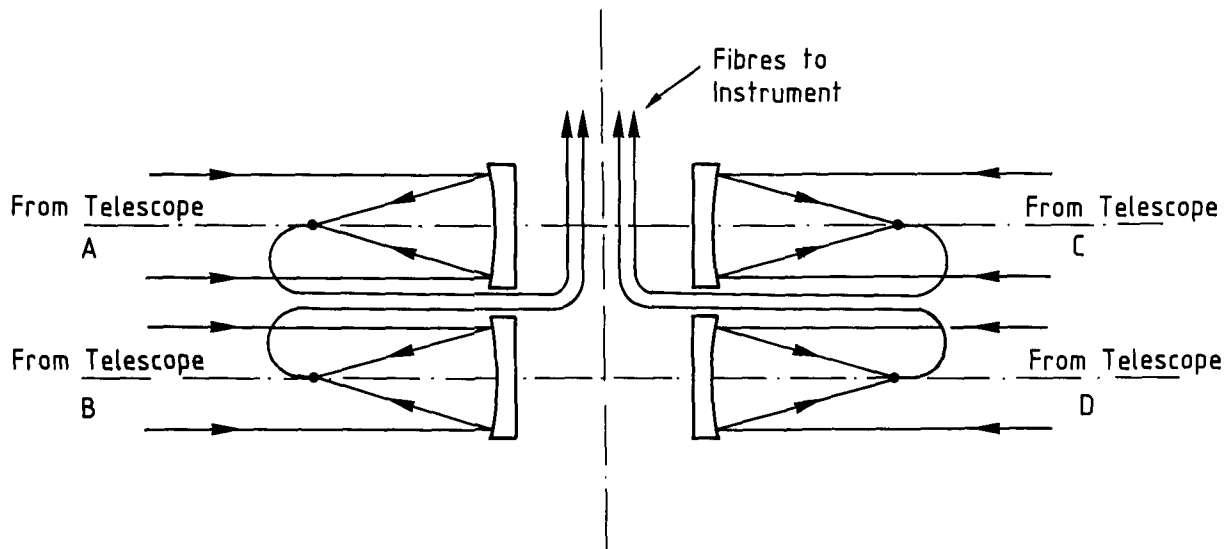


Figure 4.19: Design of a fibre optical feed for combined Coudé focus instrumentation.

The Coudé laboratory could be equipped with a special protection of the detectors against cosmic radiation. The recent progress in detector performance indicates that within the next few years the CCD arrays will have such a low noise level that cosmic radiation may determine the signal-to-noise ratio of the measurements. An increased thickness (50 to 100cm) of the Coudé laboratory ceiling made of special low radiation concrete could provide a good shielding.

## 4.2.2 Fibre Optics for Beam Combination

The application of fibre optics for the beam combination as an additional option is a very attractive approach, because of their lightness, flexibility and simplicity. This technique could save quite a number of optical elements in the beam combination train, which have, additionally, the requirement to be very stable. It would reduce the complexity and specifications on the mechanics and optics, and, thus, drastically reduce costs.

Figure 4.20 gives a possible scheme to use fibre optics between the telescope focus and a fixed collimator in the telescope base and to feed the instruments in the combined Coudé focus. This way the length of the fibre can be reduced to a few tens of metres.

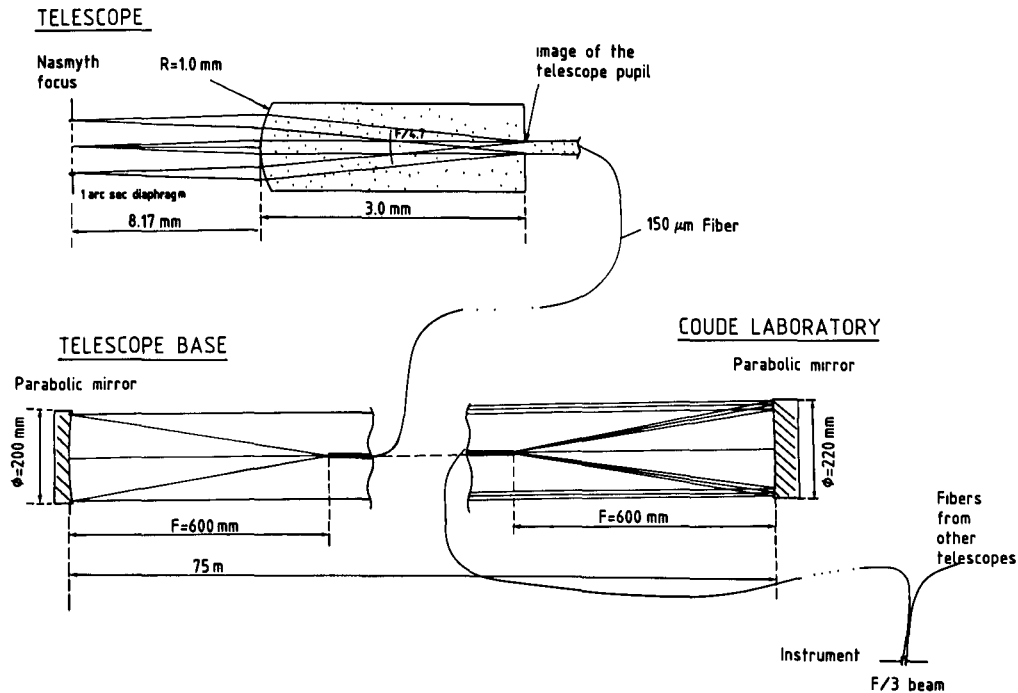


Figure 4.20: Optical train for the Coudé beam combination with optical fibres in the moving part of the telescopes and the bases, and for feeding the instruments. For the long path between the telescope bases and the Coudé laboratory a two mirror relay system has been selected in order to optimize the efficiency.

ESO has experience in the application of fibre optics in instrumentation mainly for the visible wavelength range, where they have proved to be extremely useful. An extrapolation of this experience towards a pure fibre optical beam combiner is very critical, because of the increased length of the fibres (approx. 80 metres) and the limited wavelength coverage. The application of fibre optics depends mainly on the future developments. Promising achievements have been made in the development of infrared fibres, the prospective materials, and fabrication methods.

The application of fibre optics for the VLT is under investigation, including optical design for a complete fibre combination, and the partial use of fibres only in the moving parts of the telescopes. For the time being, fibre optics do not appear competitive at least in the UV/blue and the IR with a direct optical combination and is therefore not included in the present proposal. However, if future technological developments would reverse this situation, a considerable cost saving could then be achieved. Use of coherent monomode fibres for interferometry will also be studied.

## 4.3 Coatings

### 4.3.1 Coatings for Large Telescope Mirrors

New coatings for the telescope optics are under investigation. Figure 4.21 shows first results for the reflectivities of silver and aluminium undercoated with copper and silver protected with aluminiumoxide in comparison with a standard aluminium coating. The gain of reflectivity of silver at longer wavelengths is obvious, although, there is a loss at blue and UV wavelengths. The protected silver coating is more efficient than aluminium for wavelength greater than 450nm. Samples of these coatings are exposed to real environmental conditions on La Silla, to test long timescale aging processes. Results for a overall ageing period of 18 months are shown in Figure 4.22. Silver coatings degrade rather fast in the visible but maintain a considerable gain relative to aluminium for longer wavelengths.

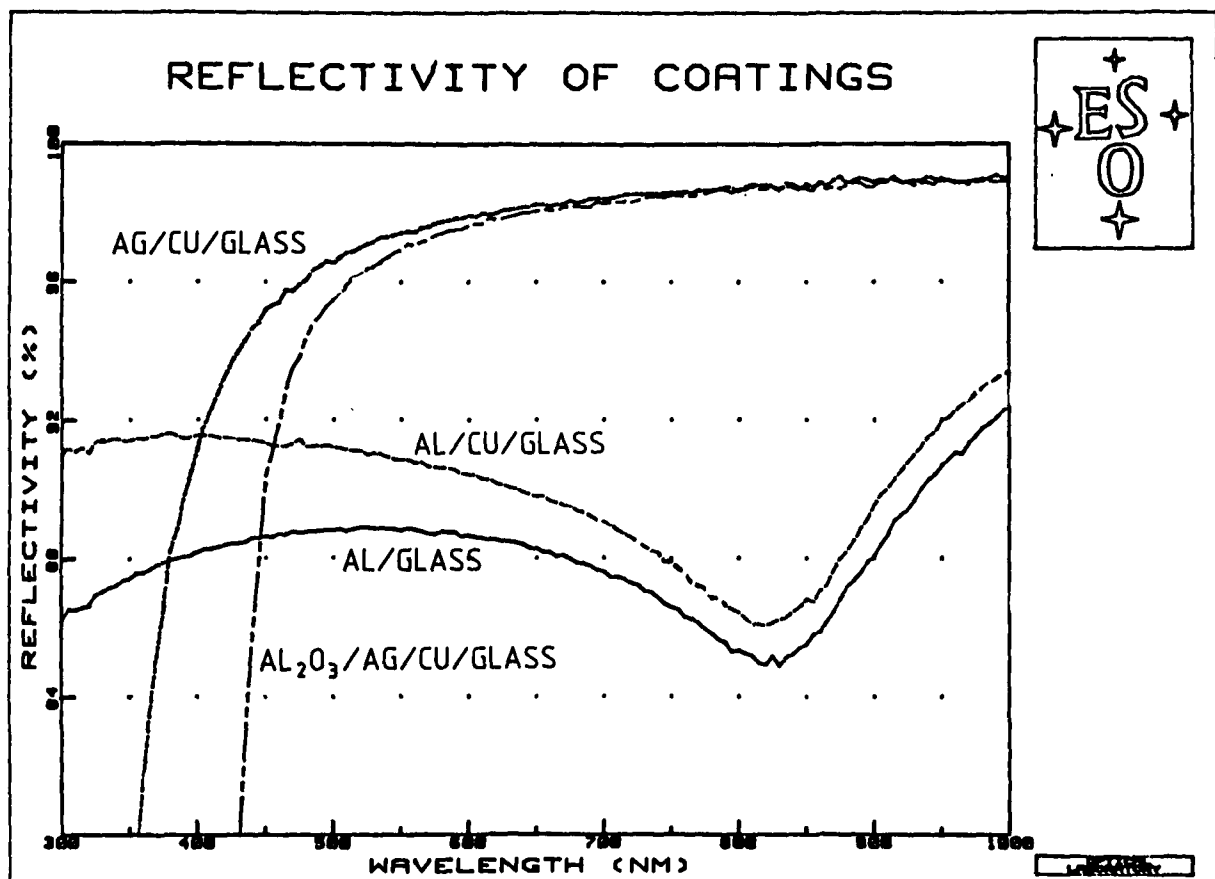


Figure 4.21: Typical reflectivity of freshly evaporated silver and aluminium coatings.

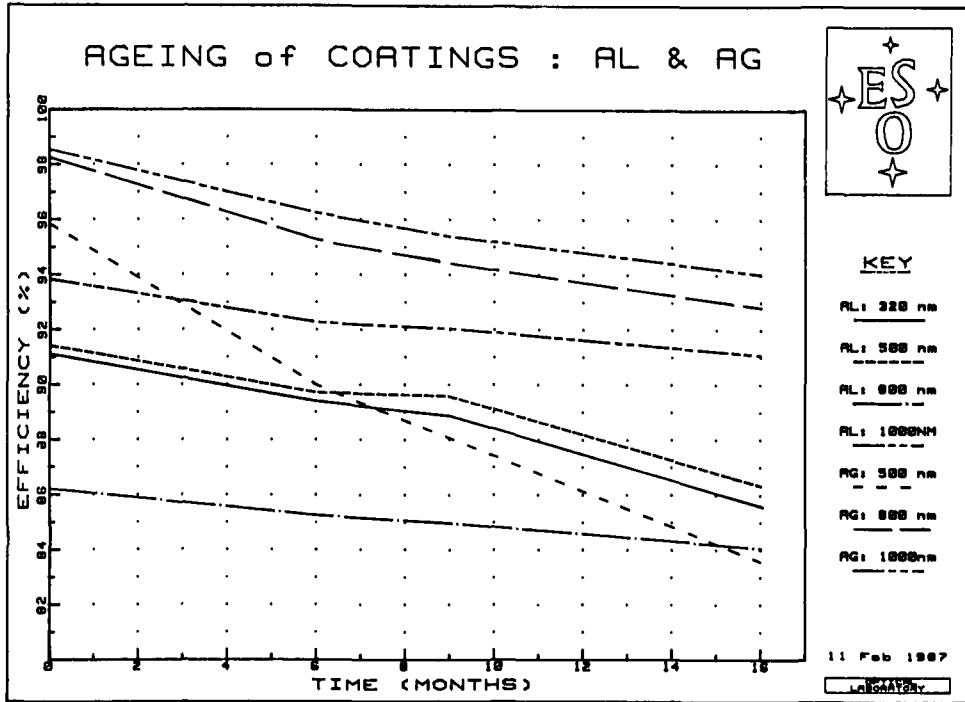


Figure 4.22: Ageing of telescope mirror coating under observatory conditions.

As far as vacuum deposition is concerned it seems that sputtering is an interesting alternative to the classical direct evaporation of metal. It requires only a short distance if a linear planar source is arranged along the radius of the mirror. The mirror rotates during the coating process for a homogeneous deposition of the material. In this case the vacuum tank would be smaller than for conventional deposition. The overall height would be about 3 metres.

### 4.3.2 Coatings for the Beam Combination Optics

The optical efficiency of the combined beam modes is of utmost importance for the array concept. It depends on the reflectivity of the various reflecting elements and the transparency of the transmissive elements of the optical combining train. Table 4.9 shows the design goals for the various wavelength ranges.

It is proposed (see Section 4.2.1) to use 3 types of optimized mirror coatings to cover the full wavelength range from near UV to the far IR. Mirrors in the visible combining train (in particular MC6) will have dielectric coatings, one set for the UV and blue and one set for the green red range. For the infrared combining train metallic silver coatings are foreseen. The Figures 4.23, 4.24, and 4.25 give the reflectance curves for coatings

TABLE 4.9

DESIGN GOALS FOR THE COATINGS OF THE BEAM COMBINATION MIRRORS			
WAVELENGTH RANGE	COATING TYPE	AVERAGE REFLECTIVITY [%]	EFFICIENCY OF THE BEAM COMBINATION
300nm–470nm	multilayer dielectric coating	> 97.6	> 0.80
470nm–700nm	multilayer dielectric coating	> 98.6	> 0.9
0.7 $\mu$ m–20 $\mu$ m	silver (eventually protected with $MgF_2$ or $Al_2O_3$ ).	> 98.8	> 0.9

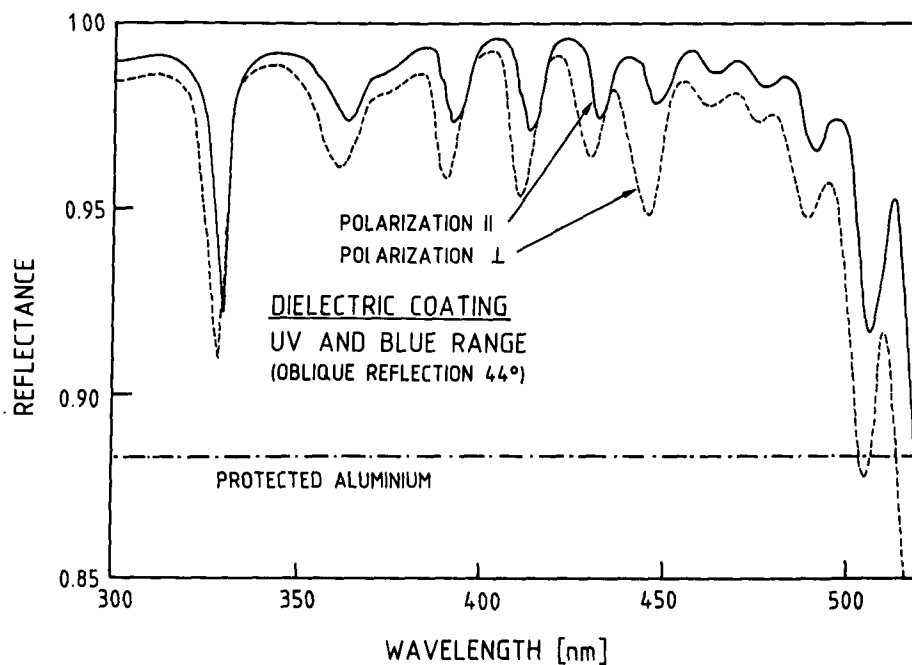


Figure 4.23: Measured reflectivity of a dielectric coating for the ultra-violet and blue wavelengths range.

4.3. COATINGS

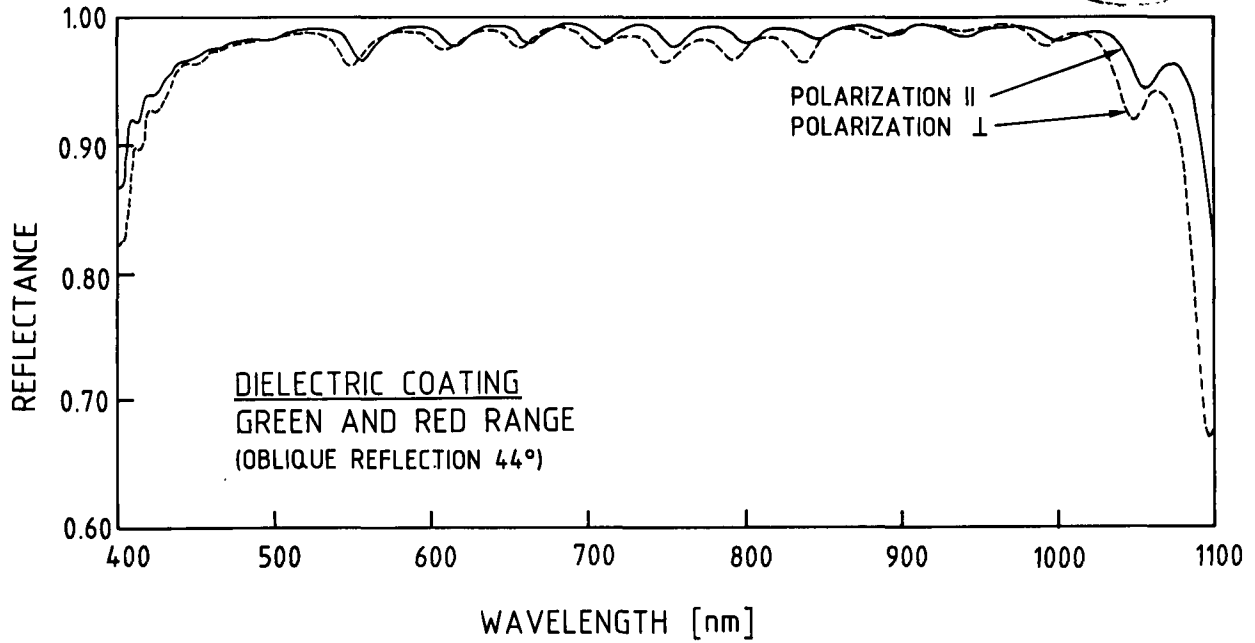
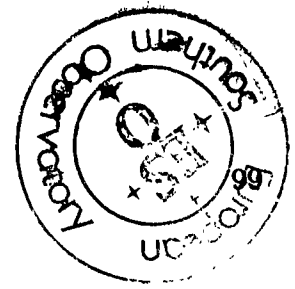


Figure 4.24: Measured reflectivity of a dielectric coating for the green and red wavelengths range.

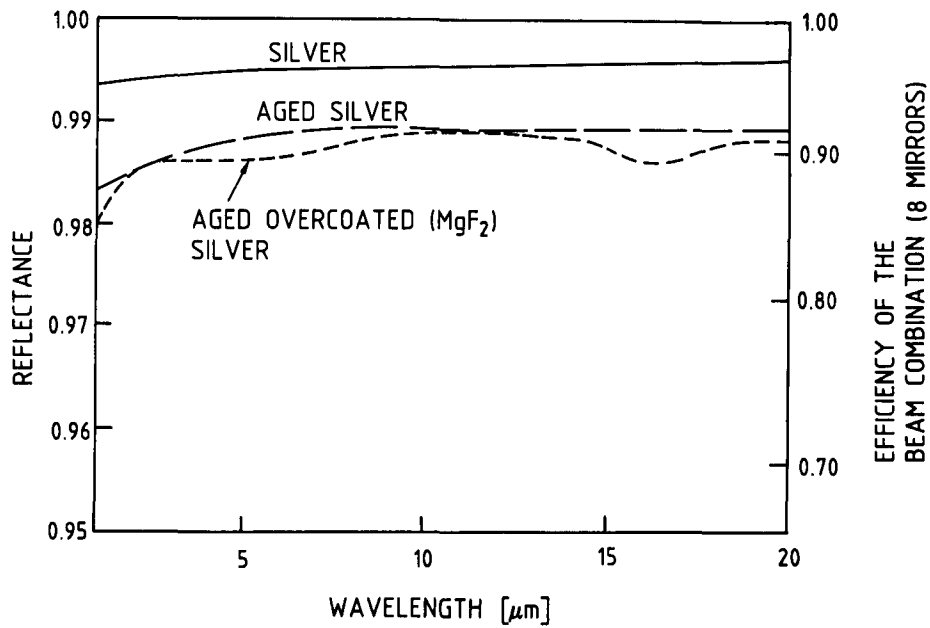


Figure 4.25: Measured reflectivity of a silver coating for the infrared wavelengths range [Burge et al., 1973, Applied Optics, 23, 47]. The right hand scale gives the optical efficiency of the design in Figure 4.14.

developed in recent years. For the silver coatings in the infrared additionally, the optical efficiency of the combining train is indicated, assuming the present concept with 8 combining elements.

For the surfaces of the prisms and lenses used in the visible beam combination path broadband antireflection coatings have to be tested. From current experience it can be concluded that the total reflection and absorption loss per prism is in the range 1.4% or less (see Figure 4.26). Measurements at ESO have shown that the absorption loss in high quality silica prisms is below 2.5% per metre optical path length.

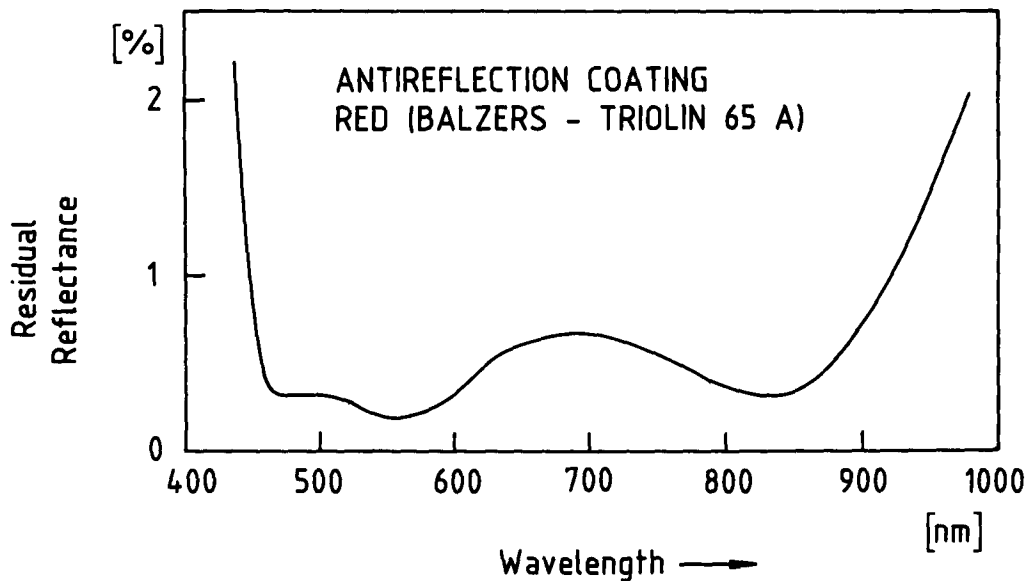


Figure 4.26: Residual reflection of a typical anti-reflection coating.

Additionally, it was investigated what optical efficiency in the visible can be reached if the optical design for the infrared beam combination (completely based on mirrors) will be used also for the visible combination. An optical set-up with 8 dielectrically coated mirrors simulated the combination path. The various angles between the mirrors had been chosen as proposed in Figure 4.14 including a rotation of the telescope. Figure 4.27 shows the efficiencies achieved with commercially available dielectric coatings in the green and yellow wavelength range. The results demonstrate that in the visible wavelength range the design goal could also be met with dielectric coatings. This test was made with off-the-shelf coatings. They can be improved to cover wider and other wavelength ranges.

The present technology for dielectric coating goes up to more than 1m substrate diameter. In the optical design attention has been paid to this point. There is no optical element in the combination path reaching this diameter, i.e. they are fully within the range available today.

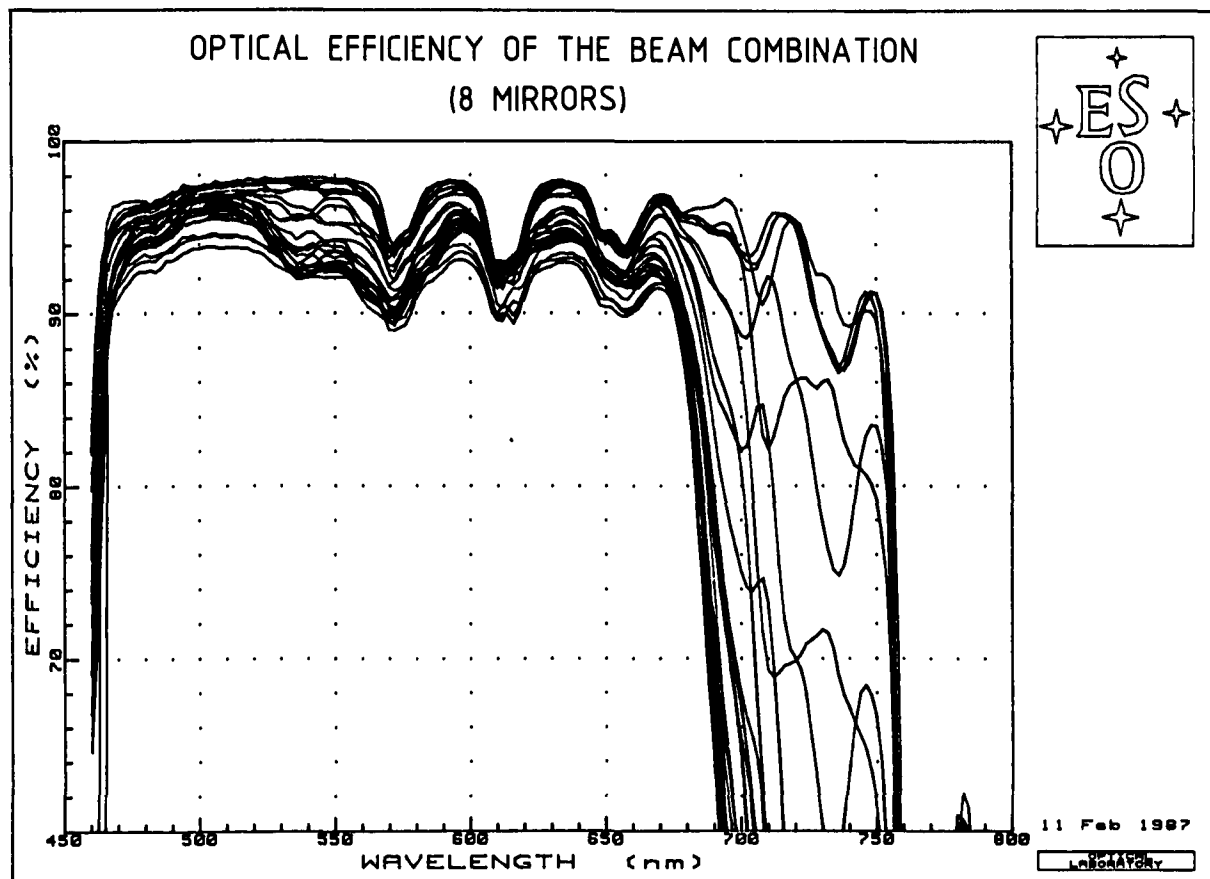


Figure 4.27: Measured efficiency of the visible beam combination in case the optical design for the infrared (Figures 4.11 and 4.14 (8 mirrors)) will be used. The various curves represent various azimuth angles of the telescopes ( $0^{\circ}$ ,  $15^{\circ}$ ,  $30^{\circ}$ ,  $45^{\circ}$ ,  $60^{\circ}$ ,  $75^{\circ}$ ,  $90^{\circ}$ , and  $180^{\circ}$ ) and polarisations (s and p). (Coatings: Spectra Physics G0235-001; manufacturer data:  $R_{avg} \geq 99\%$  for 485-700nm,  $R_{abs} \geq 98\%$  for all angles ( $0^{\circ}$  to  $45^{\circ}$ ) and both "s" and "p" polarisation.)

The life time of dielectric coatings is not exactly known but is certainly much above 10 to 20 years. From their construction principle, there is no real limitation. ESO uses high efficiency dielectric coatings on its Coudé Echelle spectrograph which are 8 years old. These coatings have been cleaned many times and were recently remeasured; no trace of degradation or loss of performance was detected. The envisaged protection of the mirrors in a neutral atmosphere offers, even for silver coatings, full guarantee that the initial efficiency of the coatings will be effectively maintained. There is no doubt, that in the visible range an average efficiency higher than 0.85, and in the infrared higher than 0.9 can be achieved.



# Chapter 5

## PRIMARY MIRRORS

### 5.1 Technologies for Large Monolithic Mirror Blanks and Options for the VLT

The cost of conventional blank procurement grows more rapidly with size than figuring costs. This explains immediately the intense activity in blank development which has emerged with projects markedly exceeding for the first time the diameter range of 3.5-5m of the last generation of "conventional", equatorially-mounted telescopes.

In view of the modern possibilities of opto-electronic control discussed below, it is essential to consider objectively what physical properties of the blank are really necessary for a modern telescope. Although a zero or near-zero expansion coefficient is clearly an advantage, modern control systems in the telescope and figuring techniques in the optician's factory can handle materials with an expansion coefficient significantly higher than that of sophisticated quasi-zero expansion glasses.

Conventional glass blanks are still bound to be expensive but the modern methods of active control permit the use of lighter and more flexible blanks. The manufacture of such light blanks presents problems of formidable technical complexity, but once these problems are overcome, production can be reasonably cheap. In fact, available cost figures show that such light mirror blanks would be cheaper per unit of area than existing massive blanks.

Because a few years ago the feasibility of very large mirror blanks using a conventional low expansion glass material such as Zerodur was doubtful, ESO has investigated the possibilities of metal for blanks. Already for the NTT it was clearly established that it was perfectly feasible to manufacture an aluminium blank coated with polishable nickel of 3.5m diameter. For the VLT aluminium remains a serious candidate but further studies have shown that non-corrosive steels, such as ferritic chrome steels or nickel steels may also be considered.

Table 5.1 gives the significant physical properties of the materials most interesting for blank production. Attention is drawn particularly to column 6 (diffusivity/expansion coefficient) which may be considered as a rough figure of merit for thermal distortions of the blank. The thermal link with the ambient air (affecting "dome seeing") will depend in a complex way on the effective cooling surface, thermal capacity and diffusivity. The most interesting blank materials and technologies of production will be considered in more detail and the options considered by ESO for the VLT analysed in Section 5.1.6.

Table 5.1

MATERIALS FOR MIRROR BLANKS									
MATERIAL	$\alpha$ [K <sup>-1</sup> ] · 10 <sup>-6</sup>	$\lambda$ [ $\frac{W}{mK}$ ]	$C_p$ [ $\frac{J}{kgK}$ ]	$\rho$ [ $\frac{kg}{m^3}$ ]	$\delta$ [ $\frac{m^2}{s}$ ] · 10 <sup>-6</sup>	$\frac{\epsilon}{\alpha}$ [ $\frac{m^2K}{s}$ ]	E [ $\frac{N}{mm^2}$ ] · 10 <sup>3</sup>	$\nu$ {-}	K [m] · 10 <sup>3</sup>
Aluminium	23	227	879	2700	95	4.16	72	0.34	3074
Steel 13/4	11	25.1	502	7750	6.45	0.59	210	0.28	2997
Invar	1	10	500	8130	2.46	2.46	145	0.30	1998
Borosilicate	3.2	1.13	1047	2230	0.48	0.15	68	0.20	3238
Fused Silica	0.55	1.38	750	2202	0.84	1.52	74.5	0.17	3550
Silica (ULE)	0.05	1.31	770	2200	0.77	15.4	66	0.17	3149
Zerodur	0.05	1.64	821	2530	0.79	15.8	91	0.24	3891
CFRP (UHM-quasi-isotropic)	0.2	10	712	1800	7.8	39.0	105	0.32	6625

$\alpha$ :	thermal expansion	$\lambda$ :	thermal conductivity
$C_p$ :	specific heat	$\rho$ :	specific mass
$\delta = \frac{\lambda}{C_p \rho}$ :	thermal diffusivity	$\frac{\epsilon}{\alpha}$ :	thermal insensitivity
E:	Young's modulus	$\nu$ :	Poisson's ratio
$K = \frac{E}{\rho(1-\nu^2)}$ :	mechanical bending resistance		

### 5.1.1 Zerodur (Glass Ceramic)

Schott first started the production of telescope mirror blanks with zero expansion glass ceramic Zerodur in 1969. During the past 10 years about 80% of all telescope blanks supplied in the western countries within a range of 2 to 3.6m were made of Zerodur. The possibilities of producing Zerodur blanks of 8m diameter have been the subject of a study performed by Schott for ESO.

It emerged clearly in this study that the production of blanks of this size by techniques similar to those used for existing 3.5m blanks, i.e. by casting massive blocks and machining down to required meniscus dimensions, would require investments that are commercially unacceptable. This is why the emphasis was placed in the study on structured blanks. For such blanks, Schott has analysed the following methods of manufacture:

## Casting

The technology is very difficult, the difficulty increasing with decreased wall thickness. 40mm has been achieved, 20mm may be possible.

Two basic techniques are possible:

- Direct casting whereby the liquid glass flows round the mould structures.
- Plunging a form into the liquid glass.

Because of “fold” effects where glass flowing from two sides meets, the first technique seems less promising than the “plunge” method. For 8m blanks, casting seems feasible, assuming the required temperature control during and after pouring can be achieved. The difficulty of achieving this increases rapidly with diameter.

## Bending and high temperature fusion (HTF)

Plates of 4mm thickness of vitreous Zerodur can be bent and welded to form a structure. Such plates are, however, considered too thin for an 8m blank. It is assumed that thicker plates can be HTF welded: the upper limit of thickness is, however, not yet known. The problem with HTF is that the allowable heat-up time to the melting temperature is only a few seconds, otherwise unacceptable pre-nucleation occurs. For this reason HTF is not promising for an 8m mirror with relatively thick ribs.

## Low temperature fusion (LTF)

The bonding by this process takes place at lower temperature than HTF. The fundamental problems of LTF (i.e. sufficient bond strength while maintaining acceptable stress values) can be considered to be solved. It follows that the connection of a cell structure to a faceplate, both consisting of vitreous Zerodur, by LTF to manufacture a lightweight blank of 8m diameter and weighing 15 tons will be feasible with high probability. Tests have been performed with several different wall and faceplate thicknesses. Nevertheless, a number of detailed experiments would have to be carried out. This would lead to tests up to 4m diameter. Figure 5.1 shows a test blank of about 400mm diameter realized with the LTF process.

It appears however that any of the 3 proposed technologies for making lightweight structures will need considerable development and time before it could be considered for making an 8m blank. This is the reason why Schott is considering another approach that aims at the production of a thin meniscus instead of a structure.



Figure 5.1: Lightweight mirror made of fused Zerodur elements.

### Spin casting of a thin solid meniscus

This technology is illustrated by Figure 5.2 and consists essentially of pouring the liquid glass in a spherically shaped concave mould. The mould is then spun and the centrifugal forces give the liquid glass surface the desired parabolic shape. The mould is kept spinning until the glass reaches a viscosity sufficient to maintain its shape. The blank is then annealed, machined and ceramized in a conventional way. Owing to recent progress on mould contact materials, it is possible to minimize the depth of material of poor quality that will have to be removed. A similar technique has been used by Schott since 1973/74 for the production of borosilicate glass column sections of 1m length and 1m diameter.



Figure 5.2: Spin cast thin meniscus. The glass in the rotating mould is still fluid.

The Zerodur glass volume for the 8m spin cast meniscus is similar to those used for existing 3.6m blanks. Also, much less material has to be milled off compared to conventional massive casting. The thin meniscus has also the advantage to reduce time for ceramization which is more dependent on the thickness than on the total mass of glass.

Samples of 0.8 and 1.2 metre spin cast mirror blanks of Zerodur have been produced successfully by Schott in November 1986. Thereupon a programme has been started in January 1987 to spin cast several 1.8, 2.8 and 4.1 metre meniscuses by mid 1987.

It seems likely that following the successful completion of a 4m meniscus an extrapolation to 8m may be made with confidence.

### 5.1.2 Borosilicate Glass (BSC, Pyrex, Duran 50)

The work of Angel et al. at the University of Arizona has re-awakened interest in a material which had been abandoned for telescope blanks by the professional glass making companies in favour of fused silica or glass ceramic. The interest of BSC glass is, of course, its low bulk price compared with zero expansion materials, about an order of magnitude cheaper. A massive block of such material has a thermal inertia so great that unacceptable distortions are inevitable in a passive telescope. However a thin-walled, lightweighted mirror in BSC can probably give the performance demanded of modern telescopes if air cooling is provided. Angel has produced blanks with a diameter up to 1.8m. Whether the technique will work up to 8m diameter can only be proven by actually doing it, but it seems reasonable to suppose that the chances of successful manufacture are quite good.

Most serious is the doubt concerning “print-through”: the appearance of the structure in the polished surface. The danger is probably higher during the polishing phase than during operation in the observatory. Only experiments can satisfactorily answer these questions and give clear results.

### 5.1.3 Fused Silica

Conventional fused silica ( $\alpha \sim 0.4 \times 10^{-6}$ ) has been available since the fifties in sizes suitable for blanks for large conventional telescopes. Thus the ESO 3.6m telescope has such a blank. Such blanks are not cast in a single piece as with Zerodur: they consist of a fairly small number (10-20) hexagonal elements (“boules”) produced separately and then welded together.

ULE fused silica was a later development rivaling glass ceramic in its extremely low expansion coefficient ( $\alpha$  ca.  $0.05 \times 10^{-6}$ ). It contains a significant proportion of titanium compounds. The number of individual elements is much larger in such a blank, the welded structure being correspondingly more complex.

For blanks up to about 4m, it can be argued that the possibility of direct casting for glass ceramic, giving a homogeneous solid disc, is a definite advantage over fused silica. For larger sizes, however, the situation is reversed:

- Since welding is accepted as a proven technique in existing blanks, the extension to 8m, while not a trivial operation, is simply an extension of known technology.
- In any material, welding (if acceptable) will be the simplest and cheapest technology. However, of all the potential blank materials, fused silica is the only one where welding seams in the upper surface has been proved to be acceptable. The reason for this is simple: silica, whether from natural or artificial sources, is a material of great chemical purity. By comparison, it is not certain that upper

surface weld joints would be acceptable in any metal; or even in BSC or glass ceramic.

- The basic meniscus form is relatively easy to make by first welding flat hexagonal plates together, then sagging the flat blank to the desired radius. For this latter operation the blank is simply lying on its mould and heated up to a softening temperature.
- Lightweighted fused silica mirrors have been made for space applications. A prime example is the blank for the space telescope, extremely lightweighted by welding elements of ULE silica. Welding of fused silica for structures is, of course, a delicate process, but the problems of making structured silica blanks are far less than in glass ceramic because of the danger of disturbing the delicate balance of ceramized glass.
- For passive telescopes, the effectively zero expansion coefficient of glass ceramic or ULE is an advantage; but with active control the  $\alpha$ -value for conventional fused silica (about one eighth of that BSC) is acceptable.

We can conclude then that, of all the possible technologies, fused silica (conventional or ULE) is the one where extrapolation from existing sizes is easiest and quickest.

ULE silica has an expansion coefficient close to that of Zerodur while that of pure silica is 10 times higher, yet very low compared with standard glass (see Table 5.1). However, the internal homogeneity of ULE is usually poor while that of pure silica is excellent and comparable with that of Zerodur. For this reason and for an active mirror such as for the VLT, pure silica should be preferred to ULE.

#### 5.1.4 Aluminium

Since the disappearance of speculum from the reflecting telescope about 1865, aluminium is the only material apart from glasses which has been used for telescope blanks of 1m diameter or more. Aluminium, including somewhat harder alloys, is too soft to be polished directly. Its use therefore only became practicable with the industrial development of nickel coating, usually deposited by chemical means. Such coatings, to which the trade name "Canegen" is usually applied, consists of about 90% nickel and 10% phosphorus. Canegen coats are softer than glass but have been successfully figured to the tolerances required by astronomy. Electrolytic coating is also possible but is unproven for practical mirrors.

In the 60's aluminium blanks were tried by H. Johnson. Warping of the mirrors resulted in poor image quality. We believe the failure was due to an unfortunate choice of blank form (a "vase" shape) combined with inadequate heat treatment.

A much more successful project was carried out in Italy in 1968 with the 1.37m telescope at Merate, which has an aluminium primary. ESO tested this telescope in

1983, after 14 years of normal use, and found its quality to be completely comparable with that found for similar telescopes with glass primaries. We found an astigmatism coefficient of about 1 wavelength which may or may not have been partially or entirely due to warping. With active control (see Chapter 5.3), the removal of such a term would be trivial.

In view of the positive test result for Merate, experiments in warping of aluminium blanks due to thermal cycling were carried out in the ESO laboratory. The results indicate that a variety of alloys of aluminium, or the “pure” metal, made by a variety of processes, can give very low warping provided correct heat treatment has been applied. The warping range would then be well within the range of active correction. It was therefore decided to tender formally to industry for an aluminium blank for the ESO 3.5m NTT. Several responses were received that gave us great confidence that such a blank could be manufactured to a very severe technical specification. Delivery times and price including the Canegen coating were of the order of 35% of that of a conventional Zerodur blank! It was finally decided not to order the aluminium blank for the NTT because of timing problems.

The main (but certainly soluble) technical problem that emerged was not the procurement of the aluminium blank but “breakthrough” problems due to the thinness of the Canegen coating during the figuring phase. For the VLT, therefore, attention turned to non-corrosive steels as a more promising alternative. Since these can be polished directly they avoid the problems associated with coatings.

However, reference to Table 5.1 shows that thermally aluminium is easily the best of the cheap metals. Furthermore, its low density (comparable with glass) is very favourable. Aluminium must still be considered as a back up candidate for the VLT. Production of an 8m aluminium blank would necessarily be based on welding. Two experimental blanks consisting of welded plates are being optically processed. One is made of AlMg<sub>3</sub> alloy, the other of pure (99.9%) aluminium. The welding material is identical to the plate material. Influence and acceptability of the weld joints will be investigated.

### 5.1.5 Steels

Non-corrosive steels seemed a more interesting candidate for 8m VLT blanks than aluminium because some such steels can be polished directly and do not require a coating such as Canegen. In addition, casting and other manufacturing technologies are available in larger dimensions for steels than with other metals.

The first step was to establish which non-corrosive steels were the most promising from the point of view of polishability, corrosion resistance and thermal properties. For VLT 8m blanks the current state of our development work for steel blanks is as follows:

- The most promising steels seem to be certain ferritic or martensitic steels. Small



samples have shown that with correct heat treatment, these can effectively be polished as well as glass. Austenitic steels can also be polished but have inferior thermal properties.

- Of classical production techniques, casting seems the most feasible for 8m blanks unless welded joints are accepted. Welded structures would require further work to rest their stability but, apart from that, weld seams could present a polishing problem. For this reason, methods such as casting that give a continuous faceplate are preferred at this stage. However classical casting in these dimensions raises considerable doubts concerning the homogeneity of the material from the point of view of polishing. A new technique of manufacture, originally developed for the production of high performance pressure vessels, has been proposed at ESO for making either whole blanks or faceplates. This method, in its most promising form called “build-up (BU) welding”, seems to solve completely the homogeneity problem, for any dimension. The method consists basically of piling-up welding seams in such a way that a structure is progressively built-up. The machine consists essentially of a computer controlled movable welding head. Because a very small amount of material is deposited at each pass, any variation of homogeneity of the material is automatically distributed into the blank in a random way. Whether a whole blank would be made by this process or only the top-plate is still open. Figure 5.3 shows an experimental 500mm BU blank during manufacture. The building-up of the ribs did not give particular problems. With simple equipment a blank of nearly any size can be built, the process by its nature being easily scalable.
- With the encouraging results of the first samples, several 500mm blanks have been ordered, some produced by classical welding. These have been polished spherical.

In order to be a successful candidate for 8m VLT blanks, a material and blank structure has to meet the following requirements:

- Its micro-polishability must be acceptable (i.e. comparable with glass).
- Its macro-polishability must be acceptable (i.e. the optician must be able to produce a smooth figure of adequate quality with normal effort). This is above all a question of the thermal performance.
- The long-term stability must be adequate (i.e. any warping must be of a low spatial frequency correctable by the active optics (see Section 5.3) and within its dynamic range).

Current evidence is that the first requirement has been met by the ferritic steels selected. The second requirement has been met for metal blanks with solid form or a modest lightweighting structure such as cylindrical holes, but there is doubt about thermal “print-through” for steel mirrors with relatively fine structure. The third requirement is still under investigation. The initial thermal treatment of steel blanks is,

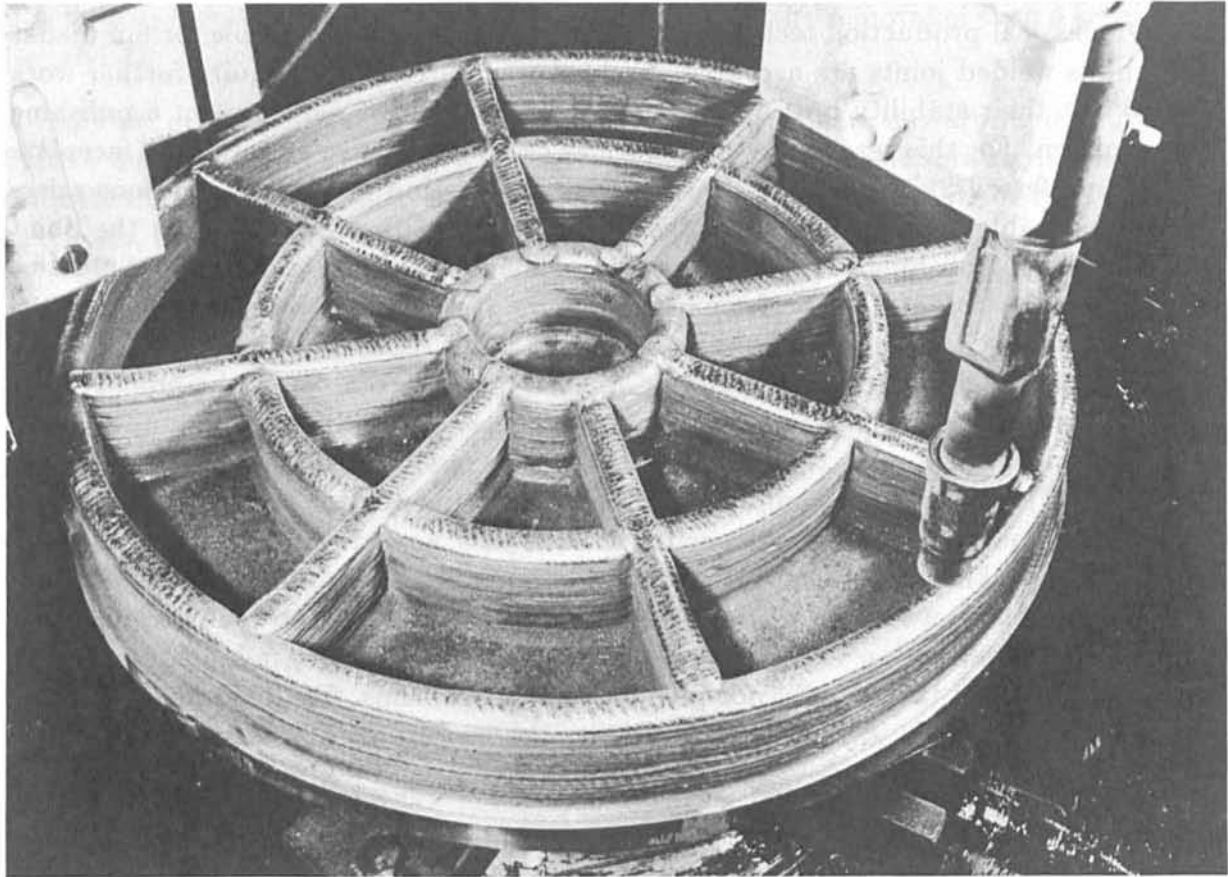


Figure 5.3: Structured steel mirror being produced by built-up welding.

as with aluminium, fundamental for stability: indeed, because of the relatively complex structure of non-corrosive steels, the thermal treatment may be more critical than for aluminium although the basic transformation temperature is higher. BU mirrors cut from a large vessel have shown, under subsequent thermal cycling tests, a form stability similar to good aluminium mirrors. But the more highly structured BU blank in Figure 5.3 has shown initially large instabilities when subjected to thermal cyclings after it underwent a “standard” annealing from  $+500^{\circ}\text{C}$  to ambient temperature before it was figured and polished (Figure 5.4). A remarkable improvement has been obtained in a second attempt during which the mirror was submitted to a combination of rest period, at moderately high and cryogenic temperatures before it was refigured and polished. Figure 5.5 shows the interferogram of the surface just after polishing and after 32 thermal cycles. The very small local surface deformations showed up after the first cycle which suggests that if an additional stabilization treatment just before the final polishing had been undertaken, it might have provided a fully stable surface.

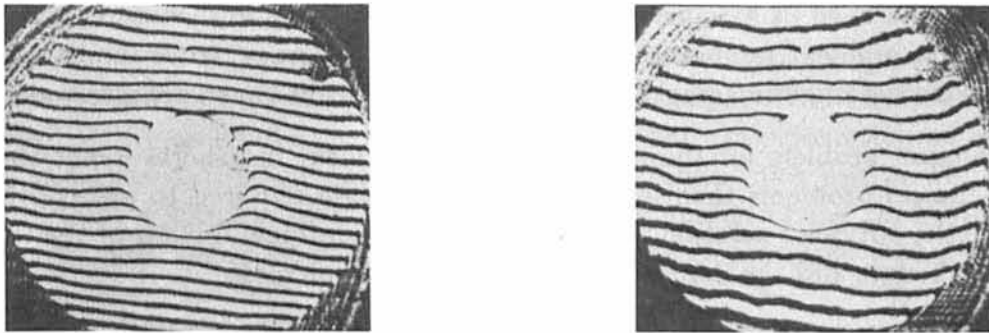


Figure 5.4: Long term stability test of a lightweight steel mirror with conventional annealing.

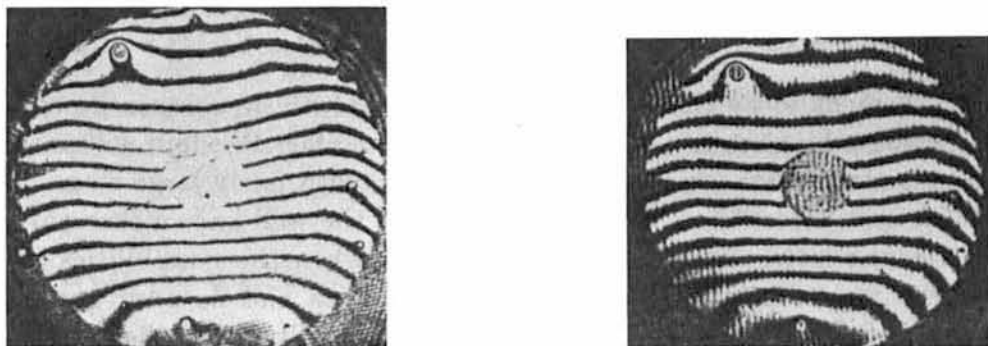


Figure 5.5: Long term stability test of a lightweight steel mirror with cryogenic temperature stabilization.

If the third requirement can be met for an acceptable structure within the limits set by the active optics system (allowing an enormous tolerance relaxation compared with passive telescopes), then the prospects for 8m steel blanks will seem to be very good. Of course, a larger test blank will be necessary. If a blank of 1.5m - 1.8m can be successfully produced with BU, the way to 8m seems relatively clear.

Some welding tests have been done with Invar which in theory would be an excellent material with a thermal insensitivity close to that of aluminium thanks to its very low expansion. The tests were however largely unsuccessful, the main difficulty being the very large difference of expansion coefficient at high temperature when the welding occurs and at ambient temperature. This difference of temperature tends to generate very high stresses and often cracks. For this reason, Invar has been definitely abandoned.

The biggest problem for the metal blank development in general is not the nature of the technical problems themselves but the time scale required to resolve them and determine the optimum solution. This poses a serious problem in view of the tight VLT planning schedule and the dominant role of the prime mirrors.

### 5.1.6 Options for the ESO VLT Primary Mirror Blanks

From the above discussion it appears that a number of materials and technologies could be considered to make large mirror blanks. New materials such as ceramics or carbon fibre based composites, foams of various types etc, could also be considered. However promising these materials may be, it is extremely unlikely that their stability, performance, cost and possibility to be manufactured in very large sizes could compete with glass or metal, within the time frame of the VLT.

Column 6 of Table 5.1 gives the thermal insensitivity of various materials which is the driving parameter for optical performance. Considering the problems of manufacture, homogeneity, support and long term stability and eliminating the materials for which there is already a negative experience one can define a preference list of materials in which Zerodur and silica would easily come up as the best.

The next element to be considered is the risk that will be necessarily encountered in manufacturing a blank much larger than any built so far. Wisdom will prompt us to consider first materials for which there is experience with fairly large sizes. These are Zerodur, silica and borosilicate. However, because of the well-known thermal problems of borosilicate, the latter should only be considered when the possibilities for using a better material are exhausted. To the extent that silica and Zerodur appear now as realistic possibilities, we have dropped (at least provisionally) borosilicate from our list of candidates. The uncertain outcome of the metal experiments as well as the lack of experience on very large sizes makes metal solutions less attractive in the short time scale of the VLT. However because such a metal mirror would be relatively cheap it has been decided to pursue the development of metal solutions in parallel to the manufacturing of a glass mirror blank. In case of (unexpected) difficulties with the glass mirror, metal

could provide a fall-back position.

The two prime solutions which are considered are therefore the following:

- Zerodur spin cast thin meniscus
- Fused silica assembled, then sagged, thin meniscus

### **Zerodur spin cast thin meniscus**

An 8m meniscus could have a thickness of 150 to 200mm. The final value will be determined by the acceptable stress during handling and transportation as well as by special constraints during the casting operation. A 175mm thick mirror would have a mass of 22 tons, a 200mm thick mirror, 25 tons. The quality of the spin-cast Zerodur blanks is not expected to be different from that of blanks produced with the existing massive casting process.

Because the blanks will directly be produced as thin shells, the time for annealing and ceramization - which is proportional to the thermal time constant, i.e. inversely proportional to the square of the thickness - will be relatively short, so that the following units could be produced at a few months intervals. The lead time for the first mirror may however be a few years because of the necessary modifications of the existing casting facility at Schott.

### **Fused silica thin meniscus**

The technology for making an 8m fused silica blank has been described in Section 5.1.4. It is based on the welding of hexagonal flat plates followed by a sagging operation at the softening temperature.

A thickness of 200mm is considered. The mass will be about 22 tons, the same as for Zerodur with a thickness of 175mm.

Lead time is mostly driven by the production of the raw material. The first blank could be produced in 3 years or less, the following units at 1 year intervals.

## **5.2 Optical Figuring**

### **5.2.1 General**

As has been stated above, the cost of figuring large glass mirrors grows less rapidly with size than that of conventional blank procurement. The technical problems engendered by size extrapolation are - while still considerable - less serious for figuring than for

conventional blank production. The pressure for radical technological innovation is therefore also less.

This is an important general conclusion: for it implies current technology is basically able to cope with the figuring of 8m glass mirrors. Of course, this does not mean that considerable efforts will not have to be made in certain specific areas. Furthermore, it does not mean that major financial investments may not be required in order to extend the technological facilities to 8m diameter.

There are only two suppliers of large precision optics in western Europe. These are REOSC in France and CARL ZEISS in West Germany. Both companies independently performed feasibility studies for the figuring of the VLT mirrors under contracts with ESO. While there are significant differences in their technologies depending on experience and performance, both firms feel entirely capable of producing the VLT optics. The optical performance that can finally be produced depends much on the active optics concept (see Section 5.3) and the limits will above all be set by the test methods.

From the technical and financial analysis performed independently by the two firms, it follows that the cost for polishing a large mirror is proportional to  $D^1 A^2$  (with  $D$  the diameter and  $A$  the focal ratio). The capital investment for buildings, machinery and tools would vary approximately as  $D^2 A^{-0.5}$ .

This first relationship is a strong justification for a project based on large monoliths, and also indicates that going to a very fast primary would become rapidly very expensive. Adding to this, the increased lead time and the risk of not attaining the stiff optical requirements implies that it may not be desirable to go much faster than  $F/2$ . An aperture of  $F/1.8$  has been selected as a trade-off between the increased cost of the polishing of the mirror and savings in the test tower as well as in the telescope building and mechanics.

The following Sections (5.2.2 to 5.2.7) will deal with the main aspects affecting the total operation of optical figuring.

## 5.2.2 Building and Test Tower

Neither firm has existing building facilities suitable for 8m blanks. Such infrastructure costs are always relatively high but most of the infrastructure, machinery and test tools can, of course, be re-used. An important matter is the question of a quasi-vacuum test tower. It seems probable that the additional investment for this is justified. REOSC however intends to use helium as a substitute. Helium has an index of refraction about 10 times lower than air and is therefore 10 times less sensitive to thermal gradients. A vertical conical tube made of modern plastic fabrics would have an acceptable leakage of less than 2 liter/m<sup>2</sup>/day. The cost of helium which is less than 30 DM/m<sup>3</sup> makes this solution attractive at least for the final polishing phase. Neither vacuum nor helium will be necessary till the mirror is close to its final shape.

Handling of the mirrors and question of overlap in the production schedule (to improve total leadtime, for example) will have a major impact on building layout. Handling of a thin glass mirror has been analysed (see Section 5.7) and found possible, although great care has to be taken.

### 5.2.3 Milling, Grinding and Polishing Machine

The most interesting modification of existing technology is the question whether it is possible, and if so the most economic solution, to mill the surface to a fair approximation to the final aspheric. The main requirement here is to maintain axial symmetry, above all to avoid an excessive residue of astigmatism which could not be easily removed in the polishing phase. A standard high accuracy machine could provide a final accuracy of 30 to 50  $\mu\text{m}$ . A better accuracy could be obtained if the azimuthal errors are kept under control. CARL ZEISS has proposed a scheme in which the run-out and tilt errors of the turntable are controlled with a laser interferometer. If the mirror is adequately supported an accuracy of a few microns could be obtained.

The smoothing, polishing and figuring processes are essentially conventional. An important aspect is the size of tools and laps which can be used. More because of the higher value of the relative aperture  $D/f$  with modern concepts (around  $f/2$  instead of  $f/3$ ) than because of the large diameter, it will not be possible to use full-size 8m tools: 4m will be about the maximum that can be envisaged. Of course, the larger the tool, the greater the smoothing effect. Highly flexible tools, or possibly active tools, will have to be considered. Computer control methods for determining lap form, pressures and speeds will clearly be used as required by the phase of work.

The relaxation of low spatial frequency tolerances, as with the NTT, will have much more significance for the VLT, since the dynamic range of active correction will be much greater and the relaxation correspondingly more. This should produce a considerable saving both of time and money. Relaxation of tolerances in the modes astigmatism and spherical aberration will probably be most significant.

### 5.2.4 Mirror Support During Figuring

The design of an adequate support system for the 8m blanks that have, in any case, a flexibility an order of magnitude higher than the NTT 3.5m blank and two orders of magnitude higher than those for conventional telescopes like the ESO 3.6m, is mandatory for the successful production of the mirrors.

The studies show that the support problem during figuring for an 8m VLT blank may be considered to have been solved. For both suppliers, the relaxation of certain optical tolerances because of active optics control will simplify support requirements. REOSC proposes a pressure variation control which is, in the manufacturing phase, to some extent similar to the concept of our own active control system for the final

telescope in function. For acceptance, the supports will have to be able to simulate the support conditions in the final telescope cell.

### 5.2.5 Nature of the Blanks and Thermal Aspects

Whatever the blank material - even in Zerodur - thermal aspects will almost certainly set the limitations of what can be achieved. CARL ZEISS has done a thermal analysis in some depth on the problems associated with the figuring process for blanks of different materials and with or without structure. As would be expected the quality of materials from the point of view of thermal warping during polishing goes from Zerodur (easily the best) through beryllium, invar, aluminium, ferritic non-corrosive steels, austenitic non-corrosive steels ("stainless steels") to BSC glass (Pyrex). Print-through is above all dependent upon the internal thermal conductivity of the blank.

For the two main options retained for the VLT blanks which are based on low expansion material and a solid meniscus form it is not expected that structure print-through problems will be encountered.

### 5.2.6 Optical Testing

If aspherics are produced by milling or grinding, test methods will be required at this stage. Various methods can be used, ranging from beam spherometry to interferometry in the visible or IR-interferometry (possibly also millimetric interferometry). In view of the fact that the precision required in this stage is not very high, no serious difficulty should arise.

In the polishing phase, the test procedure is of fundamental importance: one can only reliably correct what has been reliably measured. A two-track approach to testing is the best. For the acceptance, the following two basic methods could be used:

- Shack-Hartmann (S-H) testing, as introduced by ESO for off-line telescope tests.
- Interferometry

In each case a set-up should be used with so-called compensation or null systems. The set-up is therefore, in principle, identical and only the image analysis end is different. It should be noted that the price paid for the advantages of compensation testing of aspherics is an inevitable pupil distortion which leads to a distortion of the measured residual defects. But this can be corrected by a modification of the image analysis software.

Of course, cross-checks by other methods, including Hartmann tests with or without compensators, are possible and will be welcome, but the above two methods are seen as fundamental. The technology of compensators is therefore very important and



cross-checks with different types of compensators will be required. For the matching of primary and secondary, a supplementary method (pentaprism test) may be required. Ripple and high frequency effects will require supplementary analysis based on interferometry. The tolerance relaxation on spherical aberration, made possible by the active optics concept, means the precise matching of the aspherics is less critical. This is seen as a major advantage which will also make the production of smooth surfaces easier - reduction of higher order errors.

The specification of the "intrinsic quality" (the quality determined by high spatial frequency effects alone) which will be of the order of 80% energy in 0.10 arcsec will stretch any test method to the limit and will require extreme care in its performance. This is one reason why a quasi-vacuum or Helium test tower is probably a necessary investment, since air disturbance is one of the two major sources of error. The other major source is vibrations. Shack-Hartmann has a big advantage over conventional interferometry here, because vibration (and high time frequency air turbulence) can be integrated out. Heterodyne interferometry or equivalent dynamic procedures may bring a big gain in the precision and convenience of interferometric testing and overcome the disadvantages of static (conventional) interferometry.

At this stage, it would seem that, with the proposed test procedures, means exist to manufacture the optics to the specification envisaged.

### 5.2.7 Leadtime

The leadtime for figuring the mirrors is a steep function of the degree of optimization of the testing and figuring processes. Generally, a shorter time (hence a lower cost) can be obtained through a higher investment either in development or in machinery. For the first time in astronomy it is proposed at the beginning of a project to manufacture several mirrors. This increases the need to reduce the leadtime, but also permits the consideration of a higher initial investment which could not be considered for only one mirror but which could pay off in terms of cost and leadtime if several mirrors have to be produced. Since it is likely that additional telescopes of 8m size, will be constructed, the optimization of the production schedule is all the more important.

Estimates of the delivery time range between 2 and 3 years, but realistically cannot be expected to be much less than 3 years for the first mirror. The relaxation of tolerances on low spatial frequencies permitted by the active compensation of the mirror should normally lead to a shorter leadtime but this is difficult to evaluate accurately as there is no experience available yet on this type of mirror. The results of the figuring of the NTT mirror will certainly be important.

The nature of the mirror blank material will have an impact on the time schedule. Zerodur and silica are viewed as the best material and in any event, the only ones for which the suppliers have a direct experience. It is difficult to forecast how the lead time may be affected by the material.

By reducing the test time or by performing parallel figuring and testing of two mirrors with frequent exchanges between the polishing machine and the test tower, it should be possible to bring the manufacturing time of subsequent mirrors down to 2 years. The optical facility has to be designed according to a certain fabrication sequence. Frequent swaps of 8m mirrors may also be costly and dangerous, and one can wonder whether the best practical possibility is not to consider a double facility. In such a case, an additional delay during the figuring phase could to some extent be compensated by a fully parallel processing so that the project schedule would remain within limits. This may be the best solution if one considers the limited accuracy of the present estimates and the corresponding risk cast on the project schedule and cost.

## 5.3 Active Correction

### 5.3.1 Image Error Sources in Telescopes

The image quality of telescopes can - and normally is - reduced from the theoretical diffraction limit for visible light by the following sources of error or disturbance:

- a) Optical design (residual aberrations).
- b) Optical manufacturing errors.
- c) Theoretical support errors (those predicted by the analysis), both for individual mirrors (or optical elements) and for structure positioning them to each other: theoretical tracking or slewing induced errors of decentering or focus.
- d) Maintenance errors of above.
- e) Errors due to thermal distortions of optical elements or structure.
- f) Long term mechanical deformation due to structural or material changes of optical elements (i.e long-term warping of mirror blanks).
- g) Thermal effects of the ambient air: “dome”, “telescope” or “site” seeing (turbulence).
- h) Wind buffeting deformations of optical elements.
- i) Atmospheric seeing (turbulence).
- j) High frequency tracking errors (image motion) due to motor vibration, structural or mirror resonance or wind shake.

It is important to consider the time bandpass of these error sources:

- a) and b) are effectively dc: no change takes place with time.

- c) is dc for theoretical support errors, but time varying with telescope movement for the structure errors (focus and decentering). With tracking the bandpass is very low (of the order of  $10^{-3}$ Hz) with re-pointing (change of observing object) of the order of  $10^{-2}$ Hz or less.
- d) represents slow changes which cause deterioration over weeks or months. Very low bandpass.
- e) represents errors of very low bandpass because the thermal capacity and inertia of the system is too high to allow rapid changes.
- f) is by definition extremely low bandpass.
- g) includes effects which may cover a wide bandpass from slowly varying effects which may be stable for hours to high frequencies of many Hz similar to i).
- h) has the frequency spectrum of wind buffets filtered through the prime mirror (the deformation of other optical elements will probably be negligible in comparison with the primary). For the VLT 8m primary it is expected that the effective bandpass will lie roughly between 0,1 Hz and 2 Hz.
- i) has the large bandpass from about 0,02 Hz to 1000 Hz.
- j) has a bandpass roughly in the range 5 Hz to 100 Hz. Telescope designers try to push up the lowest eigenfrequencies to reduce the amplitude.

### 5.3.2 The Active Optics Control System: Principles

This system had its origins about nine years ago in telescope testing work done for the setting up of the ESO 3.6m telescope. Out of this has evolved the active optics control system of the ESO New Technology Telescope (NTT), which will also be the base technology for the VLT active control.

The purpose of the active optics system is to correct all the low bandpass errors, from dc up to the frequency set by the dynamic response of the system. In practice, it is expected that this might be of the order of 2 Hz for the correction of wind buffeting deformations of the primary mirror if it is fully exposed to the air stream.

At this frequency the effects cannot easily be separated from low frequency atmospheric turbulence effects (see below). Below about 1/30 Hz this separation is possible by integrating out the turbulence. This sets the bandpass upper limit of the active correction in the NTT. This is more than sufficient for the active correction of all errors a) to g). In contrast to the VLT, h) is considered negligible in the NTT. Optical design errors a) are, in practice, negligible except for field limiting aberrations which are inherent in the system and can only be influenced by field correctors, not by any active optics system. The basic principles of the active optics control are essentially identical in the NTT and VLT but the VLT requires the bandpass extension for correction of h).

In practice, the active optics correction is also limited to low spatial frequency aberrations. That this is necessary and sufficient for correction of all errors originating from elastic effects in the total system is a consequence of the Principle of St. Venant in elasticity theory. Of the error sources b) - f), only b), optical manufacture, can produce high spatial frequency errors, "ripple" being the most common example. Such high spatial frequency errors have their origins in resonance effects of the polishing movements and have nothing to do with elasticity. If a severe tolerance is applied to such high spatial frequencies for the optics manufacturer, that for the low spatial frequencies can be relaxed. The consequences for the NTT can be summed up as follows:

- A modest specification of optical manufacturing quality except for high spatial frequencies, giving major economies in manufacturing cost and leadtime. As an example, a low astigmatism value is normally very difficult to achieve but a rather large amount of astigmatism can be tolerated in an active mirror because it is possible to correct it in situ.
- A final functional specification far better than the manufacturing specifications giving a continuously maintained performance in the visible which is effectively diffraction limited (80% of the energy within 0.15 arcsec).

We are confident that we will be able to use a much wider dynamic correction range with the VLT than for the NTT and to aim for an even tighter functional specification of 80% geometrical energy within 0,1 arcsec for the primary mirror alone. The target for the complete telescope is 0.15 arcsec. The extension of the dynamic range for the VLT is discussed below in more detail in connection with the results on a 1m experiment test bench. Before considering this, however, it is necessary to review briefly the main characteristics and principles of the active optics control system.

The active optics system is shown schematically in Figure 5.6. The principles and some aspects of this system have been described in the literature. (See also in particular *Optica Acta* to be published soon.) The essential features are:

- An image analyser analyses the image of a guide star in terms of a quasi-Zernike polynomial using a small computer. There is no disturbance to the observation and the astronomer will be unaware that an analysis (or subsequent image correction) is taking place.
- The image analyser is of the Shack-Hartmann type. Combined with the software package developed at ESO for off-line telescope testing it is termed "ANTARES". For the VLT a CCD detector will be used. The system will work with stars down to ca.  $14.5^m$ , more than ample for availability of stars within the field (30 arcmin) of the VLT unit telescopes. Figure 5.7 shows the principle of the ANTARES image analyser. The exit pupil of each 8m telescope is re-imaged by an objective (3) which collimates the light from the star image. A raster of small, square, weak lenses (4) divides the pupil continuously into sub-apertures which form spots in

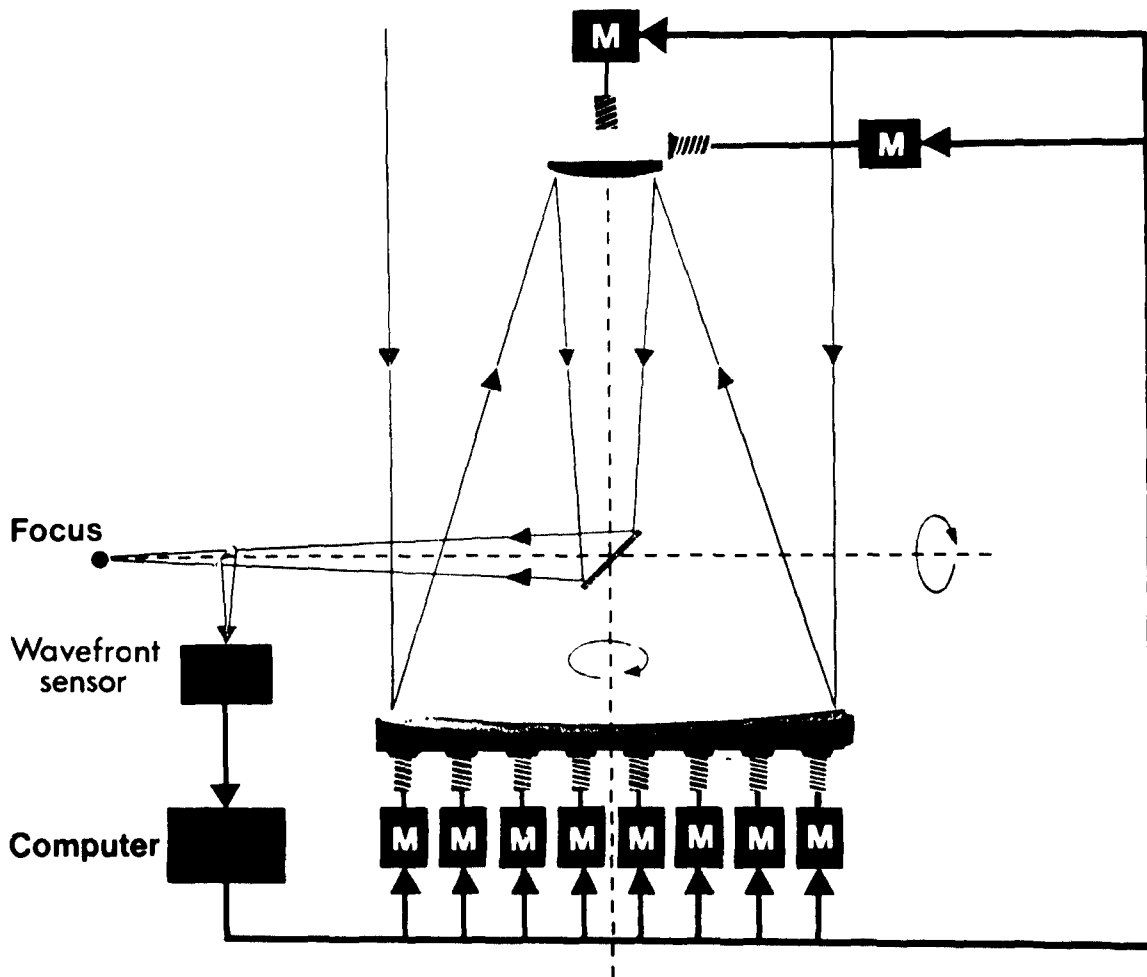


Figure 5.6: Principles of active optics.

their image plane (5). A reference source (6) sends an equivalent beam, but slightly inclined, through the system and forms a similar raster of bright spots in the image plane. Figure 5.8 shows a typical result if a photographic plate is used as the detector and is placed at (5). The raster of points over the whole area comes from the reference source; that over the circular pupil, with obstruction, is from the natural star. The reference raster eliminates errors of the transfer optics and the lens raster. The differences of the vectors separating pairs of points give the information on the transverse aberrations of the telescope. The use of a lens raster has many advantages over a simple screen with holes, in particular the gain due to light concentration which is of about 5 magnitudes. A transfer system (7) is required to reduce the image to the width of a CCD chip (8).

- The system is a force-based (soft), not position-based (hard), system. We believe it is far easier to measure and control forces with sufficient accuracy than to try

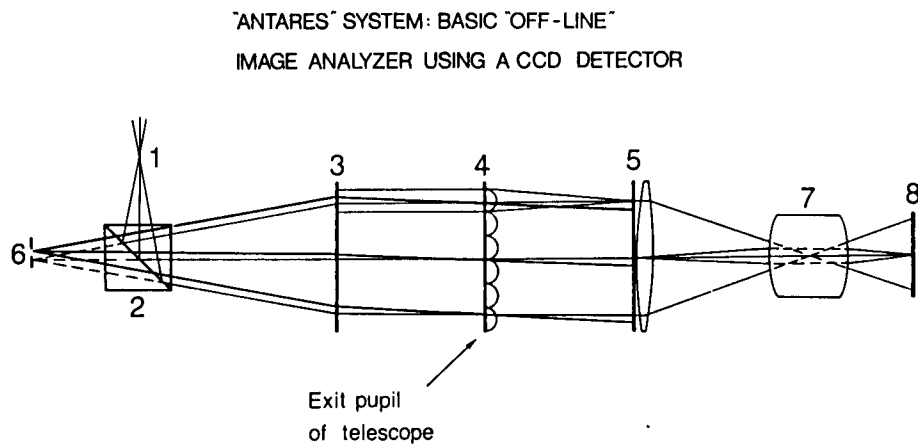


Figure 5.7: Principle of the existing ANTARES image analyser.

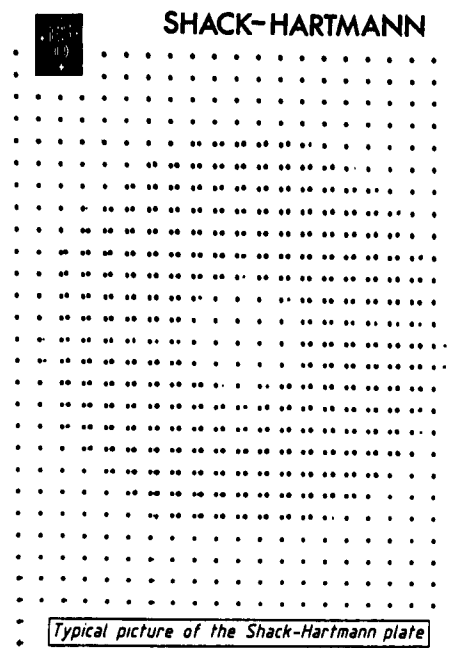


Figure 5.8: Typical image pattern produced by ANTARES image analyser.

to control the position to a small fraction of a wavelength. The correct form is assured by the natural elastic properties of the monolith under the influence of force changes.

- Decentering coma is corrected at its source by appropriate movement of the secondary mirror. All the other low spatial frequency aberrations are corrected by the active primary support.
- As with the passive support systems, the fundamental law on which the active system is based is the Linearity (Superposition) Law which is simply Hooke's Law in elasticity theory.
- Also fundamental is the application of the Principle of St. Venant in elasticity theory which leads to an analysis of the elastic modes of a telescope mirror in terms of a converging series originating from a Fourier equation mathematically identical with that leading to Zernike polynomial terms. The practical consequence is that disturbances in the system lead essentially to low spatial frequency terms which can therefore be corrected. High spatial frequency terms with significant amplitude can neither be provoked nor corrected by the support. This is why a very hard tolerance on ripple is necessary for the optical figuring.
- The Orthogonality Law of Zernike polynomial terms comes from the nature of the Fourier equation and applies equally to terms induced by elastic flexure. Combined with the linearity law, this allows linear superposition of corrections without "cross talk".
- Our system uses pre-stored information (precalibrations) in the computer from elasticity theory calculations. This avoids the necessity of a complex general matrix inversion for every correction and reduces the on-line calculation to a simple proportioning and addition of terms taking account of their azimuth phase.

In physical terms, then, the procedure consists of an image analysis giving the coefficients of the lower order polynomial terms; the computer has pre-stored information of what force corrections are required to generate a coefficient of, say, 500nm of each aberration term to be corrected by the primary support; this change is scaled linearly with the measured coefficient; the force changes for all the aberrations to be corrected by the primary support are then summed, these force changes are then applied to achieve the correction.

Instead of a linear translation of the secondary to correct third order coma, it is corrected by a rotation about its center of curvature which corrects the coma without disturbing the pointing.

### 5.3.3 The 1m Laboratory Experiment and Demonstration

The 1m experiment was intended to test, prove and demonstrate the validity of the active optics system and has been very successful.

If the three laws of physics stated in Section 5.3.2 are accepted, then the essential part of the experiment consisted in proving:

- a) That the precalibrations are sufficiently correct in scale.
- b) That the radial purity of the precalibrations is confirmed in practice.
- c) That the theoretically perfect azimuthal orthogonality is achieved in practice (cross talk between modes negligible).

In practice a) is relatively uncritical because any scaling errors detected can be at once corrected by scaling, but about 90% scaling accuracy was immediately achieved, better than expected. b) was confirmed with high precision and c) was within the detection limit of the image analysis and air turbulence disturbances.

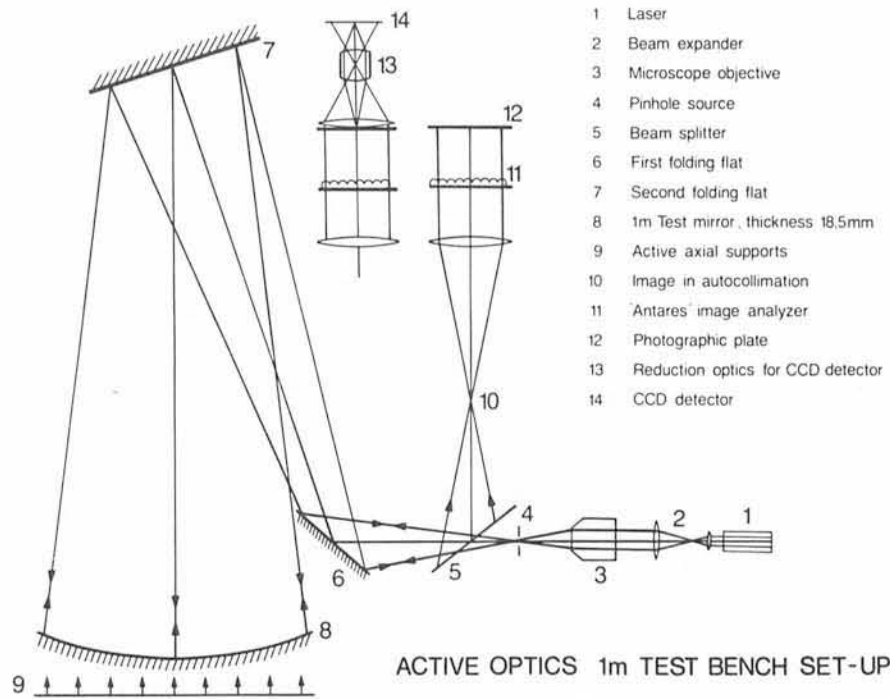
Once these three points were established, the active correction of the mirror is a trivial operation.

Figure 5.9 shows schematically the test set-up. The 1.05m diameter spherical mirror is tested at its center of curvature in autocollimation. Figure 5.10 shows the mirror after manufacture at REOSC in Paris. One can see the thinness of the mirror and its support. Although the tolerances for low frequency errors were relaxed (since they were to be corrected actively) the manufacture was nevertheless a delicate operation because the mirror is only 18.9mm thick ( $AR = 1:56$ ). The reason for this thickness is discussed in Section 5.3.4. Figure 5.11 shows the support, with the same geometry as the NTT i.e 75 active supports with 3 fixed points. Load cells measure the actual forces with high precision. For reason of simplicity, the dynamic range of active correction here is only  $\pm 10\%$  of the mean passive load. This means the experiment is appreciably more delicate than the procedure in the NTT itself, where the dynamic range in the zenith is six times greater.

A hand adjustment was first performed by adding loads to reduce the major aberrations to a point where the correction was within the dynamic range of the moveable counterweights. This hand adjustment was simply the equivalent of the dc correction with springs which will be done with the NTT.

One demonstration of the results of calibration tests with the 1m mirror will now be given. The “Antares” analysis results are expressed numerically in a computer print-out. This data, integrated as wavefront forms, is processed in the MIDAS image processing system available at ESO. The wavefront aberration is then shown in a colour system whose sensitivity can be varied at will. Figure 5.12 shows a calibration test for astigmatism, the lowest-energy mode. An arbitrary state of the mirror was used for the initial state which still had appreciable astigmatism and a residue of other aberrations. A fixed amount of astigmatism (coefficient change  $\Delta g = 838\text{nm}$ ) was added to this state using the precalibrated force changes. The result is shown in the top left corner: by chance the additional astigmatism only slightly overcorrected that still present in the initial state, so the mirror was then not far from the corrected state with little





- 1 Laser
- 2 Beam expander
- 3 Microscope objective
- 4 Pinhole source
- 5 Beam splitter
- 6 First folding flat
- 7 Second folding flat
- 8 1m Test mirror, thickness 18.5mm
- 9 Active axial supports
- 10 Image in autocollimation
- 11 Antares image analyzer
- 12 Photographic plate
- 13 Reduction optics for CCD detector
- 14 CCD detector

Figure 5.9: 1m test set-up (schematic).



Figure 5.10: 1m test mirror.

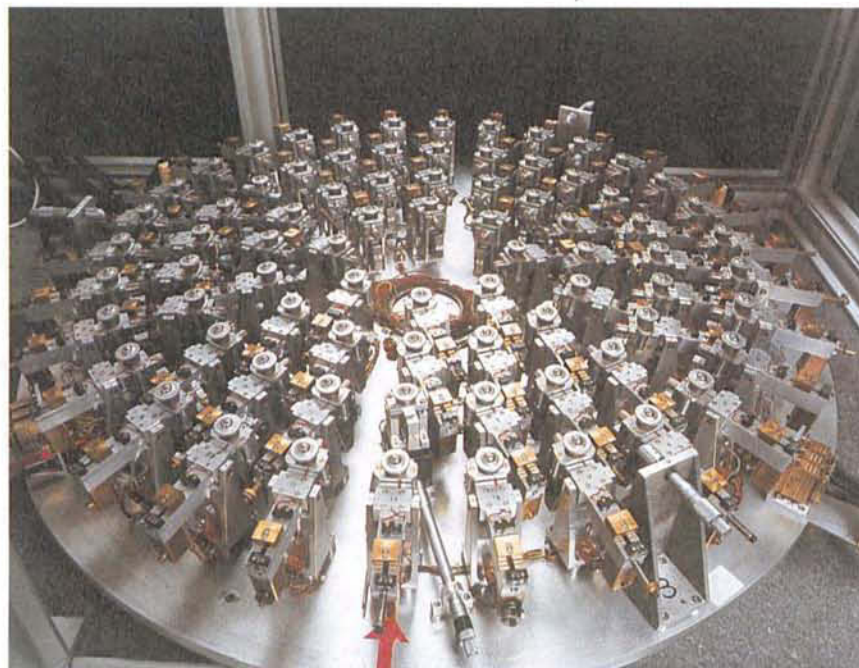


Figure 5.11: 1 metre experimental mirror support.

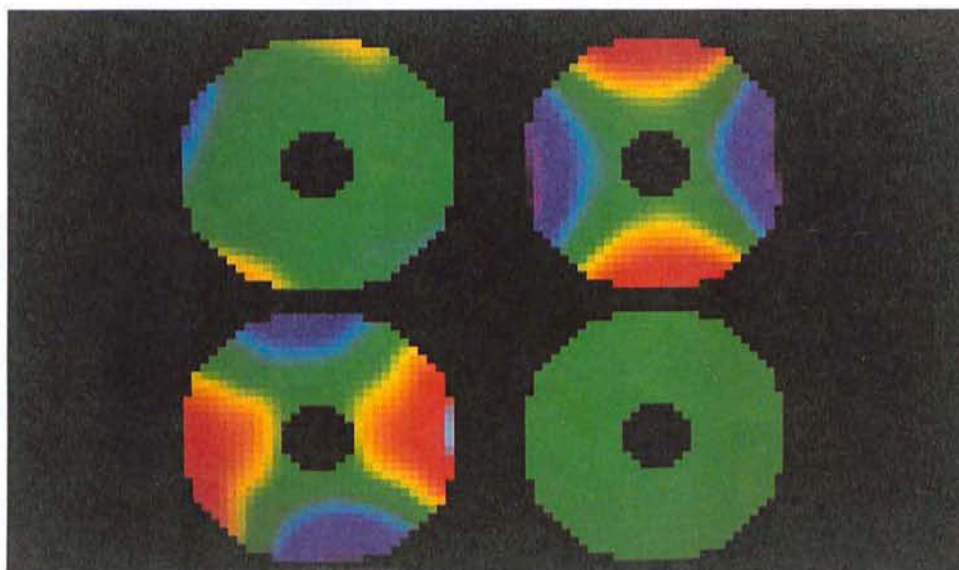


Figure 5.12: MIDAS demonstration third order variation of astigmatism with 1m test mirror.

colour detail. The residue is still largely astigmatism. In the lower left corner, the same coefficient of astigmatism was subtracted from the initial state of the mirror, thereby virtually doubling the astigmatism present. The difference of these wavefronts was now formed (top right picture) giving the total change of astigmatism in the mirror ( $2\Delta g = 1677\text{nm}$ ). It is evident from the colour appearance that this represents astigmatism in quite pure form. To test this purity, the same amount of astigmatism was artificially generated in a pure form, whereas the pictures show wavefronts actually measured with the image analyser. The pure astigmatism was subtracted from the top right corner picture to give the lower right picture. On this colour sensitivity scale, no error can be detected. This excellent purity is to be expected precisely because astigmatism is the lowest energy mode.

Figure 5.13 shows a similar demonstration with a more difficult mode, namely coma. A mixture of wavefront tilt, third and fifth order coma is introduced, the specific interest being the latter (in the NTT third order coma would be removed afterwards at the secondary). The amount of aberration corresponds to a change of fifth order coma of  $\Delta\kappa = 368\text{nm}$  and of third order coma of  $\Delta d = -748\text{nm}$ . The top left and bottom left pictures show the addition and subtraction of this coma as before, but now the bottom right picture shows the difference ( $2\Delta k = 735\text{nm}$ ). The 1-axis colour symmetry is obviously coma, the amount being modest compared with the original state of the mirror. The top right picture shows the measured coma of the bottom right again, with an increased colour sensitivity. On this scale, some error can be detected. This error residual is analysed in Figure 5.14. The top right picture is a repetition of the measured coma shown in the top right of Figure 5.13. At the top left, a pure coma combination with the same coefficients is generated artificially and subtracted from the top right to give the bottom left. This represents the residual cross-talk error in this case, on the same colour scale. It is clearly extremely small. As expected, most of this small residue is astigmatism. If this astigmatic error is subtracted, we get the bottom right picture, which shows very small random higher order residues.

Our general conclusion from the 1m experiment is that we have a practical, working system of active correction whose performance has been proven and which is quite simple to operate. The hardware of this model has functioned extremely well, limits being set finally (as should be the case) by the signal/noise limit of the image analyser. The basic algorithm, using precalibrations, has been well proven: it is very simple and requires minimum computing. We thus feel quite confident that we can go ahead with a similar system for the VLT, using a larger dynamic range of correction.

### 5.3.4 Extrapolation from the NTT to the VLT

#### Passive support

As with the NTT, the basic passive axial support geometry will be completely adequate for the active control of the VLT provided the dynamic range of active correction is not

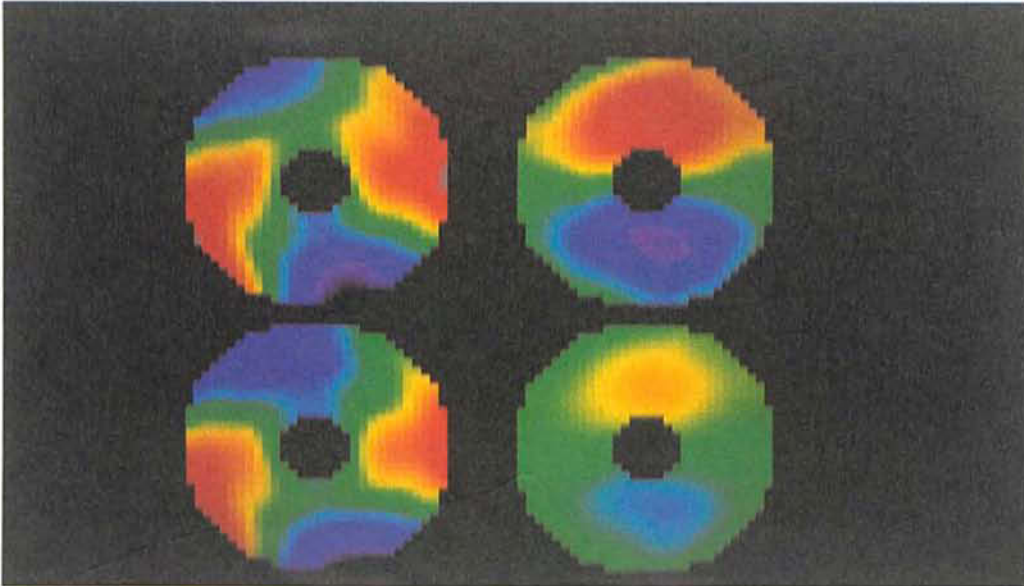


Figure 5.13: MIDAS demonstration of third order coma variation with 1m test mirror.

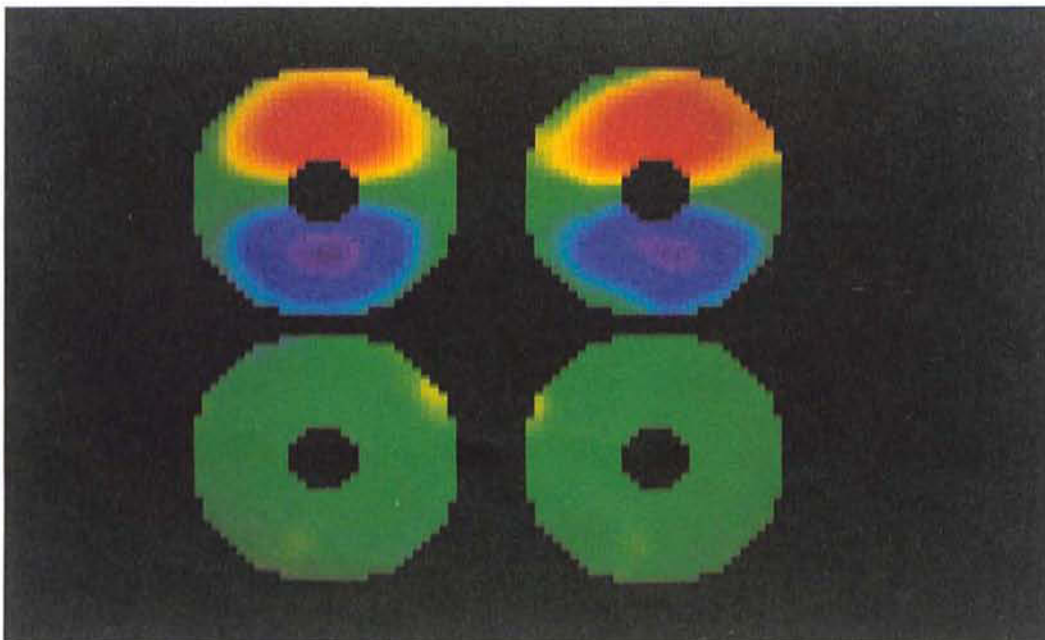


Figure 5.14: Coma demonstration (continued).

too high, which is very unlikely.

The passive support consists of an axial and a radial support system. In the NTT the radial support is a separate system operating at the edge of the mirror. In the VLT the radial support may be similar or combined with the axial support following the same basic concept as the Palomar 5m telescope. It should be remembered that active optics control can compensate all the low frequency errors in the image, whatever their origin.

The requirements of the basic (passive) axial support geometry can be deduced from quite elementary considerations. The scaling law for the bending moment action of an external force on a mirror depends on  $D^2/h^3$  ( $D$  = diameter,  $h$  = thickness). If the weight of the mirror in the gravity force field is introduced by integration over the back surface, the well-known scaling law for mirror flexibility (Couder Law) results:  $D^4/h^2$ . The 1m mirror ( $AR = 1:56$ ) was scaled from the NTT primary ( $AR = 1:15$ ) using this law so that the passive support geometry could be taken over, the loads being linearly scaled according to the weight, some correction being made for the "shell effect". Relative to its weight, the 1m mirror is then as flexible in wavefront flexure as the NTT primary. The Couder scaling law also applies to the force distributions of active control, which is simply a supplementary force field parallel to the mirror axis.

It should be emphasized here that the 1m mirror was in no way a scale model for the VLT: it was intended solely to simulate the NTT. If a solid meniscus form is chosen for the VLT, the primaries will be of the order of 30 times more flexible than the NTT primary. Such flexibility would be fatal in a passive telescope but will be entirely feasible with active control. The weight gain will be a factor of five to eight compared with the aspect ratio of conventional passive telescopes, a saving which goes through the whole telescope.

The NTT has an extremely severe geometrical optical specification leading to a number of supports which is relatively uncritical and which was also fixed from symmetry considerations. For the VLT the specification will be based on diffraction limit considerations (Strehl intensity ratio) and their link to geometrical optical specifications so the final number of supports will probably be of the order of 150 to 200.

### Active optics for the VLT: dynamic range

The purpose of the active control is essentially the same as in the NTT but the correction range, in the global sense of the range of change of aberration coefficients, is bound to be much greater because of the vastly greater flexibility of the VLT. In the stricter sense of the force range relative to a 1 g gravity field, the dynamic range  $r_{dn}$  is one of the fundamental parameters still to be fixed.

The NTT has a "push-only" axial support, so its  $r_{dn}$  is theoretically limited to 1 g. In fact, the NTT has

$$r_{dn} \leq 0.6g. \quad (5.1)$$

But the VLT will have a “push-pull” axial support, so the only theoretical limit to  $r_{dn}$  is the breakage risk (or elastic limit for metals) of the mirror, corresponding to a very large range indeed.

Table 5.2 gives an example of the correction achievable with the NTT and the corresponding values for the VLT for the cases where  $r_{dn}$  is the same (correction range extended by  $30\times$  from the increased flexibility) and where  $r_{dn}$  is increased by a factor of 10. It should be remembered that the correction range of the NTT is quite modest because it was required to have a passive specification equal to the ESO 3.6m conventional telescope and because of the “push-only” support.

TABLE 5.2

ACTIVE CORRECTION RANGE OF THE NTT AND POSSIBLE EXTENSIONS OF THIS RANGE FOR THE VLT			
TELESCOPE	$r_{dn}$	Aberration Mode	Ex. of simultaneous correction in $\lambda$ ( $\lambda = 500\text{nm}$ )
NTT	$\leq 0.6g$	SPH <sub>3</sub>	4
		AST <sub>3</sub>	3
		$\triangle$	0,8
		$\square$	0,4
VLT	$\leq 0.6g$ (AS NTT)	SPH <sub>3</sub>	120
		AST <sub>3</sub>	90
		$\triangle$	24
		$\square$	12
	$\leq 6g$ ( $10\times\text{NTT}$ )	SPH <sub>3</sub>	1200
		AST <sub>3</sub>	900
		$\triangle$	240
		$\square$	120

The Table shows that already the extension for the VLT from flexibility alone brings a very large correction range. With  $(r_{dn})$  VLT = 10  $(r_{dn})$  NTT, the correction range would be so enormous that it will certainly exceed what can be used: indeed if most were used for spherical aberration it would correspond to about half the total asphericity of the mirror! This, of course, raises the often discussed possibility of polishing the primary spherical and actively bending it to the required aspheric form. This may well be the final role of active optics, but it may be better to get an approximation to the final aspheric by stress polishing the sphere and performing perhaps a 10-20% correction with the active optics system. Bending fully to the final aspheric form would also require a significantly thinner mirror than we envisage which would require a higher number of passive supports  $N$ . This would put up the weight and complexity of the cell.

Probably  $r_{dn}$  will be chosen of the order of 1 - 2 g. In any event, the correction range will be sufficient to allow a possible conversion from a Nasmyth to a Cassegrain focus (about 10  $\lambda$  of third order spherical aberration).

Let us now consider what, in practice, will anyway set a limit to the dynamic range  $r_{dn}$ . This is the purity  $P$  of the precalibrations. Consider an example (astigmatism - Figure 5.15) of the precalibration for the NTT. This was the simplest case where the purity achieved quite easily was very high. Figure 5.16 shows a mode much less easy to generate: third order spherical aberration. In order to maximize the range of correction, some higher order errors of this function have been deliberately accepted. These errors are negligible over the correction range of the NTT. For the same wavefront aberration, the forces are about 6 times higher than for astigmatism. From the linearity law, the higher order errors will increase linearly with the dynamic range  $r_{dn}$ . The required purity of calibrations is treated in detail in the general paper to appear in *Optica Acta*.

Here we repeat briefly only some basic aspects. The theoretical calibration process for generation of a pure aberration mode  $(\Delta W_i)_{nm}$  can be written as

$$(\Delta F_j)_{nm} = A_{ji}^{-1} \cdot (\Delta W_i)_{nm}, \quad (5.2)$$

where  $(\Delta F_j)_{nm}$  is the required force distribution and  $A_{ji}^{-1}$  an inversion process (or equivalent) of the stiffness matrix  $A_{ji}$ .

The practical calibration will be done with certain tolerances on higher order impurities to give  $(\Delta \bar{W}_i)_{nm}$  as the approximation to the pure mode, thereby lowering the forces  $(\Delta \bar{F}_j)_{nm}$  required:

$$(\Delta \bar{F}_j)_{nm} = A_{ji}^{-1} \cdot (\Delta \bar{W}_i)_{nm} \quad (5.3)$$

or

$$(\Delta \bar{F}_j)_{nm} = [Q]_{nm} \cdot (\Delta \bar{W}_i)_{nm} \quad (5.4)$$

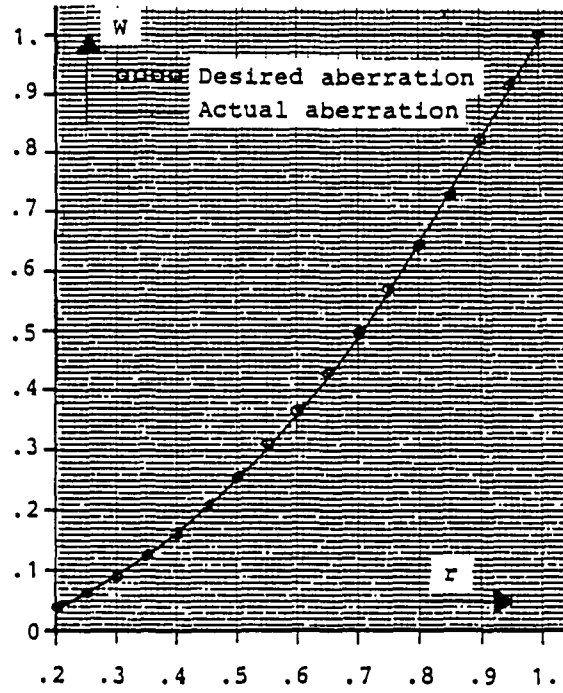


Figure 5.15: Precalibration for one wavelength (coefficient of 500nm) of astigmatism for the NTT primary.

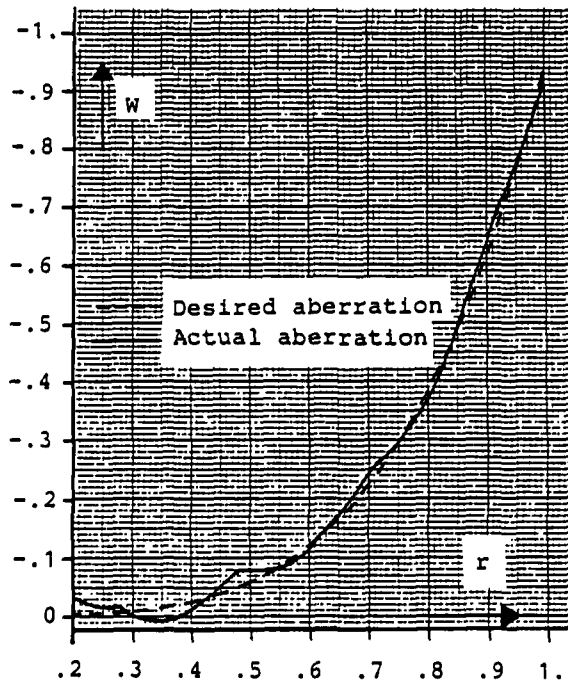


Figure 5.16: Precalibration for one wavelength (coefficient 500nm) of third order spherical aberration for the NTT primary.



$[Q]_{nm}$  is an operator formally equivalent to the matrix inversion  $A_{ji}^{-1}$ . Now it follows from the linearity law that the smaller the dynamic range  $r_{dn}$ , the larger will be the impurities that can be accepted and the lower the forces  $(\Delta \bar{F}_j)_{nm}$  will be relative to  $(\Delta F_j)_{nm}$ . A large dynamic range  $r_{dn}$  requires a high purity  $P$  and therefore higher forces for the same range of correction. We have

$$P = \frac{(\Delta W_i)_{nm}}{(\Delta W_{HF})_n} \quad (5.5)$$

where  $(\Delta W_{HF})_n$  are the higher order impurities associated with the azimuthal mode  $n$ . Also

$$P \propto r_{dn} \quad (5.6)$$

If  $r_{dn} \rightarrow \infty$ , then  $(\Delta \bar{F}_j)_{nm} \rightarrow (\Delta F_j)_{nm}$ , that is no tolerance relaxation is possible and  $P \rightarrow \infty$ . Suppose we fix as an arbitrary example

$$(r_{dn})_{VLT} = 10 (r_{dn})_{NTT} \quad (5.7)$$

then we must have

$$(P)_{VLT} = 10 (P)_{NTT} \quad (5.8)$$

for the same image quality. It follows, for the same correction range that

$$[(\Delta \bar{F}_j)_{nm}]_{VLT} > [(\Delta \bar{F}_j)_{nm}]_{NTT} \quad (5.9)$$

in other words, the correction that can be achieved for a given  $r_{dn}$  in the VLT would be less than in the NTT. The extent of the inequality of (5.9) will depend on the aberration mode: it will be much greater in the case of spherical aberration than astigmatism. This is very important if we bear in mind that a very large correction range is particularly interesting for spherical aberration.

The important conclusion for the VLT is that  $(r_{dn})_{VLT}$  must be fixed with great care and not made larger than necessary. There is a second reason for this restriction of  $(r_{dn})_{VLT}$  to only that which is technically useful; for if we choose  $(r_{dn})_{VLT} = 6g$  or some such value much greater than  $1g$ , the purity  $P$  required may not be attainable with the passive support ( $1g$ ) geometry. More supports would then be necessary than the number  $N$  for the passive support, which would bring complication, extra cost and extra weight to the axial support system.

### 5.3.5 Active Optics and Wind Buffeting

Wind buffeting deflection of the top end of the tube relative to the primary will produce theoretically both tracking errors and coma. As with any Cassegrain telescope, the sensitivity to decentering coma for the VLT is negligible compared to tracking errors. Tracking errors will be corrected with the telescope drives for lower frequencies and by the secondary mirror for frequencies beyond the bandpass of the telescope drives.

In view of its large area, a deformation of the primary mirror under wind buffets is a matter of concern.

The static wind load is however a small percentage of the gravity load. If the mirror were vertical and directly facing the wind, the total load would be  $160 \text{ N/m}^2$  for a wind of  $18 \text{ m/sec}$  which should be compared to  $4400 \text{ N/m}^2$  for gravity. Close to zenith position the load is estimated to be about 10 times less, i.e. 0.36% of gravity load. Considering that observations will be performed at much lower wind speeds and that the load increases as the square of the wind speed, the effect will probably remain unnoticed. For instance at a typical speed of  $5 \text{ m/sec}$  the wind load at the zenith will be 0.28% of the gravity and at  $45^\circ$  zenith distance only about 0.15%, a value which is close to the target accuracy for the active supports and therefore tolerable.

The dynamic load is more difficult to evaluate because a part of the load especially at higher frequencies, i.e. beyond about 2 Hz, will be aerodynamically generated by the structures of the telescope and by the mirror itself. A wind tunnel analysis is being done and is expected to bring quantitative data soon.

However, it is not expected that we will encounter major problems for the following reasons:

- the dynamic load will be anyway smaller than the static wind load. The wind power spectrum shows a peak at a frequency of about 0.01 Hz and then a continuous decrease.
- the higher the time frequency, the higher the corresponding spatial frequency. Owing to the very large area of the primary mirror the turbulence vortices which at high frequencies are small compared to the mirror, will neutralize each other. This effect is known as the aerodynamic attenuation and is given by the approximate formula:

$$\frac{1}{1 + (\sqrt{\pi} \frac{f \cdot D}{v})^{4/5}} \quad (5.10)$$

For the maximum wind speed of  $18 \text{ m/sec}$  the attenuation is 0.46 at 2 Hz and 0.17 at 10 Hz. For  $9 \text{ m/sec}$  the values are respectively 0.19 and 0.05.

- the first eigenmode of the mirror is 18.4 Hz, the following one is 43 Hz. It is very unlikely that the wind turbulence at these frequencies will be of any significance with respect to the mass of the mirror to generate any detectable vibration.

A problem with the correction of wind buffeting effects is that this bandpass of the effect no longer allows integration of the atmosphere. In principle, therefore, there is no means of separating off the wind-buffeting effects from atmospheric seeing effects. There is evidence that for telescope sizes not greatly exceeding the Fried parameter, significant low spatial frequency terms such as astigmatism occur in the atmospheric seeing. However, the VLT unit telescopes will so much exceed the probable maximum Fried parameter values that it is expected that the atmospheric seeing amplitudes of

such low spatial frequency terms will be negligible: in other words, separation of the effects would then be achieved by spatial frequency filtering instead of time frequency filtering.

The above approach seems the most promising but requires a support system capable of functioning up to 1 or 2 Hz. This seems quite feasible. Other methods which may well give useful supporting information on wind buffeting effects are under investigation, especially measurement of the reaction of the fixed points to wind buffeting.

### 5.3.6 Modal Analysis of a Thin Glass Meniscus Mirror

The knowledge of the free natural vibration modes of the primary mirror is essential for optimization of the active optics system for image correction. The force distributions necessary to correct certain image aberrations, can be derived from the eigenmodes of the mirror. Besides this it is important for the design of the support system and the mirror cell, to know the dynamic response behaviour of the mirror, due to excitation by wind gusts or telescope drives. The dynamic response behaviour depends on the lowest eigenfrequency that can be excited by the dynamic loading. As a first step of information in this complex analysis a modal analysis of the primary glass solid meniscus has been performed. For that purpose a finite element model of the full mirror which is shown in Figure 5.17, has been prepared. The model shown is a thin shell model. For comparison a flat circular plate has been analysed with the finite element method as well as with an analytical model described in the literature.

The results of all calculations are summarized in Table 5.3 for the mode Nos 1 to 10 of the flat plate model and for the mode Nos 1 to 8 of the shell model. The corresponding eigenmodes of vibration of the shell in the case of the free-free boundary conditions are shown in the isocontour plots in Figure 5.18. The displacements in z-direction  $w_z$  can be described by the following model

$$w_z(r, \vartheta) = F_{mn}(r) \cdot \cos(n \cdot \vartheta) \quad (5.11)$$

where each mode effectively consists of an orthogonal mode pair m,n

$$\begin{pmatrix} F_{mn}(r) \cos(n \cdot \vartheta) \\ F_{mn}(r) \sin(n \cdot \vartheta) \end{pmatrix}$$

and  $F_{mn}(r) = \sum C_k \cdot r^k$  is a polynomial of r.

The comparison of eigenfrequencies of plate and shell shows that only the radial modes are significantly higher in the shell due to the stiffening effect of the curvature. For example in mode 2, which is a defocusing mode, the eigenfrequency of the shell is 47% higher than the corresponding plate frequency. The same is true for mode 4 and 8. Compared with the plate, the mode Nos 6 and 7 are exchanged in their sequence.

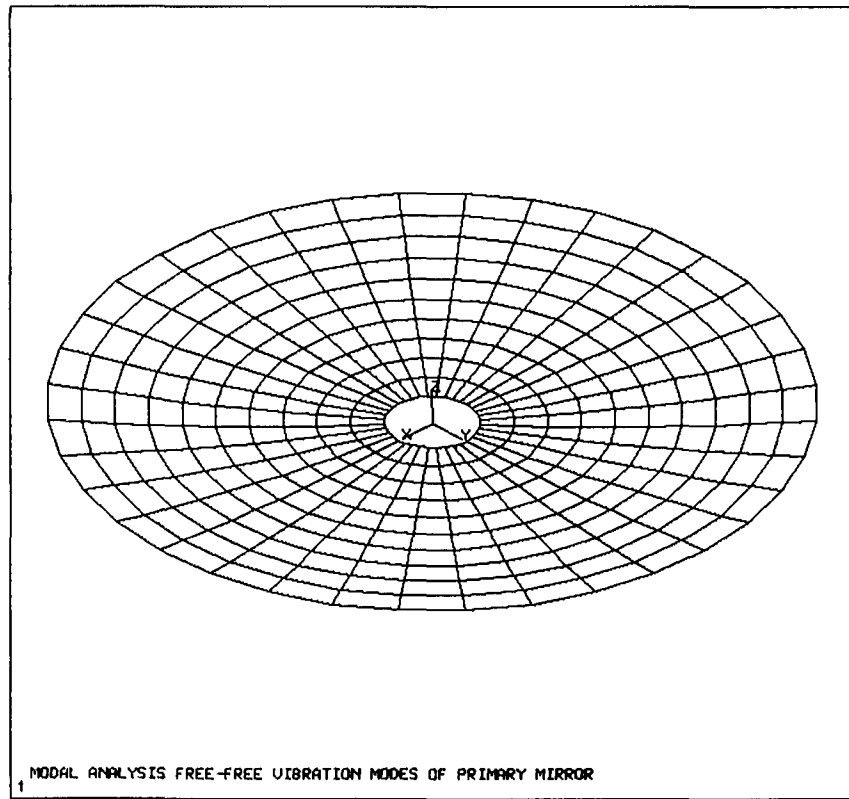


Figure 5.17: Finite element model for the modal analysis of the primary mirror.

## 5.4 Primary Mirror Support

### 5.4.1 Specification

The support system of the VLT glass meniscus primary mirror will consist of points or small pad supports as regularly distributed as possible on rings over the back surface of the blank. All supports will then carry approximately the same load.

As a good approximation the mirror can be regarded as a fairly thin shallow shell. But the stiffening effect of the shell as compared with a plate (of the order of 2 to 3 for an envisaged 8m meniscus with an f-number between 1.7 and 2.0) will only be of significance for the correction of certain aberration modes in the active state. Otherwise, the support points are so close together that, for the sag between the support points, the mirror can be regarded as an infinitely extended thick plate resting on an infinite pattern of more or less regularly distributed support points or pads.

TABLE 5.3

EIGENFREQUENCIES OF A PLATE AND SHELL MODEL OF THE PRIMARY MIRROR					
MODE No.	m	n	EIGENFREQUENCY [Hz]		
			Plate	Analyt. model	Shell (F.E.M.)
1	0	2	19.4	19.9	19.5
2	1	0	30.8	31.0	45.4
3	0	3	45.6	46.4	46.1
4	1	1	72.3	72.3	79.9
5	0	4	80.0	80.7	83.3
6	0	5	123.0	123.3	129.7
7	1	2	123.0	125.2	136.0
8	2	0	139.0	135.5	145.0
9	0	6	174.0	174.1	
10	1	3	188.0	189.4	

The pattern yielding, for a given density of support points, the lowest wavefront aberration is a grid of equilateral triangles. But, since the support points of the mirror should, naturally following the axial symmetry of the mirror, be placed on concentric rings, such a perfect distribution is not possible. Therefore, wavefront aberrations computed for a support pattern with a square geometry, yielding data which are larger by 15 to 20%, are more realistic.

For such a model of an infinitely extended thick plate resting on a regular periodic support grid we can use an analytic solution. This has been cross-checked for a few cases with a finite element solution and the differences turned out to be negligible. The results for the root mean square  $\sigma$  of the wavefront aberrations as a function of the number of supports and the thickness  $h$  of the meniscus is presented in Figure 5.19.

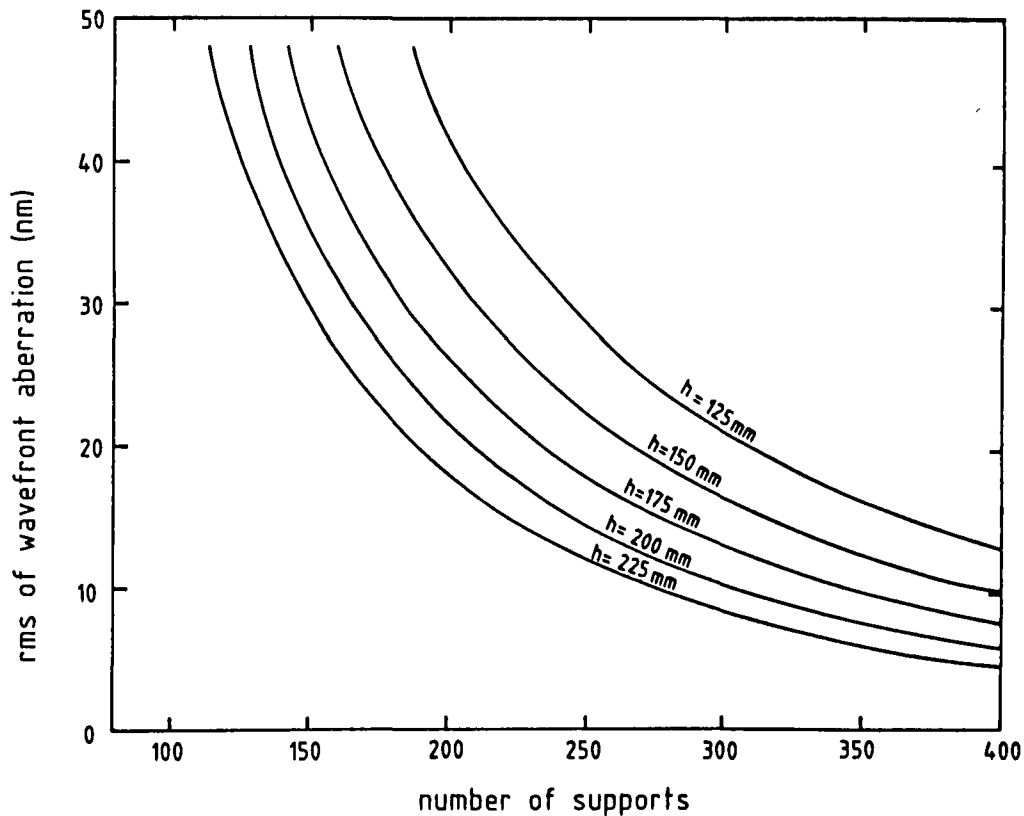


Figure 5.19: RMS wavefront aberration versus number of supports for a silica solid meniscus and for various thicknesses.

To interpret this data we first look at the values for  $\sigma$  which we would obtain if the mirror deformations were restricted to pure bending deformations. In such a simple case, which is only realistic for very thin plates, the following formula could be applied:

$$\sigma \propto \frac{1}{(h \cdot N)^2} \quad (5.12)$$

or

$$N \propto \frac{1}{(h \cdot \sqrt{\sigma})} \quad (5.13)$$

Any deviations of the real deformations of the top surface from these simple formulas are caused by effects arising from the thickness of the plate, i.e. particularly shearing stresses. Fortunately, for the range of aspect ratios (defined here as the ratio of the thickness  $h$  to the distance  $a$  between the rows and the columns of the supporting grid) which is of interest for a VLT-meniscus, the proportionality factor which has to be used to compute from the simple formula the real values does not vary too rapidly with the

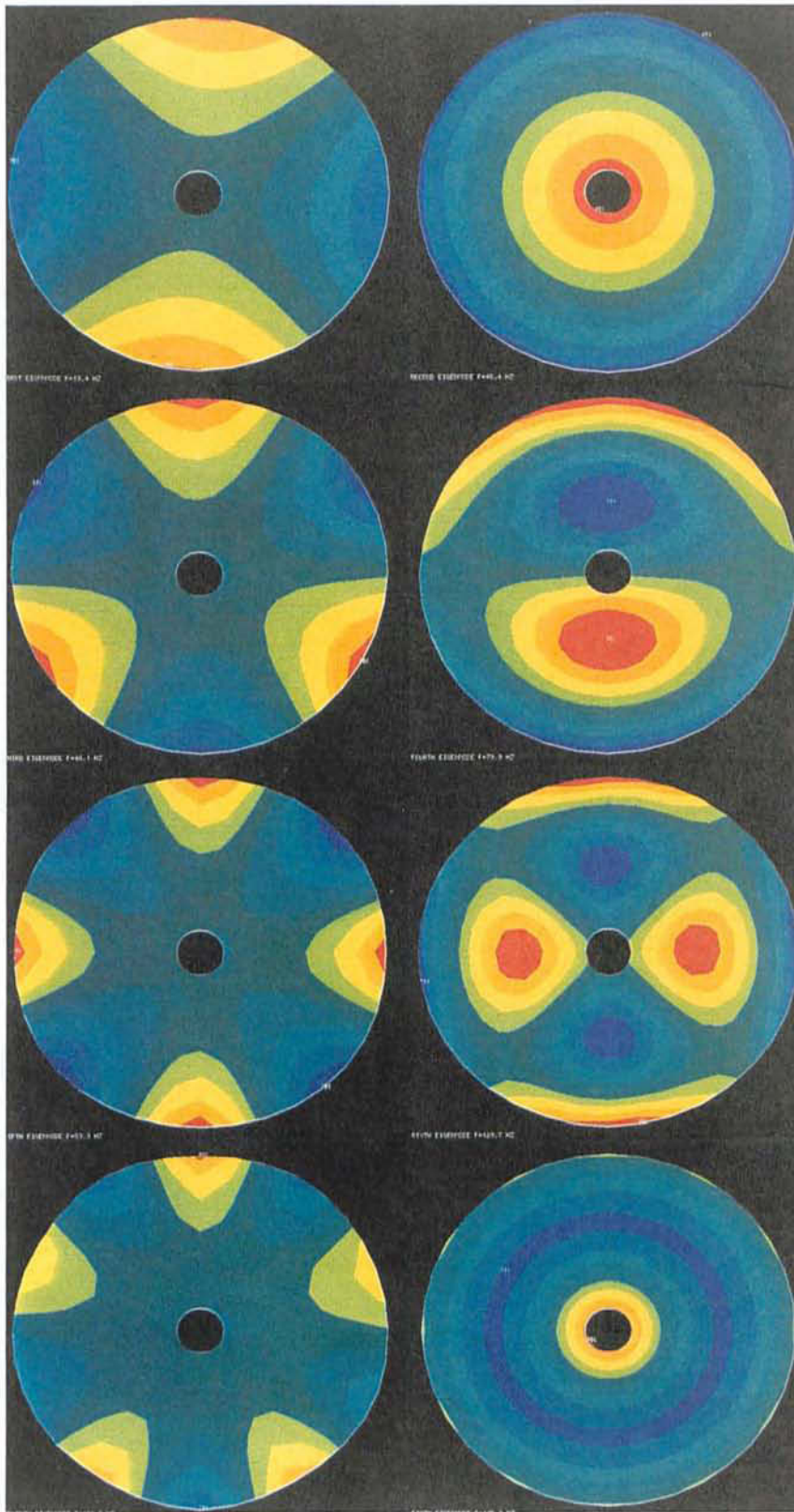


Figure 5.18: Eigenmodes (1-8) for the primary meniscus mirror.

aspect ratio. Therefore, the formula above shows quite realistically the dependence of the total number of supports on the chosen specification for  $\sigma$  and the thickness  $h$  of the meniscus.

The specification should, of course, be defined in terms of image quality. As the performance of the telescope optics will not be all that far from the diffraction limit, a computation of the image in terms of geometrical optics alone is not realistic, i.e. diffraction effects have to be taken into account. Small wavefront aberrations will affect the diffraction pattern, i.e. the image, in the following way:

- a) The diameter of the central disk, which for a perfect system contains approx. 85% energy, will not change, but it will lose part of its energy into the diffraction rings. The ratio of the residual energy in the central disk compared with the energy of the perfect system in the central disk is proportional to the Strehl ratio i.e. the ratio of the heights of the central peaks.
- b) A rotationally symmetric wavefront aberration of high frequency which can be caused by the ring structure of the supports, will transfer energy into one diffraction ring with a radius several times the radius of the central disk. The amount transferred will depend on  $\sigma^2$ .
- c) A regular wavefront aberration having the geometry of, say, our model square pattern support will similarly transfer energy to some spots again with distances from the center which are large compared with the radius of the central disk.

The real diffraction pattern will be a combination of (a), (b) and (c) together with the effect of some random variation of the wavefront. But for the large Strehl ratios, say larger than 0.8, the intensity of the diffraction outside the central disk will be, as in the case of a perfect system, negligible. Therefore, for small wavefront aberrations, the Strehl ratio is the natural criterion for the optical quality.

For the range of Strehl ratios, which are of interest for the VLT-primary, i.e. between, say, 0.75 and 1.0, the Strehl ratio can directly be related to the root mean square  $\sigma$  of the wavefront aberration.

$$s = 1 - \left( \frac{2\pi}{\lambda} \cdot \sigma \right)^2 \quad (5.14)$$

For the wavelength  $\lambda$ , we assume 500nm.

As the formula indicates, and is well-known, the Strehl ratio does not depend on the particular nature of the wavefront aberration but only on its root mean square value. Strehl ratios of 0.8 and 0.9 are equivalent to  $\sigma$ -values of 35nm and 25nm, respectively.

Figure 5.20 shows the Strehl ratio as a function of the number of supports and the thickness of the meniscus.

As a provisional specification we have fixed the maximum RMS deviation to 35nm which corresponds to a Strehl ratio of 0.8. From Figure 5.20 the corresponding number



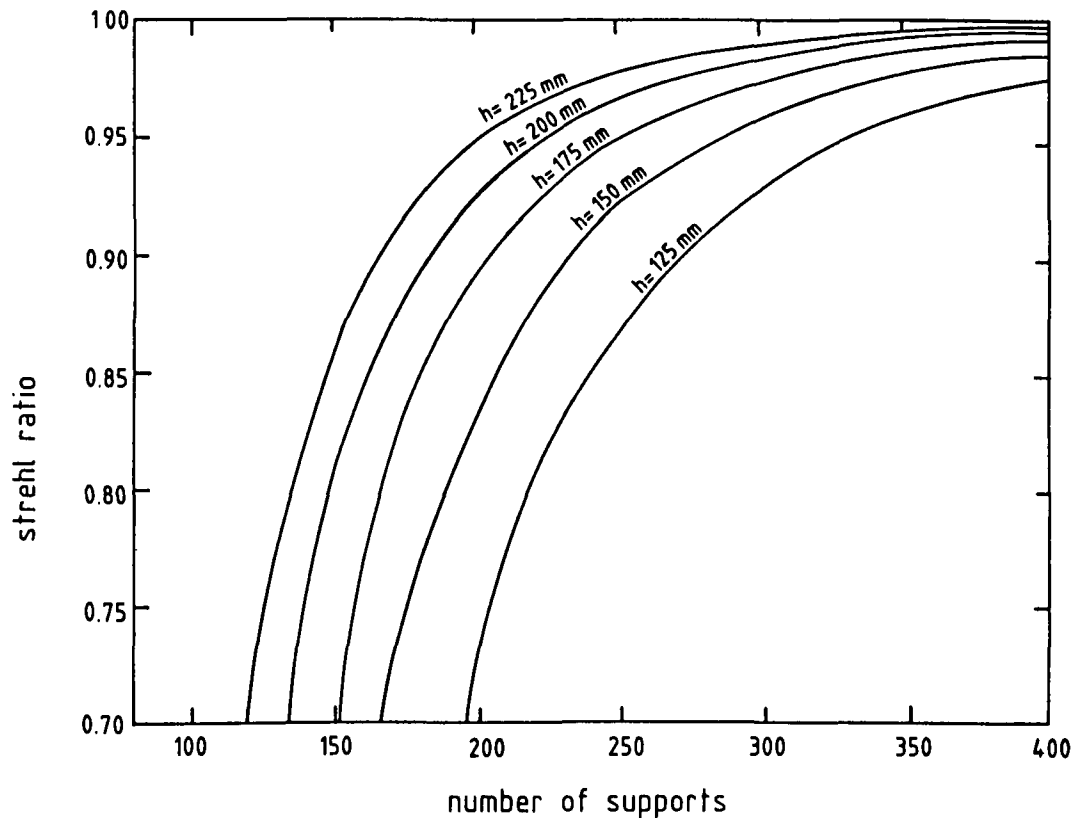


Figure 5.20: Strehl ratio versus number of supports of the image for a silica solid meniscus and for various thicknesses.

of axial supports will be about 150 for a 200mm thick mirror. The curves of Figures 5.19 and 5.20 are for silica. The results are however very similar for other types of glass.

### 5.4.2 Axial Support

The preliminary optimization of the mirror support system, which is the subject of the next chapters, is based on the following assumptions.

The primary mirror is a 200mm thick meniscus shaped mirror with an f-ratio of 1.8, an outer diameter of 8.2 metres, a central hole diameter of 1 metre and it is made of Zerodur having a Young's modulus  $E = 91000 \text{ N/mm}^2$ , a Poisson's ratio  $\nu = 0.24$  and a density  $\rho = 2.53 \text{ g/cm}^3$ .

The analysis of an optimum distribution of axial supports begins with the determination of the necessary number of support rings and the optimization of their radii.

The number of support rings can be estimated by the well known relation for the sag  $w_z$  in an infinitely extended flat plate on equally distributed support points (see Figure 5.21).

$$w_{1/2} = K_{1/2} \cdot \frac{p \cdot b^4}{D} \quad (5.15)$$

where

$$D = \frac{E \cdot h^3}{12(1 - \nu^2)} \quad (5.16)$$

is the bending stiffness of the plate and  $p = \rho \cdot g \cdot h$ , the constant area load (dead weight) of the plate. The coefficients  $K_{1/2}$  for the center point 1 and the half distance point 2 are  $K_1 = 0.00575$  and  $K_2 = 0.00431$  respectively.

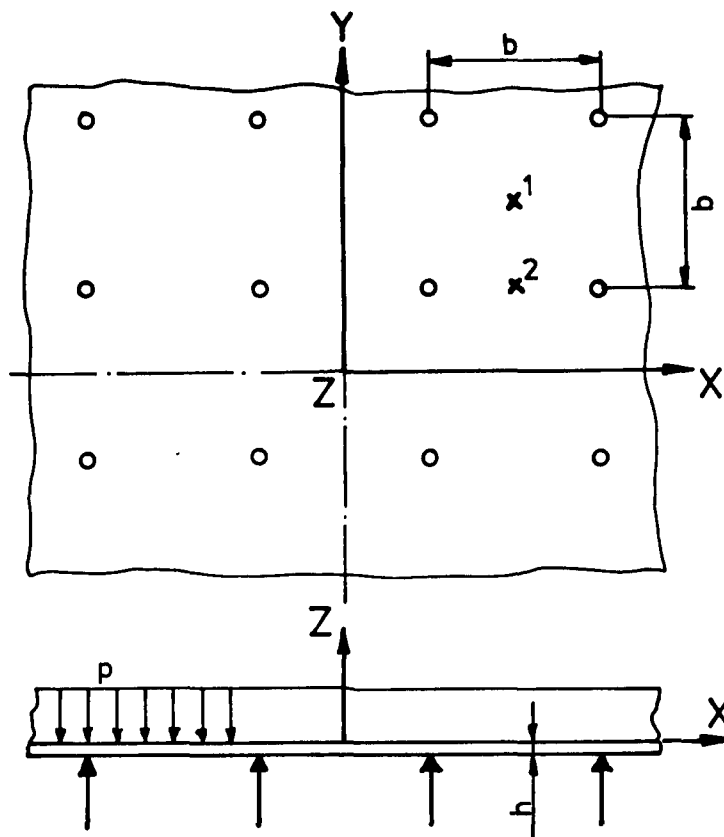


Figure 5.21: Infinitely extended plate on equally distributed supports.

Assuming a ring distance of 600mm, which corresponds to a 6 ring support system, the maximum peak-to-valley deflections would be

$$w_{z1} = 63.0nm \quad (5.17)$$

$$w_{z2} = 47.3nm \quad (5.18)$$

It has to be noted that the above estimation neither includes transverse shear nor the shell effect of the mirror. For the subsequent optimization of the support ring radii the above estimates (6 rings,  $\lambda/8$  peak-to-valley sag) have been taken as start values. In this second analysis step an axisymmetric finite element model of the mirror has been used. This model is plotted in the upper half of the Figure 5.22. The support ring radii have been optimized to get an equal sag distribution on the mirror surface. In five analysed models the support ring distance  $c$  (equidistant support rings assumed), the inner edge distance  $a$  and the outer edge distance  $b$  have been varied. The results of this optimization are summarized in Table 5.4, and the sag distribution in the final optimum model No 5 is shown in the lower half of Figure 5.22.

TABLE 5.4

<b>SUPPORT RING RADII OPTIMIZATION RESULTS OF FINITE ELEMENT ANALYSIS WITH AXISYMMETRIC MODEL</b>											
Model No.	Geometry			Axial Ring Load						Surface Deflection	
	a	b	c	1	2	3	4	5	6	p.v.t.	av.sag
	[mm]			[kg]							
1	300	300	600	1499	2659	3214	5033	5629	7672	180	42
2	255	250	619	1327	2750	3919	5142	6327	6836	56	47
3	265	250	617	1367	2746	3920	5134	6308	6830	53	46
4	275	250	615	1607	2742	3921	5125	6283	6824	52	45
5	285	245	614	1449	2744	3934	5125	6321	6736	50	46

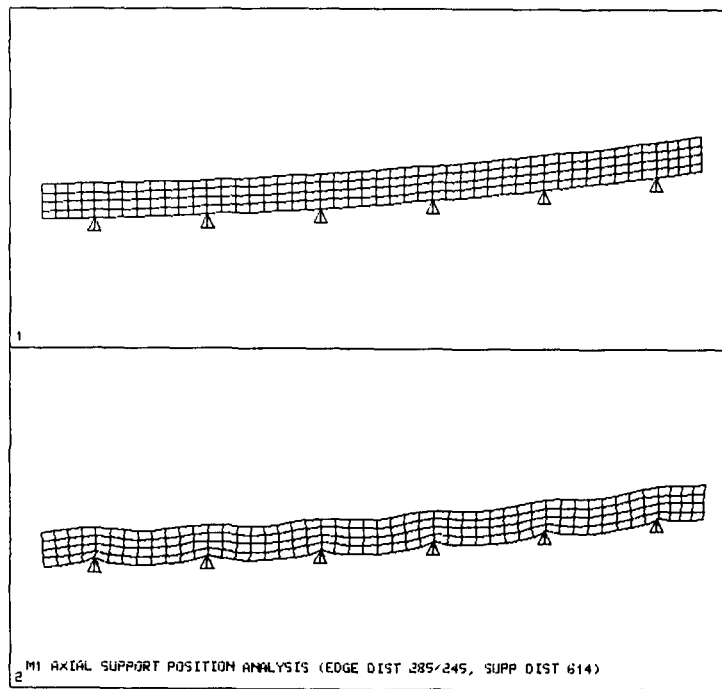


Figure 5.22: Axisymmetric finite element model for support ring radii optimization.

In addition, an analytical model which is based on the theory of a thin, shallow shell can be used for the optimization of the ring support. First, to check the agreement with the finite element calculations, the sag for the ring geometry from the finite element equal sag optimization has been calculated with the analytical model. The result is shown in Figure 5.23. Between the rings the sag is, indeed, constant, but the results differ from the finite element results (see Table 5.4, model No 5) in two points:

- The sag at the outer and inner edge is larger than the sag between the rings.
- The sag between the rings amounts to only 65% of the sag one would obtain when all physically relevant effects were included.

The reasons for the disagreements are the approximations which have been used in the analytical model:

- Shearing effects which increase the sag have been neglected.
- The sag data are averages over the thickness over the mirror instead of the surface deflections which are smaller.

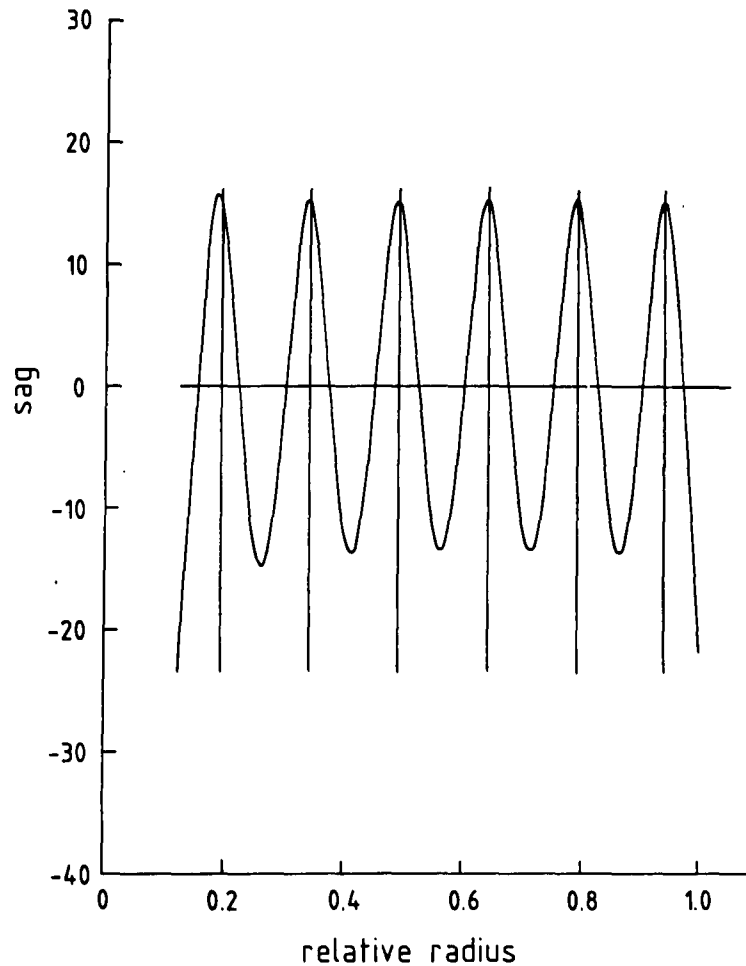


Figure 5.23: Wavefront aberration in the case of equal sag distribution optimization.

Using another three dimensional model for an infinitely extended plate supported on a rectangular pattern of slabs and choosing the distances of the slabs in one direction much smaller than in the other direction, then having effectively an infinitely extended plate on infinite parallel bars one can, by comparison with thin plate theory, estimate the effects of (a) and (b). For a thickness of a plate of 200mm and a distance of 614mm of the support bars these effects increase the sag by approximately 70% as compared with a thin plate. This brings the sag between the rings in good agreement with the finite element results. As the distances between the edges and the nearest rings (a and b of Table 5.4) are smaller than the distances between the rings (c of Table 5.4) the shear effects between the rings should be larger than near the edge. This explains why the analytical model slightly overestimates the sag near the edge as compared with the sag between the rings.

The comparison shows that the analytical model can well be used for further optimization of the ring support. The next optimization step differs from the first one in two points:

- One does not ask for constant sag but instead for a minimum root mean square value of the surface deflection.
- The overall surface deflection, i.e the deflection without the pattern of the ring support structure, is not forced to be perfectly flat but may instead follow a parabola.

The result of this optimization, which has been used for the NTT support as well, is shown in Figure 5.24. As a consequence of the relatively larger areas the sag between the outer rings is smaller than the one between the inner rings. The peculiar bending up of the surface deflection at the edge is a consequence of the fit to a parabola which would cause a change of the focal length of only 1mm. The effect of this optimization step is a reduction of the rms deflection of the surface by approximately 30% as compared with the first optimization step (Figure 5.23).

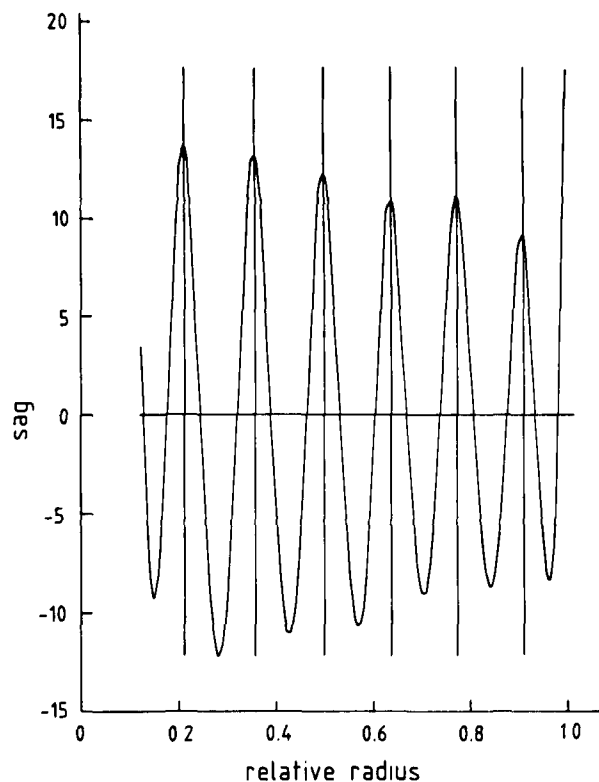


Figure 5.24: Wavefront aberration in the case of optimized rms value.

Up to now the mirror has been considered to be supported on knife edge rings. To study the effects of finite pads on the maximum sag between the supports, the axisymmetric model of the mirror has been modified as shown in Figure 5.25. Instead of point supports at the back surface, pads with a width  $d_p$  and a thickness  $t_p$  have been put under the mirror, and the element mesh of the model has been refined at the pad position, as shown in the zoomed plot in Figure 5.25. The sag between the support rings as a function of pad size is plotted in Figure 5.26. For a pad size of about 150mm the maximum sag is reduced by 35% and is of course zero for a continuous support with constant load distribution.

After having optimized the support ring geometry one has to determine the circular distribution of support points on the rings. Two main requirements constrain the optimization of the circumferential distribution of the support points: first, the sag in this direction should not exceed the one in radial direction and second, one should get at least a  $90^\circ$  symmetry in the distribution. Under these constraints a support distribution has been designed which is presented in Table 5.5. The total number of axial supports is 152 and the support pattern has a  $45^\circ$  symmetry. According to this geometry a finite element model of half the mirror has been created which is shown in Figure 5.27 together with the isocontour plot of the deformations on the mirror surface. The maximum p.t.v. deflection is 77.2nm at the outer edge of the mirror (on the x and y axes). The maximum sag between ring 1 and 2 is about 65nm.

The support forces given in Table 5.5 show first of all a good agreement between the axisymmetric analysis and the shell analysis of a half model of the mirror. The average support force is 175 kg with a variation of about 5% on the different rings. With respect to the sag between the supports this analysis is conservative because point loads are considered. As shown above, a finite pad with 150mm diameter can reduce the maximum sag by about 35%.

The active axial supports should compensate for gravity deflections (astatic effect), mirror figure correction (manufacturing low order effects, thermal effects) and wind loading. The basic idea is that the active optics scheme based on a variable distribution of forces should be extended so as to compensate also for rapidly varying effects such as the wind buffeting.

The force is measured directly from a load-cell located between the back of the mirror and the support. Position sensing from the mirror cell is not considered because the cell is likely to be more flexible than the mirror and therefore does not provide an adequate reference. Nevertheless a rigid connection between the mirror and the cell would be useful to reduce the amplitude of high temporal frequency disturbances mostly caused by wind buffeting. This approach differs from the classical flotation principle using astatic levers.

In order to increase the range of the active correction it seems desirable to adopt a push-pull system. This is only useful however, to compensate quasi-permanent errors

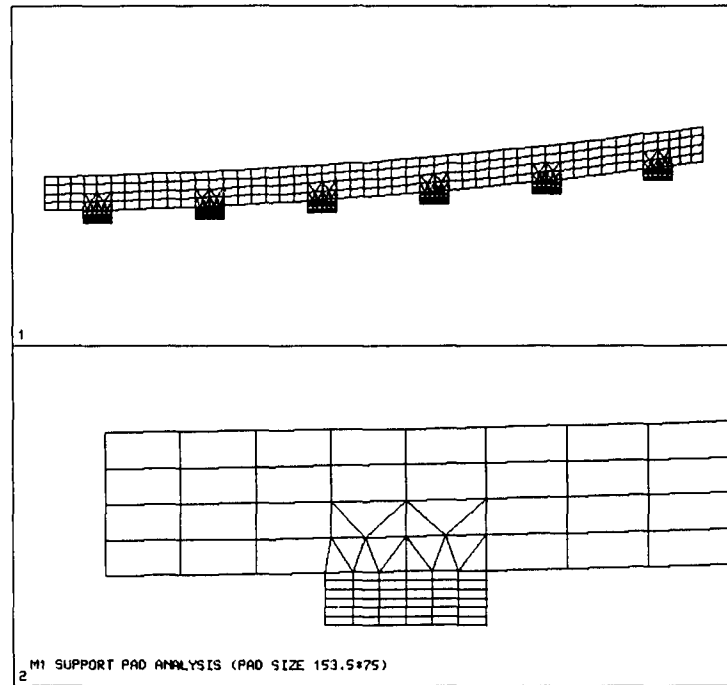


Figure 5.25: Finite element model for analysis of finite pad influence.

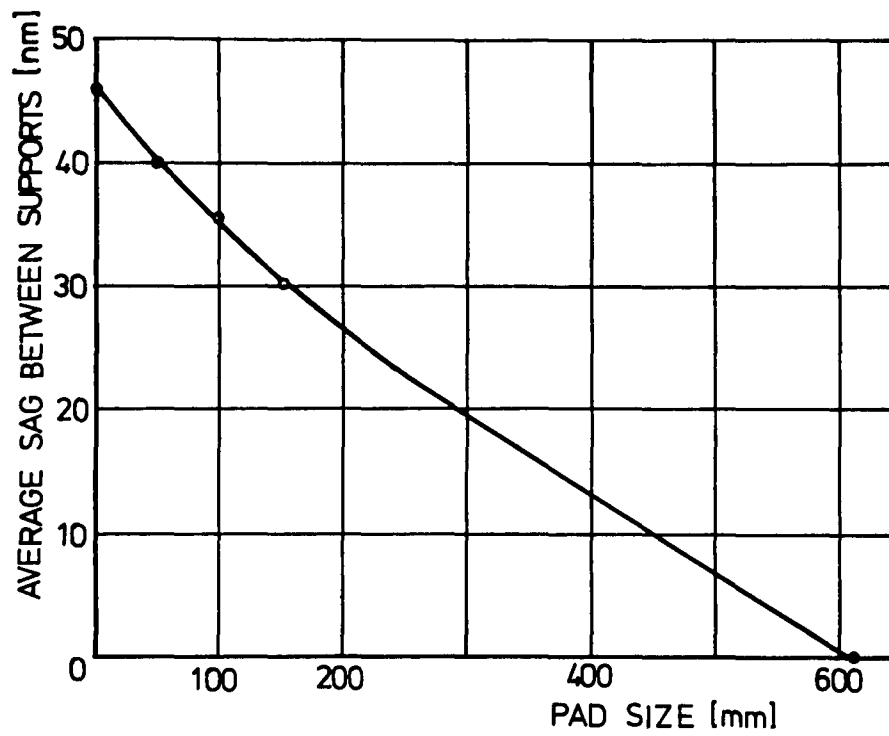


Figure 5.26: Sag between support rings as function of pad size.



TABLE 5.5

<b>AXIAL SUPPORT SYSTEM OF THE PRIMARY MIRROR WITH FORCE DISTRIBUTION</b> Comparison of axisymmetric ring force distribution with discrete point forces								
Ring No.	Radius		No. of Supp.	Angle [°]	Ring Force		Force Support [kg]	
	[mm]	[%]			[kg]	[%]	axisym	3-D model
1	785	19.15	8	45	1449	5.50	181.13	181.65
2	1399	34.12	16	22.5	2744	10.43	171.50	170.30
3	2013	49.10	24	15	3934	14.95	163.92	165.20
4	2627	64.07	28	12.86	5125	19.48	183.03	182.43
5	3241	79.05	36	10	6321	24.03	175.58	178.24
6	3855	94.02	40	9	6736	25.60	168.40	169.76
Total	4100		152		26309			

such as manufacturing errors and warping. The actual range of correction which includes the variation of gravity load with the telescope position (i.e. the astatic function from 0 to 100% of the mirror weight) may be of the order of -50%, +150% of the normal load. For the high frequency wind load correction one has considered that the system should be capable of modifying the load by 10% at a frequency of 3 Hz. The real requirements are, however, considerably less.

### 5.4.3 Radial Support

There are two different solutions for the radial support system of a thin meniscus mirror:

- Outer edge together with inner hole support.
- Distributed point support at the rear surface of the mirror or in the neutral plane.

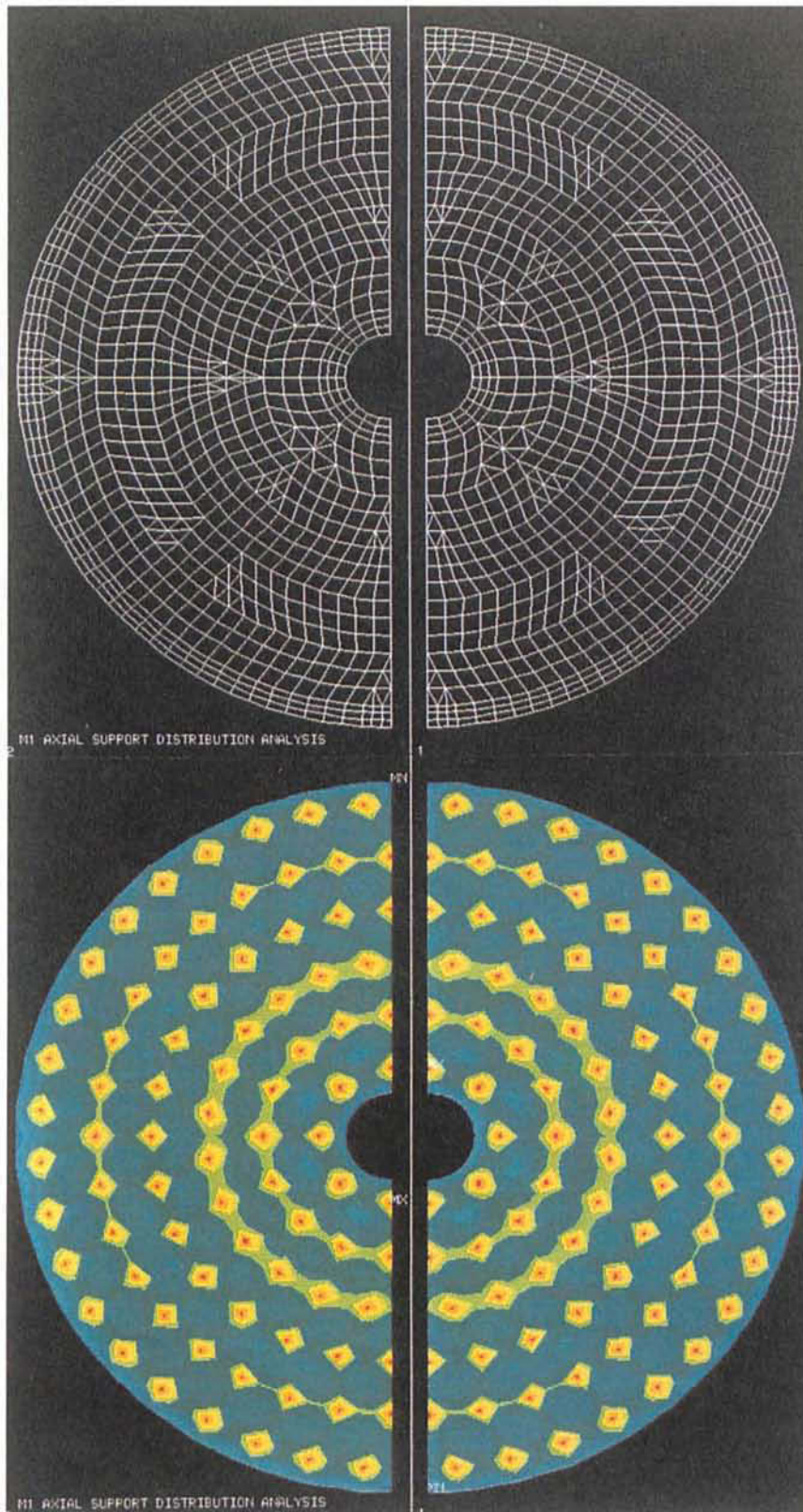


Figure 5.27: Finite element model of the axial support system - half mirror model.

Both support principles have advantages and drawbacks.

In the first solution, the edge support, a bending moment is introduced into the mirror, due to the fact that the edge support points cannot be placed in the plane of the center of mass of a thin and fast meniscus mirror. Due to that out-of-plane-loading third and fifth order coma is introduced in the mirror figure. By adding radial supports at the central hole of the mirror the bending moment and the resulting aberrations can be reduced. The advantage of the edge support is firstly, the strict separation from the axial support system which eases the design of the mirror cell and secondly, the better, because more direct, transfer of radial load to the centerpiece.

The alternative solution, to apply the radial supports at points of the rear surface of the mirror may on the one hand considerably reduce the overall bending moments in the mirror but requires on the other hand the machining of blind holes up to half the mirror thickness, which is a risky operation. Cementing blocks onto the surface for radial support fixation may be an alternative, but this way of load introduction will result in local bending moments and corresponding distortions in the mirror which cannot be corrected by active optics because of their high spatial frequency. Finally the distribution of radial supports on the rear surface also complicates the design of the mirror cell.

As active correction is foreseen for the primary mirror figure, the first solution i.e. outer edge plus inner hole radial supports, has been analysed in detail in order to determine the magnitude of forces necessary to correct the aberrations introduced by the edge support.

For the analysis of the radial support system the same finite element model as in the case of the axial support analysis has been used. At the outer edge 14 pull and 14 push supports and in the inner hole 5 push and 5 pull supports have been applied to the mirror model.

In the first analysis step it was assumed, that the mirror acts against the three axial fix points. The isocontour plot of the surface for that case is shown in the upper half of Figure 5.28. A polynomial wavefront analysis showed that the figure aberrations are predominantly 1st and 3rd order coma and to a lesser degree defocus and astigmatism. The maximum deflections occur at the lower and upper edge with  $+23\mu\text{m}$  and  $-13\mu\text{m}$  respectively.

In the second analysis step it was assumed, that the mirror figure is corrected by all axial supports to zero deflection at the support points. The resulting figure of the mirror is shown in the lower half of Figure 5.28. One can see a deflection between the two outer axial support rings with a peak of about 28nm. The maximum deflections occur at the edge beyond the 6th ring with  $\pm 80\text{nm}$ . It has to be mentioned that in the latter case of axial correction, additional axial correction forces have to be applied at the outer edge, because the deflections of the edge cannot be corrected by the outer support ring of the axial system. These additional axial forces can be applied by an astatic lever system working with a radial counterweight, so that the applied axial forces

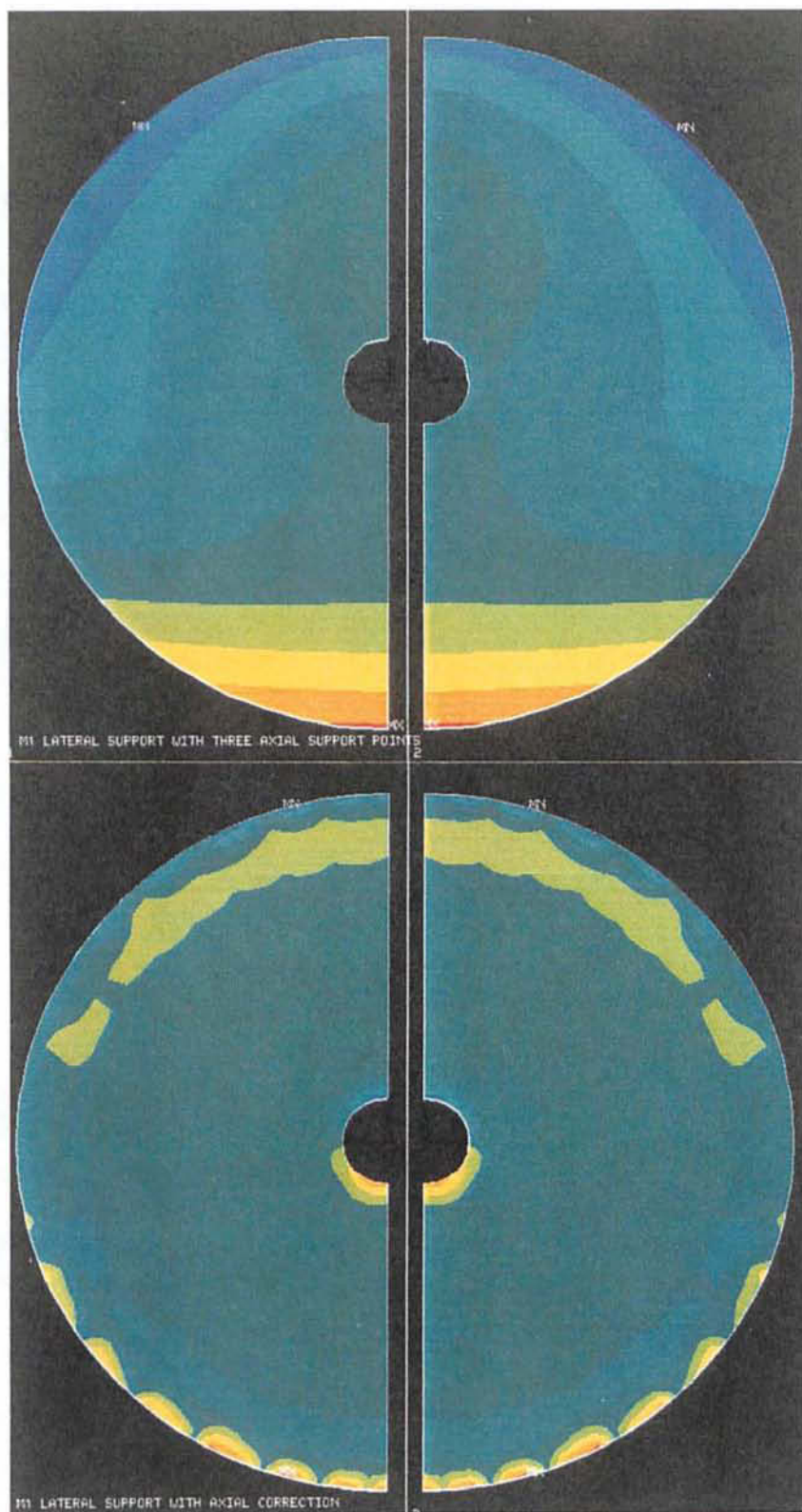


Figure 5.28: Mirror surface distortion in radial support condition. Top: Radial support-reaction on 3 axial fixed points. Bottom: Corrected surface with axial support forces.

are proportional to the sine of the zenith distance angle of the telescope. Therefore, if the mirror is in the horizontal position, the additional supports do not contribute to the axial support. They only correct aberrations produced by the radial support system. A sketch of the principle of the additional axial correction system is shown in Figure 5.29. The maximum axial edge correction force is 84 kg and the maximum active correction forces in the axial support system are  $\pm 35$  kg, which is 20% of the average passive axial force. The axial correction forces in general and the additional axial correction forces at the edge in particular can be significantly reduced if one allows a certain amount of third order coma to remain in the primary mirror. The optical effect of such an aberration can be corrected by a rotation or translation of the axis of the secondary mirror.

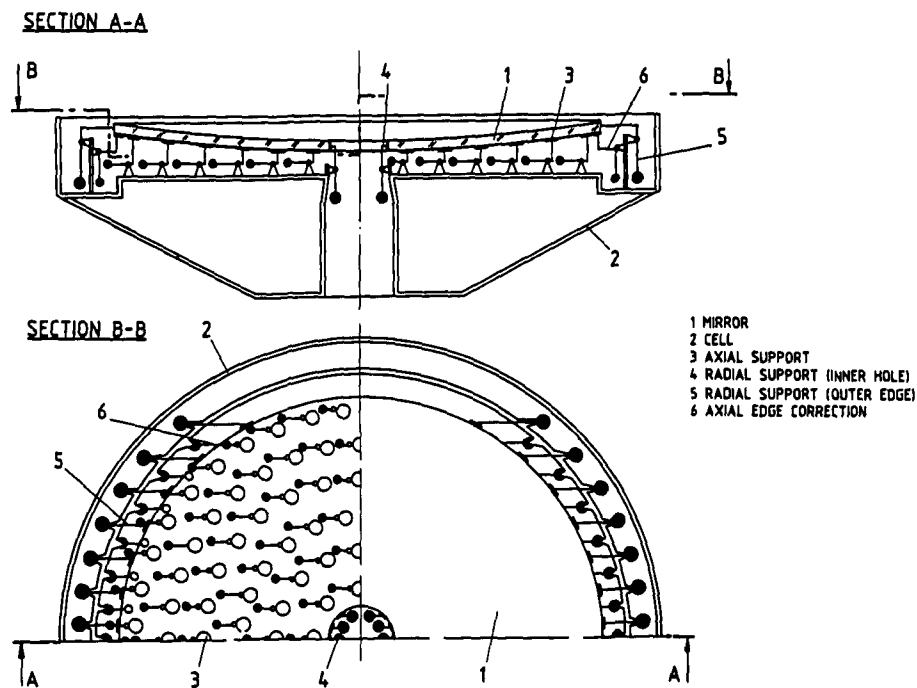


Figure 5.29: Possible support system for a thin meniscus. Radial support with axial edge correction.

The mechanical design of the radial supports could be totally conventional and use a single or multi-stage astatic lever or an astatic lever coupled to an hydraulic amplifier. A two-stage mechanical lever i.e with a reduction ratio of 20 and the above radial support system, which consists of 38 supports in total, would require counterweights of 34 kg per support.

A problem with pulling supports is their fixation at the mirror. Conventionally, pads on which the supports are then mechanically attached, are glued to the mirror back or edge. Alternatively, a wire can be cemented inside a small diameter hole drilled into the mirror. An attractive possibility presently considered for both axial and radial supports is the use vacuum chucks.

## 5.5 Mirror Cell

The mirror cell should be very stiff so that together with the use of dynamically rigid supports, a good coupling of the mirror to the cell is obtained and deformations due to quasi-static and dynamic wind loads are minimized. The structure of the primary mirror cell depends on the axial and radial support distribution of the mirror. For reasons of weight minimization and natural ventilation as well as small wind-attack cross-sections the primary mirror cell will be a space frame construction. The design concept of the mirror cell is similar to recent designs of radio-reflector support frame structures. The choice of the material depends to some extent on the material selected for the mirror blank. With a silica or Zerodur mirror, carbon fibre plastic tubes are attractive because of the good matching of the thermal expansion for both materials. For the same reason a metal mirror would be better matched with a cell made of the same metal.

For the first preliminary design and analysis of the cell structure it has been assumed that the primary mirror is a thin glass meniscus supported axially by about 220 pads, which are arranged on 7 rings and radially supported by about 70 support points distributed on the rear surface of the mirror. The last optimization of the mirror support described in the previous paragraph has shown that probably 6 rings would be sufficient. The following analysis of the cell model is therefore not strictly valid anymore. However the results are not expected to differ much, so that the reader can find hereafter an overview of the static and dynamic cell behaviour. For this configuration the total load on the cell is 25000 kg.

The main cell structure consists of 12 radial ribs, which are connected by 8 rings on the top and 4 rings at the back of the cell structure. The inner 7 rings on the top provide the base for the axial and radial supports. Vertical and diagonal bracings between the top and bottom rings stiffen the structure. The connections of the centerpiece structure are provided by tripod structures at the outer top ring of the cell. The central hole of the cell has a diameter of 2 metre and may accept a Cassegrain adapter and instrument. The overall height of the cell structure is 2.75 metres including the connection bars to the centerpiece.

The finite element model, which has been prepared for the static and dynamic analysis of the cell, is shown in Figure 5.30. The cell structure deflections have been calculated for a steel and a carbon fibre structure. The static deflections of the steel cell for zenith and horizon position due to gravity are shown in Figures 5.31 and 5.32, respectively. The maximum deformations are 1.1 and 0.79mm respectively and the mass of the structure is 5000 kg. With carbon fibre one can reduce the deflections to about 50% and at the same time reduce the mass to about 3500 kg.

When the telescope is in operation, the primary mirror cell and consequently the mirror may suffer from vibrations which are induced by the drives and the wind forces. It is important to study the dynamic performance of the cell, i.e its natural vibration modes, to make sure that no resonances can occur.

The results of the analysis are summarized in Table 5.6.

TABLE 5.6

<b>NATURAL VIBRATION MODES AND EIGENFREQUENCIES OF THE CELL</b>			
<b>Mode No.</b>	<b>Frequency (Hz)</b>	<b>Mode No.</b>	<b>Frequency (Hz)</b>
1	9.83	8	26.0
2	15.7	9	26.5
3	16.8	10	31.1
4	18.0	11	31.3
5	20.7	12	32.7
6	20.7	13	33.4
7	23.2	14	35.7

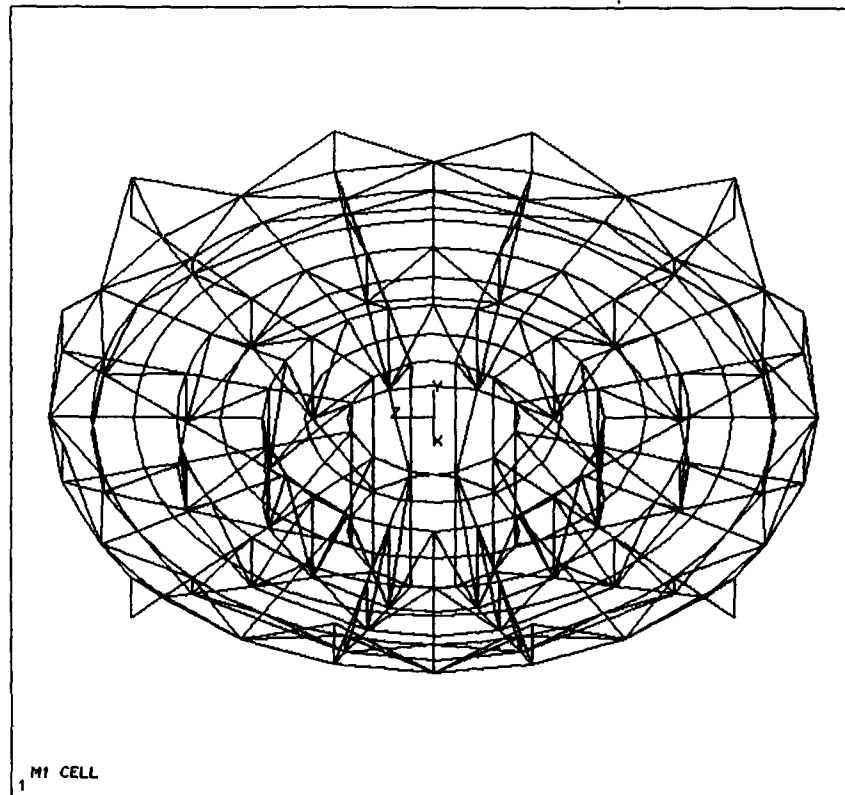


Figure 5.30: Finite element model of the mirror cell.

The eigenmodes 1 and 2 are plotted in Figures 5.33 and 5.34, respectively. The first eigenmode is a rotation in the cell structure around the optical axis (see top view of cell in Figure 5.33) and it occurs at 9.8 Hz. Since there is no component of deformation in the vertical direction, this eigenmode has no effect on the mirror and the image. The second eigenmode with a frequency of 15.7 Hz (see Figure 5.34) is a lateral cell deflection superimposed by an axial bending deflection of the cell top surface where the supports are attached. The latter deflection is similar to a coma deformation of the mirror. The higher modes are basically bending modes of higher order.

The mirror cell will include provision for washing the mirror periodically (approximately every 2 or 3 months). This is important for IR performance and to extend the life time of the coating. The washing facility will probably consist of a circular spraying device located at the mirror periphery and of a central collection of the liquid through the central hole. Mirror 3 will be washed simultaneously. Introduction of a temporary or permanent Cassegrain facility would complicate the design of the central part of the cell.

The mirror cover may be of a high strength plastic fabric rolled on one or two sides of the cell. Correctly stretched, such a cover would provide an efficient mirror protection, and would not significantly increase the weight.



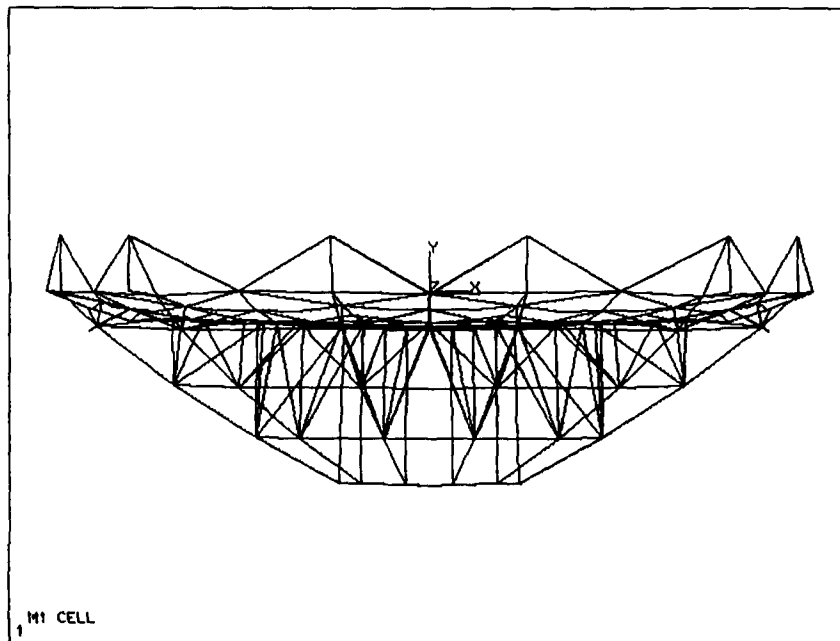


Figure 5.31: Static deflection of the cell with the tube in zenith position. Maximum deflection 1.1mm.

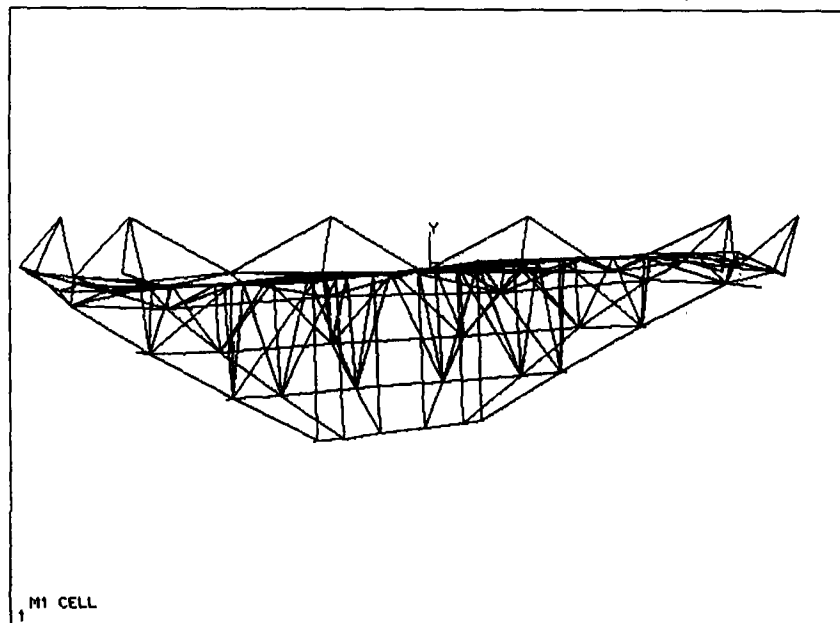


Figure 5.32: Static deflection of the cell with the tube in horizon position. Maximum deflection 0.79mm.

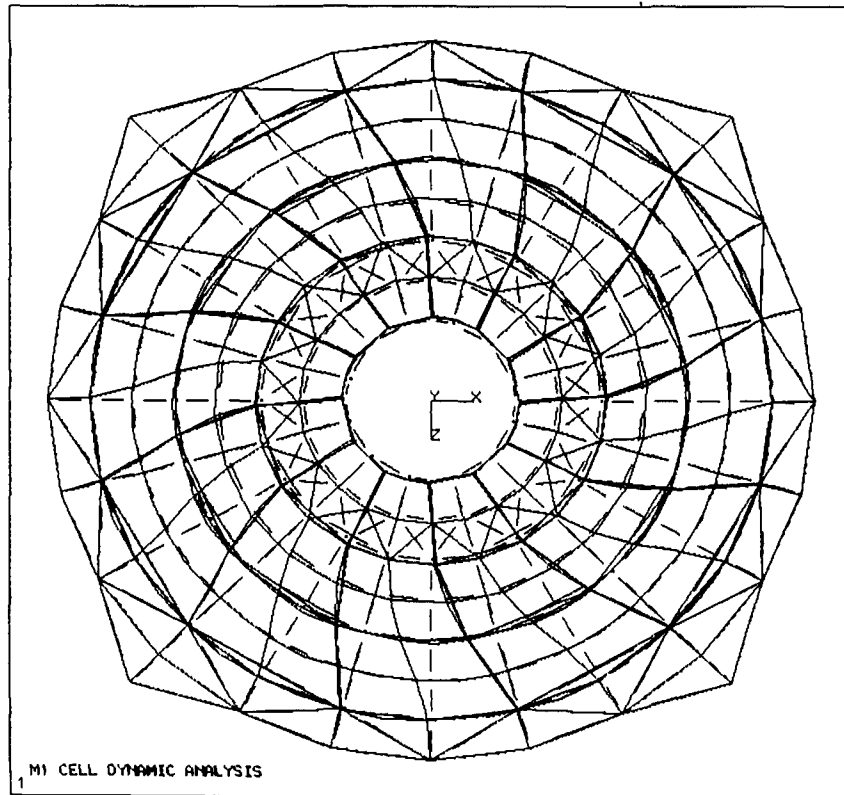


Figure 5.33: First eigenmode of the mirror cell (top view). Frequency 9.8 Hz.

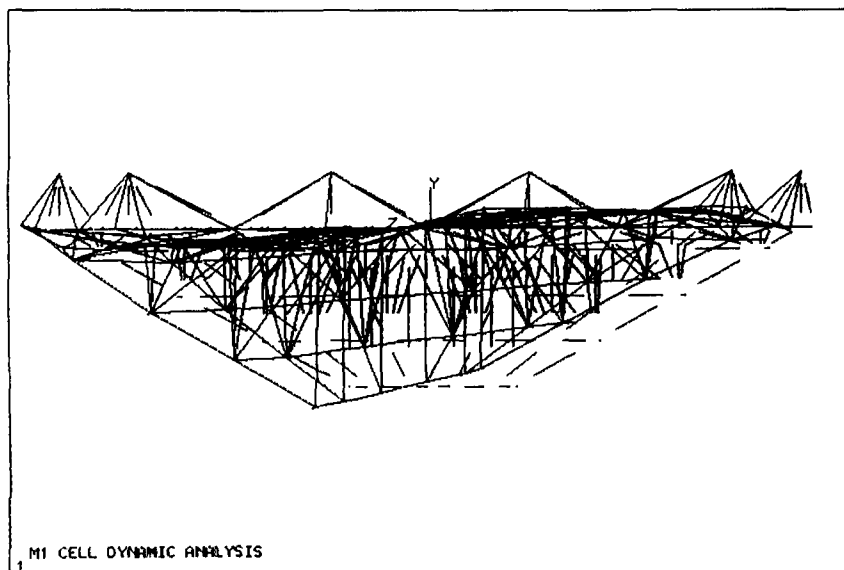


Figure 5.34: Second eigenmode of the mirror cell (side view). Frequency 15.7 Hz.

## 5.6 Thermal Aspects

Both internal and external thermal equilibrium are important. The latter has mainly an influence on thermal turbulence above the mirror which can considerably degrade the optical performance. The internal equilibrium is important to avoid figure distortions and possible print-through of the internal blank or support structure to the mirror surface.

The equilibrium of the mirror temperature with the ambient air is important when the telescope is embedded in a dome. It has been shown that  $1^{\circ}\text{C}$  of temperature difference of the mirror with respect to the air may cause about 0.5 arcsecond image degradation. With a telescope in the open air stream, differences of a few degrees will probably remain unnoticed. This is clearly demonstrated by Figure 5.35 which illustrates an experiment performed at ESO on an aluminium mirror. Though heated up to  $30^{\circ}$  above ambient, the original wavefront is nearly retrieved when the surface is slightly ventilated (about 0.2 m/sec). The problem with a solid meniscus made out of silica, which has a low thermal expansion and poor conductivity is mainly the thermal capacity and the long time constant. Nevertheless, because the thickness envisaged

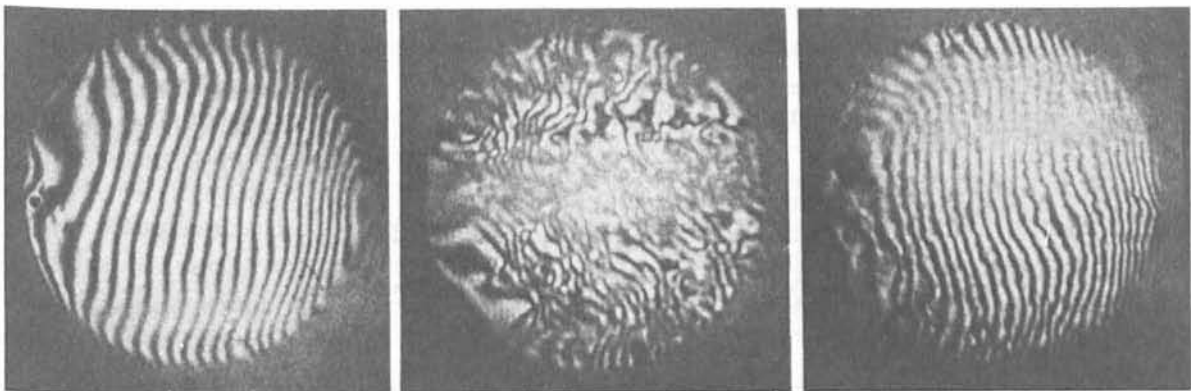


Figure 5.35: Effect of ventilation on air turbulences generated above a mirror by a difference of temperature between the mirror and the surrounding air. A 500mm aluminium mirror was heated up to  $30^{\circ}\text{C}$  above ambient. A slight ventilation almost suffices to eliminate the effect of stagnating unstable layers of air.

is nearly a factor of 3 less than that of existing conventional glass mirrors, the time constant will be nearly 10 times lower. An active control, mostly cooling will however be necessary if large temperature variations from one night to the next have to be considered. Figure 5.36a shows the effect of a moderate cooling of  $24 \text{ W/m}^2$  on the back surface for 8 hours. An internal gradient of  $1.5^\circ\text{C}$  is created but after 4 more hours has nearly disappeared. The average temperature of the blank has then decreased by 2 degrees. It is not expected that the night air temperature would vary by more than that over 24 hours intervals. To the extent that night temperature can be predicted, it is possible with an air cooling to bring the temperature of the mirror to the average night temperature. Figure 5.36b shows the mirror temperature assuming only free convection exchanges on both faces and radiative cooling on the mirror surface. Radiative cooling is low because of the reflective coating but corresponds nevertheless with a 2% emissivity to about  $6 \text{ W/m}^2$ . Internal gradient is less than  $0.3^\circ\text{C}$  and the average temperature difference with air less than  $1^\circ\text{C}$ .

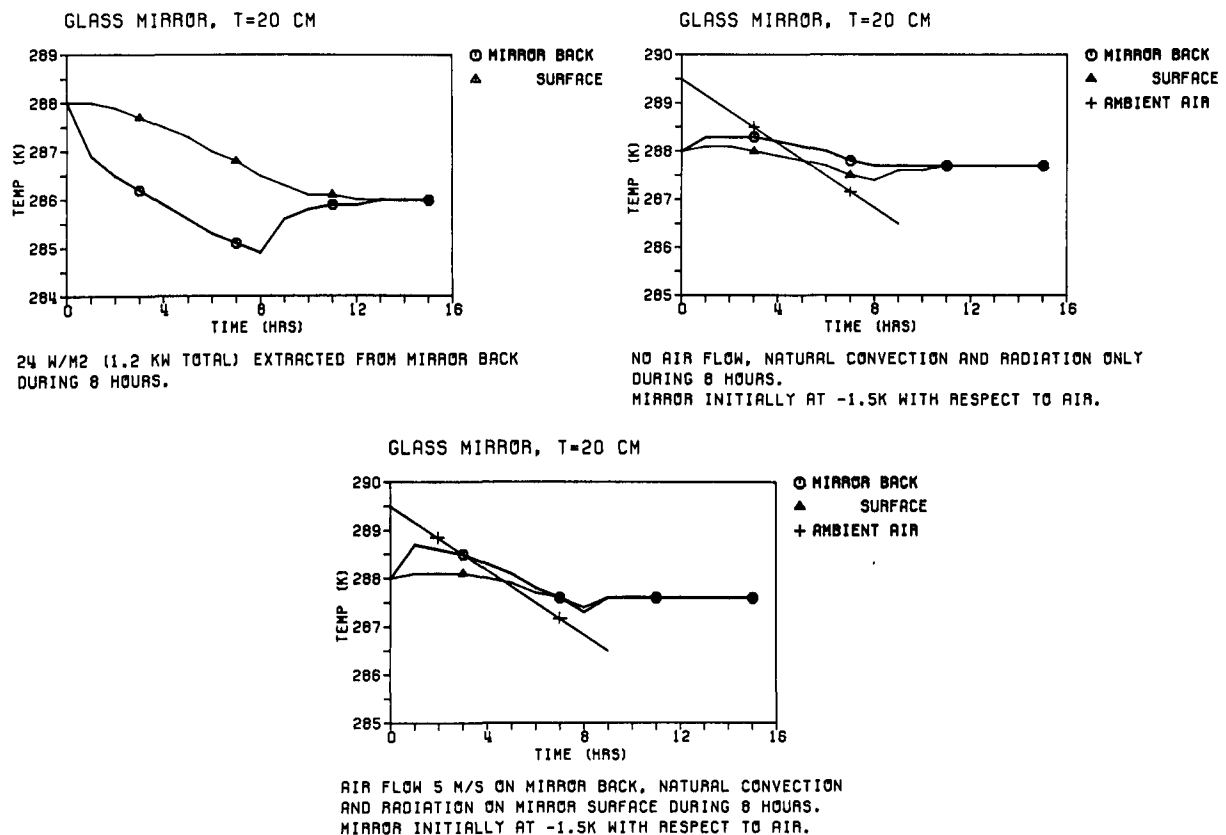


Figure 5.36: Thermal behaviour of a glass meniscus mirror; 36a (upper left), 36b (upper right), 36c (lower).

A perhaps more realistic case is shown by Figure 5.36c where one has assumed a natural air flow at 5 m/sec on the back face. Starting from a mirror temperature 1.5°C below air at the beginning of the night one gets a temperature equilibrium after 5 hours.

The strategy for a solid meniscus would then be to rely on an active cooling of the back face during the day to bring the mirror temperature to the expected midnight temperature and during observing to rely only on natural convective and radiative couplings. Neither the remaining internal gradient nor the temperature difference with ambient air are expected to be a limitation because of the low expansion of the material and of the open air operation of the VLT.

## 5.7 Handling

During its lifetime the primary mirror will experience several different handling operations which begin with the lifting of the blank out of the mould. After that the mirror has to be carried and transported to the optical shop, where it will be lifted and turned several times for final figuring before it is integrated into the mirror cell for installation in the telescope.

The nature of the risk in handling the primary mirror depends on the material and on the structure of the mirror.

For metal mirrors the risk is not of breakage but of permanent deformations that could occur if the microyield strength (MYS) is approached. A maximum stress of 50% of MYS is considered appropriate to avoid any permanent deformation. Preliminary analysis shows that with proper handling procedure, this limit should not be exceeded either with aluminium or with steel.

The situation is more complex with glass which in theory is perfectly elastic up to the point of fracture. The maximum stress value corresponding to a fracture cannot be easily determined because it depends on several factors such as the surface quality (possibility of propagation of cracks) of the time the load is applied, and the dimension of the surface under stress. For instance Schott indicates for Zerodur a 0.5% probability of fracture for a surface of 1 m<sup>2</sup> submitted to a load of 22 N/mm<sup>2</sup> during a full year. A practical limit of 5 N/mm<sup>2</sup> is recommended for handling stresses although a higher load applied for a short time is extremely unlikely to produce a failure.

For silica, Corning recommends a maximum stress of 7 N/mm<sup>2</sup> which is higher but comparable to the 5 N/mm<sup>2</sup> for Zerodur.

For a 200mm thick Zerodur meniscus blank a handling stress analysis has been performed for three different handling configurations, namely: lifting at 3 points, lifting in a carrying frame where the mirror is kept at the outer and inner edge, and upside down turning in a frame with 2 x 9 axial pads and a radial support belt at the outer edge. For the stress analysis a special finite element model Figure 5.37, with three

dimensional volume elements of half the mirror has been established.

A summary of the results of these analyses is given in Table 5.7, which shows the support configurations, the maximum peak-to-valley deformations that occur and the maximum and minimum principal stresses together with the equivalent stress which is given by the relation

$$\sigma_e = \frac{1}{\sqrt{2}} \cdot [(\sigma_1 - \sigma_2)^2 + (\sigma_2 - \sigma_3)^2 + (\sigma_3 - \sigma_1)^2]^{1/2}. \quad (5.19)$$

The absolute maximum stresses are the compression stresses ( $\sigma_3$ ) which occur directly at the load introduction points. This is also illustrated in the isocontour plots of the stress component  $\sigma_3$  in the lower half of the plots in Figure 5.38, which shows the results of the analysis for the 3-point support and the lifting device. In the upper half of the plots the surface sag is shown. The maximum compression stresses are indicated by the dark blue spots on the surface of the mirror.

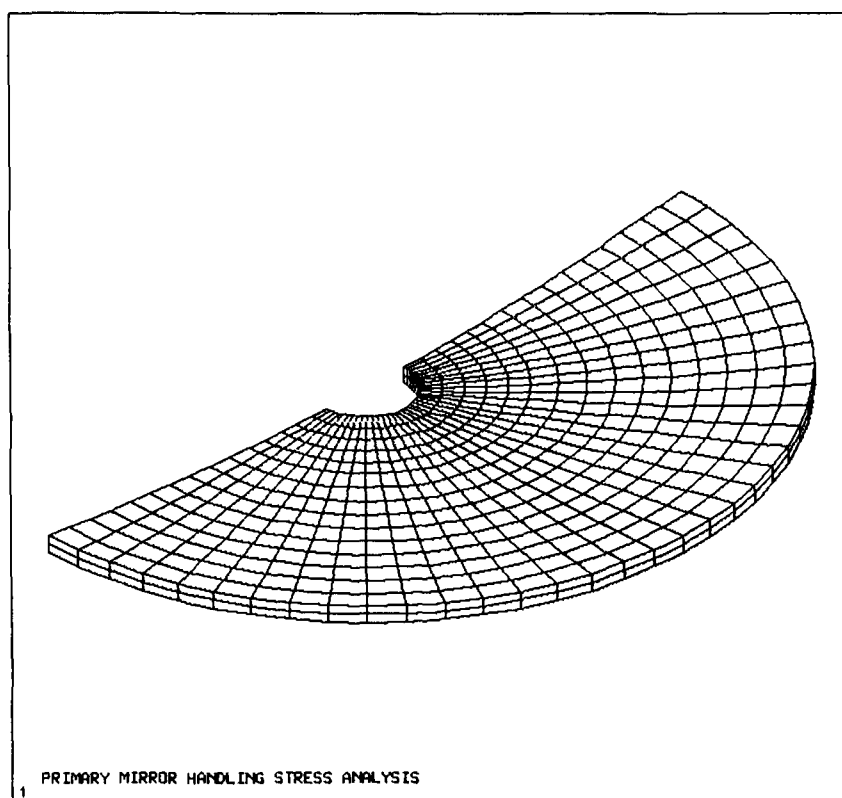
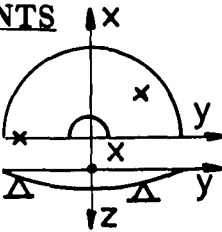
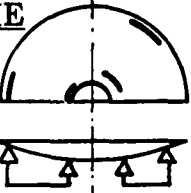
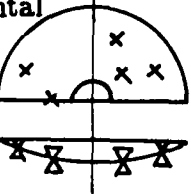
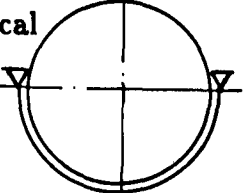


Figure 5.37: Finite element model for handling stress analysis.

TABLE 5.7

<b>HANDLING STRESSES AND MAXIMUM DEFLECTIONS IN THE PRIMARY MIRROR</b>					
for three different handling conditions					
HANDLING DEVICE CONFIGURATION	LOAD DIRECTION	MAXIMUM DISPLACEM. $\Delta\delta$ [mm]	MAXIMUM STRESSES		
			EQUIV. $\sigma_e$ [ $\frac{N}{mm^2}$ ]	PRINCIPAL	
				$\sigma_1$ [ $\frac{N}{mm^2}$ ]	$\sigma_2$ [ $\frac{N}{mm^2}$ ]
<b>3 POINTS</b> 	+1g	1.06	3.64	3.48	-4.38
<b>CARRYING FRAME</b> 	+1g	0.41	2.72	1.82	-2.74
	-1g	0.41	2.53	2.79	-1.89
<b>TURNING FRAME</b> horizontal 	+1g	0.50	2.25	2.03	-2.91
	-1g	0.50	2.45	2.26	2.74
	vertical 	1g	0.23	0.61	0.37

It has to be pointed out that the analysis is conservative in the sense that the load introduction into the mirror is considered to be realized by point or knife edge supports. The use of adequate pads will considerably reduce the stress level as has been shown in Section 5.4.2 for the axial support case.

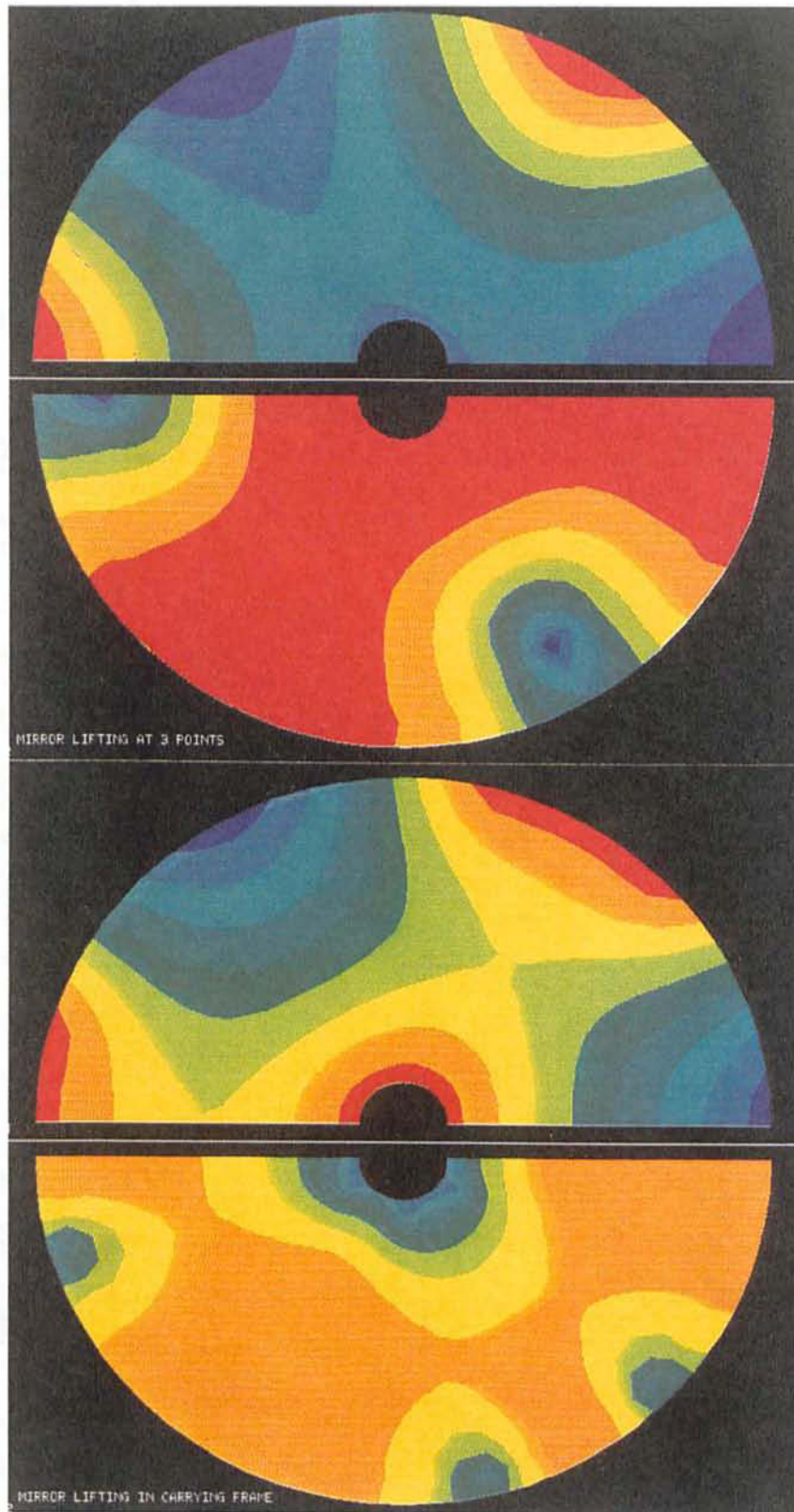


Figure 5.38: Deformation (upper half) and principal stress  $\sigma_3$  (lower half) plots for 3 point and carrying frame support.



Nevertheless, the maximum stresses calculated with the conservative point support approach are already below the acceptable stress level of  $5 \text{ N/mm}^2$  for Zerodur. But one has to be careful when specifying allowable additional loads, i.e. by shocks, especially in the case of a 3-point support of the mirror.

For transportation, the load can be spread uniformly over the mirror surface so that even large accelerations could be applied. Transport of the mirrors to the main optical suppliers premises from a waterway has been investigated and found possible up to 8 metres. A 10 metre mirror would on the contrary pose much more drastic difficulties and would involve a much higher cost for transportation.

# Chapter 6

## MECHANICAL DESIGN

### 6.1 General

The unit 8m telescopes have alt-azimuth mounts of relatively classical architecture. The open air operation, which will reduce the cost of the building and improve the local seeing, has an important impact on the design of the mechanical structure.

The main design drivers for the telescope structure are:

- low cost lightweight structure,
- low thermal inertia,
- small wind attack cross-section,
- high reliability and
- rapid availability

The present design is based on standard steels available in commercial sizes. In a subsequent study phase, the use of composite materials will be analysed. It is already clear that carbon fibre reinforced plastic materials would be of great advantage for the construction of the mirror cell and the M2 and M3 spiders and are likely to be used. Other parts of the structure could also be built with composite materials if their cost would go down by a significant factor during the forthcoming years.

The two main parts of the alt-azimuth 8 metre telescope structure are the tube and the fork, together with the interface support ring to the concrete pillar.

The tube of the telescope serves as an optical support structure with the task to ideally maintain a zero-pointing error condition when the telescope moves in the gravity field. The design of the tube follows the principle of stiffness and weight optimization in order to minimize the static elastic deflections due to gravity loading and consequently

the hysteresis effects, which cannot easily be corrected by a pointing model. Concerning the dynamic behaviour of the telescope tube, the first structural eigenfrequencies should be as high as possible, in order to maximize the frequency response of the telescope drives. In order to minimize the effect of wind loading on the structure, the design was concentrated on space frame type structures instead of closed box type structures, wherever possible. Besides the better performance with respect to wind loading the truss design concept offers the advantage of low thermal inertia. In the design of the tube structure, the optical elements, i.e. the primary mirror cell, the secondary and tertiary mirror units, are regarded as "black boxes" with geometrical interfaces and masses as given below:

Primary mirror unit M1:

- diameter of cell	9.5	metre
- height of cell	2.75	metre
- total mass	30.000	kg (incl. the mirror)

Secondary mirror unit M2:

- diameter of unit	1.2	metre
- diameter of mirror	1.27	metre
- height of unit	1	metre
- total mass	2.000	kg

Tertiary mirror unit M3:

- diameter of unit	1.0	metre
- diameter of mirror (projected)	1.14	metre
- height of unit for spider attachment (appr.)	1	metre
- total mass	2.500	kg

During the design of the tube structure, the possibility of exchanging top units was not considered as mandatory, but, if necessary, the conceptual design allows without major alterations the exchange of top units and/or complete top ring assemblies. In order to provide observation on two Nasmyth stations the M3 mirror should be able to rotate 180° around the optical axis. The necessary free beam path diameter in the altitude bearing shafts is 1.2 metre, which defines the minimum size of the altitude bearings.

When moving the telescope from zenith to horizon, the tube structure has to keep the mirrors in place within tolerances or allowable static deflections which are given in the following Table:

Mirror	Deflection	Tilt Angle
M1	2 mm	20 arcsec
M2	2 mm	1 arcmin
M3	1 mm	1 arcmin

The deflections, which are perpendicular to the optical axis, are assumed to compensate so that the resulting net deflection between M1 and M2 is less than 1mm. This can be reduced to zero during final optimization. The specified tilt angles are around the altitude axis. The static deflections and rotations of the optical elements specified above are not critical, because active correction of the primary and secondary mirror is foreseen in the design of these units.

The fork serves as a support structure for the tube. Its main functions are to carry the telescope tube, to transfer the load from the altitude to the azimuth bearings, to carry the Nasmyth platforms, to transfer the load of the Nasmyth instruments to the azimuth bearings, and to provide the attachment for the Coudé tubes. The design goal for the fork structure was to optimize the stiffness-to-weight ratio in order to minimize the elastic deflections and consequently the hysteresis effects, which are related to the deflections. The structure has to be sufficiently stiff to guarantee a proper tracking stability under all loading conditions. As in the case of the telescope tube the fork is designed as a truss structure in order to minimize the reactions to wind loading and to provide a thermally fast structure.

The fork design allows a rotation of the telescope around the azimuth axis of  $\pm 270^\circ$ . The two Nasmyth platforms attached to the fork can carry loads up to approximately 4 tons per platform. The interface support ring to the concrete pillar of the VLT building provides the support for the track of the azimuth axial bearing.

A drawing of the telescope structure including the support ring and azimuth tracks is shown in Figures 6.1 and 6.2.

## 6.2 Tube

### 6.2.1 Structure

The design of the tube structure (see Figure 6.1 and 6.2) is based on the classical solution with Serrurier struts for the upper tube and flexion bars for the attachment of

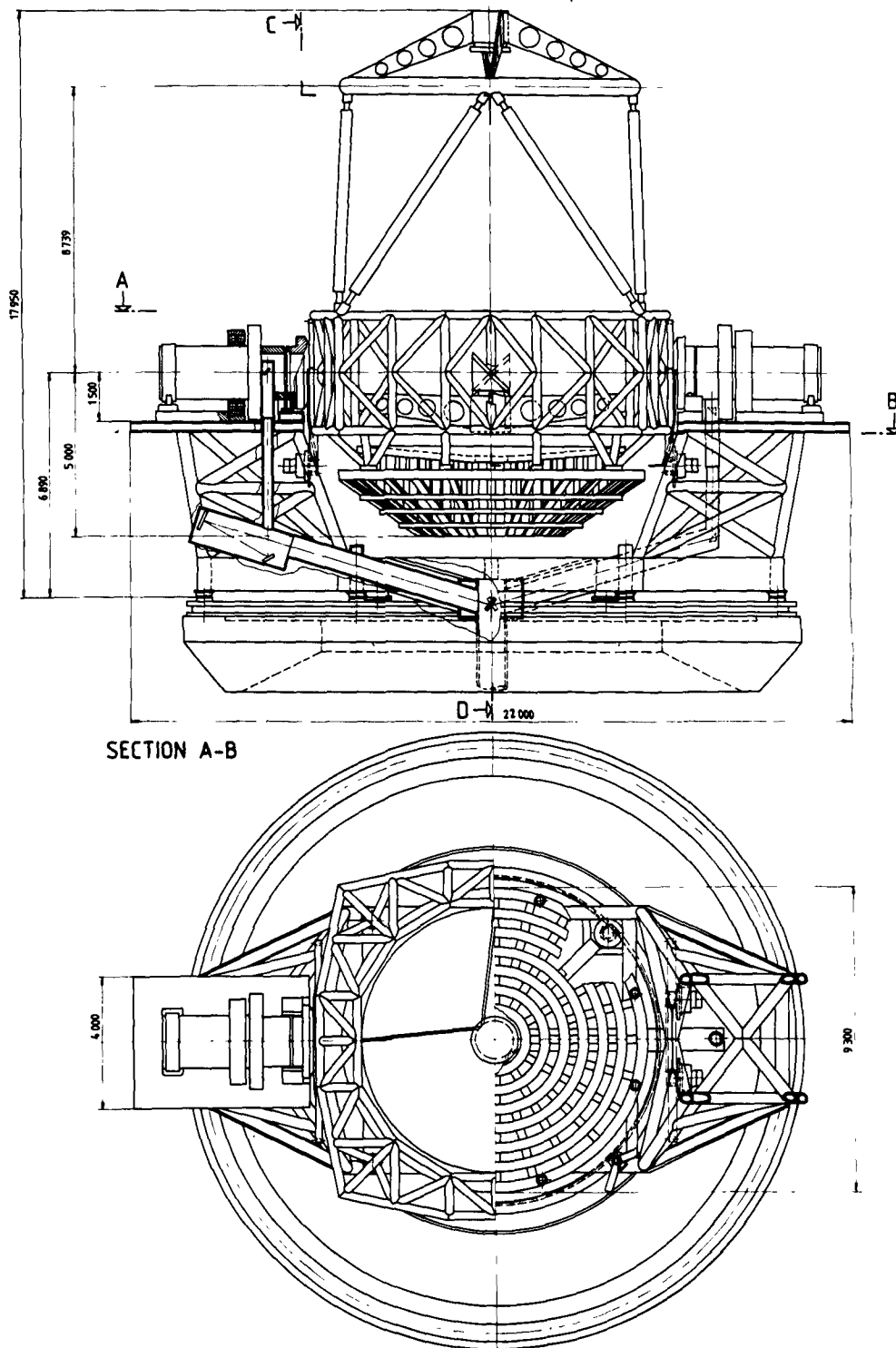


Figure 6.1: Design of the telescope structure. (Front view and top view). This drawing corresponds to the latest optimization (January 1987); the structure differs slightly from the model shown in Chapter 2.

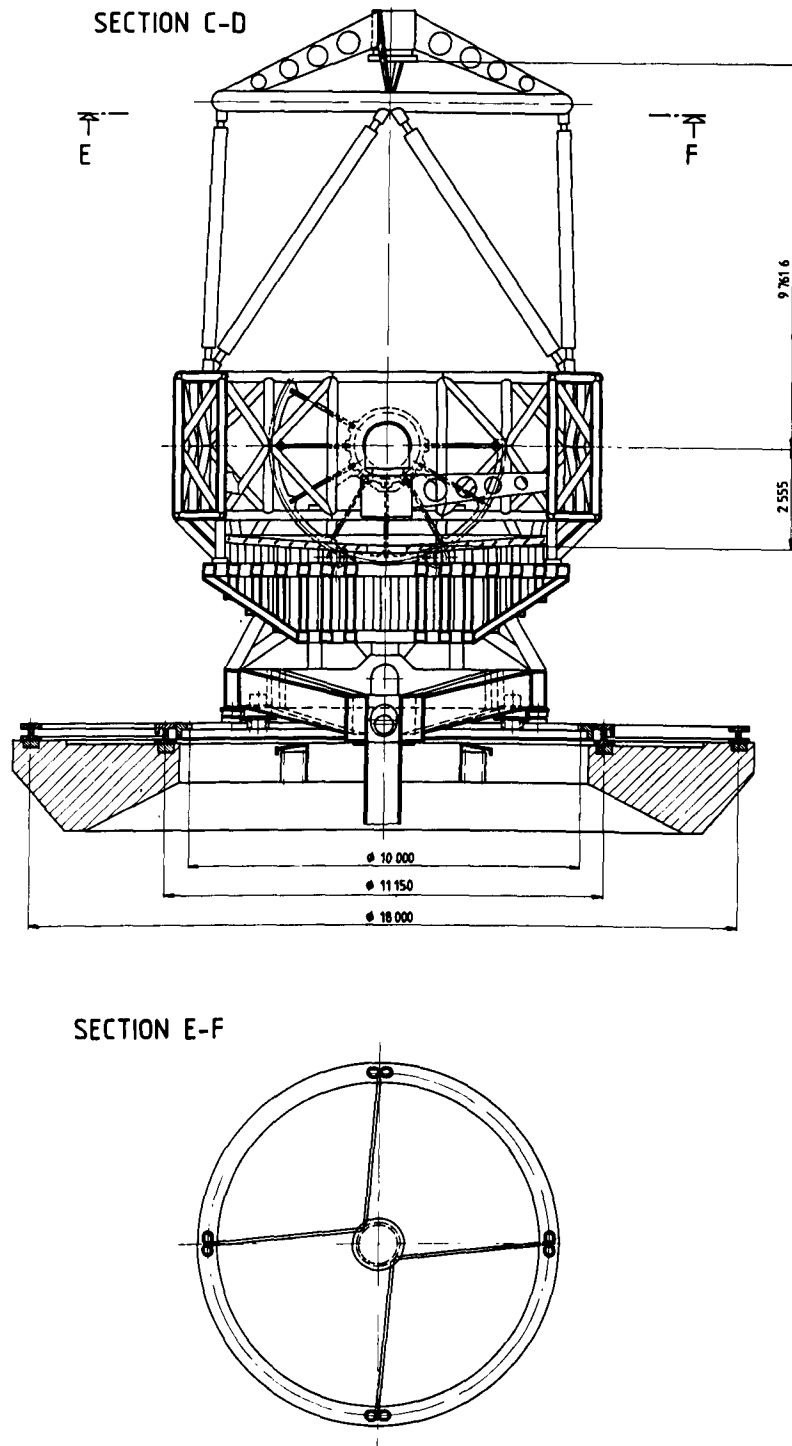


Figure 6.2: Design of the telescope structure. (Side view).

the primary mirror cell. To enhance the stiffness of the M1-cell-to-centrepiece connection, 8 additional structural members were added. The Serrurier struts are made of circular tubes.

The centrepiece is an open truss design with tubular members which are systematically arranged along the system lines. The tube joints are welded connections without any additional connecting elements like gusset plates. With its final dimension of 10.8 metres in diameter and a height of 3.5 metres, the centrepiece has a size where assembly and welding of the entire trusswork on site is the most economic procedure. A breakdown of the structure into four subassemblies can be envisaged when a preassembly in Europe is required.

In the case of a field erection of the centrepiece, the pre-cut truss members and the fixing tube for the altitude bearing trunnion are assembled and welded on-site without a final stress annealing of the entire trusswork. The fixing tubes for the bearing trunnions are annealed and machined in the workshop before shipping. The fixing points for the Serrurier struts and flexion bars are welded to the centrepiece. No extra mechanical machining is necessary, because the design of the connecting structures will allow for minor position deviations due to welding distortions.

In the case of a preassembly of the centrepiece, the entire trusswork is welded in the workshop, including fixing tubes and connection points, and thereafter split into 4 subassemblies. The 4 subassemblies are annealed and the connecting surfaces of the fixing tubes and connecting points are machined individually. The final assembly of the four parts on-site can be done either by welding or by bolting, provided the subassemblies are equipped with flanges at the field joints.

In order to minimize the wind drag force on the structure, the top ring is made of circular tubes. It is divided by 4 bolted field joints for dismantling in 4 transportable units, which are individually annealed and the connecting surfaces machined.

The connections of the Serrurier struts to the centrepiece will be bolted joints with ball sockets. The possibility of alignment of the top ring to the centrepiece during final erection is foreseen.

The spiders of the M2 and M3 units are arranged so that they are connected by pairs to the two attachment points at the mirror unit, this provides the highest torsional stiffness. In order to minimize the wind torque and the rotational inertia moment of the tube about the elevation axis, the spider of the M2 unit has been designed as a quadrupod so that the moments of wind and gravity loads are smaller. This also has the advantage of increasing axial stiffness which is important to reduce the path length variations, critical for the interferometry. Both spiders are welded sandwich plates with holes to minimize the weight and the surface exposed to the wind. The altitude bearing trunnion is a hollow shaft with 1.2 metres free inner diameter and flange mounted to the fixing tubes via high-strength friction grip bolted connections.

A detailed mass breakdown of the telescope tube is given in the following table:

Item	Mass [kg]
Centrepiece	25050
Flexion bars	2100
Serrurier struts	4300
Spider M2	860
Spider M3	860
Top ring	4300
Hollow shafts	11630
Gear wheels	12000
Data wheels	3600
Subtotal	64700
M1 unit	30000
M2 unit	2000
M3 unit	2500
Additional equipment	10000
Subtotal	44500
GRAND TOTAL	109200

### 6.2.2 Mirror Units

The primary mirror cell structure is described in Section 5.5. The primary mirror cell is connected to the centrepiece by means of 4 modified flexion bars made of 3 trusses arranged in a triangular pyramid plus 8 single bars along the sides (two per side). In total there are 12 joints, designed as bolted connections with ball sockets.

The secondary mirror unit consists of a 1.27 metre convex mirror (4435mm radius of curvature), the support system and mirror cell, and a mechanical unit. The overall outer dimensions of the M2 unit will be minimized to present the lowest cross-section to the wind and the mechanics will be completely in the shadow of mirror M2. The secondary mirror unit will provide the following functions: an axial positioning (focus) and a centring of the secondary with respect to the primary mirror, a fast tilt correction of small tracking errors induced by wind buffets and possibly a square wave chopping between two angular positions for background subtraction in the infrared. This last function is subject to a feasibility study.

The tertiary mirror unit consists of a 1.62 metre flat mirror (elliptical rim), the mirror support system and a mechanical unit, which provides the 180° rotation of M3 to serve the two Nasmyth instrument stations and Coudé trains. A mechanism for



removing M3 out of the optical path in case of a Cassegrain focus has not yet been investigated.

## 6.3 Azimuthal Structure

### 6.3.1 Fork Structure

The design of the fork structure (see Figure 6.1 and 6.2) is optimized in order to transfer in the most efficient way the load of the tube from the altitude to the azimuth hydrostatic bearings.

The fork consists of two individual pedestals supported on the concentric series of hydrostatic pads. The two pedestals are connected by a truss structure which provides the bending and torsional stiffness. The distance between the altitude axis and the plane of the azimuthal pads has been minimized in order to obtain the highest dynamic performance. The total mass of the fork is 110000 kg with the following breakdown:

Item	Mass [kg]
Fork structure (steel)	66360
Alt bearings	13000
Az bearings	11500
Alt drives	6000
Az drives	4500
Coudé mirror supports	3000
Miscellaneous	6000
Total fork	110360
Instruments	8000
Tube (see Section 6.2)	109200
Total moving mass	227560

### 6.3.2 Support Ring and Azimuth Tracks

The support ring structure is the interface between the moving part of the telescope and the concrete pillar of the telescope building. Since the axial azimuth bearings are provided by hydrostatic pads, which are fixed to the fork structure, the support ring

serves as basement for the two concentric circular azimuth tracks, with diameters of 11 and 18 metres respectively. The tracks consist of 8 or 12 elements which are bolted together. For final positioning and alignment an adjustment system is foreseen; the expected accuracy of the bearing surfaces is about  $\pm 0.05\text{mm}$ . The recent measurement technique is able to resolve 0.03mm of level differences on an 18 metres diameter ring. The inner track with approximately 11 metres diameter has on its outer side the surface for the radial centring bearing, and on its inner side the gear rim for the azimuth drives. On both tracks an oil recovering system is provided. The tracks are protected by rubber covers, which are lifted up by appropriate devices at the locations of the hydrostatic pads.

### 6.3.3 Bearings and Oil System

Axial and radial support of both telescope axes is provided by means of hydrostatic bearings.

The hydrostatic solution has been selected for the baseline concept because of its favourable stiffness to friction ratio compared with a rolling contact bearing. One could also envisage a ball or roller bearing for the altitude axis as an alternative, when the friction is brought to an acceptable level. However, hydrostatic bearings represent a relatively cheap and reliable solution and they have been used for the existing 4m class telescopes without any problem. At this stage there is no clear advantage in favour of ball or roller bearings and it seems preferable to rely on the conventional but fully proven hydrostatic solution.

The altitude axis is supported radially by 4 hydrostatic pads, 2 on each side of the telescope tube, mounted at an angle of  $35^\circ$  from the vertical direction (see Figure 6.3). With an assumed total weight of the tube of 1200 KN, the nominal load for one radial hydrostatic pad is 366 KN. The radial pad will have 4 rectangular pockets, each fed by a throttle from the piston room. The supporting head with the 4 pockets is provided with a ball pivot in order to allow for a self adjustment of the bearing. The sphere takes about 10% of the nominal load of the pad, while 90% is supported by the oil pressure in the piston chamber.

The axial support of the altitude axis is provided by 2 hydrostatic pads, 1 on each side of the telescope tube, acting towards the centre of the tube (see Figure 6.3). The axial hydrostatic bearing is of the bladder type. In this design the supporting head floats on the hydraulic cushion in the rubber bladder and is thus able to align itself to the running surface. The two opposite axial bearings are prestressed against each other with about 25% of the operational load in order to provide a centring force. Additionally, this bearing design allows an active adjustment of the position of the bearing of a few millimetres by inflating the bladder. The supporting head consists of 4 pockets, each fed by a throttle from the main oil line. The nominal operating load for each axial pad is 125 KN and the maximal load is 200 KN (corresponding to a loading due to 100 km/h wind speed in the direction of the altitude axis with the tube in zenith position).

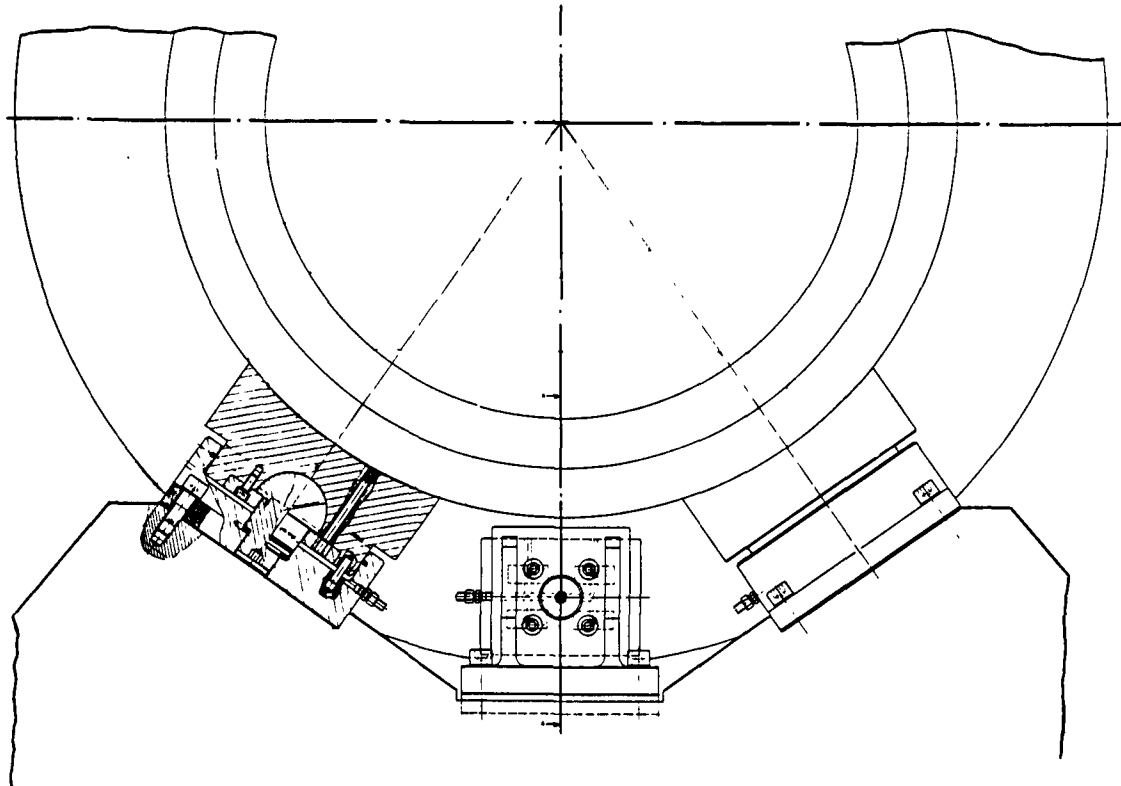


Figure 6.3: Drawing of altitude bearings.

The azimuth axis is supported axially by 8 hydrostatic pads. With an assumed total moving weight of the telescope of 2600 kN, the nominal load for each hydrostatic axial bearing is 325 kN. The azimuth axial bearing design is identical to the altitude radial bearings (see Figure 6.4).

The radial centring of the azimuth axis is provided by 4 hydrostatic pads attached to the 4 inner axial support points. The outer rim of the inner axial bearing track (with a diameter of 11 metres) is fitted with a radial bearing surface. In order to produce a centring force, the 4 radial bearings are prestressed against each other. The nominal operational load per pad is 175 kN including 25 kN preloading. The design of the radial azimuth bearings is identical to the one of the axial altitude bearings. For all pads the nominal oil feed pressure is about 30 bar and the oil flow through the nominally 50  $\mu\text{m}$  ring gap is about 1.2  $\ell/\text{min}$ .

In order to optimize the dynamic stiffness of the hydrostatic bearings, the oil pumps have to be placed as close as possible to the bearings. There will be several oil supply units in the vicinity of a group of bearings. These individual oil supply units must not dissipate heat nor transmit any vibrations to the telescope fork structure on which they

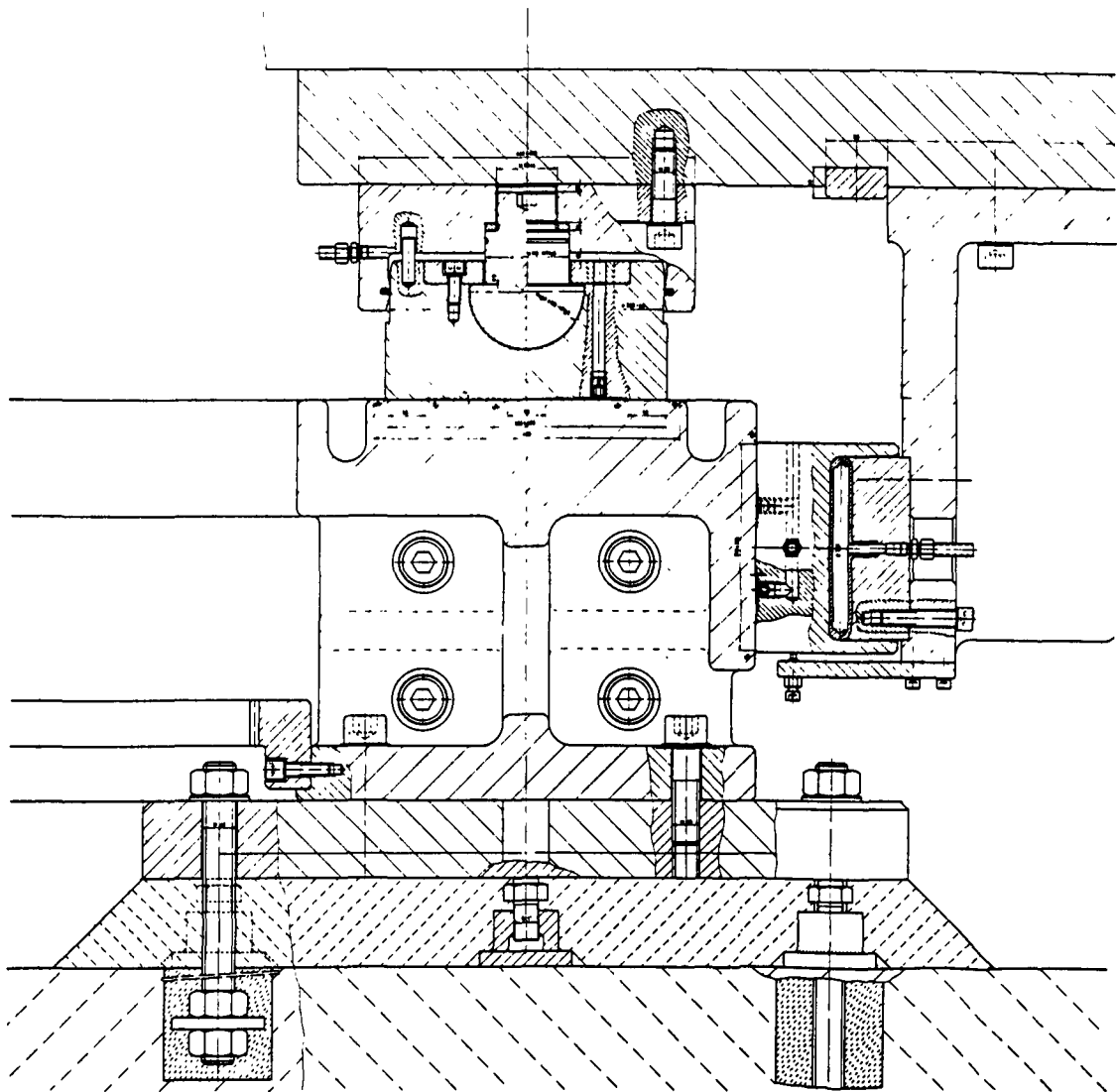


Figure 6.4: Drawing of azimuth bearings.

are mounted. For this purpose low vibration pumps are chosen, short pieces of damping rubber hoses are inserted in the oil and cooling liquid ducts, the whole supply system is rubber pad suspended, the oil is cooled and controlled to approximately  $1.5^{\circ}\text{C}$  below ambient temperature, the electric motors (as the main heat dissipators) are mounted in an insulated and ventilated box which at its end has an air cooler controlled to ambient temperature, and the whole system is thermally insulated. The oil will be of low viscosity type and will be precooled to a temperature about  $1.5 - 2^{\circ}\text{C}$  cooler than the ambient temperature. When the oil is throttled down in the hydrostatic bearings, it escapes with ambient temperature.

## 6.4 Drives and Encoders

The basic concept for the altitude and azimuth drive is the gear rim-pinion drive.

For the altitude axis, the diameter of the precision gear rim with hob-milled teeth is approximately 5.5 metres. The compact drive units, which consist of torque motor, brake and tachometer, are rigidly flange-mounted to the fork structure. The transmission ratio between motor and telescope axis is about 30. Four drive units are provided for altitude drive, 2 on both sides of the telescope tube bias torqued for backlashfree drive. The necessary adjustment of meshing between gear rim and drive requires an alignment system in the fixing flange of the drive units.

For the azimuth axis, the same drive system will be used. The gear rim will be mounted on the inner azimuth track which has a diameter of 11 metres. The transmission ratio for the azimuth axis is about 50. The 4 drive units for the azimuth axis are located close to the corners of the central connecting structure of the fork, where the radial azimuth centring bearings are mounted.

An interesting alternative for the telescope drives could be the use of an assembly of curved segments of linear motors arranged around the axis (eventually several in parallel) to form a continuous direct drive system.

For pointing and tracking of the telescope, two different encoder systems will be used in the 8 metre unit telescope. For positioning of the telescope, incremental strip encoders, and for tracking, friction roller coupled incremental encoders are provided for both axes.

An attractive alternative technique is to use an active ring laser gyro as angular encoder. This system measures the angular velocity with an accuracy of approximately 0.01 arcsec/sec which is expected to be improved by one order of magnitude in the near future. The ring laser gyro system is based on the effect of pathlength differences of two laser light beams running in opposite directions in a closed optical path system, which is rotating at a certain angular velocity. When the two light beams are interfered, the frequency of the resulting signal can be related to the angular velocity of the system. Two one-dimensional gyro systems would be required in the telescope, one for altitude and one for azimuth encoding. Since the system will not give absolute angular positions, an initialization procedure as in the case of incremental encoders is necessary.

## 6.5 Structural Performance

### 6.5.1 Static Performance

The telescope structure has to provide adequate structural stiffness in order to withstand the static gravity and quasi-static wind loads within the specified limits.

For the static analysis of the telescope, two finite element models, one with the tube in vertical (zenith) and the other with the tube in horizontal position, have been established. Each model consists of 423 nodal points and 956 beam elements which gives a total number of 2518 degrees of freedom. A three-dimensional view of the models is shown in Figure 6.5.

The gravity load case has been analysed for both models. The deformations at the mirror units and at the altitude bearings due to gravity loading are given in Table 6.1. In the zenith position the deflections at all mirror units are of nearly the same magnitude (1mm in the direction of the optical axis of the tube). The bending deformation of the centrepiece results in a tilt of the axis of 67 arcsec at the altitude bearings. In the horizontal tube position the bending of the centrepiece gives a tilt of 42 arcsec at the altitude bearings. The difference of 25 arcsec bending deflection between vertical and horizontal position will give a position dependent loading on the axial altitude bearing and will be covered by the prestressing of the bearings.

TABLE 6.1

STATIC PERFORMANCE - GRAVITY LOADING				
Location	Displacement [mm]		Rotation [arcsec]	
	Vertical	Horizontal	Vertical	Horizontal
M1	1.16	0.79	-	1.0
M2	1.22	1.52	3.5	6.9
M3	1.04	0.74	13.7	25.0
Alt Bearing	0.20	0.21	67.2	41.9

The maximum deformation at the top unit M2 in horizontal tube position is 1.52mm, including 0.21mm deflection of the altitude bearings. With respect to mirror M1, the net deflection in the tube structure is 0.73mm (M2 - M1). Plots of the deformed telescope structure are shown in Figures 6.6 and 6.7.

Quasi-static wind loading of the telescope structure with the tube in vertical position has been analysed. For the wind velocity of 14 m/s the resulting force at the top unit M2 is about 3000 N when the wind is blowing in a plane perpendicular to the optical and altitude axes. The maximum deformation due to that wind load is 0.23mm at the top unit M2.

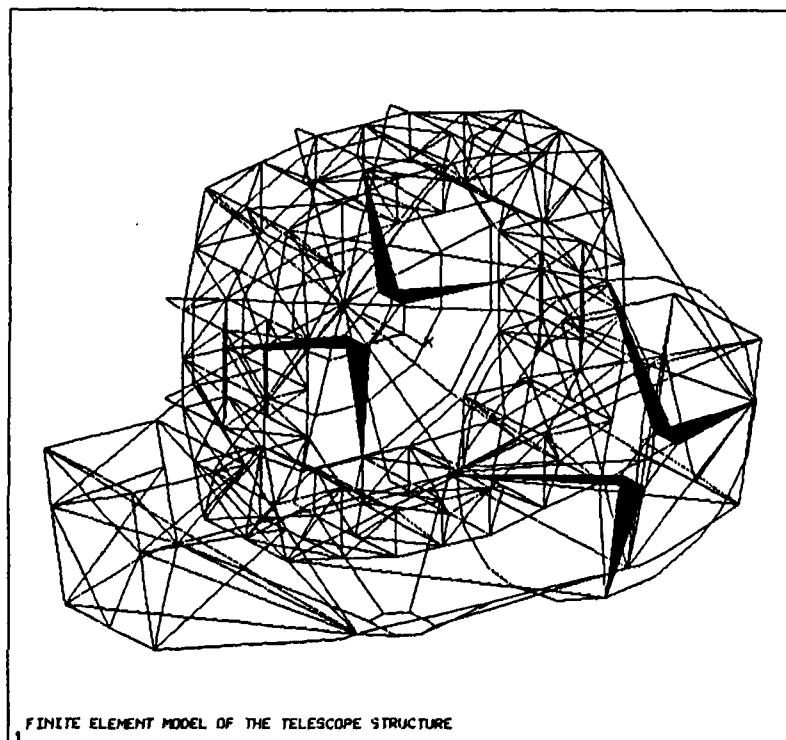
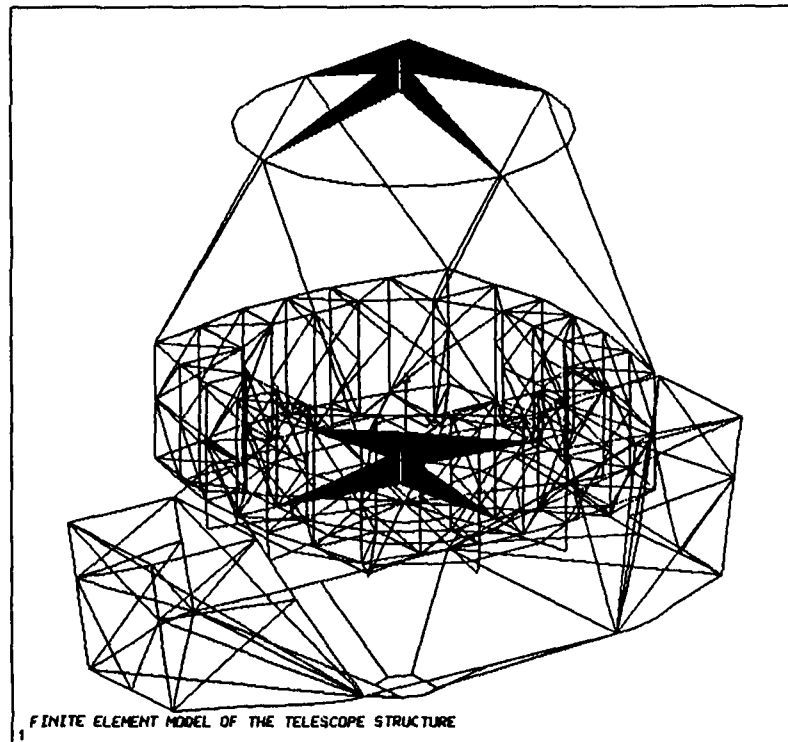


Figure 6.5: Finite element model of telescope structure.

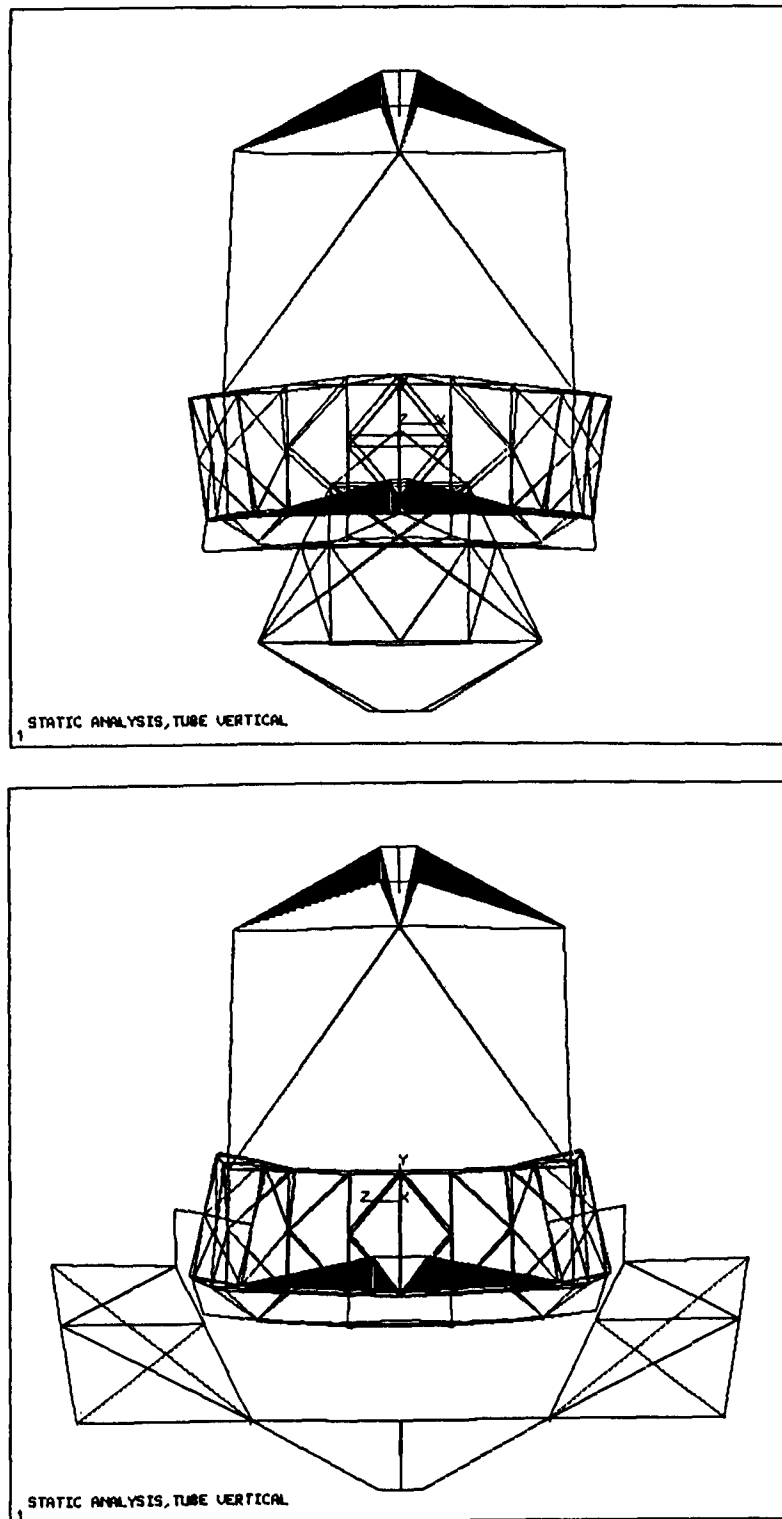


Figure 6.6: Static performance - tube vertical.



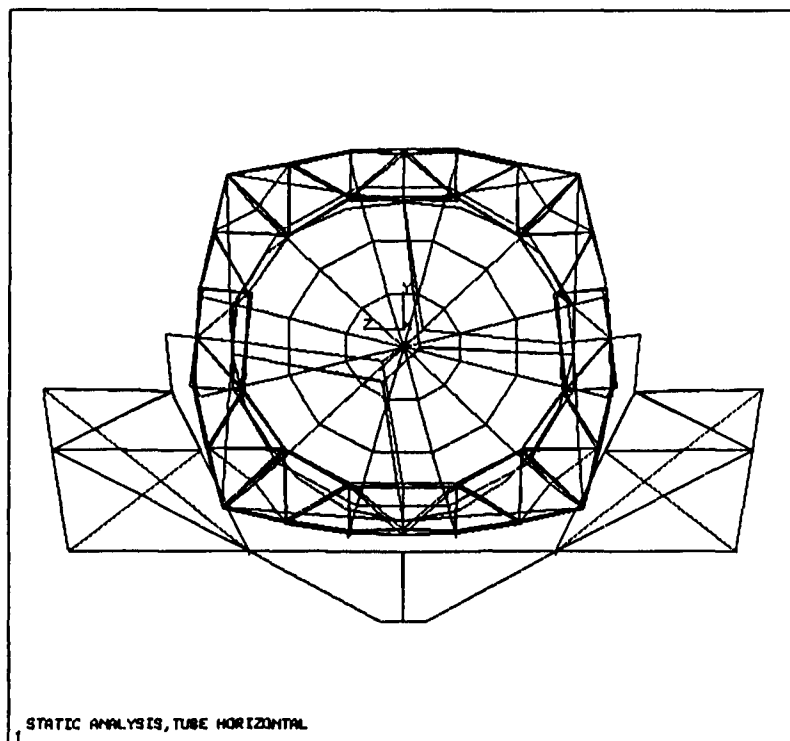
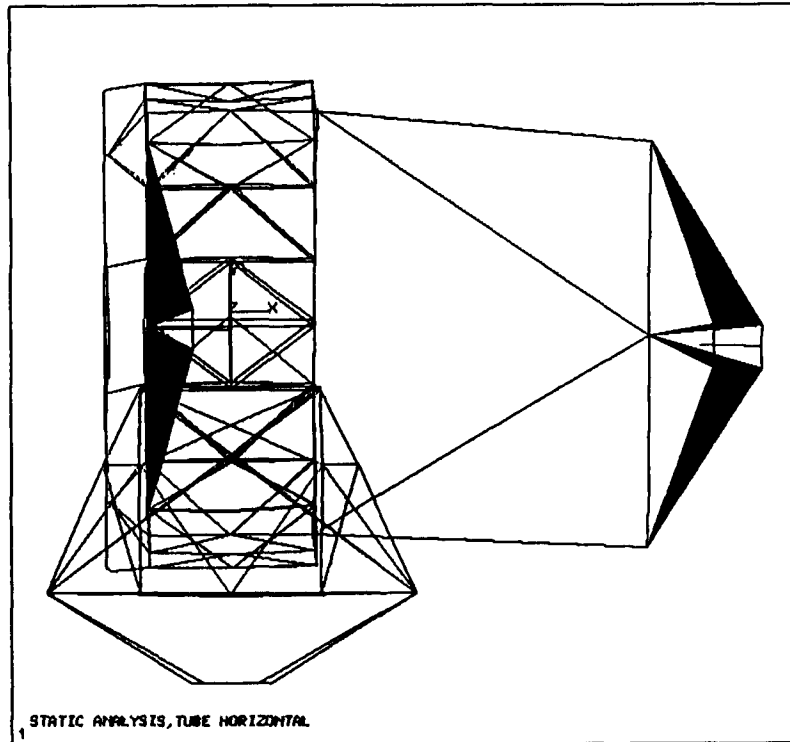


Figure 6.7: Static performance - tube horizontal.

### 6.5.2 Dynamic Performance

The knowledge of the dynamic response of the telescope structure to transient external loading i.e. wind or drive forces, is important for the design of the active elements in the structure, like the active primary mirror, as well as the drives themselves.

First the structural resonances, i.e. eigenfrequencies and corresponding eigenmodes, have to be examined in order to find the bandwidth limitations for the control systems of the telescope. For this purpose, a dynamic finite element model of the telescope including the gear rim-pinion drives as well as the hydrostatic bearings has been established. The model is identical to the static model with the tube in vertical position, except that the total number of degrees of freedom has been reduced to about 500 dynamic degrees of freedom by means of a dynamic matrix condensation. The system has been solved for the first eight eigenfrequencies and mode shapes. A summary of the results of the modal analysis is given in Table 6.2. The first eigenfrequency of the telescope is a rigid body rotation of the tube about the altitude axis with a frequency of 6.5 Hz.

TABLE 6.2

DYNAMIC PERFORMANCE - EIGENFREQUENCIES		
Mode No.	Frequency [Hz]	Eigenmode Description
1	6.5	Tube rotation about alt axis (locked rotor)
2	8.5	Tube lateral movement in the alt axial supports
3	14.6	Tube bending in altitude axis direction
4	14.8	Top ring bending (in-plane)
5	15.0	Centrepiece bending (unsymmetric)
6	15.0	Centrepiece bending (symmetric)
7	19.4	Fork rotation around azimuth axis
8	21.4	Top ring twisting (out of plane)

This locked rotor frequency for the altitude axis is in the present design determined by the torsional stiffness of the shaft and gear-stages of the altitude motors. The second eigenmode of the telescope is a lateral bending of the telescope tube structure (in direction of the altitude axis) with a frequency of 8.5 Hz. This resonance frequency is determined by the lateral stiffness of the altitude bearings. The third eigenmode is the lateral bending of upper tube with a frequency of 14.6 Hz, and the fourth eigenmode is a local top ring bending with 14.8 Hz. The mode shapes of the first four structural resonances are shown in Figures 6.8 to 6.11. The higher modes are local vibrations in the tube and fork structures.

One of the most important aspects in the dynamic performance of the telescope is the response of the structure to dynamic wind loads.

In a statistical analysis, using the random vibration theory, the r.m.s. response of the telescope structure, including the drives, to a wind force spectrum (Figure 6.12) acting at the top unit has been calculated. The wind force spectrum in Figure 6.12 has been derived from a typical wind speed time history measured at La Silla. The sample selected is the worst case with a mean and maximum wind speed of 18 m/s and 27 m/s (= 97km/h). The mean square response  $\sigma^2$  of the structure to the wind force spectrum  $S(f)$  follows from

$$\sigma^2 = \int_{f_1}^{f_2} S(f) |H(f)|^2 df, \quad (6.1)$$

where  $H(f)$  is the harmonic response spectrum of the telescope structure. The harmonic response of the telescope is shown in Figure 6.13 for a structural damping of 1%. The peak occurs exactly at the first resonance frequency of the telescope i.e. 4.7 Hz (see Figure 6.8), and the magnification factor is about 3. The displacement response spectrum of the structure (see Figure 6.14) shows a very small resonance peak at the locked rotor resonance frequency of 4.7 Hz.

When equation (6.1) is integrated from 1 to 15 Hz, the r.m.s. response is  $10\mu\text{m}$  at the M2 unit, which corresponds to 0.2 arcsec pointing error at the sky. One has to note that this first wind response analysis has been based on the assumption of an  $f/2$  primary mirror, a wind speed equivalent to red light condition at La Silla and a servobandpass of 1Hz. By reducing the length of the tube ( $f/2 \rightarrow f/1.8$ ), increasing the first resonance frequency of the telescope to about 7 - 8Hz and increasing the servoband pass to 2Hz, the r.m.s. pointing error due to dynamic wind loading can be reduced to less than 0.1 arcsec. An additional way to improve the dynamic behaviour of the telescope, namely a tracking correction with the secondary mirror, is discussed next in Section 6.6.

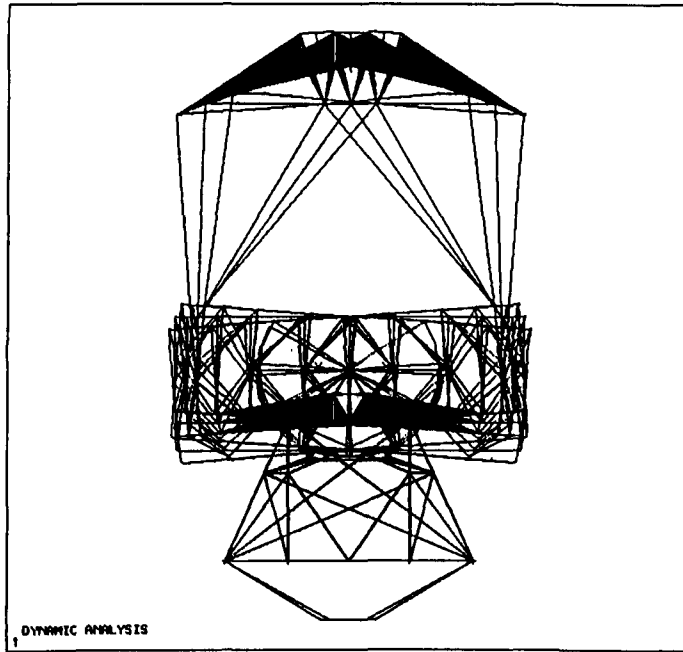


Figure 6.8: Dynamic performance - first eigenmode.

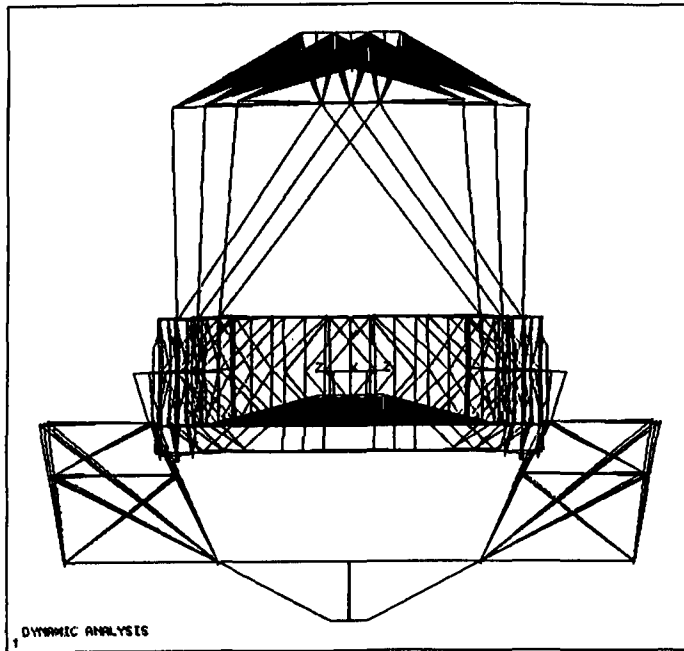


Figure 6.9: Dynamic performance - second eigenmode.

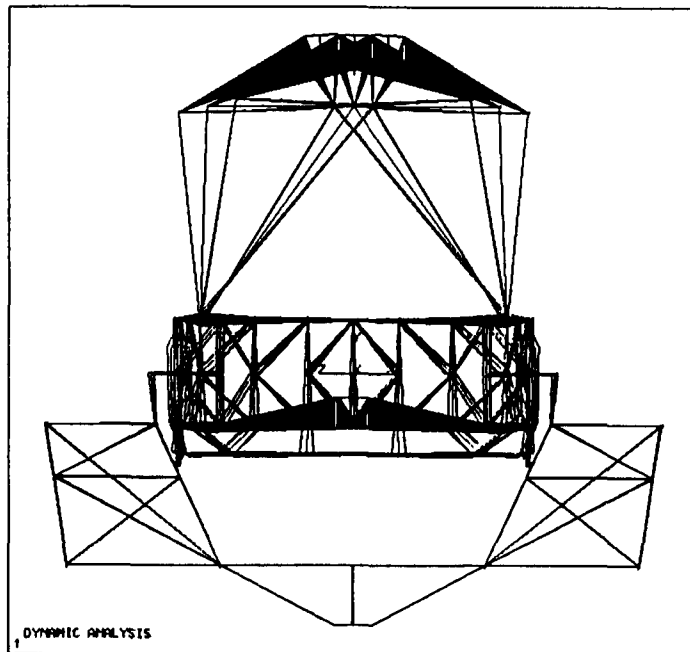


Figure 6.10: Dynamic performance - third eigenmode.

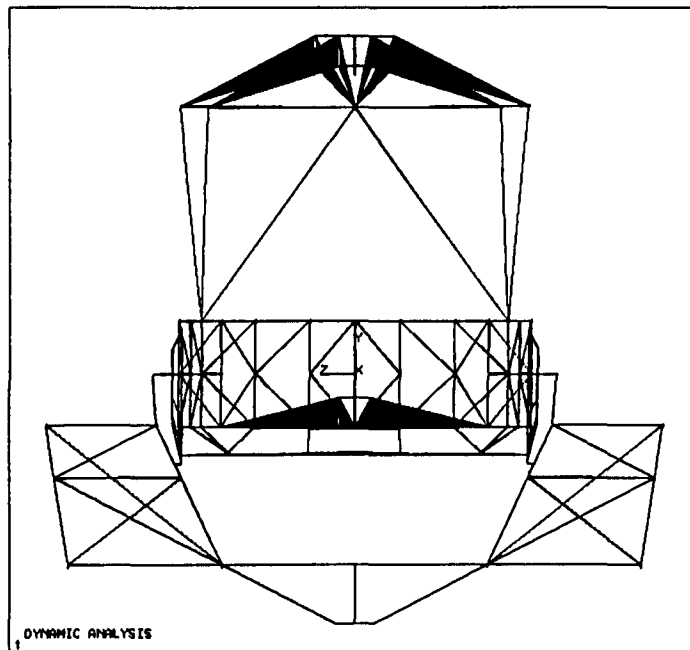


Figure 6.11: Dynamic performance - fourth eigenmode.

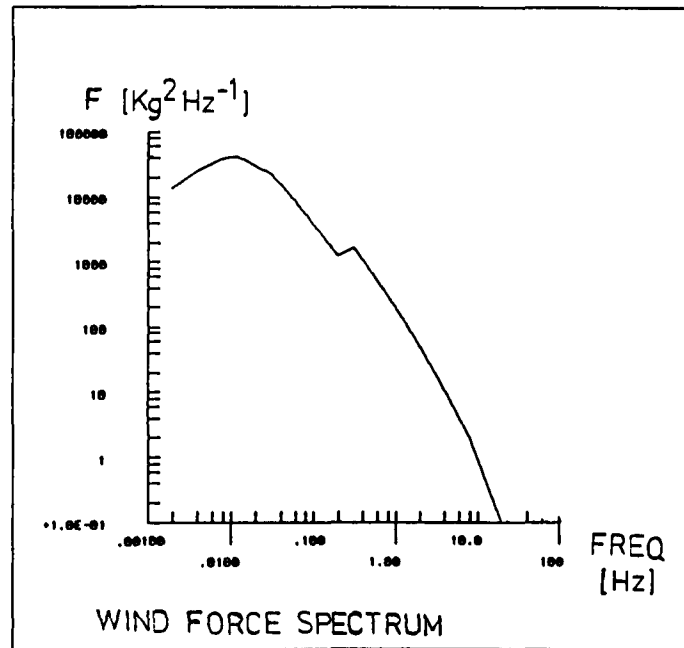


Figure 6.12: Wind force spectrum at M2 (measured at La Silla;  $V = 18$  m/sec).

## 6.6 Tracking Simulation

### 6.6.1 Model

In order to obtain information about the dynamic performance of the servo system, the altitude axis has been simulated in a closed loop configuration. The objectives were primarily to investigate the position setting and tracking performance and secondly to assess the behaviour of the telescope under influence of strong wind.

The control of the altitude axis is achieved with two separate servo systems. The main servo system controls the position of the tube by means of a conventional position controller. In order to compensate the unavoidable errors from this servo, a further correction is done by the M2 mirror unit. The M2 mirror can tilt slightly under control of a second servo system. Since the position error of the main system is known from the encoder and autoguider, the M2 mirror can be commanded to compensate this error, and the overall tracking performance can be considerably improved.

In all the following simulation runs, the performance of the altitude axis is shown with and without the M2 mirror compensation. Curve 1 always shows the result with the main servo system, i.e. this corresponds to the normal expected tracking and position setting errors for a telescope. Curve 2 shows the resulting system performance, including the correction from the M2 mirror.

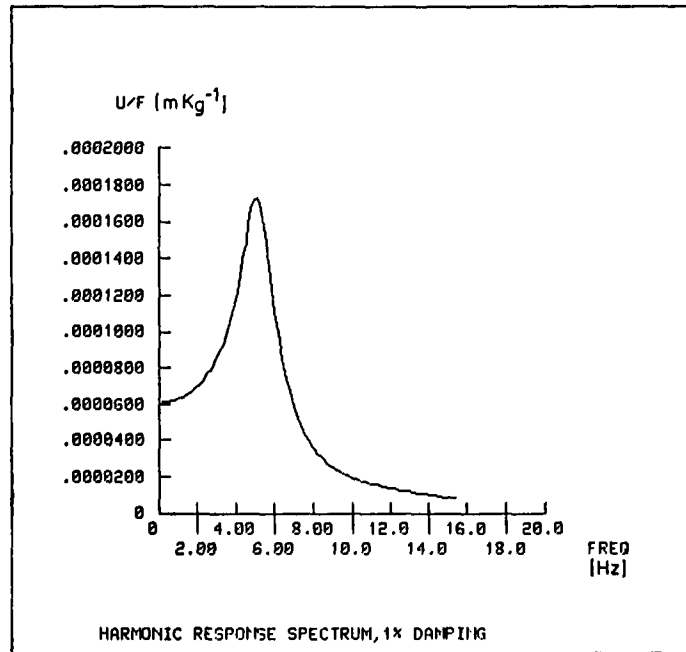


Figure 6.13: Harmonic response spectrum (1% damping).

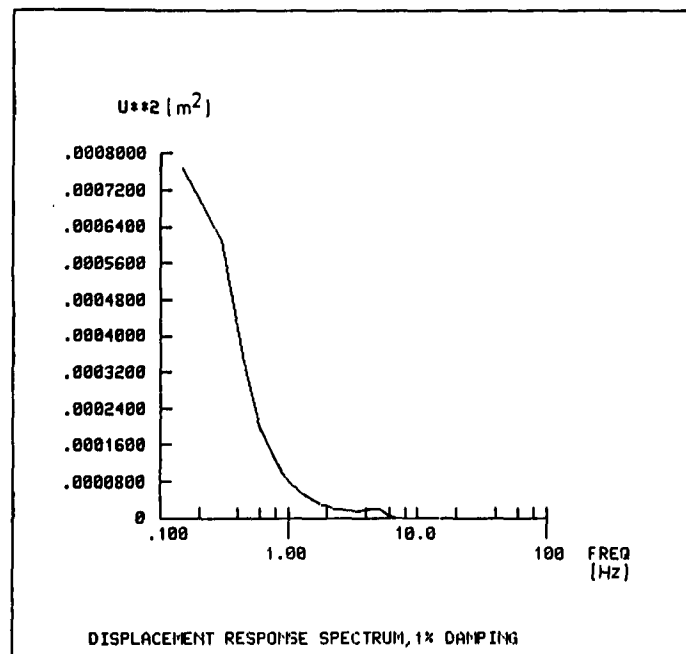


Figure 6.14: Displacement response spectrum (1% damping).

The following assumptions have been made for the main servo system:

- The telescope structure is represented by a model with 7 degrees of freedom. The characteristic of the model is an undamped antiresonance at 4.7Hz, the so-called “locked-rotor” resonance frequency. The first real structural resonance occurs at 8.9Hz. These two resonances determine the obtainable bandwidth of the control system. For numerical reasons a relative structural damping of 0.001 has been added.
- Friction has been added to the motors. Due to the lack of reliable data concerning the angular slip speed (defined as the speed for which the friction becomes independent of velocity), the friction model represents a worst case situation. The angular slip speed is 50 arcsec/sec at the motor axis, corresponding to 1.7 arcsec/sec at the telescope axis. This means that the friction influence is pronounced at the interesting tracking speeds between 0.1 to 1 arcsec/sec.
- No other friction sources have been assumed, due to the use of hydrostatic main bearings.
- The controller is a conventional cascade proportional-integral type with a velocity loop cascaded with the position loop. This type is in common use and has the advantage of being relatively insensitive to changes in parameters, i.e. change in friction and stiffness.

For the M2 mirror control system, the assumptions are:

- The M2 unit structure is represented by a model with 2 degrees of freedom. The first resonance frequency is assumed to be 150Hz.
- Relative damping is 0.001.
- No friction has been assumed.
- The controller is a simple proportional control of position and velocity. The bandwidth of the system has deliberately been set low, namely 13Hz.

It should be noted that all the errors mentioned in this Chapter are arising from the control system only. For example, deflection due to gravity is not taken into account.

### 6.6.2 Results

Three different types of simulations are presented in the following, namely:

- Position setting accuracy.



- Tracking performance for 0.1 arcsec/sec and 1 arcsec/sec (tracking speed is not constant with an alt-az telescope).
- Performance under wind load.

### Position setting

The position setting accuracy which can be expected from the feedback control system was simulated by step offset reference inputs. Curve 1 in Figure 6.15 shows the positioning error versus time for an offset step of 5 arcsec. Due to friction, it takes about 1 second for the main servo system to reach a position error of ca. 0.2 arcsec. Of interest is also the first limit cycle occurring at  $T = 3.8$  seconds. Limit cycles are characteristic for non-linear systems, i.e. the system will never come to zero error, but only oscillate around zero.

Curve 2 in Figure 6.15 shows the system performance, including the M2 mirror compensation. The performance is considerably improved. The overshoot has been reduced by a factor 2.5 and the limit cycles have practically been eliminated.

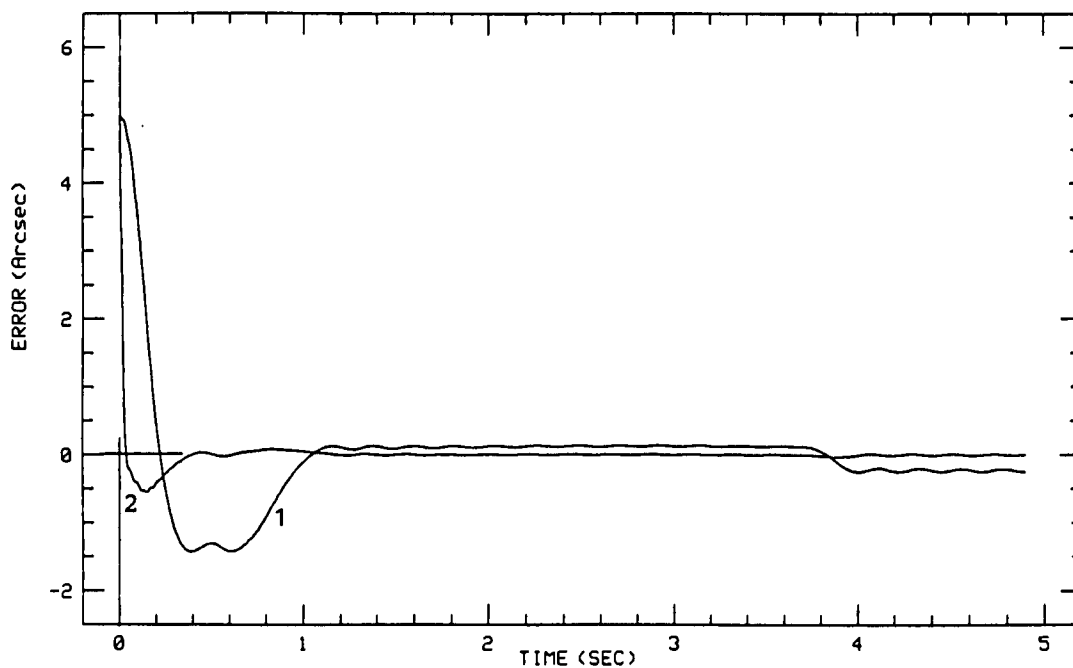


Figure 6.15: Position setting error for a 5 arcsec offset step.

## Tracking

The tracking performance was checked using a linear ramp as input reference to the system. The tracking performance is measured as the error between the ramp reference and the actual tube position. Figures 6.16 and 6.17 show the tracking at 0.1 arcsec/sec and 1.0 arcsec/sec, respectively.

### *0.1 arcsec/sec tracking speed*

From Curve 1 in Figure 6.16, it can be seen that the telescope does not move continuously, but stepwise. The first ca. 1.5 seconds are used to build up a big enough error signal and thereafter the telescope moves. After the first movement oscillations are induced in the telescope structure. The oscillations occur exactly at the locked rotor resonance, 4.7Hz. The oscillations are very poorly damped but this is due to the simple control scheme which has been used.

Curve 2 in Figure 6.16 shows the system performance using M2 mirror compensation. The saw tooth error has been nearly removed, but the M2 mirror cannot compensate the small oscillations at 4.7Hz because of the limited bandwidth of M2. However, the overall performance is considerably improved. The RMS tracking error is 0.11 arcsec without M2 and 0.009 with M2 correction.

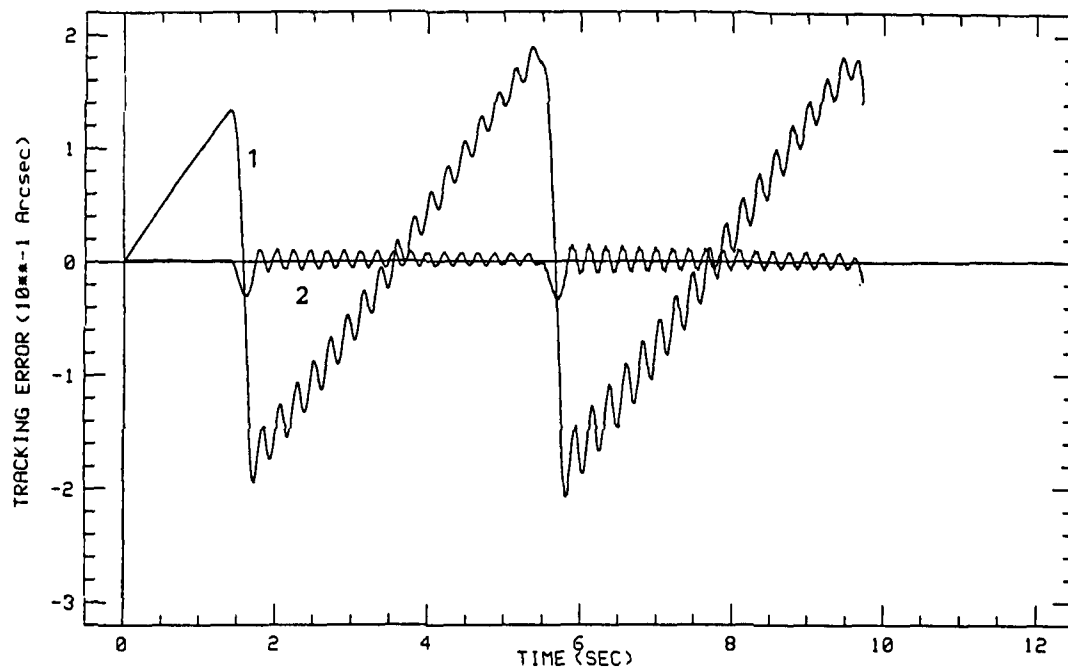


Figure 6.16: Tracking error for a 0.1 arcsec/sec reference input.

*1 arcsec/sec tracking speed*

Curve 1 in Figure 6.17 shows that after 0.5 seconds the telescope starts to move. After about 3 seconds the initial transient error has died out but the system will infinitely oscillate around zero tracking error with an amplitude of  $\pm 0.1$  arcsec. It must be emphasized that these oscillations do not indicate instability of the servo system. The behaviour stems from the non-linear friction. At higher tracking speeds they will disappear.

Curve 2 in Figure 6.17 shows the system performance after compensation. Even though the oscillations are not fully eliminated, the overall RMS error is reduced by more than a factor 10. It is 0.13 arcsec with the telescope drives only and 0.011 arcsec with the additional correction by M2.

Figures 6.16 and 6.17 show some of the worst case limit cycles which can be expected. As the tracking speed increases the phenomenon will disappear. Above 5 arcsec/sec limit cycles cannot be noticed any more. The reason is that the stick-slip effect for the bearing friction in the motors disappears beyond 50 arcsec/sec on the motor axis which is equivalent to 1.7 arcsec/sec on the telescope axis.

Figure 6.18 shows the tracking speed for the 2 axes and for various declinations and hour angles.

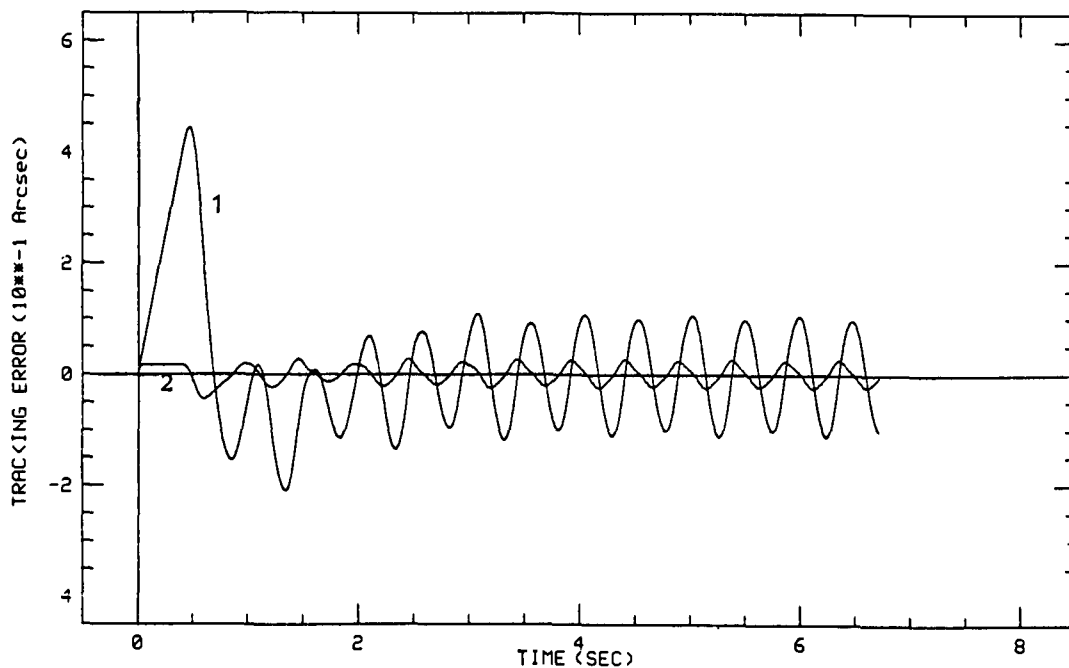


Figure 6.17: Tracking error for a 1.0 arcsec/sec reference input.

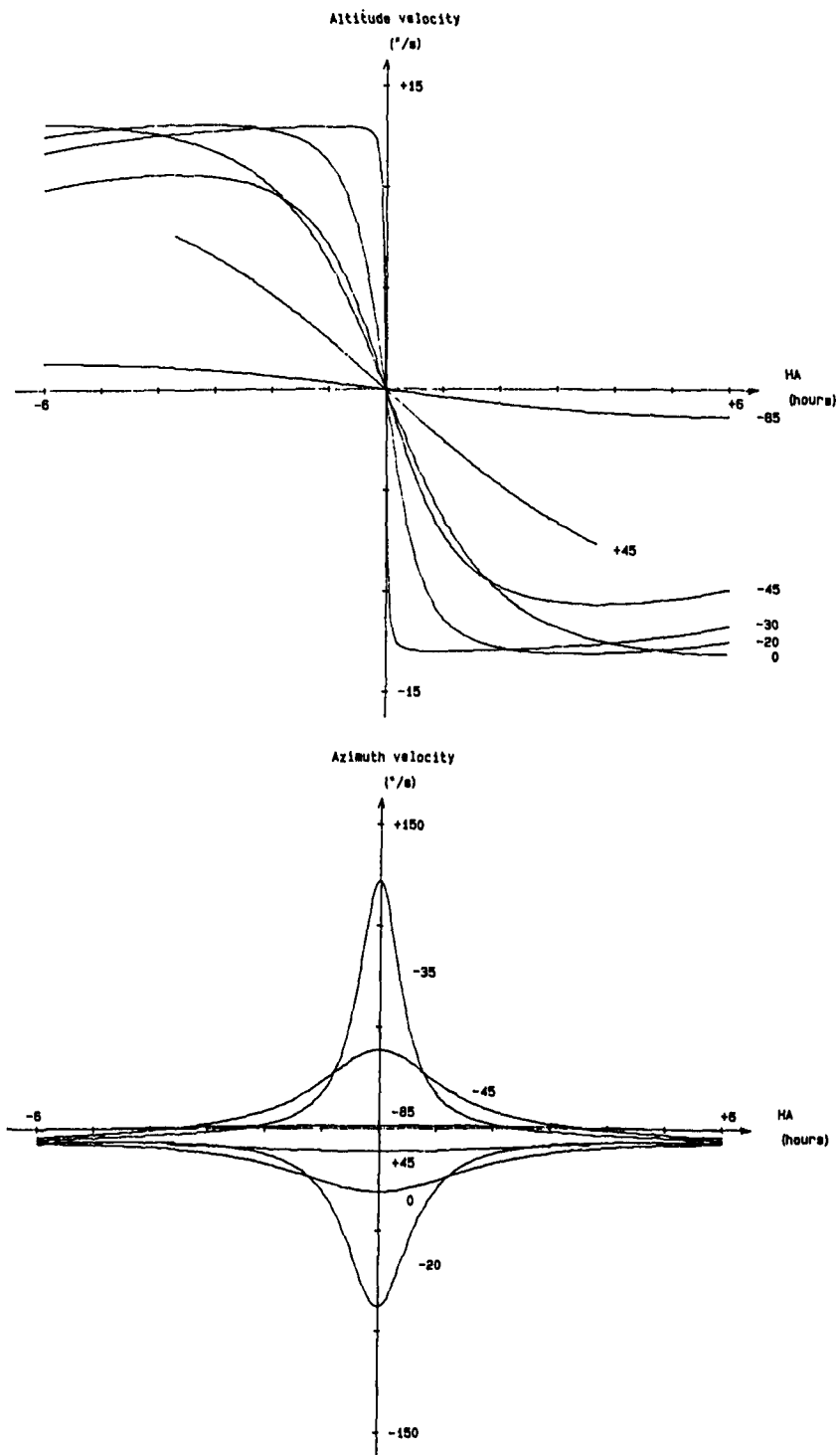


Figure 6.18: Tracking speed for an alt-az mounted telescope (latitude  $-30^{\circ}$ ).

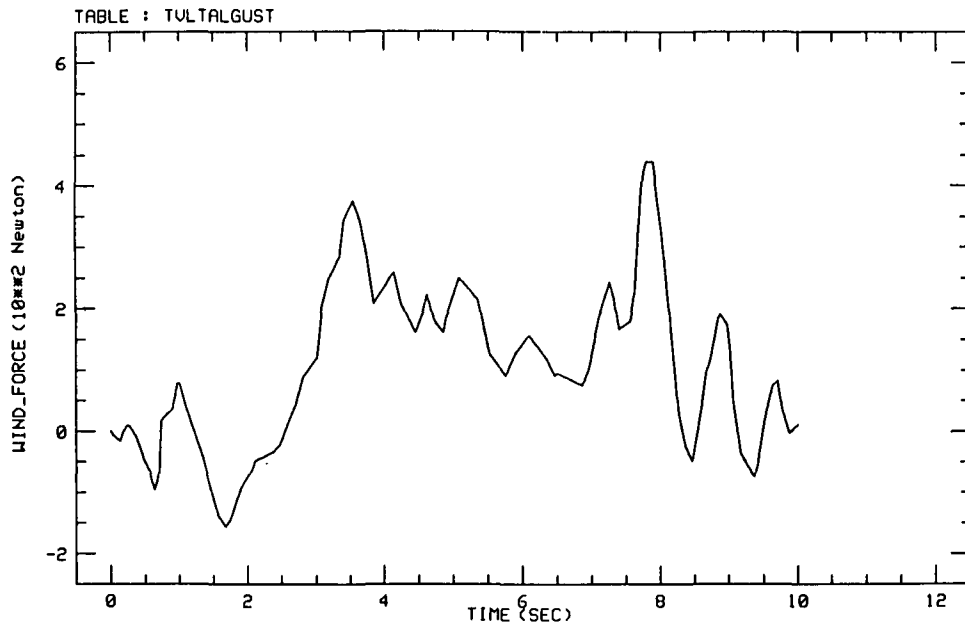


Figure 6.19: Wind force input (measured at La Silla).

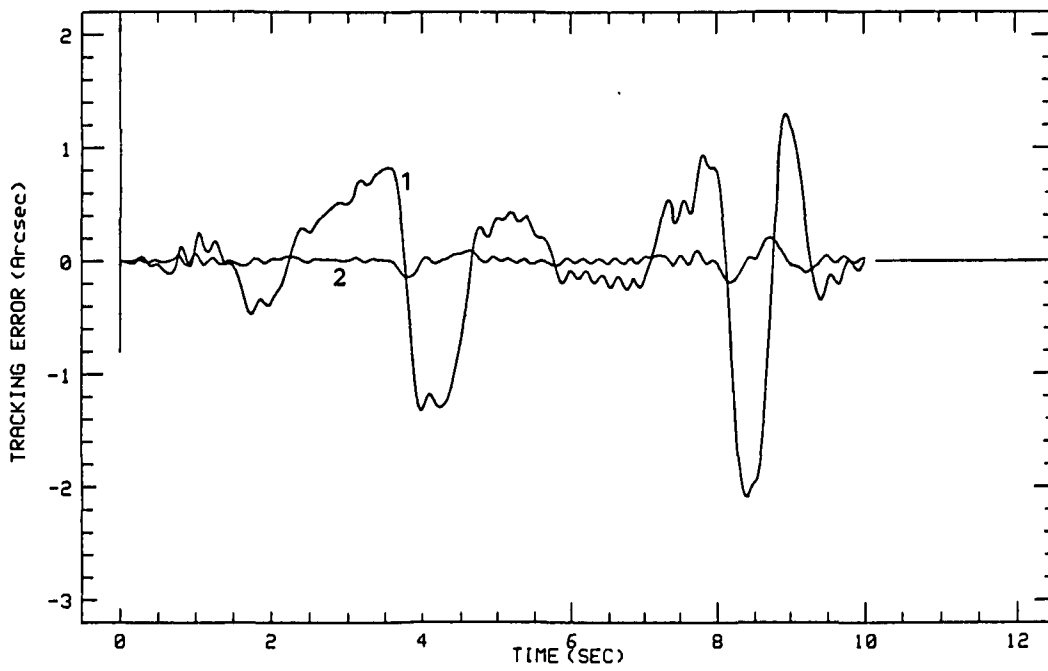


Figure 6.20: Tracking error under wind load.

### Wind load

One of the characteristics of the VLT is that it operates in open air. The wind forces, which act mostly at the top-ring, will influence the tracking performance. Slow changes in the wind speed can be fully compensated by the servo system. Rapidly changing wind gusts, however, are more serious. Reliable data for wind speed at La Silla is today available. Therefore, a worst case wind gust has been selected and transformed into an equivalent force acting at the top-ring (Figure 6.19).

The telescope behaviour under the influence of the above wind force sequence can be seen in Figure 6.20. Curve 1 shows that the strong wind buffets arrive at times equal to 4 seconds and 8 seconds and provoke tracking errors as large as 2 arcsec. However, the overall pointing performance with mirror 2 correction is excellent, as can be seen from Curve 2. Without M2 correction, the r.m.s. tracking error over this particular period is 0.58 arcsec, with M2 correction it is only 0.038 arcsec.

Taking into account the huge mechanical structure of the VLT, the position setting, tracking and wind loading simulations show rather satisfying performance for the main servo system. Considering the ambitious goals set for the VLT, it is nevertheless not sufficient and - unless the telescope drive response can be improved - an active tracking correction with the secondary mirror will be necessary. An improvement of a factor of 10 to 15, depending on the dominant type of disturbances, can be expected.

Solutions for an active secondary mirror are being studied. The goal set for these studies is not only to correct for tracking errors, but also to use the secondary mirror as a chopping mirror for the IR. It is not yet certain that this last function can be successfully achieved with a rather large mirror, but there is little doubt that the correction, to about 0.05 arcsec r.m.s. of tracking errors up to a few arcsec, can be achieved over bandpasses of at least 10Hz. Full open-air operation therefore seems possible, even when considering rather important wind loads.

# Chapter 7

## CONTROL SYSTEM

### 7.1 Introduction

The VLT with its four unit telescopes, each with active optics, with beam combination and with unprecedented specifications, will be a complex instrument to control. At the same time, it is so expensive that a significant percentage of down time is hardly acceptable. As a consequence very high demands will be made on the reliability of the control system.

On the basis of the experience obtained at La Silla, it would seem that this is best achieved with dedicated electronics incorporated locally into the electro-mechanical units. This is the concept of distributed microcontrollers shown by Figure 7.1. It has the advantage that large numbers of cable connections are avoided which frequently cause trouble, and it moves most of the real-time problems into dedicated microprocessors.

In addition, reliability is much improved when instrumental exchanges are avoided. It is foreseen to have most instruments continuously under power and computer connected and to send the light beam to the desired instrument by a simple switching of mirrors. The switching on and off of instruments, the changing of their operating temperature and the disconnecting of large numbers of cables have been regular sources of trouble and will be largely avoided at the VLT.

The 3.5m New Technology Telescope is being developed as a prototype in which many of these concepts will be extensively tested.

### 7.2 Distributed Microcontrollers

The microprocessors are distributed in such a way that the cabling between motors, tachos, encoders and their dedicated electronics is minimized in length and in the

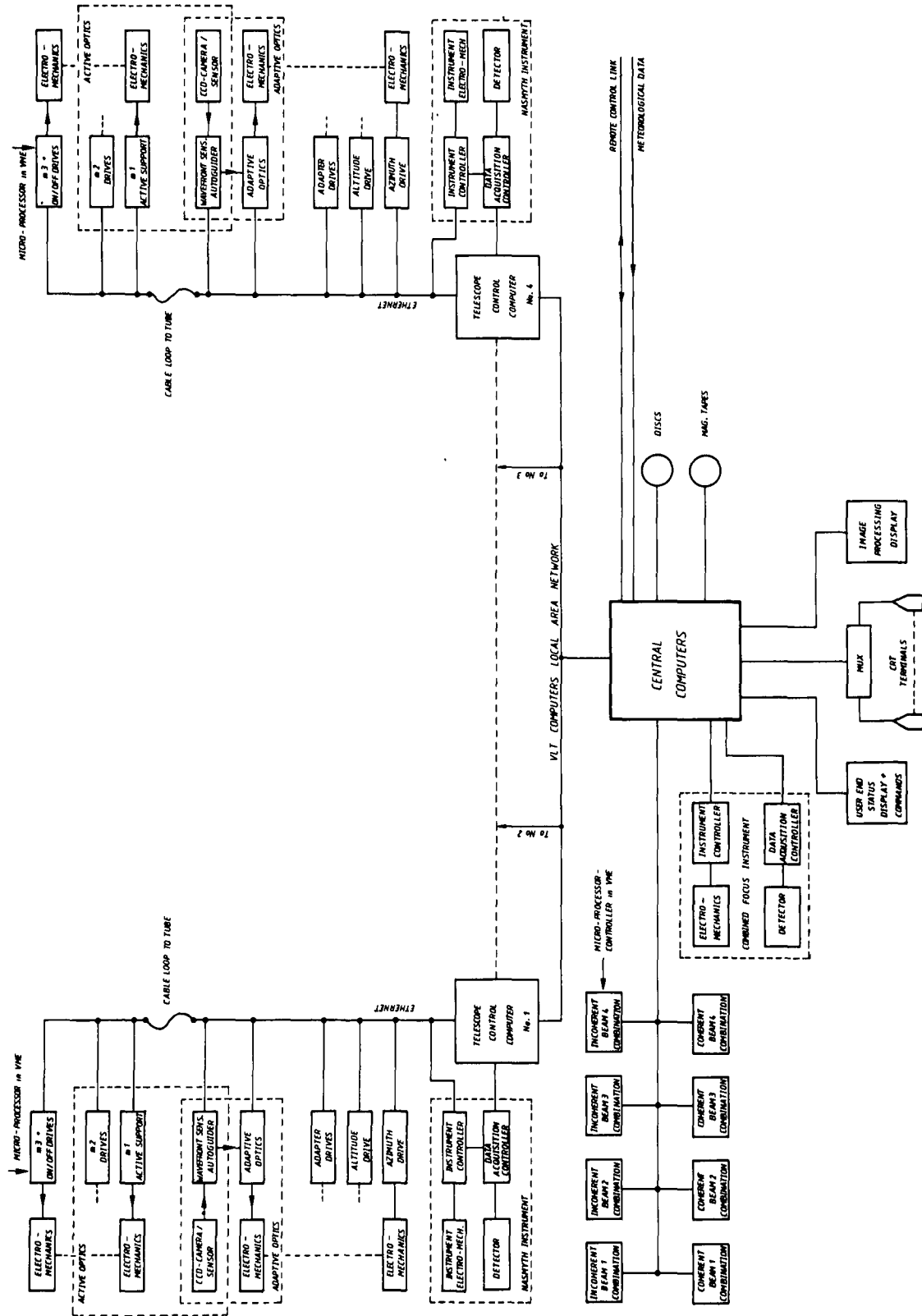


Figure 7.1: VLT control system.



number of interconnections. Control electronics will mostly be incorporated into the electro-mechanical units. The only interconnections which are needed will be one cable for the data transmission (Local Area Network) and one for the power supply. Heavy and voluminous cable twists are avoided in this way.

Incorporating the electronics into the electro-mechanical units has also the advantage that after dismounting they can easily be tested on a bench.

The principle of distributed electronics and the Local Area Network connection will already be tested at the NTT.

### 7.2.1 Hardware

The microprocessors and the main part of the electronics will be housed in VME chassis. VME is an internationally standardized and commercially available system for industrial process control. VME bus has become a standard, high performance bus structure through several years of intensive design activity. It supports data transfers as high as 24 Mbytes in the expanded 32 bit configuration.

VME bus has a master/slave asynchronous non-multiplexed data transfer structure, seven levels of priority interrupt, four levels of data bus arbitration and rapid fault detection and control for bus, system and AC failures. One of the many features of the 32 bit configured VME bus system is that the bus dynamically senses whether 8-, 16- or 32-bit data paths are needed and adjusts automatically. In integrating 8-, 16- and 32-bit system components, VME bus is well adaptable to new technologies. Large scale (LSI) and very large scale integration (VLSI) are providing interface and peripheral chip functions that vastly increase the functionality/cost ratio of VME bus modules.

Most of the modules needed for telescope control are commercially available (i.e. micro controller, D/A converter, A/D converters, I/O modules). Some modules like the PID controller for the velocity feedback and the encoder interfaces which are very special to telescope control, had to be developed in house already for the NTT and are presently being tested. The control unit for the Mirror 1 support system is shown in Figure 7.2.

### 7.2.2 Microprocessor Software

Another advantage of the principle of distributed microprocessors is that real time problems like position control will be handled by the microprocessors. This keeps the telescope computers free for fast data acquisition and image processing. The telescope computer and the distributed microprocessors will work on the basis of a master-slave principle. Normally microprocessors will not communicate directly with each other. Each microprocessor will pass its information first to the telescope computer which will process the data and redistribute it as needed.

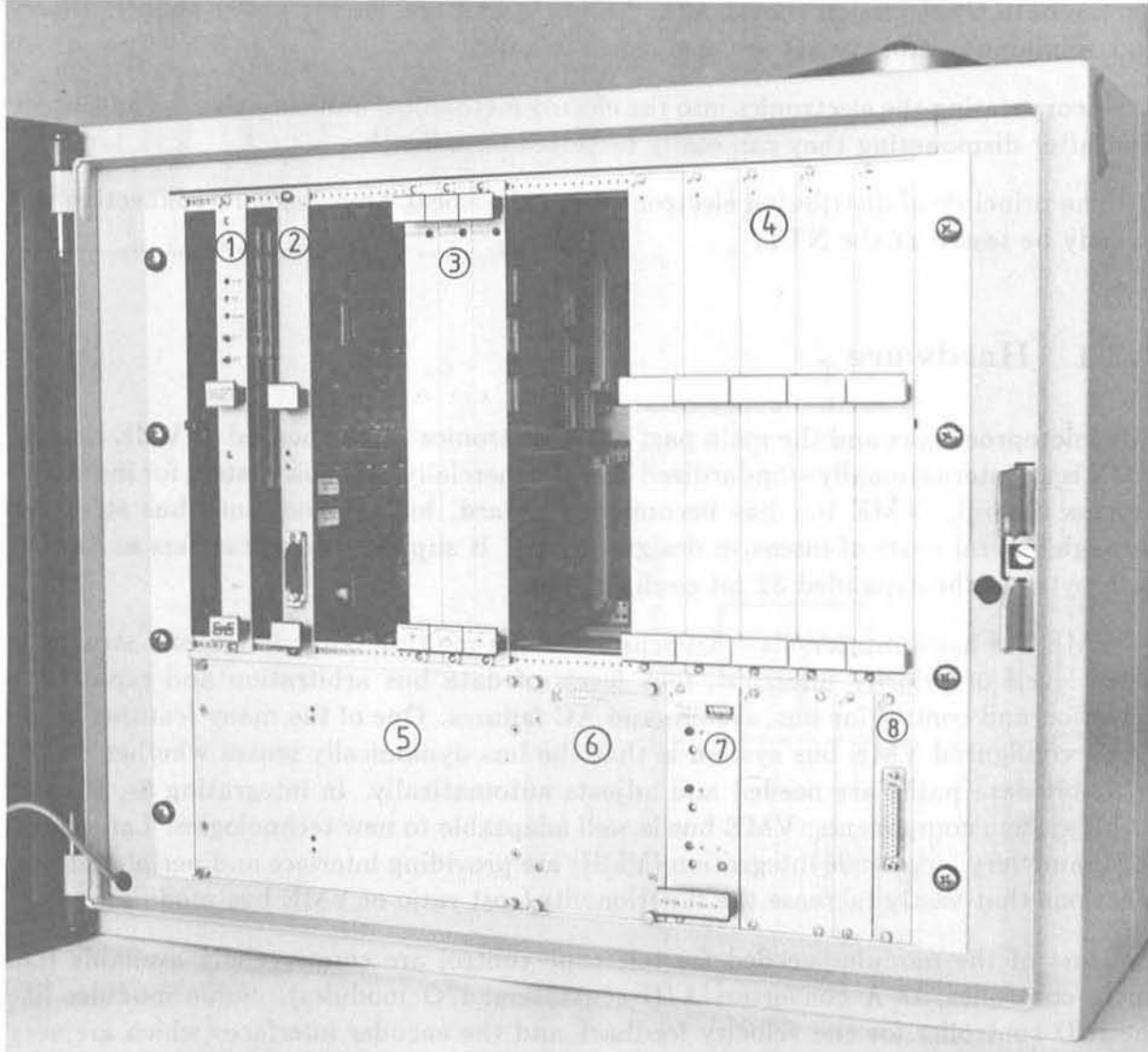


Figure 7.2: Mirror I support system controller for the NTT. (1) Microprocessor unit (CPU). (2) Ethernet interface. (3) Three digital I/O interfaces. (4) Five motor controllers. (5) Motor power supply. (6) VME power supply (digital circuits). (7) VME power supply (analogue circuits). (8) Terminal interface (RS 232 serial links).

The microprocessor software is built around a multitasking real time kernel. The kernel supports all necessary functions for task control (creation, scheduling, suspending, etc.), memory allocation and management, messages for task to task communication and semaphores for task synchronization and resource sharing. Scheduling is done on priority basis with up to 255 priority levels. Interrupt handling and a basic I/O system are available. It is possible to generate the kernel for different hardware configurations.

The following tasks will be implemented on the microprocessors:

- Debug task for debugging application programmes, for remote control either from the central computer or from the terminal interface on the CPU board.
- Application tasks like motor control task.
- Hardware diagnostic task.

The application programmes are supported by a set of libraries like: interfacing to the real time kernel, I/O library and motor control library.

A terminal interface makes it possible to give commands to the application programmes, to debug programmes or to make hardware diagnostics from a terminal connected to the CPU board. This is especially useful when a central computer is not available like in the case of:

- Testing an electro-mechanical unit at the factory.
- Control the support system during the polishing process of mirrors.
- Separating communication problems from electro-mechanical functional problems.

Data are transmitted on the bus in packets. The packet consists of a header, data block and trailer. The header consists of source address, destination address, control code and byte count for number of bytes in the data block. The trailer is the 16-bit CRC checksum of header and data block.

### 7.2.3 Local Area Network (LAN)

The microprocessors controlling the telescope are linked together to the telescope computer via Ethernet, which is an internationally standardized local communication network. It provides a communication facility for high speed data exchange among computers and other digital devices located within a moderate-sized geographic area. Its primary characteristics include:

- Physical Layer:

- Data rate: 10 Mbits/sec
- Maximum station separation: 2.8 kilometres
- Maximum number of stations: 1024
- Medium: shielded coaxial cable, baseband signaling

- Topology: branching non-rooted tree; bus
  
- Data Link Layer:
  - Link control procedure: fully distributed protocol, with statistical contention resolution.
  - Message protocol: variable size frames, best effort delivery.

Ethernet was chosen for the NTT, as it is the only system which is world wide standardized and supported by a big number of firms. It was primarily developed for use in office automation, distributed data processing, terminal access and other applications requiring economical connection to a local communication medium which carries traffic at high-peak data rate bursts. As, at the moment, many developments are going on in the field of Local Area Networks, the market needs to be surveyed in a year or two to see whether another well tested system is appearing which would be especially suited for process control on the VLT.

### 7.3 Main Axes Servos

The most demanding servo systems on the telescopes are the two main axes ones for azimuth and altitude, especially under the condition of exposing the telescopes to full windload. The calculated maximum windtorques for the VLT will be 14 times higher than at the NTT. Due to the size of the telescopes, the reduction factor in a one stage spur gear can be 2 to 3 times higher than at the NTT. Torque motors with 5 or 7 times the torque of the NTT motors are available. One problem with such big motors is their power dissipation. To avoid warm spots at the telescope, disturbing the seeing conditions, the motor coils have to be cooled efficiently. A solution comparable to that of the NTT drives would also be feasible for the VLT. As the heat is produced in the motor coils which are normally mounted on the rotor, the motor principle is changed in such a way that the rotor is fixed to the telescope structure and the stator is turning. The cooling of a non-rotating piece can be done much more efficiently. At the NTT the temperature rise of the motor coils under full load with water cooling will be only 10°C in comparison to 120°C without cooling. When applying this principle, the motor power has to be supplied via slip rings. The application of brushless motors is also being considered as they now exist on the market with a similar torque range as conventional torque motors. It would simplify the mechanical design and the cooling. On the other hand it increases the complexity of the electronics.

As the diameter of the light beam through the altitude axis is much bigger than for the NTT, a different solution for the encoding has to be used. For the VLT it is therefore proposed to use incremental strip encoders for the positioning of the telescopes, combined with friction roller coupled incremental encoders for the tracking.

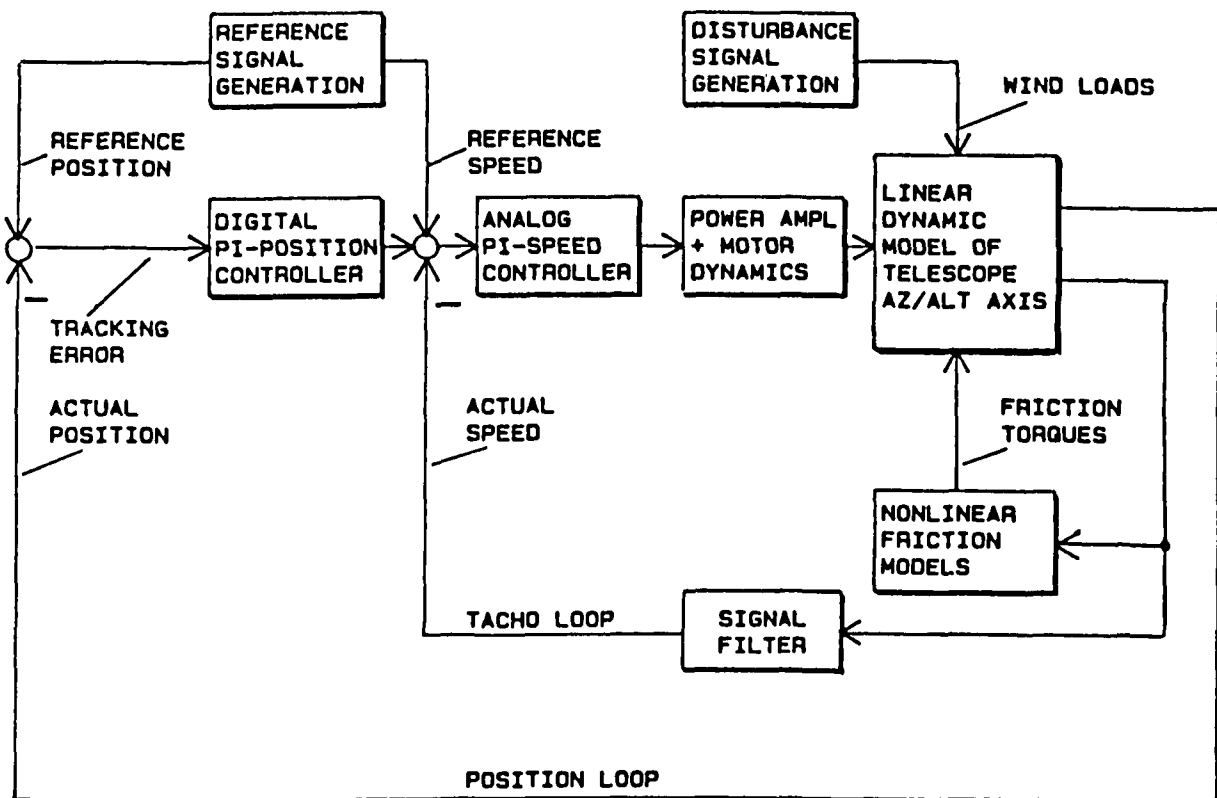


Figure 7.3: Structure of the control system.

The possible application of Laser gyros as an encoding system will be checked in the near future. A test at the 3.6m telescope will give information about stability, the reproducibility and the equidistance of the Laser gyro pulses. The use of Laser gyros would very much simplify the high precision mechanics. As the telescope will be exposed to nearly full wind load, special care has to be taken to push the resonance frequencies (locked rotor and free rotor) and the eigenfrequencies of the structure as high as possible in order to improve the tracking performance. A possible scheme of the servo system with a cascaded controller is shown in Figure 7.3. During the adjustment procedure additional loops may be installed as needed to improve the telescope response (i.e. accelerometer feedback).

## 7.4 TV-Image Analysis

In principle it should be possible to use one single intensified CCD detector to derive all the necessary information for autoguiding, active optics and adaptive optics. But the

differences needed in resolution, sensitivity and real time performance may require two different guide probes and two detectors.

In Chapter 6 it is proposed to improve tracking performance under high dynamical windloads by tilting Mirror 2. The necessary information for the M2 tilt (which is already a part of adaptive optics) and for the autoguiding can probably be derived easily from one detector. To avoid conflicts between the telescope and M2 movements, a cascaded correction should be used. The first loop will be closed between the detector and the M2 tilt movements, thus performing the fast corrections and the autoguiding. As the tilt range of M2 will be limited, the mean deviation of the tilt after some seconds (defined by the lowest resonance frequency of the telescope drives) has to be checked and if it is bigger than 0.1 arcsec, an offset correction has to be performed by the telescope axis.

The required real time performance of the adaptive optics will probably be the first case where a special hardware connection between CCD-microprocessor and the processor for the control of the adaptive optics will be needed, thus not following the master-slave principle. The adaptive optics is controlled by each telescope computer, while the optical beam combination is controlled by the central computer.

## 7.5 Instrument Control and Data Acquisition

### 7.5.1 Hardware

Figure 7.1 shows the distribution of the instruments on the VLT. The meaning of instrument here is any electro-mechanical unit where movable parts are computer controlled. As previously explained, all such units will be microprocessor controlled via a distributed control system. This means that on the LAN connecting the different microprocessor systems for telescope control, there will also be other microprocessors controlling instrumental functions. The microprocessors will have to be capable of on-line control of all instrumental functions of the VLT, taking away from the control computers the real-time demands in the range of about 1-300 msec. The function of the telescope control computer will be then to set-up and periodically check microprocessors in order to convey all the needed information to the user. The information exchanged on the LAN will contribute only modestly to the traffic due to telescope control operations. This is why even a LAN like Ethernet will be adequate: its bandwidth of 10 Mbit/sec is so high that there will be no danger of collisions (i.e. non deterministic behaviour of the LAN).

Quite a different demand will be imposed by the detectors, which might easily provide several Mbytes per exposure. Because of this, detectors like CCD's are today directly coupled to the minicomputer (normally via CAMAC), so that data can be quickly secured on disc and tape. Here is where the real-time and I/O capabilities of today's control minis play an important role. In any case, the data readout always

takes several seconds. Therefore an easy improvement is to perform data acquisition via distributed control, once more via a microprocessor system. This should be capable of buffering/staging the acquired data in their entire volume (all the burst of raw data corresponding to one exposure). Later on, data will be passed to the control computer for archiving on tape and for evaluation by means of on-line image processing.

A further advantage of using a dedicated microprocessor for data acquisition is that it can also perform preliminary data screening and compress data. This would allow for example to remotely transmit data directly in a standard format, while the archiving of data locally goes on in parallel.

What has been said so far shows that everything can be controlled and acquired by a set of micros in a network. This would much reduce the role of the control computer, if it were not for links to other computers in the VLT and for the interface with the user. In reality the picture is still more complex. In instrumentation control there are "cross-functions" which require coordination of different parts of the equipment. In data acquisition there are the "continuous flow" detectors, where readout has to be done all the time and reduction has to be done on-line. Even in this case, like in photon counting, images can be pre-processed by a micro and possibly chopped into parts, but the degree of on-line cooperation with the control computer is higher. This means that while the desirable trend will be to confine all time critical functions to the micros, in practice it will also be necessary that the control computers have some real-time capabilities, although certainly less so than today's control minicomputers. To cope with the data volume of detectors, a separate LAN will be required. A high bandwidth deterministic (i.e. token passing) LAN will fulfil these needs better than Ethernet but standardization is as yet far away in this area. This LAN will also connect the telescope control computers to the central computer(s), allowing data acquisition there in case of beam combination with synchronous set-ups at the 4 telescopes.

## 7.5.2 Software

Software control and data acquisition systems serve the purpose of managing telescope, instrument, detector and image processing operations in a way which has to be comprehensive and clear to the user. The higher the degree of checking, interlocking and modularity allowed, the better it is. At the same time the higher the degree of integration of different parts into a unique and friendly user interface, the better is the success of the system. The need for a data acquisition system has been recognized and implemented in La Silla some years ago. However, it is a rapidly evolving field in which new needs inevitably develop, as soon as users see a possibility to perform their work more efficiently. The requirements for data acquisition are also evolving as a result of the increased complexity of instruments and telescopes. At the NTT, the presence of two instruments at the same time on the telescope and the need to cope with instruments like EMMI, with two detectors, have dictated a new design of the NTT acquisition system. The aim of this is also to test features needed on the VLT. On the VLT the list of general requirements for the control/acquisition system will comprise:

- Multi-user operation,
- Multi-instrument operation,
- Multi-telescope operation,
- Automatic observing procedures,
- Computer assisted programme evaluation,
- Integration with image processing,
- Access to catalogues and previous data, and
- Remote observing (see Section 7.8).

All these requirements will have to be incorporated into a set of programmes, libraries of subroutines and protocols to control communication between the different parts, namely the VLT control/acquisition system. Architecturally this system will have to be a completely distributed one, jumping two steps ahead of the present single computer, single-user system.

However, many of the above features will be already present in the NTT control/acquisition system.

### **Multi-user operation**

This means that while one user is using some equipment (i.e. instrument and telescope), one or more others are doing other activities, even on the same telescope. One of these could be to simply monitor what the first user is doing, another could be to work off-line looking at what is going on in the system. The third activity could be to test, set-up a different equipment (i.e. a second instrument), but this case is covered under the multi-instrument operation.

### **Multi-instrument operation**

This means that while one instrument is used for astronomy, another can be maintained or tested. This can be another equipment on the same telescope. It is assumed as a prerequisite that all instrumentation is mounted all the time and that the computer is capable to interface to the whole of it.

Instrument programmes have to share hardware/software “resources”.

Testing instruments which do not have the telescope beam must be possible without disturbing the real observation.



Some part of the control system has to take precautions that other instrument programmes do not send illegal commands, for example, to the telescope. The control system should decide if an instrument switching can be done at all. "Hot standby" of the other instrument programmes should be foreseen, so that it should be possible to prepare an integration on one instrument while an integration on another instrument is going on (a dark exposure, for example).

### Multi-telescope operation

This is first of all the need that the various telescopes perform independently. At the same time, users at various sites (central computer, Garching, etc.) must be capable of taking part in the observing at different levels as described under the multi-user Section.

Alternatively, control of the various telescopes has to be coordinated in the case of optical beam combination. Data acquisition will be done at the central computer but with synchronisation constraints on the four telescope computers.

The more demanding requirement is for simultaneous observation at the different telescopes. Here data acquisition is done by the various control computers and there will then be an electronic beam combination. This can have different characteristics, like superposition of acquired exposures or pixel by pixel reconstruction at the central computer.

### Automatic observing procedures

Whoever the user of the VLT telescope will be, a visiting astronomer or an operator, a large number of parameters have to be controlled for the smooth running of an observing night. Already today sequences of exposures are executed by the control computer.

This is complex enough under normal conditions, but will be even more critical, should a telescope or equipment part present problems and therefore be excluded. A reconfiguration of the set up must be possible, by letting all other activities proceed to a maximum extent while repairs are undertaken. All this should be automatic with alternative solutions being presented to the user for approval/rejection.

On the NTT, and as an intermediate step towards an intelligent user interface, the fixed forms and menus provided up to now will be replaced by a user definable interface. This means that there will be tools whereby the assisting staff in La Silla will be able to modify the interface to the system (telescope, instrument, detectors), without re-coding the control programmes involved. In keeping with this, the procedures for automatic observing will have to be prepared in such a form as to be directly computer executable.

### Computer assisted programme allocation

The optimization of telescope time use will be possible, due to flexible scheduling and remote control (see below). This will be most effective, if alternative observing programmes are fully specified and therefore can be started in the course of a night, should weather conditions change.

Here again computers can help a lot by offering advice to the person in charge of the VLT about: more suitable programme to be executed under the given conditions, alternative existing programmes, checking of existing programmes with respect to present weather conditions and operational status of telescope and parts available.

### Integration with image processing

This is obviously needed and should allow full integration of MIDAS on-line. The areas where developments will have to be made in order to realise this, are:

- availability of same system and commands both in Garching and on La Silla, off- and on-line,
- direct and efficient access to the image processing data base for storage of data at data acquisition time,
- fast quick look procedures, particularly developed for on-line work,
- on-line feedbacks of image analysis in the form of parameters affecting the running of automatic observing procedures, and
- integration of telescope/instrument/detector/atmospheric parameters with astronomical data (i.e. NTT pool system containing control parameters and MIDAS table system to be closely related and accessible in similar ways).

At the moment image processing integration is achieved on-line by putting both the data acquisition system and the image processing system on the same computer.

This is also a possibility for the VLT case, based on the UNIX portable version of MIDAS and so every telescope computer would have its own image processing system.

An alternative that will be considered in depth and which is made possible by the development of local area networks, is to keep control/acquisition and image processing on different computers, instead of making compromises which limit both.

### Access to catalogues and previous data

Data archiving is being organized at ESO for all its telescopes. Subject to possible limitations of rights, access to this data base may also be possible on-line from the VLT

computers, as quick comparisons with previous observations might be of great value and affect the actual run.

Even more important for on-line work is the availability of a large catalogue of objects, from which the computer will automatically select candidate guide and reference stars.

## Conclusions

From the previously specified requirements, it is possible to deduce a set of general functions which must be fulfilled by the control/acquisition system of the VLT:

- communication between different programmes and micro-, minicomputers, i.e. message system and protocols,
- coordination functions whereby programmes (i.e. telescopes, detectors, instruments) can send commands to each other according to certain rules, i.e. booking system (where exclusive booking of vital parts, like light beam and corresponding equipment will be guaranteed and protected from independent use of other parts of equipment, for maintenance, preparation, etc.),
- pool of central parameters, containing all auxiliary non-astronomical data available: about telescope, instruments, etc., and
- on-line interfaces to image processing.

## 7.6 User End

The subject of the user end is largely connected to the feasibility of remote control. Today, users go to the observatory, since only there can they have full on-line information about what is going on. On the VLT there will be many user ends, some at the VLT, others in Garching and others at some European institutes. It is important that the user end be the same (even if simplified) at all locations. This does not mean that all users will see the same data and even less that they will see the same presentation of the data. There is no need for this, because there are different categories of users: astronomers, assistants, programmers, maintenance staff.

However:

- the information available to every user station has to be the same,
- the user must be capable of selecting an appropriate set-up for the information he needs, and

- astronomical data may undergo cutting, compression, etc. and be available only with delays at the various stations.

From the hardware viewpoint, user stations should be identical, so that there can be one for every telescope of the VLT and one more in Garching with the same hardware. The “specialisation” of the user end will be done by software, by simply choosing different graphics, labels and pages.

An interesting point in this connection, and fully confirmed by our first tests on remote control, is that it does not entail additional costs to have such a comprehensive workstation in Garching, as the load on the remote link represented by the control data is only a small fraction of that represented by the astronomical data.

This then also allows to consider having a set of workstations in Garching as the user ends for the individual/combined use of the VLT telescopes. A night assistant in Garching can help astronomers or an ESO astronomer can observe on their behalf, fully from Garching. Users will see Garching as their station, with basically no need to go to the VLT site, except for special observations.

## 7.7 Computers

### 7.7.1 Control/Instrumentation Minicomputers

Going back to Figure 7.1, we see the fundamental components of the control/data acquisition system of VLT. The four telescope control computers shown there and the central computer are linked via the LAN. From the viewpoint of the hardware, they fall into the category of very large, real-time minicomputer configurations, with computation performances well inside the range of current superminis. Their purpose will be the coordination of telescope control functions (transformation of coordinates, corrections for flexures, etc.), instrumentation control and data acquisition.

Other very important aspects for computers to be installed at the VLT site will be the behaviour with altitude and maintainability. A suitable solution for the VLT would be a 32 bit UNIX based minicomputer with real-time capabilities.

### 7.7.2 User End Workstations

When the user end was described, some basic needs became clear at the user side which have an impact on the computers used there:

- The user interface has to be like for the NTT, a flexible, adaptable interface with colours, graphics, menus, tables, etc.

- Image processing (MIDAS) has to be accessible on-line.
- Some “Expert System” features would be desirable to cope with access to catalogues, previous data, etc.
- Some stations (control stations) will need more of this computer aided expertise when advice on observing programmes or repairs is needed.
- One or more stations will have to be expert systems helping off-line for automatic programme preparation and checking.
- A number of these stations must exist at the VLT site and in Garching.

All the above requirements should be compatible and coexist in one computer. Work is already going on in ESO in defining a desirable UNIX workstation for MIDAS and in parallel to enter the area of expert systems. For the users, the user end workstations would be the successors of today’s terminals, also for control/acquisition.

In conclusion the foreseeable picture of the computer configuration is that there will be three layers of computers on the VLT:

- the control/acquisition microprocessors on different control LANs,
- the control/acquisition minicomputers, and
- the user end workstations.

While the relation between control minicomputers and micros will be hierarchical, the minis and workstations will be at the same level on the LAN and the remote link.

The user end stations will be dynamically configurable to become: operator consoles, data acquisition or image processing stations, or all three at the same time.

The splitting of roles between various CPU’s will present no problem as long as well established computers with LAN interconnect capabilities are chosen. However LAN performance is crucial to allow the proposed split in functionality between control and user end computers. Should speed on the LAN not be satisfactory, one will have to fall back to the present approach of putting both control and image processing functions on one computer.

## 7.8 Remote Observing

The concept of “remote observing” has been applied to cover anything from interactive observing from a distant control room (in which sense we shall use it) to absentee observing (carried out by a resident observer for someone else). Satellite observations

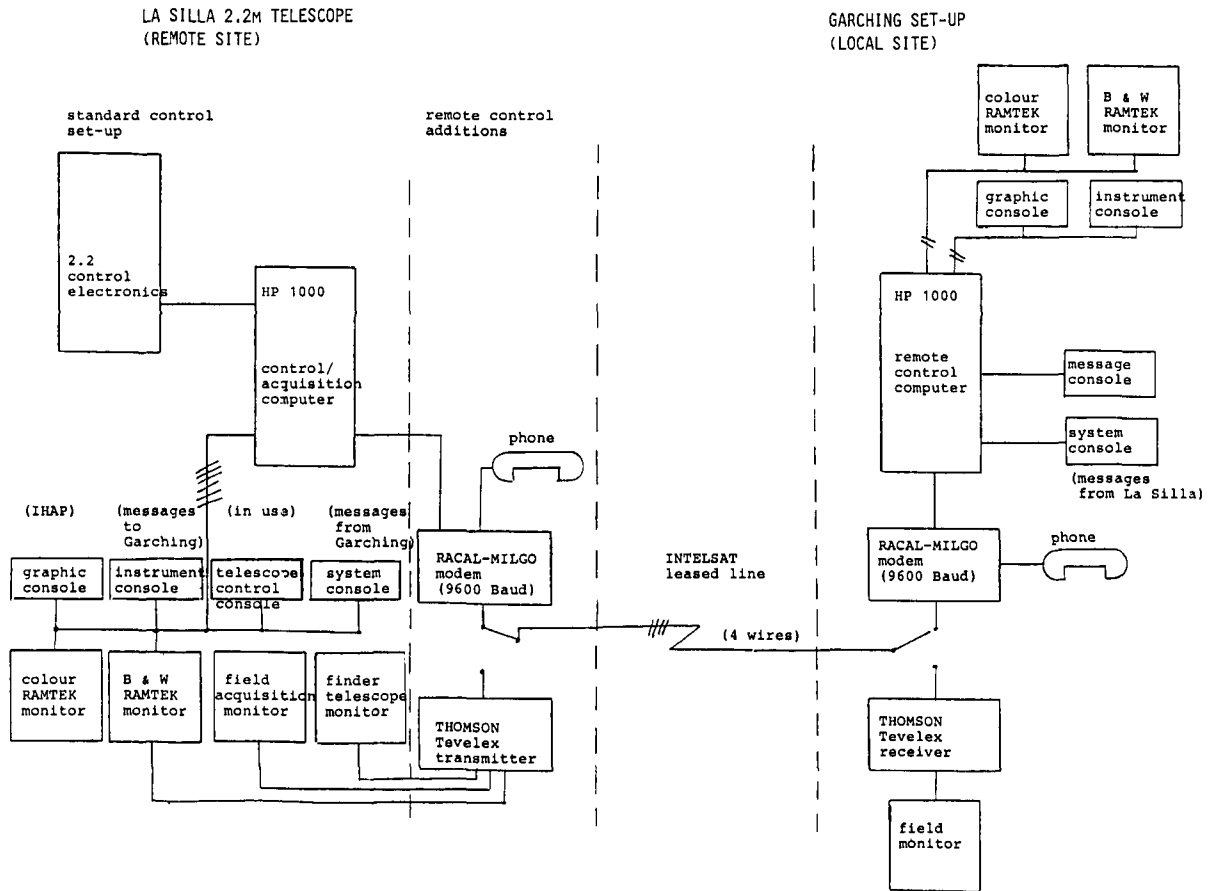


Figure 7.4: Remote control configuration; 2.2 metre telescope.

often come closer to the latter although some degree of interaction is allowed to the astronomer through an operator; this could also be an interesting operating mode for the VLT.

Successful tests with remote observing have been made at ESO, in which the 2.2m telescope at La Silla was controlled from Garching (Figure 7.4). Much may be expected to be learned during the coming years, especially on global reliability, observing efficiency and the suitability for different types of programmes, see also the Chapter on Remote Control in the Proceedings of the Second ESO VLT Workshop (Venice, 1986).

In the near future, computers at European institutes will be networked to Garching in order to enable access, also to the ST/ECF data base. As soon as remote observing from Garching becomes a possibility, this should allow scientists at these institutes to indirectly carry out the same from their home institute. It will of course in general not be possible to reproduce a complete control station at every astronomical institute, but observers should be able to monitor on-line what is happening, and with some delay and compression, to receive data.

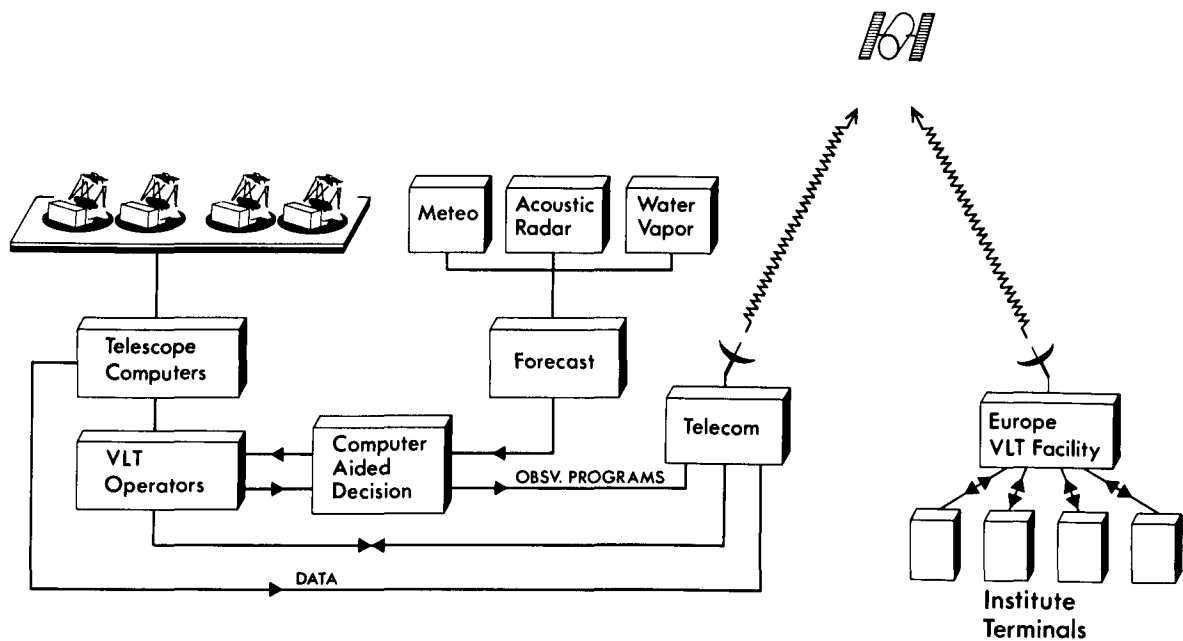


Figure 7.5: Possible operating scheme for the VLT.

The principal advantage of remote observing is that it allows flexible scheduling as a function of atmospheric conditions. All too frequently at the moment someone travels to La Silla for a programme which requires excellent seeing to have only some mediocre nights, while another astronomer a week later experiences superior conditions which his programme does not need. With the VLT such wasteful procedures cannot be accepted. In Figure 7.5 a global view is given of the local/remote operation of the VLT.

# Chapter 8

## BUILDING

### 8.1 General

A number of requirements, many of them common to all telescope projects, some others specific to the VLT concept of a linear array, have been considered for the design of the VLT building.

- A stable base is required for each of the four telescopes.
- The concept must include laboratories and in general adequate space for instrumentation and supply equipment, considering both joint and independent modes of operation of the telescopes. Control of the four telescopes should be performed from a central location.
- Effective protection must be provided for the telescopes, when they are not in operation.
- A protection may also be necessary in order to limit the wind loading on the telescope structures, so as not to penalize the structural design or decrease the amount of available observing time.
- For most applications, an outstanding seeing quality is essential. Sites with particular good seeing are envisaged. Consequently, the seeing must not be degraded by the enclosure arrangement.

The general configuration must also be convenient from the point of view of logistics and handling, as well as transport of heavy equipment, in particular of the primary mirrors. The available surface will in any case be limited in practice by the amount of rock that can be blasted within a reasonable frame of expenditure.

Two main considerations have driven the elaboration of the present concept for the VLT enclosure. The first one is the choice of an open air arrangement of the telescopes



during observation, as a solution that would in the end both ensure optimum seeing conditions and minimize the enclosure cost. This configuration is now considered feasible, in particular in view of the performance expected from key elements of the telescopes such as the drives and the mirror supports, and the associated control systems. The second main concept driver is the fact that the telescopes will be controlled from a central location, which reduces considerably the volume and service requirements that often constrain the definition of telescope buildings. Thus the shelters needed for the telescopes, when they are not in operation, have only a protecting function and can be completely opened or removed for the observations.

The problems of seeing and wind loading are central to the design of the enclosures, cf. VLT Reports nos. 41, 44 and 46. What concerns the seeing, it has been recognised that a moderate wind flow is more favourable to optimum seeing conditions than the nominally stable and controlled environment inside a classical dome. In fact, if the telescope is exposed to the wind, whatever heat is transferred from the surfaces to the air is quickly swept away and does not affect the optical properties in the field of view. Minor temperature differences between surfaces and air, of the order of a few tenths of a degree, which in a closed dome suffice to create unfavourable seeing effects, become irrelevant in a continuous air flow.

However, although wind exposure will have a very positive effect on the seeing performance, the wind loading on telescope structures and mirrors is an important constraint on the VLT design. In this connection, the open air concept of the VLT profits from the fact that in the mountains of northern Chile where the VLT may be located, the wind blows predominantly from north. The telescope, which for the purpose of interferometry should preferably be oriented in East-West direction, will naturally be facing the prevailing wind, so that turbulence caused by one unit will not affect the others.

The telescopes will be designed to perform adequately at least up to the average wind loading conditions of the site. A fixed linear wind screen placed normally to the predominant wind direction will then ensure an acceptable telescope performance under the more severe conditions.

Moreover, a number of operational requirements have been considered in the definition of the VLT enclosure. For instance, a separate laboratory, parallel to the array, is foreseen for performing interferometric measurements. This is viewed as an important feature of the VLT configuration which should allow:

- Easy switching to interferometry with no further disruption of normal observing.
- Independent use of the interferometer with smaller auxiliary telescopes.

In summary, the general enclosure arrangement which resulted from the feasibility studies (VLT Report no. 46) is shown in Figure 8.1. We consider here the case of a compact array where the four telescopes are placed approximately equidistantly and close to one another.

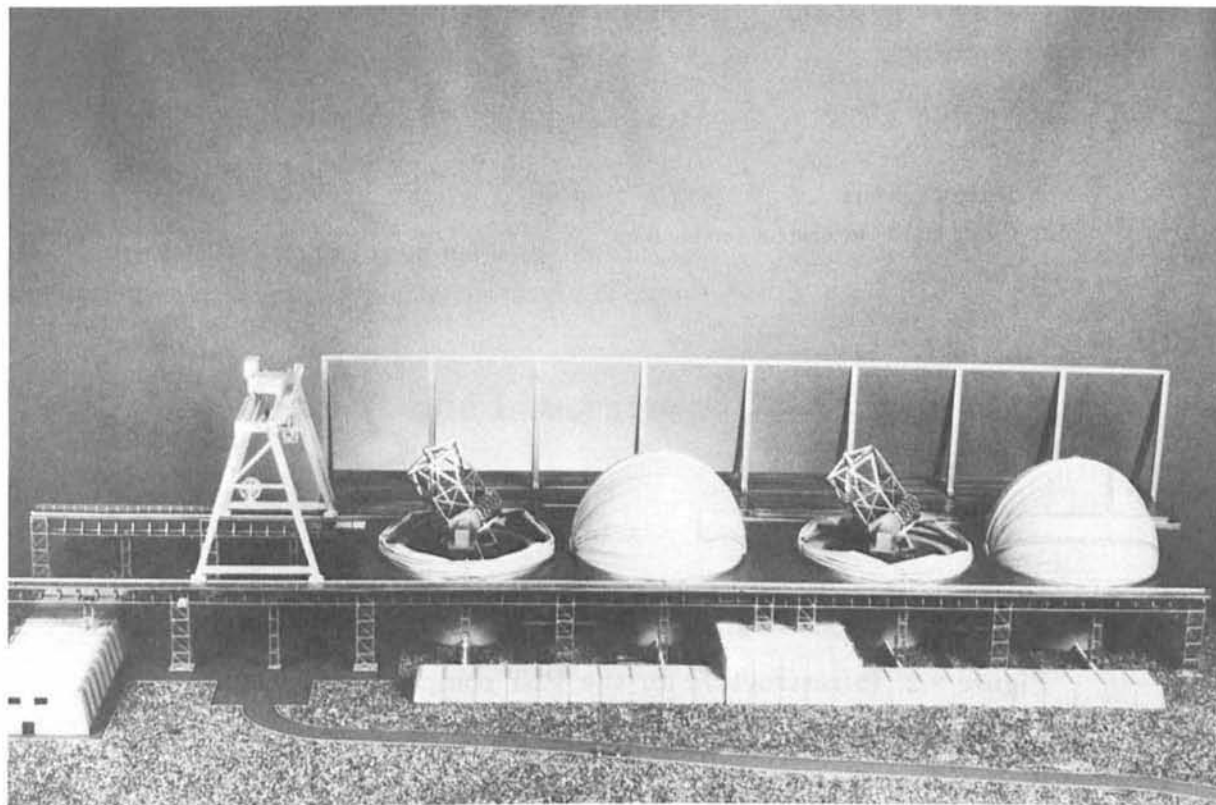


Figure 8.1: Model of the VLT arrangement.

There will be four independent telescope pillars. A building containing the main control room and the Coudé laboratory for incoherent beam combination will be placed near the centre of the array. Another separate building with the interferometric laboratory will be set parallel to the telescope array. A platform-like structure will surround each telescope, providing access, support for the shelters and the crane, and some insulation from thermal and aerodynamic influence of the ground and the structures below. In front of this platform, in the upwind direction, a wind screen will protect the telescope array in case of strong winds. The telescope shelters will be inflatable domes, a novel design derived from the experience of large antenna radomes.

From a functional point of view, the enclosure complex of the VLT may be divided in two major subsystems: an infrastructure with the pillars, control rooms and laboratories, and an upper structure which includes the enclosure, wind screen, handling equipment, etc.

The individual components are now described in more details in the next Sections.

## 8.2 Infrastructure

The infrastructure of the VLT (see Figure 8.2) includes the four telescope pillars, whose main function is to support the telescopes, and the buildings required to house control rooms and laboratories.

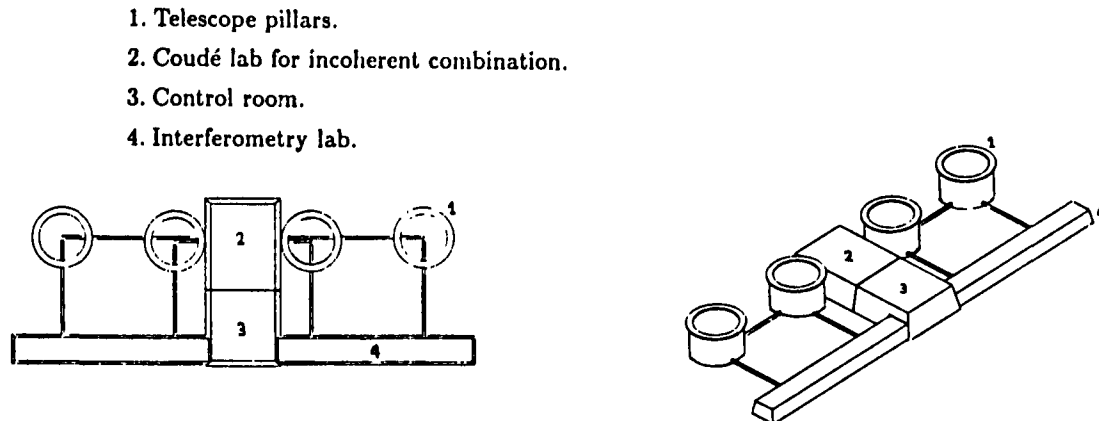


Figure 8.2: Infrastructure for the VLT compact configuration.

The layout of these constructions is essentially determined by volume and location requirements. The Coudé Laboratory, where incoherent beam combination will take place, is therefore located at the centre of the array, between the bases of telescopes 2 and 3. The Interferometric Laboratory, a long, narrow building, is placed along and parallel to the linear array. This laboratory will house the special equipment needed to combine the beams, e.g. delay lines, combining mirrors, etc. The Control Room, from which all four telescopes will be controlled, is presently annexed to the Coudé Laboratory, although it may actually be placed anywhere, depending, in particular, on the site configuration.

### 8.2.1 Telescope Pillars

The pillars of the telescopes are concrete structures of cylindrical shape. The diameter, as required for supporting the telescope, is about 16 metres.

The optimum height of the pillars will ultimately be fixed by an analysis of ground induced seeing and near ground wind turbulence. Preliminary measurements of near-ground thermal turbulence indicate that the elevation axis of the telescope may have to be placed about 10 to 15 metres above the ground in order to ensure that the optical performance is not affected by ground effects. In this case the height of the pillar, considering the dimension of the telescope yoke, will be between 5 to 10 metres.

The large diameter of the pillars allows to attain a very high rigidity with a relatively light structure. For a preliminary dimensioning, a bending rigidity (EI) of  $5 \cdot 10^{12}$  Nm<sup>2</sup> (e.g. ten times the value specified for the ESO NTT) was adopted, resulting in a cylindrical wall in reinforced concrete of 30 cm thickness. Two possibilities are presently envisaged:

- Standard cylindrical shell of thickness 30 cm.
- Twelve-sided cylinder made of pre-fabricated elements.

Figure 8.3 illustrates, in some more detail, the configuration of the first option, in particular with a service platform for maintenance purpose.

### 8.2.2 Combined Coudé Laboratory

The Coudé Laboratory is located in a building placed between telescopes 2 and 3.

Dimensions of the internal space: Length: 20 m  
Width: 20 m  
Height: 5 m

If needed, this building can be divided into four instrument spaces ( $10 \times 10 \times 5$  m) around a central hole (diameter 3 m, depth 3 m) which, like the floor, is unconnected to the main structure. Four removable partitions may effectively separate the instrument spaces.

Corridors allow to reach the four instrument spaces. Thermal control and stable conditions are achieved by a cooled floor. In the solution presented in Figure 8.4, the main walls, slabs and beams are pre-fabricated elements in reinforced concrete. The preliminary design also considered the possibility of placing 1-m thick concrete blocks on the roof as a cosmic ray shield.

### 8.2.3 Control Room

The Control Room is situated beside the Coudé Laboratory, transversally with respect to the array alignment which bridges the Interferometric Laboratory.

Main dimensions: Surface: 200 m<sup>2</sup>  
Height: 3.2 m above the false floor (30 cm)

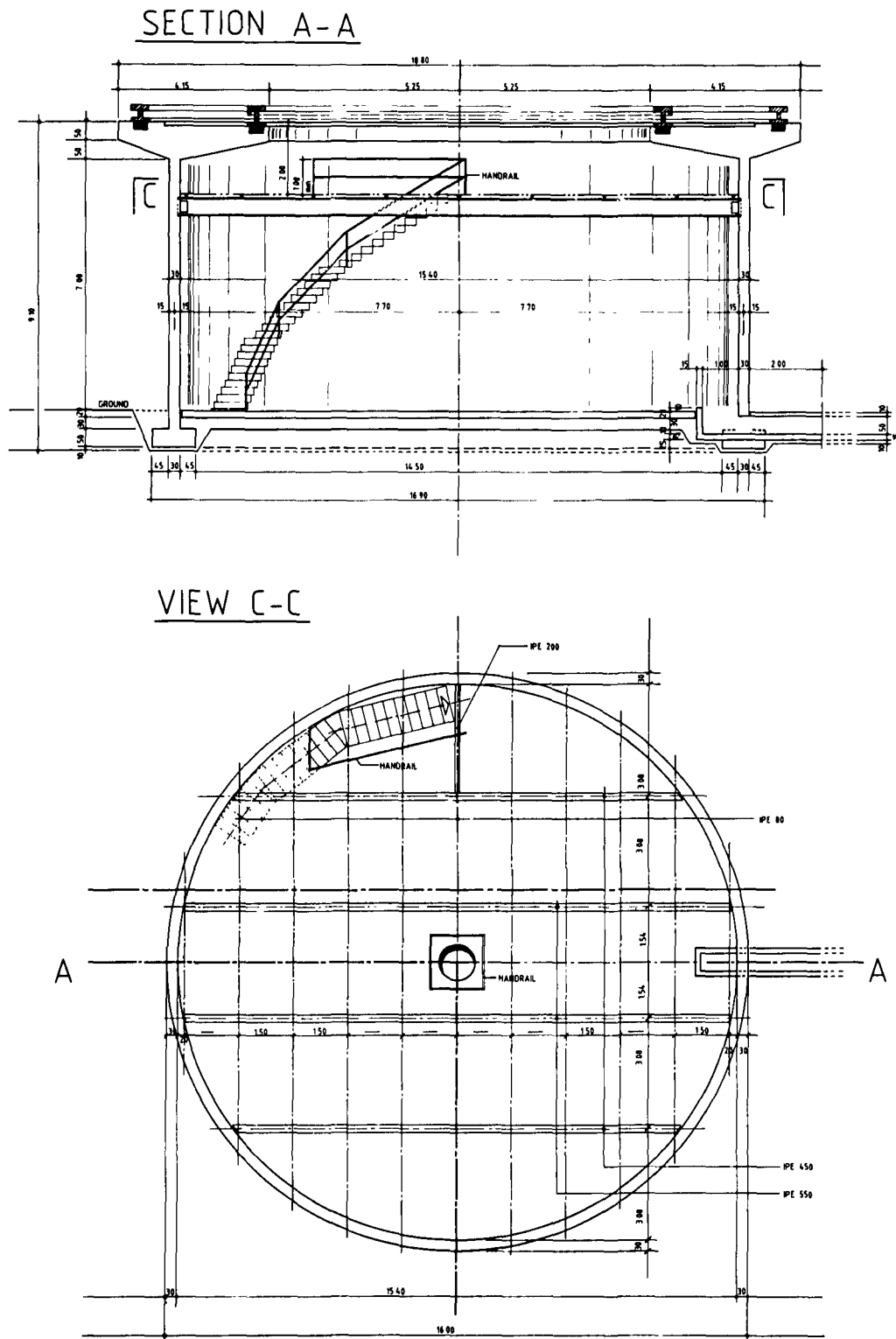


Figure 8.3: Telescope pillar with internal equipment.

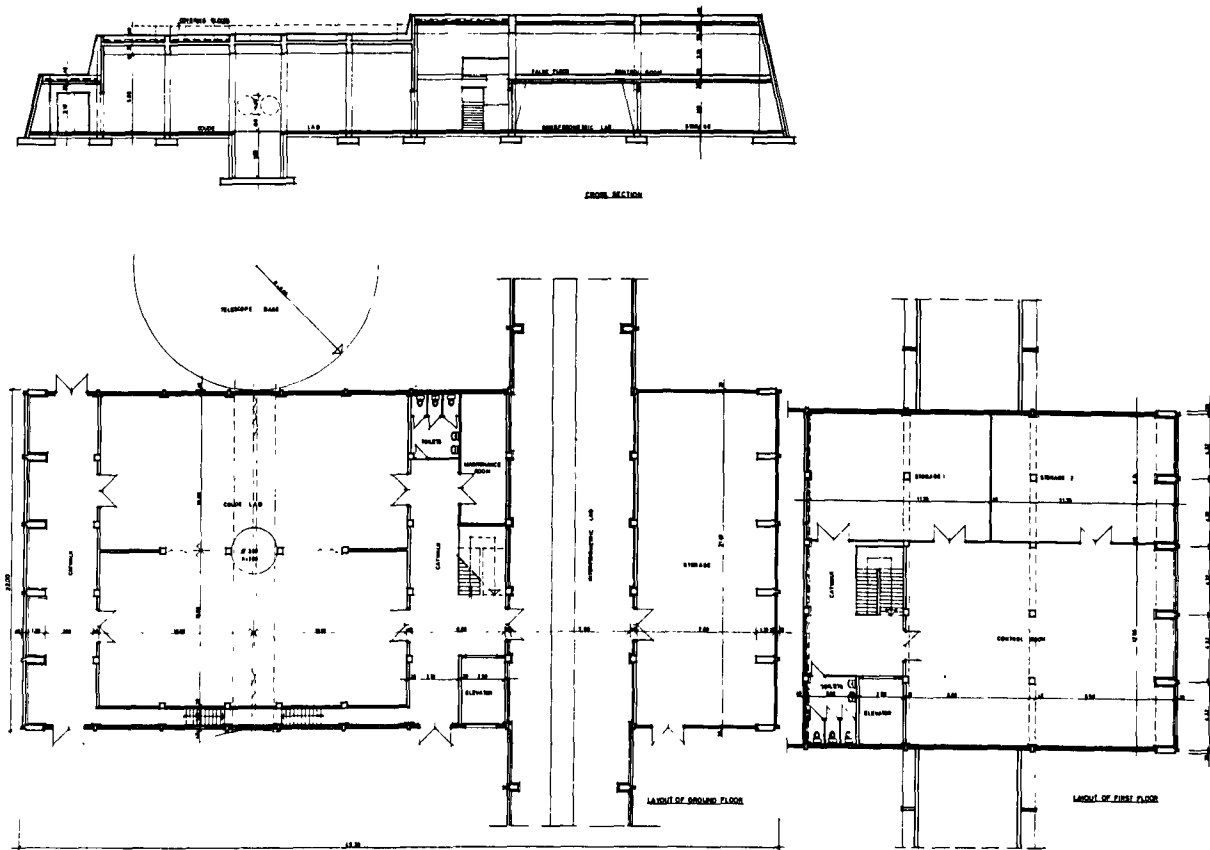


Figure 8.4: Coudé Laboratory and Control Room.

In the solution presented here, the main walls, slabs and beams are pre-fabricated elements in reinforced concrete. Direct access by a staircase is provided to the Coudé Laboratory.

Two 100 m<sup>2</sup> storage and service rooms are situated at the same level as the control room. Another storage room is situated underneath at the ground level.

### 8.2.4 Interferometric Laboratory

The Interferometric Laboratory consists of a long building situated parallel to the array. Its actual length will depend on the total distance between the four telescopes. Here a length of about 120 m is assumed. In the solution illustrated in Figure 8.5, the main walls, slabs and beams are pre-fabricated elements in reinforced concrete and high insulation.

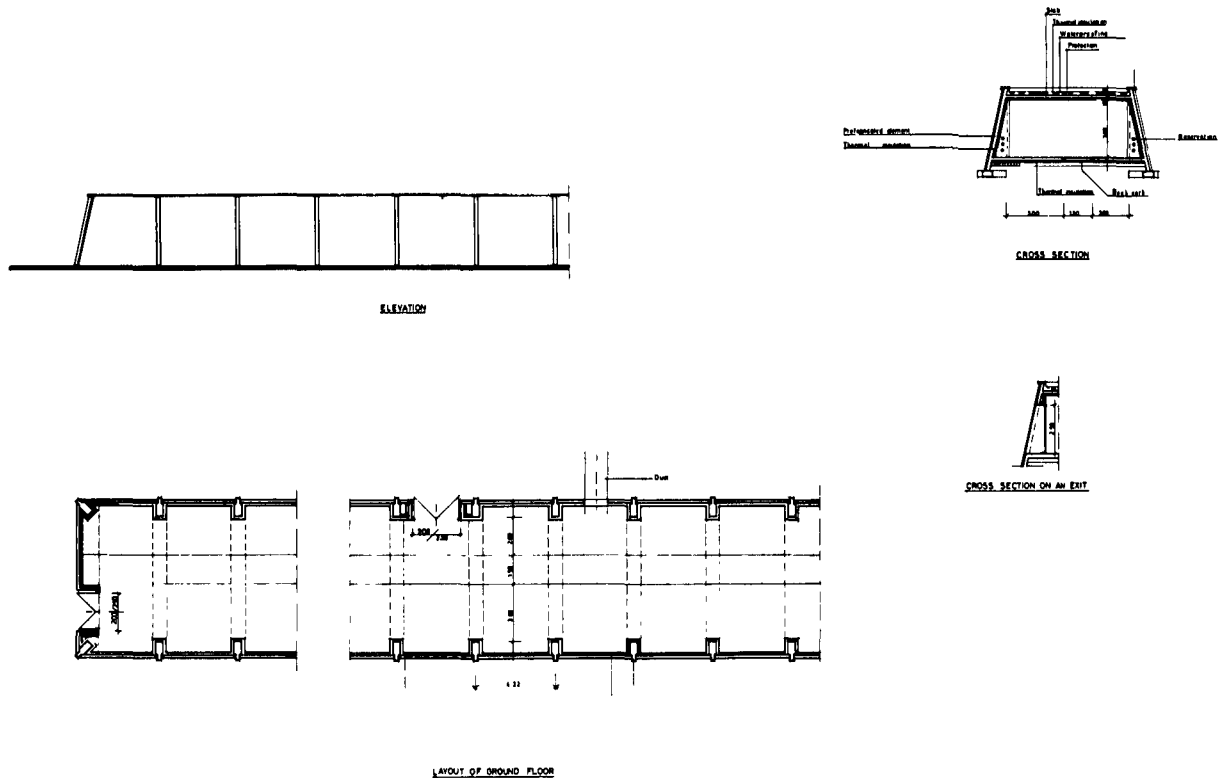


Figure 8.5: Interferometric Laboratory.

The ground slab consists of three parts: two working spaces ( $2 \times 120$  m on the telescope-side and  $3 \times 120$  m on the opposite side) separated by a ground slab resting on cork aggregate for optimal damping, and receiving the interferometric set-up. One entrance is situated at one end, with four more doors ( $2 \times 2.5$  m) near the incoming light beams. A cooled floor will ensure thermal control and a stable environment. Walls and slabs will be painted; a special anti-dust paint will be used on the floor.

### 8.2.5 Mirror Maintenance Building

A building for mirror maintenance will be part of the VLT complex. It will, however, be relatively independent from the other elements and its location will mainly depend on the ground configuration.

Dimension of the internal space: Length: 52 m  
 Width: 14 m  
 Height: 7.5 m

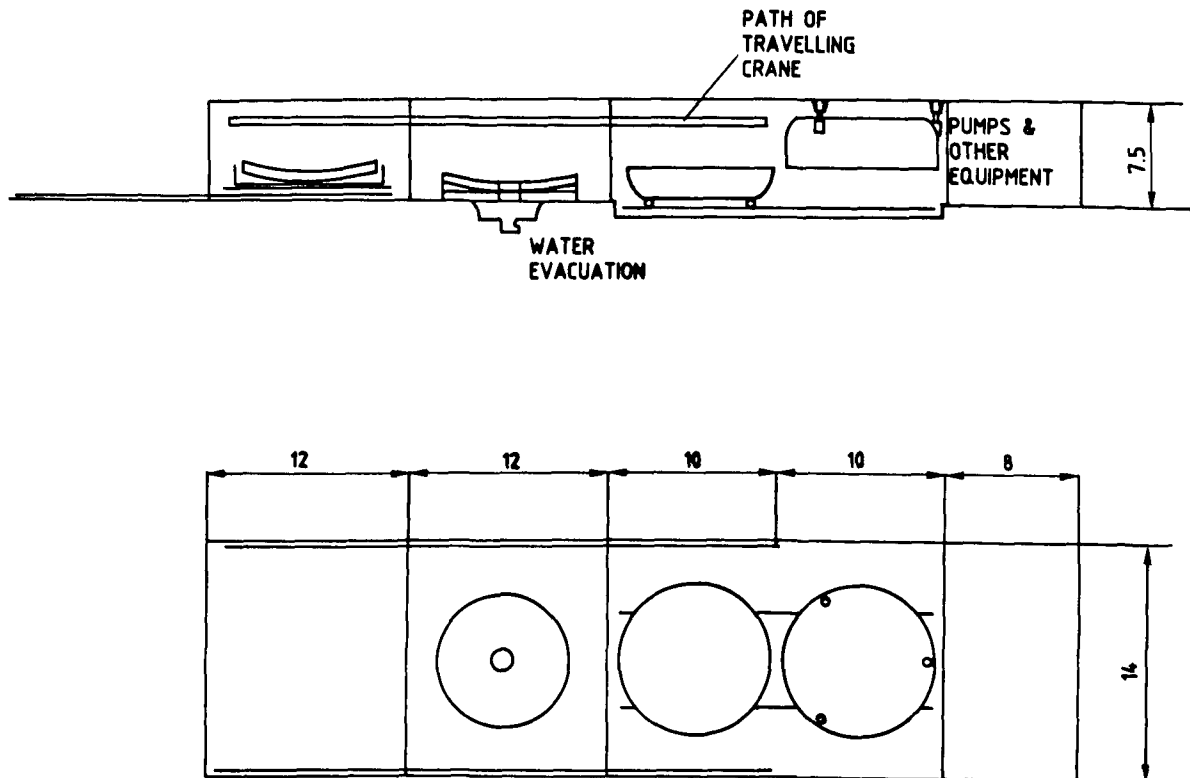


Figure 8.6: Schematic of mirror maintenance building for the VLT.

The building is divided into four sections as illustrated in Figure 8.6:

- 1) Storage:  $12 \times 14 \times 7.5$  m
- 2) Cleaning:  $12 \times 14 \times 7.5$  m
- 3) Aluminization:  $20 \times 14 \times 7.5$  m
- 4) Services:  $8 \times 14 \times 4.5$  m for pumps and other equipment.  
 $8 \times 14 \times 3$  m at first floor for offices.

Main walls, slabs and beams are pre-fabricated elements in reinforced concrete. A travelling crane (load 35 tons) will allow handling and transport of the mirror from the storage to the aluminizing section.

It is presently envisaged to aluminize the VLT mirrors with the sputtering process which requires a relatively low aluminization tank. With this technique, a large size target is located at a close distance from the substrate and bombarded by ions generated by a plasma. Collision with ions causes the target material to evaporate and deposit on the substrate. The main advantage will be good uniformity of the coating and reduced



dimensions of the tank. In view of the high flexibility of the mirror and the risk of handling, it appears preferable to leave the mirror in a horizontal position during the entire procedure, beginning with its removal from the telescope and ending with its return.

Figure 8.7 shows a pre-design of the tank. The mirror will be placed on a rotating table and the sputtering sources located along a radius. The tank will also accommodate classical evaporation sources. The possibility is presently being studied of not separating the mirror from its cell, in order to simplify the handling procedures; this may require a division of the tank into two stages.

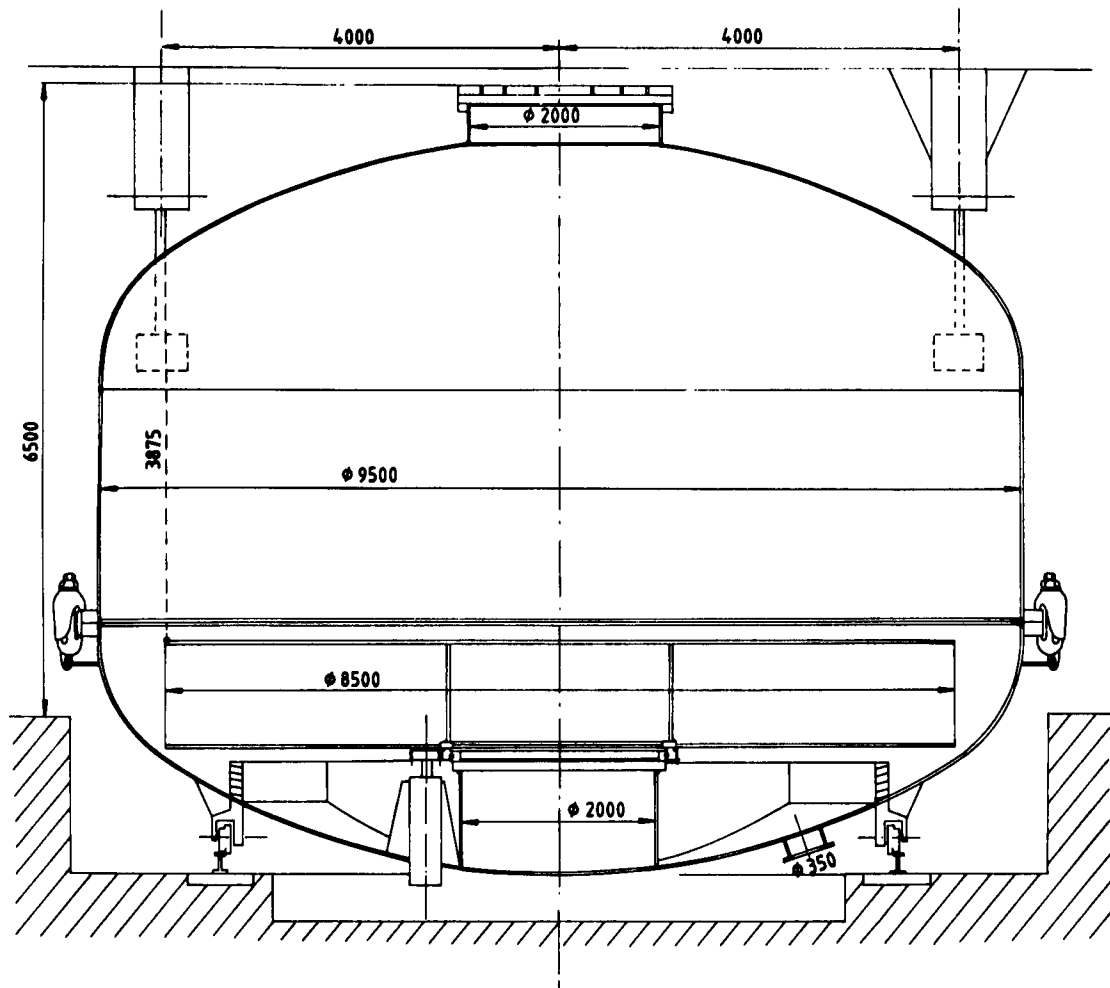


Figure 8.7: Pre-design of a coating plant for 8-metre mirrors.

## 8.3 Upper Structure: Telescope Shelters, Wind Screen, Handling Equipment

This part of the VLT enclosure assumes the function of telescope protection, reduction of wind loads and handling facilities for construction and maintenance. It should be noted that it is the combination of these requirements within one construction that results in the complexity of a classical dome and adds to its size. Contrarily, we have tried in the VLT project to separate the main functions required by different hardware elements. In this way design procedures become simpler since it is possible to optimize separately the individual components. Moreover, a greater flexibility is retained when adapting the overall configuration to an evolving VLT project.

### 8.3.1 Telescope Shelters

The two concurrent aspects of open air operation and control from a (relatively) remote central location permits to define shelters that have only a protecting function, and which can and shall be completely opened or removed during observation time.

During the initial phase of this project, an inflatable dome structure was proposed for the telescope shelters (see Figure 8.8 and 8.9). After further studies, this has been retained as the present nominal solution for the VLT. The inflatable domes of the VLT will be much lighter and cheaper than comparable metallic structures. Their design can profit from the considerable experience already existing with large antenna facilities, which have similar requirements.

In order to establish the validity of the concept, a 15-metre evaluation model is being built and will be erected at La Silla. This model, with a scale of about 1:2 relative to the size required for the VLT, will be used for housing optical tests connected with the VLT project, and it will permit to judge the quality and reliability of the overall concept.

A brief description of the system proposed for the VLT is given below. More extensive descriptions of the concept have been published in the proceedings SPIE 628 342 and 2<sup>nd</sup> Workshop on ESO's VLT (Venice) 379. Each dome (see Table 8.1) consists of a double-wall fabric hemisphere supported by rigid hoops that open and close in two symmetrical parts. The principle of the structure is to use air for inflating the double wall cover and, once the shelter is closed, the internal volume. The strength and stability are directly related to the inflation pressure which may vary from 3 to 30 mbar, according to the wind load acting on the structure. When opened, the shelters are stowed within the platform structure. Three types of hoops are used for supporting the fabric:

- Two main hoops that take up most of the loading, especially during maneuvering.

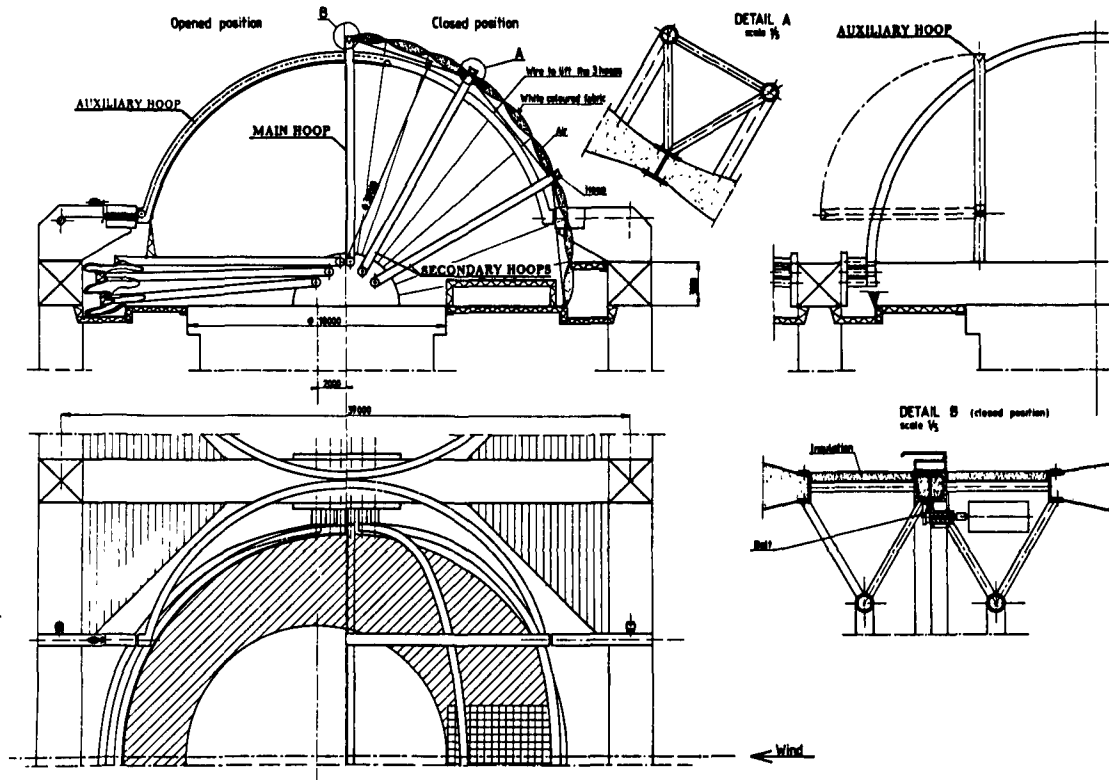


Figure 8.8: Preliminary assembly drawing of the inflatable dome.

- Four secondary hoops that maintain the overall shelter shape when there is no internal pressure.
- Two auxiliary hoops that provide two intermediate support points for the other hoops guiding them and which therefore decrease the loading during opening and closing. These auxiliary hoops will be tilted on the platform when the shelter is open.

Each of the two sections of the double-wall cover consists of nine inflatable ribs of lenticular cross-section. This double-wall solution gives a high reliability to the shelter: If the main blower fails with an ensuing drop in internal pressure, the inflated ribs keep the fabric tensioned. If the external fabric is torn or leaks, the internal fabric is forced against the external one, thereby keeping the external shape, which is very important to resist high wind loadings. Blowers provide pressure both inside the shelter and in the double cover (which is slightly pressurized with respect to the interior). The



Figure 8.9: Photograph of an existing inflatable dome similar to the one proposed for the VLT.

TABLE 8.1

<b>30-METRE INFLATABLE DOME</b>	
<b>WEIGHTS</b>	
• STEEL FRAME	35 tons
• COVER	5 tons
• BLOWERS	2 tons
• MANEUVER SYSTEM, ACCESSORIES	5 tons
• <u>TOTAL</u>	47 tons
<b>POWER</b>	
• BLOWERS	5 kW
• DRIVES (MAIN)	20 kW
• DRIVES (AUX)	12 kW
• AIR CONDITIONING	10 kW

inflation pressure must vary according to the wind speed, the principle being that the internal pressure remains at all times greater than the wind dynamic pressure so that no instabilities can occur on the surface.

The hoop hinges will be set close to the platform level, so that when open and folded, the shelter is completely stowable within the platform, thereby minimising aerodynamic perturbations on the telescope. From the point of view of wind loading during opening/closing operations, it should be more convenient to set the hoop axis normally to the main wind direction. In case of strong wind, the upwind half can be raised first, thus protecting the operation of the second half. The inflatable shelter is stowed in a recess of the service platform formed of a peripheral structure all around the central hole and a floor, supported by short cantilever beams toward the inside of the hole. The floor is designed to be easily air-tightened.

### 8.3.2 Service Platform

A service platform around each telescope (see Figure 8.10) gives a solution to various requirements: access to the telescopes, support and closing floor for the telescope shelters, support for the crane. This platform is presently defined as a light-weight steel lattice structure which reaches the level of the telescope base, from which the inflatable domes rise.

Structural, aerodynamic and thermal considerations will drive the final design. From the point of view of structural design, the definition of the platform is dictated by the support requirements for the telescope shelters and the gantry crane. The aerodynamic aspect favours a lattice structure, largely transparent to the wind and also, for its high convective transfer coefficients and low thermal inertia, favourable from the thermal point of view.

These thermal aspects of the platform surrounding the telescope are particularly important, as they may affect the seeing performance, and they have been the object of a preliminary study. The service floor inside the domes will be treated for low emissivity: cladding with standard aluminium sheeting is proposed. In this way, during the day, almost no heat is transmitted by radiation between the internal surface of the dome and the inside structures and the only source of heat to the telescope may come from the temperature of inside air which can be effectively controlled.

For the platform outside the domes, which is also exposed to daylight, an aluminized coating with low solar absorptivity is proposed. During the day, heating would be limited to 3°C above air with a 5 m/s wind. During the night the maximum cooling would be 1.3°C below air temperature with the same assumptions. Such a temperature difference, which would be serious inside a classical dome, will not have significant effects in open air.

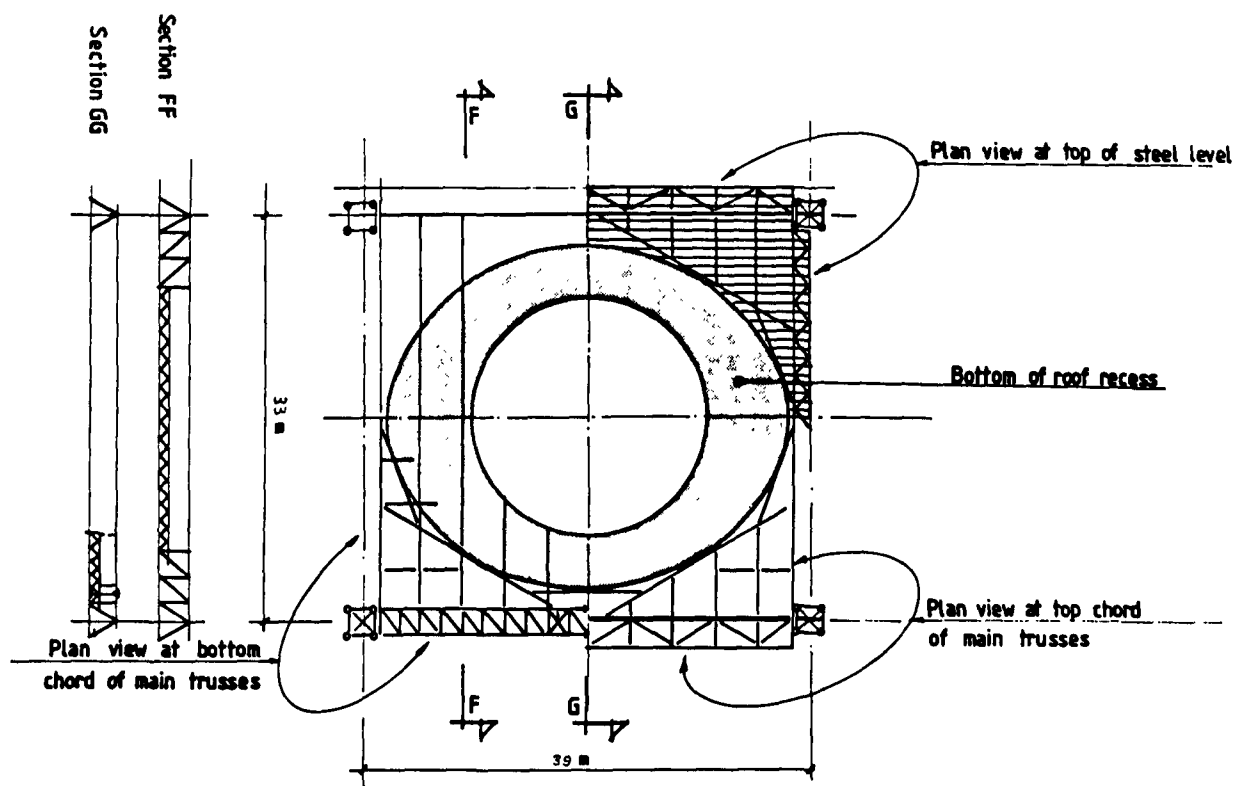


Figure 8.10: Schematic view of one unit of the VLT service platform.

### 8.3.3 Wind Screen

As it has been mentioned in Section 3.5, a limit of 9 m/s has been tentatively specified on the incident wind velocity on the telescope, in order not to penalise excessively the telescope structure design, which has already quite ambitious and severe requirements. Therefore some kind of wind shield to the telescopes will be required to be effective when the mean wind velocity is between 9 and 18 m/s. 18 m/s (which in fact means close to 28 m/s or 100 km/hr gust velocity) is the present limit for telescope operation on La Silla. Following a survey of experimental data available of the subject and an analysis by means of a finite element fluid model, the present definition for the wind screen is a 50% semi-permeable structure rising up to about 3 metres above the telescope top unit and wide enough to shield the telescopes without edge effects.

The presently considered design solution is illustrated in Figure 8.11. It consists of an array of semi-permeable screens that can be set in vertical position or removed horizontally. The screen elements are 20 metres wide. They are supported by a steel frame structure. The actual height of the structure may vary according to the height at which the telescopes will be placed.

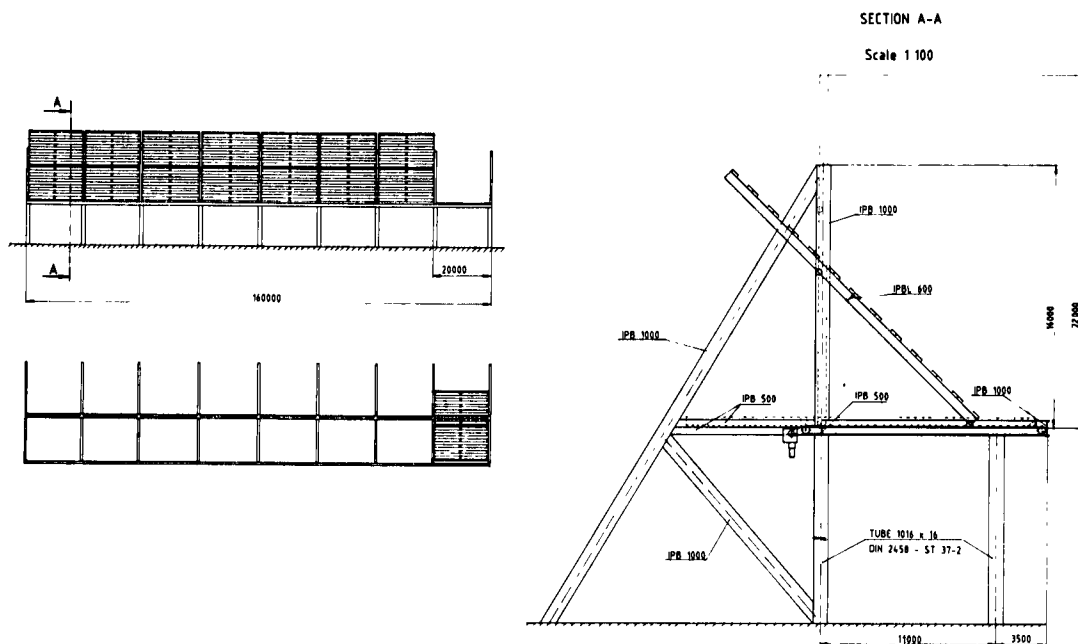


Figure 8.11: VLT wind screen.

With respect to a louvers solution, which was also considered initially, the proposed configuration has some advantages :

- Low winds are left undisturbed, as in such cases the screen is removed. Therefore no unnecessary turbulence or thermal effects are created. Also the obstacle to a very low angle of view is removed, except for the support poles, which rise lower than the screens.
- The screens are not exposed to storms, hence saving structural weight and cost.
- Less mechanisms, lower complexity, thus cheaper.

Each screen element is made of a frame which integrates panels made of 1-m wide plates with a 2-m spacing. The weight of each screen element will be of about 29 tons. The power required to move one screen element is estimated at about 20 kW. Eight 20-metre elements are required for the VLT configuration.

### 8.3.4 Gantry Crane and Other Lifting Equipment

Most telescope buildings include a crane for maintenance operations which adds considerably to the size of the building. In the case of the VLT, an analysis of maintenance operations led to the conclusion that the combination of a single external crane, which will then work with the shelters open, and some smaller equipment within the shelters (lifts, a small mobile crane) would be a reasonable compromise in view of the cost saving with respect to having a bridge crane inside each shelter. A gantry crane moving on the service platform is presently considered but a mobile crane on the ground level eventually combined with a system of lifting carriages could become an interesting option in case of a low telescope pillar (cf. Section 8.4). Indeed the optimal configuration of handling equipment will strongly depend on the area and arrangement of the site.

Once the telescopes are completed, the main handling operation to occur routinely will be the removal of a mirror cell. The procedure presently envisaged for the removal of the cell from the telescope is illustrated in Figure 8.12. The cell can then be lifted by the gantry crane or, alternatively, by a mobile crane or a rail carriage, and be brought within the coating facility.

For the transport of personnel and small loads up to the telescope level, a series of lifts will be installed near each telescope.

## 8.4 Alternatives

It must be noted that the enclosure described above is only the presently nominal solution within a general concept, where many possibilities and options are still open. The final configuration will depend in particular on some very general operational parameters of the telescopes:

1. Distance between the four telescopes.
2. Optimum height of the telescopes above the ground. The actual height of the telescope pillars is of course related to the geometry of the telescope fork.
3. Sensitivity of telescopes to wind loading.

Point 1 is essentially determined by the requirements of interferometry. Point 2 is a question of evaluating seeing dependency upon the general aerodynamic behaviour and weigh it with the cost of the required structures. Measurements of site conditions and



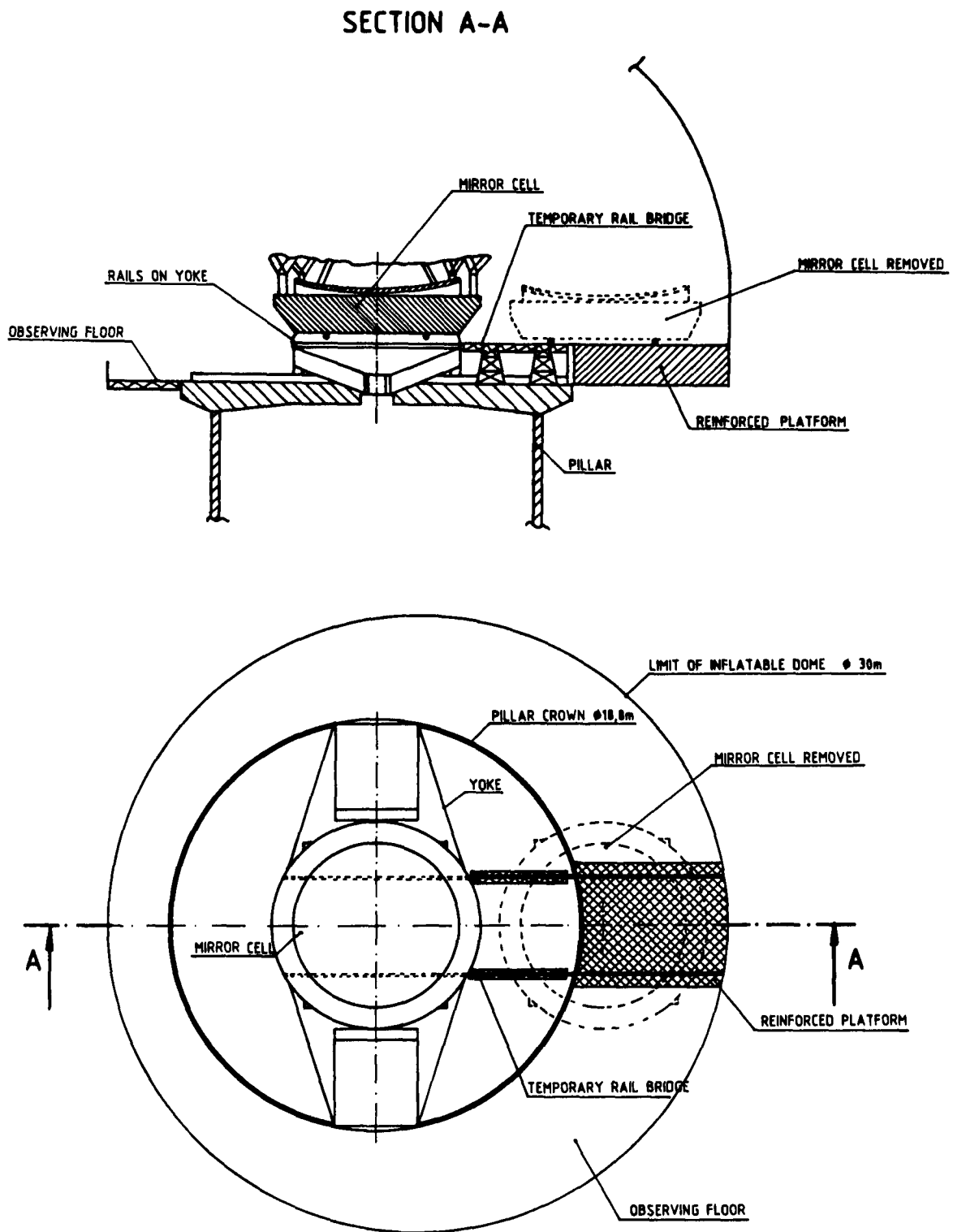


Figure 8.12: Removal of primary mirror.

wind tunnel tests will provide most answers to this point. Point 3 is mainly a matter of technology development: if, however, the performance of the control systems required to let the telescope operate optimally in average free air conditions can not be achieved, the design of the enclosure will be significantly affected. This may be illustrated by the variant shown in Figure 8.13 which was conceived on the following assumptions:

1. The primary mirror must be shielded from direct wind flow.
2. The telescope can be placed at the minimum height from the ground compatible with the path of the light beams.
3. Minimization of the diameter of the inflatable shelter.

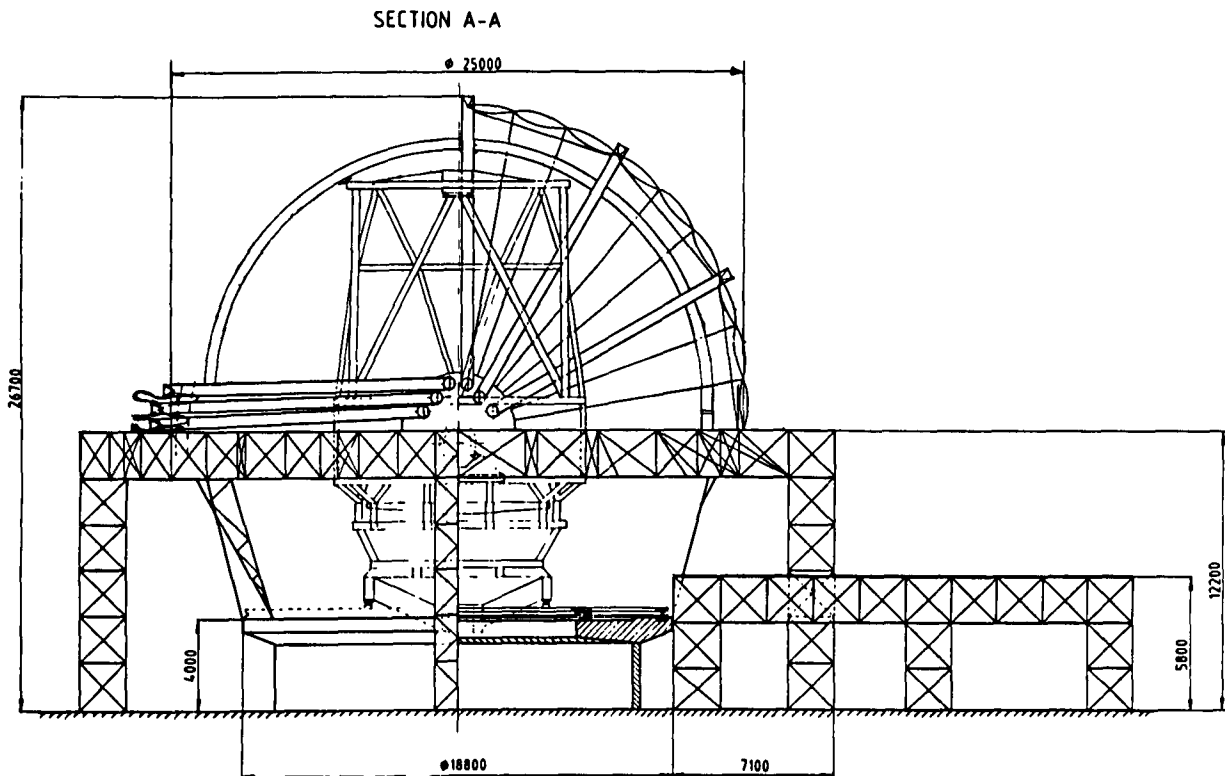


Figure 8.13: Alternative VLT enclosure.

Note that in this case each telescope is surrounded by an independent platform which supports the inflatable dome. The primary mirror is removed to the lower platform at the side. Being only 6 m from the ground level, the mirror cell can then be picked up by a movable lifting carriage, thus avoiding the need of a permanent gantry crane. This is an example of a possibility quite different from the nominal proposal, which becomes

attractive if some of the design conditions presently assumed (Section 8.1) are reviewed in the course of the project.

Also within the presently assumed conditions, several alternatives are possible for the single components as described in VLT Report No. 46. It is worth to mention here the possibility of movable shelters. Although they are heavier and more expensive than the inflatable domes, they will be a reliable backup solution if any development problem should arise with the inflatable domes.

# Chapter 9

## SITE

### 9.1 Requirements for a Site for the VLT

The requirements for astronomical sites have been often described. The ideal site should have low atmospheric turbulence, low water vapor and dust content, a low frequency of clouds, low wind and a small daily (and particularly nightly) temperature variation. Absence of atmospheric pollution and nearby sources is also important.

The present ESO site at La Silla is one of the world's better sites with respect to these criteria. Although the atmospheric water vapor is rather high, there are also periods with less than 2mm precipitable H<sub>2</sub>O. The site was chosen almost 25 years ago on the basis of then valid criteria which included, apart from astronomical considerations, questions like availability of water, nearness to a reasonably large city etc. In view of magnitude of the VLT investment, it is not clear that the latter criteria should have the same weight today. Consequently, a new search has been made to see if substantially better sites than La Silla exist, without considering ease of operation, infrastructure requirements, or personal comfort for the staff. Only when the facts are known does it become reasonable to make the tradeoffs between the astronomical and other aspects.

### 9.2 Possible Sites

#### 9.2.1 Introduction

From all that is known to-date, there are no suitable sites in Australia. While the surveys made by ESO and others in the fifties and sixties have located some good sites in southern Africa, none appeared to be fully comparable to La Silla. The new ESO surveys have therefore been concentrated on various sites in Chile. Since conditions at the Northern and Eastern borders of Chile are inferior to the best sites in that country, other South American sites cannot be expected to have superior quality. For a further

description of these surveys and the equipment used reference may be made to various papers in "ESO Workshop on Site Testing for Future Large Telescopes" and in the Venice Workshop Proceedings.

The principal conclusion to be drawn from surveys conducted since September 1983 is that both the cloudiness and the atmospheric water vapor content are particularly low in a coastal area of northern Chile centered around Antofagasta. Towards the central Andes in the East, cloudiness increases even though at altitudes of 5000-6000 meters very low water vapor values may be found more frequently. Towards the North, cloudiness and water vapor both increase. In the coastal area there are few high mountains, except some 100km south of Antofagasta where altitudes above 2500 meters are reached at less than 15km from the Pacific coast. It is important to remember that generally atmospheric turbulence (resulting in deterioration of astronomical image quality, "seeing") is better at coastal and island sites than further inland (Walker, ESO Workshop on Site Testing).

Had the very high sites in the Andes had unsurpassed conditions, it might have been worthwhile to study more closely the severe environmental and accessibility conditions. Since this appears to be not at all the case, we have concentrated attention on the coastal sites and in particular on Cerro Paranal, an isolated small mountain at geographical longitude  $70^{\circ} 24'$  and latitude  $-24^{\circ} 37'$ . A permanently manned observing station was installed there in September 1983, and continuous meteorological records have been obtained both there and at La Silla to evaluate the relative quality between the two sites.

### 9.2.2 Comparison between Paranal, La Silla and Other Sites

The essential data are given in Figures 9.1 and 9.2. Figure 9.1 gives the monthly percentage of photometric nights (at least 6 consecutive hours of clear sky) at La Silla and Paranal for the period 1 October 1983 - 31 December 1986. While La Silla has poor conditions during winter, Paranal's quality is relatively constant during the year. Over the 3 1/4 year period the La Silla average is 57%, compared to 82% at Paranal. The La Silla values are comparable to long term (up to 20 years) averages of about 60% at the three observatories Tololo (70km south of La Silla), La Silla and Las Campanas (30km north of La Silla). Other sites in the world appear to have comparable values. The conclusion appears to be that the Paranal area is unique among astronomical sites in the world with regard to low cloudiness.

Atmospheric water vapor content has been measured (from its IR emission) at Paranal since September 1983, while at La Silla more fragmentary data are also available. In Figure 9.2 are given the monthly percentages of nights with less than 2mm H<sub>2</sub>O. Results from earlier daytime data at Mauna Kea in Hawaii are also given. The great superiority of Paranal over La Silla in this respect is clear. Upon multiplication with the percentage of usable nights it is found that 37% of all nights at Paranal observations may be made with less than 2mm H<sub>2</sub>O. The same percentage is obtained at

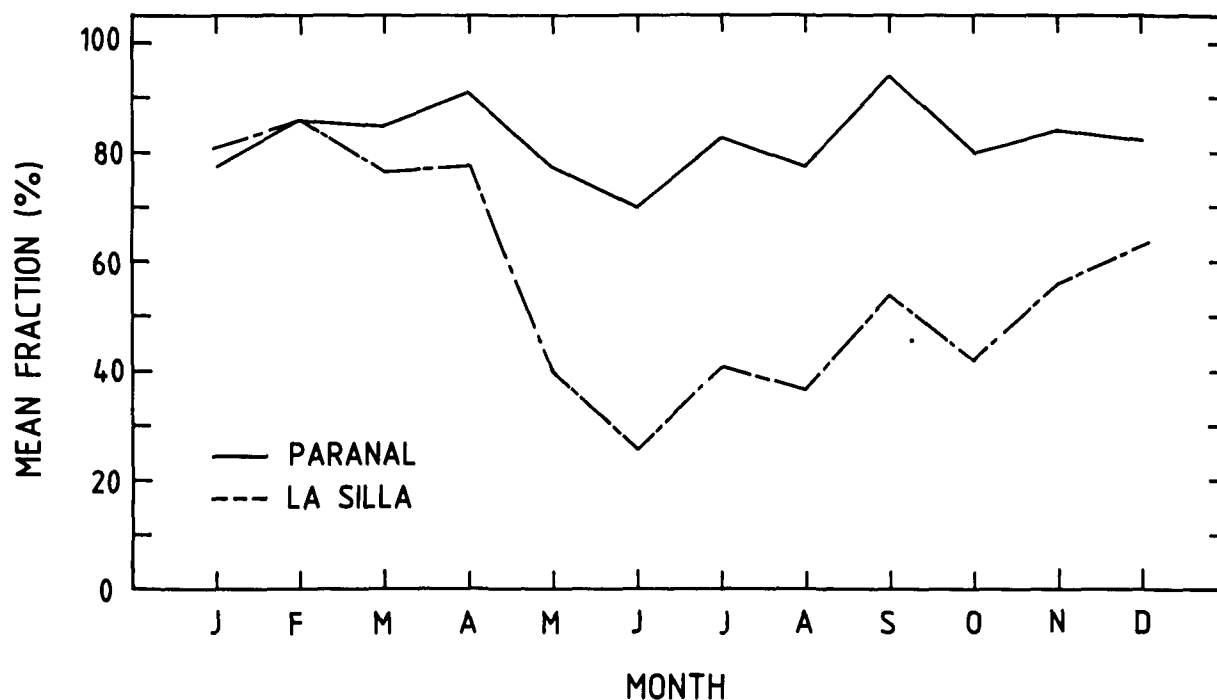


Figure 9.1: Fraction of photometric nights at Paranal (upper curve) and at La Silla from October 1983 till December 1986.

Mauna Kea, which has been considered the world's best year round astronomical site for infrared work. It is to be noted that Mauna Kea is 1400 meters higher than Paranal, with consequently more difficult operational conditions.

Other relevant meteorological parameters do not seem to show important differences between La Silla and Paranal. Wind speeds, temperatures and nightly temperature gradients are not very different. However, rain or snow typically falls at La Silla half a dozen times a year (< 35mm annually in all), while at Paranal in 3 1/4 years some rain or drizzle has been registered only 3 times.

Long term (50-100 years) variations in rainfall appear to occur in the La Silla area. Evidence for this is partly anecdotal (tall grass at Pelicano 50 years ago) or archeological (remnants of irrigation systems and more extensive farming etc.); it seems to be confirmed by some hydrological data. Since La Silla is situated in a region of strong gradients, it is plausible that a small displacement in the main atmospheric pressure systems would have relatively important effects. Since Paranal is situated more centrally in one of the driest areas in the world, less variability would perhaps be expected. This

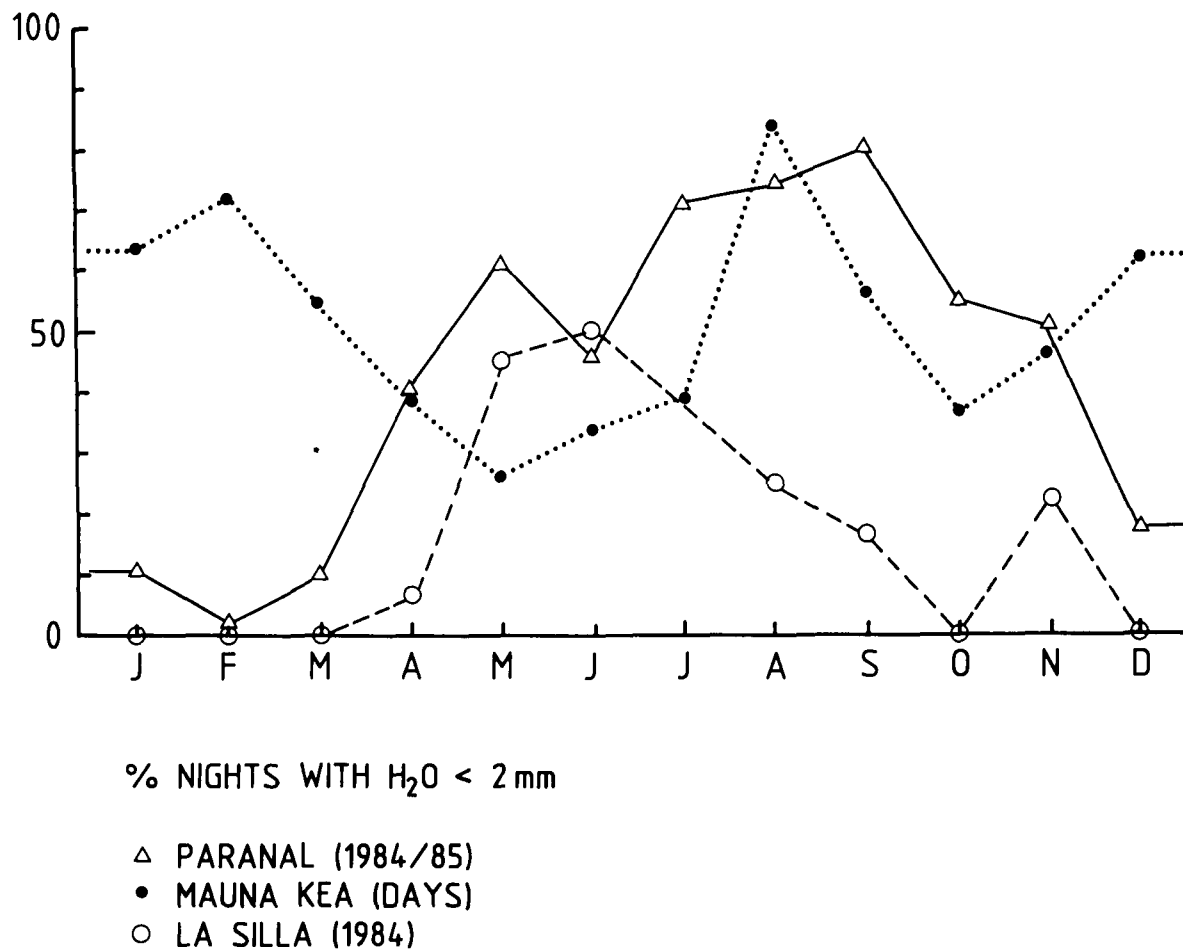


Figure 9.2: Percentage of observing periods with less than 2mm H<sub>2</sub>O at Paranal (nights Oct. 1983 - Dec. 1985), at La Silla (nights 1984) and at Mauna Kea (daytime).

appears to be confirmed by the state of preservation of various archeological remains in the oases 200km to the east which is claimed to indicate the absence of any significant rain over the last few thousand years. While no very firm conclusions are possible, it seems that the chance of changing conditions during the next decades is definitely lower at Paranal than at La Silla.

On the basis of the evidence available so far, it seems that Paranal is sufficiently superior to La Silla to consider electing it as the site for the VLT. However, the most important measurements pertaining to seeing quality have not yet been made at Paranal. This will be done starting in March 1987 and significant results should become available soon. The necessary equipment has been extensively calibrated at La Silla. Included are microthermal sensors to measure ground turbulence up to 30 meters height, an acoustic

sounder to measure boundary layer turbulence from 30m to about 1km, a scintillometer to study the higher layers, and a differential image monitor to evaluate the total "seeing" somewhat more directly. Results obtained at La Silla appear to indicate that at times the boundary layer there makes an important contribution; since the boundary layer is particularly sensitive to local topography, this suggests that more favourable locations may well exist. The rather pointed shape of Paranal could be particularly favourable in this respect. While the seeing measurements are needed to arrive at a definitive scientific choice between La Silla and Paranal as the site for the VLT, it is of interest also to consider the suitability of the two sites from the point of view of the general infrastructure of a site development at Paranal.

The situation at La Silla is well known: With two hours driving distance from the small town of La Serena and with a two-hour flight from Santiago by small plane to Pelicano at the foot of La Silla, access does not pose major problems. A complete infrastructure is available: 25km access road, electricity connection to the Chilean electricity net with a 26km cable, water wells at Pelicano and a 20km pipe with pump stations to bring it up to the mountain. At the top of the mountain, there are hotel facilities, a warehouse, car repair workshops, mechanical, electronic and optical workshops. The various telescopes placed on the La Silla ridge have taken most of the available place, and while a VLT location could be created there by removing some telescopes, it would lead to a decade of disturbed conditions and a consequent reduction of the scientific productivity of the present telescopes.

The La Silla ridge, however, extends further east, and about 5km further there is another area (Cerro Vizcachas) where ample space for the VLT would be available. The cost of making this site suitable for the VLT and for connecting it to the La Silla infrastructure has been estimated at about DM 5,000,000.

At Paranal nothing exists at this moment. However, a good dirt road passes by at 10km. Driving distance to Antofagasta is 2 hours, and also an airstrip could very easily be made. Antofagasta is a relatively large harbor town (250,000 inhabitants). An electricity connection would involve a line of about 80km length. The region is extremely dry, and if no water were found locally, the simplest would be to bring it in by truck, as is done in some surrounding communities. Some workshops and hotel accommodation would have to be built near Paranal, but in view of the very different mode of operating the VLT (remote observing, few instrument exchanges, etc.), these should be much more restricted than at La Silla, especially if a larger part of the infrastructure requirements were dealt with by personnel residing in Antofagasta rather than at Paranal.

Paranal is a rather small mountain which would have to be enlarged in area by removing a 20-30 meter area at the top. While the smallness is a disadvantage in an operational sense, it is likely to be an advantage for the seeing quality. A possible layout of the VLT at Paranal is shown in Figure 9.3. Figure 9.4 indicates the position of Paranal with respect to the main towns, coast and communication facilities.

Because of the exceptional characteristics of Paranal, the cost of its development (DM 25,000,000) has been foreseen in the VLT budget. It would seem, however, to be



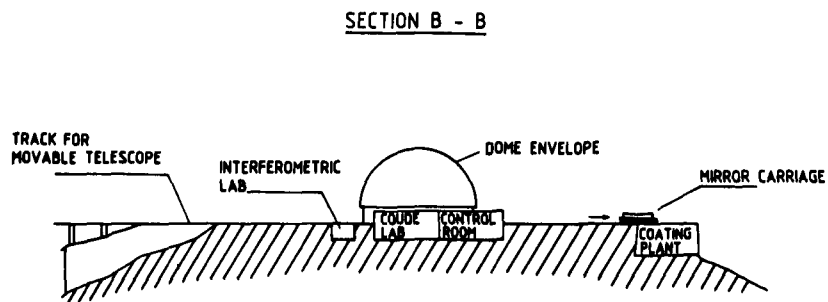
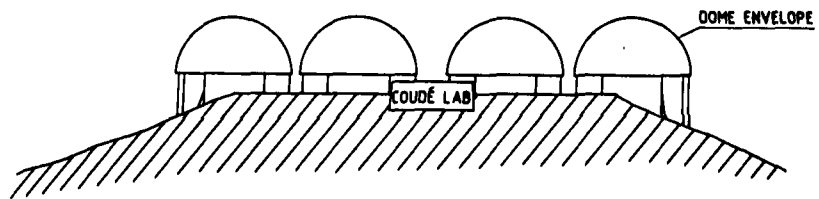
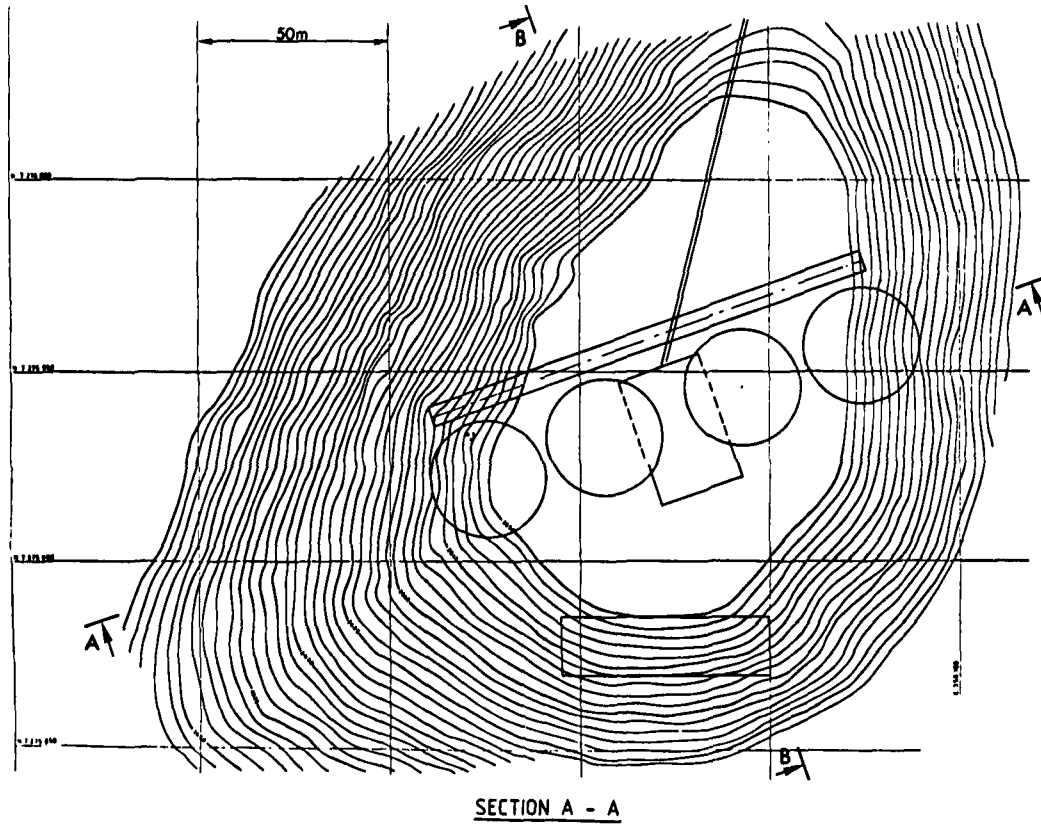


Figure 9.3: A possible layout of the VLT at Paranal.

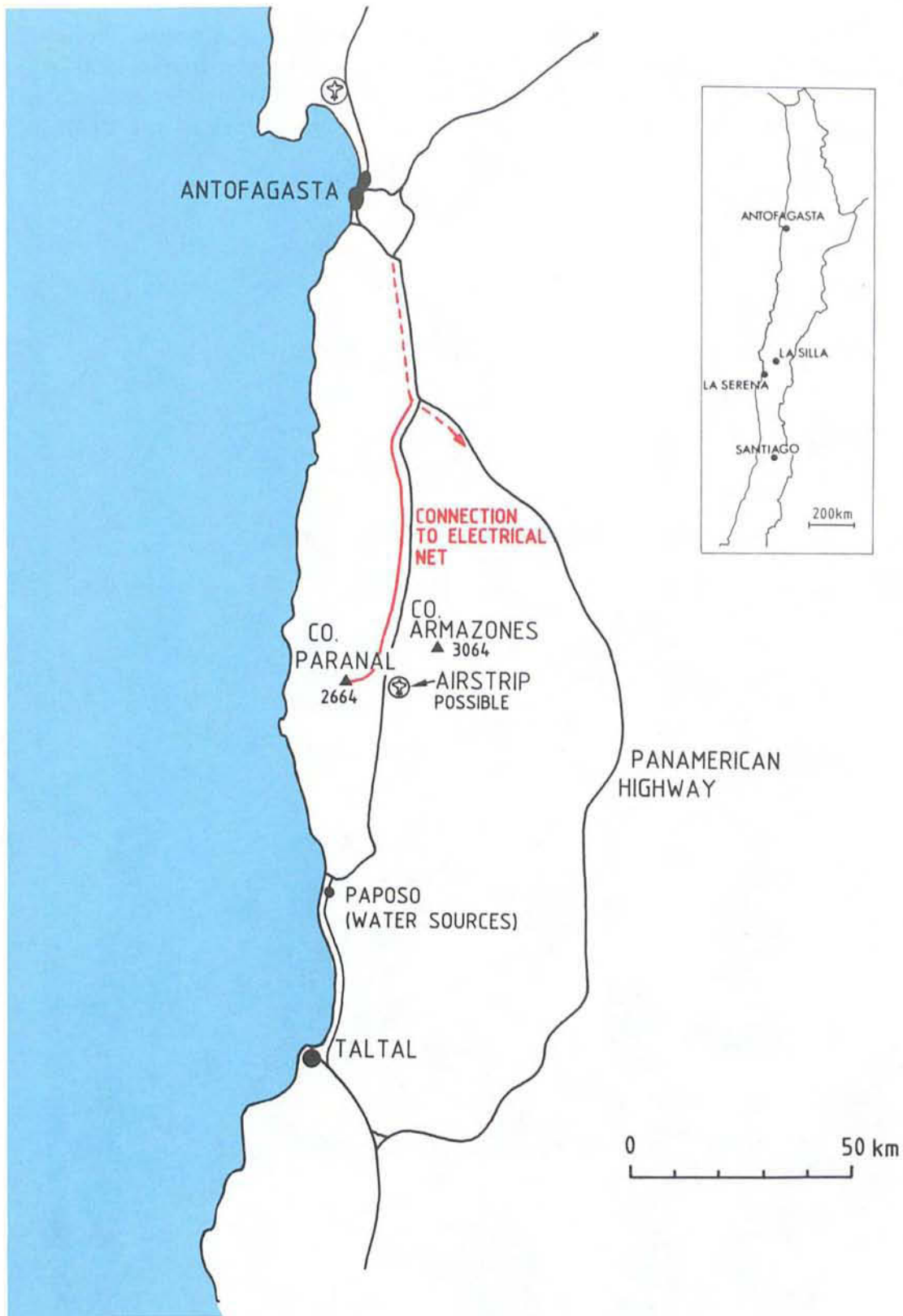


Figure 9.4: Geographical position of Paranal.

(DM 25,000,000) has been foreseen in the VLT budget. It would seem, however, to be advantageous to postpone a definitive choice of site until some time in 1990 so that the available data on which a decision is to be based will be as complete as possible. Before that time, there would in any case be little need for much work on the VLT site.

# Chapter 10

## INSTRUMENTATION

### 10.1 Introduction

Auxiliary instrumentation has been considered by the VLT Working Groups on Infrared Aspects, Low Resolution Spectroscopy and Imaging, High Resolution Spectroscopy and Interferometry. Based on the requirements and wishes included in the final WG reports submitted in July 1986, a preliminary model instrumentation package was outlined at the Venice Workshop in October 1986; it covered the main areas of interest, except interferometry. Most of these instruments were based on designs, already proven in existing instruments at La Silla or being built for the NTT. This approach was well received by the participants who were also virtually unanimous in their view that a basic instrumentation package should be funded as part of the VLT project and that ESO should undertake the responsibility for its procurement. Therefore, an updated proposal for the basic instrumentation is presented here, taking into account the views expressed in Venice as well as further optical design work conducted in the meantime. While complete instrument designs cannot be presented at this stage of the project, it is felt that the optical designs have now advanced to a point where the basic feasibility and the possibility of matching these instruments to the VLT can be demonstrated. Various options still remain open for some of these instruments and alternative solutions exist in other cases. Final designs therefore must await further discussions within the ESO community, as well as the final definition of the telescope parameters.

### 10.2 Instrumentation Interfaces

#### 10.2.1 Available Telescope Foci

Like most giant telescopes of the new generation, the VLT will set new requirements for its instrumentation. In addition, because of its cost and greater dependence upon

observational conditions as compared to smaller telescopes, it is necessary to optimise its use - in particular its scheduling - and to limit the cost of operation.

Both of these requirements can be better approached with a combination of remote observing and flexible scheduling, implying that instrument and telescope changeovers be reduced or preferably, entirely eliminated. Adaptation of the observing programme to the prevailing conditions - particularly seeing - should be made possible by switching instruments, or instrument modes, very rapidly. Since the number of available foci will be always less than the desirable number of instruments, it will be necessary to combine several instrumental modes inside the same housing. This approach has been followed with good results for recent instruments developed for the ESO 3.6m and NTT telescopes.

The change of telescope configuration is usually most critical and time consuming. To avoid this difficulty, the VLT is based on single-focus telescopes. They have two Nasmyth foci only (in addition to the possibility of being converted into Cassegrain operation). Coudé operation is achieved through an optical relay of the Nasmyth focal plane to the combined focus and does not necessitate a change of the telescope configuration.

In addition to the Nasmyth and combined foci, there is access to an individual Coudé focus in the base of each telescope.

Table 10.1 gives the main characteristics of the various foci. It is not foreseen to implement the Cassegrain focus at the beginning of the VLT operation. Because of space limitation for the Cassegrain adapter and of greater field aberrations, the F.O.V. will be limited at that focus to 15 arcmin.

Individual Coudé foci may have a F.O.V. of 0.5 to 2 arcmin, depending on the final solution that will be selected, cf. Section 5.2. The final combined Coudé design has been based on 30 arcsec F.O.V. for the visible and 1 arcmin for the IR which seems adequate for most applications. The four images at the combined focus have the same orientation but the large instruments will have to rely on optical derotators if the field rotation has to be compensated.

The provisional value being considered for the combined beam aperture, is  $F/18.9$  for the IR and  $F/26$  for the visible. The final value will be set according to the instrumental requirements. The characteristics of the beam combination for interferometry are still very much in discussion and cannot be defined at this stage.

## 10.2.2 Nasmyth Platforms

The two Nasmyth platforms are essentially identical in their conception. One will be dedicated to IR instruments, the other to instruments for the visible. The platform for the optical instrumentation will be equipped with an atmospheric dispersion compensation.

TABLE 10.1

VARIOUS FOCI OF THE VLT					
FOCUS	F.O.V.	F/No.	FIELD ROTATION COMP.	ADC	INSTRUMENTS
NASMYTH 1 (Optical)	30 arcmin	F/15	Yes	Yes	Imaging/ Spectroscopy 0.3 - 1 $\mu$ m
NASMYTH 2 (IR)	30 arcmin	F/15	Yes	No	idem 1 - 10 $\mu$ m
(CASSEGRAIN)	15 arcmin	F/13.3	Yes	No	tbd (Later Implementation)
INDIVIDUAL COUDÉ					Specific Instruments/ Experiments
- Visible	0.5	F/74	Possible	No	
- Infrared	2 arcmin	F/32	Possible	No	
COMBINED COUDÉ					
- Visible	30	F/26	No	No	High Resolution
- Infrared	60 arcsec	F/18.9			0.3 - 5 $\mu$ m
INTERFEROMETRY	3 arcsec	tbd	Possible	Yes	Interferometric Set-up

Figure 10.1 shows the present concept for the instrument support and rotator. The pick-up mirror for the Coudé beam is located before the adapter which has the advantage of not interfering with the Nasmyth instrument and adapter. The pick-up mirror will be moved outside the F.O.V. during Nasmyth operation. Instrument and adapter may be supported by a cradle attached to the platform and aligned properly with respect to the elevation axis or attached to the elevation shaft. Bulky instruments may also be supported by a free rotating bearing at the other end of the cradle.

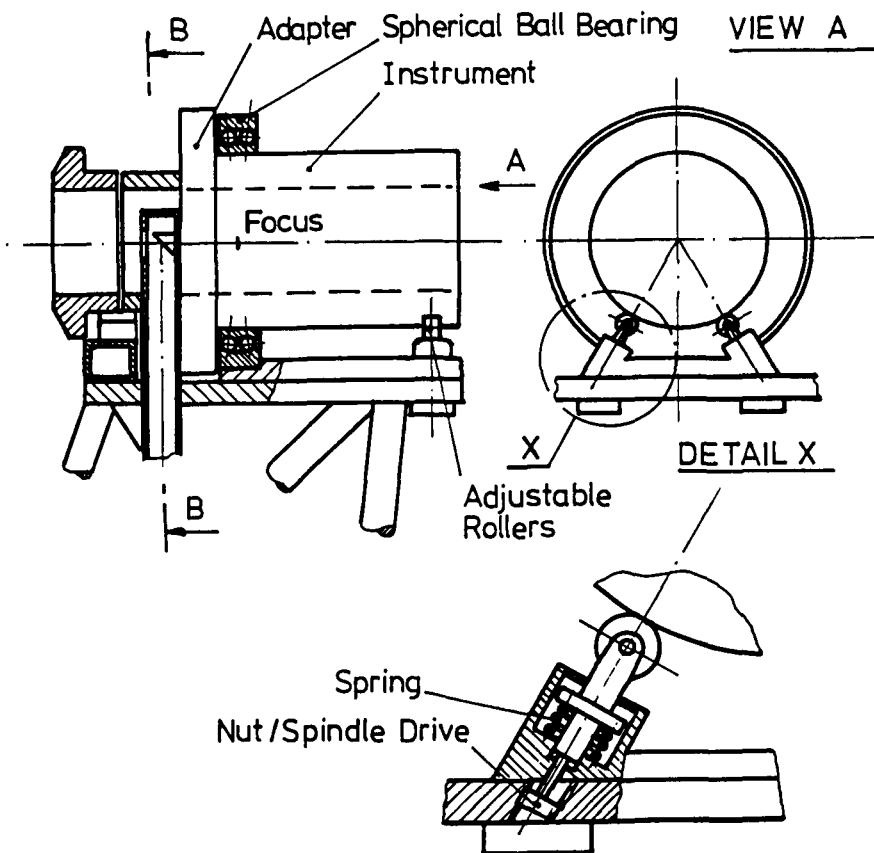


Figure 10.1: Nasmyth platform. Possible arrangement for the instrument and adapter attachments to the telescope structure. In this solution, the pick-up mirror for the Coudé beam is set before the adapter.

The specifications for the Nasmyth instruments are:

- maximum weight is about 3 tons,
- maximum radial dimension of a rotating instrument is 1.4m measured from the telescope axis (diameter 2.8m)
- maximum length is about 3 metres.

Electronic racks for the instrumentation will be located along the sides of the platforms or below them. Excessive heat dissipated by the electronics will be removed through a water-cooled heat exchanger.

It is conceivable, either to cover the whole platform with panels which will provide a sealed and temperature controlled area equivalent to a Coudé lab or to leave the instruments exposed to the free air. The first solution looks more attractive but has the slight drawback of increasing the wind cross section.

### 10.2.3 Instrument Adapters and Rotators

The adapter is the interface between the telescope and the instrument. Because of the field rotation and the necessity to operate the VLT in a blind mode, the accuracy and stability of the adapter functions are particularly critical.

Each telescope has two identical adapters, one on each platform. Each consists essentially of optical probes which together can cover the entire field of view. The probes provide information on:

- Pointing and tracking errors, and
- Wavefront deformations for the correction of the telescope optics.

It is not clear whether the detection of tracking errors and of wavefront distortions for the active correction and possibly the adaptive system can be achieved with the same probe. Although in principle one reference object could provide all the information required, it may be convenient to separate the functions of guiding and wavefront measurement in two separate off-axis units. In any case, both units should be able to reach the telescope axis for the purpose of calibration and field acquisition.

Because the VLT will observe objects so faint that they cannot be detected without a long integration, it is necessary that blind pointing from a nearby reference source be possible with an accuracy of  $\pm 0.05$  arcsec. This puts extremely severe requirements on the accuracy and stability of the off-axis guiding unit.

The alt-az mount of the unit telescope generates a field rotation at all foci. This field rotation can only be compensated by a similar counter-rotation of the instrument or possibly - and only when the field of view is very small - with an optical derotation.

Figure 10.2 shows the position and velocity of the instrument when the fixed reference is the Nasmyth platform. The accuracy required for the instrument rotation depends on the field of view. Typically, for a 10 arcmin F.O.V. it will be about 40 arcseconds and can be easily met.

The instrument should ideally rotate around the elevation axis. Assuming that the azimuth and elevation axes are perfectly squared and that the instrument optical axis is perfectly aligned with the axis of rotation, the telescope pupil would remain centered on the instrument pupil while it rotates. In practice there may be a misalignment which will result in a motion of the sky on the entrance aperture of the instrument. This may be corrected for by appropriate pointing corrections. In addition, there may be a progressive shift of the 2 pupils which would be most detrimental to performance, particularly in IR. Instruments for alt-az telescopes may consequently require some kind of alignment adjustment. A simple solution may consist of inserting a LED in the center of the secondary mirror and to check and correct (in a closed loop mode or at distant intervals) the instrument's proper alignment with a position sensor located in the center of the instrument internal stop, in the shadow of the central obstruction.



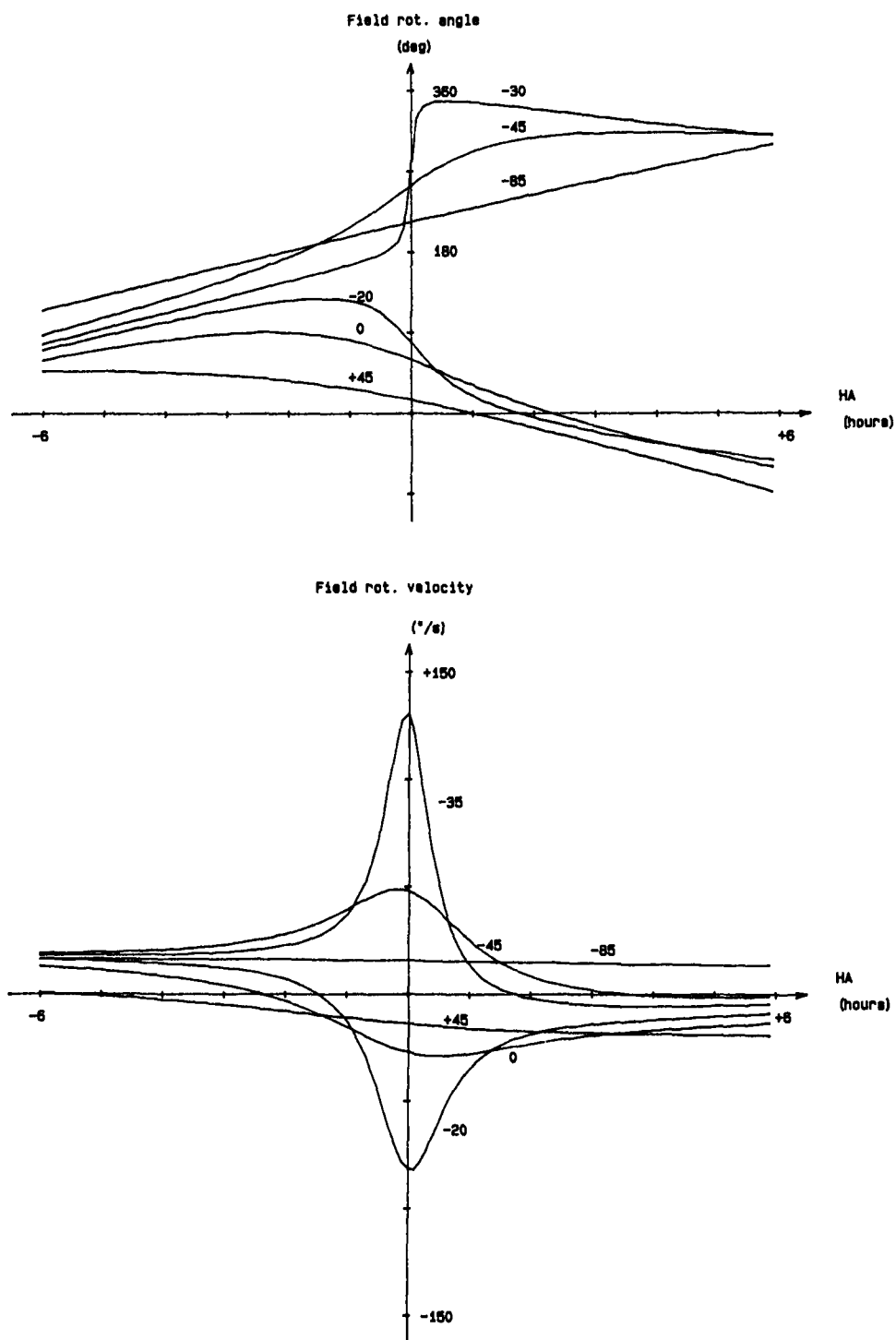


Figure 10.2: Compensation of image rotation at the Nasmyth focus for different declinations and hour angles. Upper: Instrument angular position. Lower: Instrument angular velocity.

### 10.2.4 Compensation of Atmospheric Dispersion

For observing in the UV/visible, it may often be required to correct the atmospheric dispersion. Refraction through the atmosphere causes a dispersion of the light which typically for  $60^\circ$  zenith distance is 1.7 arcsec between the B and R bands (450-680nm). Even for more narrow bandpasses, atmospheric refraction can induce a noticeable degradation of image quality and important light loss in spectroscopy whenever a narrow entrance aperture is used to eliminate sky background.

Many optical designs have been proposed which usually consist of prisms rotating against each other. They provide an acceptable compensation for practical zenith distances ( $< 60^\circ$ ).

The main question is what field of view should be corrected. It is tempting to consider the correction of the entire F.O.V. so that the off-axis guiding unit also works with a corrected image. The size of the corrector would then exceed 1 metre. Its cost would be high despite the fact that - located close to the image - the requirement on surface accuracy is not extremely high.

A simple solution proposed for the ESO NTT is based on a set of fixed small prisms which compensate the dispersion over a limited range of zenith distances only. A set of 4 prisms will be sufficient to cover the  $0^\circ - 60^\circ$  range. Each prism is made of 2 parts (Silica and Fluorine) cemented together. A similar system is considered for the VLT. In spectroscopy, it would cover only the useful field of view of the instrument and would be placed before the focal plane. When there is no sky limiting aperture, a similar device can be located in a parallel beam, inside the instrument.

### 10.2.5 Individual Coudé Foci

They will be located in the telescope bases. The Coudé optical path is defined by 4 mirrors or prisms. The final beam is vertical along the azimuth axis. It is foreseen to have access to a horizontal flange from which the back focal distance will be about 200mm. Cassegrain type instruments would be directly attached to the flange. It is possible to fit out a laboratory within the base to accommodate larger instruments. The space available is roughly a cylinder of 16 metres diameter and a few metres high.

### 10.2.6 Combined Coudé Focus

The details of the instrument feed are still being discussed and would depend heavily on the number and type of instruments that will be built.

There are two possibilities, based on a pure optical combination and on fibre optics, respectively. The former is made of 2 mirrors. The largest, which is the combining mirror, is about 1m diameter. With fibre optics one mirror only is sufficient. Fibre

optics may induce some coupling loss, but on the other hand, one would benefit from a better photometric stability owing to the scrambling effect.

The unvignetted field of view will be about 30 arcsec for the visible, 1 arcminute in the IR, and the F/ratio of each beam will be between F/15 and F/30. The instrument requirements will lead to the final definition of the F/number. Provisional values are F/26 for the visible and F/18.9 for the IR.

The central building has been described in Chapter 8. The space available for instrumentation will be about  $20 \times 20 \times 5$  metres.

## 10.3 Instruments for Observations in the UV/Visible Spectral Region (320-1000 nm)

### 10.3.1 Definition of General Characteristics of Instruments for Nasmyth and Cassegrain Foci

The background for the definition of instruments to do deep imaging and low-to-medium resolution spectroscopy at the individual 8m telescopes, is provided by the recommendations of the VLT Working Groups, as specified in the Proceedings of the Venice Workshop. An upgraded version of EFOSC, the ESO Faint Object Spectrograph and Camera, scaled up to the VLT has been mentioned there as a possible route to take.

EFOSC, in operation during the past two years at the 3.6m telescope, has been generally praised by the users for its efficiency, versatility and reliability. Many observatories have or are in the process of building similar devices. With its six modes of operation (imaging, long slit grism spectroscopy, grism field spectroscopy, echelle spectroscopy, multi-object spectroscopy and field polarimetry), EFOSC is an extremely effective tool to study faint emission nebulae, galaxies at large redshifts, QSO's and faint stars. These objects are among the main targets for observations with a 16m telescope. A battery of EFOSCs at all or at some of the individual 8m telescopes would be a unique way to attack fundamental cosmological problems, such as the structure and evolution of the universe at earlier epochs, cf. Chapter 3.

The resolving power of a VLT-EFOSC, as will be shown in the next Section, could hardly exceed the value of 2000. The Working Groups have stressed that the high collecting power of the 8m telescopes could offer for the first time the possibility to do medium resolution work ( $R \sim 10^4$ ) on relatively faint objects ( $m_V \simeq 18$ ). Again reference was made to an ESO instrument, EMMI, as a possible way to achieve such a performance, which would open new prospects in many research fields.

EMMI is the multimode camera-spectrograph being built for the Nasmyth focus of

the New Technology Telescope; Figure 10.3 shows the optical layout. EMMI will be used for imaging over a 10 arcmin square field with a 54mm square detector and for multiobject spectroscopy with moveable slitlets at low (red channel only) and medium ( $R = 2 \cdot 10^4$ ) resolution. The instrument is split in a red and a blue channel with optimized coatings and detectors to achieve a high overall efficiency despite the large number of optical elements. It appears that EMMI will be an efficient and versatile instrument. However, it is still in the construction phase and modifications and improvements may be suggested from the experience over the next few years.

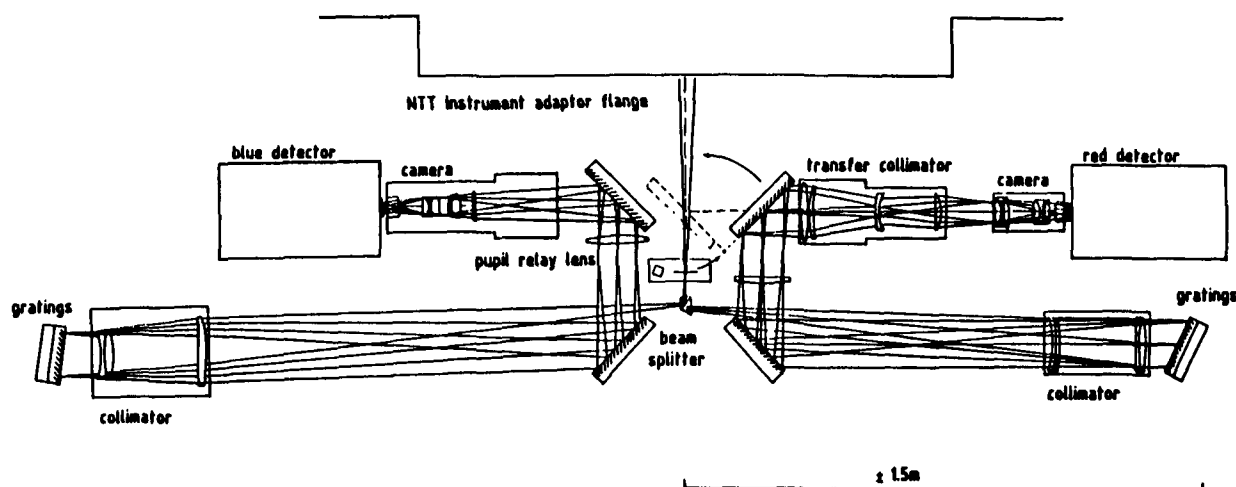


Figure 10.3: Optical layout of EMMI, the two channel camera-spectrograph for the Nasmyth focus of the ESO New Technology Telescope.

A simple extrapolation of the EMMI design to match the VLT seems, however, not to be possible with today's state-of-the-art in glass technology. The optical characteristics of the Nasmyth focus for the 8m telescope make the matching of a wide field instrument to the telescope much more difficult. An additional constraint is imposed by the need to accommodate at the Nasmyth the mirror to feed the Coudé and the combined foci.

In the next Section, a possible layout is given for an instrument which is more restricted in performance than EMMI but still combines the imaging and the low resolution with a medium resolution possibility. From the point of view of the instrumentation design, it might be easier and possibly more efficient to split the imaging and low resolution modes (to be done with an EFOSC type instrument) from the medium resolution mode (to be achieved most likely with an echelle grating and a larger size instrument).

An important factor in the definition of an instrument is the choice of the detector and, above all, its overall size and pixel dimensions. No definitive statement can be made on the detectors which will be available in the early 1990s. Expectations in this field have often not been fulfilled. Cullum has reviewed the present status and the development plans at the Venice Workshop. There are some interesting prospects, both for Charge Coupled Devices (CCDs) and Photon Counting Detectors (PCDs), the two types of detectors which are likely to be used for different observing modes in the next decade. For a project of the size of the VLT, development work will have to be started in collaboration with European industry and laboratories, to reach the desired specifications. ESO has already made steps in this direction, supporting the production of buttable CCDs by Thomson CSF and the development of PCD prototypes by national laboratories. For the planning of the VLT optical instruments, we have assumed the availability of detectors with  $25 \mu\text{m}$  pixels and dimension of up to  $50 \times 50\text{mm}$ , a reasonable hypothesis for the state of the art, seven years from now.

### 10.3.2 Optical Layouts and Performance of Instruments for Nasmyth/Cassegrain Focus

We consider first the case of a focal reducer with spectroscopic capability like EFOSC. Table 10.2 shows the pixel matching, the field and the largest size of the optics which are required with different camera apertures and detectors  $25 \times 25$  or  $50 \times 50\text{mm}$  in size and  $25\mu\text{m}$  pixels.

TABLE 10.2

DETECTOR MATCHING WITH THE VLT					
CAMERA APERTURE	SCALE AT DETECTOR pixel/arcsec	DETECTOR			
		size 25x25mm		size 50x50mm	
		field (arcmin)	optics (mm)	field (arcmin)	optics (mm)
5	7.8	2.1	104	4.2	208
2.5	3.9	4.3	213	8.6	426
2	3.1	5.3	262	10.6	524
1.5	2.3	7.2	356	14.4	712

As discussed by D'Odorico et al. at the Venice Workshop, pixel matching requirements and the state of the art in glass technology suggest the choice of a F/2.5 camera and a 25 x 25mm detector. Four of these systems could be mounted in parallel to increase the field. The coatings should be optimised either for the UV-blue or the visual-red band in order to achieve high efficiency. Table 10.3 and Figure 10.4 illustrate the optical layout of the VLT-EFOSC.

TABLE 10.3

<b>EFOSC TYPE INSTRUMENT FOR THE VLT</b>	
Camera Focal Lengths	150mm
Final Aperture of single channel	F/2.5
Collimator Focal Lengths	900mm
Diameter of the parallel beams	60mm
Field coverage	8.6 x 8.6 arcmin
Maximum resolving power (using 1 arcsec slit)	1800 with transmission echelle 800 with prism

The present set-up is conceived for the Nasmyth focus of the VLT, but could be adapted to the Cassegrain in the present design for the telescope. The corrected field at the Nasmyth is larger, but optical quality at the Cassegrain would still be satisfactory within a 10 arcmin diameter field.

Based on the knowledge of coating properties as acquired from the manufacturing of EMMI, an efficiency of the optics for the VLT-EFOSC channels between 80 and 90% is computed; a value which compares well with present instruments.

Let us now consider the medium resolution spectrograph ( $R \simeq 2 \cdot 10^4$ ). As mentioned in the previous paragraph, the EMMI design (see Figure 10.3) can hardly be extrapolated to a VLT. The layout of a spectrograph still based on the white pupil concept, with two channels, and incorporating the EFOSC option mentioned above, is shown in Figure 10.5 and specified in Table 10.4. The instrument would reach a resolving power

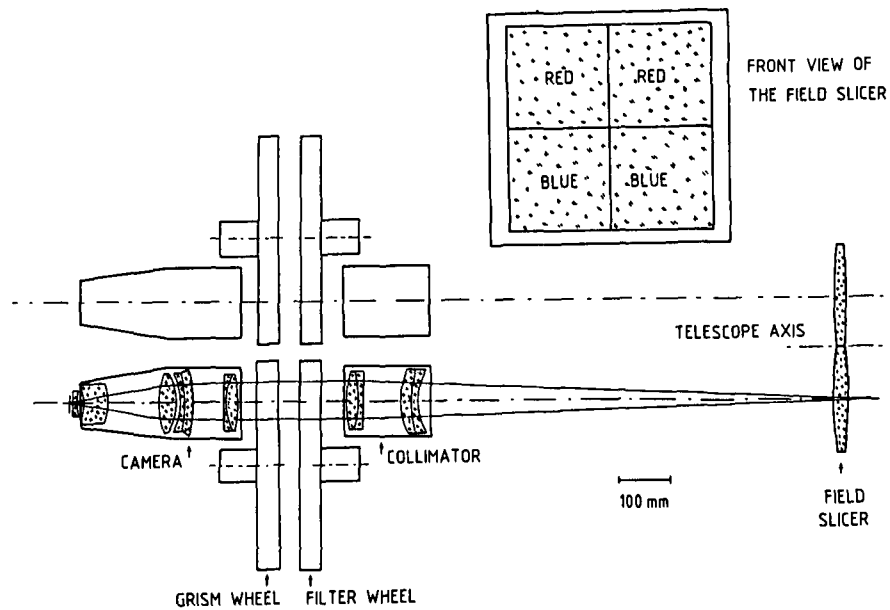


Figure 10.4: Layout of the EFOSC type instrument for the Nasmyth focus of the VLT. A field of 8.6 arcmin square is split in four channels with coatings optimised for different spectral regions.

TABLE 10.4

MULTI-MODE INSTRUMENT AT THE NASMYTH FOCI	
RED PATH (4500-10000 Å)	BLUE PATH (3000-4500 Å)
F collimator $\simeq 2\text{m}$ $\phi \simeq 140\text{mm}$	F collimator $\simeq 2\text{m}$ $\phi \simeq 140\text{mm}$
Echelle grating size 140x130mm	Echelle grating size 140x130mm
Grating $31.6 \ell/\text{mm}^{-1}$ $\beta = 63^\circ$	Grating $79 \ell/\text{mm}^{-1}$ $\beta = 63^\circ$
Cross dispersion required = $200 \text{ \AA}/\text{mm}$	Cross dispersion required = $100 \text{ \AA}/\text{mm}$
Separation of orders = 0.4mm	Separation of orders = 0.6mm
Linear dispersion $\simeq 5 \text{ \AA}$ at $\lambda 6000 \text{ \AA}$	Linear dispersion $\simeq 3 \text{ \AA}$ at $\lambda 4000 \text{ \AA}$

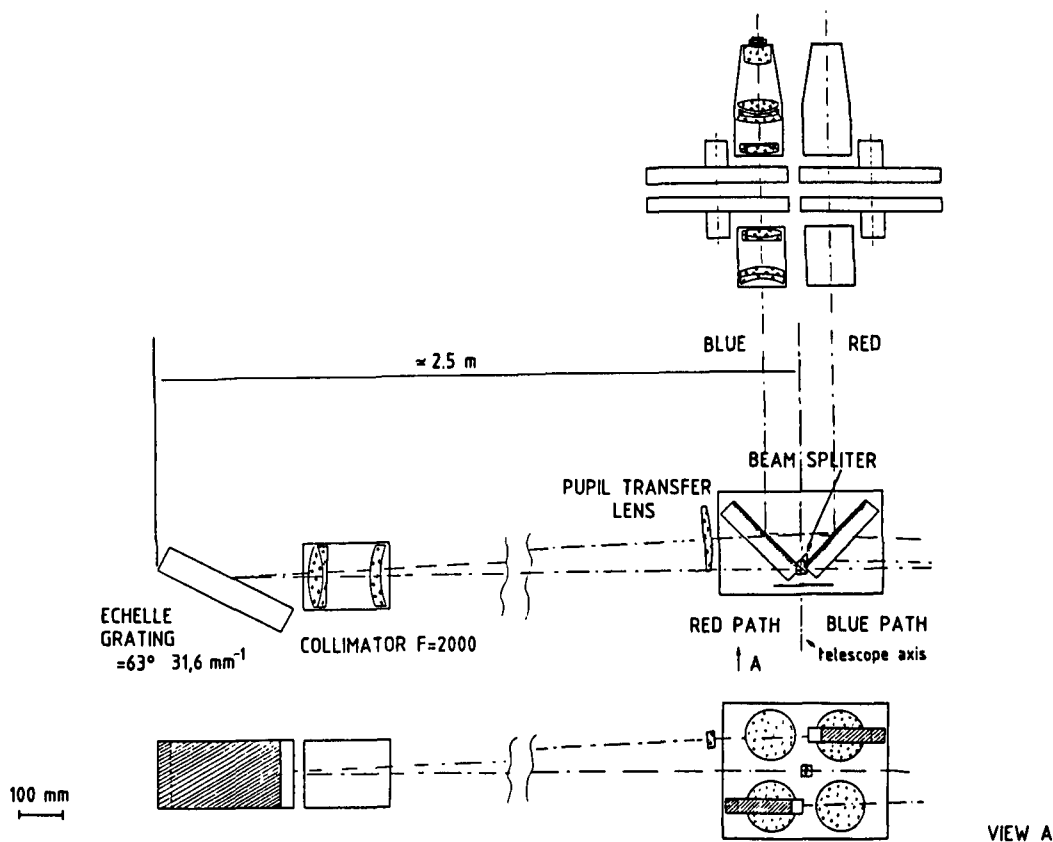


Figure 10.5: A preliminary layout of a multimode instrument for the Nasmyth focus of the VLT. In the medium resolution mode ( $R = 15000$ ) the field slicer which feeds the array of focal reducers of the EFOSC type is replaced by a slit and a dichroic beam splitter. The red and blue arms mount double-pass collimators and echelle gratings. The spectra are finally reimaged on the detectors through two EFOSC channels. Cross dispersion is provided by grisms. The medium dispersion arms are stationary and the instrument will work on axis in that mode.

of the order of  $1.5 \cdot 10^4$  with a 1 arcsec slit. The efficiency of the two channels would compare well with that of EMMI. The instrument would basically serve most of the scientific objectives outlined by the Imaging and Low Resolution Working Groups.

There are alternative designs which would provide a similar resolving power, i.e. a scaled down version of the dual beam echelle spectrograph considered for the Keck telescope or the configuration suggested by J. Solf at the Venice Workshop. A more detailed design has to be produced to define size, weight and exact performance of these alternative solutions, but there should not be problems of feasibility. However, these solutions do not provide the imaging, low resolution mode. A separate instrument would have to be built for that purpose and exchanged at the Nasmyth focus.



Clearly, one of the main purposes of the detailed feasibility studies to be performed is to provide all the information needed for an optimal trade-off between the different solutions based on capabilities, costs and mode of operation.

### 10.3.3 A High Resolution Instrument for the Incoherent Combined Focus

High resolution spectroscopy ( $\lambda/\Delta\lambda \simeq 10^4 - 10^6$ ) is one of the most important techniques for observing the physical parameters (temperature, density, pressure, gravity, chemical abundances, velocity) of astronomical objects. In these types of observations, the radiation flux is distributed over a large number of detector elements, and the use of a large collecting area is needed to obtain a sufficient signal-to-noise ratio, if one does not want to be limited to study of the brightest objects.

Figure 10.6 exemplifies the signal expected in a resolution element of a high resolution spectrograph with  $(\lambda/\Delta\lambda) = 50000$  mounted on an 8m telescope as a function of stellar magnitude and compares it with the sources of noise. Readout noise becomes important in the spectra of objects fainter than about  $17^m$ . Photon statistics dominate the other sources of noise for brighter objects. The effect of increasing resolution or longer exposure times can be easily deduced. Sky subtraction would be needed in the observations of the fainter targets at the time of full moon.

In the report of the ESO High Resolution Spectroscopy Working Group and in similar studies for other large telescope projects, spectroscopy at high resolving power has been unanimously considered as a primary mode of operation of a VLT and it has been shown that the expected gain in magnitude over the 4m class telescope will allow a variety of new research possibilities.

The type of instruments to be built changes with the resolving power one wants to achieve. The Working Group on High Resolution Spectroscopy identified three main instruments: a Nasmyth echelle spectrograph for  $R < 20000$ , eventually to be replicated at the four telescopes, a grating spectrograph for  $2 \cdot 10^4 < R \leq 10^5$  and an FTS for  $R > 10^5$ . The medium resolution spectrograph outlined in the preceding Section matches well the first request. An FTS could easily be matched to a 16m aperture. Several existing instruments could serve as a starting base. The feasibility of such an instrument has been amply demonstrated, but a detailed optimization study remains to be made. For the grating spectrograph with  $R < 10^5$ , its dimension will be so large that it has to be planned for the combined focus or for a Coudé focus at a unit 8m telescope.

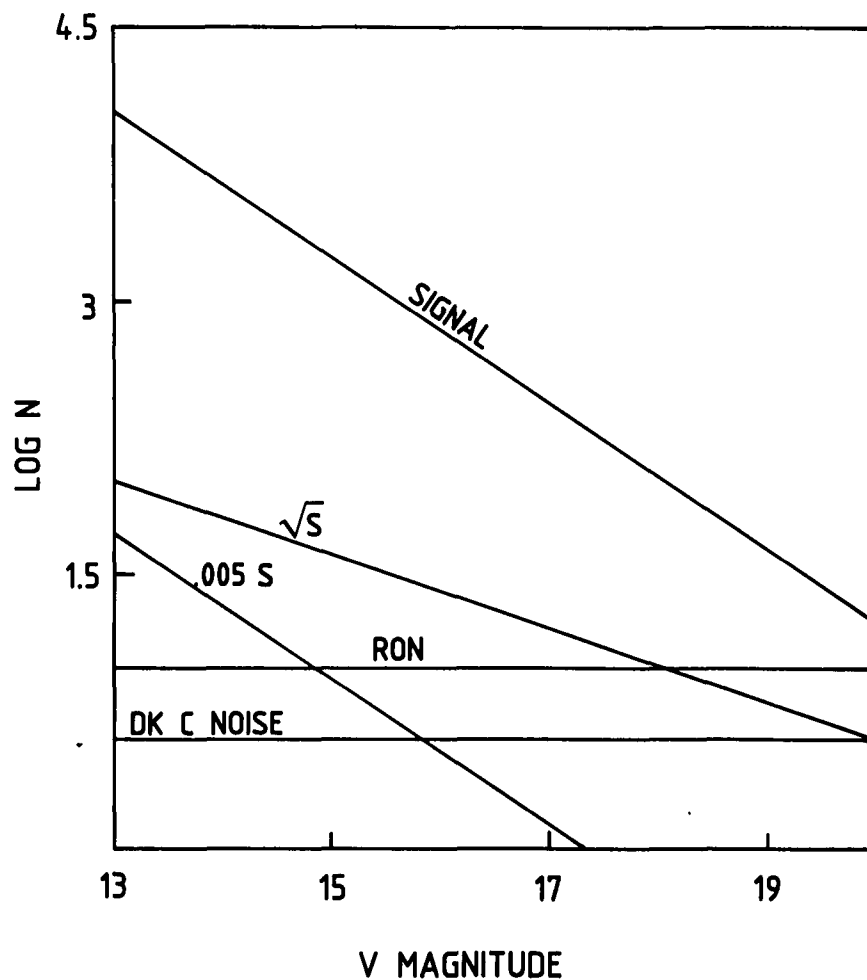


Figure 10.6: Expected photons from stars of different visual magnitudes and noise sources per pixel computed for a two-hour exposure with an 8m telescope at  $0.055 \text{ \AA}/\text{pixel}$ . The efficiency of the telescope-spectrograph-detector combination is taken as 0.05 and the energy per wavelength bin is spread over 4 pixels perpendicular to the dispersion. The read-out noise of the detector is assumed 10 el/pix, the dark current 10 el/pix/hour. The line corresponding to 0.5% accuracy in the intensity calibration is also indicated.

The problem of matching an 8m telescope to a spectrograph for high resolution work has been discussed extensively, i.e. in the Proceedings of the First ESO VLT Workshop in Cargèse and of IAU Colloquium No. 79. There are many ways to formulate the

so-called spectrograph law which relates the maximum resolving power, the telescope diameter, the slit width, the grating size, the camera focal length and the detector pixel size. Let us just remember here that the resolving power is directly proportional to the size of the beam (or grating width), to the tangent of the diffraction angle, and inversely proportional to the slit width and the telescope diameter. With an 8m telescope and a 1 arcsec slit, an echelle grating of 80cm width and  $63^{\circ}.5$  blaze angle, gives  $R \simeq 5 \cdot 10^4$ . As the current state of art limits the grating groove length to about 40cm, a mosaic would be needed. ESO and other institutes have successfully built mosaics of smaller gratings (Figure 10.7) and the extrapolation to larger sizes should be possible. A configuration which needs to be explored as an alternative would be based on a holographic grating working in a lower order.

We have initially investigated a possible design for the high dispersion grating spectrometer to prove the feasibility of such an instrument. Table 10.5 and Figure 10.8 summarise the characteristics of the proposed layout which assumes an incoming beam at  $F/26$ . A predisperser is used in combination with a second slit to select the wavelength range. It is based on a single lens collimator and a backside reflecting prism. A double pass collimator (white pupil configuration) illuminates a grating mosaic of 9 echelles, each 200 x 400mm in size. The grating is used in the Littrow configuration. Two different collimators, a blue and a red one, are used alternatively. Separate blue and red dioptic cameras are also employed to optimize the efficiency through the use of appropriate coatings. The stellar images from the four telescopes are aligned along the entrance slit of the spectrograph and prisms are used after the slit to superpose the pupil of the 4 telescopes on the grating. The final spectrum is sliced into three parts to use small optics in the camera and the detectors with linear size of about 25mm. The expected efficiency of the optics of the spectrograph is 40%.

The resolving power with a 1 arcsec slit is about  $6 \cdot 10^4$  at  $\lambda 5000\text{\AA}$ . This solution appears more attractive than one based on the use of a cross disperser necessarily as large as the echelle and with an additional 40% loss in efficiency. The mosaic of echelle gratings also seems easier to build and is more efficient than the large holographic grating or mosaic of gratings that would be needed to achieve the same dispersion.

It is worth stressing again that the main aim of this exercise is to demonstrate that a high dispersion spectrograph for an array of 8m telescopes can be built with good efficiency and modest extrapolation of current technologies. It is of course clear that the solution outlined here has to be investigated in more detail and further optimized.

The cost of the combined focus spectrograph is difficult to estimate without more detailed studies. A global estimate based on the experience with smaller high dispersion instruments suggests a value of 10 MDM.

The combined focus solution has been compared with the possibility of building high dispersion spectrographs at the individual telescopes. With a global efficiency of the relay of 85%, the combination of the light from the four telescopes would be advantageous with respect to post detection addition of the spectra from the four separate telescopes,

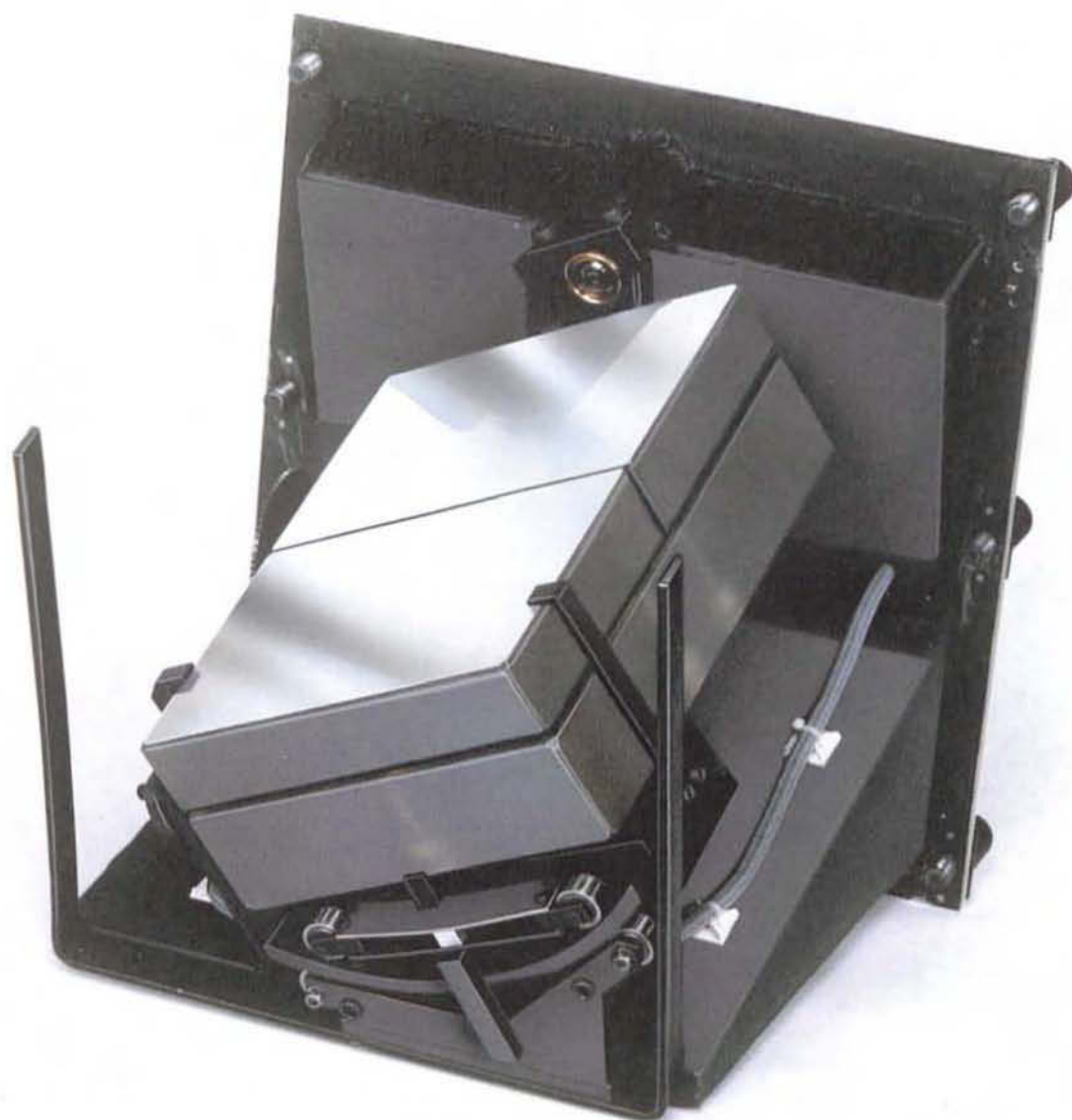


Figure 10.7: The mosaic of two 180 x 250mm gratings in use as cross-disperser in the ESO CASPEC spectrograph. In the mounting of the two components, coplanarity was achieved and maintained during operation at the 2 fringe level. For the same spectrograph, a mosaic of four smaller echelle gratings was also successfully constructed.

TABLE 10.5

<b>HIGH RESOLUTION SPECTROMETER FOR THE COMBINED COUDÉ FOCUS</b>	
Entrance aperture	F/26
Entrance slit	4x10mm
Predisperser	Focal length: 5m Dispersion: 25 Å/mm at $\lambda = 5000 \text{ \AA}$ Collimator size: 200mm Prism angle: 29° Incidence angle: 45° Material: silica
Predisperser slit	Width 4mm at $\lambda = 5000 \text{ \AA}$ for 75 Å bandpass
Collimator	Focal length: 15m Size: 600x1200mm
Grating mosaic	9 x (200x400mm) echelle gratings $\beta = 63^\circ$ 79 gr/mm Intermediate spectrum length: 750mm $D = 0.08 \text{ \AA/mm}$
Spectrum slicer	Divides the intermediate spectrum in 3 parts
Cameras	Magnification: 0.1 F/2.5 Diameter: 60mm
Detector	25x25mm 25 $\mu$ m pixels Used area: 4x25mm Pixel matching: 1 arcsec = 4 pixels = 100 $\mu$ m
Performance	Dispersion: 0.8 Å/mm $R = 62500$ at $\lambda = 5000 \text{ \AA}$ (1 arcsec slit)

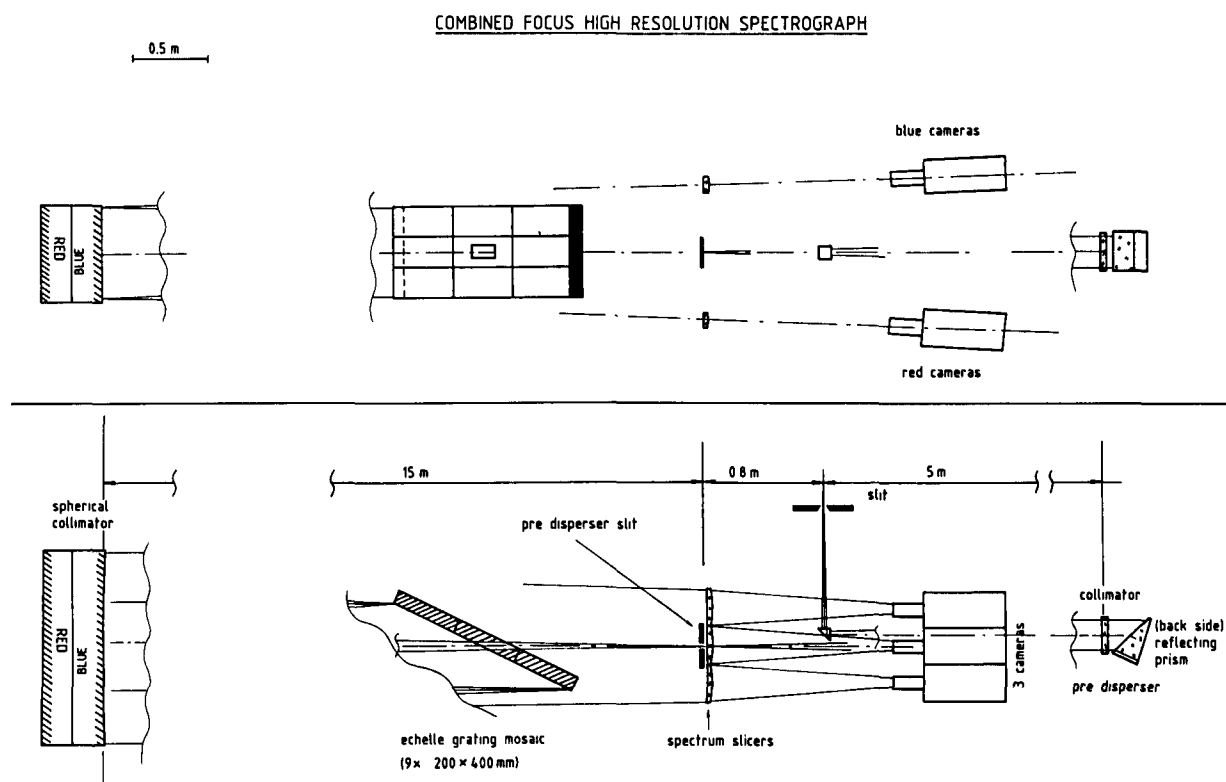


Figure 10.8: Possible optical scheme for a high resolution spectrometer for the combined Coudé focus.

especially in the observations of the faintest objects or at the highest resolution where the noise of the individual detector becomes important. The full light gathering power of the equivalent 16m aperture would then be used at the combined focus for unique observations which can not be made with the unit 8m telescope.

Another strong argument in favour of the combined focus is based on cost considerations. A high dispersion spectrograph at the individual 8m telescope would be as difficult and expensive to build as the one at the combined focus. The total cost of four copies would then be unnecessarily high.

## 10.4 Infrared Instrumentation

It is clear from the Working Group Reports that full scientific exploitation of the VLT for Infrared Astronomy would require instruments for imaging photometry and polarimetry, spectroscopy and interferometry in all the groundbased "windows" between  $1\mu\text{m}$  and  $20\mu\text{m}$  and with some capability even at longer wavelengths if the site chosen were to be extremely dry. With respect to defining a basic instrumentation package, however, highest priority has been afforded to near infrared spectroscopy; to achieving telescope diffraction limited angular resolution between  $1\mu\text{m}$  and  $20\mu\text{m}$  (by means of speckle interferometry, adaptive optics and direct imaging - depending on wavelength) plus long baseline interferometry. For these infrared imaging observations, the diameter of the VLT telescopes is important not only with regard to light gathering power, but additionally due to the gain in angular resolution possible with respect to the existing smaller groundbased telescopes and the even smaller telescopes, which can be operated in space (e.g. the ESA 0.6m Infrared Space Observatory).

In order to satisfy the above requirements in an optimal way on the VLT, a basic instrument package is described below which follows a modular, multimode approach and also makes use of the flexibility in choice of focal station inherent in the present VLT concept. The basic elements in this proposal are 2D imaging cameras. In this regard it should be noted that the panoramic detectors needed, are now becoming available. Compared with the single detectors used in the past, these devices are of course already revolutionizing the capability of infrared instrumentation and the development of such detectors, both in sensitivity and size, may proceed extremely rapidly during the next few years. While an exciting prospect in terms of scientific potential this of course complicates the task of designing instruments too far in advance. For reasons of immediate purpose the availability of  $64 \times 64$  pixel arrays for all the groundbased windows is therefore either explicitly or implicitly assumed. This appears to be the largest format currently available for astronomical applications but it is known that, at some wavelengths, much larger arrays are already technically feasible.

Considerations including field, telescope emissivity and interest in fully utilizing the first unit telescope led the WG on Infrared Aspects to recommend that the unit telescope foci be primarily instrumented for imaging. Such instruments should be relatively small and can conceivably be duplicated on all unit telescopes in which case the sensitivity achievable by electronic combination exceeds that possible at the combined focus while the angular resolution is the same. The WG also stressed the need for sky chopping and, in addition, felt that for some purposes access to a Cassegrain focus might be an advantage.

In this proposal a possible approach is outlined for fulfilling the high priority imaging requirements and for additionally providing for polarimetric and medium resolution spectroscopic capability under the baseline assumptions of Nasmyth foci and sky chopping by means of the F/15 secondaries. However, the instrumental considerations would not be substantially changed, if at a later stage it were decided to implement the Cassegrain focus option.

For high resolution spectroscopy ( $R > 5 \cdot 10^3$ ) in the near infrared, the WG on Infrared Aspects proposed use of the combined focus on the following grounds:

1. high efficiency combining optics should be possible in the infrared
2. telescope emissivity is relatively unimportant at  $\lambda < 3\mu\text{m}$ , and
3. the instrument is likely to be too large and perhaps complex to duplicate.

Here some preliminary ideas are presented of what is technically feasible. Actual designs are more difficult at this stage, because the combining option adopted might depend on the actual array detector formats available in the future. Possible alternative solutions such as Fourier Spectroscopy (possibly using a combined visible/infrared Michelson interferometer) also need to be studied in more detail.

#### 10.4.1 Imaging at the Nasmyth Foci

As already mentioned above, imaging in the infrared has only recently become possible with the availability of 2D array detectors. ESO has nevertheless already gained some interesting experience through the use of a 1-5  $\mu\text{m}$  camera at the 2.2m telescope on La Silla which was built at the Observatoire de Meudon and which utilizes an 8 x 8 InSb CID array produced by SAT in France. A 32 x 32 pixel version of this camera has subsequently been built in Meudon for use on the ground and also as part of the development programme for a camera to be flown on the Infrared Space Observatory. In relation to this latter project, it should be noted that other institutes in the ESO member countries are also working with industry to produce a variety of array detectors for this ESA spacecraft.

At present, ESO is also finalising the design of a near infrared camera to be used at the F/35 foci of the 3.6m and 2.2m telescopes on La Silla. In the former case, the scale is very similar to that at the F/15 VLT Nasmyth foci. The choice between InSb arrays with CID and direct readout systems, or HgCdTe arrays with CCD readouts has not yet been made but promising results have recently been obtained in the laboratory with a 32 x 32 pixel version of the latter on loan from Mullards (Philips). This company already makes 64 x 64 pixel arrays and is planning for formats of 128 x 128. In principle, similar HgCdTe arrays can also be used in the 10 $\mu\text{m}$  window. Doped silicon arrays have also been produced for this wavelength range and out to the 20 $\mu\text{m}$  window. Development work on Ga:Si arrays is well advanced in France in relation to ISO. It is expected therefore that with 2, or at most 3 different arrays, it will be possible to cover the complete 1-20 $\mu\text{m}$  region.

Figure 10.9 shows a possible design for a 1-5 $\mu\text{m}$  camera at the VLT Nasmyth focus derived from that made for the 3.6m and 2.2m telescopes. Its main features are an input optical system producing a well defined and small pupil image, followed by a number of interchangeable (on a wheel) relay optical systems providing for a range of scales at



the array. A filter wheel close to the pupil image carries both standard broad-band filters and CVF (circular variable filter) segments which allow narrow band ( $R \simeq 50$ ) imaging over most of the wavelength range. In the design actually shown, the largest scale of 0.5 arcsec/pixel (assumed  $48\mu\text{m}$ ) is close to an upper limit, but there is no difficulty at the smaller values. This basic camera could therefore be used for direct imaging, in a speckle mode or with an adaptive optics system to achieve diffraction limited performance. The complete camera is extremely small and thus relatively easy to integrate into standard cryostats for cooling to  $\text{N}_2$  or He temperatures. It is also relatively straightforward to replicate. Systems for the  $10\mu\text{m}$  and  $20\mu\text{m}$  windows would be essentially identical, except for the choice of optical materials.

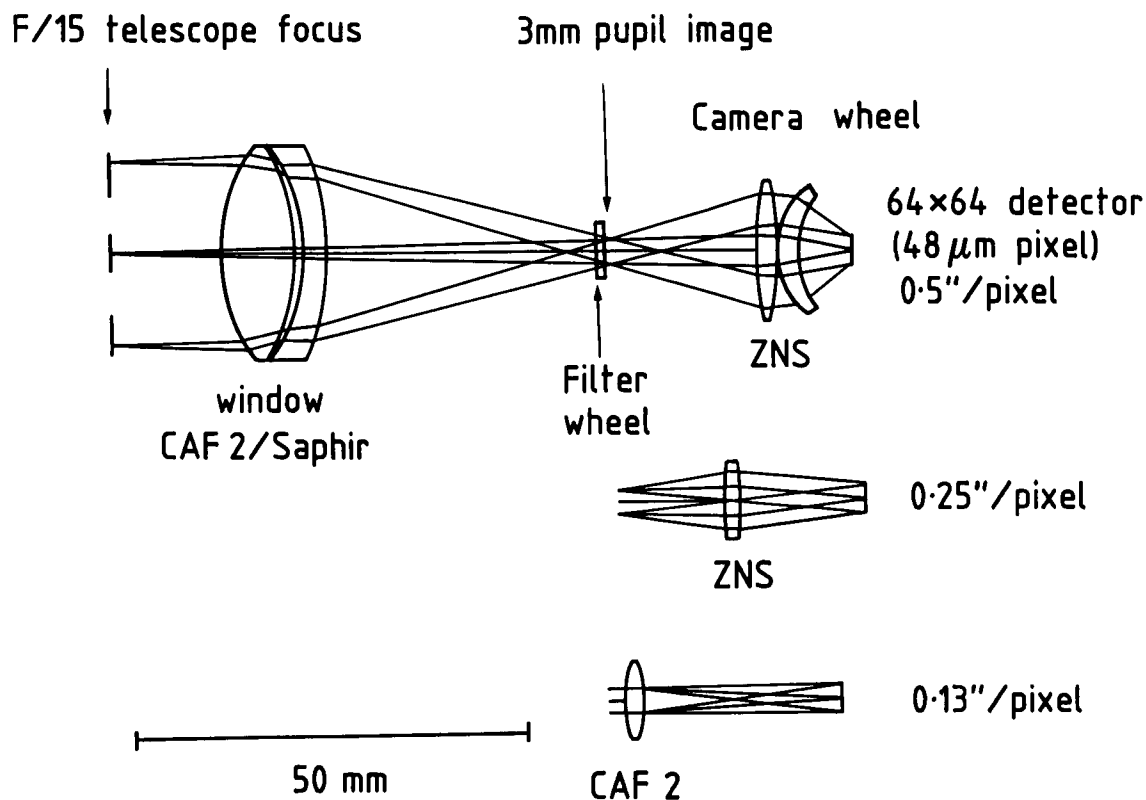


Figure 10.9: Possible design for an infrared camera at the Nasmyth focus. Provides for broad and narrow ( $R \simeq 50$ ) band imaging between  $1\mu\text{m}$  and  $5\mu\text{m}$  at a variety of scales  $\leq 0.5$  arcsec/pixel. A similar design could be adapted for imaging in the  $10\mu\text{m}$  and  $20\mu\text{m}$  atmospheric windows.

### 10.4.2 Spectroscopy and Polarimetry Options at the Nasmyth Foci

Adopting the above camera modules, polarimetric capability can be added simply by either including polarising filters in the filter wheel or by adding an insertable rotating analyser module in the input beam. With CVF's, the cameras already provide a basic narrow band imaging capability at  $R \simeq 50$ . This could be increased to  $R \sim 5 \cdot 10^3$  by including a scanning Fabry Perot etalon or even higher with a tandem FP system. This would slightly complicate the final design, but it introduces no additional matching problems and the etalons themselves and the scanning electronics are commercially available. In order to accommodate "long slit" moderate resolution ( $R \simeq 10^3$ ) spectroscopy in the near infrared, the design shown in Figure 10.10 has been made as an example of how the same basic camera could be combined with a "white pupil" grating spectrometer which is of the EMMI type, except for the mirror collimators and the fact that the grating has to be scanned for full wavelength coverage. The design characteristics are summarized in Table 10.6.

TABLE 10.6

IR IMAGING SPECTROMETER IRIS	
Grating	3 or 4 interchangeable, 80x50mm ruled area
Dispersion	$\simeq 95 \text{ \AA/mm}$
Collimators	Spherical mirrors with $f = 750\text{mm}$
Camera	64x64 with $48\mu\text{m}$ pixels
Slitwidth	1 arcsec (2 pixel matching)
Slitlength	30 arcsec
Resolving power	$\simeq 2 \cdot 10^3$

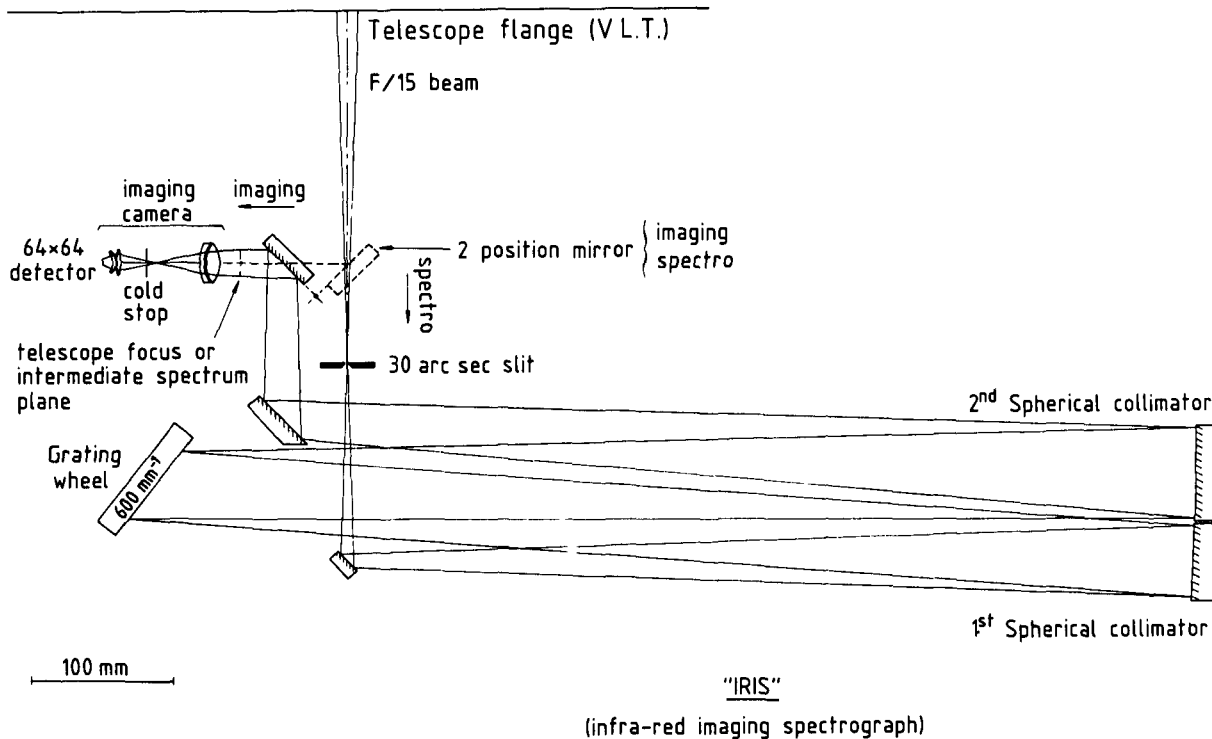


Figure 10.10: IR imaging spectrometer (IRIS) yields  $R \simeq 2000$  between  $1\mu\text{m}$  and  $5\mu\text{m}$  with the camera shown in Figure 10.9 and a 1 arcsec slit.

The physical size of the instrument as shown is in fact slightly smaller and the collimated beam is only half that of the ESO IRSPEC cooled grating spectrometer now installed on the 3.6m telescope. From the technical point of view there are no doubts that an instrument of this type can be constructed and operated at cryogenic temperatures (80K in this case).

### 10.4.3 Near Infrared Spectroscopy at the Combined Focus

The VLT has an enormous potential for high resolution spectroscopy in the near infrared atmospheric windows. Space telescopes are not competitive in this region and ISO, for example, has no capability at  $\lambda < 3\mu\text{m}$ . In the near infrared at  $\lambda < 2.5\mu\text{m}$ , measurement noise will be most likely dominated either by OH sky emission (shot noise and/or fluctuations) or electronic readout noise and the telescope emissivity is relatively unimportant. As even simple metal coatings yield high reflectivities, it should therefore be possible to employ almost the full collecting power of the array (particularly necessary

at these resolving powers) at the combined focus, thus avoiding the difficulty, additional expense and operational complexity of replicating a relatively large and complex spectrograph for the individual Nasmyth foci. (For observations limited by electronic read noise, the S/N ratio achievable at the combined focus is in fact higher than what could be obtained by electronic combination of four Nasmyth instruments).

The Working Group on Infrared Aspects has requested resolving powers of up to at least  $10^5$  based on the requirements for some of its high priority scientific objectives. This is not considered feasible with a dispersive spectrometer alone, due to the extremely large size of the gratings or mosaics of gratings required which will have to be scanned (because of the small array sizes and wide spectral range) and also cooled for operation at wavelengths  $> 2\mu\text{m}$ . The baseline instrument proposed here therefore is a cooled grating spectrometer which can be used alone at  $R \leq 10^4$  or, in combination with a scanning Fabry Perot etalon, at  $R \geq 10^5$ .

Assuming the same array detector as above, it is possible to achieve  $R = 10^4$  with a 1 arcsec slit, using an already commercially available grating of 300 x 400mm. This could be incorporated in a scaled up version of the IRIS spectrometer for the Nasmyth focus shown in Figure 10.10. As the collimator focal length would be  $\sim 5\text{m}$ , however, it may not be practicable to cool the whole instrument in this case. Alternatively therefore the design shown in Figure 10.11 is proposed, based on an inverted Cassegrain system used both as collimator and to image the spectrum at the camera. At this resolving power, the required beam diameter is large enough for the central obstruction to be made smaller than that in the telescopes. The result is an extremely compact instrument which it should be possible to cool, using a continuous flow  $\text{N}_2$  system similar to that developed for IRSPEC.

Because their resolving power is proportional to beam diameter squared, Fabry Perot etalons of a few cm in diameter in front of the grating spectrometer are sufficient to achieve  $R > 10^5$ . Such etalons are now available commercially for use in the infrared up to  $\lambda \sim 15\mu\text{m}$ . The grating spectrometer is necessary for order separation and if the ratio of the resolving powers is chosen to be close to the finesse of the Fabry Perot it should be possible to combine the instantaneous wavelength coverage of the grating with the resolving power of the FP.

The detailed design of such an instrument will depend to some extent on the actual array detectors available in a few years time and on the precise beam combination scheme adopted. However, because the field at the combined focus is expected to be small, it appears most attractive at this stage to consider using the 4 telescopes effectively as an image slicer to align the images along the slit. In this case it is then possible to re-image the telescope pupils on top of each other in the spectrometer and thus minimize the grating size.

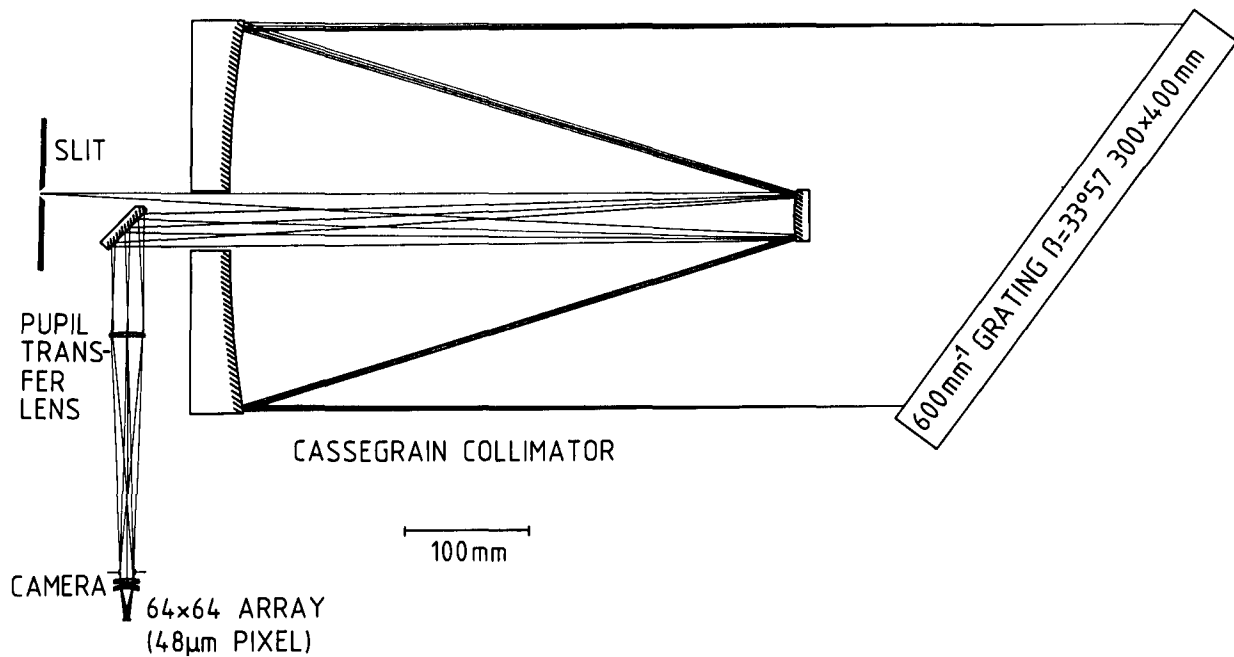


Figure 10.11: Design of a near infrared grating spectrometer capable of  $R = 10^4$  with a 1 arcsec slit at the combined focus. The use of an inverted Cassegrain system both as collimator and to image the spectrum at an interchangeable camera results in an extremely compact and flexible instrument.

#### 10.4.4 Summary of Infrared Instrumentation

The modular approach outlined above allows for many combinations of imaging, polarimetry and spectroscopy. As a realistic example, it is proposed to equip one Nasmyth focus on each telescope as follows:

- Near IR ( $1\text{-}5\mu\text{m}$ ) camera for imaging at  $\leq 0.5$  arcsec/pixel with fast speckle mode, broad band filters, CVF filters and rotating polarizer.
- An IRIS type grating spectrometer yielding  $R \sim 2000$  in conjunction with the near IR camera.
- A mid ( $8\text{-}20\mu\text{m}$ ) camera for imaging at  $\leq 0.5$  arcsec/pixel either direct or using adaptive optics, with broad band filters, CVF filters, a rotating polarizer and a Fabry Perot scanning etalon for imaging at  $R \simeq 5 \cdot 10^3$

and the combined focus with

- A grating spectrograph for  $R \leq 10^4$  between  $1\mu\text{m}$  and  $2.5\mu\text{m}$  (possibly out to  $5\mu\text{m}$  depending on available arrays).
- A Fabry Perot system to be used in conjunction with the above for special applications requiring  $R \geq 10^5$ .

## 10.5 Conclusions

It has been shown in this Chapter that a coherent instrument package can be constructed which can be matched efficiently to the VLT, and which can be built at a reasonable cost (see Chapter 13).

A natural distribution of instrumentation at the different foci would be:

- Nasmyth foci 1: optical instrumentation - imaging and spectroscopy up to medium to high resolution ( $R = 20.000$ ).
- Nasmyth foci 2: infrared instrumentation - imaging and spectroscopy up to  $R \simeq 5.000$ .
- Individual Coudé foci: reserved for specific visitor instruments and experimental developments that do not require a large field of view.
- Combined Coudé focus: bulky instruments that could not fit on a Nasmyth platform and which are too expensive or too complex to be built for each telescope and used in a post detection combination mode. Instruments which need the 16m light collecting power.
- The Cassegrain focus, if implemented, could accommodate instrumentation for visible-infrared imaging and low-resolution spectroscopy.

We have indicated that for some instruments, more than one option exists. For some modes of observation, alternative - and more attractive - solutions might still be proposed.

It would certainly be premature to freeze the instrumentation six years before the first telescope will be completed. The final design must await further discussions within the ESO community, taking into account the technological developments which are currently taking place, in particular in the detector area.

# Chapter 11

## ADAPTIVE OPTICS

This Chapter describes the technology of adaptive optics and its application in the VLT project. Adaptive optical techniques are closely related to active optics which was described in Chapter 5. Both techniques apply a real-time closed-loop correction to the wavefront. In the case of *active optics*, it is the compensation of wavefront aberrations due to primary mirror and telescope effects introduced by gravity, temperature, wind buffeting, etc. In this case the corrections are applied directly to the aberrated optical elements. In the case of *adaptive optics*, wavefront aberrations due to optical propagation effects in the atmosphere are compensated in real-time with an additional optical element, usually a deformable mirror. A major difference in these two applications of the same general principle is in the control bandpass. Typical frequency ranges are DC to 5Hz for active optics and 1Hz to 200Hz for active optics.

The technology of adaptive optics has been developed in the past 10 to 15 years mainly for laser propagation applications. Recently, the first projects have been initiated with the aim of applying it to astronomical observations. It can be expected that this technology will progress even more rapidly in the coming years. Therefore, it is important to take into account future developments and to implement them in the final design of the VLT adaptive system.

The imaging quality of ground-based telescopes is degraded by the transmission of the light from the astronomical object through the turbulent atmosphere of the earth. The reason for this degradation is a random spatial and temporal wavefront perturbation induced by the turbulence in the different layers of the atmosphere. In addition to this, the aberrations of the optical elements of the telescope also contribute to the degradation. All these wavefront perturbations together result in a complex phase aberration

$$\Phi(\vec{r}, t) - iA(\vec{r}, t)$$

of the light beam. The real part  $\Phi(\vec{r}, t)$  represents the phase shift of the wavefront, usually called "seeing", while the imaginary part  $A(\vec{r}, t)$  is a measure of the intensity fluctuations across the aperture plane, called "scintillation".

It is possible to correct the phase shift by adaptive optics. The basic principle of adaptive optics is to use a phase shifting optical element, which can be controlled in space and time in order to compensate the atmospheric phase shift (see Figure 11.1). A correction of the scintillation would require a spatially and temporally controllable apodization element. Thus, a system for the full correction of the aberrations applies a compensation equal to

$$-\Phi(\vec{r}, t) + i\mu A(\vec{r}, t)$$

where  $\mu$  is a dimensionless intensity scaling factor. For most of the imaging problems, especially with very large telescopes, the phase correction part is sufficient and for technical reasons its realization is much easier than the correction of the intensity fluctuations.

The first suggestions for the construction of an adaptive optical correction device came from astronomy in 1953. But up to now, no astronomical observatory operates an adaptive optical system. A more detailed description about the application of adaptive optics in astronomy and the VLT is given in VLT Report No. 47.

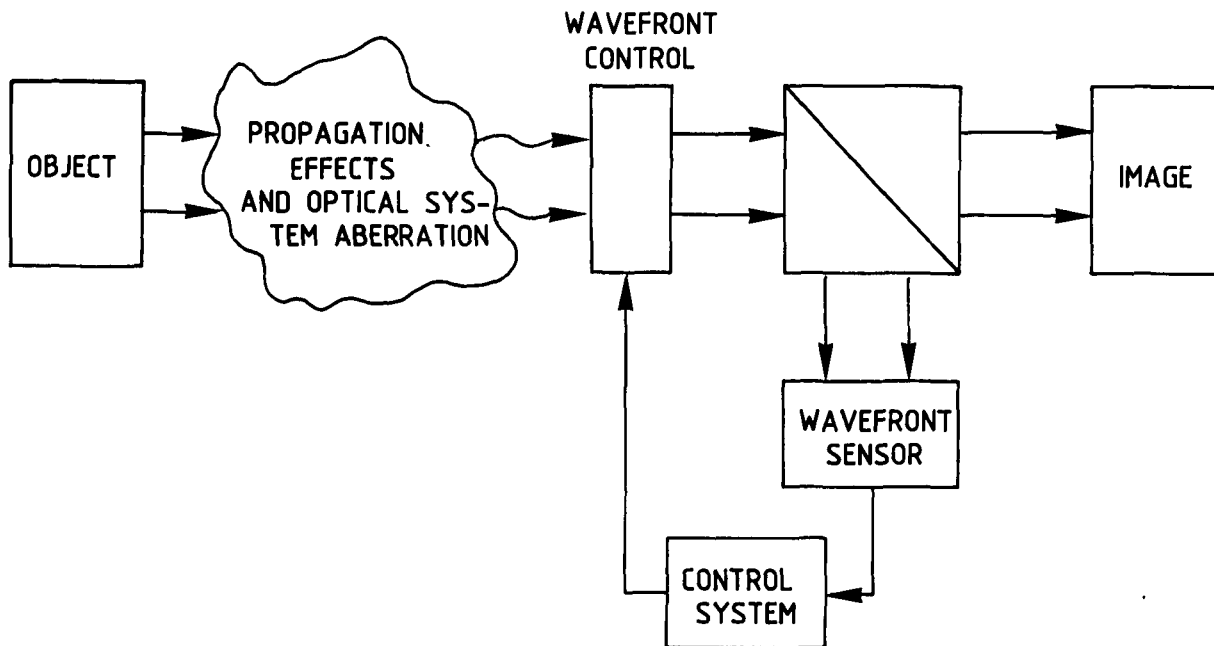


Figure 11.1: Principle of an adaptive optical correction system.



## 11.1 Principle of Adaptive Optics

An adaptive optical system for astronomical applications (see Figure 11.2) contains four basic elements: an optical train and image detector, a wavefront sensor, a servo-control system, and a phase-shifting optical element. The distortion of the received wavefront is usually compensated by reflecting the light beam on a deformable mirror. The surface of this mirror is adjusted in real-time to compensate the path length aberrations. The information required to deform the mirror is obtained by analyzing the light beam with a wavefront sensor. A map of wavefront errors is then derived at each instant of time. Using this error map, the control system determines the signals required to drive the phase shifting optical element and to null the phase aberrations by closing the adaptive loop. The phase correction values can be obtained by expanding the phase-correction function

$$\Phi(\vec{r}, t) = \sum_{n=1}^N a_n(t) f_n(\vec{r})$$

in space ( $f_n(\vec{r})$ ) and time ( $a_n(t)$ ) dependent functions. The spatial functions might represent zones or modes of the aperture, resulting in a zonal or modal correction strategy. The complexity and design of an adaptive system depends on the aperture size  $D$  of the telescope, the direction of the optical path specified by the zenith angle, and the atmospheric conditions. The atmospheric conditions are usually described with the atmospheric turbulent refractive-index structure constant  $C_n^2$ , which is a function of the height  $h$  above the ground, or a derived integral value  $r_0$ , called Fried's parameter.

The number of necessary subapertures  $N$  for an adaptive system with a deformable mirror as active element is given by

$$N \approx \left(\frac{D}{r_0}\right)^2 .$$

The temporal development of the wavefront depends on the transit time of the atmospheric perturbations. It is usually described by the so-called correlation or life time

$$\tau \simeq \frac{r_0}{\Delta v} ,$$

where  $\Delta v$  is a measure for the velocity dispersion of the turbulent atmospheric layers.

For the 8m telescopes of the VLT the necessary wavefront correction range is

$$\Delta z \simeq \pm 12.5 \mu m ,$$

and is independent of the wavelength.

The number of subapertures ( $N$ ) (degrees of freedom), the correction rate ( $1/\tau$ ), and the wavefront correction range ( $\Delta z$ ) are the basic design parameters for an adaptive system. Typical values of these parameters for different wavelengths at an average astronomical site (assuming a telescope diameter of 8 metres), are given in Table 11.1.

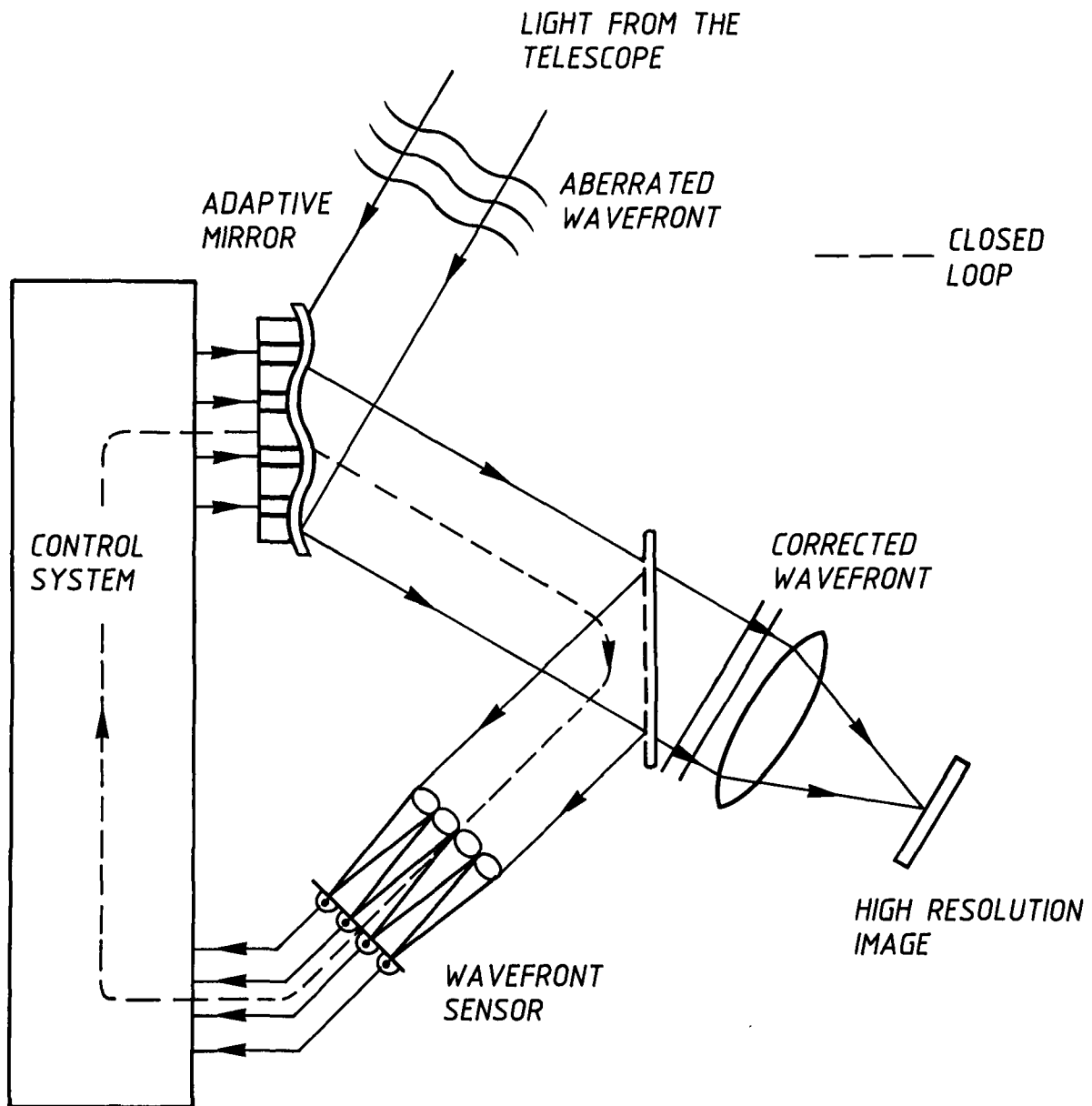


Figure 11.2: Principle of the application of adaptive optics in astronomy.

It is seen, that for an 8m telescope this would lead to more than 6000 controlled subapertures and correction rates higher than 170Hz. A realistic aim for an adaptive system which can be available in the early phase of the operation of the VLT, is a full wavefront compensation at infrared wavelengths ( $\geq 4\mu\text{m}$ ) with a system of 150 to 200 subapertures and a minimum correction rate of at least 20Hz. This satisfies

the requirements shown in Table 11.1. A spatial oversampling (more subapertures) is important for a sufficient fitting quality between the aberrated wavefront and the mirror surface. In order to reach this rate an effective bandwidth of the control loop of 150 to 250Hz is necessary.

Table 11.1

<b>PARAMETERS FOR AN ADAPTIVE SYSTEM</b>				
Telescope diameter: 8m				
$\lambda$ [ $\mu\text{m}$ ]	0.5	2.2	5.0	10
$r_0$ [cm]	10	60	160	360
N	6400	180	12	4
$\tau$ [ms]	6	35	95	220
$\Theta$ [arcsec]	1.8	10	30	70

A perfect adaptive optical system will perform diffraction limited imaging on the optical axis. For off-axis parts in the image which have different viewing angles with respect to the optical axis, the correction is limited due to the limited atmospheric correlation length. The angular range wherein the light suffers from the quasi-identical atmospheric disturbance is called the isoplanatic angle  $\Theta$ . This parameter, together with  $r_0$ , completely determines the optical properties of the turbulent layer at points on the ground. The expressions for  $r_0$  and  $\Theta$  are based on plane and spherical wave theory, respectively. They describe a model for which measurements have shown sufficient evidence. Table 11.1 displays some typical values of the isoplanatic angles for different wavelengths.

## 11.2 Strategy for Seeing Optimization

The shape of an optical wavefront may be represented in two different ways: (1) using an array of independent, localized zonal functions, or (2) using a set of orthogonal, whole-aperture modal functions. Analytically, the two systems are equivalent in terms of the number of degrees of freedom required to specify a given wavefront to a certain precision. However, there are major practical differences, especially in the implementation of wavefront sensors and compensation devices. All practical wavefront sensors

and most of the deformable mirrors use the zonal approach. With zonal mirrors, the main variable is the shape of the influence function of each zone.

For modal compensation, the well-known Zernike polynomials, which correspond to systematic optical aberrations such as defocus, astigmatism, etc. encountered in conventional optical components, may be employed as the spatially dependent function  $f_n(\vec{r})$ . The strategy of modal correction is already applied at ESO for the active correction of the primary mirror in the NTT, and is also proposed for the active correction of the VLT primaries as described in Chapter 5.

In a modal concept, the single steps in the closed-loop procedure are (see Figure 11.3):

- Measurement of the local slope of the wavefront.
- Computation of a wavefront map.
- Computation of the modal coefficients (e.g. Zernike coefficients).
- Computation of the control signals for the wavefront correction device.
- Conversion of control signals to the required drive signal for each subaperture of the correction device.

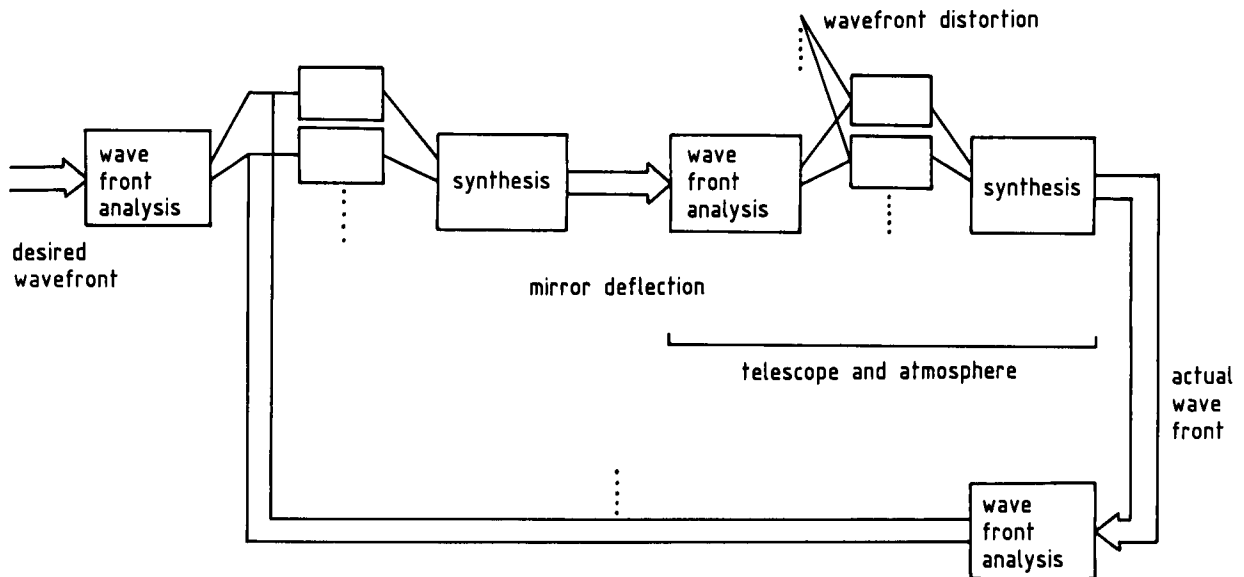


Figure 11.3: Schematics of the modal closed-loop wavefront compensation strategy.

If the modal approach is used rather than a zonal decomposition, image improvement is possible, even with a limited number of modes. This is one of the essential advantages of the modal correction strategy. The goal for the future investigations is to determine the optimum algorithms for the adaptive correction with large telescopes in astronomy.

## 11.3 Elements of an Adaptive System

The main elements of an adaptive optical system are the wavefront correction device, the wavefront sensor, and the control computer.

### 11.3.1 Wavefront Correction Device

The wavefront can be controlled, either by changing the velocity of propagation or by changing the optical path length. The former is achieved by varying the refraction index of a medium, while the latter is implemented by moving a reflective surface such as a mirror or by generating a grating as in a Bragg cell.

At the present time, reflective devices are the most successful and widely used as wavefront correctors. The problem with the other devices are mainly the limited range of refraction index change, the spectral absorption, and nonuniform transmission. On the other side mirror coatings are available with high efficiencies over wide spectral ranges, and because the optical path is confined to one side of the mirror surface, a great variety of substrates and methods of deforming the mirrors are available. Finally, the wavefront deformation is a true optical path length change, independent of wavelength. Figure 11.4 shows the basic types of adaptive mirrors, and Figure 11.5 gives examples of adaptive mirrors which have been developed in Europe.

For the correction of atmospheric perturbation in an astronomical telescope with adaptive optics, the continuous thin-plate mirrors with discrete position actuator or the bending moment actuators seem to be the most favourable ones.

### 11.3.2 Wavefront Sensor

It is not possible to measure directly the phase of an optical wavefront, as no existing detector will respond to the temporal frequencies involved. For the application in astronomy with the severe intensity problems, a shearing interferometer or a Shack-Hartmann sensor seems to be adequate.

The Shack-Hartmann sensor is based on the well-known Hartmann test for checking the figure of large optical elements. Figure 11.6 shows the schematics of a Shack-Hartmann sensor. The wavefront is divided into a number of zones,

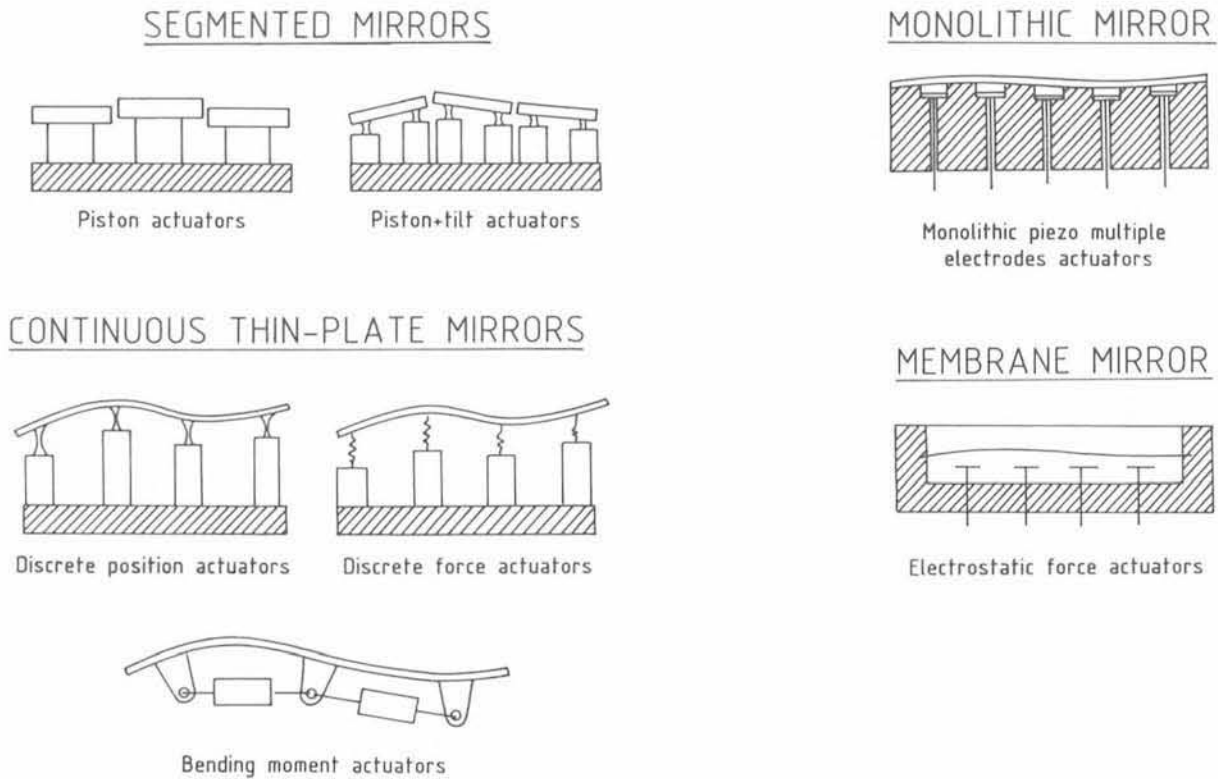


Figure 11.4: Different types of deformable mirrors.

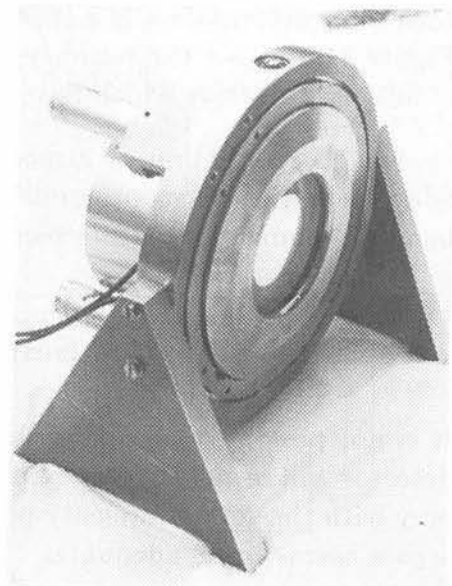
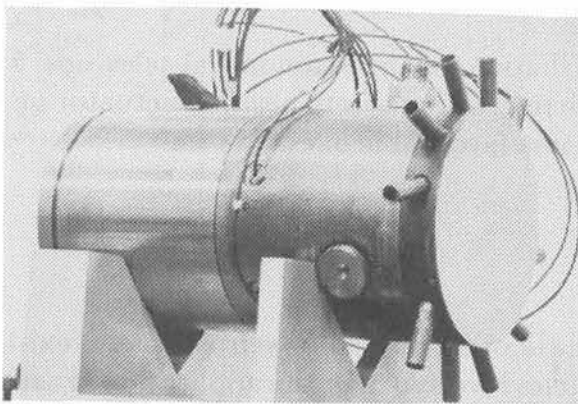


Figure 11.5: Deformable mirrors developed in Europe. left: CGE mirror (France) with piezoelectric actuators (with permission of CGE, DRET), right: University of Heidelberg mirror with a thin electrostatically deformable membrane.

usually contiguous and of equal size. The light from each zone is brought to a separate focus and the position of the centroid of each focus is measured in two dimensions by a photoelectric device, e.g. a quadrant detector or an array detector camera. Figure 11.6 also shows a typical focus pattern of a Shack-Hartmann lenticular array developed at ESO. The position measurements reveal the mean wavefront slope over each zone. A CCD camera or a Reticon type array will be used as detector to determine the position of the individual foci, e.g. by calculating the centre of gravity within a subarray of the detector array. In this case typically 10 x 10 elements are used. The residual wavefront curvature over each zone is not measured, and in fact tends to degrade the signal-to-noise ratio, due to a slight defocus.

The mechanical requirements on the stability of the individual imaging lenses and detector elements are severe. However, by combining the beam to be analyzed with a reference beam, for example representing a plane wavefront, it is possible to overcome the precise optical alignment requirements (see Figure 11.6). At ESO this technique was first implemented in 1979. Such a system can be self-calibrating, even during observation.

Hartmann type sensors are unique when compared to other systems, such as interferometers with chopper wheels, because they collect and sample virtually 100% of the light entering the optical system. Additionally, the wavefront tilt over the subapertures can be measured even when the phase of the light from one side of the subaperture to the other side exceeds  $2\pi$ . Hartmann-type sensors can also detect wavefront tilts of white light beams, because they are independent of wavelength. They measure the tilt angles of wavefronts, and not optical phase differences which makes them robust and therefore well suited for adaptive optical systems. This tilt angle is exactly what is needed to compensate for optical path errors independent of wavelength.

### 11.3.3 Control System

All slope-measuring wavefront sensors require a reconstruction of the wavefront itself. Normally, two orthogonal wavefront slope measurements are made for each actuator location. In other words, there are twice as many measurements as unknowns, so that a least-squares fit can be performed with beneficial effect on error propagation. Several reconstruction operations have been used or proposed in the literature.

All of these algorithms require very high computation powers in order to meet the temporal and spatial requirements of the astronomical application. With special dedicated hardware or hybrid systems this problem can be approached successfully. At the present time first prototype systems are available. These systems are based on microprogrammable parallel structures, controlled by a general purpose host processor.

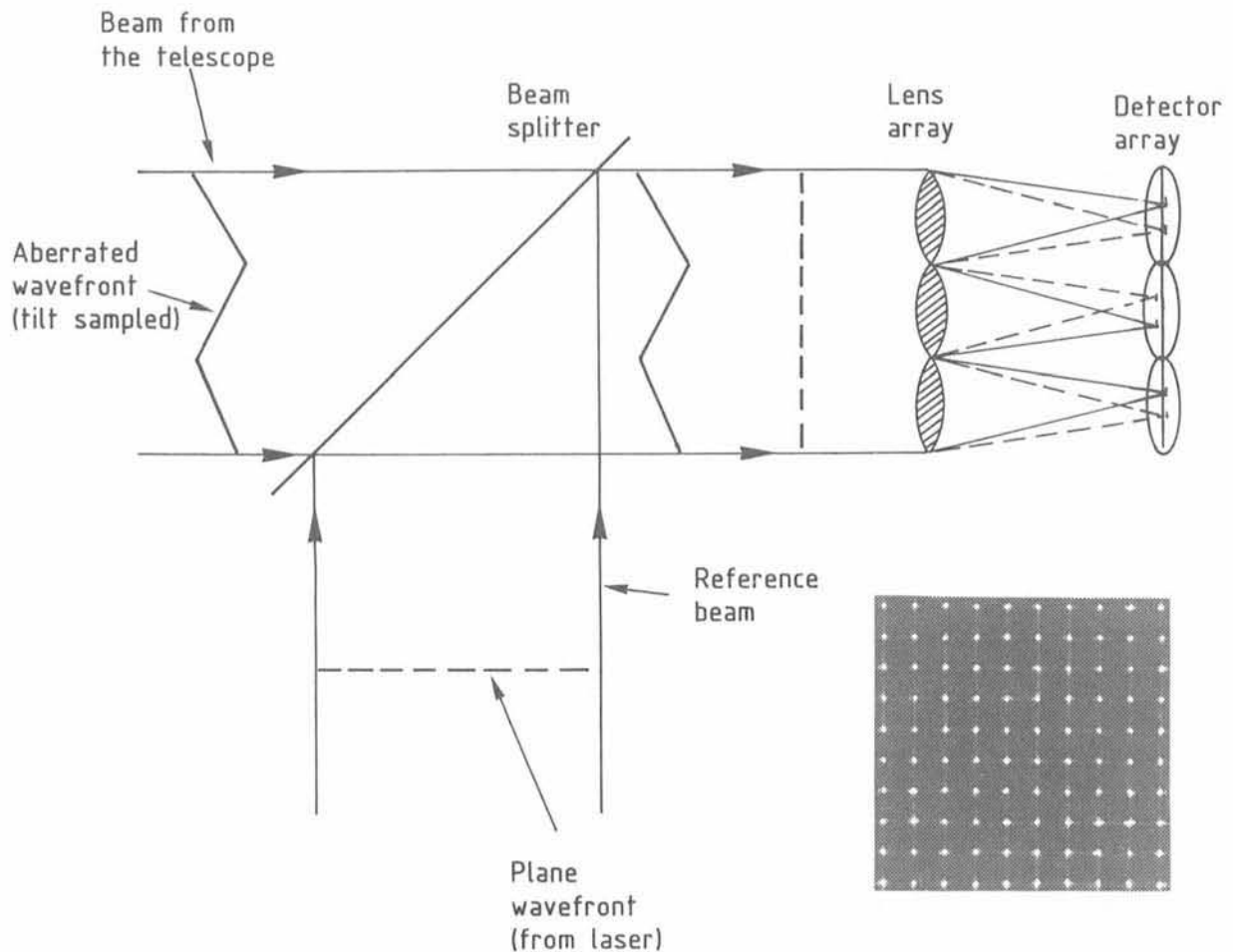


Figure 11.6: Principle of the Shack-Hartmann wavefront sensor with a reference beam for self-calibration and a typical Shack-Hartmann focus pattern.

## 11.4 Performance of an Adaptive System

The main sources for errors in the model of adaptive optics are *wavefront fitting errors* ( $\sigma_F^2$ ), which depend on how closely the wavefront corrector can match the actual wavefront error, the *detection error* ( $\sigma_D^2$ ), which is essentially reciprocal to the signal-to-noise ratio of the wavefront sensor output, and the *prediction error* ( $\sigma_P^2$ ), which is due to the time delay between the measurement of the wavefront disturbances and their correction. The overall residual error ( $\sigma_R^2$ ) is then given by:

$$\sigma_R^2 = \sigma_F^2 + \sigma_D^2 + \sigma_P^2$$



## 11.5 Requirements for Adaptive Correction in Astronomy

Any correction requires a measurement of the effect which shall be corrected. This is the major problem in relation to the application of adaptive optics in astronomical observation. The observed sources are in most cases so faint that their light is insufficient for the correction. A brighter nearby reference source within the same isoplanatic patch is seldom available. Figure 11.7 gives the density of stars in dependence of its magnitude for the galactic pole and the galactic equator. At the present time a large scanning programme of photographic plates (obtained with the Palomar, SERC and ESO Schmidt telescopes) is being carried out in order to provide a database for the guide star catalogue of the Hubble Space Telescope. This resulting star lists will be of great importance also as a reference source for active and adaptive optics. Initial results seem to indicate that the actual star density is higher than previously described in the literature.

Although the coverage with reference stars thus may be denser than earlier assumed, it is by far not sufficient for the operation of an adaptive optical system at visible wavelengths for any source. Under the assumption that 100 photons per subaperture are sufficient for a wavefront measurement with an integration time of less than 10msec, the limiting magnitude  $m_{lim}$  would be by far too bright. However, for infrared wavelengths the situation becomes more favourable because of the increase of the isoplanatic angle as shown in Table 11.2.

Table 11.2

<b>LIMITING MAGNITUDES AND SKY COVERAGE FOR ADAPTIVE OPTICS</b>				
$\lambda$ [ $\mu\text{m}$ ]	0.5	2.2	5.0	10
$r_0$ [cm]	10	60	160	360
$m_{lim}$	7	13	15.5	17
$C_P$ [%]	$\approx 0$	0.1	30	100
$C_E$ [%]	$\approx 0$	0.3	100	100

Theoretically, there is a correlation between the atmospheric MTF at visible and

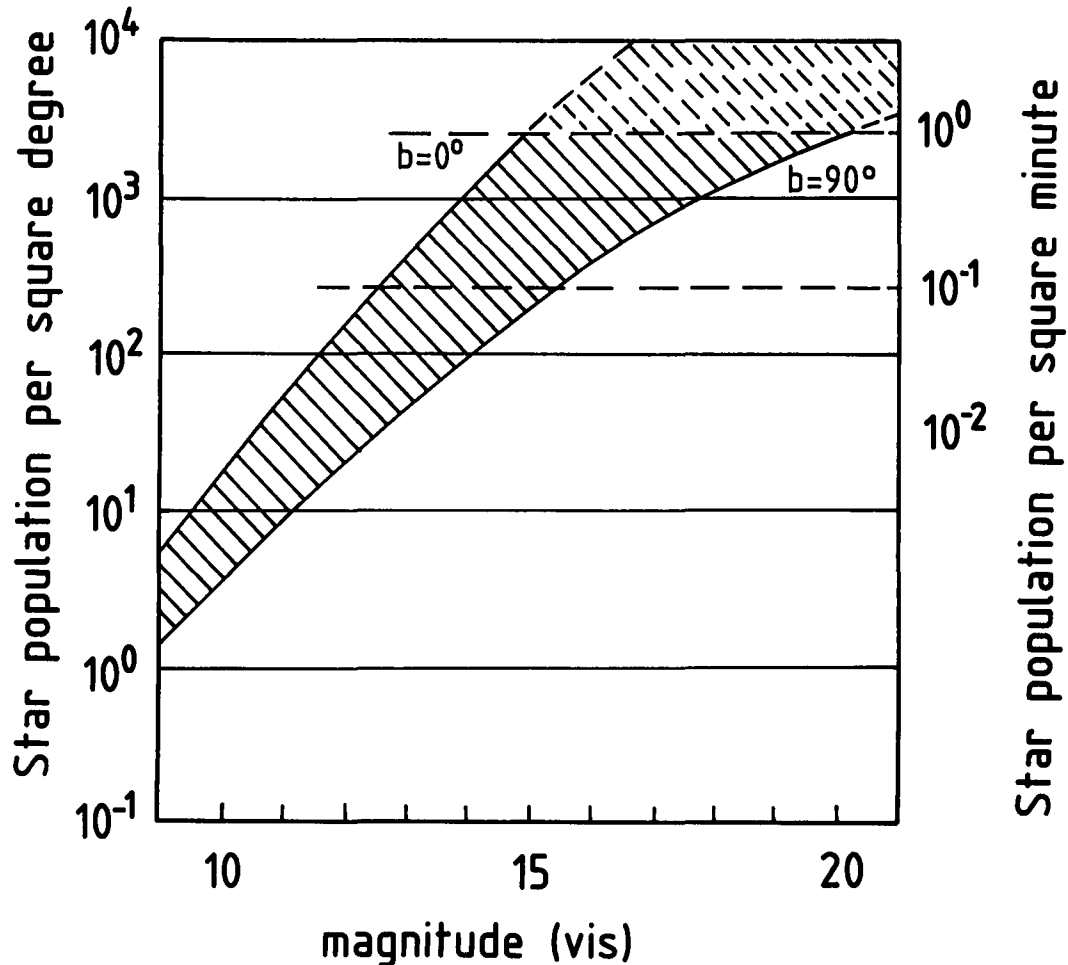


Figure 11.7: Star density as a function of visual magnitude, at the galactic poles ( $90^\circ$ ) and equator ( $0^\circ$ ).

infrared wavelengths. The first measurements on La Silla indicate that the low spatial frequencies in the visible MTF are correlated with the infrared MTF. This correlation opens the possibility of measuring the wavefront in the visible range and to compensate for infrared wavelengths. This makes adaptive optics in the infrared much easier because the technical realization of a wavefront sensor in the infrared would be much more complicated and expensive. Table 11.2 gives the limitation for adaptive optics in the visible and for selected infrared wavelengths, and the resulting sky coverage at the galactic pole ( $C_P$ ) and the galactic equator ( $C_E$ ).

Recently, new techniques to overcome the reference source problem even in the visible range have been proposed. With a LIDAR like technique an artificial reference source

is generated using resonance scattering of yellow laser light in the mesospheric sodium layer (see Figure 11.8). A powerful dye laser could be an appropriate light source. These artificial reference sources have to be generated within the isoplanatic angle of the astronomical source at a repetition rate synchronous to the adaptive correction rate. It would require to gate the astronomical detector during the wavefront sensing time, which means a small loss compared to the high gain of the adaptive correction. The test of this technique will be included in the further investigations for adaptive optics.

## 11.6 Adaptive Optics for the VLT

It is intended to equip each individual VLT telescope with independent active and adaptive optical systems (see Figure 11.9). To point out the major differences between the two techniques, we here briefly recall active optics. The active optics will be used for the figure compensation of the telescope optics. For the optical figure correction, it is important to measure the wavefront by integrating over the atmospheric fluctuations in order to get only the optical system aberrations due to gravitational, thermal, and wind effects on the telescope optics and structure. Also here a Shack-Hartmann sensor is foreseen as wavefront sensor and located in an image of the primary pupil. The wavefront sensor for the active optics has to be arranged on a scanning system in order to set it on a suitable reference source. There is basically no isoplanicity problem for this active optical system. Also the wavefront computation problems are relaxed because of the low temporal frequencies.

The atmospheric compensation is foreseen in separate adaptive optical systems which will be installed in the yoke of the unit telescopes. They can be switched in and out of the infrared Coudé beams. A two mirror system seems to be favourable; one mirror to compensate tip-tilt aberrations and another piezoelectrically actuated deformable mirror to correct all higher order aberrations. As wavefront sensor, the Shack-Hartmann type again seems to be the most adequate one. As mentioned above, the active and adaptive optics will have separate wavefront sensors, due to the different isoplanatic angles and the different time constants for the corrections. At the moment, an adaptive system with 150 to 200 subapertures and a bandwidth for full compensation (0 dB) of 20Hz is the target for future investigations. Figure 11.10 shows a possible configuration with a 187 actuator deformable mirror and a  $16 \times 16$  Shack-Hartmann wavefront sensor array. By extrapolating currently available technology with stacks of piezoelectric material as actuators, the diameter of this mirror would be approximately 300mm.

This adaptive system will serve the instrumentation at the individual Coudé foci as well as the combined Coudé focus. These adaptive systems will offer diffraction limited observation for the infrared Coudé images at wavelengths greater than  $4\mu\text{m}$  and a partial correction at shorter wavelengths. The importance of adaptive optics for interferometry is pointed out in Chapter 12; it is concluded that it is mandatory. For long baseline interferometry with the VLT, the gain of the 8m apertures is only given

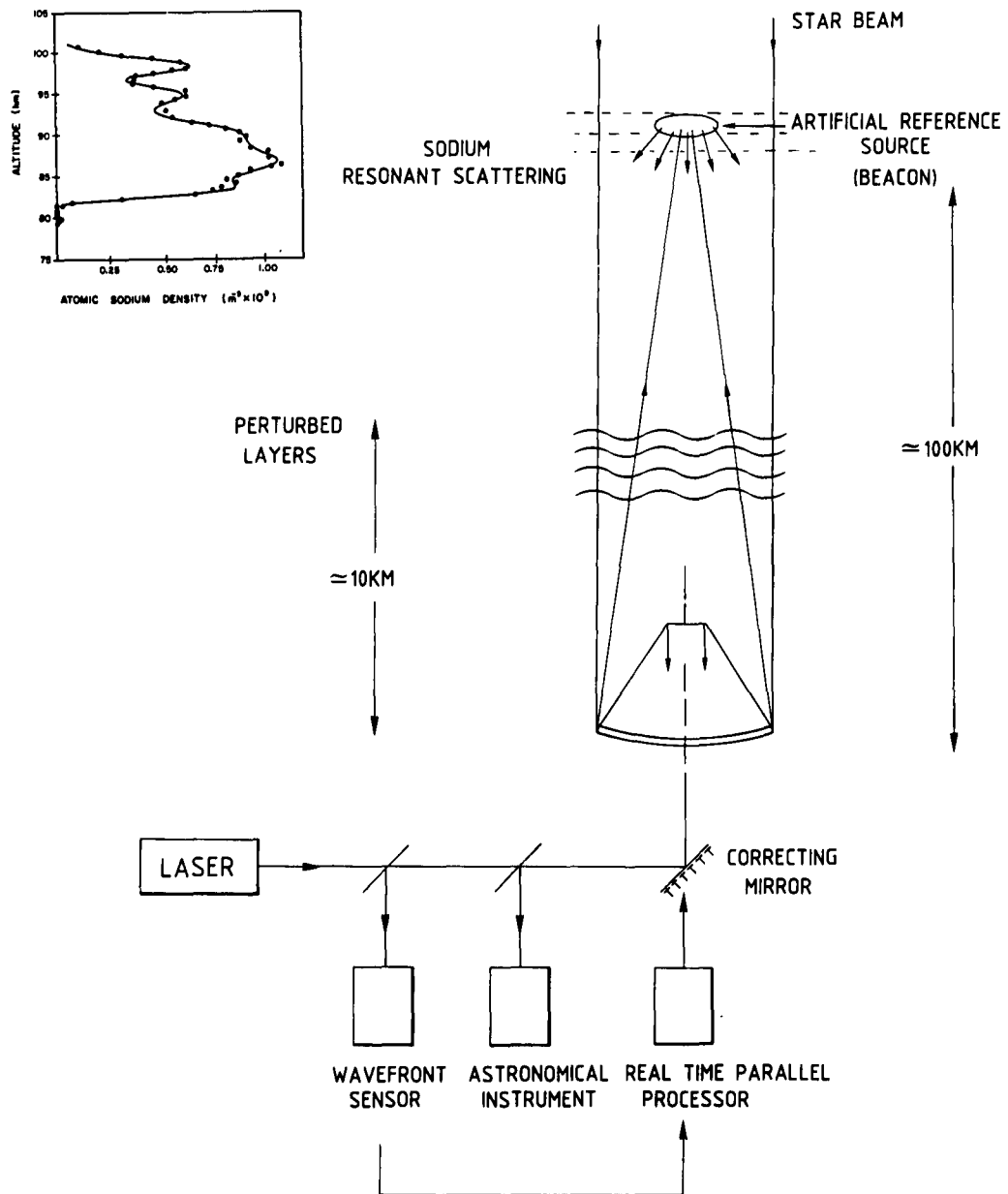


Figure 11.8: Generation of an artificial reference source by resonance scattering of a laser beam in the mesospheric sodium layer. The insert shows the sodium concentration vrs. altitude.

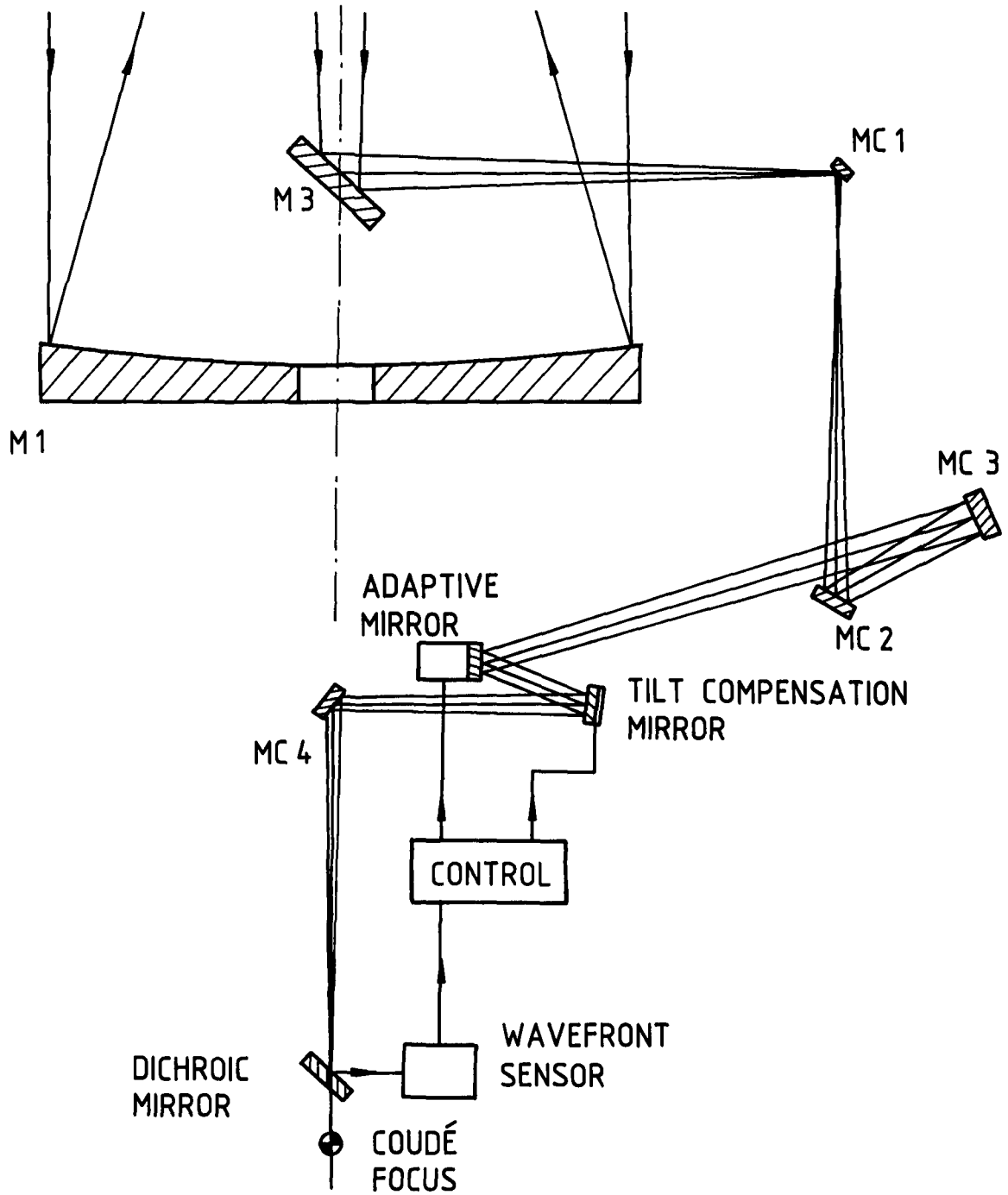


Figure 11.9: Schematic diagram of the adaptive system for the VLT.

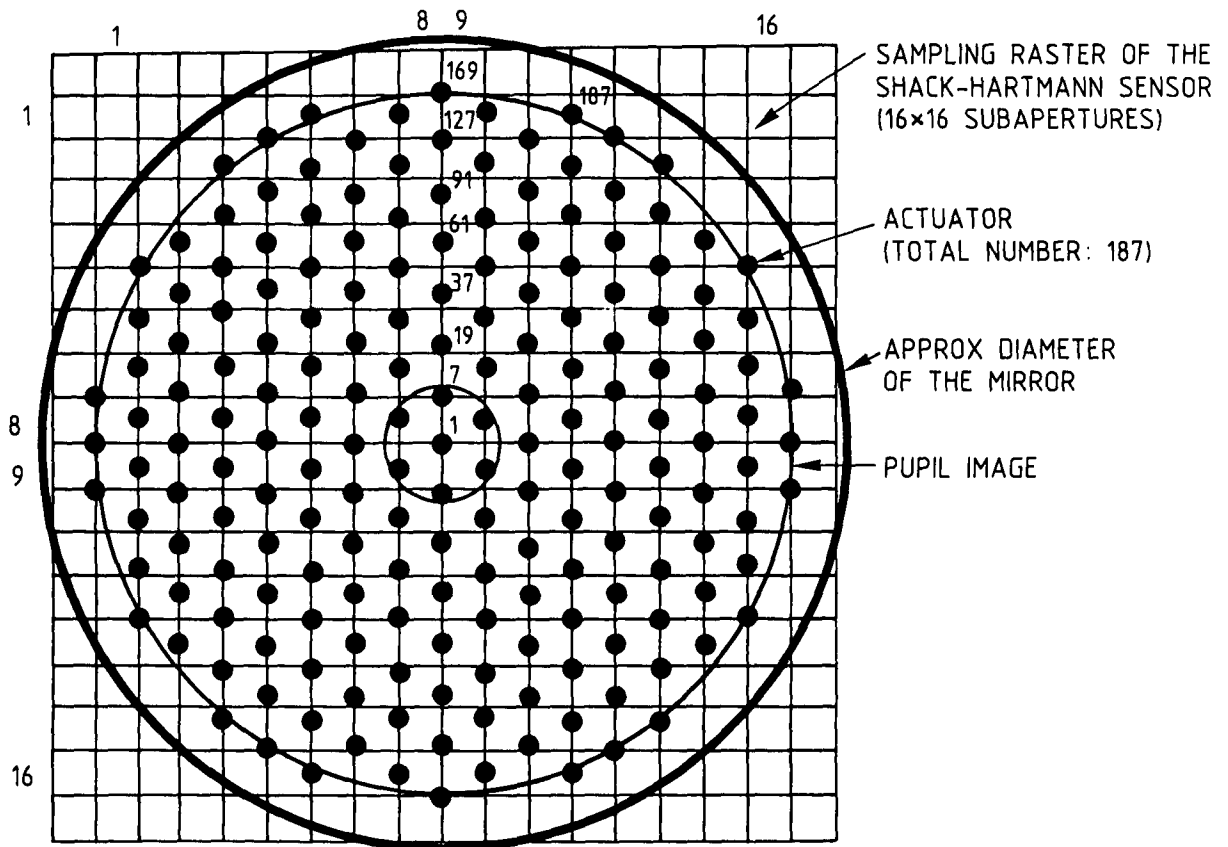


Figure 11.10: Possible configuration of a 187 actuator driven deformable mirror and the corresponding  $16 \times 16$  subaperture raster of the Shack-Hartmann sensor.

in combination with adaptive optics. Otherwise the signal-to-noise ratio will not be improved, as compared to interferometers with smaller apertures.

As an initial step by ESO into the field of adaptive optics, a 19 actuator prototype adaptive system is currently in the design phase in collaboration with other institutions. This system will serve as a testbench for the various elements of an adaptive system and the control algorithms. In a second step, a 37 to 61 subaperture adaptive device could serve as the intermediate scale system towards the large units required for the VLT.

The experience gained with the planned smaller scale systems is of great importance not only for the realization of the proposed adaptive system, but also for the active optical system. Because of the similarity of the control procedure and strategy, identical or at least similar algorithms and hardware could be developed and applied, improving the performance and reliability of the systems.

It should be mentioned, that the proposed adaptive system is based on currently available technology. New developments indicate that much more complex systems will have become available when the VLT goes into operation.

# Chapter 12

## INTERFEROMETRY

The linear array concept of the VLT offers a unique possibility for astronomical observations with very high angular resolution by operating the telescopes as an infrared and/or visible long-baseline interferometer. In the proposed, compact linear array configuration with a

- baseline of 104 metres -

between the centres of the most extreme telescopes, resolutions up to approximately 45 milliarcsec at  $20\mu\text{m}$  wavelength and approximately 0.75 milliarcsec in the blue could be reached.

Interferometry with two or more telescopes is only at its beginning, but its potentials have been well demonstrated by recent measurements with small existing prototypes. As a result, several ground and space based projects have been proposed, or are already in the design or realization phase.

The impact of interferometry on the global concept of the VLT should be limited, because interferometry is neither the prime, nor the only driver of this project. But the baseline concept, with its incoherent beam combination system, already offers many of the necessary features for a long-baseline interferometer. With limited effort and cost, it will be possible to equip the VLT additionally with an interferometric operation mode.

In order to optimize the interferometric operation mode within the general frame of the linear array concept, different options have been under discussion. These options and various combinations of them included the following basic configurations (for more details see VLT Report No. 49 of the VLT Working Group on Interferometry):

- a linear array with one large telescope movable parallel and/or perpendicular to the array axis,
- a non-redundant array configuration (unequal spacings between the unit telescopes) with spacing ratios of 1:3:2, and two smaller telescopes (one of which can



be moved parallel and the other perpendicular to the linear array axis), and

- a redundant array with equal spacing between the telescopes and again two smaller auxiliary telescopes.

The discussions converged towards the latter solutions (see Figure 12.1), which present a maximum of flexibility. The last solution has the smallest impact on the site and space requirements and is therefore considered in this Chapter.

Interferometry requires the phasing of the VLT unit telescopes. This sets much tighter specifications to the mechanics and optics, than if the four telescopes would only be incoherently combined. From the beginning it can be excluded that the linear array and its unit telescopes offer a passive stability sufficient for interferometry, with vibrational amplitudes of less than a tenth of a wavelength, even at wavelengths of 10 or  $20\mu\text{m}$ . Therefore, it is important to develop techniques for an active stabilization of the the light beams, after they have left the unit telescopes. Nevertheless, the unit telescopes should be as stable as possible in order to limit these stabilization efforts. Therefore, a first and realistic target for the operation of the VLT in the interferometric

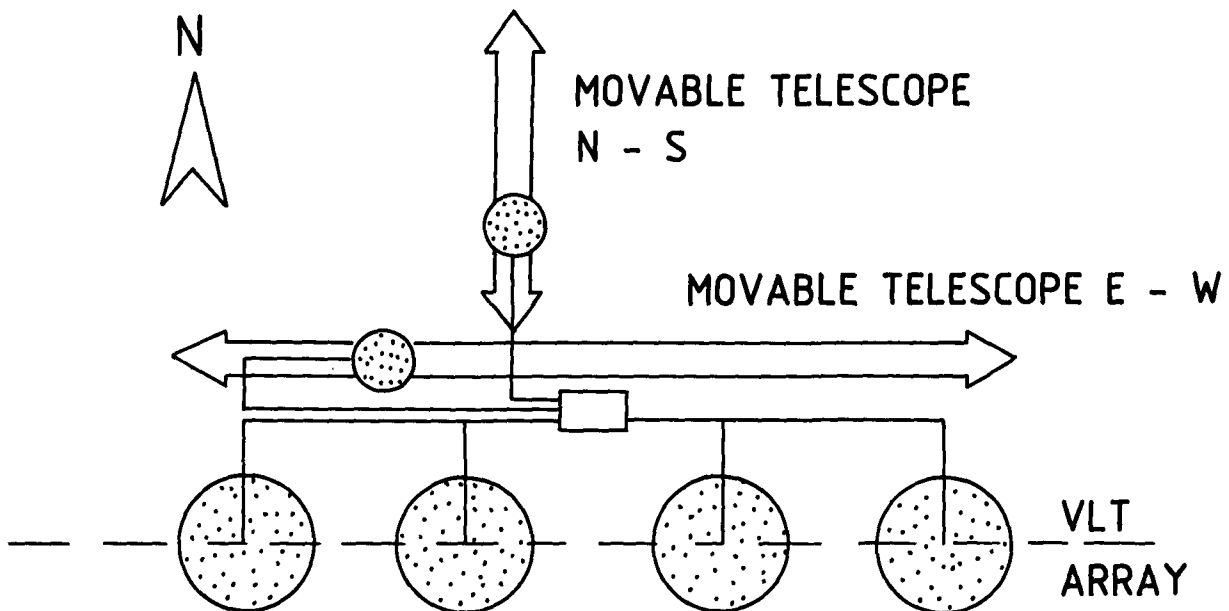


Figure 12.1: Schematic configuration of the VLT as a long baseline interferometer. The linear array is arranged in East-West (or quasi-East-West) orientation. Two smaller auxiliary telescopes are added to the array. They are movable, one parallel to the array axis (E-W) and one perpendicular in the North-South direction.

mode is the infrared wavelength range from 3.5 to 20 $\mu$ m, where the tolerances are already in the submicron range and this over distances in the range of 50 m. Later, after sufficient experience at longer wavelengths has been gained, and as a second phase of interferometer operation, a gradual expansion towards shorter wavelengths should be envisaged.

Obtaining images or spectra at the diffraction limit from the ground, either with a single large pupil or with two or more smaller pupils, suffers basically from the same limitation: the fluctuations of the index of refraction of the atmosphere. In the interferometric mode, the full gain of the 8 metre single apertures of the VLT is, however, only obtained, if adaptive optics is applied for a real-time partial or full phase compensation of the degradations due to atmospheric turbulences. This technique has been discussed in detail in Chapter 11. Additionally, a great deal of knowledge has been accumulated during the last years in the treatment of images distorted by atmospheric turbulence in the visible and infrared, respectively, providing a firm basis for the planing of the performance and the operation of a ground-based optical interferometer.

The auxiliary movable telescopes are mainly selected for spatial frequency coverage reasons, but would also allow a full-time use of the interferometric instrumentation, while the large telescopes are used for other observation modes. The finally selected arrangement depends strongly on the available site. The current configuration is the most compact arrangement. If a larger mountain top will be considered, it can be easily expanded.

Interferometry with the VLT offers such a novel field for science that it is difficult to forecast the discoveries associated with the two to three orders magnitude leap in angular resolution. VLT Report No. 49 of the WG on Interferometry discusses the scientific aspects of a VLT interferometer in detail and gives specifications and recommendations for the optical and mechanical design. A rather conservative assumption is that interferometry will progress in steps, measuring in the beginning only the visibility amplitudes, and moving progressively towards visibility phases, better (u-v) coverage, and complete image restoration. Infrared wavelengths may be covered first, and with progressive use of adaptive optics the range will be pushed towards shorter wavelengths. Visible wavelengths may follow. Therefore it is important to examine how the linear array concept with auxiliary small movable telescopes will ultimately provide images.

## 12.1 Image Formation in Interferometry

A single telescope provides a spatial frequency coverage which is the two-dimensional autocorrelation function of the pupil measured in units of wavelength. The diffraction limited image contains all spatial frequencies from zero to the cut-off frequency of the telescope  $\lambda/D$  ( $D$  = telescope diameter), weighted by the monotonously decreasing MTF. The spatial frequency domain is called the (u-v) plane. The atmospheric turbulences introduce random phase errors over the pupil, which produce a speckle image

(seeing disk). The atmospheric MTF is a random function, which strongly attenuates the high spatial frequencies.

Aperture synthesis for image formation with sampled wavefronts is well known in radio astronomy. If two telescopes are separated by the baseline  $L$ , the  $u$ - $v$  plane is sampled at the frequency  $L/\lambda$ , and gives only one value in the object spectrum, called the complex visibility (amplitude and phase). The  $u$ - $v$  coverage is obtained by varying the baseline  $L$  projected on the sky, by moving the telescopes or by letting the diurnal motion do it, or both. The coverage is usually incomplete, leaving holes or empty stripes in the ( $u$ - $v$ ) plane. Figure 12.2 demonstrates this in the 1-dimensional case for the linear array. The treatment of radio signals is easy, due to the existence of phase stable amplifiers. The final image is obtained by Fourier inversion of the measured visibility data. The feasibility and quality of this image reconstruction process depends on the following factors: ( $u$ - $v$ ) coverage, amount and quality of phase information, noise in the visibility data, and complexity of the object itself.

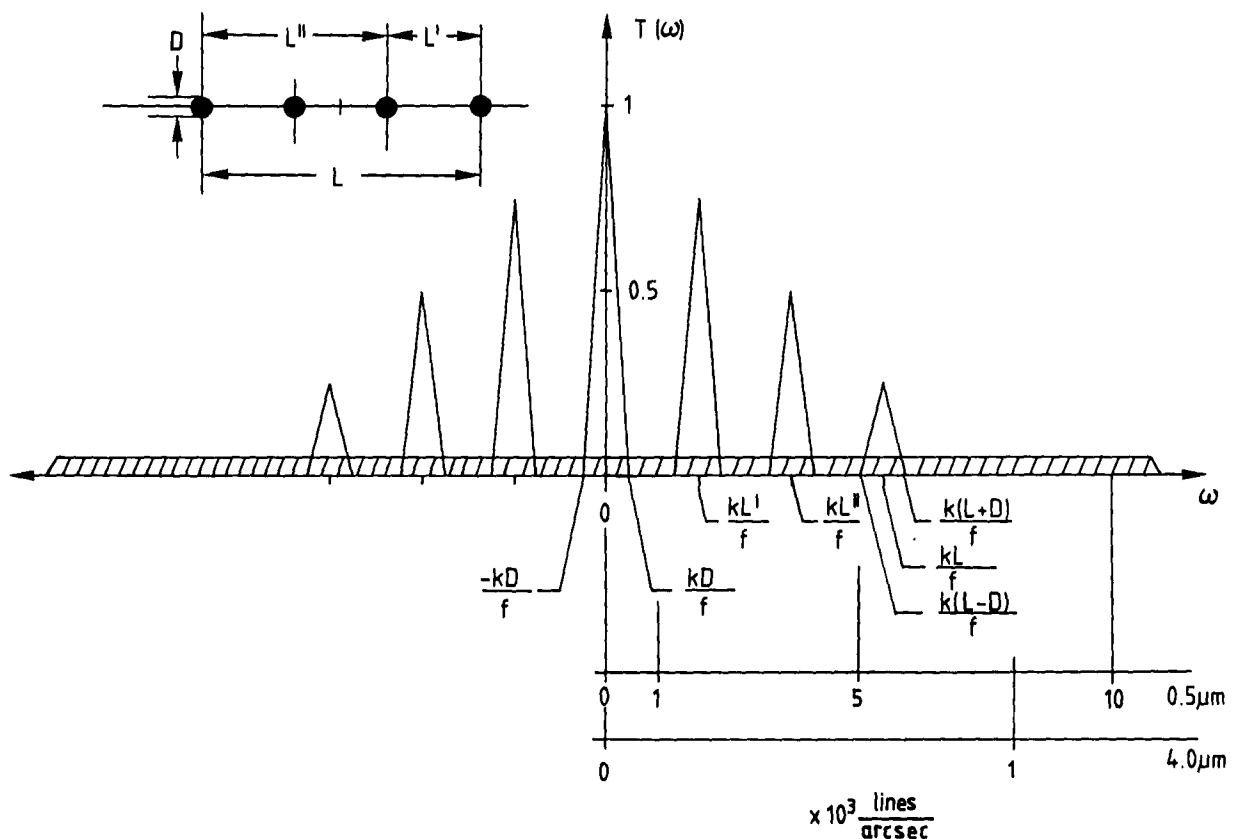


Figure 12.2: One-dimensional spatial frequency coverage of the VLT array in the array axis for 2 different wavelength ( $D=8\text{m}$ ;  $L=104\text{m}$ ;  $L'=33\text{m}$ ;  $L''=71\text{m}$ ;  $k=2\pi/\lambda$ ;  $f$ : focal length of the camera). The shaded area indicates the filling of the ( $u$ - $v$ ) plane by adding a smaller movable telescope (1.5m aperture; motion parallel to the array axis) to the array. See also Figure 12.4.

At optical wavelengths, the problems are much more complex than in radio astronomy, due to the atmospheric effects: the phase of the wavefront from a point source is in general no longer constant over the surface of each pupil, these phases are randomly varying with time (timescale: 10 to 100 msec), and even when the wavefront is constant over each pupil, a temporally varying global phase difference is present between the individual pupils. Measuring the amplitude of the complex visibility (or fringe contrast) is straightforward, but atmospheric phase disturbances prevent a direct phase measurement. The situation is more favourable for longer wavelengths in the infrared, where the size of the atmospheric coherence area ( $r_0$ ) becomes comparable with the size of the pupil itself, while the phase excursions, measured in units of wavelength, are much smaller.

At shorter wavelengths, where the telescope diameter is much larger than the atmospheric coherence area adaptive optics is a technique to overcome these problems and to restore in real-time full coherence over the whole pupil. In this sense adaptive optics (Chapter 11) is a must for long baseline interferometry. Whenever the full coherence of the wavefront can not be achieved over each pupil, one is forced to break the pupil into subpupils, which are coherent. But the final result has a poorer signal-to-noise ratio.

In the presence of rapidly varying atmospheric phase errors, consecutive measurements will have different errors (unless some methods of phase tracking are applied). The only way to reduce the number of independent phase errors in this case is to measure a number of visibilities simultaneously. There are several ways to do this:

- With a single interferometer (2 telescopes), one can measure the phase difference between two (u-v) points that are less than one telescope diameter apart. In practice this provides the phase derivative.
- With only two telescopes, it is also possible to measure the visibility at multiple frequencies by dispersing the light. Since the (u-v) coordinates are measured in wavelengths, each frequency corresponds to a different (u-v) point.
- An array of N telescopes can provide  $N(N-1)/2$  different interferometers. If all measurement errors can be assigned to the individual telescopes, the number of independent errors is N, which is smaller than  $N(N-1)/2$  for  $N \geq 3$ . The measured phases can be combined to build error-free quantities called closure phases.

Current optical interferometers only measure amplitudes. The use of phase derivatives with respect to spatial frequency is well developed in speckle interferometry (e.g. Knox-Thompson algorithm). The feasibility of other well known radio astronomy techniques, such as phase derivation with respect to the wave frequency (spectral phase derivatives) or as phase closure at optical wavelengths, has recently been successfully demonstrated.

### 12.1.1 Measuring the Visibility Amplitude

The achievements of speckle interferometry in terms of sensitivity are extremely good and close to the theoretical limits. Since the limiting factors - mostly the atmospheric effects - are basically the same, there is no reason to doubt the efficiency of an interferometer. It is nevertheless necessary to treat separately the visible and infrared case, because the limiting factors have a different impact on the final sensitivities and accuracies.

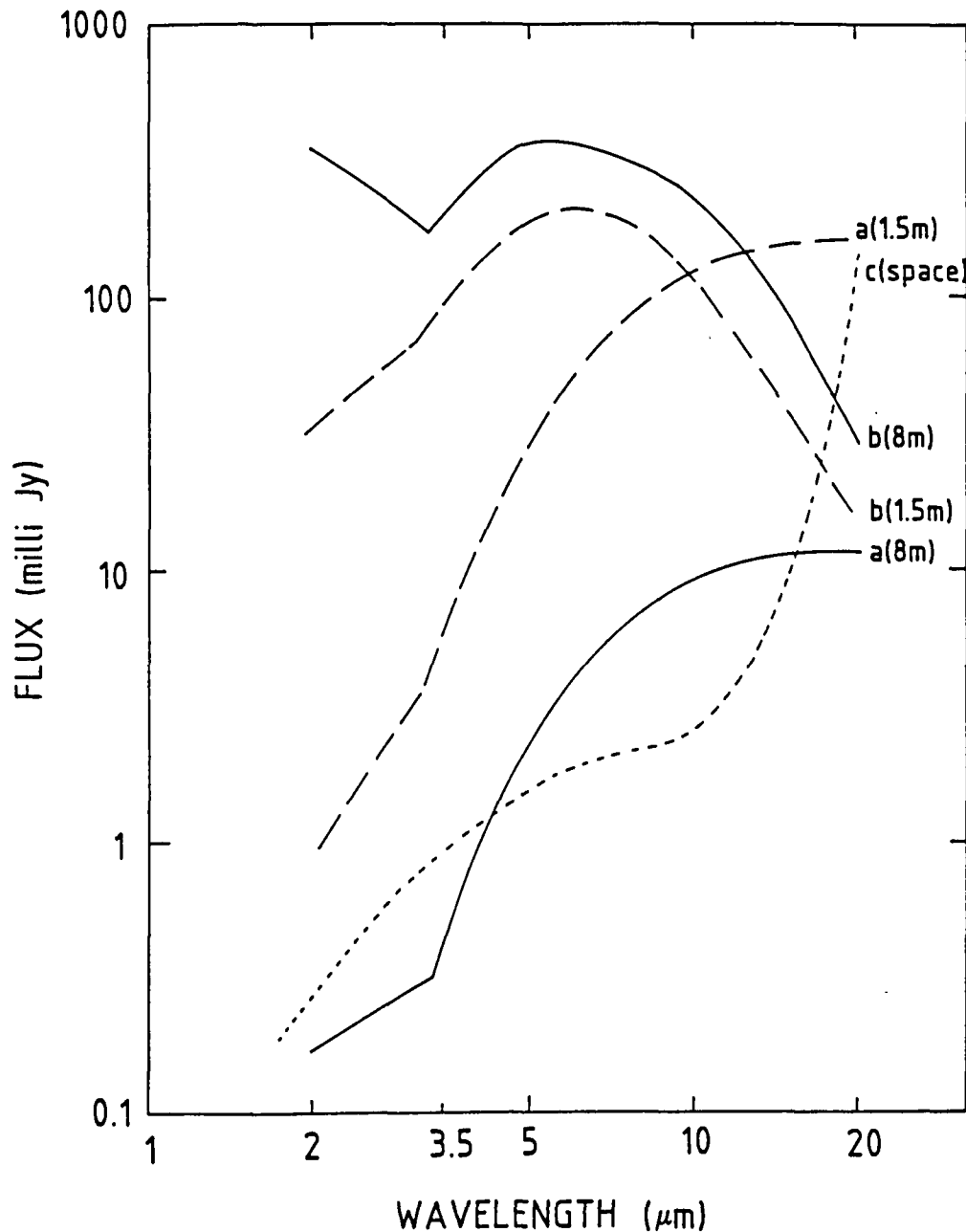
#### Infrared case

With image stabilization, a stable interference pattern for long baselines is obtained within the coherence time  $\tau$ . Under rather reduced spectral coherence requirements, the short exposure limiting magnitude depends mainly on the value  $\tau$  and on the noise. This is the case for short infrared wavelengths. At longer wavelengths where thermal noise limits the sensitivity, array detectors become very useful: the coherence areas within the telescope pupils are not averaged out by one detector. Image stabilization as well as phase tracking require a minimum signal-to-noise ratio. It eventually helps to use the object at another wavelength region or a nearby source. Figure 12.3 shows the limiting flux using image stabilization, array detectors and short integration times ( $\approx 1$  sec), determined by the temporal coherence time  $\tau$ . This time is indicative for a visible seeing of 1 arcsec and wind velocities up to 5 m/sec.

A considerable gain is obtained as soon as adaptive optics is used. It is only under this condition that the interferometric use of a telescope of 8-10m attains its full value. Long time integration (hours) with phase drift control requires more developments but would lead to a much higher sensitivity. This long integration is made difficult due to the presence of random phase variations between the pupils.

#### Visible case

At visible wavelengths, detector noise becomes completely negligible, but the atmospheric coherence area is small. Fast detectors with a large number of pixels are therefore necessary. Limiting magnitudes have been estimated for typical seeing conditions (1 arcsec), assuming that the fringes can be frozen for 0.02 sec. Several cases were considered. The limiting magnitude is found to be in the order of  $m = 4$  for visual fringe detection, independently of the telescope size. Photoelectric fringe tracking should allow to observe objects up to at least  $m_V = 9$ , possibly  $m_V = 14$ , with very little dependence on the telescope diameter, while absolute phase tracking and multispectral observations may push this limit to  $m_V \approx 20$ . The improvement given by the large telescopes becomes significant when adaptive optics reduces the number of speckles per image. Bright objects ( $m_V < 9 - 14$ ) would be easily accessible with the VLT interferometer, but faint objects definitely require more sophisticated developments, before they can be



Curves a:  $F_{oA}(\lambda, D)$ . Limiting flux, with fully phased pupils.

Curves b:  $F_{oT}(\lambda, D)$ . Threshold flux, array detector of  $N_S$  elements.

Curves c:  $F_{oS}(\lambda)$ . Sensitivity of a space Interferometer,  $D = 1$  m.

Figure 12.3: Infrared sensitivity of the VLT interferometer (8m apertures) without time integration with (a) and without (b) adaptive optics in comparison with a medium sized interferometer (1.5m apertures; a and b) and a space interferometer (1 m aperture; cooled to 100K). For details see VLT Report No. 49.

measured. For bright objects, the use of a large telescope compared to a smaller one essentially brings a favorable gain in observing time: the time required to obtain a given signal-to-noise ratio for the visibility varies as the inverse of the telescope area.

### Comparison of the VLT interferometer with space platforms

The interferometric mode of the VLT has the great advantage that it can yield higher angular resolution than the space projects in the foreseeable future. At visible wavelengths, an interferometer placed in space is only suffering from phase errors due to relative drifts of the individual telescopes. The sensitivity is therefore greatly enhanced. In the infrared the factor which limits the sensitivity is not so much the atmosphere, as the thermal background noise due to the thermal emission of the telescope. A space instrument brings significant gain only when it is cooled. This is illustrated in Figure 12.3. Cooling of the entire optical system in space is a costly and difficult task, and it appears ground based interferometry with large apertures is therefore an important and most interesting step.

#### 12.1.2 Measuring the Visibility Phase and Image Restoration

An array of individual telescopes provides a  $(u-v)$  coverage which is time and declination dependant. For a given source declination, fixed telescopes offer a fixed coverage. Movable telescopes will extend this coverage, but the ultimate goal is to achieve a roughly circular point spread function (see Figure 12.4). At visible and infrared wavelengths, the atmospheric absorption prevents from tracking down to the horizon (limits are approximately at 2 airmasses) and, thus, to use fully the earth rotation for the image synthesis. This means that a one dimensional array will always have large sectors missing in the  $(u-v)$  coverage, even for high declination sources. This makes it imperative for a useful optical interferometer to have a 2-D coverage.

As mentioned above, atmospheric phase fluctuations prevent the direct determination of the phase of the complex visibility. But in case of large telescopes at infrared wavelengths, interferences between subareas of the individual pupils provide the phase derivative of the object in a given domain (spatial phase gradient estimate). There is no direct equivalent to radio astronomy, since there the beam through-put always uses the full pupil area.

## 12.2 Optics

The general overview in Figure 12.1 shows schematically the proposed interferometric configuration. In order to combine the light beams from the unit telescopes and the movable auxiliary telescopes, they have to be decoupled from the telescope reference

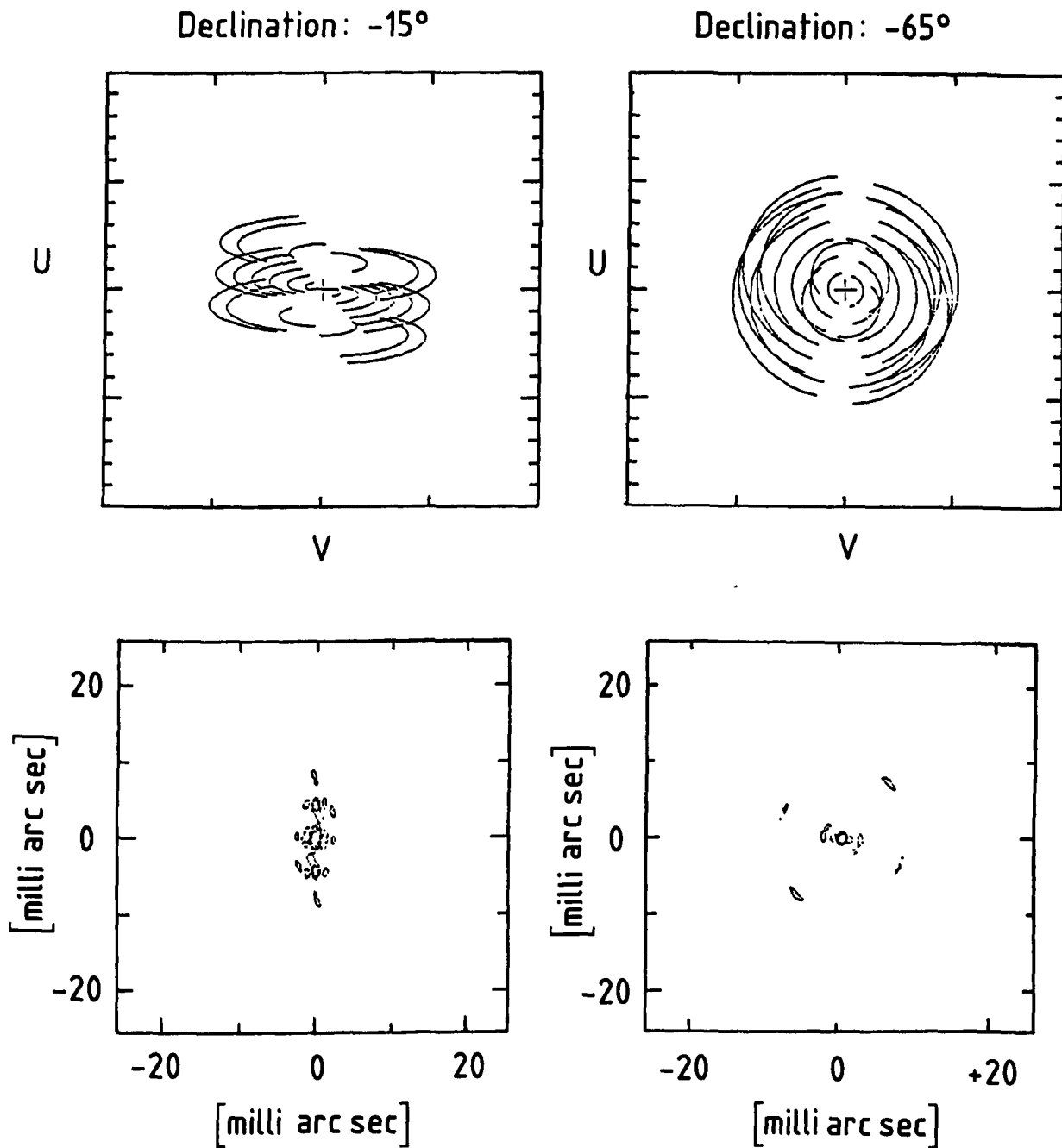


Figure 12.4: Spatial frequency ( $u-v$ ) coverage of the VLT linear array in quasi East-West orientation with two additional telescopes in North-South orientation and a separation of 100m is shown in the upper diagrams for two different declinations of the source. The lower diagrams show the corresponding point spread functions at  $1 \mu\text{m}$  wavelength.



system. It is planned to use for the large telescopes the same optical path as for the individual infrared Coudé foci (see Section 4.1.8) and infrared incoherent beam combination (see Section 4.2), in order not to increase unnecessarily the complexity and cost of the opto-mechanical system. The light beams are then deflected perpendicular to the array axis into the interferometric laboratory, which houses a large optical platform, aligned parallel to the telescope array (see Figure 8.5). All optical elements for the final beam combination and beam co-phasing are installed on this platform.

In order to guarantee phasing on-axis as well as off-axis for an array of telescopes, the Lagrange invariants of the individual telescopes including their combining trains must be equal, and additionally the overall Lagrange invariant of the array must be conserved. The co-phasing of an array of independent telescopes differs significantly from the requirement for telescopes arranged in the same mechanical mount (like MMT type interferometers). This has a major impact on the optical design of the final combination optics.

With the independently mounted telescopes, the entrance pupils ( $P_A$  and  $P_B$ ) are not coplanar as the telescope points off the zenith (see Figure 12.5). Additionally, pointing off the zenith with more than one telescope results in a pupil foreshortening, which decreases the synthetic pupil diameter  $L$ . To maintain the geometrical scaling of the lateral pupil geometry, the exit pupil separation  $l$  at the combining optics has to be adjusted according to the zenith angle  $\Theta$ . The longitudinal pupil position needs also a correction due to the change of the relative locations of the optical elements in the combining train with respect to the wavefronts. The exit pupils  $p_A$  and  $p_B$  are also no longer coplanar. Besides these pupil corrections, which determine the off-axis phasing, the overall on-axis phase difference between the telescopes to be combined has to be compensated. This pathlength compensation is indicated schematically in Figure 12.5 as a shift of the beam combiner to the left.

The external pathlength difference  $D_e$  between the two entrance pupils of the interferometer is demonstrated in Figure 12.6.  $D_e$  is a function of the zenith angle  $\Theta$  and the field angle  $\alpha$ .

$$D_e = L \cdot \sin(\Theta + \alpha).$$

For small angles  $\alpha$ ,  $D_e$  can be written as

$$D_e \approx L \cdot \sin\Theta + L \cdot \cos(\Theta) \cdot \alpha - \frac{1}{2} \cdot L \cdot \sin(\Theta) \cdot \alpha^2 + \dots$$

The internal path difference  $D_i$  is shown in Figure 12.7.

$$D_i = -d \cdot \frac{1}{\cos\alpha'} - (l - d \cdot \tan\alpha') \cdot \sin(\alpha').$$

The distance  $d$  describes the difference in pathlength from the output pupil  $p_B$  to output pupil  $p_A$ .  $\alpha'$  is the angular off-axis distance in the afocal combining beams with

$$\alpha' = M \cdot \alpha$$

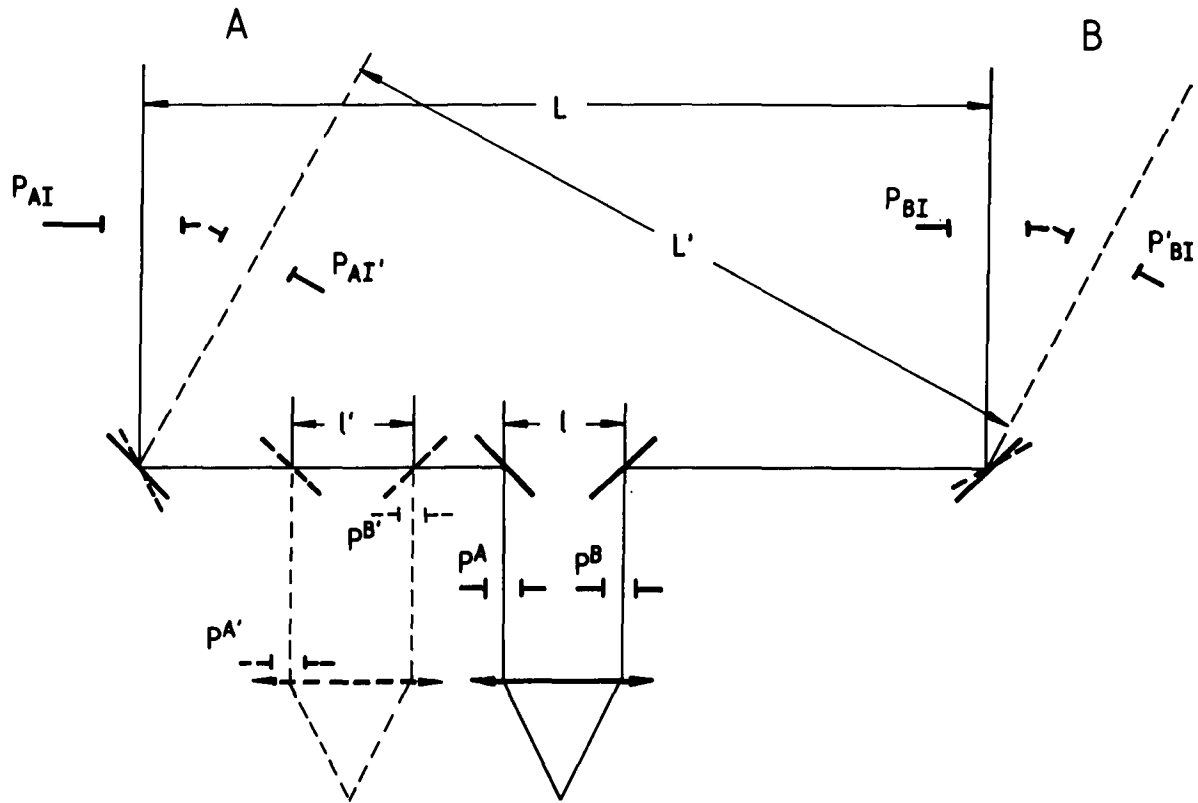


Figure 12.5: The figure shows the principle of an interferometer with independent telescopes for the zenith position (solid lines) and an off-zenith position (broken lines).

( $M$  is the magnification of the telescopes). For small field angles,  $D_i$  can be simplified to

$$D_i \approx -lM \cdot \alpha + d \frac{M^2}{2} \cdot \alpha^2 + \dots$$

In order to phase the interferometer, the external pathlength difference  $D_e$  has to be compensated by an internal path difference  $D_i$ :

$$D_e + D_i = 0.$$

Considering only on-axis compensation ( $\alpha = 0$ ) this leads to the condition

$$d = L \cdot \sin\Theta.$$

This expression describes the need for an optical pathlength compensator. For a fixed zenith position, it has constant value and in this case there would be no need for pathlength compensation. This situation is approximately fulfilled when the interferometer

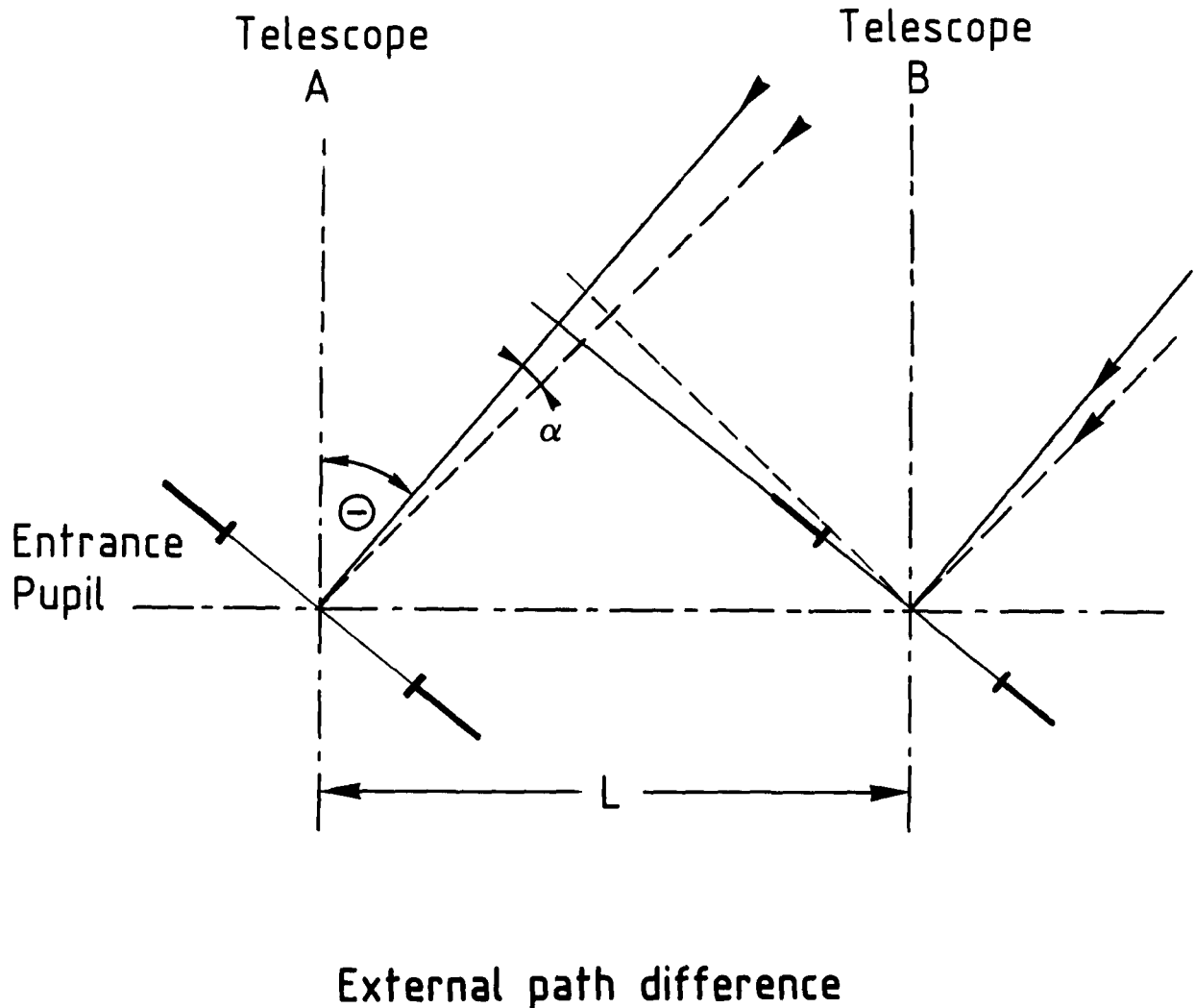
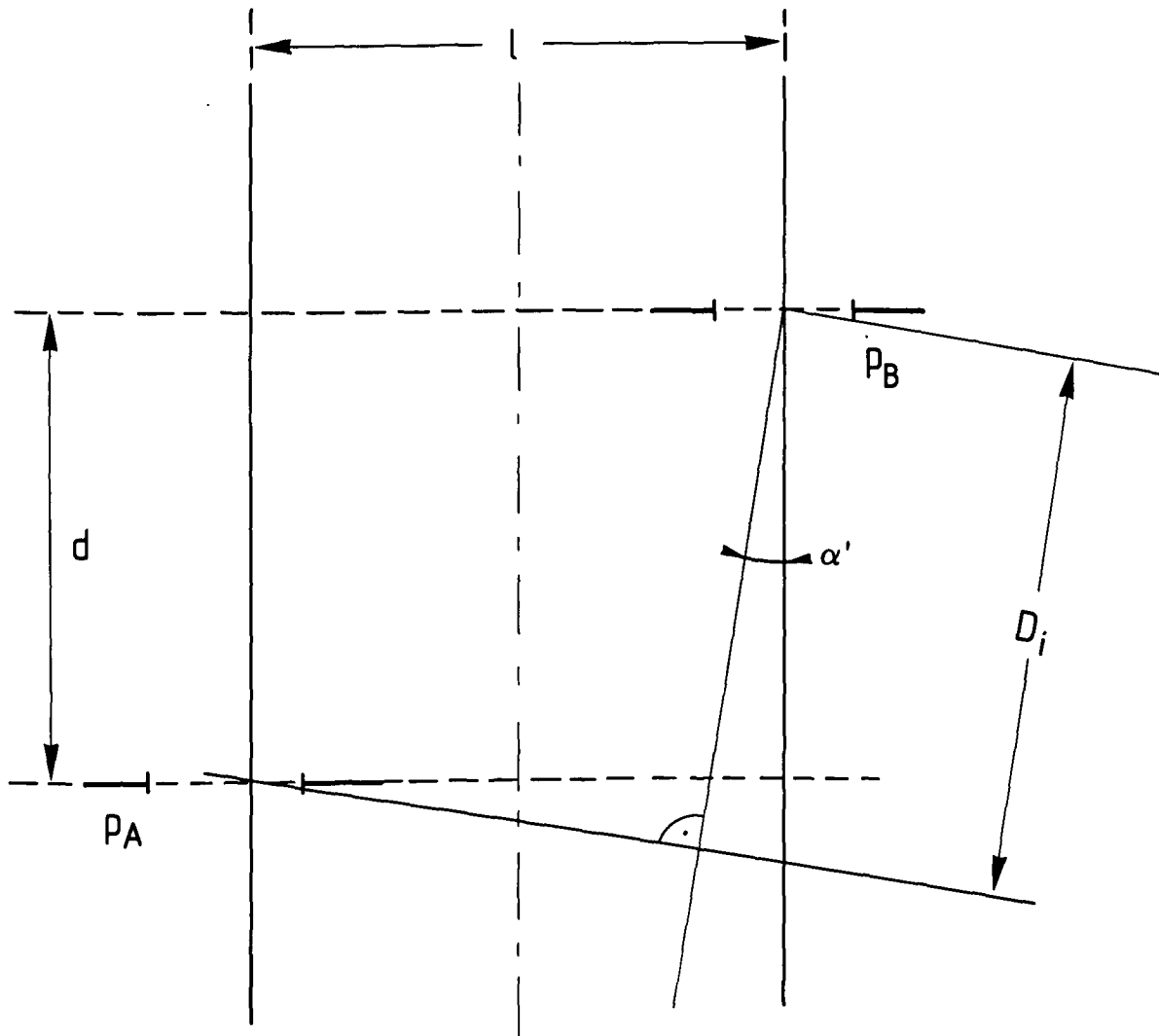


Figure 12.6: External pathlength differences on- and off-axis for an interferometer with independently mounted telescopes.

is arranged in North-South orientation and one observes objects moving through the meridian. In case of a quasi East-West arrangement as for the VLT, the zenith angle  $\Theta$  changes rapidly, making mandatory a fast and accurate pathlength compensator. Therefore optical delay lines are proposed for each telescope (see Section 12.2.1).

On-axis compensation is not sufficient. A field of at least 3 arcsec is requested for proper identification of small details in a somewhat larger source. A first order



### Internal path difference

Figure 12.7: Internal pathlength differences of an interferometer with independently mounted telescopes for on- and off-axis beams.

correction is achieved by changing  $l = L/M$  to

$$l' = l \cdot \cos\Theta = \frac{L \cdot \cos\Theta}{M}.$$

Now the sum of the linear terms (terms with  $\alpha$ ) is zero. This condition expresses the need for the output pupil to be an image of the entrance pupil, scaled by a factor  $1/M$ .

The impact of this condition for the VLT interferometer is, that it requires, additionally to the pathlength compensation, a continuous adjustment of the output pupil separation (see Section 12.2.2). The co-phased field of view is significantly increased by this correction step, but by far not sufficient for a wide application of the interferometer.

A second order correction (terms with  $\alpha^2$ ) requires a compensation for the expression

$$\frac{1}{2} \cdot \alpha^2 L (M^2 - 1) \cdot \sin \Theta = 0.$$

A correction of this second order term is essential for a reasonably sized (several arcsec) field of view, due to the quadratic dependence on the field angle  $\alpha$ . A nearly full compensation of this term is possible by re-imaging the output pupil with a continuously variable optical element, e.g. a small deformable mirror (see Section 12.2.3).

The diagrams of Figure 12.8 summarize the efficiency of the above discussed correction schemes for the VLT case. The phase differences are linear with the baseline length  $L$ . For optical design reasons a magnification of 50 has been selected. The curves show the pathlength difference between the two wavefronts versus the field angle  $\alpha$  for different zenith angles  $\Theta$ . With pure on-axis pathlength compensation, there is basically zero field available (dotted curves). Introducing a compensation for the transversal pupil imaging improves the situation (dashed curves). A sufficient ( $\geq 3$  arcsec) phased ( $\leq \lambda/10$ ) field of view can only be achieved by applying a variable pupil re-imaging (solid curves). Therefore, the above demonstrated pathlengths and pupil corrections are mandatory for the VLT interferometer and have been used as the basic guidelines for the optical design (see Section 12.2.4).

### 12.2.1 Delay Lines

Possible solutions for the pathlength compensations are the use of optical delay lines in the combining beams of the individual telescopes and a stationary combining system, or the use of a moving combining system to ensure equal path length for both beams. The latter method is limited to the combination of only one pair of telescopes at a time. Therefore, this option has been dropped, because multibeam combination is of high importance for the image formation and has to be kept as the final, even if long term, goal. Figure 12.9 shows the general scheme of the proposed delay lines.

For a baseline of 104m length, East-West orientation and a maximum zenith angle of  $45^\circ$  (for interferometry) a total path difference of

$$D_e = 73.5m$$

has to be corrected. With double path delay lines in each beam to be combined, this leads to total translation range of

$$D_{dl} = \pm 18.4m.$$

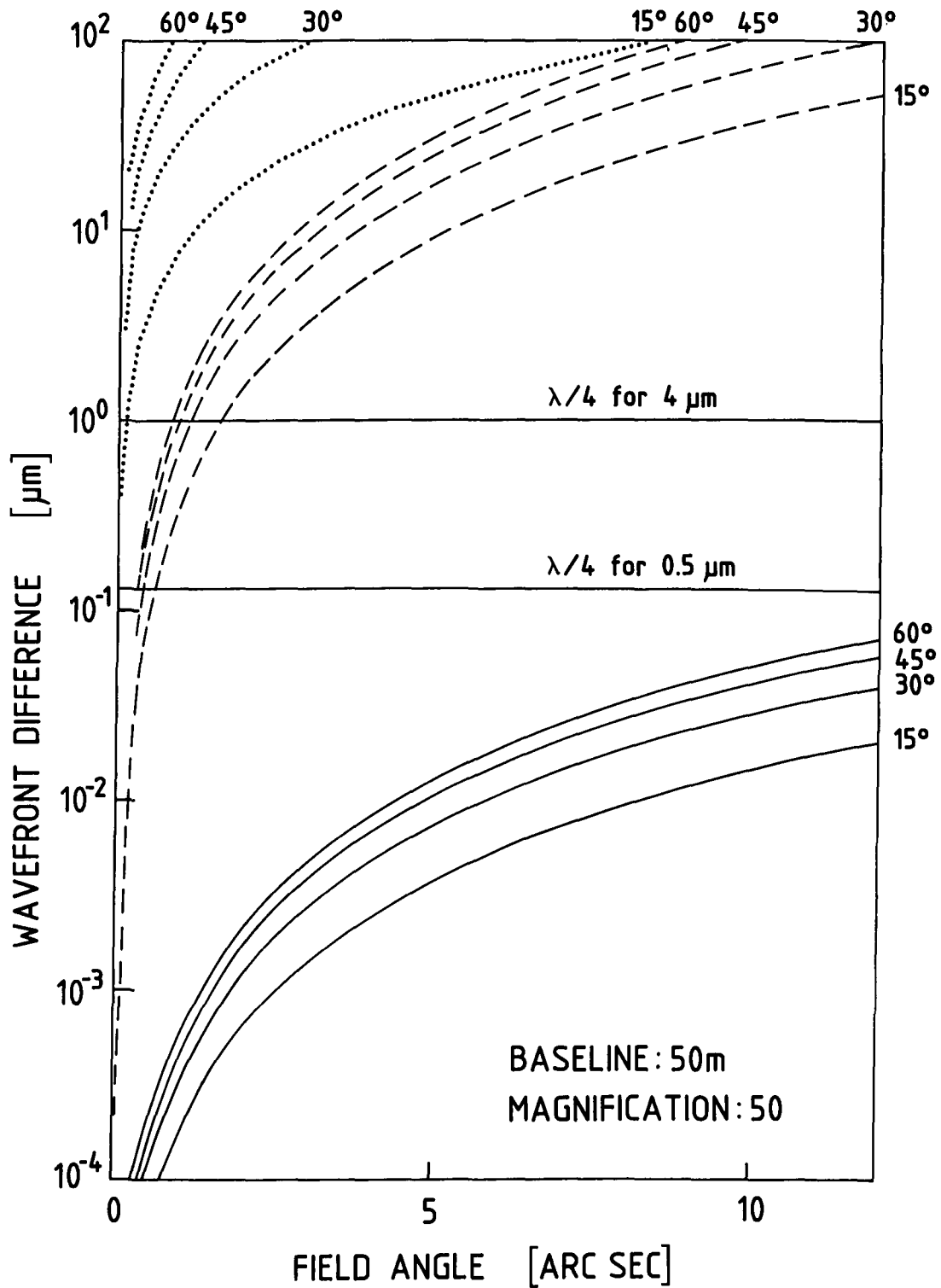


Figure 12.8: The phase difference between two wavefronts is displayed versus the field angle for different compensation steps and zenith angles. Dotted lines: on-axis compensation. Dashed lines: pupil transversal position correction. Solid lines: pupil axial position correction.

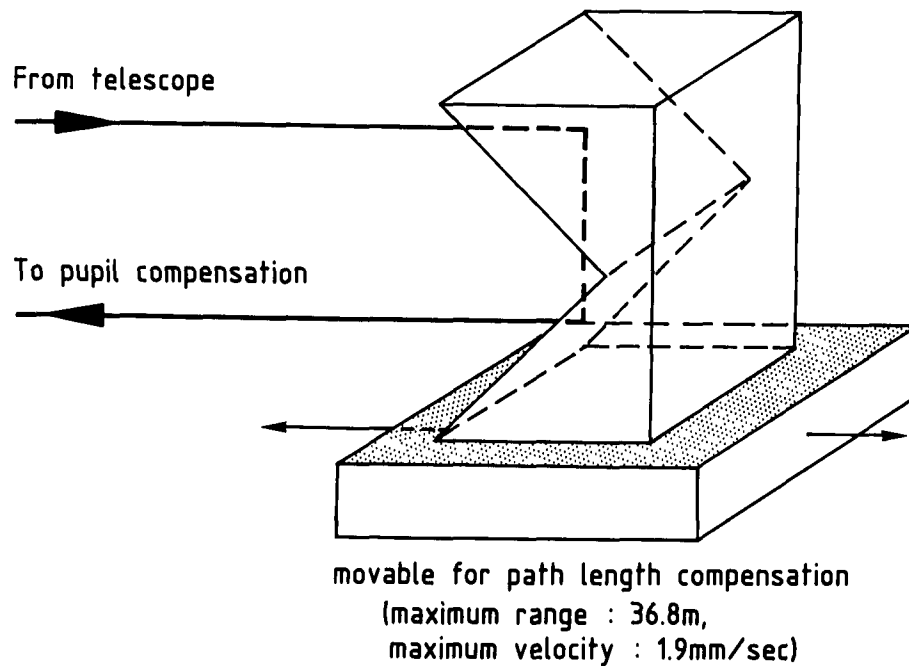


Figure 12.9: Schematics of the proposed delay lines.

The phase difference in the wavefronts changes with a maximum velocity of

$$\left(\frac{dD_e}{dt}\right)_{max} = 7.6mm \cdot s^{-1}.$$

As mentioned above, each of the beams to be combined will have its own delay line, i.e. two double path compensations occur. This reduces the maximum delay line velocity to

$$\left(\frac{dD_{dl}}{dt}\right)_{max} = 1.9mm \cdot s^{-1}.$$

It is important that the delay lines follow the wavefront motion within a limit of  $\pm\lambda/10$ . These are the values for the combination of the two most extreme telescopes. If the total baseline is increased by using the auxiliary telescopes, it is necessary to scale the above values accordingly. For the North-South axis, the correction requirements are much more relaxed.

It is proposed to mount the optical elements which have to be translated during the observation on a carriage supported by air cushions or magnetic bearings. This support has to ensure a smooth motion with low pitch and yaw errors and a high vertical and horizontal linearity. Linear brushless DC motors would meet the specifications for a homogeneous slip stick free motion. The use of magnetic suspension might be preferable, because airbearings could cause turbulence problems with the exhausted air.

It is unlikely that the above mentioned precise motion of the delay lines can be achieved with a single control system. It is therefore proposed to perform a coarse motion control with the delay line carriage and a fine correction with piezo driven mirror positioning systems. It depends on the final optical layout where this could be installed. A control is possible by fine adjustment of the mirror reflecting the intermediate image or with the folding mirror in front of the beam combiner (see Figure 12.10). It should be noted, that current Fourier transform spectrometers in use at large telescopes require significantly higher accuracies for precise translation motions up to several metres.

### 12.2.2 Lateral Pupil Geometry

To maintain the geometrical scaling of the lateral pupil geometry at the combining optics, the positions of the folding mirrors at the input of the beam combiner are continuously adjusted parallel to the interferometric axis as derived in Section 12.2. For the proposed configuration (baseline 104m; maximum zenith angle 45°; magnification 50) this results in a maximum translation range for the extreme mirrors of

$$\Delta d = 305mm.$$

The maximum velocity is then

$$\left(\frac{d\Delta d}{dt}\right)_{max} = 0.055mm \cdot s^{-1}.$$

The precision of this motion is much less critical than for the pathlength compensation and can be easily achieved with commercially available translation stages. The major requirement is a smooth motion and a high mechanical stability. A possible layout is shown in Figure 12.10.

### 12.2.3 Longitudinal Pupil Position

It is proposed to correct for the required longitudinal pupil position with a variable optical element. A deformable field mirror will be used to continuously relay an image of the pupil to the fixed position of the entrance pupil of the beam combiner (see Figure 12.10). The present design foresees a spherical, continuously deformable mirror with a focal length range from X m to X m close to the entrance pupil of the beam combiner.

### 12.2.4 Optical Design

Figure 12.11 shows the optical layout of the VLT interferometer. The field of view is limited to approximately 3 arcsec. It is based totally on reflecting elements (protected silver) in order not to restrict the infrared application by transmissive elements and to



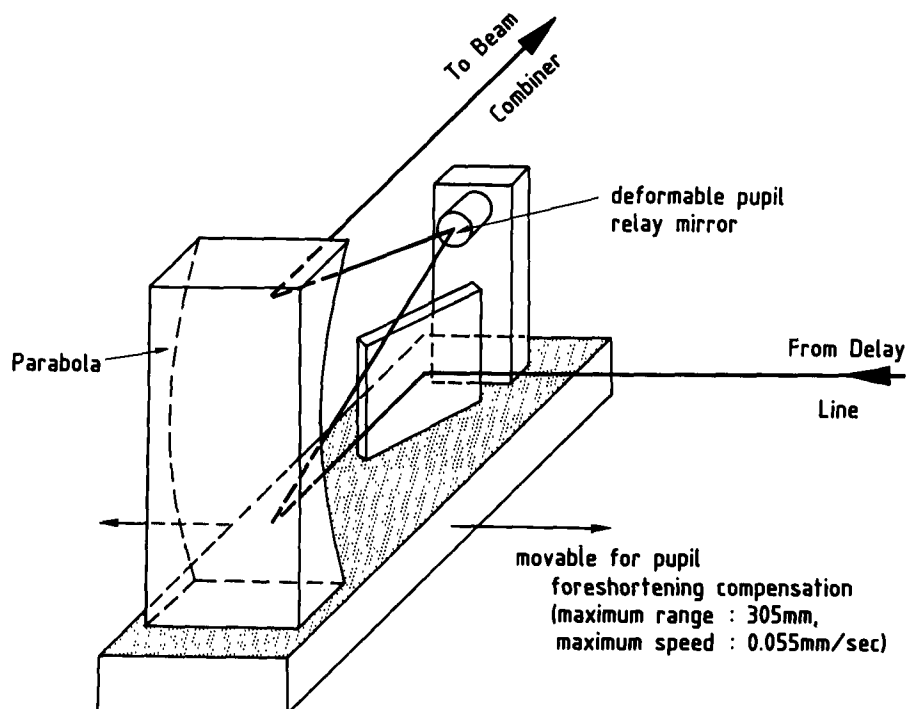


Figure 12.10: The lateral position of the entrance pupils of the beam combiner is correctable by translating the whole stage carrying the beam folding mirrors. With a deformable mirror in an intermediate image it is possible to correct additionally the lateral pupil position. A translation of this mirror could be used for fine pathlength control.

allow its use at any wavelength above 450nm. One goal for the further optimization of the combining path is the reduction of the number of optical elements. The design of the final beam combining camera is considered as instrumentation and depends strongly on the final image analysis and detection techniques. It is foreseen to equip the interferometer with a visible (red) and an infrared instrument (see Section 12.2.7).

It is proposed to compensate the field rotation whenever necessary by a rotating the instrument in order to avoid optical beam rotators. Such elements would unnecessarily increase the number of reflecting surfaces.

Silver coatings are foreseen because they cover efficiently the wavelengths range from 800nm to  $20\mu\text{m}$  (see Section 4.3.2). Due to the relatively high number of reflecting elements, special care has to be taken to keep the mirrors clean. Further investigations have also to cover polarisation effects.

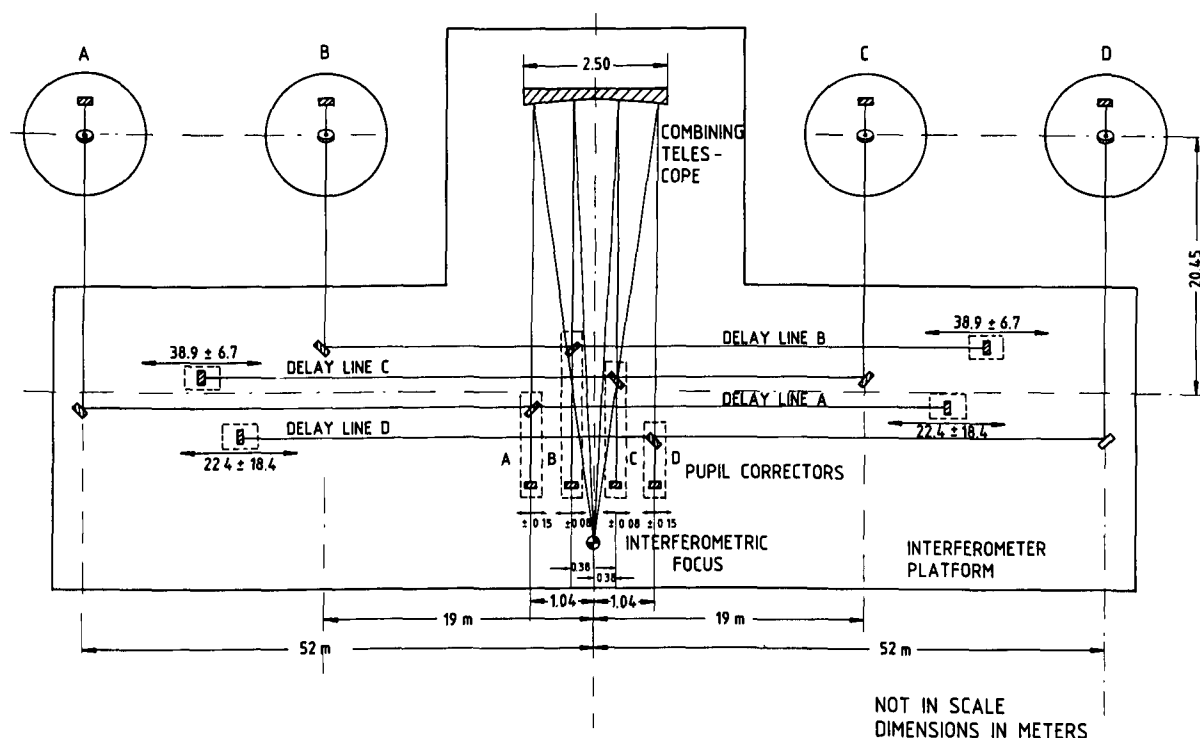


Figure 12.11: Optical design of the interferometric beam combination path.

Interferometry depends on a very high imaging quality. This is not without impact on the mechanical stability and optical quality of the individual telescopes and the combining paths. The technical challenge is augmented by the movable optical components. In addition to the quality and stability aspects, the optical path is influenced by atmospheric effects. The temporal power spectrum of these fluctuations is seeing-dependent. A considerable gain in sensitivity of the interferometric mode can be expected if the atmospheric distortions are partially or fully corrected with adaptive optics.

### 12.2.5 Adaptive Optics

The technology of adaptive optics has been described in more detail in Chapter 11. Phasing at least partially the individual pupils of the VLT is a fundamental requirement for the efficient use of the large aperture interferometer. As shown before, it is most likely that a full adaptive correction for wavelengths  $> 3.5 - 4 \mu\text{m}$  will be available when the VLT goes in operation.

The isoplanatic angle of atmospheric distortion limits the phased field of view. Figure 12.12 demonstrates this effect. It gives the fringe contrast versus the field angle in case of a full on-axis phasing of the individual pupil with adaptive optics. It is obvious that for wavelengths  $> 3.5 - 4\mu\text{m}$  the full field of 3 arcsec is phased. For the shown diagrams, it is assumed that the large scale atmospheric effects which can be considered as piston type phase errors between the telescopes are corrected by a separate device. This type of wavefront aberration can not be detected and corrected by the individual adaptive systems of the unit telescopes.

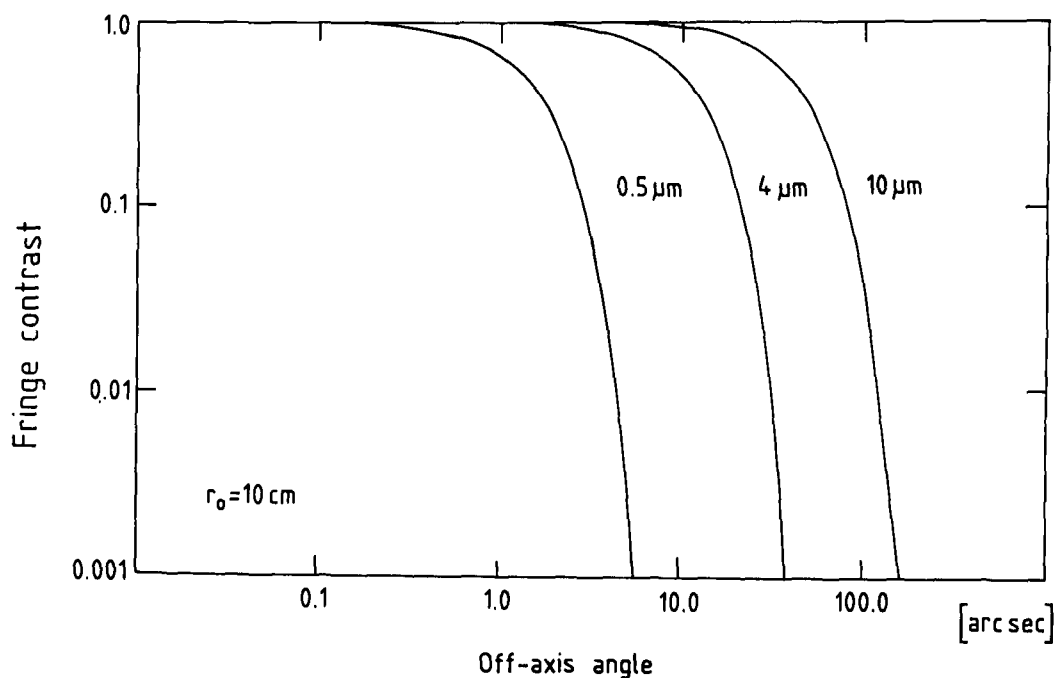


Figure 12.12: Theoretical fringe contrast versus field angle after correction of the individual pupils with adaptive optics.

Large scale atmospheric wavefront aberrations (after phasing the individual pupils) have to be corrected by a measurement of the relative phase between the telescopes to be combined (see Figure 12.13). The same correction system which is used to compensate phase fluctuations due to mechanical vibrations could be used, provided it is fed by an error signal derived from a sufficiently bright source or part of the object whenever available. Fringe tracking methods will be most efficient by allowing long time integration and giving a considerable sensitivity gain. Therefore, they have to be foreseen in the detailed design from the beginning.

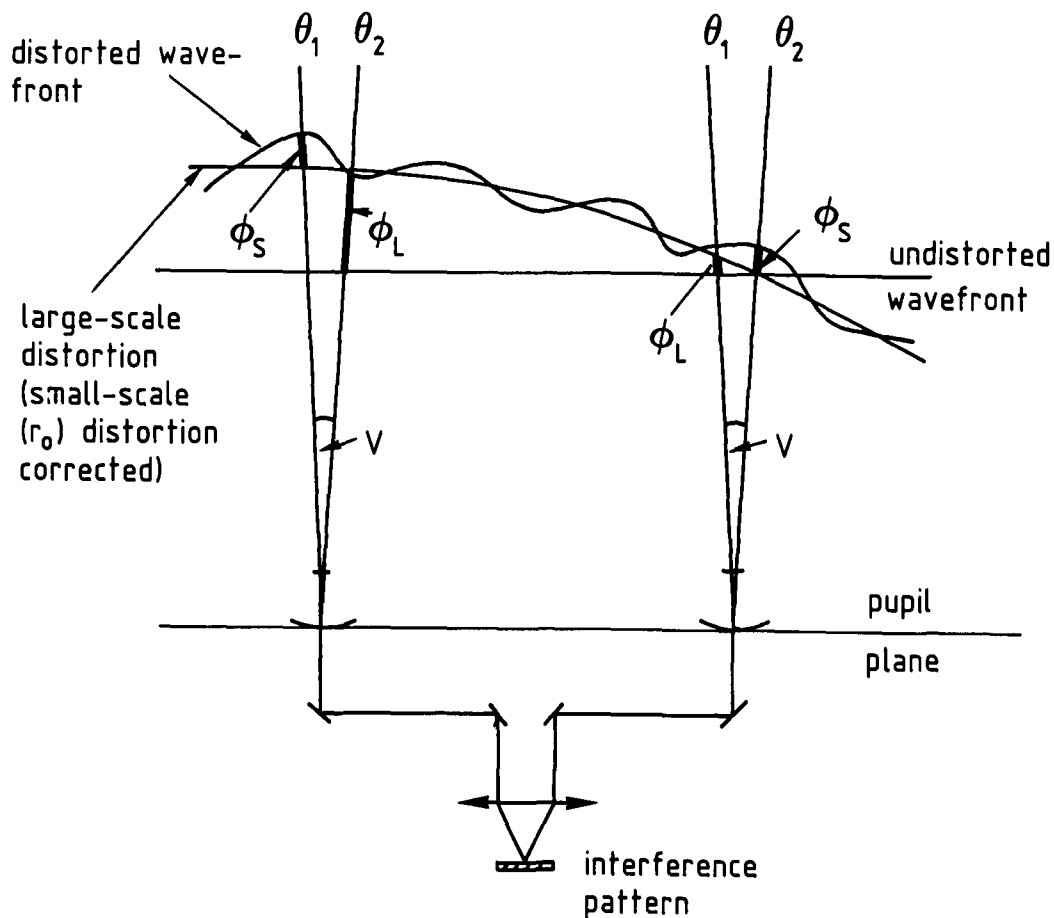


Figure 12.13: Principle of the atmospheric effect on the wavefront. Phase variations within the pupil can be corrected by adaptive optics. The residual effect is a piston error in the wavefronts between the telescopes.

### 12.2.6 Fibre Optics for Interferometry

The application of fibre optics for the interferometric beam combination has been discussed. Currently there are some activities at various observatories, mainly in combination with smaller telescopes. It has to be investigated whether an additional or alternative combining system based on optical fibres will be scientifically useful. From the technical point of view, it is an interesting option because of its simplicity. But up to now no fibres are available for the infrared wavelengths which are comparable in their efficiency to the proposed beam combination. Fibre optics could be a first step

into the visible wavelengths range, since reasonable quality fibres already exist for this application. For more details on fibre optics, see Section 4.2.2.

### 12.2.7 Instrumentation

The design of the beam combination optics allows a flexible use of the phased beams. Depending on the design of the combining instrument and the wavelength image plane as well as pupil plane, interferometry are possible with the VLT interferometer (see Figure 12.14).

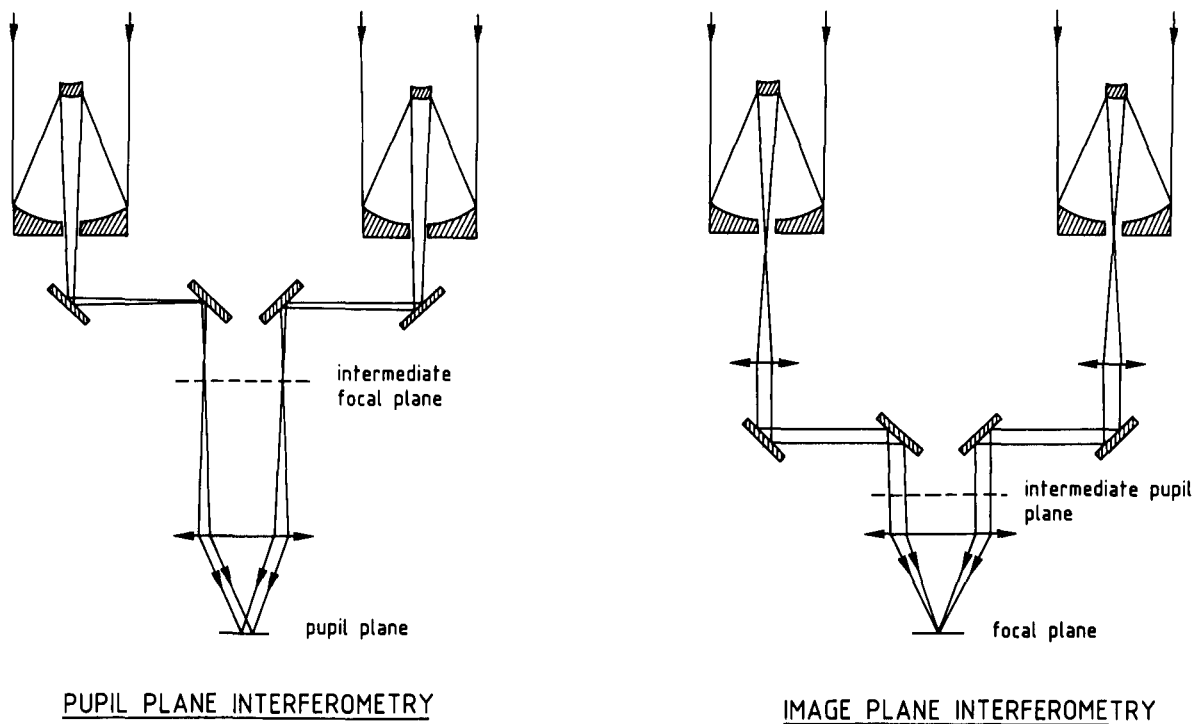


Figure 12.14: Principle of image plane and pupil plane interferometry.

### Instrumentation for the infrared wavelengths

The infrared beam combining instrument shall be based on array detectors with a limited number of pixels.  $32 \times 32$  or  $64 \times 64$  arrays will be fully sufficient and are already available with excellent sensitivity. Spectral resolution is obtained with techniques directly derived from classical Fourier spectroscopy, where spatial and spectral information are multiplexed. The real-time data compression requirements are modest and the associated dedicated computer will be conventional.

### Instrumentation for the visible wavelengths

Multi-speckled images and the required spectral resolution at visible wavelengths require photon-counting detectors with about  $2000 \times 2000$  pixel resolution or several arrays of 10000 pixels (one detector per observed wavelength). The necessary number of detector pixels depends on seeing (adaptive optics may not be available for the visible), on the beam combination technique, and on the number of observed spectral channels. The proposed instrumentation package for visible wavelength consists of the beam combining optics for two or more beams, an image slicer and spectrograph for recording spectrally dispersed long baseline interferograms, the photon-counting detector, and the data acquisition equipment, with an array processor for real-time data compression.

## 12.3 Mechanical Stability

The light beams leaving the unit telescopes suffer from the following perturbations: the wavefront has path fluctuations with respect to the fixed ground, induced by vibrations and motions of the mechanical structures.

The mechanical vibration constraints must be discussed in comparison to the optical path fluctuations induced by the atmosphere. It is sufficient to keep the time spectrum of the mechanically induced fluctuations below the spectrum of the atmospherically induced fluctuations. This means that the rms values of the mechanical fluctuations of the optical path should lie below the lines indicated in Figure 12.15. At high frequencies, the limit is a horizontal line corresponding to fluctuations of  $\leq 0.025\mu\text{m}$  ( $\lambda/20$ ) for visible wavelengths. For infrared observations at  $2.2\mu\text{m}$ , amplitudes of the order of  $0.1\mu\text{m}$  would be acceptable at frequencies higher than about 1 Hz (for details see VLT Report No. 49).

The required stability is only achievable with closed loop active control systems. It might be possible to use a laser beam in the central obstruction of the light path for directional stabilization of the beams.

For the pathlength control of the telescope and combining optics laser interferometers with closed loop active stabilization of the opto-mechanical system are proposed. The complexity of the total control process makes further studies necessary.

## 12.4 Auxiliary Movable Telescopes

The discussion on image reconstruction has shown, that the (u-v) coverage should be as filled as possible and certainly 2-dimensional. It is therefore highly important to add moving telescopes to the basic VLT linear array. It is proposed to join two 1.5m movable telescopes to the array, one movable in parallel to the array axis (quasi East-West) and

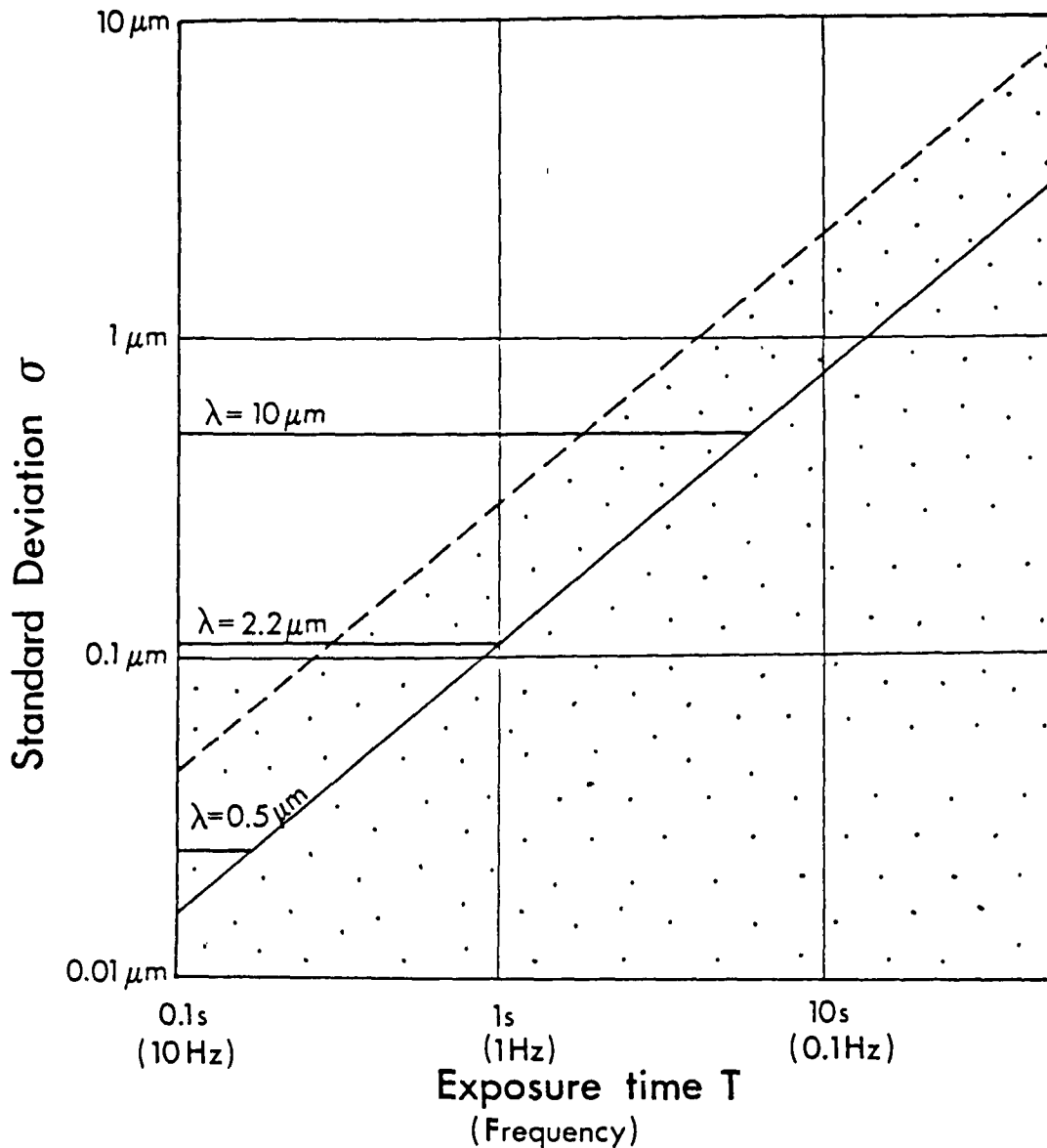


Figure 12.15: Expected standard deviation of the optical path fluctuations during the exposure time (solid line: lucky observer model; dashed line: average model). The dotted range gives the stability requirements for  $2.2\mu\text{m}$  operation with average seeing.

one perpendicular (quasi North-South). This would allow to close the (u-v) plane, to stay with the basic VLT concept, and to use the entire interferometric instrumentation permanently. Especially the last point is of importance, because the use of the large

telescopes for interferometry will be limited to observation programmes requiring their full sensitivity. The smaller auxiliary telescopes could be optimized for interferometry.

The ESO experience with the Coudé Auxiliary Telescope (CAT) (see Figure 12.16) is very helpful. The alt-alt mounting is very useful for interferometry, because it limits to three the total number of mirrors for an afocal decoupled beam. From the general concept of an alt-alt mounting, there is no restriction to design a special carriage for moving smoothly this type of telescope on special tracks. The use of the small telescopes together with the interferometric instrumentation will allow a gradual build-up of the interferometric capabilities.

## 12.5 Site Aspects

There is a compromise between the maximum resolution and a good (u-v) coverage. The array should not be too thin. It can be shown that the signal-to-noise ratio drops rapidly when the object is fully resolved. The resolution of the array should therefore be adapted to the size of the objects to be studied, and an extension of 100 to 150m appears to be appropriate, i.e. a more than ten-fold gain in resolution over the large unit telescopes.

In addition to the size, the site should have the best possible seeing. The signal-to-noise ratio varies with the inverse second to fourth power of the seeing disk size, therefore giving a high weight to sites which at least occasionally have exceptionally good seeing. The signal-to-noise ratio depends also on the so-called wavefront boiling time which is related to the wind, mainly at high altitude. Sites with low windspeed are therefore preferred. High altitude turbulence also reduces the size of the isoplanatic patch in which high angular resolution can be restored. Therefore, a good site should have a minimal high altitude turbulence.

It is important that the seismicity of Cerro Paranal or any other potential site is carefully investigated, because microseismic effects may have a significant impact on the interference fringe stability. Preliminary measurements from other astronomical sites seem to indicate that they remain at fully tolerable levels.

## 12.6 Conclusions

The interferometric operation of the VLT must proceed as a gradual build-up of a new potential. In the initial infrastructure all site and building impacts of interferometry have to be foreseen, because any future modification at the site will be costly and entail undesirable risks for the large telescopes.

The progressive implementation of the small telescopes and of the interferometric instrumentation allows to solve most of the technical problems without interference with



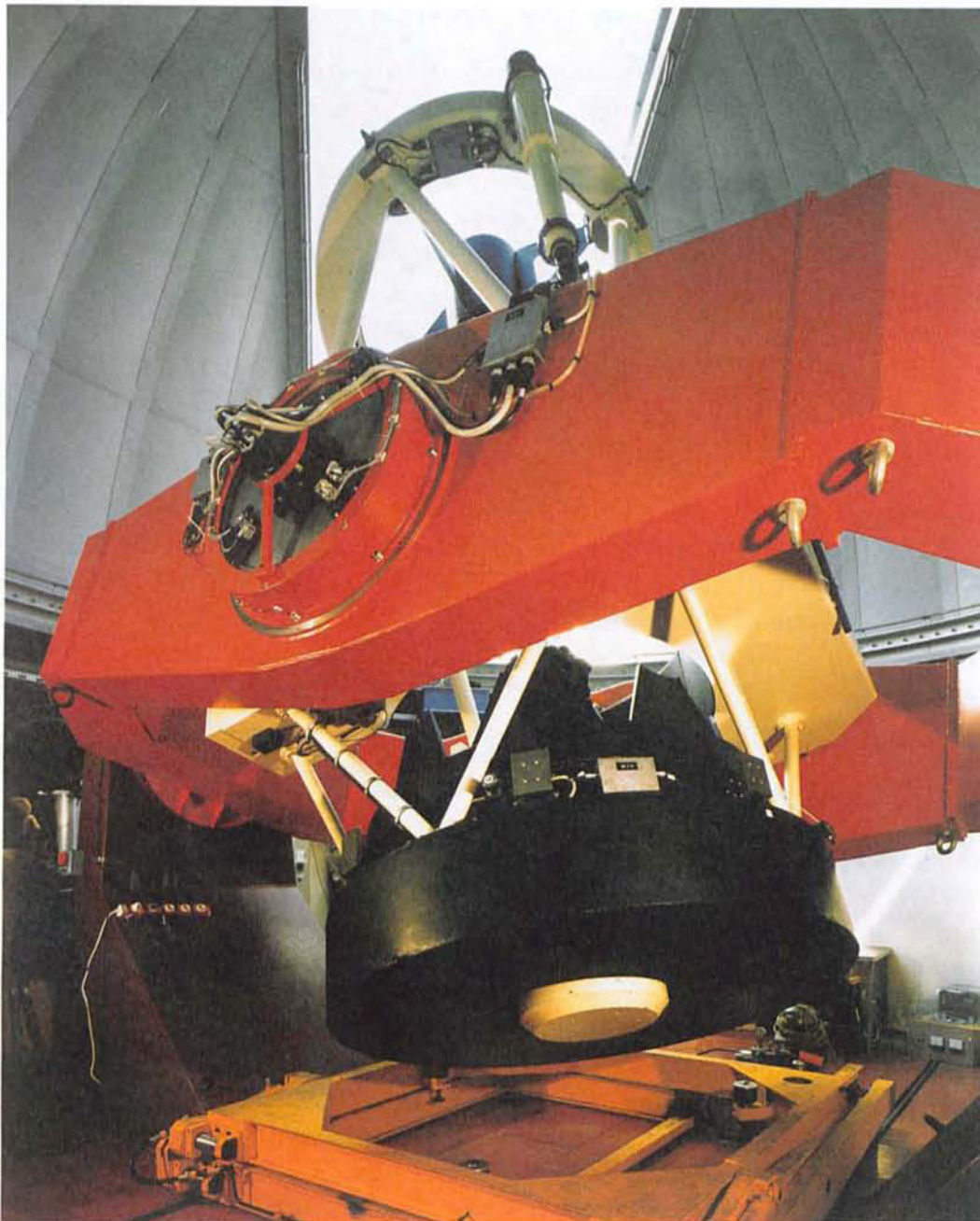


Figure 12.16: The ESO Coudé Auxiliary Telescope design can be adopted for the development of dedicated movable telescopes for interferometry.

the large telescopes. Gradual use of the large telescopes will allow to reach sensitivities which will not be challenged for a long time to come. Table 12.1 illustrates the major steps in the interferometry development programme.

Table 12.1

<b>DEVELOPMENT STEPS FOR INTERFEROMETRIC OPERATION</b>	
<input type="radio"/>	<u>COMBINATION OF 2 TELESCOPES</u> <ul style="list-style-type: none"><li>• 2 × 1.5 METRE TELESCOPES FIXED</li><li>• 2 SMALL TELESCOPES MOVABLE</li><li>• 1 LARGE AND 1 SMALL TELESCOPE FIXED</li><li>• 2 LARGE TELESCOPES</li></ul>
<input type="radio"/>	<u>COMBINATION OF MORE THAN 2 TELESCOPES</u> <ul style="list-style-type: none"><li>• 2 LARGE AND 1 SMALL TELESCOPE FIXED</li><li>• 2 LARGE AND 1 SMALL TELESCOPE MOVABLE</li><li>• 4 LARGE TELESCOPES</li><li>• 4 LARGE AND 2 SMALL TELESCOPES FIXED</li><li>• 4 LARGE AND 2 SMALL TELESCOPES MOVABLE</li></ul>

In parallel to this gradual build-up in sensitivity, a progressive move towards shorter wavelengths, starting at 10 and  $5\mu\text{m}$ , will be more demanding on accuracy, stability, instrumentation, and data processing, but it will widen the range of observable astronomical sources. The fraction of VLT time devoted to interferometry will depend on the ability of this mode to substantially contribute to discoveries.

# Chapter 13

## MANAGEMENT, SCHEDULE AND COST

### 13.1 Management: ESO Project Experience, Means and Organisation

The ESO international staff establishment consists of 142 positions distributed among four main divisions: Scientific, Technical Project and Administrative divisions in Europe (Garching) and the Observatory at La Silla in Chile. To the international staff should be added more temporary positions such as Associates and Fellows, Students and Auxiliaries which number about 50 in all. At La Silla ESO employs also about 120 local staff.

The Technical Project Division which will have the main responsibility to carry out the VLT programme, is at present employing 55 persons distributed in 3 main activities: instrumentation developments, telescope projects (NTT and VLT) and electronics (hardware and software for instrumentation and telescopes). In the instrumentation area, some involvement from the Scientific Division is also foreseen.

Since the setting up of ESO in its definitive European headquarters in Garching, the data processing facilities as well as various laboratories, workshops and general services have been considerably expanded. Largely because of this concentration of means and of the permanent feed back from the operation and maintenance groups at La Silla as well as from the observers, ESO has been able to constantly improve the quality and performance of its instruments and to propose novel concepts. Since already quite a few years ESO is recognised as a leading organisation in the development of instruments for astronomy. By its financial size, its advanced technology and the necessity to coordinate research, development and construction activities in eight European member states, the VLT represents a new challenge and ESO will have to adapt its internal organisation to this new task. However, since the construction of the 3.6m telescope, ESO has continuously developed its technical and management abilities: owing to a

deliberate policy to concentrate the internal activities to those aspects for which no suitable experience could be found in industry or which were related to the specificity of the astronomical projects, ESO has built up a unique expertise in a few key areas such as optics, detectors, cryogenics, control, etc., and acquired a great experience in the management of complex projects involving many industrial and scientific partners.

For the previous projects, including the 3.5m New Technology Telescope, ESO has assumed full responsibility for the conception, integration, erection and management. The manufacturing - except for electronics - has been systematically contracted out in packages of variable sizes. The detailed design has often been contracted out, in a greater proportion, however, for telescopes than for instrumentation.

This approach has been highly successful in terms of quality and performance of the instruments that have been produced as well as in terms of cost; the same approach will be followed for the VLT. Because of the complexity of the project, it is, however, thought that for the parts which can be clearly defined and whenever an adequate expertise exists in the ESO member states, the contracting should be done at a system level. As an example, the complete secondary mirror unit, in which the performance depends on the combination of several advanced technologies, is envisaged to be developed under one single contract. This contract will include detailed conception and production and will be preceded by feasibility and definition studies. Acceptance will be based on the performance of the entire system.

In this way, it will be possible to carry out the VLT project without adding more than about a dozen persons to the present T.P. division.

The development of the VLT instrumentation may follow a slightly different scheme to the extent that national institutes could and should effectively collaborate with ESO, if a basic set of instruments is to be made available on time for the first telescope.

As to the optical and infrared instruments completed in the past years, ESO has generally done the designs as well as most of the construction drawings in-house and tendered the mechanical manufacture to firms in the member countries. A few, however, have been designed and built by national institutes, with the ESO contribution limited to the interface to the telescope and the control computer.

In the case of the VLT instrumentation, several sophisticated major instruments will have to be built in parallel. It is clear that a much larger share of the responsibility in the design and construction phases will have to be distributed to national institutes and laboratories, or to consortia of the same.

One can foresee that following the approval of the VLT project, the ESO staff, in collaboration with specialists from different locations in Europe, will have first to define in more detail the instruments which have been outlined and given first priority by the VLT Working Groups.

The degree of participation and the way in which such a participation will be solicited and organized will probably vary from instrument to instrument. In cases where

ESO itself has extended and successful expertise, the overall design could be ESO's responsibility and only sub-units and/or components could be contracted outside; in other cases a more general call for proposals could be issued and full responsibility for the completion of the project could be left to the successful bidder. Clearly, ESO will closely follow and participate in the work in this latter case as well, to insure that the instrumentation budget is properly used to procure a balanced set of instruments in time and according to the original specifications.

The budget for instrumentation included in the VLT proposal is intended to cover the hardware costs of a basic set of instruments as outlined here, but the personnel costs will have to be borne by the national institutes.

The task of building instruments for the VLT is exciting, but it is worth emphasizing that it is a very difficult one. Very few groups have built instruments for 4-meter class telescopes in Europe, and devoted teams will have to be set up to participate in such an enterprise for a VLT. In some European countries, this requirement is being seriously considered and the appropriate steps for the planning of future activities related to astronomical instrumentation are being taken.

## 13.2 Schedule

As has frequently been the case in telescope development, the schedule is driven mostly by the lead-time for producing the primary mirror.

An 8m blank made of fused silica could be produced and delivered in about 3 years and subsequent units produced at 1 year intervals.

For Zerodur, the lead-time for the first mirror might be slightly longer, but the delivery of the following units could be faster. The precise schedule can only be set upon completion of the test programme currently in progress.

As mentioned in this proposal, the metal mirror development will be pursued as a back-up solution, so that, should difficulties appear with the supply of a glass blank, at least a provisional solution would be available that would keep the project on schedule owing to the shorter lead-time for a metal mirror blank.

The lead-time for developing an optical facility to figure and polish the mirrors is about 3 years, including initial testing and debugging and is thus compatible with the shortest blank delivery time.

The proposed schedule is based on a 3 year lead-time for the first blank and on the availability of 2 polishing machines, so that 2 mirrors can be processed simultaneously. Alternatively two mirrors may be swapped between the test tower and the polishing machine in which case one machine would be sufficient.

The polishing and figuring of the first mirror is estimated to take 3 years. The experience acquired should allow to achieve it in 2 years for the subsequent units. The possibility to polish the mirrors "round the clock" will also be investigated and could lead to important cost savings through a better use of the initial industrial investment.

The other parts of the project are less critical; the charts (Figures 13.1 to 13.3) indicate the timing for the main activities. A finalization of the detailed general specifications is foreseen at the beginning of 1989. This means that the technical sub-systems performance and the way they relate to the telescope scientific performance will then be definitely fixed. The interfaces between the different parts will also be frozen at that time.

In Figure 13.1, the first telescope is shown to be completed by the end of 1993. A one year interval is foreseen between the completion of the first telescope and the construction of the next units in order to keep the possibility to introduce minor modifications that would appear necessary.

The detailed planning of the construction of the 3 subsequent units is basically a matter of optimizing the cost. Some parts may be constructed simultaneously, some others sequentially.

The project would be completed in 1998, if a decision is taken in 1987.

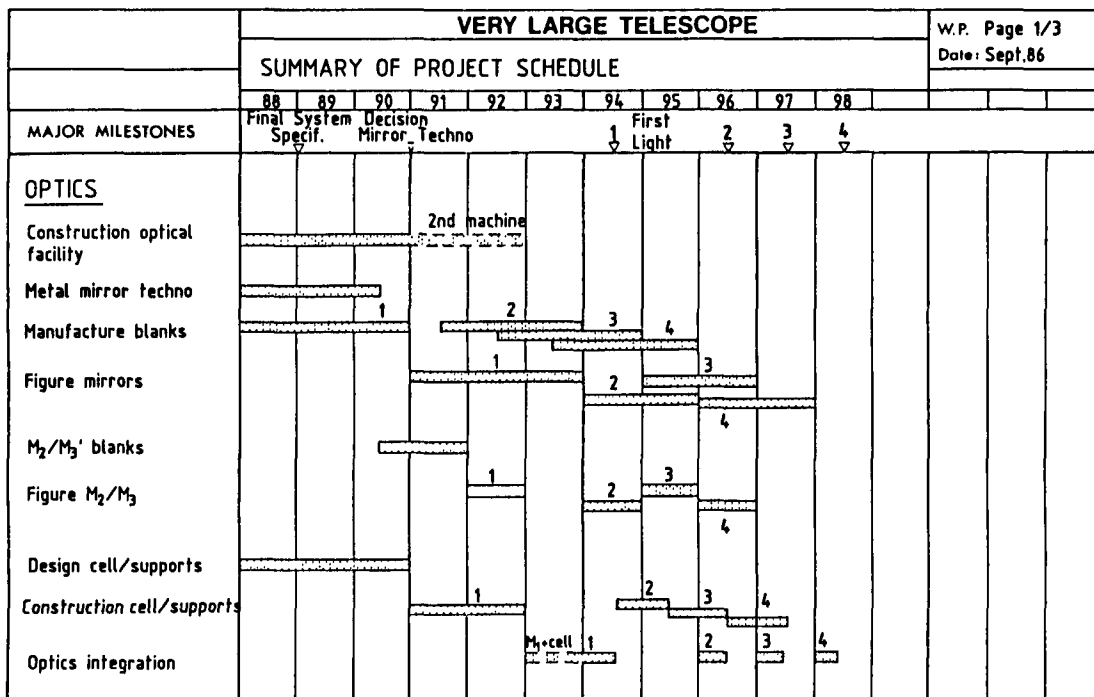


Figure 13.1:

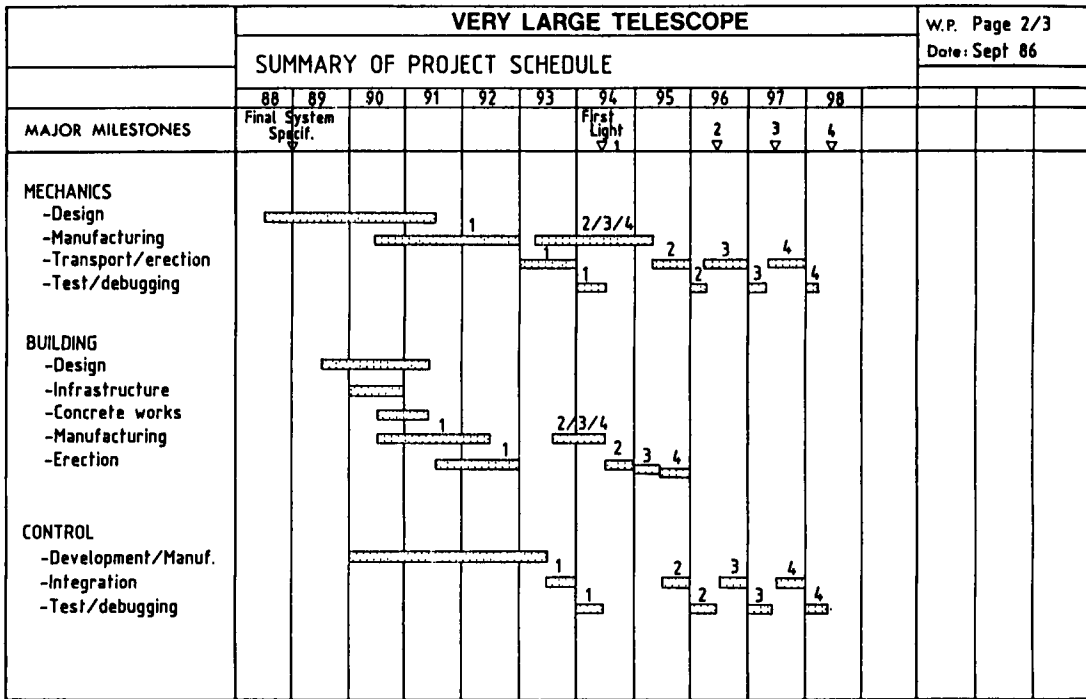


Figure 13.2:

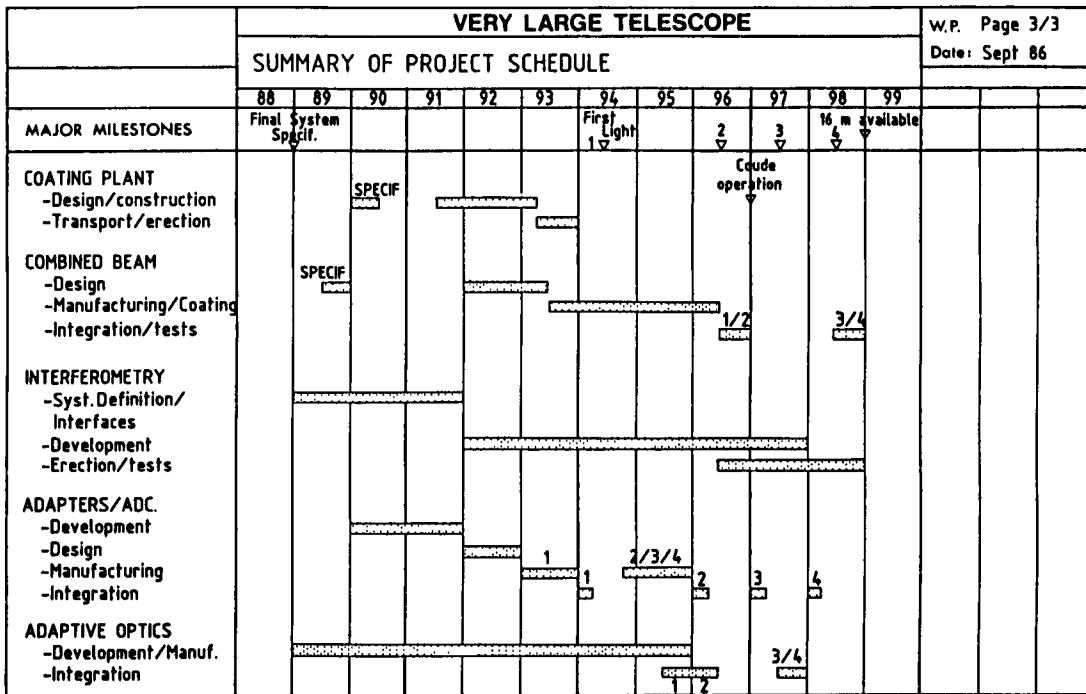


Figure 13.3:

TABLE 13.1

GLOBAL BUDGET (KDM 1986)		
	Sub-Total	Total Sub-System
PRIMARY MIRRORS		98800
- Glass blanks	44000	
- Optical figuring	36500	
- Handling/transport	5000	
- Cells + active supports	13300	
SECONDARY MIRRORS		9100
NASMYTH MIRRORS		4300
TELESCOPES		61900
- Tubes	15800	
- Yokes + bearings	27000	
- Other tel. functions	4100	
- Drives + encoders	9800	
- Computers + controls	5200	
AUXILIARY FUNCTIONS		65200
- Beam combination	11000	
- Adapters + wavefront sensors + ADC's	11000	
- Coating plant	7200	
- Adaptive optics	12000	
- Interferometry	25000	
BUILDING AND SITE		41800
- Tel. bases and labs	9900	
- Tel. shelters + platform	20000	
- Wind screen	6900	
- Local groundwork + equipping	5000	
TOTAL TELESCOPE		281100
CONTINGENCY 10%		28100
TOTAL VLT		309200
SITE DEVELOPMENT PARANAL		25000
INSTRUMENTATION		48000
TOTAL VLT PROGRAMME		382200



## 13.3 Budget

Table 13.1 gives a summary breakdown of the project cost, based on the latest information available.

Many technical options remain open and the estimate is based on the solutions which appear the most realistic at the present stage of the study. It is possible that new solutions will emerge, leading to savings which could cover unforeseen difficulties that may occur in other areas. In addition, a general 10 per cent contingency has been added for the telescope.

Budgets for the development of Paranal and for instrumentation are also given.

More details about the costing are given in Section 13.4. The schedule for the required cash flow during the execution of the project is given in Table 13.2.

TABLE 13.2

REQUIRED CASH FLOW IN MDM (1986) DURING THE EXECUTION OF THE PROJECT				
YEAR	VLT	INSTRUMENT. DEVELOPMENT	PARANAL DEVELOPMENT	TOTAL
1989	18			18
1990	21			21
1991	32	6	10	48
1992	37	6	6	49
1993	40	4	5	49
1994	40	5	4	49
1995	33	7		40
1996	33	7		40
1997	33	7		40
1998	22.2	6		28.2
	309.2	48	25	382.2

### 13.4 Detailed Cost Estimates (KDM 1986)

(transport included when not explicitly mentioned)

#### Primary Mirrors

Blanks	44000
Optical figuring	36500
Handling equipment	1000
Transportation of mirrors	4000
Mirror cells	6000
Active supports	4100
Development, tests, assembling of mirror cells and supports	3200
<hr/> <u>Total</u>	<hr/> <u>98800</u>

#### Secondary mirror units

Development	1000
Mirror blanks and active supports	3000
Optical surfaces (polishing or replicas)	1900
Mechanical units	3200
<hr/> <u>Total</u>	<hr/> <u>9100</u>

#### Nasmyth mirror units

Development	300
Mirrors and cells	3000
Mechanical units	1000
<hr/> <u>Total</u>	<hr/> <u>4300</u>

**Telescope mechanics**

<u>Tubes</u>	
Structure (steel)	8500
Bearing journals	3000
Altitude drive wheels	4300
M1 cover	900
Miscellaneous equipment	1500
<u>Azimuth structures</u>	
Fork structure (steel)	12000
Support rings/gear wheel	11000
Hydrostatic bearings	4000
Miscellaneous equipment	1700
<hr/>	
<u>Total</u>	<u>46900</u>

**Control**

Computers	2200
Drives (incl. motors)	8000
Encoders	1300
M1 support system	1600
Other functions	1900
<hr/>	
<u>Total</u>	<u>15000</u>

**Beam combination**

Mirrors and other optical components	4500
Coatings	1500
Mirror mounts	2500
Tubes and mechanics for switching the beams. Alignment system	2500
<hr/>	
<u>Total</u>	<u>11000</u>

**Adapters and ADC's**

Mechanical units	5500
Optics	800
Detectors (auto-guiders and wavefront sensors)	4000
ADC's	700
<u>Total</u>	<u>11000</u>

**Coating plant**

Mirror cleaning equipment	500
Vacuum tank	3900
Pumps and internal equipment	2000
Transportation	800
<u>Total</u>	<u>7200</u>

**Adaptive optics (IR only)**

Adaptive mirrors	5400
Wavefront sensors	1800
Processors	4800
<u>Total</u>	<u>12000</u>

**Interferometry**

Combining optics	2200
Path stabilization	1800
Delay lines	2400
Control	1600
Auxiliary telescopes (1.5m)	15400
Tracks	1600
<u>Total</u>	<u>25000</u>

**Buildings**

Concrete bases	3000
Coudé laboratory and control room	3000
Interferometric lab	1900
Mirror maintenance building (including internal handling equipment)	2000
Inflatable shelters	8000
Support for shelters (platform)	6000
Enclosures internal equipment (lifts, lighting, air conditioning etc.)	4300
Wind screen	6900
Foundations and local equiping (connections to power, water lines, air conditioning etc)	5000
Handling equipment (crane)	1700
<hr/> <u>Total</u>	<hr/> <u>41800</u>

**Site Development (Paranal)**

Levelling of mountain top (60.000m <sup>3</sup> )	5400
Access road (last kilometer paved)	4400
Water supply (local storage and distribution net)	2200
Electrical connection to Chilean net	2800
Emergency generator	600
Infrastructure buildings (offices 200m <sup>2</sup> , lodging 50 persons, workshops 500m <sup>2</sup> , kitchen-restaurant, warehouse 1000m <sup>2</sup> , furniture, communication equipment)	8100
Air strip	1500
<hr/> <u>Total</u>	<hr/> <u>25000</u>

**Instrumentation**

Focal reducers for imaging and low resolution spectroscopy (4 Nasmyth foci)	6000
Multimode spectrometers (4 Nasmyth foci)	8000
High resolution spectrometer for the combined focus	10000
FTS spectrometer (combined focus)	2500
IR imaging spectrometer (4 Nasmyth foci)	8000
IR grating spectrometer (combined focus)	5000
IR and visible interferometric set-ups (coherent combined focus)	2000
Instrument support and handling devices at Nasmyth foci	1500
Computers and data acquisition	2500
Remote control facility in Garching	2500
<hr/> <u>Total</u>	<hr/> <u>48000</u>

**13.5 Annual Costs**

It is of course difficult to make reliable estimates of the annual costs to operate, maintain and upgrade the VLT during its operational phase. No similar telescope exists. Moreover, developments in communication technology are so rapid that it is not possible to predict at present what the remote control environment will be more than a decade from now. The following estimates therefore have a somewhat global character.

According to the budget presented before, the initial instrumentation will be built in ten years at a cost of 48 MDM, corresponding to 4.8 MDM/year on the average. Since undoubtedly additional instrumentation will be needed after completion of the VLT, while also the then existing instrumentation will have to be updated, it would seem reasonable to foresee continuing investment in instrumentation at the same rate at least for the first five years of full VLT operation and maybe half as much thereafter. Additional investments in the telescope itself should also be foreseen. On the basis of the experience with the 3.6 m telescope, it may be estimated that about 1% of the VLT cost would be required initially, or 3.1 MDM/year, to further increase the VLT performance. This may seem low, but it should be remembered that much of the VLT cost is in large items (mirrors, etc.) which will not undergo further change. Again, after the first five years half as much would suffice. The annual investments needed to upgrade the VLT and its instrumentation are therefore estimated at 7.9 MDM for the first five years (1999 - 2003) and about 4.0 MDM thereafter.

Annual operating expenses (maintenance, replacement of parts, power, etc.) may

be estimated at about 3 MDM, to which 2 MDM should be added for satellite links between the VLT site and the remote control terminals in Garching. Total operating expenses therefore would amount to 5 MDM/year.

At the VLT site, the dedicated VLT staff would consist of 12 highly qualified engineers and about 18 technicians and operators. In addition, some 8 operators would be needed in Garching, augmented with 2 supervisory schedulers. Total personnel cost would be about 4 MDM/year.

Adding these amounts it would seem that the total annual running cost of the VLT during the first five years would be 16.9 MDM and thereafter 13 MDM (see Table 13.3).

TABLE 13.3

ANNUAL RUNNING COST OF THE VLT (MDM 1986)		
	1999-2003	2004 and after
Personnel	4	4
Operations	5	5
Investment	7.9	4
<b>Total</b>	<b>16.9</b>	<b>13</b>

It is important to note that these amounts are not necessarily net increases in the ESO budget. The 1987 budget of ESO contains 3.4 MDM for VLT studies. In addition, it seems reasonable to assume that instrumentation activities related to the present telescopes at La Silla would be reduced and their operation simplified, which would lead to a further reduction of perhaps 1.6 MDM. The net requirement is therefore reduced to 11.9 MDM during the first five years and 8 MDM thereafter.

It may not be unreasonable to consider the closing of some of the present telescopes upon completion of the VLT. In this case, additional savings become possible. It seems premature, however, to make quantitative estimates before the appropriate cost-benefit analyses have been made.

## SUMMARY OF VLT DESIGN PARAMETERS

### CONCEPT

- 16m equivalent light collecting power
- Linear arrangement of 4 x 8m alt-az telescopes

### OBSERVING MODES

- Combined Coude focus
- Combined observation at unit telescopes with distributed instrumentation
- Single telescope independent observation
- Interferometry using 2, 3 or 4 telescopes and 2 auxiliary 1.5m telescopes

### OPTICAL CHARACTERISTICS OF THE 8m UNIT TELESCOPES

- Ritchey-Chretien optical system
- 2 Nasmyth foci: F/15; 0.5 degree unvignetted field-of-view
- Scale at the Nasmyth foci: 1.72 arcsec/mm
- Primary mirror: effective diameter 8m. Aperture: F/1.8. Solid meniscus, thickness 175 to 200mm depending on material.  
Options considered:
  - Zerodur produced with spin casting
  - fused hexagons of pure silica
  - metal as back-up solution
- On-line active correction of the primary mirror based on wavefront sensing and active supports.



- Active axial supports: push-pull systems using hydraulic or electromechanical actuators
- Image quality target: 80% encircled energy within 0.15 arcsec at  $\lambda = 0.5\mu\text{m}$ . Diffraction limited at  $\lambda = 5\mu\text{m}$
- Field rotation compensation by rotating the instruments
- Active tracking with auto-guider and close-loop correction using the telescope drives and the secondary mirror. Accuracy 0.05 arcsec. Bandpass 10 Hz
- Pointing: 1 arcsec RMS; 0.5 degree blind offsets: +/- 0.05 arcsec
- Unbaffled secondary mirror
- Central obstruction: less than 3%
- Possibility of conversion to Cassegrain focus at F/13.3 by removing the Nasmyth mirror unit

## MECHANICAL CHARACTERISTICS OF THE 8m UNIT TELESCOPE

- Designed for open air operation
  - lightweight structure with low thermal inertia and low wind drag
  - high stiffness
- Tube:
  - mass 109 T
  - first eigenfrequency  $\simeq 10$  Hz
  - maximum static wind deformation at secondary mirror 0.1mm at 9 m/sec windspeed
  - maximum obscuration of spiders 1.5%
- Fork:
  - mass 110 T
  - first eigenfrequency  $\simeq 9$  Hz
  - load on each Nasmyth platform 4 T
- Bearings: hydrostatic bearings for both elevation and Azimuth axes

- Drives: DC-motors; large diameter gear wheel
- Encoders: large diameter absolute strip encoder and incremental high resolution encoder for fine tracking and pointing. (Alternative laser gyros)
- Maximum rotation angle:
  - elevation:  $-5$  to  $+90$  degrees
  - azimuth:  $\pm 270$  degrees

## BEAM COMBINATION

- Optical train using 3 sets of mirrors with optimised high efficiency coatings:

UV:	300 to 400nm (multi-dielectric)	R > 98%
Visible:	380 to 700nm (multi-dielectric)	R > 98.5%
IR:	> 700nm (silver)	R > 99%

- Beam protection: helium filled sealed tubes
- Visible = 5 total reflexion prisms, 1 lens, 1 mirror, FOV: 30 arcsec
- IR: 8 silver mirrors, FOV up to 1 arcminute
- Built-in laser aligning system
- Alternative fiber optics scheme to replace 4 mirrors

## BUILDING

- Designed for open air operation of the telescopes during the night and environmental and thermal protection during day-time
- Telescope enclosure: Inflatable shelters. Double skin inflatable envelope supported by a steel structure
- Combined platform and windscreen to optimise wind load and local seeing conditions
- Central building independent of telescopes including Control room and Coudé laboratory
- Separate building for interferometric recombination
- Separate mirror maintenance facility

## INTERFEROMETRY

- Combination of one or several pairs of telescope beams in a separate laboratory
- Path length compensation by delay lines or displacement of the beam combiner
- Atmospheric turbulence compensation with adaptive optics
- Active stabilisation of beam and phase
- Redundant configuration: 104m baseline
- Auxiliary telescopes: A pair of specialised movable 1.5m telescopes provide full U-V plane coverage in two dimensions as well as full-time use of the interferometer independently of the large telescope

## ASTRONOMICAL OPERATION

- Flexible scheduling: fast change of observing modes and instruments (less than 5 minutes); selection of observing program according to prevailing atmospheric conditions
- Remote observing through permanent data and communication link between on-site telescope operators and remote observers
- IR optimisation:
  - minimisation of obstruction to  $< 3\%$
  - optimised pupil imaging for cooled baffling inside the instruments
  - low emissivity coatings
  - built-in mirror washing facility
  - possibility of conversion to Cassegrain operation
  - chopping with standard secondary
- Minimisation of down-time: elimination of change-over with single focus, fixed configuration telescopes and stationary instrumentation.
- Operating conditions for optimum performance:
  - without windscreen: up to 9 m/s average wind speed
  - with windscreen: up to 18 m/s average wind speed

## VLT NOTES AND REPORTS

### 1980

- 1 ESO telescope plans for the future. Optical and IR telescopes for the 1990's. KPNO Proceedings. W. Richter

### 1981

- 2 Image quality and high resolution in future telescopes ESO conference - high angular resolution March 81 R.N. Wilson
- 3 Comparison of space and ground based telescope systems for optical telescopes, Nov. 81 (Internal Report) E.G. Wampler
- 4 Brief note on detector matching and image scales for large telescopes, Nov. 81 (Internal Report) M. Cullum

### 1982

- 5 Long baseline interferometry with large ground based telescopes, June 82. (Internal Report) O. Citterio
- 6 Signal to noise considerations in Fourier Transform spectroscopy of faint objects, March/Sept 82. Includes remarks from L. Debouille Aug. 82. (Internal Report) R.H. Miller
- 7 Very large telescope studies at ESO, April 82. 2nd ESO IR Workshop, proceedings. J.P. Swings
- 8 VLT versus space, April 82 2nd ESO IR Workshop, proceedings. A.F.M. Moorwood
- 9 Aperture synthesis in the IR, April 82 2nd ESO IR Workshop, proceedings. P. Léna

- 10 Estimation des performances que l'on peut attendre de l'interférométrie optique à longue base avec de grands télescopes au sol, Juin 82. Internal report published later, together with the following report in J. of Optics 1984, vol 15. F. Roddier
- 11 Perspectives de l'interférométrie IR directe avec de grands télescopes au sol, Sept 82. (Internal Report) P. Léna
- 1983  
[Notes 12 to 33 correspond to contributions published in the proceedings of the workshop on ESO VLT - Cargèse (May 1983)]
- 34 Optical Telescopes of the Future, Florence meeting Dec. 83 L. Woltjer
- 1984
- 35 Comparison of the Alt-Alt and Alt-Az mountings in the case of an array of four 8m telescopes, Feb. 84, VLT. (Internal Report) D. Enard
- 36 Optical System Analysis of various MMT concepts and comparison with a corresponding array, March 84. (Internal Report) D. Enard
- 37 Instrument matching in spectroscopy and direct imaging. IAU colloquium 79, proceedings. April 84. D. Enard
- 38 The Linear Array concept IAU colloquium 79, proceedings. April 84. D. Enard
- 39 The ESO VLT Project - Major concept discriminations. Minden meeting, Sept 84. D. Enard
- 40 Preliminary analysis of an 8m steel mirror blank for the ESO VLT. M. Schneermann
- 1985
- 41 A first evaluation of the effects of wind loading on the concept of the ESO Very Large Telescope June 85 L. Zago

- 42 Aperture synthesis (spatial interferometry) with the Very Large Telescope. Interim report of the working group on interferometry. Oct 85.
- 1986
- 43 Site testing at Cerro Paranal, results from 1983 A. Ardeberg
- 44 Very Large Telescope: interim report of the ESO study group.
- 45 Site testing at Cerro Paranal results from 1984 A. Ardeberg
- 46 Enclosure and building for the ESO VLT L. Zago
- 47 Adaptive optics for ESO's VLT project F. Merkle
- 48 Comparison of meteorological conditions on Chilean sites - annual summary 1985 M. Sarazin
- 49 Interferometric imaging with the VLT. Report from the ESO working group on interferometry.
- 50 VLT Working Group on high resolution spectroscopy (final report)
- 51 VLT Working Group on infrared aspects (final report)
- 52 Report to the ESO VLT project of the working group on imaging and low resolution spectroscopy
- 53 Proceedings of the second workshop on ESO's Very Large Telescope, Venice, 29 Sept - 2 Oct 86

## Appendix 3

## INSTITUTES AND INDUSTRIAL FIRMS WHICH HAVE CONTRIBUTED TO VLT STUDIES

ADES	B
ADS Italia s.r.l.	I
AHC Oberflächentechnik GmbH	D
AMOS	B
ALLEGA AG	CH
BCV Progetti s.r.l.	I
CNRM	F
Dr. Ing. V. Caramaschi	I
CNES	F
CERGA	F
CERN	
CGE (Laboratoire de Marcoussis)	F
COPPI Ugo s.r.l.	I
CREUSOT-LOIRE Industrie SA	F
DALIC SA	F
DANALITH A/S	DK
Albert DECAMPS	F
DELTA MARINE Consultants B.V.	NL
DORNIER Systems GmbH	D
Ecole Polytechnique Federale de Lausanne	CH
ESCHER-WYSS	CH
Fol et Duchemin	CH
HERAEUS Quarzschmelze	D
HONSEL-Werke AG	D
IRAM	D/F
Instituto di Fisica Cosmica, CNR, Milano	I
LEYBOLD-HERAEUS	D
LINDE	D
M.A.N AG	D
MATRA SA	F
MONTUPET SA	F
NEYRPIC SA	F
NEYRTEC SA	F
Observatoire de MEUDON	F
ONERA	F
POLY-NEDERLAND	NL
REMTECH	F
REOSC SA	F

Heinrich Schnarr GmbH	D
SCHOTT Glaswerke	D
SODETEG SA	F
STEIGER SA	CH
SULZER Brothers Ltd	CH
THYSSEN Schwerkomponenten GmbH	D
University of LUND	S
Universitat MUNCHEN	D
Universite de NICE	F
Universite de ROUEN (CORIA)	F
CARL ZEISS	D